

NOAA Technical Memorandum OAR ARL-268

doi:10.7289/V5VX0DHV



PROJECT SAGEBRUSH PHASE 1

D. Finn
K.L. Clawson
R.M. Eckman
R.G. Carter
J.D. Rich
T.W. Strong
S.A. Beard
B.R. Reese
D. Davis
H. Liu
E. Russell
Z. Gao
S. Brooks

Air Resources Laboratory
College Park, Maryland
July 2015

NOAA Technical Memorandum OAR ARL-268

doi:10.7289/V5VX0DHV

PROJECT SAGEBRUSH PHASE 1

D. Finn¹
K.L. Clawson¹
R.M. Eckman¹
R.G. Carter¹
J.D. Rich¹
T.W. Strong¹
S.A. Beard¹
B.R. Reese¹
D. Davis¹
H. Liu²
E. Russell²
Z. Gao²
S. Brooks³

Field Research Division¹
Idaho Falls, Idaho

Laboratory for Atmospheric Research²
Washington State University

The University of Tennessee Space Institute³
Tullahoma, Tennessee

Air Resources Laboratory
College Park, Maryland
July 2015



**UNITED STATES
DEPARTMENT OF COMMERCE**

Penny Pritzker
Secretary

**NATIONAL OCEANIC AND
ATMOSPHERIC ADMINISTRATION**

Dr. Kathryn D. Sullivan
Under Secretary for Oceans
and Atmosphere/Administrator

**Office of Oceanic and
Atmospheric Research**

Craig McLean
Assistant Administrator
Oceanic & Atmospheric
Research

NOTICE

This report was prepared as an account of work sponsored by an agency of the United States Government. Neither the United States Government nor any agency thereof, or any of their employees, makes any warranty, expressed or implied, or assumes any legal liability or responsibility for any third party's use, or the results of such use, of any information, apparatus, product, or process disclosed in this report, or represents that its use by such third party would not infringe on privately owned rights. Mention of a commercial company or product does not constitute an endorsement by NOAA/OAR. Use of information from this publication concerning proprietary products or tests of such products for publicity or advertising is not authorized.

TABLE OF CONTENTS

NOTICE	ii
TABLE OF CONTENTS	iii
FIGURES	vii
TABLES	xix
ABSTRACT	xxi
INTRODUCTION	1
EXPERIMENTAL PLAN	7
Grid 3 Dispersion Array and Release	7
Bag Sampling	8
Fast Response Tracer Gas Analyzers	9
Aircraft Operations	10
Meteorological Equipment	13
IOP Summaries	14
THE SF ₆ TRACER RELEASE SYSTEM	15
Accuracy	17
SF ₆ Release Summary	18
SF ₆ Release Quality Control	21
Data File Format	23
BAG SAMPLING	25
Description of Equipment	25
Description of Bag Sampling Grid	26
Sampler Cartridge Analysis	27
Sampler Handling and Chain of Custody	29
Quality Control Procedures and Measurement Quality Objectives	33
Final Bag Sampler Data Files and Format	64
Final Data File Quality Control Flags	64
FAST RESPONSE TRACER ANALYZERS	67
Quality Flags	68
Instrument Description	69
Calibration and Concentration Determination	71
MLOD/MLOQ	72

Accuracy Verification Tests	73
Quality Control (QC)	75
METEOROLOGICAL MEASUREMENTS	83
Grid 3 Tower (GRI)	85
NOAA ARLFRD	87
Sonic Anemometers	87
Experimental Setup	87
Quality Control	88
Data File Formats	91
Other Measurements	95
Configuration	95
Quality Control	96
Data File Formats	96
WSULAR	97
Sonic Anemometers	97
Experimental Setup	97
Quality Control	98
Data File Formats	98
Other Measurements	104
Experimental Setup	104
Quality Control	105
Data File Formats	105
Meteorological Towers on Sampling Grid	106
Experimental Setup	106
Quality Control	108
Data File Formats	108
Sonic Anemometers on Sampling Grid	110
Experimental Setup	110
Quality Control	110
Data File Formats	111
Sodars	111
Experimental Setup	111
Quality Control	112
Data File Formats	112
Radar Wind Profiler and RASS	113
Experimental Setup	113
Quality Control	114
Data File Formats	114
Flux Station	115
Experimental Setup	115
Quality Control	116
Data File Formats	117

Radiosondes	121
Experimental Procedures	121
Quality Control	123
Data Files and Results	123
NOAA/INL Mesonet	130
Configuration	130
Quality Control	131
Data File Formats	131
 SUMMARY OF INDIVIDUAL IOPs	 133
Introduction	133
IOP1	134
Date/Time and General Description	134
Winds and Quality Assurance	135
Turbulence	144
Stability	156
Radiosonde Results	156
Concentration Results and Analysis	157
IOP2	170
Date/Time and General Description	170
Winds and Quality Assurance	170
Turbulence	180
Stability	192
Radiosonde Results	192
Concentration Results and Analysis	193
IOP3	206
Date/Time and General Description	206
Winds and Quality Assurance	206
Turbulence	215
Stability	227
Radiosonde Results	227
Concentration Results and Analysis	228
IOP4	243
Date/Time and General Description	243
Winds and Quality Assurance	243
Turbulence	251
Stability	263
Radiosonde Results	263
Concentration Results and Analysis	264

IOP5	275
Date/Time and General Description	275
Winds and Quality Assurance	275
Turbulence	283
Stability	295
Radiosonde Results	295
Concentration Results and Analysis	296
PRELIMINARY ANALYSIS	307
DETERMINATION OF σ_Y	307
Methods for Determining σ_Y	307
Comparison of σ_y Results by the Three Methods	308
σ_y Comparisons Between PSB1 and Previous Work	311
PSB1 σ_θ and Turbulence Intensity Measurements	318
Miscellaneous Observations and Calculations of σ_y	321
DETERMINATION OF σ_Z	324
TOWER DATA COMPARISONS	328
FAST RESPONSE ANALYZER ANALYSES	329
REFERENCES	335

FIGURES

Figure 1. Location of Grid 3 (star) on the INL in SE Idaho.	1
Figure 2. Google Earth image of the Grid 3 area.	4
Figure 3. Photo from Grid 3 tower looking northeast toward the tracer sampling array along the radial road through the tracer sampling array. The command center (COC) tower and wind profiler installation (PRO) are visible in the right center of the photo.	4
Figure 4. Photo of the Grid 3 tower.	5
Figure 5. Configuration of PSB1 field tracer experiments. The 3-character labels are defined in the text.	7
Figure 6. Photo of bag sampler mounting.	8
Figure 7. Photo of Piper Navajo airplane used for airborne sampling of tracer.	10
Figure 8. Flight pattern used during Phase 1. The aircraft started at the 3200 m downwind distance (black circle) and then made successive passes closer to the source. After the closest pass at 200 m downwind, the aircraft flew downwind along the plume centerline before exiting the pattern (black arrow). The full pattern was repeated at several levels above the ground. The hatched areas labeled ATRC and INTEC are building complexes that the aircraft was required to avoid.	12
Figure 9. The SF ₆ release system inside the cargo trailer including the SF ₆ bottles, mass flow controller, computer data acquisition and control system, and electronic scales under the bottles.	15
Figure 10. The cargo trailer where the release system was housed on location at the Grid 3 facility.	15
Figure 11. Schematic of SF ₆ tracer release system.	16
Figure 12. Liquid SF ₆ certificate of analysis.	17
Figure 13. SF ₆ release rate for IOP1.	19
Figure 14. SF ₆ release rate for IOP2.	19
Figure 15. SF ₆ release rate for IOP3.	20
Figure 16. SF ₆ release rate for IOP4.	20
Figure 17. SF ₆ release rate for IOP5.	21
Figure 18. Bag sampler with cover and cartridge removed.	25
Figure 19. Sampler cartridge.	25
Figure 20. Bag sampler with sampler cartridge installed.	26
Figure 21. ATGASs in lab.	27
Figure 22. ATGASs in lab with computer	27
Figure 23. Schematic of sample loop fill with column 1 (pre-column) in the back-flush position.	28
Figure 24. Schematic of injection to column 1 (pre-column) and on to column 2 (main column).	28
Figure 25. Timewand.	29
Figure 26. Sampler servicing procedure A: Placing a sampler at a location.	30
Figure 27. Sampler servicing procedure B: Retrieving a sampler.	30
Figure 28. Sampler servicing procedure C: Replacing a cartridge.	31

Figure 29. Example of Sampler Servicing Record. This was from cartridge removal after Test 1.	32
Figure 30. Cartridge cleaning apparatus.	36
Figure 31. Comparison between measured and NIST-certified standard concentrations for all lab control (CCV) samples.	43
Figure 32. Linear regression of rerun against original values for all laboratory duplicates. ...	45
Figure 33. Linear regression field control samples.	48
Figure 34. Linear regressions for all field duplicate samples.	49
Figure 35. Example of Raw Data Summary sheet.	51
Figure 36. Example of first page of quality control sheet.	52
Figure 37. Example of last page from quality control sheets.	53
Figure 38. Example of chromatogram and calibration curve check sheet.	54
Figure 39. Example of laboratory notebook page.	55
Figure 40. Example of data package Data Verification sheet.	56
Figure 41. Example of Analysis Summary sheet.	57
Figure 42. Example of bubble/dot plot for examining consistency of concentrations between neighboring locations and identifying suspicious values.	60
Figure 43. Example of cartridge time series plots used for identifying suspicious values.	61
Figure 44. Example of output from program used to assign flags to values in final data set and final check for possible errors.	62
Figure 45. FRD mobile, fast response, tracer gas analyzer consisting of a data acquisition system, a TGA-4000 below the data acquisition system, and a calibration gas cartridge (foreground) installed in the passenger side seat.	70
Figure 46. Fast response tracer gas analyzer system installed in Piper Navajo aircraft.	71
Figure 47. Operating checklist for fast response analyzers.	76
Figure 48. An example of a fast response analyzer Settings Record.	77
Figure 49. Example of a fast response analyzer QC sheet.	80
Figure 50. Schematic representation of the 62 m Grid 3 tower instrumentation. All anemometers mounted transverse to the prevailing wind direction on booms extending from the tower. Barometric pressure, rain gauge, and soil heat flux not shown.	86
Figure 51. A closeup picture of an R. M. Young Ultrasonic 81000 (left) and a Gill Windmaster Pro (right) used during PSB1.	87
Figure 52. An Acumen data collection bridge (white device inside box) is used to collect data from the sonic anemometers.	88
Figure 53. 30 m command center meteorological and tracer sampling tower (COC).	107
Figure 54. Photo of the ASC sodar, collocated with radar wind profiler at PRO.	111
Figure 55. Photo of the radar wind profiler and RASS.	114
Figure 56. Photo of the flux station.	116
Figure 57. Photo of releasing the radiosonde.	121
Figure 58. Example balloon profile data diagram from IOP1, Launch 1, with atmospheric pressure (green), relative humidity (orange), air temperature (blue), balloon ascent rate	

	(black), wind speed (red), and radiosonde height AGL (black) plotted as a function of time after launch. The time stamp is the start of the ascent in UTC.	124
Figure 59.	Example thermodynamic (Stueve) diagram from IOP1, Launch 1, with relative humidity (orange), air temperature (blue), wind direction (black), and wind speed (red) plotted as a function of geopotential height MSL. The time stamp is the start of the ascent in UTC.	125
Figure 60.	Example tephigram from IOP1, Launch 1, with air temperature (blue), wet bulb temperature (red) and dew point temperature (orange) plotted on a temperature/potential temperature graph. The time stamp is the start of the ascent in UTC.	126
Figure 61.	Example Skew-T diagram from IOP1, Launch 1, with air temperature (blue) and dew point temperature (orange) plotted on a temperature/pressure graph. The time stamp is the start of the ascent in UTC.	127
Figure 62.	Example emagram from IOP1, Launch 1, with air temperature (blue) and dew point temperature (orange) plotted on a temperature/pressure graph. The time stamp is the start of the ascent in UTC.	128
Figure 63.	Example altitude diagram from IOP1, Launch 1, with wind speed (red), relative humidity (orange), temperature (blue), and wind direction (black) plotted as a function of height. The time stamp is the start of the ascent in UTC.	129
Figure 64.	ARLFRD wind speed and direction comparisons in the vertical at GRI and COC for IOP1.	136
Figure 65.	Standard deviation in wind direction σ_{θ} (σ_A) using the wind vanes at GRI, COC, and TOW for IOP1.	137
Figure 66.	ARLFRD wind speed and direction comparisons in the horizontal at 2 and 10 m during IOP1.	139
Figure 67.	ARLFRD wind speed and direction comparisons in the horizontal at 30 and 45 m during IOP1.	140
Figure 68.	ARLFRD wind speed and direction comparisons in the horizontal at 60 and 160 m during IOP1.	141
Figure 69.	Time-height cross-section of wind speed and direction at ASC sodar during IOP1.	142
Figure 70.	Time-height cross-section of wind speed and direction at ART sodar during IOP1.	143
Figure 71.	Time-height cross-section of wind speed and direction at wind profiler (PRO) during IOP1.	144
Figure 72.	ARLFRD sonic anemometer 10-minute averages for σ_w , TKE, u^* , kinematic heat flux, and $1/L$ during IOP1 (G1, G2, R2, R3, and R4).	145
Figure 73.	ARLFRD sonic anemometer 30-minute averages for σ_w , TKE, u^* , kinematic heat flux, and $1/L$ during IOP1 (G1, G2, R2, R3, R4, and FLX).	146
Figure 74.	Time-height cross-section of σ_w at ASC sodar during IOP1.	147
Figure 75.	Time-height cross-section of TKE at ASC sodar during IOP1.	148
Figure 76.	Time-height cross-section of σ_w at ART sodar during IOP1.	148
Figure 77.	Time-height cross-section of TKE at ART sodar during IOP1.	149

Figure 78. Time-height cross-section of virtual temperature at the RASS during IOP1. Temperatures are in degrees C.	149
Figure 79. Vertical profiles of wind speed and direction from sonic anemometer measurements at GRI during IOP1. ARLFRD instruments were at 4 and 30 m; WSULAR instruments were at 2, 8, and 16 m. Times in legend are start times for the 10 minute interval (hhmm MST).	151
Figure 80. Vertical profiles of turbulence intensity and σ_w from sonic anemometer measurements at GRI during IOP1. ARLFRD instruments were at 4 and 30 m; WSULAR instruments were at 2, 8, and 16 m. Times in legend are start times for the 10 minute interval (hhmm MST).	152
Figure 81. Vertical profiles of turbulent kinetic energy (TKE) and u^* from sonic anemometer measurements at GRI during IOP1. ARLFRD instruments were at 4 and 30 m; WSULAR instruments were at 2, 8, and 16 m. Times in legend are start times for the 10 minute interval (hhmm MST).	153
Figure 82. Vertical profiles of wind speed and direction from cup anemometer and wind vane measurements at GRI during IOP1. Times in legend are start times for the 10 minute interval (hhmm MST).	154
Figure 83. Vertical profiles of σ_θ (from cup and vane) and aspirated air temperature measurements at GRI during IOP1. Times in legend are start times for the 10 minute interval (hhmm MST).	155
Figure 84. Pre and post IOP radiosonde potential temperature profiles for IOP1.	156
Figure 85. Pre and post IOP radiosonde specific humidity profiles for IOP1.	157
Figure 86. Bag sampling results (a-f, bags 1-6) for IOP1 with color-coded concentration markers for each 1 m AGL bag sampling location and contour lines of normalized concentration. The color scheme for the markers and contours is described in the Introduction to this section.	158
Figure 87. Cross-sections of concentration along each arc for each 10-minute bag sampling period during IOP1. The individual plume cross-section layouts are arranged to illustrate the variation in time, across 40 minutes per layout (bags 1-4), and the simultaneous variation with distance across all four arcs.	161
Figure 88. Vertical concentration profiles (a-f, bags 1-6) at the towers at 201, 408, and 499 m downwind for all 10-minute bag sampling intervals for IOP1. Round black markers show the average concentration obtained from aircraft measurements at the plotted height. The approximate downwind distance of the aircraft measurement is indicated in the legend.	165
Figure 89. Time series of SF ₆ concentrations measured by the fast response analyzers at the specified arc and arc angle location during IOP1.	167
Figure 90. Time series of aircraft height and SF ₆ concentrations measured by the onboard fast response analyzer during IOP1. Heights are approximate AGL calculated by subtracting the elevation at the release from the aircraft altitude.	168
Figure 91. Color-coded concentrations along the aircraft flight path during IOP1 for (a) the overall flight path and (b) zoomed in over the bag sampling array. The color scheme and significance of the black markers are described in the Introduction to this section. They are linked to the black markers in Fig. 88 where b# is bag number and avgloc is average	

location.	169
Figure 92. ARLFRD wind speed and direction comparisons in the vertical at GRI and COC for IOP2.	172
Figure 93. Standard deviation in wind direction σ_θ (σ_Λ) using wind vanes at GRI, COC, and TOW for IOP2.	173
Figure 94. ARLFRD wind speed and direction comparisons in the horizontal at 2 and 10 m during IOP2.	175
Figure 95. ARLFRD wind speed and direction comparisons in the horizontal at 30 and 45 m during IOP2.	176
Figure 96. ARLFRD wind speed and direction comparisons in the horizontal at 60 and 160 m during IOP2.	177
Figure 97. Time-height cross-section of wind speed and direction at ASC sodar during IOP2.	178
Figure 98. Time-height cross-section of wind speed and direction at ART sodar during IOP2.	179
Figure 99. Time-height cross-section of wind speed and direction at wind profiler (PRO) during IOP2.	180
Figure 100. ARLFRD sonic anemometer 10-minute averages for σ_w , TKE, u_* , kinematic heat flux, and $1/L$ during IOP2 (G1, G2, R2, R3, and R4)	181
Figure 101. ARLFRD sonic anemometer 30-minute averages for σ_w , TKE, u_* , kinematic heat flux, and $1/L$ during IOP2 (G1, G2, R2, R3, and R4).	182
Figure 102. Time-height cross-section of σ_w at ASC sodar during IOP2.	183
Figure 103. Time-height cross-section of TKE at ASC sodar during IOP2.	184
Figure 104. Time-height cross-section of σ_w at ART sodar during IOP2.	184
Figure 105. Time-height cross-section of TKE at ART sodar during IOP2.	185
Figure 106. Time-height cross-section of virtual temperature at the RASS during IOP2. Temperatures are in degrees C.	186
Figure 107. Vertical profiles of wind speed and direction from sonic anemometer measurements at GRI during IOP2. ARLFRD instruments were at 4, 30, and 45 m; WSULAR instruments were at 2, 8, 16, and 60 m. Times in legend are start times for the 10 minute interval (hhmm MST).	187
Figure 108. Vertical profiles of turbulence intensity and σ_w from sonic anemometer measurements at GRI during IOP2. ARLFRD instruments were at 4, 30, and 45 m; WSULAR instruments were at 2, 8, 16, and 60 m. Times in legend are start times for the 10 minute interval (hhmm MST).	188
Figure 109. Vertical profiles of turbulent kinetic energy (TKE) and u_* from sonic anemometer measurements at GRI during IOP2. ARLFRD instruments were at 4, 30, and 45 m; WSULAR instruments were at 2, 8, 16, and 60 m. Times in legend are start times for the 10 minute interval (hhmm MST).	189
Figure 110. Vertical profiles of wind speed and direction from cup anemometer and wind vane measurements at GRI during IOP2. Times in legend are start times for the 10 minute interval (hhmm MST).	190

Figure 111. Vertical profiles of σ_θ (from cup anemometers and wind vanes) and aspirated air temperature measurements at GRI during IOP2. Times in legend are start times for the 10 minute interval (hhmm MST).	191
Figure 112. Pre and post IOP radiosonde potential temperature profiles for IOP2.	192
Figure 113. Pre and post IOP radiosonde specific humidity profiles for IOP2.	193
Figure 114. Bag sampling results (a-f, bags 1-6) for IOP2 with color-coded concentration markers for each 1 m AGL bag sampling location and contour lines of normalized concentration. The color scheme for the markers and contours is described in the Introduction to this section.	194
Figure 115. Cross-sections of concentration along each arc for each 10-minute bag sampling period during IOP2. The individual plume cross-section layouts are arranged to illustrate the variation in time, across 40 minutes per layout (a-d, bags 1-4), and the simultaneous variation with distance across all four arcs.	197
Figure 116. Vertical concentration profiles (bags 1-6) at the towers at 201, 408, and 499 m downwind for all 10-minute bag sampling intervals for IOP2. Round black markers show the average concentration obtained from aircraft measurements at the plotted height. The approximate downwind distance indicated of the aircraft measurement is indicated in the legend.	201
Figure 117. Time series of SF ₆ concentrations measured by the fast response analyzers at the specified arc and arc angle location during IOP2.	203
Figure 118. Time series of aircraft height and SF ₆ concentrations measured by the onboard fast response analyzer during IOP2. Heights are approximate AGL calculated by subtracting the elevation at the release from the aircraft altitude.	204
Figure 119. Color-coded concentrations along the aircraft flight path during IOP2 for (a) the overall flight path and (b) zoomed in over the bag sampling array. The color scheme and significance of the black markers are described in the Introduction to this section. They are linked to the black markers in Fig.116 where b# is bag number and avgloc is average location.	205
Figure 120. ARLFRD wind speed and direction comparisons in the vertical at GRI and COC for IOP3.	207
Figure 121. Standard deviation in wind direction σ_θ (σ_A) using wind vanes at GRI, COC, and TOW for IOP3.	208
Figure 122. ARLFRD wind speed and direction comparisons in the horizontal at 2 and 10 m during IOP3.	210
Figure 123. ARLFRD wind speed and direction comparisons in the horizontal at 30 and 45 m during IOP3.	211
Figure 124. ARLFRD wind speed and direction comparisons in the horizontal at 60 and 160 m during IOP3.	212
Figure 125. Time-height cross-section of wind speed and direction at ASC sodar during IOP3.	213
Figure 126. Time-height cross-section of wind speed and direction at ART sodar during IOP3.	214

Figure 127. Time-height cross-section of wind speed and direction at wind profiler (PRO) during IOP3.	215
Figure 128. ARLFRD sonic anemometer 10-minute averages for σ_w , TKE, u_* , kinematic heat flux, and $1/L$ during IOP3 (G1, G2, R2, R3, and R4).	216
Figure 129. ARLFRD sonic anemometer 30-minute averages for σ_w , TKE, u_* , kinematic heat flux, and $1/L$ during IOP3 (G1, G2, R2, R3, and R4).	217
Figure 130. Time-height cross-section of σ_w at ASC sodar during IOP3.	218
Figure 131. Time-height cross-section of TKE at ASC sodar during IOP3.	219
Figure 132. Time-height cross-section of σ_w at ART sodar during IOP3.	219
Figure 133. Time-height cross-section of TKE at ART sodar during IOP3.	220
Figure 134. Time-height cross-section of virtual temperature at the RASS during IOP3. Temperatures are in degrees C.	220
Figure 135. Vertical profiles of wind speed and direction from sonic anemometer measurements at GRI during IOP3. ARLFRD instruments were at 4, 30, and 45 m; WSULAR instruments were at 2, 8, 16, and 60 m. Times in legend are start times for the 10 minute interval (hhmm MST).	222
Figure 136. Vertical profiles of turbulence intensity and σ_w from sonic anemometer measurements at GRI during IOP3. ARLFRD instruments were at 4, 30, and 45 m; WSULAR instruments were at 2, 8, 16, and 60 m. Times in legend are start times for the 10 minute interval (hhmm MST).	223
Figure 137. Vertical profiles of turbulent kinetic energy (TKE) and u_* from sonic anemometer measurements at GRI during IOP3. ARLFRD instruments were at 4, 30, and 45 m; WSULAR instruments were at 2, 8, 16, and 60 m. Times in legend are start times for the 10 minute interval (hhmm MST).	224
Figure 138. Vertical profiles of wind speed and direction from cup anemometer and wind vane measurements at GRI during IOP3. Times in legend are start times for the 10 minute interval (hhmm MST).	225
Figure 139. Vertical profiles of σ_θ (from cup and vane) and aspirated air temperature measurements at GRI during IOP3. Times in legend are start times for the 10 minute interval (hhmm MST).	226
Figure 140. Pre and post IOP radiosonde potential temperature profiles for IOP3.	227
Figure 141. Pre and post IOP radiosonde specific humidity profiles for IOP3.	228
Figure 142. Bag sampling results (a-f, bags 1-6) for IOP3 with color-coded concentration markers for each 1 m AGL bag sampling location and contour lines of normalized concentration. The color scheme for the markers and contours is described in the Introduction to this section.	229
Figure 143. Cross-sections of concentration along each arc for each 10-minute bag sampling period during IOP3. The individual plume cross-section layouts are arranged to illustrate the variation in time, across 40 minutes per layout (a-d, bags 1-4), and the simultaneous variation with distance across all four arcs.	232
Figure 144. Vertical concentration profiles (a-f, bags 1-6) at the towers at 201, 408, and 499 m downwind for all 10-minute bag sampling intervals for IOP3. Round black markers show	

the average concentration obtained from aircraft measurements at the plotted height. The approximate downwind distance of the aircraft measurements is indicated in the legend. 236

Figure 145. Time series of SF₆ concentrations measured by the fast response analyzers at the specified arc and arc angle location during IOP3. 239

Figure 146. Time series of aircraft height and SF₆ concentrations measured by the onboard fast response analyzer during IOP3. Heights are approximate AGL calculated by subtracting the elevation at the release from the aircraft altitude. 241

Figure 147. Color-coded concentrations along the aircraft flight path during IOP3 for (a) the overall flight path and (b) zoomed in over the bag sampling array. The color scheme and significance of the black markers are described in the Introduction to this section. They are linked to the black markers in Fig. 144 where b# is bag number and avgloc is average location. 242

Figure 148. ARLFRD wind speed and direction comparisons in the vertical at GRI and COC for IOP4. 244

Figure 149. Standard deviation in wind direction σ_{θ} (σ_A) using wind vanes at GRI and COC for IOP4. 245

Figure 150. ARLFRD wind speed and direction comparisons in the horizontal at 2 and 10 m during IOP4. 246

Figure 151. ARLFRD wind speed and direction comparisons in the horizontal at 30 and 45 m during IOP4. 247

Figure 152. ARLFRD wind speed and direction comparisons in the horizontal at 60 and 160 m during IOP4. 248

Figure 153. Time-height cross-section of wind speed and direction at ASC sodar during IOP4. 249

Figure 154. Time-height cross-section of wind speed and direction at ART sodar during IOP4. 250

Figure 155. Time-height cross-section of wind speed and direction at wind profiler (PRO) during IOP4. 251

Figure 156. ARLFRD sonic anemometer 10-minute averages for σ_w , TKE, u^* , kinematic heat flux, and $1/L$ during IOP4 (G1, G2, R2, R3, and R4). 252

Figure 157. ARLFRD sonic anemometer 30-minute averages for σ_w , TKE, u^* , kinematic heat flux, and $1/L$ during IOP4 (G1, G2, R2, R3, and R4). 253

Figure 158. Time-height cross-section of σ_w at ASC sodar during IOP4. 254

Figure 159. Time-height cross-section of TKE at ASC sodar during IOP4. 255

Figure 160. Time-height cross-section of σ_w at ART sodar during IOP4. 255

Figure 161. Time-height cross-section of TKE at ART sodar during IOP4. 256

Figure 162. Time-height cross-section of virtual temperature at the RASS during IOP4. Temperatures are in degrees C. 256

Figure 163. Vertical profiles of wind speed and direction from sonic anemometer measurements at GRI during IOP4. ARLFRD instruments were at 4, 30, and 45 m; WSULAR instruments were at 2, 8, 16, and 60 m. Times in legend are start times for the 10 minute interval (hhmm MST). 258

Figure 164. Vertical profiles of turbulence intensity and σ_w from sonic anemometer

	measurements at GRI during IOP4. ARLFRD instruments were at 4, 30, and 45 m; WSULAR instruments were at 2, 8, 16, and 60 m. Times in legend are start times for the 10 minute interval (hhmm MST).	259
Figure 165.	Vertical profiles of turbulent kinetic energy (TKE) and u^* from sonic anemometer measurements at GRI during IOP4. ARLFRD instruments were at 4, 30, and 45 m; WSULAR instruments were at 2, 8, 16, and 60m. Times in legend are start times for the 10 minute interval (hhmm MST).	260
Figure 166.	Vertical profiles of wind speed and direction from cup anemometer and wind vane measurements at GRI during IOP4. Times in legend are start times for the 10 minute interval (hhmm MST).	261
Figure 167.	Vertical profiles of σ_θ (from cup and vane) and aspirated air temperature measurements at GRI during IOP4. Times in legend are start times for the 10 minute interval (hhmm MST).	262
Figure 168.	Pre and post IOP radiosonde potential temperature profiles for IOP4.	263
Figure 169.	Pre and post IOP radiosonde specific humidity profiles for IOP4.	264
Figure 170.	Bag sampling results (a-f, bags 1-6) for IOP4 with color-coded concentration markers for each 1 m AGL bag sampling location and contour lines of normalized concentration. The color scheme for the markers and contours is described in the Introduction to this section.	265
Figure 171.	Cross-sections of concentration along each arc for each 10-minute bag sampling period during IOP4. The individual plume cross-section layouts are arranged to illustrate the variation in time, across 40 minutes per layout (a-d, bags 1-4), and the simultaneous variation with distance across all four arcs.	268
Figure 172.	Vertical concentration profiles (a-f, bags 1-6) at the towers at 201, 408, and 499 m downwind for all 10-minute bag sampling intervals for IOP4. No aircraft measurements were available.	271
Figure 173.	Time series of SF ₆ concentrations measured by the fast response analyzers at the specified arc and arc angle location during IOP4.	274
Figure 174.	ARLFRD wind speed and direction comparisons in the vertical at GRI and COC for IOP5.	276
Figure 175.	Standard deviation in wind direction σ_θ (σ_A) using wind vanes at GRI and COC for IOP5.	277
Figure 176.	ARLFRD wind speed and direction comparisons in the horizontal at 2 and 10 m during IOP5.	278
Figure 177.	ARLFRD wind speed and direction comparisons in the horizontal at 30 and 45 m during IOP5.	279
Figure 178.	ARLFRD wind speed and direction comparisons in the horizontal at 60 and 160 m during IOP5.	280
Figure 179.	Time-height cross-section of wind speed and direction at ASC sodar during IOP5.	281
Figure 180.	Time-height cross-section of wind speed and direction at ART sodar during IOP5.	282
Figure 181.	Time-height cross-section of wind speed and direction at wind profiler (PRO) during IOP5.	283

Figure 182. ARLFRD sonic anemometer 10-minute averages for σ_w , TKE, u^* , kinematic heat flux, and $1/L$ during IOP5 (G1, G2, R2, R3, and R4).	284
Figure 183. ARLFRD sonic anemometer 30-minute averages for σ_w , TKE, u^* , kinematic heat flux, and $1/L$ during IOP5 (G1, G2, R2, R3, and R4).	285
Figure 184. Time-height cross-section of σ_w at ASC sodar during IOP5.	286
Figure 185. Time-height cross-section of TKE at ASC sodar during IOP5.	287
Figure 186. Time-height cross-section of σ_w at ART sodar during IOP5.	287
Figure 187. Time-height cross-section of TKE at ART sodar during IOP5.	288
Figure 188. Time-height cross-section of virtual temperature at the RASS during IOP5. Temperatures are in degrees C.	288
Figure 189. Vertical profiles of wind speed and direction from sonic anemometer measurements at GRI during IOP5. ARLFRD instruments were at 4, 30, and 45 m; WSULAR instruments were at 2, 8, 16, and 60 m. Times in legend are start times for the 10 minute interval (hhmm MST).	290
Figure 190. Vertical profiles of turbulence intensity and σ_w from sonic anemometer measurements at GRI during IOP5. ARLFRD instruments were at 4, 30, and 45 m; WSULAR instruments were at 2, 8, 16, and 60 m. Times in legend are start times for the 10 minute interval (hhmm MST).	291
Figure 191. Vertical profiles of turbulent kinetic energy (TKE) and u^* from sonic anemometer measurements at GRI during IOP5. ARLFRD instruments were at 4, 30, and 45 m; WSULAR instruments were at 2, 8, 16, and 60 m. Times in legend are start times for the 10 minute interval (hhmm MST).	292
Figure 192. Vertical profiles of wind speed and direction from cup anemometer and wind vane measurements at GRI during IOP5. Times in legend are start times for the 10 minute interval (hhmm MST).	293
Figure 193. Vertical profiles of σ_θ (from cup and vane) and aspirated air temperature measurements at GRI during IOP5. Times in legend are start times for the 10 minute interval (hhmm MST).	294
Figure 194. Pre and post IOP radiosonde potential temperature profiles for IOP5.	295
Figure 195. Pre and post IOP radiosonde specific humidity profiles for IOP5.	296
Figure 196. Bag sampling results (a-f, bags 1-6) for IOP5 with color-coded concentration markers for each 1 m AGL bag sampling location and contour lines of normalized concentration. The color scheme for the markers and contours is described in the Introduction to this section.	297
Figure 197. Cross-sections of concentration along each arc for each 10-minute bag sampling period during IOP5. The individual plume cross-section layouts are arranged to illustrate the variation in time, across 40 minutes per layout (a-d, bags 1-4), and the simultaneous variation with distance across all four arcs.	300
Figure 198. Vertical concentration profiles (a-f, bags 1-6) at the towers at 201, 408, and 499 m downwind for all 10-minute bag sampling intervals for IOP5. No aircraft measurements were available.	303
Figure 199. Time series of SF_6 concentrations measured by the fast response analyzers at the specified arc and arc angle location during IOP5.	305
Figure 200. Comparison between σ_y calculated by the three methods using shifted, aligned, and	

	combined plume cross-sections for IOPs (T) 2, 3, 4, and 5. For ‘xsig’ the value of $b=1.0$; for ‘xsigb’ the value of $b=0.894$. The bold line is a 1:1 reference.	309
Figure 201.	σ_y calculated using the $x^b\sigma_\theta$ and second moment methods for b equal to (a) 1.0, (b) 0.894, and (c) 0.85.	310
Figure 202.	σ_y calculated using second moment method with individual PSB1 10-minute intervals classified by σ_A P-G stability class (EPA 2000c) with linear fit compared to σ_y P-G curves calculated from Turner (1969, 1970).	311
Figure 203.	Calculated σ_y with best-fit lines for stability classes A, B, C, and D including all averaging periods for each class. Truncated profiles excluded.	313
Figure 204.	Plots of PSB1 σ_y results for qualifying profiles binned by stability class (A, B, C, D) and averaging period (10, 20, 30, 40, 60 minutes). Project Prairie Grass (PPG) results and the dispersion model curves for Markee, P-G, and Briggs are shown for comparison.	314
Figure 205.	Calculated PSB1 σ_y results for qualifying profiles binned by averaging period (10, 20, 30, 40, and 60 minutes).	315
Figure 206.	Comparison between σ_y calculated from the Taylor theory relationship $\sigma_y = \sigma_v t$ for sonics G1, G2, R2, R3, and R4 to the class A and D stability class dispersion curves from Markee, P-G, and Briggs.	316
Figure 207.	5-minute average cup and vane σ_θ for all IOPs from COC and GRI at 10 m AGL as function of wind speed.	318
Figure 208.	Wind vane anemometer measurements of σ_θ during IOPs 2, 3, and 4 during PSB1.	319
Figure 209.	Comparisons between GRI cup and vane (CV) σ_θ measurements, converted to radians, and sonic anemometer measurements of turbulence intensity for each 10-minute period of IOPs 2, 3, and 4. Times indicated in the legends are MST start times	320
Figure 210.	σ_y calculated by second moment method on non-truncated profiles for IOPs 2-5 as a function of σ_θ for different distances and averaging periods (dist_ap).	322
Figure 211.	Plot of σ_y/σ_θ for non-truncated cross-sections. These results are roughly consistent with the “universal” relation posited by Pasquill (1976) although they tend to lie near or just above the upper bound of the range shown there.. . . .	322
Figure 212.	σ_y calculated on non-truncated cross-sections by the second moment method as a function of the stability parameter z/L for the five downwind distances in PSB1. The z/L were determined at the sonic anemometers R3 and R4 on the 3200 m arc.	324
Figure 213.	Calculated σ_z with linear best-fit lines for stability classes A, B, C, and D including all averaging periods for each class. Truncated profiles excluded.	326
Figure 214.	Plots of PSB1 σ_z results for qualifying profiles binned by stability class (A, B, C, D) and averaging period (10, 20, 30, 40, 60 minutes). The dispersion curves for Markee and PG (Turner, 1969, 1970; Martin, 1976) are shown for comparison.	327
Figure 215.	Calculated PSB1 σ_z results for qualifying profiles binned by averaging period (10, 20, 30, 40, and 60 minutes).	328

Figure 216. Comparison between concentrations measured at the towers to concentrations calculated by the Gaussian plume formula for IOPs 2 and 5. 329

Figure 217. Intermittency (no zeros fraction) and unconditional (U) and conditional (C) concentration fluctuation intensities for IOPs 1 (a) and 2 (b). Intermittency is equivalent to time in plume. 331

Figure 218. Unconditional (U) and conditional (C) concentration fluctuation intensities and 95th percentile P:M as a function of intermittency (fraction of time in plume). 333

TABLES

Table 1. IOP Summary.	14
Table 2. Point source SF ₆ tracer release summary for all IOPs. ‘MFC’ is the flow rate measured by the mass flow controller. ‘Scale’ is the difference in mass of the SF ₆ cylinder between the start and end of the release.	18
Table 3. Arc and arc angle location of field duplicate, field control, and field blank samplers.	26
Table 4. Measurement quality objectives (MQO) for the bag sampling Data Quality Indicators.	34
Table 5. Summary of project instrument sensitivity and low end instrument bias.	39
Table 6. ATGAS analytical ranges.	40
Table 7. Summary of project laboratory control (CCV) results.	42
Table 8. Summary of results for lab background checks (room air).	43
Table 9. Summary of RPD results for laboratory duplicates.	44
Table 10. Summary of results for lab background checks (room air).	46
Table 11. Combined ATGAS field control results expressed in terms of standard concentration and IOP number.	47
Table 12. Summary of field duplicate sampler results.	49
Table 13. Estimates of MLOQ using field duplicates, field blanks, and field controls.	59
Table 14. Summary of data completeness by IOP with contribution to analyses by individual GC.	63
Table 15. Method Limit of Detection (MLOD) and Method Limit of Quantitation (MLOQ) for fast response analyzers during PSB1.	74
Table 16. Percent recovery of SF ₆ concentrations by real-time analyzers sampling known mixtures as unknowns.	74
Table 17. Meteorological instrumentation used during PSB1.	84
Table 18. Summary of radiosonde launch dates, times, durations and calculated variables. .	122
Table 19. Meteorological conditions during IOP1. Wind speeds, directions, σ_{θ} , and P-G stability class determinations (EPC, 200c) are from COC at 10 m. Solar radiation measurements are from FLX. R3 and R4 indicate sonic anemometer data from their respective locations.	134
Table 20. Meteorological conditions during IOP2. Wind speeds, directions, σ_{θ} , and P-G stability class determinations (EPA, 200c) are from COC at 10 m. Solar radiation measurements are from FLX. R3 and R4 indicate sonic anemometer data from their respective locations.	170
Table 21. Meteorological conditions during IOP3. Wind speeds, directions, σ_{θ} , and P-G stability class determinations (EPA, 2000c) are from COC at 10 m. Solar radiation measurements are from FLX. R3 and R4 indicate sonic anemometer data from their respective locations.	206

Table 22. Meteorological conditions during IOP4. Wind speeds, directions, σ_θ , and P-G stability class determinations (EPA, 2000c) are from COC at 10 m. Solar radiation measurements are from FLX. R3 and R4 indicate sonic anemometer data from their respective locations. 243

Table 23. Meteorological conditions during IOP5. Wind speeds, directions, σ_θ , and P-G stability class determinations (EPA, 2000c) are from COC at 10 m. Solar radiation measurements are from FLX. R3 and R4 indicate sonic anemometer data from their respective locations. 275

Table 24. Summary of fast response analyses. Peak:Mean (P:M) values of 19.9 represent ratios ≥ 20 . ‘U’ represents unconditional calculations (all valid values), ‘C’ represents conditional calculations (zeros excluded), and ‘c’ represents concentration. 330

ABSTRACT

The Field Research Division of the Air Resources Laboratory (ARLFRD) of the National Oceanic Atmospheric Administration (NOAA), in collaboration with the University of Tennessee Space Institute (UTSI) and the Laboratory for Atmospheric Research at Washington State University (WSULAR), conducted a tracer field experiment at the Idaho National Laboratory (INL) during October 2013. It is the first of a series of new tracer experiments to study dispersion from continuous sources in flat terrain using technologies not available during earlier dispersion studies of the 1950s and 1960s. These releases are collectively being called Project Sagebrush. The October 2013 study is designated Project SageBrush phase 1 (PSB1).

Five tests were conducted during PSB1, all during the daytime with conditions ranging from near neutral with higher wind speeds to unstable with low wind speeds. Each experimental period consisted of a continuous 2.5 hour SF₆ tracer release with consecutive 10-minute average bag sampling over the last two hours of the tracer release period. Bag sampling was done on four arcs of almost 90 degrees each ranging in distance from 200 to 3200 m from the source, depending on the stability conditions and aircraft availability. The bag sampling measurements were complemented by six fast response tracer analyzers, an airborne fast response analyzer, and an extensive suite of meteorological measurements. This included a 60 m tower arrayed with seven 3-d sonic anemometers and five sets of cup anemometers and wind vanes. Two additional towers at 10 and 30 m height had cup and vane anemometers mounted at 2 and 3 levels, respectively. Three additional sonic anemometers were arrayed on the 3200 m arc to examine the issue of horizontal homogeneity. Additional meteorological measurements were made by two sodars, a radar wind profiler, and radiosondes released just prior to and just after the two hour sampling period.

Preliminary analyses have identified some key results. The PSB1 results for the horizontal plume spread parameter σ_y tended to be larger than the daytime σ_y found in Project Prairie Grass and those determined from stability class model dispersion schemes (e.g., Pasquill-Gifford curves). The discrepancies increased with increasing downwind distance. However, the σ_θ and turbulence intensities measured during PSB1 were similar to those measured during the daytime in Project Prairie Grass. The result is that the PSB1 ratios of σ_y/σ_θ tended to fall near the upper limit or somewhat above the historical range of values found in previous field studies. Another key point is that the evidence suggests that σ_y becomes independent of σ_θ for σ_θ greater than about 18 degrees. Finally, an investigation extending the comparison of σ_θ values into stable nighttime conditions found that the values of σ_θ reported during Project Prairie Grass and PSB1 differed significantly.

This page is intentionally left blank.

INTRODUCTION

The Field Research Division of the Air Resources Laboratory (ARLFRD) of the National Oceanic Atmospheric Administration (NOAA), in collaboration with the University of Tennessee Space Institute (UTSI) and the Laboratory for Atmospheric Research at Washington State University (WSULAR), conducted a tracer field experiment at the Idaho National Laboratory (INL) during October 2013 (Fig. 1). It is intended to be the first of a series of new tracer experiments to study dispersion from continuous sources in flat terrain using technologies not available during earlier dispersion studies of the 1950s and 1960s. These releases are collectively being called Project Sagebrush. The October 2013 study is designated Project SageBrush phase 1 (PSB1).

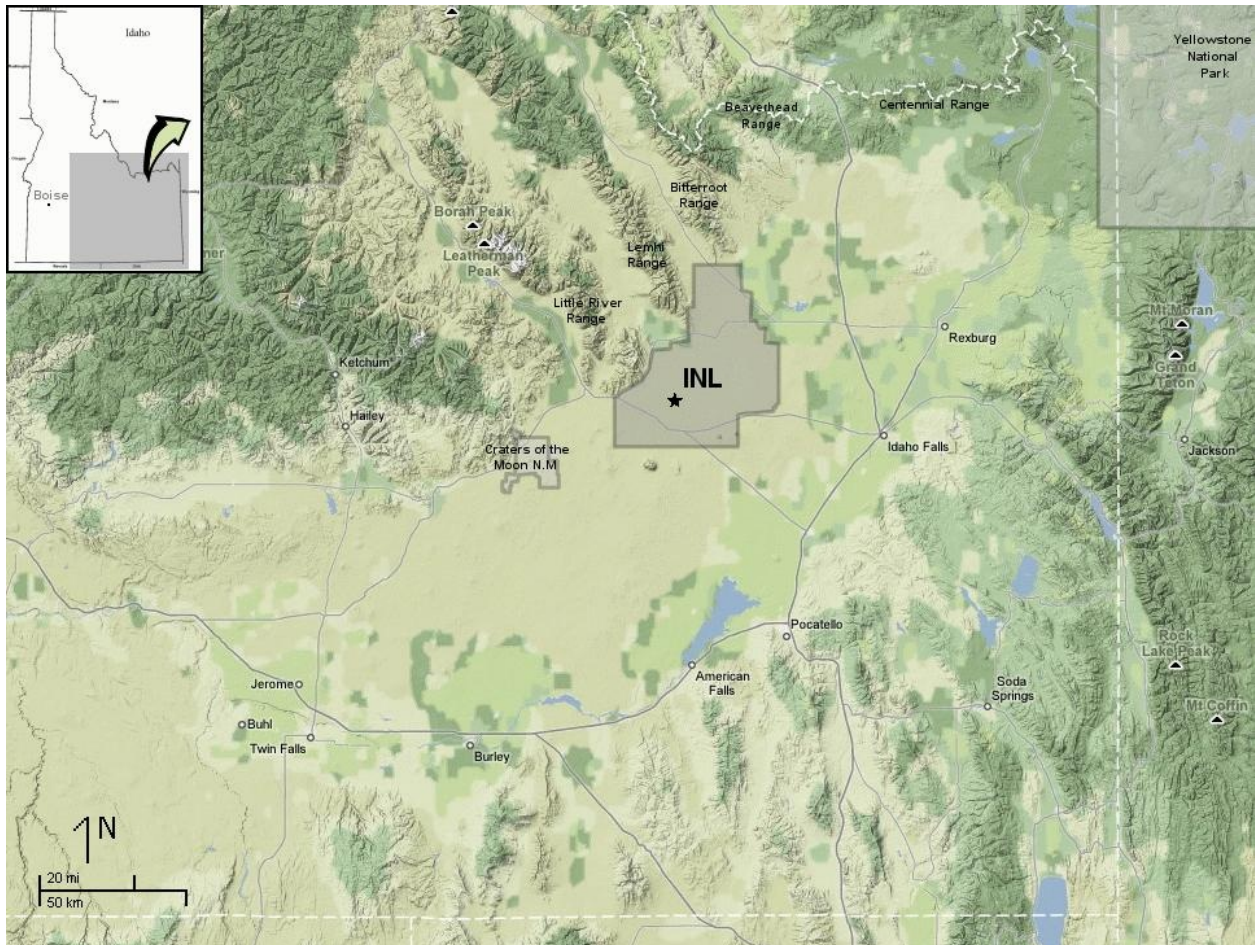


Figure 1. Location of Grid 3 (star) on the INL in SE Idaho.

Tracer studies are a relatively expensive but effective method for collecting field data on atmospheric dispersion. Rudimentary studies of this type extend all the way back to the 1920s (Pasquill, 1974) but became more common in the 1950s and 1960s as interest in air pollution increased and better tracer measurement technology appeared. Many of the “classical” tracer experiments involving short-range dispersion from continuous near-surface sources were

conducted during these two decades. Perhaps the best known is the 1956 Project Prairie Grass in Nebraska (Barad, 1958). Other early near-surface experiments include Project Green Glow (Fuquay et al., 1964), Projects Ocean Breeze and Dry Gulch (Haugen and Fuquay, 1963), and a series of Uranine dye releases at the INL (formerly National Reactor Testing Station) in Idaho (Islitzer and Dumbauld, 1963). Slade (1968) provides a comprehensive listing of these early tracer experiments.

Because of the expense of tracer studies, funding agencies have been reluctant to support new studies that appear to replicate the terrain, meteorology, and source configurations found in previous studies. There has been a tendency to assume a single tracer study “solves” a specific dispersion problem, so later studies should move on to something different. While there is certainly a need to understand dispersion in varying conditions, the inherent variability of dispersion due to its turbulent nature leads to basic questions regarding the repeatability of results from individual studies.

In science there is a basic requirement that experimental results be repeatable. Much of our experimental knowledge of atmospheric dispersion at short ranges is based on a small number of studies conducted over 40 years ago. Project Prairie Grass (Barad, 1958) remains one of the most used tracer studies for flat terrain, but many users are unaware of its limitations. The entire study took place during a dry period in Nebraska during July and August 1956. Information on vertical dispersion came from a single set of towers 100 m downwind of the source, with a maximum tracer measurement height of 17.5 m above ground level. Estimates of boundary-layer stability and surface fluxes were derived from mean wind and temperature profiles, since the state of instrument development available at that time severely limited the ability to measure fluxes directly. The SO₂ tracer used in Prairie Grass is both reactive and depositing, which may affect the interpretation of the results. Did Prairie Grass and other classical short-range tracer studies produce results that are repeatable and generally applicable to other regions? Would tracer studies using modern meteorological instrumentation and nonreactive tracers produce similar results to the classical studies?

Further inspiration for new studies comes from a 2008 tracer experiment ARLFRD conducted at the INL (Finn et al., 2010). The focus of this 2008 experiment was the effects of roadside sound barriers on vehicle pollution, but a subset of the data was compared to the Prairie Grass results and shows interesting deviations (Venkatram, 2011, personal communication). One justification for a new study is therefore to help determine the repeatability and replicability of the dispersion results from the classical studies. Are the observed deviations due to different surface roughnesses at the two sites, different methods of measuring boundary-layer stability, random variability, seasonal differences, or perhaps something else? Will further tracer releases continue to show deviations from the Prairie Grass results?

As a result of the issues identified above, the science objectives of Project Sagebrush are to:

1. Improve the understanding of short-range dispersion from continuous near-surface releases in nearly flat terrain using modern meteorological sensors and tracer technology.
2. Improve the understanding of concentration fluctuations within continuous plumes.
3. Assess the overall repeatability and applicability of individual tracer studies by comparing the new tracer results to classical tracer experiments.
4. Develop improved parameterizations linking plume widths to observed boundary-layer structure.
5. Develop improved dispersion models for both mean concentrations and concentration fluctuations.
6. Provide a new high-quality data set for testing and validating existing dispersion models.

ARLFRD will use newer technologies to go beyond the older studies. The current ARLFRD tracer bag samplers each contain 12 bags controlled by a programmable computer processor. This allows mean concentrations to be collected over a range of averaging times. ARLFRD also has fast response tracer gas analyzers capable of sampling concentration fluctuations at about 1 Hz. These analyzers can measure the concentration frequency distribution at specific points within the tracer plume. With these measurements it is possible to investigate such issues as peak-to-mean ratios (with the peak value being defined, for example, as the 95th percentile concentration). During PSB1 a nearby 62 m mesonet tower was additionally instrumented with seven 3-d sonic anemometers and other equipment by ARLFRD and WSULAR for fully characterizing the state of the boundary layer. This was augmented by two sodars, a 915 MHz radar profiler, an energy balance flux station, radiosondes, and the remaining 33 towers of the NOAA/INL Mesonet (Clawson et al. 2007).

The INL is located across a broad, relatively flat plain on the western edge of the Snake River Plain in southeast Idaho. Elevations across the INL are approximately 1500 m above mean sea level (MSL). Several parallel mountain chains with peaks exceeding 3000 m MSL dominate the western side of the plain. These chains are separated by a series of tributary valleys that feed into the Snake River Plain. The mountains and benches forming the eastern side of the plain are somewhat lower in elevation, with mountain peaks at roughly 2200 m MSL. Several tributary valleys also feed into the plain from the east, but they are not as regularly spaced as those to the west.

The Grid 3 area on the INL was selected for Project Sagebrush for several reasons (Figs. 2 and 3). The Grid 3 area was originally designed to conduct transport and dispersion tracer studies in the 1950s. Numerous tracer and other atmospheric studies have been conducted at Grid 3 since that time (Start, et al. 1984; Sagendorf and Dickson, 1974; Garodz and Clawson 1991, 1993). Conducting Project Sagebrush at Grid 3 allows ARLFRD to include valuable knowledge from previous work gained over the years. Deployment of the experiment to the INL has the added benefits of simplifying logistics (thereby minimizing some of the costs) and the availability of meteorological measurements already in place utilizing the NOAA/INL Mesonet.

Notable among these is the proximity of the Grid 3 tall tower that provided vertical profiles of wind, turbulence, fluxes, and temperature during PSB1 (Fig. 4). Analyses of data from this tower showed that the near-surface wind often blows parallel to the axis of the Snake River Plain, with southwest winds common during the day and northeast winds at night. Hence, although the INL lies about 13 km southeast from the nearest mountains, the NOAA Grid 3 tracer test facility usually has a relatively flat, uniform fetch extending many tens of kilometers upwind. The boundary layer under such conditions is expected to be close to equilibrium. Two INL building complexes are located about 1.6 km from the tracer facility and are the closest potential flow obstructions. One is nearly south at a true azimuth of 165° and the other almost west at 255° . Wind rose analysis prior to PSB1 indicated these complexes are usually not a factor except perhaps for winds out of the WSW.

The Big Lost River is a visible feature of the aerial photo seen meandering across the right portion of Fig. 2. This is usually a dry river bed that only contains water during spring runoff in wet years. Old river channels also are visible

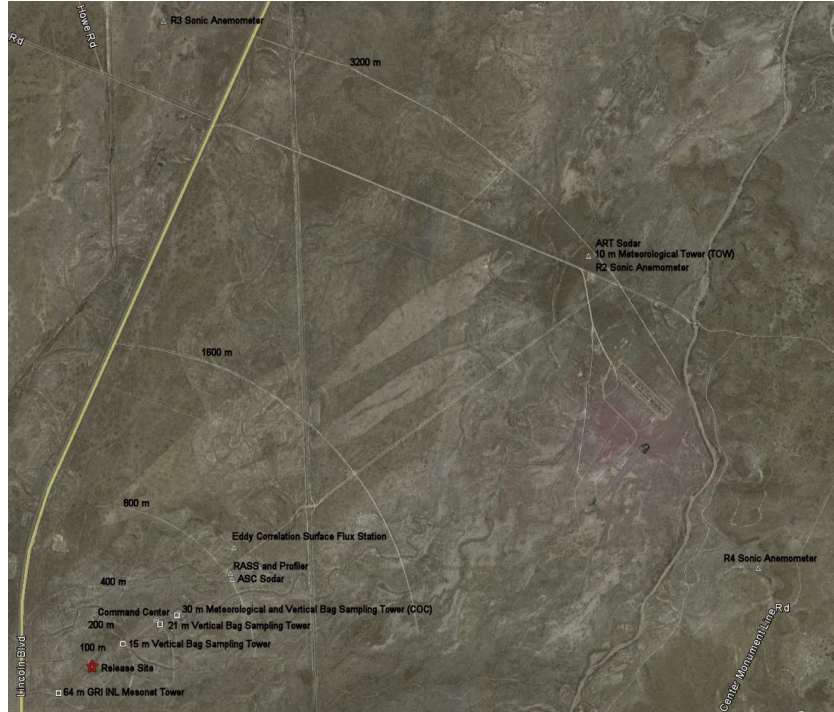


Figure 2. Google Earth image of the Grid 3 area.

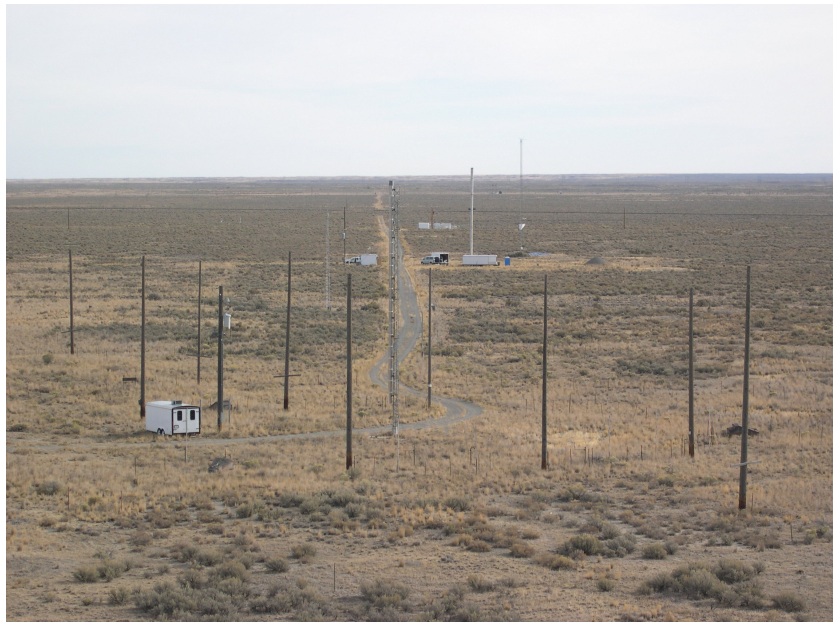


Figure 3. Photo from Grid 3 tower looking northeast toward the tracer sampling array along the radial road through the tracer sampling array. The command center (COC) tower and wind profiler installation (PRO) are visible in the right center of the photo.

to the northwest of the current bed. These channels create only minor topographic variations. They could have a minor influence on the air flow over the tracer facility when winds have more of a westerly component. The streaks of lighter vegetation with a southwest-northeast orientation in Fig. 2 are burn scars from wildfires. Fires typically kill the darker sagebrush and leave lighter-colored grasses as the dominant vegetation until the sagebrush can recover.

The site also offers relatively uniform aerodynamic characteristics across the Grid 3 area (Fig. 3). The canopy is mostly sagebrush and grass. The Grid 3 tower has routine wind measurements at 2, 10, 15, 45, and 60 m above the ground. Wind profiles from this tower in near-neutral conditions have been used in a statistical algorithm to estimate the roughness length z_0 at the tracer facility. For SW winds common during the day the median z_0 is 3 cm, with a 90% probability interval of 2.5–3.5 cm. For NE winds common at night the median z_0 is 3.8 cm

with a 90% probability interval of 3.3–4.4 cm. The slightly higher roughness length for NE winds may be due to the old river channels and low terrain undulations to the north of the facility. Estimates of the displacement height d were also computed from the Grid 3 profiles, but the values are not significantly different from zero. A small displacement height of a few centimeters probably exists but is not detectable with the current observations on the tower.

A Piper Navajo aircraft from UTSI was used to assist in measuring the vertical dispersion of the SF₆ tracer during PSB1. For this reason, it was desirable to conduct tracer releases and



Figure 4. Photo of the Grid 3 tower.

sampling during unstable atmospheric conditions. Unstable conditions were necessary to provide sufficient vertical dispersion of the tracer such that measurable concentrations could be readily detected at aircraft flight levels. Pasquill-Gifford stability classes A and B were considered ideal but classes C and D were deemed acceptable for Intensive Observational Periods (IOPs) during which the aircraft was available. Due to some unavoidable logistical and planning issues, it was not possible to begin PSB1 until early October. Unfortunately, this time of the year was not optimum for obtaining frequent unstable conditions. Stability classes C and D were much more common during the experiments than classes A or B.

The release rate was adjusted for the anticipated stability condition of each IOP in an attempt to ensure it was high enough such that concentrations aloft could be readily measured by the aircraft but low enough such that the concentrations at the surface did not overwhelm the dynamic range of the fast response sensors there. There were five SF₆ tracer releases and IOPs conducted during PSB1. The aircraft was available only during IOPs 1-3. As a consequence, release rates during IOPS 1-3 were much higher than for IOPs 4 and 5.

This report covers PSB1, the first phase of Project Sagebrush. It includes the entire tracer release and measurement data sets collected by ARLFRD and UTSI and the complete meteorological data sets collected by ARLFRD and WSULAR. It also includes information about the experimental design, SF₆ tracer release system, time integrated bag samplers, fast response real-time tracer gas analyzers, meteorological instrumentation, and summaries of each IOP as well as some preliminary data analyses. In addition, this report details the data formats found on the accompanying data CD.

EXPERIMENTAL PLAN

Five tracer release tests or Intensive Observational Periods (IOPs) were conducted from 2 October to 18 October, 2013 as part of PSB1. Since unstable conditions were desired and the prevailing winds during unstable conditions were from the SW, the study domain was located primarily on the northeast quadrant of the Grid 3 dispersion array. Figure 2 shows a Google Earth image of the study area. Figure 5 is a more detailed image showing the configuration of PSB1.

Grid 3 Dispersion Array and Release

Tracer sampling arcs are visible in Fig. 2 both to the NE and SW of the center point of the Grid 3 dispersion array. The arcs at 400, 800, 1600, and 3200 m from the source are labeled, but arcs are also present at 50, 100, and 200 m. These arcs contain surveyed markers at 1°

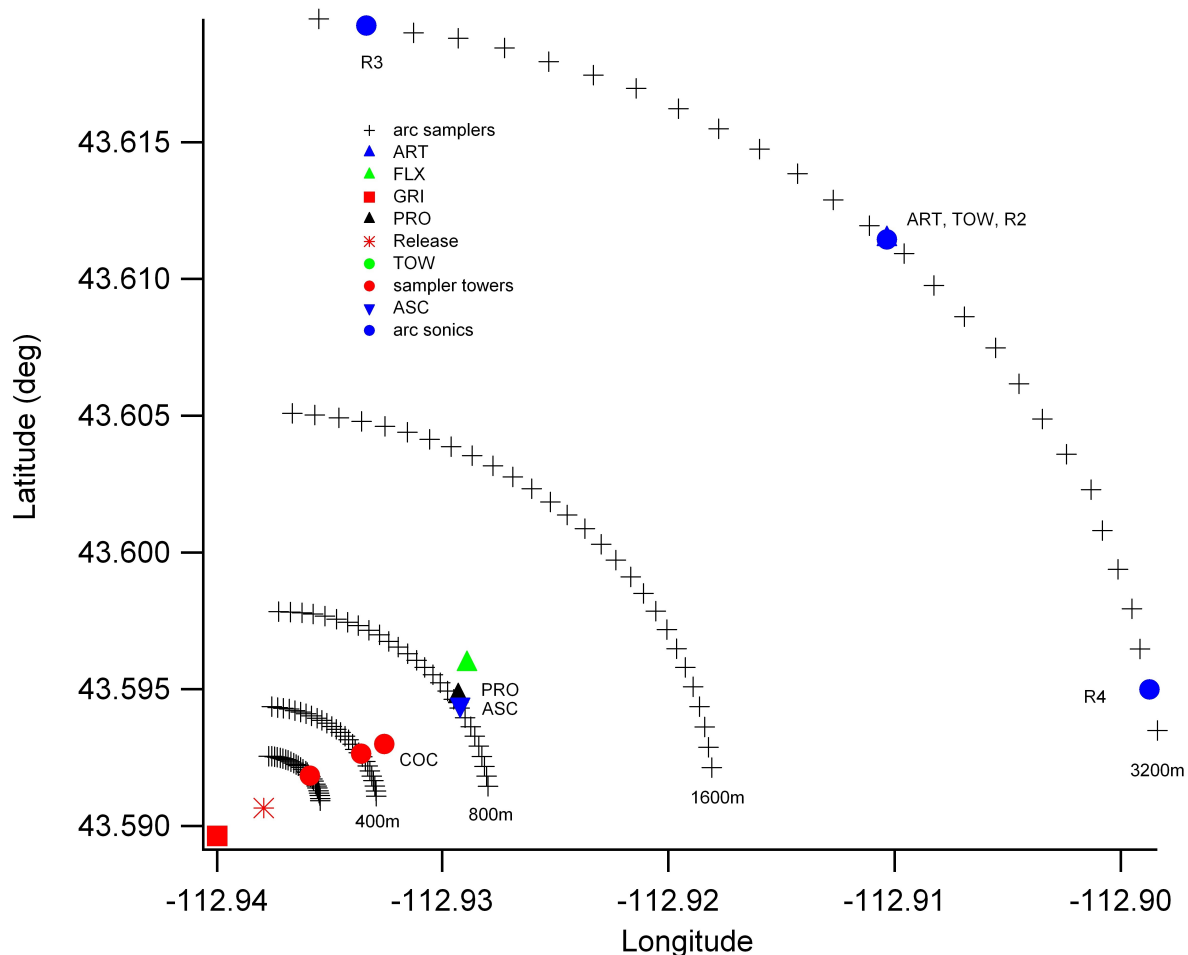


Figure 5. Configuration of PSB1 field tracer experiments. The 3-character labels are defined at the beginning of Meteorological Measurements section and Table 17.

intervals to facilitate the placement of tracer samplers. Bag sampling was conducted at 3° intervals from 4° azimuth to 85° azimuth on the 400, 800, and 1600 m arcs during all IOPs.

Depending upon the release rate, bag sampling was also conducted along either the 200 m arc (low release rate) or 3200 m arc (high release rate). The inner arcs are a full circle, but the 800, 1600, and 3200 m northeast arcs were truncated at 85° on the south end of the arcs. The original 1600 and 3200 m arcs were truncated on their north ends by a highway. The arcs truncated on the north were extended at 3° increments to 4° azimuth by a survey prior to the start of PSB1 for consistency with the inner arcs.

Continuous releases of SF₆ tracer gas were made at a constant rate from a point source at the center of the Grid 3 dispersion array for each IOP during PSB1. The releases began one-half hour prior to the start of sampling on the dispersion array to establish a quasi-steady state SF₆ concentration field out to the most distant sampling arc. The release then continued at a constant rate for the two-hour duration of the sampling in the IOP. Release rates were set based upon preliminary calculated estimates of concentrations at different heights and distances, the anticipated atmospheric stability conditions, and whether the aircraft would be making tracer measurements during an IOP.

Bag Sampling

The bag sampling measurements were the most essential feature of the experiment. Nominally, 150 samplers were deployed for each IOP. Twenty-eight samplers were placed along each of the 4 arcs designated for an IOP. These were either the 200, 400, 800, and 1600 m arcs or the 400, 800, 1600, and 3200 m arcs, depending upon the release rate as previously described. They were mounted atop plastic boxes at 1 m AGL and stabilized from toppling in the wind by hooking the carrying handle over the metal post marking the sampling location (Fig. 6). They were placed at 3° intervals from 4° azimuth to 85° azimuth (i.e., 4, 7, 10, ..., 82, 85°).



Figure 6. Photo of bag sampler mounting.

Three towers were available for vertical sampling to the northeast of the source. The first of these was 15 m (50 feet) tall and located at the intersection between the 55° azimuth radial road (visible in Figs. 2 and 3) and the 200 m arc. Samplers were mounted at 1, 5, 10, and 15 m on this tower. The second tower was 21 m tall and located at the intersection of the radial road and the 400 m arc. Samplers were mounted at 1, 5, 10, 15, and 20 m on this tower. The third tower was 30 m tall (100 feet) and located 499 m from the source at about 60° azimuth. This tower served the dual purpose as the meteorological tower for the nearby command center (COC). Samplers were mounted at 1, 5, 10, 15, 20, 25, and 30 m on this tower.

The locations were designated with a 4-digit code. The first digit represents the arc or tower location (2 = 200 m, 4 = 400 m, 8 = 800 m, 6 = 1600 m, 3 = 3200 m, 1 = 30 m COC sampling tower, 5 = 15 m sampling tower, 7 = 21 m sampling tower). Quality control (QC) was integral to the experimental plan and called for the use of blank, control and duplicate samplers. Field blank and field control samples were designated with '9' in the first digit. The second digit specified whether the sample was designated as a primary (0) or duplicate (1) sampler. For field blank and control samples the second digit specified the arc location. There were 4 duplicate samplers per arc, a total of 16 per IOP. The last two digits designated the position along either the arc (degrees azimuth) or height on the tower (m agl). There were 16 duplicate, 3 field blanks, and 3 control samplers designated for QC purposes per IOP.

The SF₆ samplers operated by pumping air into Tedlar bags with each bag being filled sequentially for 10 min. Thus the analysis of the bags provided 10-min average concentrations. Tracer concentrations from 2 parts per trillion volume (pptv) to 1 part per million volume (ppmv) could be analyzed. A complete discussion of bag sampler operation, timing, analysis, and QC can be found in the Bag Sampling chapter.

Fast Response Tracer Gas Analyzers

Six fast response SF₆ analyzers were deployed during PSB1. Five of these were mounted in vehicles and driven to a bag sampling location on the sampling arcs. One analyzer was mounted in an airplane during IOPs 1, 2, and 3. The analyzer measured SF₆ as the airplane flew across wind and downwind routes above the experiment area. During IOPs 4 and 5, the airplane was not available so this analyzer was relocated to an equipment building on the 800 meter arc at approximately 57 degrees.

The primary purpose of the fast response analyzers was to measure concentration fluctuations at about 1 Hz. These stationary analyzers were used to determine the concentration frequency distribution at specific points within the tracer plume and made it possible to investigate such issues as peak-to-mean ratios.

The sites for the ground-based analyzers were selected to: 1) be near the centerline or margins of the plume and 2) avoid instrument "railing" artifacts where the concentration levels were higher than the analyzer could quantify. For IOPs during which the aircraft was available, it was necessary to try to set release rates low enough to avoid railing but high enough to provide

for measurable concentrations at aircraft flight levels. Nominally, the fast response analyzers had a dynamic range from a few tens pptv to about 10,000 pptv, depending on the characteristics of the individual analyzer. Some of the analyzers were equipped with a dilution system that made it possible to measure concentrations up to about 20,000 pptv. Over ranging was not a problem for the bag samplers. In consultation with the command center, it was sometimes necessary to move one or more analyzers during an IOP. This could have been due to a sustained shift in forecast wind directions leaving the analyzer persistently outside of the plume. A move could also be made further away from the plume centerline to minimize the possibility of railing.

To ensure data quality, a complete QC program was followed during operation of the fast response real-time analyzers. A more complete description of the fast response analyzer operations can be found in the Fast Response Analyzer chapter.

Aircraft Operations

Airborne fast response SF₆ sampling was done using a twin-engine Piper Navajo airplane (Fig. 7). The crew consisted of a pilot, co-pilot, observer from UTSI, and an analyzer operator from ARLFRD.



Figure 7. Photo of Piper Navajo airplane used for airborne sampling of tracer.

The flight path of the aircraft was determined ahead of time based upon preliminary calculated estimates of concentrations at different heights and distances using existing dispersion curves (Fig. 8). The flight pattern consisted of crosswind traverses across the dispersion array moving successively toward the source after each crosswind pass. Each crosswind pass was approximately the same downwind distance as the arcs designated for sampling during the IOP (400, 800, 1600, and 3200 m). After completing the innermost arc the plane banked and returned downwind along the estimated centerline of the plume. This flight pattern was then repeated at the next highest level. The sampling heights were nominally 100, 200, and 300 m above ground, although the analyzer operator had the discretion to direct the pilot to cancel passes at the upper heights if concentrations were low or undetectable. The outward to inward pattern was intended to minimize any effects of turbulence artificially generated by the aircraft on tracer dispersion.

The aircraft was utilized in IOPs 1-3 but was unavailable for IOPs 4 and 5. For IOPs 1-3 the plume patterns observed by the aircraft were consistent with plume patterns observed in the bag sampling data. For IOPs 1 and 2 the aircraft vertical profiles showed lift off from the surface of the vertical plume centerline. For IOP 3 the aircraft data showed that this plume rise was significantly suppressed with no evidence of liftoff. Without the aircraft, the results of IOPs 4 and 5 showed conflicting and inconclusive evidence for liftoff of the plume centerline. During most of IOP1 and some of IOP2, the plume was often truncated by the ground sampling arcs. The flight paths of the aircraft were modified in real time to extend aircraft sampling lines to the NW and SE, respectively, to avoid this truncation. During IOP4 the plume was also sometimes truncated by the ground arrays, but the aircraft was not available.

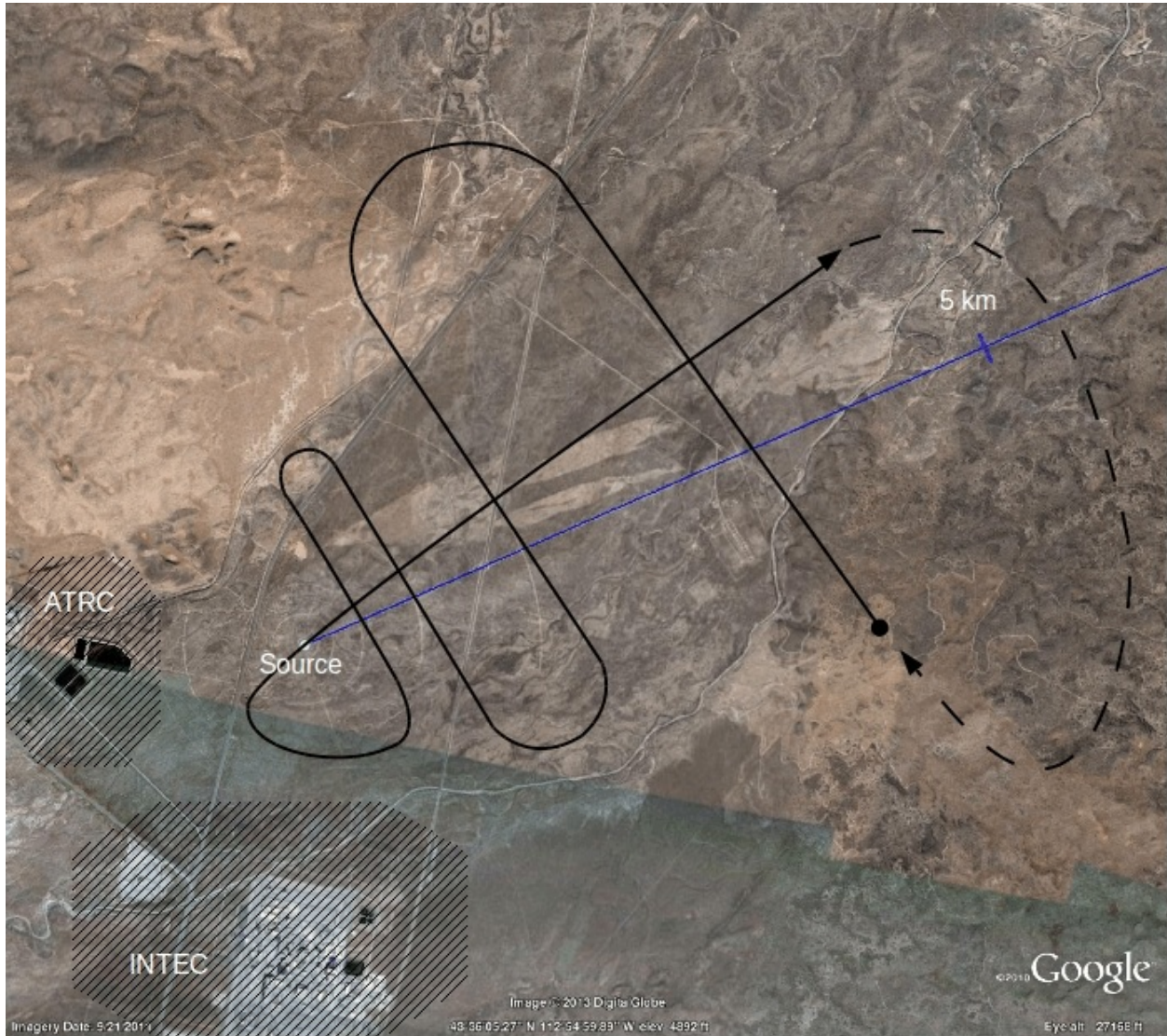


Figure 8. Flight pattern used during Phase 1. The aircraft started at the 3200 m downwind distance (black circle) and then made successive passes closer to the source. After the closest pass at 200 m downwind, the aircraft flew downwind along the plume centerline before exiting the pattern (black arrow). The full pattern was repeated at several levels above the ground. The hatched areas labeled ATRC and INTEC are building complexes that the aircraft was required to avoid.

Meteorological Equipment

ARLFRD made every effort to fully characterize the conditions and structure of the boundary layer during PSB1 for the purpose of identifying all possible meteorological factors controlling tracer dispersion. This included:

- Wind speed and direction in the horizontal and wind speed the vertical
- Vertical profiles of turbulence and turbulent fluxes (including sensible and latent heat fluxes)
- Temperature profiles
- Horizontal homogeneity of the turbulence field
- Soil temperatures, moisture, and heat fluxes
- Solar radiation, net radiation, and energy balance
- Barometric pressure

To this end, ARLFRD, in collaboration with WSULAR, used a broad array of meteorological instrumentation and measurements on the Grid 3 tower during PSB1:

- 62 m Grid 3 tower – cup anemometer and wind vanes at 6 levels; 3-d sonic anemometers at 7 levels, 2-d sonic anemometers at 6 levels, air temperature/RH at 14 levels, infrared gas analyzers at 4 levels, solar radiation, barometric pressure at 3 levels, net radiometer at 2 levels, infrared radiometer, soil heat flux at 2 levels, soil moisture and temperature at 5 levels

Other meteorological measurements included:

- Three 3-d sonic anemometers arrayed along the 3200 m arc
- 30 m Command Center (COC) meteorological tower – cup anemometers and wind vanes at 3 levels
- 10 m meteorological tower at 3200 m arc – cup anemometer and wind vanes at 2 levels
- SoDARs at 800 and 3200 m (winds at 30-200 m AGL)
- Boundary Layer Radar Wind Profiler and RASS at about 800 m arc (winds up to 2.9 km height, temperatures up to about 1 km height; both usually much less)
- Radiosondes before and after each IOP
- Flux station at about 900 m on the dispersion array – 3-d sonic anemometer, infrared gas analyzer, solar radiation, net radiometer, air temperature/RH, barometric pressure, soil temperature at 2 locations, soil moisture, soil heat flux at 4 locations
- 33 other (in addition to Grid 3 tower) meteorological stations of the NOAA/INL Mesonet

A complete description of the meteorological instrumentation, measurements, QC procedures, and data file formats can be found in the Meteorological Measurements chapter.

IOP Summaries

A brief summary of IOP test dates and times, release rates, meteorological conditions, and atmospheric stability is listed in Table 1. A more comprehensive discussion of each IOP and sampling period is included in the Summary of Individual IOPs chapter.

Table 1. IOP Summary.

IOP	Date	Start Time (MST)	Release Rate (g s^{-1})	Stability	Aircraft	Meteorological Summary
1	02-Oct-13	1430	10.177	Unstable ^a	Yes	Mostly sunny with cirrostratus haze. Very light and variable winds.
2	05-Oct-13	1300	9.986	Unstable ^a	Yes	Mostly sunny. Light-moderate SW winds.
3	07-Oct-13	1300	9.930	Neutral	Yes	Mostly sunny. Moderate-strong SW winds.
4	11-Oct-13	1400	1.043	Weakly Unstable	No	Mostly sunny. Moderate SW winds.
5	18-Oct-13	1300	1.030	Weakly Unstable	No	Mostly sunny. Moderate SW winds.

a. Estimates of stability vary.

THE SF₆ TRACER RELEASE SYSTEM

The SF₆ tracer release system was custom built for PSB1 by ARLFRD engineers and technicians. The system was placed in a cargo trailer to simplify deployment, provide a reasonably controlled environment for operation, and to simplify removal of the release system when the field deployment was complete. The complete release system (Fig. 9) was entirely self-contained in the cargo trailer (Fig. 10) and only required a 115 VAC 20 ampere power source. This was provided from an adjacent power pole.

The ARLFRD tracer release system was engineered to release a constant amount of SF₆ from a single point source at the center of the Grid 3 tracer facility (43.59066 N, -112.938 W). Each SF₆ point source release during PSB1 lasted a total of 2.5 hours. The first half-hour of each release period was dedicated to obtaining steady-state dispersion conditions over the entire sampling area before sampling began. Each release then continued at the initial release rate for the next two hours of the actual 2-hour long tracer sampling period.

During all SF₆ releases, the gaseous tracer flowed from a cylinder containing SF₆ through



Figure 9. The SF₆ release system inside the cargo trailer including the SF₆ bottles, mass flow controller, computer data acquisition and control system, and electronic scales under the bottles.



Figure 10. The cargo trailer where the release system was housed on location at the Grid 3 facility.

the mass flow controller, through a visible flow meter, and into a garden hose. The outlet end of the garden hose served as the dissemination point. The garden hose outlet was placed at a height of 1.5 m AGL and attached to a tower at the center of the sampling grid. It was oriented horizontally to avoid imparting any vertical momentum to the tracer. A heater was used to maintain constant pressure in the SF₆ cylinder and to assist with the vaporization of the liquid SF₆. A schematic of the of the release mechanism is shown in Fig. 11. The first K-size cylinder of SF₆ tracer was provided the by Norco, Inc. The certified concentration of the liquid SF₆, as reported by Norco, was >99.9%. A copy of the certificate of analysis is shown in Fig. 12. Concorde Specialty Gas of New Jersey supplied the remainder of the K-type SF₆ cylinders used during experiment with the same specifications.

SF₆ Release Mechanism

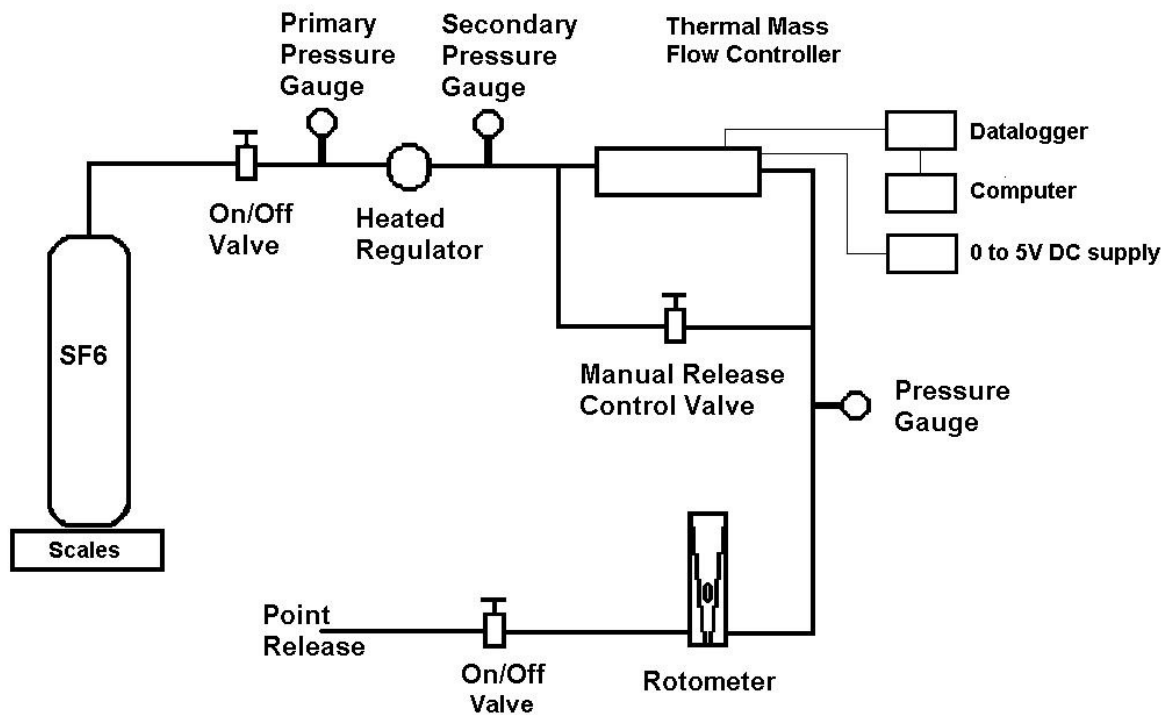


Figure 11. Schematic of SF₆ tracer release system.

The heart of the SF₆ tracer release system was the thermal mass flow controller (Hastings Teledyne, Model HFC-203). The mass flow controller was responsible for monitoring and controlling the tracer leaving the SF₆ cylinder. During a release, a voltage was applied to the mass flow controller that was proportional to a given SF₆ flow rate. This voltage could be manually controlled to obtain any desired release rate between a set range. The voltage and the flow rate from the mass flow controller were continuously monitored and recorded with a datalogger.



Calibration Gases & Equipment

CERTIFICATE OF ANALYSIS

September 3, 2013

Norco, Inc
Idaho Falls Warehouse
3450 N. 25th East
Idaho Falls, ID 83401

Cust Number WH020
Order Number 31377025
P.O. Number SAGE BRUSH

Lot Number 3-133-304
Part Number SPG KCOMSF
Product Sulfur Hexafluoride, Commercial
Cylinder Size K
Pressure N/A

Date Analyzed 7/12/2013
Expires 7-2016

Cylinder Number(s)
4G386L

Component	Reported Concentration	Requested Concentration
Sulfur Hexafluoride	≥ 99.9%	≥ 99.9%
Water	< 5.0 ppm	< 5.0 ppm
Nitrogen	< 700 ppm	< 700 ppm

Storage: Keep away from heat, flames, and sparks. Store and use with adequate ventilation. Close valve when not in use and when empty. Never allow cylinder temperature to exceed 125 degrees F.

Minor constituents tested with standards traceable to NIST by mass or comparison to SRM's (Standard Reference Materials).

Approved:


Aaron Schwenken
Lab Technician

898 W. GOWEN ROAD • BOISE, IDAHO 83705
Phone (208) 336-1643 • Fax (208) 331-3038 • 800-657-6672

Figure 12. Liquid SF₆ certificate of analysis.

Accuracy

The mass flow controller was calibrated at the factory and subsequently double-checked outdoors at our office in Idaho Falls. Calibration was needed to correlate the tracer flow rate to the applied voltage. Several verification tests were conducted after the factory calibration to ensure proper functioning of the mass flow controller.

SF₆ Release Summary

A total of 5 tracer tests (IOPs) were conducted. The releases were always conducted from the center of the sampling grid. The target SF₆ release rates for the first three IOPs was 10.0 g s⁻¹. This release rate was selected in order to provide tracer concentrations sufficiently high enough to be sampled by the real-time analyzer installed in the aircraft. The aircraft was used for sampling the vertical distribution of the tracer plume during the first three IOPs but was not available for the last two. A much lower release rate was used for the remaining tests. The target SF₆ release rate for these tests was 1.00 g s⁻¹.

The tracer dissemination summary, including release date and time, target release rate, actual average release rate from the mass flow meter, and the total mass of SF₆ released for each period are listed in Table 2. Actual release rates differed only slightly from the target release rates. For the first three tests, the actual release rates ranged from 9.93 to 10.18 g s⁻¹, which were anywhere from 0.7% less than to 1.8% greater than intended. For the last two tests, the actual release rates ranged from 1.030 to 1.043 g s⁻¹, which were anywhere from 3.0% to 4.3% greater than intended. The standard deviations of the actual flow rates for the first three tests ranged from 0.01 to 0.26 g s⁻¹. Standard deviations of the actual flow rates for the last two tests ranged from 0.007 to 0.010 g s⁻¹. The low standard deviations indicated very steady flow rates throughout the entire 2.5-hr continuous release periods. The total amount of SF₆ tracer material that was disseminated during field deployment was 289,905 g.

Table 2. Point source SF₆ tracer release summary for all IOPs. ‘MFC’ is the flow rate measured by the mass flow controller. ‘Scale’ is the difference in mass of the SF₆ cylinder between the start and end of the release.

Test	Date (2013)	Start time (MST)	End Time (MST)	Total SF ₆ Release Scale (g)	Total SF ₆ Release MFC (g)	Correction (Scale/MFC)	Target Release Rate (g s ⁻¹)	Measured 2-hr Release Rate (g s ⁻¹)	Release Rate Standard Deviation (g s ⁻¹)	Release Rate Error (%)
1	02-Oct	14:00	16:30	91600	89,049.1	1.0286	10.0	10.177	0.260	1.77
2	05-Oct	12:30	15:00	89900	89,509.2	1.0044	10.0	9.986	0.200	0.14
3	07-Oct	12:30	15:00	89400	89,604.6	0.9977	10.0	9.930	0.010	0.70
4	11-Oct	13:30	16:00	9525.4	9,063.9	1.0509	1.0	1.043	0.010	4.30
5	18-Oct	12:30	15:00	9480	9,030.9	1.0497	1.0	1.030	0.007	3.00

Graphs of the release rates, together with the cumulative amount of SF₆ tracer released during each test are shown in Figs. 13-17. The release traces indicate very steady release rates, with the exception of IOPs 1 and 2. At approximately 1 hr 20 minutes into these release periods, the source of the SF₆ tracer was switched from a near-empty bottle to a full bottle. While the trace indicates a large flow excursion, this is an artifact of the mass flow controller. Visual monitoring of the rotometer showed only a minor and very short-lived flow disruption. For all practical purposes, the flow rate remained steady. This is also indicated by the cumulative trace of disseminated SF₆ tracer, which shows only a steady increase for those two tests.

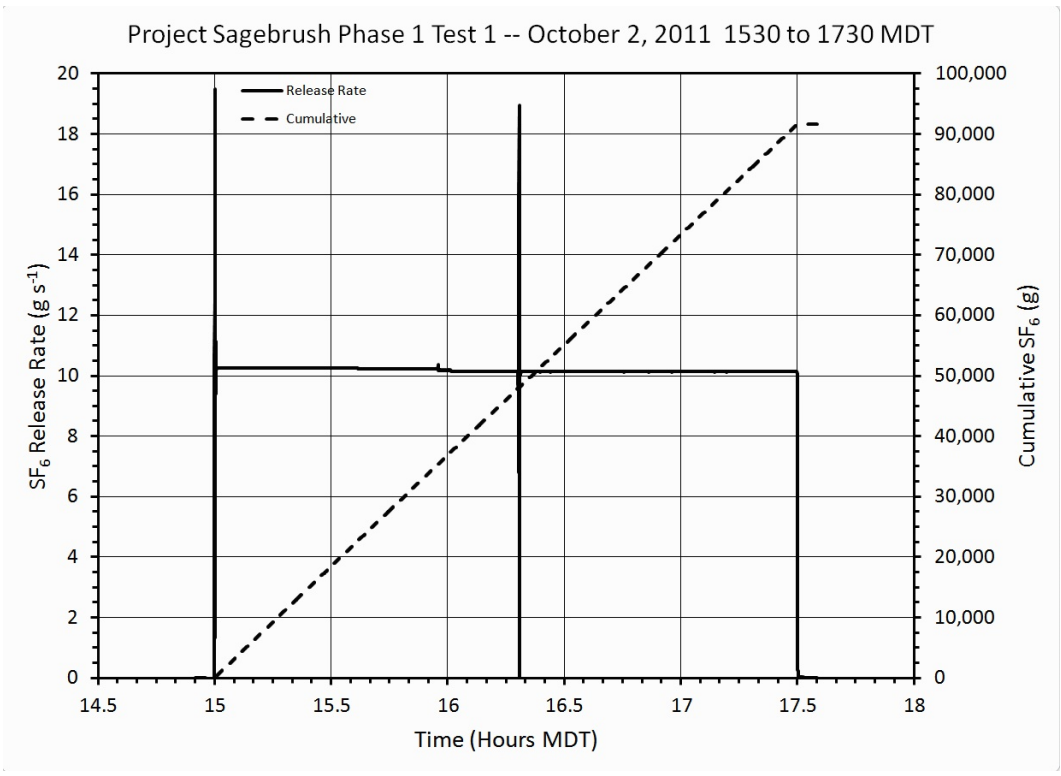


Figure 13. SF₆ release rate for IOP1.

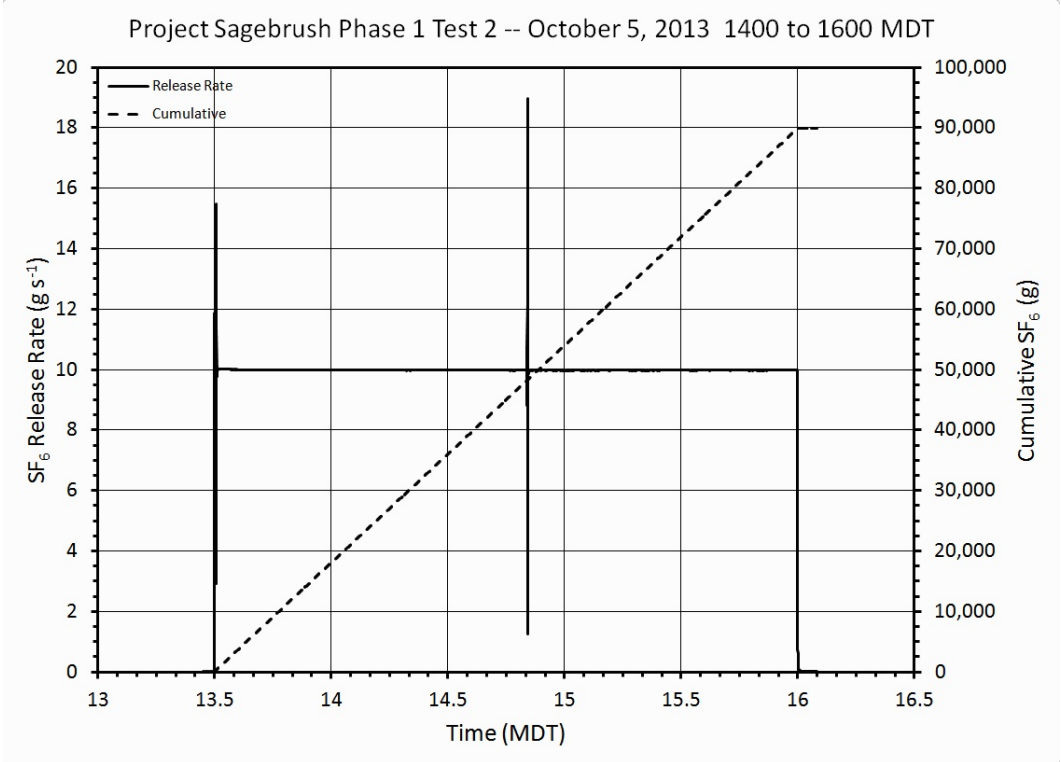


Figure 14. SF₆ release rate for IOP2.

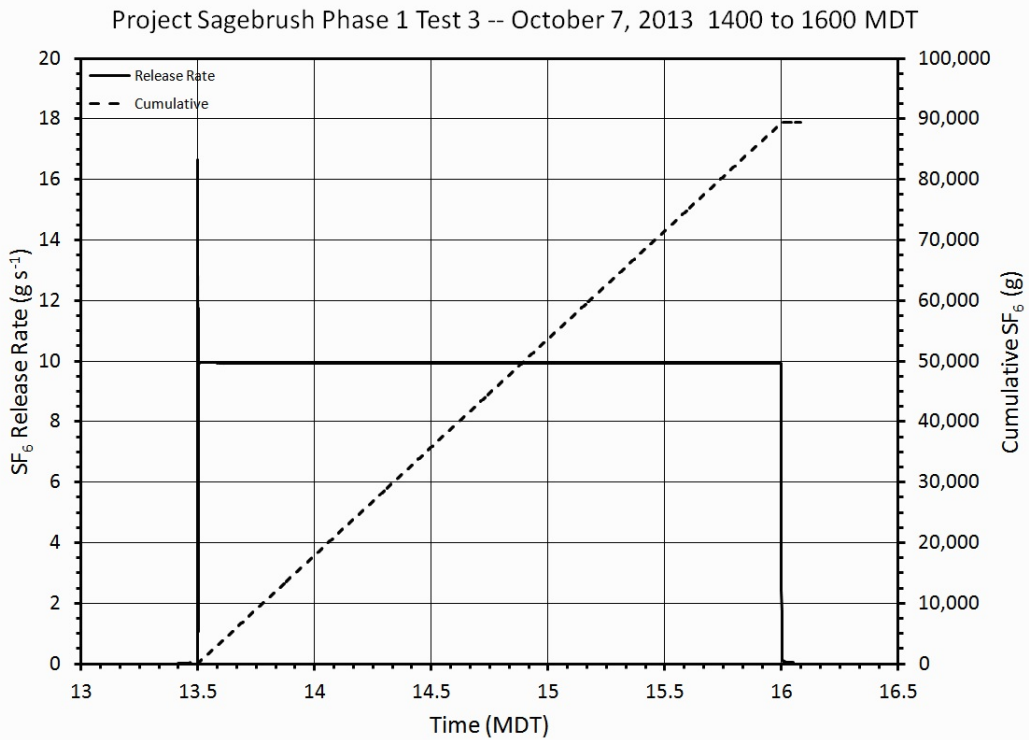


Figure 15. SF₆ release rate for IOP3.

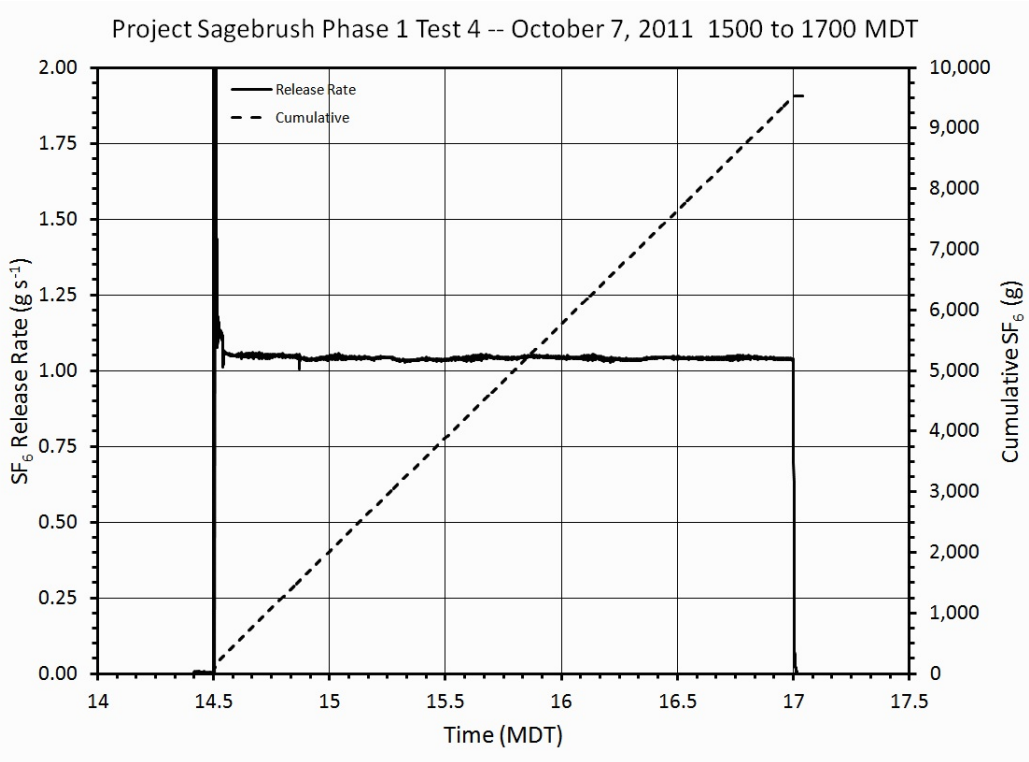


Figure 16. SF₆ release rate for IOP4.

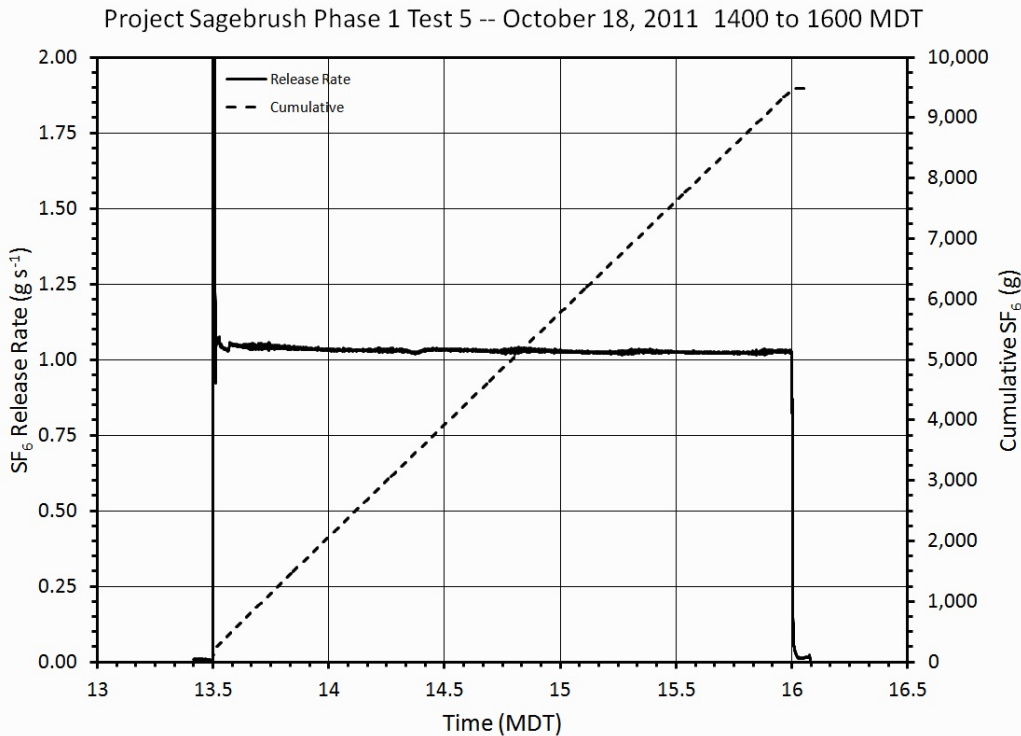


Figure 17. SF₆ release rate for IOP5.

SF₆ Release Quality Control

The quality control program for the SF₆ tracer release consisted of the 8 steps outlined below:

1. Pre-project preparation.
2. Pre-test procedures.
3. Monitoring of key operational parameters during the test.
4. Post-test procedures.
5. Post-test data screening and processing.
6. Verification of all calculations and data by a second analyst.
7. Identification of data problems and setting of QC flags.
8. Review of final data files.

1. Pre-project preparation.

Before the experiment, the SF₆ release mechanism was constructed and thoroughly tested to ensure all systems were in good working order. Prior to the release system construction, the mass flow controller was calibrated at the factory and again at the FRD office/laboratory facility to correlate the actual flow rate with the indicated flow rate. After construction, the system was

tested from end to end for flow accuracy. The release system released 99.9% pure SF₆ without dilution.

2. Pre-test procedures.

On the day of a test, the release system operator was required to follow established procedures for preparing the release mechanism. These procedures were based on the experience of previous tracer projects. The procedure included checking for loose connections, visually inspecting the release line, calibrating the scale, setting the clock, setting the mass flow controller output to zero, and verifying that data was recording on the computer. These actions were recorded in the release logbook.

3. Monitoring of key operational parameters during the test.

During the test, the mass flow controller and weight of the SF₆ bottle were monitored for a stable and correct flow rate. These values were recorded approximately every 10 minutes in the release logbook. The release system operator was able to adjust the flow rate on the release mechanism if necessary. Note: The mass flow meter was accurate enough that it did not require additional adjustment after initial setting at the beginning of each test.

4. Post-test procedures.

After a test was complete, the release system operator followed end of release procedures for shutting down the release mechanism and collecting the data. Weight loss from the SF₆ bottle(s) was recorded in the release logbook. Release data that had been recorded on the computer was backed up onto a compact memory stick and returned to the FRD office for processing.

5. Post-test data screening and processing.

Once the memory stick was returned to FRD, the data was uploaded onto the network for processing. Release rate data was graphed and reviewed for any spikes or anomalies in the recorded data that would indicate deviations from a stable flow rate. Release rate data from the mass flow controller was compared to the actual weight of the released tracer, as measured by the scales, to ensure that the flow rate was within five percent of the mass flow set point. The mass flow output data was adjusted (corrected) to match the total amount released using the precision balance scale data.

6. Verification of all calculations and data by a second analyst.

The plots of the new data were reviewed and verified by a second analyst.

7. Identification of data problems and setting of QC flags.

The release logbook entries and the plots of the data were carefully reviewed by the data analysts. No problems were found. If any problems had been found, they would have been annotated with the appropriate flag and recorded in the final data files. The data flags would indicate unstable or varying flows, spikes in the release rate, or missing data.

8. Review of final data files.

The data files were carefully reviewed for any problems and checked for the correct flags.

Data File Format

The one second readings from the mass flow controllers are provided in data files on the CD accompanying this report. The files are named RELEASEx_PSB1.csv, where “x” is replaced by the IOP test number. The files contain five columns:

1. date (month/day/year)
2. time (hhmm in MST)
3. seconds
4. corrected tracer flow rate (grams per second)
5. quality flag

The files are all comma separated variable format. The first line of each file contains headers for each column. Quality flags are 0 for good data, 1 for suspect data.

This page intentionally left blank.

BAG SAMPLING

Description of Equipment

Stationary time-integrated sampling of SF₆ for PSB1 was performed using programmable bag samplers. These samplers acquired time-sequenced air samples in bags that were subsequently analyzed for the concentration of the SF₆ tracer. The samplers collected 12 samples by sequentially pumping air into each of 12 individual Tedlar® bags. The integrated sampling time for each bag in the study was 10 minutes resulting in 12 individual experiments within each of the five 2-h Intensive Observational Periods (IOPs).

The bag sampler housing is constructed from durable double-wall polypropylene manufactured by Mills Industries Inc. and measures 61 cm x 41 cm x 33 cm (Fig. 18). The mounting of the sampler was shown previously in Fig. 6. The other component of the bag sampler assembly is a cardboard sampler cartridge (Fig. 19). One hundred thirty five of the sampler boxes utilize Motorola microprocessors (model MC68HC811E2). An additional 15 new samplers were built for PSB1 using Texas Instruments MPS430 series microprocessors, making 150 bag samplers in total. All sampler boxes contain 12 microprocessor-controlled air pumps designed to start sequentially filling the bags at a time and duration specified for each bag. The sampling period for each bag and the delay before each bag can be independently specified to create a sampling program customized for each situation. The cartridge box contains 12 Tedlar® bags.

Prior to deployment, a sample cartridge was placed into each sampler box (Fig. 20) and connected by R-3603 tubing to the sampler pumps. The much more durable R-3603 tubing was used to replace old latex tubing prior to the



Figure 18. Bag sampler with cover and cartridge removed.



Figure 19. Sampler cartridge.

experiment. The latex tubing was prone to degradation and cracking. With its cover in place (Fig. 6), each sampler box and sampler cartridge assembly had a total mass of approximately 4 kg and was powered by a single D-cell battery. The microprocessor and air pump components of the sampler design have been used successfully in field experiments for many years and are known to be free of artifacts (e.g. Clawson et al. 2004, 2005). The material used for the bag sampler housing represents a recently improved design that was extensively tested for reliability and potential sampling artifacts in 2007 and also found to be free of artifacts.



Figure 20. Bag sampler with sampler cartridge installed.

Description of Bag Sampling Grid

A total of 112 primary bag samplers were deployed on four out of five of the sampling arcs shown in Fig. 5 during each IOP. For IOPs 1-3 these samplers were deployed on the 400, 800, 1600, and 3200 m arcs. For IOPs 4 and 5 the samplers were deployed on the 200, 400, 800, and 1600 m arcs. The arc samplers were mounted atop plastic boxes and secured in place with bungee cords attached to metal fence posts. Sample inlet tubes were at about 1 m AGL. In addition, 16 bag samplers were deployed on 3 towers for the measurement of vertical concentration profiles. Four bag samplers were deployed on the 15 m (50 ft) sampling tower shown at 201 m (1, 5, 10, and 15 m AGL), 5 samplers were deployed on the 21 m (70 ft) sampling tower shown at 408 m (1, 5, 10, 15, and 20 m AGL), and 7 samplers were deployed on the 30 m (100 ft) meteorological and sampling tower at 499 m (1, 5, 10, 15, 20, 25, and 30 m AGL). The locations of each bag sampler were specified by (1) latitude and longitude and (2) distance of the arc from the release location at the center of the arc array and an angle in degrees clockwise from north along each arc. In addition to these 128 primary samplers, an additional 22 samplers were deployed for quality control (QC) purposes. This included 16 field duplicate, 3 field control, and 3 field blank samplers. The arc angle positions of these QC samplers are listed in Table 3.

Table 3. Arc and arc angle location of field duplicate, field control, and field blank samplers.

Arc (m)	Arc Angle Position (degrees)		
	Duplicate	Control	Blank
200	16, 31, 55, 73		
400	7, 37, 55, 82	43	31
800	16, 25, 49, 85	40	70
1600	10, 34, 52, 76	70	58
3200	13, 37, 55, 76		

Sampler Cartridge Analysis

Sample cartridges were analyzed at the Tracer Analysis Facility (TAF) in Idaho Falls, ID. The TAF hosts four gas chromatographs (GC), each housed within its own autosampler module and connected to a computer which acts as the master data acquisition system. The complete configuration with GC, autosampler, and data acquisition system is called an Automated Tracer Gas Analysis System (ATGAS) (Figs. 21, 22). A dedicated small black handheld computer, visible atop each GC in Figs. 21 and 22, was used to set the operational parameters on each ATGAS.

Each GC housed two Supelco 60/80 Molecular Sieve-5A columns (5' x 1/4" and 2' x 1/4"), a 10-port sample valve, and a sample loop. These columns were maintained at 65 C inside their respective ovens. Two columns (pre-column and main column) were used to reduce analysis time and to vent interfering species, i.e. oxygen, that can damage the columns and detector. After the SF₆ sample was injected onto and eluted by the first 2-foot (610 mm) pre-column (Fig. 23), the gas flow was switched to back-flush the precolumn while the sample loop was filled with the next sample (Fig. 24). The SF₆ continued on to the main 5-foot (1520 mm) column where further separation occurred before being passed to the detector. Detection of SF₆ was accomplished using a Valco Instrument Co., Inc., Model 140BN electron capture detector (ECD) containing 5 millicuries of Ni-63. The ECD operating temperature was kept at 170 C. The ECDs and columns were protected by a Supelco High Capacity Gas Purifier tube heated inside an oven to remove oxygen, water, carbon monoxide, and carbon



Figure 21. ATGASs in lab.



Figure 22. ATGASs in lab with computer

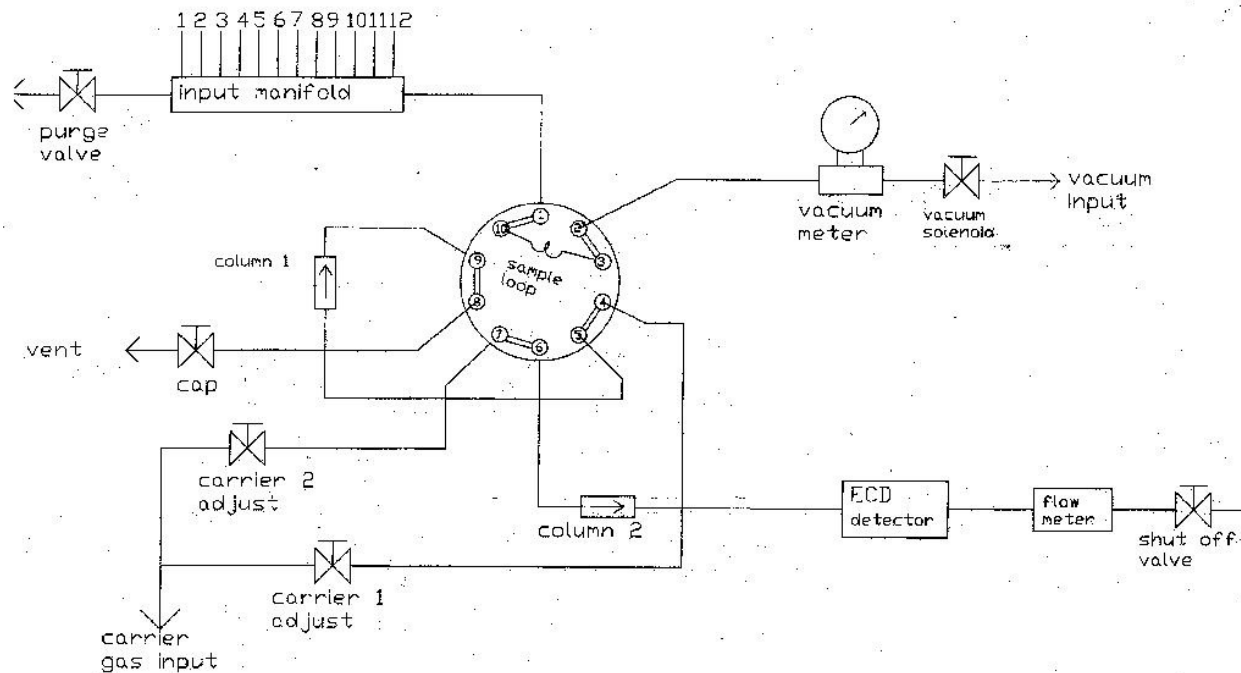


Figure 23. Schematic of sample loop fill with column 1 (pre-column) in the back-flush position.

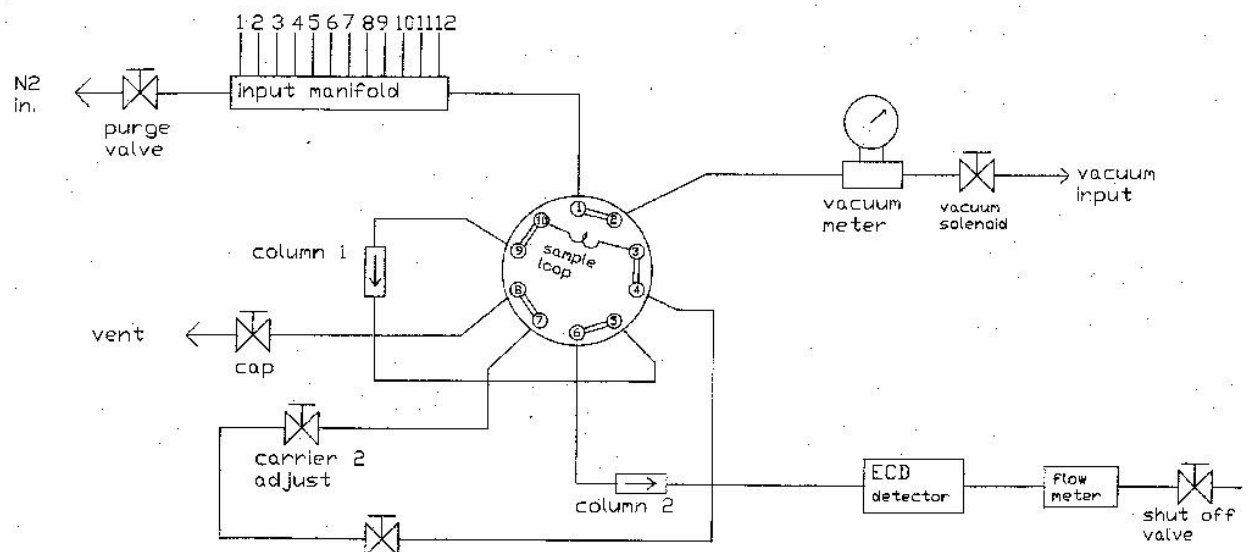


Figure 24. Schematic of injection to column 1 (pre-column) and on to column 2 (main column).

dioxide in the carrier gas as well as a Supelcarb HC hydrocarbon trap to remove organic impurities. Ultra high purity (UHP) nitrogen served as the carrier gas and filtered compressed air was used as the valve actuator gas. Concentration ranges from 2 pptv to about 1 ppmv have been analyzed using this methodology.

The ATGAS computer software (Carter, 2003) was developed in-house and was used to analyze the tracer gas chromatograms, calculate concentrations, and perform quality control functions. The software incorporates a history file system that records all operations performed on each ATGAS.

Sampler Handling and Chain of Custody

A history file in the master ATGAS computer maintained a complete and comprehensive record for each sampler cartridge. The scheme for maintaining the comprehensive history file was based upon unique bar coded serial numbers attached to both samplers and sample cartridges. In addition, prior to the start of the project, each field sampling location was identified and tagged with a location number that consisted of a weatherproof bar code label. These were affixed to the metal fence posts installed at each sampling location. A file with a list of the locations was uploaded to the ATGAS computer in the TAF. The bar code labels for the samplers, cartridges, and locations were used to automatically generate a chain of custody record for each sample.

In preparation for each test, a sample cartridge was placed inside each sampler and then transported to the field. Samplers were deployed at each location, the tubing was connected, clips were opened, and a sampling program downloaded into the memory of each sampler's microprocessor. The latter was accomplished with the use of a small hand-held computer (Videx Timewand II) shown in Fig. 25. The Timewands were programmed with sample start and stop times for each bag prior to each test using a dedicated laptop computer in the TAF. They were then used in the field to download the sampling program and acquire and record the location number, sampler number, and cartridge number. The complete field download records were later retrieved from the Timewands and transferred into the history file on the ATGAS computer in the TAF prior to the start of cartridge analysis.

Details of these field sampling servicing procedures are shown in Figs. 26, 27, and 28. These procedures were developed after years of prior field experience. Personnel responsible for deploying the samplers in the field received classroom and hands-on training in Idaho Falls prior to the experiment. It was also required that handwritten Sampler Servicing Record sheets be completed in the field for each removed or installed cartridge (Fig. 29). These records were created to



Figure 25. Timewand.

Sampler Procedure A: Placing a Sampler at a Location

1. Place the cartridge in the sampler and
 - connect the tubes securely and in the correct order
 - open the clips, making sure that the tubing is fully opened and the clip slides easily on the tube. Press on the tube with a finger or blunt end of a pen if necessary.
 2. On the Sampler Servicing Record Sheet, fill in the
 - Location number
 - Sampler number
 - Time (available by pressing "+" on the Time Wand)
 - Cartridge installed
 3. Check the sampler inlet tubes to be sure they have not been pushed back into the sampler.
 4. Make sure there is a battery in the sampler. If you need to insert one, do so carefully so that the battery clips are not damaged.
 5. Plug the Time Wand II cord into the sampler. Verify that the right LED is blinking.
 6. With the Time Wand II, scan the sampler serial number, the cartridge serial number, and the location serial number. These may be scanned in any order. Make sure you use the **correct location number** for each sampler. The Time Wand II will now download the program into the sampler. The left LED will light to indicate a successful download. Make sure the left LED is on before removing the cable!
- NOTE: In emergencies only, the serial numbers may be entered with the keypad. (Type the 6-digit code and then press the "=" key.) Since this is very error prone, do not use this method unless there is absolutely no other way!**
7. Disconnect the Time Wand II.
 8. Record any problems on the Sampler Servicing Record Sheet. **If there are problems noted, place a mark on the metal bracket in the cartridge with a Sharpie permanent marker so that lab analyst will know to check the Sampler Servicing Record Sheet.**
 9. Place the lid on the sampler and put it on the hanger.

Figure 26. Sampler servicing procedure A: Placing a sampler at a location.

Sampler Procedure B: Retrieving a Sampler

1. Retrieve the sampler from the hanger and remove the lid.
2. On the Sampler Servicing Record Sheet, fill in the
 - Location number
 - Sampler number
 - Cartridge Removed
 - Time (available by pressing "+" on the Time Wand)
3. Verify that the cartridge was connected correctly and the bags were filled. Record any problems on the Sampler Servicing Record Sheet. **If there are problems noted, place a mark on the metal bracket in the cartridge with a permanent marker so that lab analyst will know to check the Sampler Servicing Record Sheet.**
4. Close the clips on the cartridge.
5. Disconnect the tubes.
6. Cartridge may now be removed from the sampler or transported in the sampler.

Figure 27. Sampler servicing procedure B: Retrieving a sampler.

Sampler Procedure C: Replacing a Cartridge

1. Retrieve the sampler from the hanger and remove the lid.
2. On the Sampler Servicing Record Sheet, fill in the
 - Location number
 - Sampler number
 - Cartridge Removed
 - Time (available by pressing "+" on the Time Wand)
3. Verify that the cartridge was connected correctly and the bags were filled. Record any problems on the Sampler Servicing Record Sheet. **If there are problems noted, place a mark on the metal bracket in the cartridge with a permanent marker so that lab analyst will know to check the Sampler Servicing Record Sheet.**
4. Close the clips on the cartridge.
5. Disconnect the tubes and remove the cartridge.
6. Plug the Time Wand II cord into the sampler. Verify that the right LED is blinking.
7. With the Time Wand II, scan the sampler serial number and the sampler flush code **FL0406**. The sampler will now run each pump for about 4 seconds to flush the pump and the tubes.

NOTE: In emergencies only, the numbers may be entered with the keypad. (Type the 6-digit code and then press the "=" key.) Since this is very error prone, do not use this method unless there is absolutely no other way!
8. Place the new cartridge in the sampler and when the pumps have finished running:
 - connect the tubes securely and in the correct order
 - open the clips, making sure that the tubing is fully opened and the clip slides easily on the tube. Press on the tube with a finger or blunt end of a pen if necessary.
9. On the Sampler Servicing Record Sheet, fill in the
 - Cartridge installed
10. Check the sampler inlet tubes to be sure they have not been pushed back into the sampler.
11. If you have been instructed to replace the battery, do so carefully so that the battery clips are not damaged.
13. With the Time Wand II, scan the sampler serial number, the cartridge serial number, and the location serial number. These may be scanned in any order. Make sure you use the **correct location number** for each sampler. The Time Wand II will now download the program into the sampler. The left LED will light to indicate a successful download. Make sure the left LED is on before removing the cable!
14. Disconnect the Time Wand II.
15. Record any problems on the Sampler Servicing Record Sheet. **If there are problems noted, place a mark on the metal bracket in the cartridge with a Sharpie permanent marker so that lab analyst will know to check the Sampler Servicing Record Sheet.**
16. Place the lid on the sampler and put it on the hanger.

Figure 28. Sampler servicing procedure C: Replacing a cartridge.

Sampler Servicing Record Sheet

Each line represents a single visit to a sampler location. Each sheet represents a single traverse of a sampler route. Start a new sheet each time you start your sampler route.

Project: Sage Route: 1600 m Date: 10/2/13
 IOP(s): 1 TimeWand: _____ Name: Jason + Dennis

Location	Sampler	Cartridge Removed	Time	Cartridge Installed	Comments or Problems
LC 6004	GF 206	SN 1196	1830	SN	Bags a little flat (O.k.)
LC 6007	GF 84	SN 4367		SN	O.k.
LC 6010	GF 101	SN 5028		SN	O.k.
LC 6110	GF 41	SN 00120		SN	O.k. (little light)
LC 6013	GF 63	SN 0105		SN	O.k.
LC 6015	GF 16	SN 1031		SN	O.k. #9 click wants to open
LC 6019	GF 314	SN 4373		SN	O.k. (little light)
LC 6022	GF 208	SN 1212	1841	SN	#3 + 10 little low (O.k.)
LC 6025	GF 318	SN 1259		SN	O.k. (little light)
LC 6028	GF 30	SN 0389		SN	O.k.
LC 6031	GF 17	SN 0177		SN	#1 Low
LC 6031	GF 312	SN 0031		SN	Looks Good
LC 6034	GF 85	SN 0042		SN	#6 Flat
LC 6134	GF 26	SN 1299	1851	SN	OK
LC 6037	GF 998	SN 1275		SN	OK
LC 6040	GF 212	SN 0231		SN	OK
LC 6043	GF 102	SN 0085		SN	OK
LC 6046	GF 57	SN 1169		SN	OK
LC 6049	GF 999	SN 4364		SN	OK
LC 6052	GF 319	SN 4317		SN	OK
LC 6152	GF 87	SN 0310		SN	OK
LC 6055	GF 36	SN 4307	1903	SN	OK
LC 6058	GF 22	SN 4359		SN	OK
LC 9658	GF 263	SN 1264		SN	OK
LC 6061	GF 996 996	SN 0112		SN	#10 Low a few others low too
LC 6064	GF 207	SN 4388		SN	OK

Sampler 996 #'s on outside ~~are~~ are transposed ⁽⁹⁶⁶⁾ need fixed.

Figure 29. Example of Sampler Servicing Record. This was from cartridge removal after Test 1.

provide the TAF analyst with details of potential problems pertaining to each cartridge and sample bag. In combination with the history files, these records were invaluable as a reference for sample check-in and/or later for QC flagging of data. The Sampler Servicing Records were given to the laboratory analyst after sampler collection and delivery were performed. All record sheets were organized and placed in a binder for future reference.

The sample cartridges were transported back to the TAF at the completion of each IOP and analyzed within a few days of sampling. They were all checked in prior to analysis using a bar code scanner to record each cartridge bar code. During this process each bag was inspected and the following flags were entered into the computer for each bag:

- B = Too big (overfilled)
- G = Good
- L = Low
- F = Flat
- D = Damaged clip or bag
- I = Improper hookup (tubes crossed, clip open, etc.)

These flags were used later for querying, sorting and generating final QC flags as well as for monitoring sampler performance and checking for mistakes by field personnel.

Each cartridge bar code was again scanned when it was attached to the ATGAS prior to analysis. This linked the GC identity and the acquired chromatogram and calculated concentration data to the computerized data previously collected in the field that specified the project identification, test number, grid location number, grid location coordinates, sampling start time, the sample time per bag, and sampling type (primary or quality control sample). The record also included the cartridge check-in record and cleaning records. Thus a complete computer-generated chain of custody is available for each bag sample as well as automatically linking via unique bar codes all field, chromatogram, concentration, and quality control data into one comprehensive data record that could be readily reviewed. This minimized the possibility of errors caused by mistakes in manually recording, copying, or entering of location information and provided an invaluable source of information in the event of a discrepancy or a question about the data.

Quality Control Procedures and Measurement Quality Objectives

The following are detailed descriptions of the quality control and quality assurance methods followed for the sampling, analysis, and reporting of the PSB1 time-integrated bag sampler tracer data. Protocols established in the Environmental Protection Agency's (EPA) Guidance for Data Quality Assessment (EPA 2000a), the general requirements for the competence of calibration and testing laboratories of International Standards Organization/IEC Guide 25 (ISO 1990), the quality systems established by the National Environmental Laboratory Accreditation Conference (EPA 2000b), and the Department of Defense Quality Systems Manual for Environmental Laboratories (DOD 2002) provided a basis for quality assurance and

quality control procedures followed during analysis. Instrument and method limits of detection (ILOD/MLOD) were calculated based upon 40 CFR Part 136, Appendix B and the American Chemical Society (ACS) Committee on Environmental Improvement’s paper titled, “Principles of Environmental Analysis” (Keith et al. 1983). ACS principles relative to detection limit calculations in 40 CFR Part 136, Appendix B are documented in “Revised Assessment of Detection and Quantitation Approaches” (EPA 2004). Although our research-based automated analysis of tracer gases has no specified method performance or regulatory criteria, compliance with the established quality control procedures stated above were followed, where applicable, to provide high quality data that is both accurate and reliable.

The laboratory procedures followed were designed to ensure meeting the stated Measurement Quality Objectives (MQO) for the project shown in Table 4. This table will be referenced as the results for each procedural step are described below.

Table 4. Measurement quality objectives (MQO) for the bag sampling Data Quality Indicators.

Data Quality Indicator	Objectives (MQO)	How Determined
Instrument Sensitivity	Instrument Limit of Detection (ILOD) < 4 pptv	Lab blanks and low concentration calibration checks
Between Instrument Precision	RSD ¹ < 10%	Lab background checks
Low End Instrument Bias	<1 pptv	Lab blanks
Instrument Precision	RPD ² < 5% RSD < 10%	Lab duplicates above MLOQ Lab controls above MLOQ
Instrument Accuracy	RPD ³ < 20% (< 50 ppt) RPD ³ < 10% (< 50 ppt)	Required by calibration check and recalibration protocol
Low End Method Bias ⁴	< MLOQ ⁵	Field Blanks
Method Sensitivity	Method Limit of Detection (MLOD) < 12 pptv	May be calculated from field blanks, low concentration field controls, field duplicates, or background samples
Method Precision	RPD ² < 15% RSD < 15%	Field duplicates above MLOQ Field Controls
Completeness %	90%	Percentage of samples producing good measurements

¹ RSD is relative standard deviation: standard_deviation/average

² RPD is relative percent difference: for duplicates is (measure_1 – measure_2)/average_of_1&2

³ RPD is relative percent difference: for known concentrations is (measure – actual)/actual

⁴ “Method” is entire sampling method including sampling and analysis.

⁵ Method Limit of Quantitation

Quality control issues pertaining to procedures for sample handling in the field and chain of custody were described in the previous section. Pre-project and laboratory QC procedures are described below and consisted of the following 22 steps:

1. Pre-project maintenance of bag samplers.
2. Testing of all sample bags.
3. Pre-project cleaning and analysis checks of all sample bags.
4. Development of analysis protocols for the expected sample concentration ranges.
5. Use of a written standard operating procedure (SOP).
6. Pre-project calculation of instrument limit of detection (ILOD) and instrument limit of quantitation (ILOQ).
7. Holding time studies.
8. Daily calibration of the ATGAS.
9. Initial ATGAS Calibration Verification (ICV).
10. Continuing ATGAS Calibration Verification (CCV) and analysis of laboratory controls.
11. Atmospheric background checks of SF₆ at the tracer analysis facility (TAF).
12. Analysis of laboratory (instrument) blanks.
13. Analysis of laboratory duplicates.
14. Analysis of field blanks.
15. Analysis of field controls.
16. Analysis of field duplicates.
17. Software quality control checks.
18. Data verification.
19. Post-project determination of MLOD and MLOQ.
20. Final data review.
21. Data handling.
22. Summary of Data Completeness.

1. Pre-project maintenance of the bag samplers.

Prior to deployment to the field, each of the original 135 bag samplers was extensively tested to ensure proper operation in the field and to ensure the collection of an adequate sample volume. This mainly involved checking the function of the microprocessor and pumps. Fifteen new bag samplers were built for PSB1 using Texas Instruments MPS430 series microprocessors and similarly tested.

2. Testing of all sample bags.

Experience has shown that almost all leaks in sample bags occurred around the fitting used for attachment to the sample tubing. To rectify this problem prior to PSB1, the seam between the fitting and the bag was permanently sealed in all sample bags using Pliobond 30. All bags were also inspected and if there were any holes or suspected holes besides the fitting seam, they were discarded prior to gluing. Previously bags had been checked for leaks using the procedure

detailed in Clawson et. al. (2004, 2005, 2009) but the bag sealing resulted in a lower failure rate than had been achieved by the leak checking procedure of the past.

3. Pre-project cleaning and analysis checks of all sample bags.

After the bags were leak checked, but prior to deployment to the field, all bags in the sampler cartridges were cleaned. The bags were cleaned by repeatedly filling them with UHP nitrogen and then evacuating them on the cartridge cleaning apparatus seen in Fig. 30. The apparatus consisted of a nitrogen tank and vacuum connected to a system that fills and evacuates the sample bags by changing valves. Seventy-two bags in 6 cartridges were cleaned at one time. The computer mounted underneath the cleaning apparatus was used to create cartridge cleaning records. This information was then uploaded into the ATGAS history file. An 8-step cleaning protocol was used to clean the bags:

1. Connect all tubes to the cleaning machine.
2. Open all clips.
3. Make sure the cleaning machine valves are set so that nitrogen can flow into all connected cartridges.
4. Evacuate bags.
5. Fill all bags with nitrogen and then evacuate. Repeat until all bags have been evacuated 5 times.
6. Fill all bags with nitrogen for analysis.
7. Scan all cartridge bar codes with the bar code scanner and upload the data to the ATGAS PC.
8. After analysis, place the cartridges back on the cleaning machine, evacuate the nitrogen, disconnect the tubes and wait 30 seconds before closing clips.



Figure 30. Cartridge cleaning apparatus.

This protocol was developed after significant testing to ensure that bags containing concentrations in the expected high range of up to 150,000 pptv or more could be cleaned to less than background levels. After cleaning, the bags were filled with UHP nitrogen and analyzed to ensure there was no contamination from previous tests or from long-term storage. Any bags with a concentration greater than 5 pptv were re-cleaned and re-analyzed. All but 23 out of 6,744 bags (562 cartridges) were successfully cleaned below 5 pptv in the initial cleaning and none were greater than 10 pptv. The vast majority were below the instrument limit of detection and within 0.1-0.2 pptv of zero. The 23 exceptions were successfully re-cleaned and analyzed. All bags were stored evacuated until their use.

4. Development of analysis protocols for the expected sample concentration ranges.

Analysis protocols were developed to optimize instrument performance, accuracy and efficiency during the project. In particular, each GC was configured to optimize the detection of the lowest possible concentrations in line with the expectation that the planned tracer release rates would result in mostly low to moderate concentrations and relatively fewer very high concentrations. Larger volume sample loops were selected in anticipation of measuring mostly lower concentrations. However, smaller volume sample loops were also evaluated to characterize the dynamic range available for measuring high concentrations on each GC in the event these were encountered. Analysis parameters were adjusted to account for the magnitude of concentration ranges that were expected. One set of parameters dealt with the worst case scenario carryover issue resulting from measuring extremely low concentration samples immediately following extremely high concentration samples. Nitrogen purge and vacuum times and the number of purge-vacuum cycles of the GC were set to ensure no carryover of high concentrations. Other parameters controlling the timing of the injection, switch to back-flush, and total length of the analysis cycle were set to ensure that oxygen and other contaminants were back-flushed before reaching the ECD to avoid any interferences. Electron capture detector attenuation adjustments were also tested at different concentration levels to provide quick adjustments to the instruments in the case of unexpected concentration ranges.

5. Use of a written standard operating procedure (SOP).

A written SOP entitled, “Standard Operating Procedure for Sampling and Analysis of Sulfur Hexafluoride Using Programmable Integrating Gas Samplers (PIGS) and Automated Tracer Gas Analysis Systems (ATGAS)” was used by all personnel performing SF₆ analysis so that all analyses were performed consistently. The SOP contained the following sections:

1. Scope and Application.
2. Summary of Method.
3. Health and Safety Warnings.
4. Interferences.
5. Personnel Qualifications.
6. Equipment and Supplies.
7. ATGAS Setup.

8. Sample Collection.
 9. Cartridge Check-In.
 10. Analysis Preparation.
 11. Analysis.
 12. Sample Handling and Holding Times.
 13. Data Analysis and Calculations.
 14. Quality Control and Quality Assurance.
 15. Data and Records Management.
 16. Trouble-shooting.
 17. References.
6. Pre-project calculation of instrument limit of detection (ILOD) and instrument limit of quantitation (ILOQ).

Prior to the start of the project, the ILOD and ILOQ were established for each ATGAS to provide information on instrument performance. The ILOD is the instrument's limit of detection and is defined as the lowest concentration that can be determined to be statistically different from zero. It is a measure of instrument sensitivity and based upon the specific instrument's ability to differentiate a low level concentration standard from instrument noise. One bag filled with a low level standard was analyzed on each of the 12 autosampler ports on each ATGAS. The analysis at each port was preceded by the analysis of a higher concentration standard of at least 10,000 pptv to evaluate any possible carryover effects. The ILOD was calculated as three times the standard deviation of a low level standard that was analyzed twelve times. The ILOQ is the instrument's limit of quantitation and is defined as the lowest concentration that can be determined within 30% of the actual concentration. The ILOQ was calculated as ten times the standard deviation of the same low level standard analyzed 12 times. Since using different concentrations will yield different ILOD and ILOQs, the analyst selected the lowest concentration standard to meet as many of the following criteria as possible:

- Has a relative standard deviation (RSD), i.e., the standard deviation divided by the mean multiplied by 100 of less than 15%.
- Has a signal to noise (S/N; the mean divided by the standard deviation) between 3 and 10 (a higher value does not invalidate the result; rather it indicates that a lower concentration standard can be used).
- Has a percent recovery (analyzed value divided by the certified value multiplied by 100) between 90% and 110%.

Results for the pre- and post-project estimation of ILOD and ILOQ for each ATGAS are shown in Table 5. All initial ILOD were less than 1 pptv and much less than the stated

Table 5. Summary of project instrument sensitivity and low end instrument bias.

ATGAS	1	2	3	4 w. outlier	4 no outlier	All
Pre-Project (3.11 pptv)						
Number	12	12	12	12		
Mean	3.44	3.37	3.46	3.25		
S.D.	0.08	0.16	0.16	0.20		
RSD	2.33	4.75	4.62	6.15		
S/N	43.00	21.0625	21.625	16.25		
ILOD	0.24	0.48	0.48	0.60		
ILOQ	0.80	1.60	1.60	2.00		
Lab Blank						
Number	174	132	174	96		
Mean	0	0	0.24	0		
S.D.	0	0	1.47	0		
ILOD	0	0	4.41	0		
ILOQ	0	0	14.70	0		
Lab Control (3.11 pptv)						
Number	81	75	99	57	56	311
Mean	3.02	3.03	3.21	2.74	3.00	3.065
S.D.	0.45	0.59	0.62	2.04	0.42	0.53
ILOD	1.35	1.77	1.86	6.12	1.26	1.59
ILOQ	4.50	5.90	6.20	20.40	4.20	5.30
Post-Project (3.11 pptv)						
Number	12	12	12	12		
Mean	3.25	3.14	3.20	3.12		
S.D.	0.095	0.15	0.16	0.26		
RSD	2.92	4.78	5.00	8.33		
S/N	34.21	20.93	20.00	12.00		
ILOD	0.285	0.45	0.48	0.78		
ILOQ	0.95	1.50	1.60	2.60		

measurement quality objective (MQO) of less than 4 pptv outlined in Table 4. All initial ILOQ were less than 2 pptv. No carryover effects were observed.

7. Holding time studies

Holding time studies are determinations of the length of time a sample can be held in its container before the sample concentration changes appreciably. Holding time studies are conducted whenever the method or sampling container is changed in any way prior to commencement of a project. These studies are used to determine what effect degradation of the materials will have on sample results. Knowledge of the length of time the samples can be held will help in planning the analysis schedule for the samples in the field. Holding time studies

performed in 2004 on the new sample bags and tubing showed no appreciable change in sample concentration for up to six months if stored indoors and away from temperature extremes.

Artifact studies on the Pliobond-sealed bag sample fittings and R-3603 tubing were performed in 2011 and early 2013 and showed no evidence of sample contamination or bag leakage. All samples were initially analyzed within a week of sampling for this project.

8. Daily calibration of the ATGAS.

In order to quantify the concentration of the samples, each of the four ATGASs was calibrated at the beginning of each analysis day using 10 to 18 NIST-traceable SF₆ standards. The number of standards used was dependent upon the concentration range available to each ATGAS as they were configured for this experiment. Each ATGAS was configured to optimize the ability to detect very low concentrations, principally by choice of a sufficiently large sample loop. This low end optimization had the effect of restricting the ability to quantify higher concentrations without changing sample loops. The analytical range for each ATGAS as configured for the experiment are shown in Table 6. Differences relate to sample loop size and the specific performance characteristics of each ATGAS.

The routine calibration standards used ranged from 3.11 pptv to 36,900 pptv and covered

Table 6. ATGAS analytical ranges.

ATGAS	Loop Volume	Calibrated Range	Number of Standards
1	1 ml	ILOD - 52,600 pptv	18
2	5 ml	ILOD - 75,100 pptv	19
3	500 ul	ILOD - 158,200 pptv	initial 20
3	500 ul	ILOD - 210,700 pptv	final 23
4	1 ml	ILOD - 36,900 pptv	17

most of the range of field sample concentrations encountered. There were a few exceptions that required the use of an additional 7 standards ranging up to 210,700 pptv to quantify these samples (run on GC3). Two standards were depleted and replaced by standards with similar concentrations prior to the start of analyses of test samples (24.8 replaced with 19.19 pptv; 307 replaced with 301 pptv). Three other standards were depleted and replaced by standards with similar concentrations during analyses of the test samples (3110 replaced by 3140 pptv; 5220 replaced by 4980 pptv; 8300 replaced by 8270 pptv). A UHP nitrogen zero point was also used in the calibration since it is very difficult to find UHP air with undetectable amounts of SF₆.

Concentrations of samples were calculated using a point-to-point fit calibration of the standards. The calibration curve was examined for "wild fits" and an error message was displayed if such an event occurred so that the analyst could more closely examine the curve and decide if it was appropriate to use.

9. Initial ATGAS calibration verification (ICV).

After each calibration was completed and reviewed, the curve was validated by analyzing the same calibration standards as if they were field samples. This validation demonstrated that sample concentrations within the calibration range could be quantified correctly. The recoveries were required to be within $\pm 12\%$ (for < 50 pptv) or $\pm 7\%$ (for > 50 pptv) of the certified value or the standards were re-analyzed. If the recoveries still did not meet the acceptance limits, the bags were refilled and analyzed again. If the recoveries were still not acceptable, the instrument was re-calibrated and ICV was attempted again.

10. Continuing ATGAS calibration verification (CCV) and laboratory controls.

The validity of the ATGAS instrument calibration curves were regularly checked by re-analyzing calibration standards as if they were field samples. This procedure, called continuing calibration verification (CCV), was performed to provide evidence that instrument drift had not caused the calibration to be unable to correctly quantify sample results within the MQO acceptance level. Standards were chosen to cover the concentration range of samples that had been analyzed since the last calibration verification. The standards were required to have a recovery of $\pm 20\%$ (for < 50 pptv) or $\pm 10\%$ (for > 50 pptv) of the certified value for that section of the curve to be considered valid (Table 4). If any of the standards were not within the acceptance window, the instrument was re-calibrated and the curves were re-validated. All data within the unacceptable concentration range, from the point of the last acceptable CCV, were flagged and re-analyzed.

There was a tendency for the responses of the GCs to become more stable with continued operation but all of them exhibited some susceptibility to drift of the calibration. The frequency of CCVs ranged from less than 1 to about 3 h depending on the GC and how long it had been in operation with a relatively stable calibration for any given day. In general, calibration checks were done more frequently in the first few hours of operation and less frequently after that if the GC was exhibiting stable behavior. Recalibrations were usually done if the response had drifted significantly ($>$ about 6-8%) as there was a tendency that once drift had commenced it often continued and raised the prospect of performing analyses that would have to be redone due to violating the MQO requirements of $\pm 10\%$ or $\pm 20\%$ for > 50 pptv and < 50 pptv, respectively. Furthermore, the intent was to keep all results within 10%. Following any recalibration, responses were often stable within $\pm 5\%$ for the remainder of the day. In some cases it was not necessary to recalibrate after the initial calibration although it was common for GCs 1 and 3 to be recalibrated once a few hours into the day and then remain stable for an extended period of time. GCs 2 and 4 were the most susceptible to problematic calibration drift but even they sometimes had stable calibrations. Considerable time was spent in calibration and recalibration of the GCs to ensure achieving MQO, especially GCs 2 and 4. There was also some analysis time lost due to the necessity to rerun some sets of sample cartridges due to failure to achieve the requisite CCV recoveries.

The CCV serve as laboratory control samples and measures of instrument precision and instrument accuracy (Table 4). Results for the combined laboratory control samples (CCV) are summarized in Table 7. With the exception of the lowest standard (3.11 pptv), all of the RSD were well below the 10% limit specified in the MQOs and indicated excellent instrument precision. The excellent agreement between the measured and actual NIST-certified standard values is also shown in Fig. 31. The slope (1.007) and intercept (28.6) indicate no appreciable bias and the Pearson's r correlation value of 0.9995 shows excellent precision. The average recoveries are indicative of excellent accuracy across the full range of concentrations used and are easily with the 100±20% requirement.

Table 7. Summary of project laboratory control (CCV) results.

Concentration		S.D.	Avg. % Recovery	RSD %	S/N	#
Actual	Measured (Avg.)					
0	0.21	0.91				222
0	-0.05	4.05				223
3.11	3.13	0.36	100.6	11.5	8.7	306
10.1	10.14	0.46	100.4	4.5	22.0	277
19.19	19.48	1.02	101.5	5.2	19.1	276
35.1	34.91	1.46	99.5	4.2	23.9	268
88.7	89.5	2.99	100.9	3.3	29.9	266
301	304.2	9.33	101.1	3.1	32.6	264
504	509.9	16.81	101.2	3.3	30.3	268
818	829.6	30.4	101.4	3.7	27.3	267
1,550	1,583.1	71.13	102.1	4.5	22.3	265
3,110	3,154.8	113.99	101.4	3.6	27.7	133
3,140	3,257.5	123.45	103.7	3.8	26.4	127
4,980	5,105.3	214.01	102.5	4.2	23.9	125
5,220	5,302.4	195.01	101.6	3.7	27.2	135
8,270	8,406.4	264.22	101.6	3.1	31.8	85
8,300	8,346.0	343.8	100.6	4.1	24.3	150
9,730	9,920.9	424.13	102.0	4.3	23.4	217
16,370	16,582.7	784.08	101.3	4.7	21.1	210
21,720	21,928.9	727.61	101.0	3.3	30.1	185
36,900	37,062.9	1,655.32	100.4	4.5	22.4	179
52,600	53,275.1	1,238.15	101.3	2.3	43.0	139
75,100	75,652.7	1,964.19	100.7	2.6	38.5	36
90,100	90,670.2	2,581.11	100.6	2.8	35.1	14
103,600	103,528.4	3,077.36	99.9	3.0	33.6	14
152,300	153,541.6	3,254.72	100.8	2.1	47.2	9
179,300	178,952.1	3,129.02	99.8	1.7	57.2	2
210,700	210,492.1	1,562.92	99.9	0.7	134.7	2

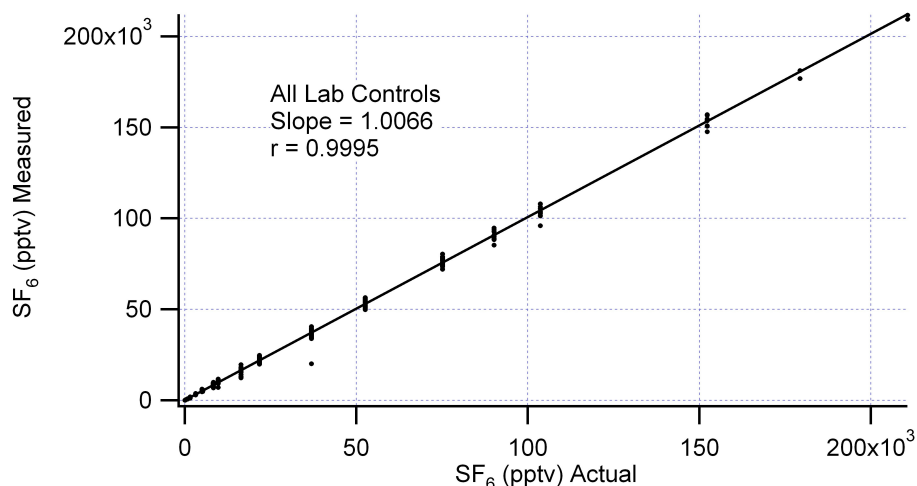


Figure 31. Comparison between measured and NIST-certified standard concentrations for all lab control (CCV) samples.

11. Atmospheric background checks of SF₆ at the tracer analysis facility (TAF).

A background atmospheric check of SF₆ in the TAF consisted of analyzing three samples of the room air in the TAF on each GC every analysis day. This information was used to determine if there was any leakage in the analysis system when compared to the instrument blanks that were subsequently analyzed. The data provided for an inter-comparison between GCs that were being used on the same day to check the between instrument precision. The results were also used to reveal discrepancies between GCs to indicate a problem that otherwise might go undetected. The results shown in Table 8 indicate that there was good precision between the 4 GCs. The average concentration for all background checks was 8.3 pptv with a standard deviation of 0.74 pptv. With the exception of GC3, the combined and individual RSD values are all less than the 10% MQO specified in Table 4 (“Between Instrument Precision”). GC3 was susceptible to baseline instabilities at very low concentrations. One consequence of that is the larger standard deviation associated with the measurement of room air.

Table 8. Summary of results for lab background checks (room air).

RoomAir	#	Mean	s.d.	RSD
GC1	48	8.30	0.62	7.5
GC2	37	8.38	0.83	9.9
GC3	48	7.96	1.69	21.2
GC4	24	7.92	0.73	9.2
All	157	8.27	0.74	8.9

12. Laboratory (instrument) blanks.

A laboratory or instrument blank was analyzed on each ATGAS each analysis day to verify that there was no contamination or leaks within the analysis system as compared to the

background checks analyzed that day, that there was no carry-over from previously analyzed high concentration standards, and to ensure carrier gas purity. The blank sample consisted of a cartridge of 12 bags that were each filled with ultra high purity (UHP) nitrogen. The concentration results of all bags were required to be less than the lowest calibration standard and close to a concentration of 0 pptv. If the concentration of one or more of the bags was higher than the acceptable range, the bag was re-filled and re-analyzed. If the concentration still was not within acceptable limits, the instrument was re-calibrated and re-verified or the samples were flagged and re-analyzed. If there were still indications of contamination, the problem was identified and fixed before analysis continued.

The laboratory blank results for each ATGAS and its corresponding ILOD and ILOQ are included in Table 5. The average results indicate no contamination or leakage problems within any of the ATGASs as well as no carryover issues and meet the MQO of <4 pptv (Table 4). The higher mean and standard deviation for ATGAS 3 reflect its sensitivity to the effect of very small changes in baseline on the peak integration at very low level concentrations. This feature also shows up in some calculations of the ILOD and ILOQ for ATGAS 3 (Table 5).

13. Laboratory duplicates.

Analyses of laboratory duplicates were performed each day to provide evidence of instrument precision. Each day at least one primary field bag sampler cartridge was analyzed in duplicate on each ATGAS. The sample cartridge and its duplicate were analyzed at least 3 hours apart in order to ensure an appropriate estimation of instrument precision over time. The duplicate cartridges were selected to encompass as much variation and range of concentration as possible within the concentration range bracketed by the calibration curve for each ATGAS.

The mean of the absolute value of the relative percent differences (RPD), $RPD = (100 * (\text{measure\#1} - \text{measure\#2}) / \text{average}(\#1 \text{ and } \#2))$ were required to be within 5% (Table 4). Any result not within the acceptable limits was flagged and re-analyzed. If the result was still not within acceptable limits, the analysis was terminated until the ATGAS precision could be re-established.

The |RPD| laboratory duplicate results are shown in Table 9 and, excepting GC4, are all less than 5% indicating excellent instrument precision. A regression analysis of the laboratory duplicates is shown in Fig. 32.

Table 9. Summary of RPD results for laboratory duplicates.

Laboratory Duplicates			
GC #	#	Mean % RPD	Mean % RPD
1	235	-0.10	2.1
2	362	1.70	3.6
3	262	0.35	3.4
4	354	-1.80	6.4

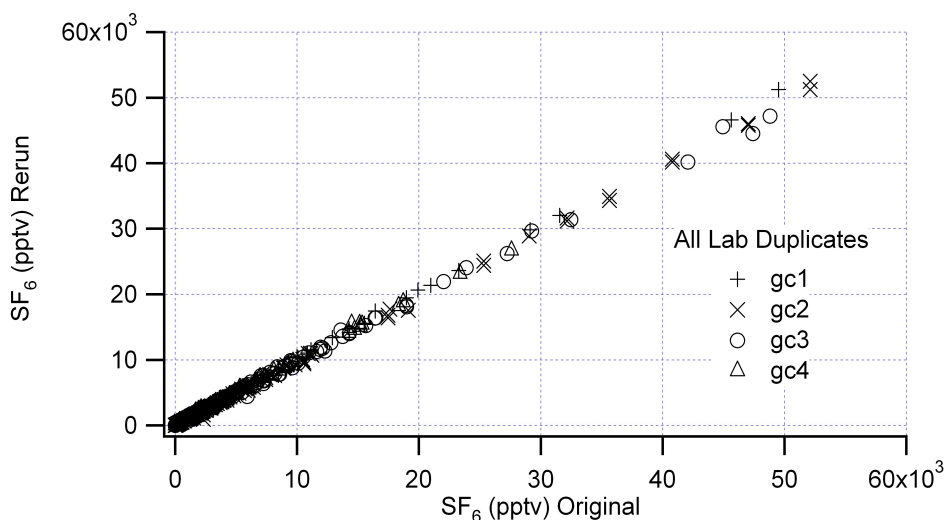


Figure 32. Linear regression of rerun against original values for all laboratory duplicates.

14. Field blanks.

Field (method) blanks were sampled and analyzed to indicate if there was any contamination or leakage introduced by any part of a bag sample's history from sampling, handling, and transport through to the final analysis. For example, isolated instances of high concentrations of SF₆ in the field blanks can indicate holes in the sampling bag, clips not properly closed, wrong location number, or other operational problems. Consistently high concentrations would indicate a sampling method that could not measure null concentrations accurately.

Three field blank samplers were deployed during each IOP as described in the section above (Description of Bag Sampling Grid). A field blank consisted of a sampler containing a cartridge filled with ultra high purity (UHP) nitrogen. Each sampler was deployed at its designated location and collocated with a regular sampler with the tubes connected and clips left open. Software requirements of the sampling program made it necessary for the pump on the first bag to turn on for one short pulse. However, after that, all pumps were left off and there was no additional filling of any of the bags. At the end of each test, the clips on the blank cartridges were closed and the cartridges were collected, transported, and stored along with all the regular sample cartridges. With the exception of the special sampling program, the field blanks were treated identically to the regular samples.

A summary of the results is presented in Table 10. The means and standard deviations for IOPs 1, 4, and 5 are all very low indicating no contamination or sample handling problems. The non-zero mean and larger standard deviation for IOP2 is attributable to the use of GC3 for one cartridge of blanks. The non-zero mean and larger standard deviation for IOP3 is likely attributable to one cartridge that was deployed where it was in the plume with high concentration values for extended periods of time. It is likely that small amounts of tracer diffused into the

Table 10. Summary of results for lab background checks (room air).

IOP	#	Mean	s.d.	MLOQ
1	36	0	0	0
2	35	-1.46	2.76	27.6
3	36	1.95	3.33	33.3
4	36	0.01	0.05	0.5
5	36	0	0	0

sample bags through the open, unclipped tubing. However, even this cartridge did not have any bags with values greater than 10 pptv.

The consequences of these observations are considered more fully in the determination of final MLOQ for the project results (step 19 below). Briefly, the field blank results adversely affected some of the project MQOs (Table 4): (1) They sometimes indicated values for MLOD greater than 12 pptv in some cases (“Method Sensitivity”) and (2) the field blanks were often greater than the nominal MLOQ.

15. Field controls.

Three field control samplers were deployed during each IOP as described in the section above (Description of Bag Sampling Grid). The cartridge for each control sampler was filled with NIST-certified tracer concentrations ranging from 14.79 pptv to 5170 pptv. Bags 1-3 contained 5170 pptv, bags 4-6 contained 199.5 or 283.9 pptv, bags 7-9 contained 14.79 pptv, and bags 10-12 contained 1571 pptv. During IOP5, bag 9 was inadvertently filled with 1571 pptv instead of 14.79 pptv. Each sampler was deployed at its designated location and collocated with a regular sampler with the tubes connected and clips left open. Software requirements of the sampling program made it necessary for the pump on the first bag to turn on for one short pulse. However, after that, all pumps were left off and there was no additional filling of any of the bags. At the end of each test, the clips on the control cartridges were closed and the cartridges were collected, transported, and stored along with all the regular sample cartridges. With the exception of the special sampling program, the field controls were treated identically to the regular samples.

The field control samplers served two primary purposes. First, they checked for any biases or inaccuracies introduced during the sampling, handling, and storage of the samples. Second, recall that the standards used to calibrate the GCs (up to 210,700 pptv) were all NIST-certified. The tracer concentrations used to fill the control bags also came from NIST-certified standards but they were different from those used in the calibration of the ATGASs. As a consequence, the field control samples serve as a semi-independent measure of quality control of the overall process, essentially a method audit.

The results for the field control samples expressed in terms of the individual ATGAS are shown in Table 11. In general there was a very good comparison between the NIST-certified

Table 11. Combined ATGAS field control results expressed in terms of standard concentration and IOP number.

	IOP1	IOP2	IOP3	IOP4	IOP5	All
14.79 pptv						
#	9	9	9	9	8	44
Mean	15.10	14.71	15.62	15.81	15.33	15.31
s.d.	0.41	0.41	1.42	0.27	0.19	0.54
Avg. Recovery	1.02	0.99	1.06	1.07	1.04	1.04
Mean RPD	2.04	-0.57	5.10	6.66	3.55	3.36
Mean RPD	2.18	1.97	7.94	6.66	3.55	4.46
RSD	2.71	2.77	9.07	1.72	1.25	3.50
S/N	36.90	36.09	11.02	58.28	80.29	44.52
199.5 pptv						
#	9	9	9	9	3	39
Mean	178.70	171.62	163.59	177.21	173.87	173.00
s.d.	3.42	8.65	15.19	3.21	4.69	7.03
Avg. Recovery	0.90	0.86	0.82	0.89	0.87	0.87
Mean RPD	-11.01	-15.13	-20.15	-11.85	-13.75	-14.38
Mean RPD	11.01	15.13	20.15	11.85	13.75	14.38
RSD	1.91	5.04	9.29	1.81	2.70	4.15
S/N	52.24	19.85	10.77	55.24	37.06	35.03
283.9 pptv						
#					6	6
Mean					284.55	284.55
s.d.					4.31	4.31
Avg. Recovery					1.00	1.00
Mean RPD					0.22	0.22
Mean RPD					1.04	1.04
RSD					1.51	1.51
S/N					66.07	66.07
1571 pptv						
#	9	9	8	9	10	45
Mean	1,497.44	1,454.86	1,428.45	1,488.10	1,446.75	1,463.12
s.d.	33.35	43.97	86.39	39.12	20.97	44.76
Avg. Recovery	0.95	0.93	0.91	0.95	0.92	0.93
Mean RPD	-4.82	-7.72	-9.66	-6.06	-8.24	-7.30
Mean RPD	4.82	7.72	9.66	5.45	8.24	7.18
RSD	2.23	3.02	6.05	2.63	1.45	3.08
S/N	44.90	33.09	16.53	38.04	68.98	40.31
5170 pptv						
#	9	9	9	9	9	45
Mean	5,265.70	5,187.80	5,275.19	5,194.93	4,941.64	5,173.05
s.d.	65.02	186.84	181.54	74.37	64.76	114.51
Avg. Recovery	1.02	1.00	1.02	1.00	0.96	1.00
Mean RPD	1.83	0.29	1.96	0.17	-4.52	-0.05
Mean RPD	1.83	2.91	2.97	1.27	4.52	2.70
RSD	1.23	3.60	3.44	1.43	1.31	2.20
S/N	80.99	27.77	29.06	69.86	76.30	56.79

standards used in the field controls with the NIST-certified standards used to develop the calibration curves for the GCs. One notable exception was the 199.5 pptv field control standard. The measured results for that standard were consistently lower. The measured results for the 1571 pptv standard also had a low bias but were within the $\pm 5\%$ uncertainty of each standard and were much closer than for the 199.5 pptv standard. Linear regression on the combined field control samples calculated a slope of 1.004, an intercept of 38.5, and a Pearson's r value of 0.999 indicating that overall there was no significant overall bias and good precision (Fig. 33).

With the exception of 199.5 pptv for IOP3, the mean |RPD| and the RSD MQO requirements were all satisfied and mostly by very comfortable margins ($<20\%$ and $<15\%$, respectively; Table 4).

16. Field duplicates.

Sixteen field duplicate samplers were deployed for each IOP during PSB1 as described in the section on Description of Bag Sampling Grid (above). The duplicate samplers were handled identically to the primary samplers with which they were collocated. They were mounted at the same height at sites within a few feet laterally from the primary sampler. A summary of the results is provided in Table 12.

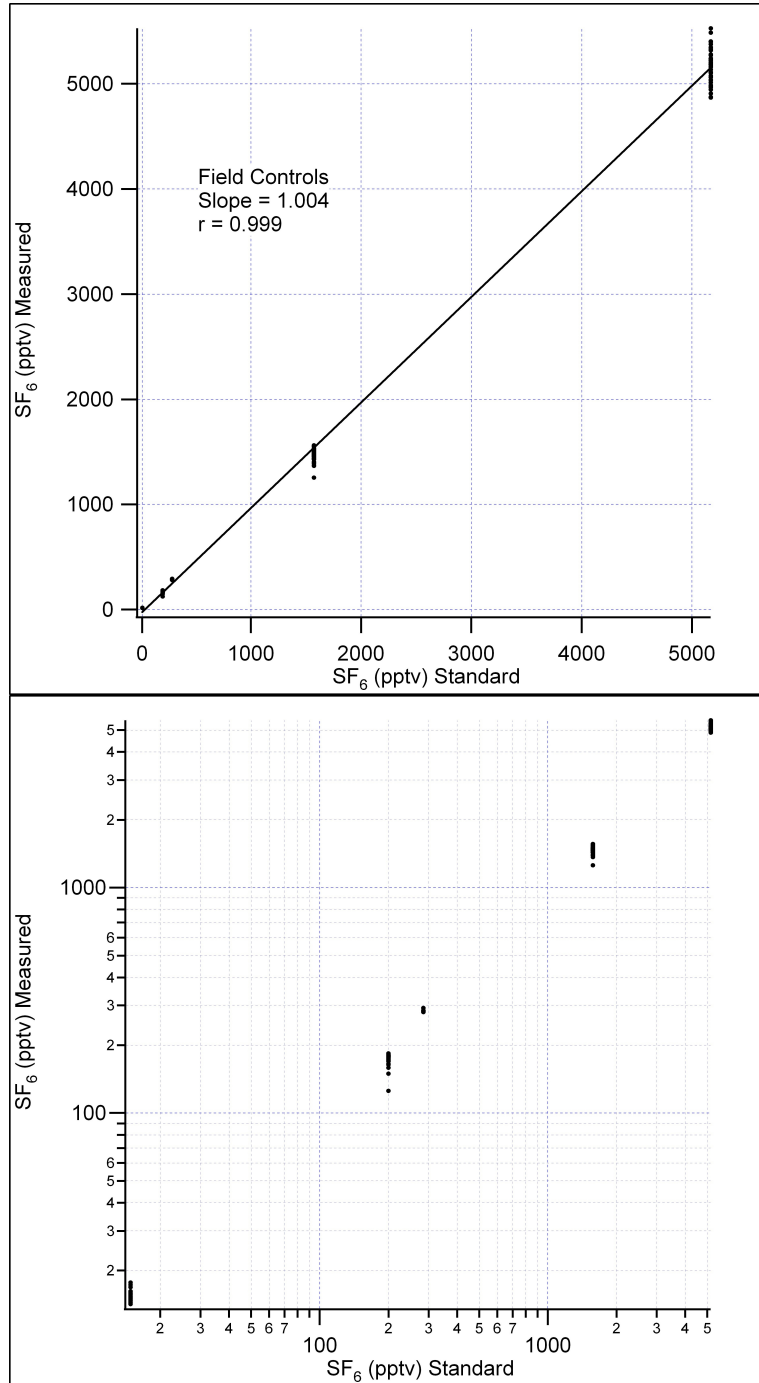


Figure 33. Linear regression field control samples.

Table 12. Summary of field duplicate sampler results.

Test	# Number	Avg. % RPD	Avg. % RPD
1	185	-3.6	10.2
2	177	-0.5	12.5
3	187	-4.0	12.8
4	182	-4.5	12.2
5	189	1.4	10.2
Combined	920	-2.2	11.6

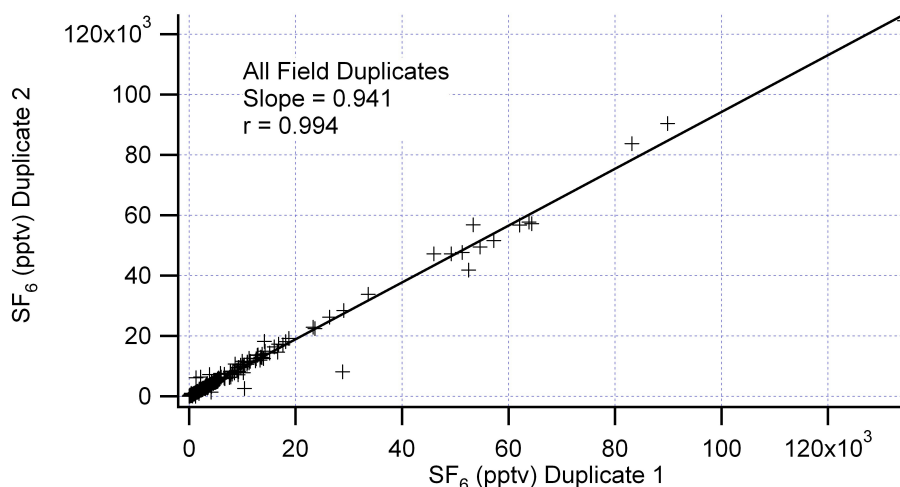


Figure 34. Linear regressions for all field duplicate samples.

Overall, it is apparent that there was good agreement between collocated samplers. The MQO mean |RPD| requirement was satisfied for all IOPs (<15%). This is confirmed by the linear regression shown in Fig. 34 (slope=0.941, intercept=38.5, r=0.994).

17. Software quality control checks.

Several important quality checks were built into the software to efficiently aid the TAF analyst in ensuring that the ATGAS instruments were functioning correctly during analysis.

- Since the concentration is dependent upon the temperature of the ATGAS ovens, it is critical that oven temperatures do not fluctuate widely during analysis. Temperature acceptance limits were set (± 2 °C) and the software produced a pop-up window to alert the analyst in case of unacceptable oven temperature readings. All samples obtained using the incorrect oven temperatures were re-analyzed.

- To check for instrument drift, the software alerted the analyst to validate the calibration curve when more than three hours had elapsed from the last CCV. The analyst had the option of overriding the alert or checking the calibration and re-starting the 3-hour clock. This option was always exercised except on a few occasions near the end of the analysis day when only 1-2 more cartridges required analysis. Even then this was only done on ATGASs that had previously been exhibiting consistently stable response for extended periods of time during that day.
- In order to verify the calibration curve in the area of interest and to save time, the software produced on the computer screen a record of the highest and lowest concentrations measured since the last CCV. The analyst had only to re-analyze calibration samples within that range. However, the complete calibration range was routinely done to most fully evaluate the current status of instrument response and performance.
- Several data flags were shown immediately on the computer screen to aid the analyst in deciding whether the data for each bag was “good” or re-analysis was necessary. For example, the low pressure flag alerted the operator to a problem with the analysis that was almost invariably due to pinched tubing restricting sample flow.
- The software kept track of which ATGAS field duplicate was analyzed on and directed the analyst to use the same GC for the duplicate cartridge. This helped to quantify the variability of the field analysis without adding the extra variability of analyzing on a separate ATGAS. However, due to limitations imposed by the restricted calibration ranges of ATGASs 2 and 4, it was not uncommon for the field duplicates to be done on different ATGASs.
- The software alerted the analyst if any calibration points did not meet pre-determined acceptance criteria. The analyst could then review the calibration curve to determine the acceptable course of action.

18. Data verification.

Data verification was performed to ensure that the samples met all QC acceptance limits and that all samples had been analyzed for that particular test. Transcription and calculation errors were reduced by automated data reduction techniques such as automated flagging of results outside acceptable limits, raw data summary sheets (Fig. 35), auto-generated quality control sheets (Figs. 36 and 37), auto generation of chromatogram plots including calibration curves (Fig. 38), and electronic transfer of data from the ATGASs to Excel spreadsheets. The analyst and at least one other person familiar with the data analysis process reviewed all data packages. All data packages were batch processed per run on each ATGAS. All data packages included the raw data sheets, quality control sheets that summarized the results of all QC data generated for that batch, plots of all chromatograms and calibration curves, a copy of the laboratory notebook pages for that analysis (Fig. 39), and a data verification sheet (Fig. 40) to ensure the verifier checked all QC parameters. Software produced an Analysis Summary (Fig. 41) that was utilized to ensure that there was at least one acceptable result for each bag for each location that was downloaded for each IOP. Any samples noted by the software were re-analyzed

131015	1035	SN0397	SAGE13	2	58	3	1	14304.62	65	653.	0	0	G	
131015	1036	SN0397	SAGE13	2	59	4	1	84.44	65	653.	0	0	G	
131015	1037	SN0397	SAGE13	2	60	5	1	912.44	65	653.	0	0	G	
131015	1038	SN0397	SAGE13	2	61	6	1	311.52	65	653.	0	0	G	
131015	1040	SN0397	SAGE13	2	62	7	1	22023.60	65	653.	0	0	G	
131015	1041	SN0397	SAGE13	2	63	8	1	3692.82	65	653.	0	0	G	
131015	1042	SN0397	SAGE13	2	64	9	1	16482.13	65	653.	0	0	G	
131015	1043	SN0397	SAGE13	2	65	10	1	11621.93	65	653.	0	0	G	
131015	1044	SN0397	SAGE13	2	66	11	1	15636.64	65	653.	0	0	G	
131015	1045	SN0397	SAGE13	2	67	12	1	32469.91	65	653.	0	0	G	
131015	1049	SN0289	SAGE13	2	68	1	1	1225.11	65	653.	0	0	G	
131015	1050	SN0289	SAGE13	2	69	2	1	347.32	66	653.	0	0	G	
131015	*1051*	SN0289*	SAGE13	2	70*	3	1*	17.10*	65	652.	0	3	F	**** unusable
131015	1052	SN0289	SAGE13	2	71	4	1	162.98	66	653.	0	0	G	
131015	1053	SN0289	SAGE13	2	72	5	1	52.92	66	653.	0	0	G	
131015	1054	SN0289	SAGE13	2	73	6	1	101.49	66	653.	0	0	G	
131015	1055	SN0289	SAGE13	2	74	7	1	8.51	65	652.	0	0	G	
131015	1056	SN0289	SAGE13	2	75	8	1	8.55	65	652.	0	0	G	
131015	1057	SN0289	SAGE13	2	76	9	1	8.96	65	652.	0	0	G	
131015	1058	SN0289	SAGE13	2	77	10	1	8.39	65	653.	0	0	G	
131015	1059	SN0289	SAGE13	2	78	11	1	8.53	66	653.	0	0	G	
131015	1100	SN0289	SAGE13	2	79	12	1	8.64	65	653.	0	0	(L)	low bag
131015	1105	SN4383	SAGE13	2	80	1	1	7.92	66	653.	0	0	G	fdp
131015	1106	SN4383	SAGE13	2	81	2	1	7.93	65	653.	0	0	G	fdp
131015	1107	SN4383	SAGE13	2	82	3	1	3006.30	65	653.	0	0	G	fdp
131015	1108	SN4383	SAGE13	2	83	4	1	81.52	65	653.	0	0	G	fdp
131015	1109	SN4383	SAGE13	2	84	5	1	1019.18	65	652.	0	0	G	fdp
131015	1110	SN4383	SAGE13	2	85	6	1	15.42	65	653.	0	0	G	fdp
131015	1111	SN4383	SAGE13	2	86	7	1	4791.56	65	652.	0	0	G	fdp
131015	1112	SN4383	SAGE13	2	87	8	1	853.01	65	652.	0	0	G	fdp
131015	1113	SN4383	SAGE13	2	88	9	1	26366.36	65	652.	0	0	G	fdp
131015	1115	SN4383	SAGE13	2	89	10	1	9346.58	65	652.	0	0	G	fdp
131015	1116	SN4383	SAGE13	2	90	11	1	10919.11	65	652.	0	0	G	fdp
131015	1117	SN4383	SAGE13	2	91	12	1	45963.54	65	652.	0	0	G	fdp
131015	1121	SN4329	SAGE13	2	92	1	1	10.47	65	652.	0	0	G	
131015	1122	SN4329	SAGE13	2	93	2	1	56.15	65	652.	0	0	G	
131015	1123	SN4329	SAGE13	2	94	3	1	40.29	65	652.	0	0	G	
131015	1124	SN4329	SAGE13	2	95	4	1	203.30	66	652.	0	0	G	
131015	1125	SN4329	SAGE13	2	96	5	1	62.75	65	652.	0	0	G	
131015	1126	SN4329	SAGE13	2	97	6	1	69.57	65	652.	0	0	G	
131015	1127	SN4329	SAGE13	2	98	7	1	446.45	65	652.	0	0	G	
131015	1128	SN4329	SAGE13	2	99	8	1	10.06	65	652.	0	0	G	
131015	1129	SN4329	SAGE13	2	100	9	1	8.61	65	652.	0	0	G	
131015	1130	SN4329	SAGE13	2	101	10	1	7.92	65	652.	0	0	G	
131015	1131	SN4329	SAGE13	2	102	11	1	8.55	65	652.	0	0	G	
131015	1132	SN4329	SAGE13	2	103	12	1	8.56	66	652.	0	0	G	
131015	1137	SN4343	SAGE13	2	104	1	1	4425.70	65	652.	0	0	G	
131015	1138	SN4343	SAGE13	2	105	2	1	1017.25	66	652.	0	0	G	
131015	1139	SN4343	SAGE13	2	106	3	1	142.95	66	652.	0	0	G	
131015	1140	SN4343	SAGE13	2	107	4	1	162.84	66	652.	0	0	G	
131015	1141	SN4343	SAGE13	2	108	5	1	408.26	66	652.	0	0	G	
131015	1142	SN4343	SAGE13	2	109	6	1	488.85	65	652.	0	0	G	
131015	1143	SN4343	SAGE13	2	110	7	1	38.70	66	652.	0	0	G	
131015	1144	SN4343	SAGE13	2	111	8	1	715.22	65	652.	0	0	G	
131015	1145	SN4343	SAGE13	2	112	9	1	34.68	66	652.	0	0	G	
131015	1146	SN4343	SAGE13	2	113	10	1	9.30	65	652.	0	0	G	
131015	1147	SN4343	SAGE13	2	114	11	1	9.78	65	652.	0	0	G	
131015	1148	SN4343	SAGE13	2	115	12	1	9.53	65	652.	0	0	G	
131015	1153	SN0007	SAGE13	2	116	1	1	9.21	66	652.	0	0	G	
131015	1154	SN0007	SAGE13	2	117	2	1	8.01	66	652.	0	0	G	

Figure 35. Example of Raw Data Summary sheet.

National Oceanic and Atmospheric Administration
 Air Resources Laboratory Field Research Division
 Quality Control Sheets

Analyst: Dennis Finn et. al.
 Date: 10/16/2013
 Project: SAGE13
 GC# 1
 Parameter: SF6
 Data file: G1131016.r01

Verified by: Roger G. Carter
 Date: 23 Oct 2013

Calibration Verification (+7%; <50 ±12%)		Lab Blank (<lowest cal)		Calibration Check (+10%; <50 ±20%)		Background Level		
Bag	True Value	Result	%Recovery	Area	Bag	Result	Bag	Result
#01	0.00	0.56	?	686	#01	0.00	#01	10.268
#02	3.11	3.39	109	2974	#02	0.00	#02	10.316
#03	10.10	10.37	103	10965	#03	0.00	#03	10.058
#04	19.19	19.77	103	22180	#04	0.00	Average	10.214
#05	35.10	35.04	100	33412	#05	0.00	Sample	
#06	88.70	87.98	99	116748	#06	0.00	Min=	0.00
#07	301.00	297.95	99	450292	#07	0.00	Max=	51066.39
#08	504.00	500.72	99	736517	#08	0.00	Temperature	
#09	818.00	822.40	101	1093385	#09	0.00	Min=	62.6
#10	1550.00	1556.80	100	1684523	#10	0.00	Max=	67.4
#11	3110.00	3070.56	99	2307952	#11	0.00		
#12	5220.00	5213.41	100	2951101	#12	0.00		
#01	8300.00	8292.34	100	3564852				
#02	9730.00	9736.86	100	3876774				
#03	16370.00	16663.88	102	4793330				
#04	21720.00	21817.29	100	5350192				
#05	36900.00	37147.07	101	7161377				
#06	52600.00	51719.08	98	8810498				
#07	75100.00	74834.21	100	10969928				

Final Calibration Verification (+10%; <50 ±20%)		Comments/Corrective Actions	
Bag	True Value	Result	%Recovery
#01	0.00	0.20	?
#02	3.11	3.21	103
#03	10.10	10.33	102
#04	19.19	19.85	103
#05	35.10	35.58	101
#06	88.70	90.92	102
#07	301.00	305.47	101

SN0378 #06 was low
 SN0378 #08 was low
 SN1265 #09 should be re-run
 SN1265 #10 should be re-run
 SN1265 #8 should be re-run

Figure 36. Example of first page of quality control sheet.

#07 75100.00 75798.70 101 10505549 52600.00 53943.86 103
 75100.00 76633.05 102

Final Calibration Verification(±10%; <50 ±20%) Comments/Corrective Actions

Bag True Value Result %Recovery

Bag	True Value	Result	%Recovery
#01	0.00	-0.37	?
#02	3.11	3.15	101
#03	10.10	9.66	96
#04	19.19	17.89	93
#05	35.10	33.12	94
#06	88.70	85.39	96
#07	301.00	292.01	97
#08	504.00	494.74	98
#09	818.00	825.60	101
#10	1550.00	1632.51	105
#11	3110.00	3279.07	105
#12	5220.00	5484.06	105
#01	8300.00	8379.71	101
#02	9730.00	9816.35	101
#03	16370.00	16746.16	102
#04	21720.00	22060.15	102
#05	36900.00	35925.72	97
#06	52600.00	52720.06	100
#07	75100.00	73595.19	98

Duplicates

cart	Bag	Result 1	Result 2	RPD
SN0203	#01	10074.35	10291.76	-2.1
SN0203	#02	11150.15	11397.22	-2.2
SN0203	#03	3430.90	3504.70	-2.1
SN0203	#04	11137.65	11522.75	-3.4
SN0203	#05	14273.24	14722.13	-3.1
SN0203	#06	6227.48	6405.37	-2.8
SN0203	#07	20973.62	21356.79	-1.8
SN0203	#08	18979.41	19477.15	-2.6
SN0203	#09	16407.46	17464.74	-6.2
SN0203	#10	23266.80	23634.66	-1.6
SN0203	#11	939.91	965.06	-2.6
SN0203	#12	2976.72	3057.99	-2.7
SN0238	#01	3067.30	3194.99	-4.1
SN0238	#02	1725.45	1851.00	-7.0

Figure 37. Example of last page from quality control sheets.

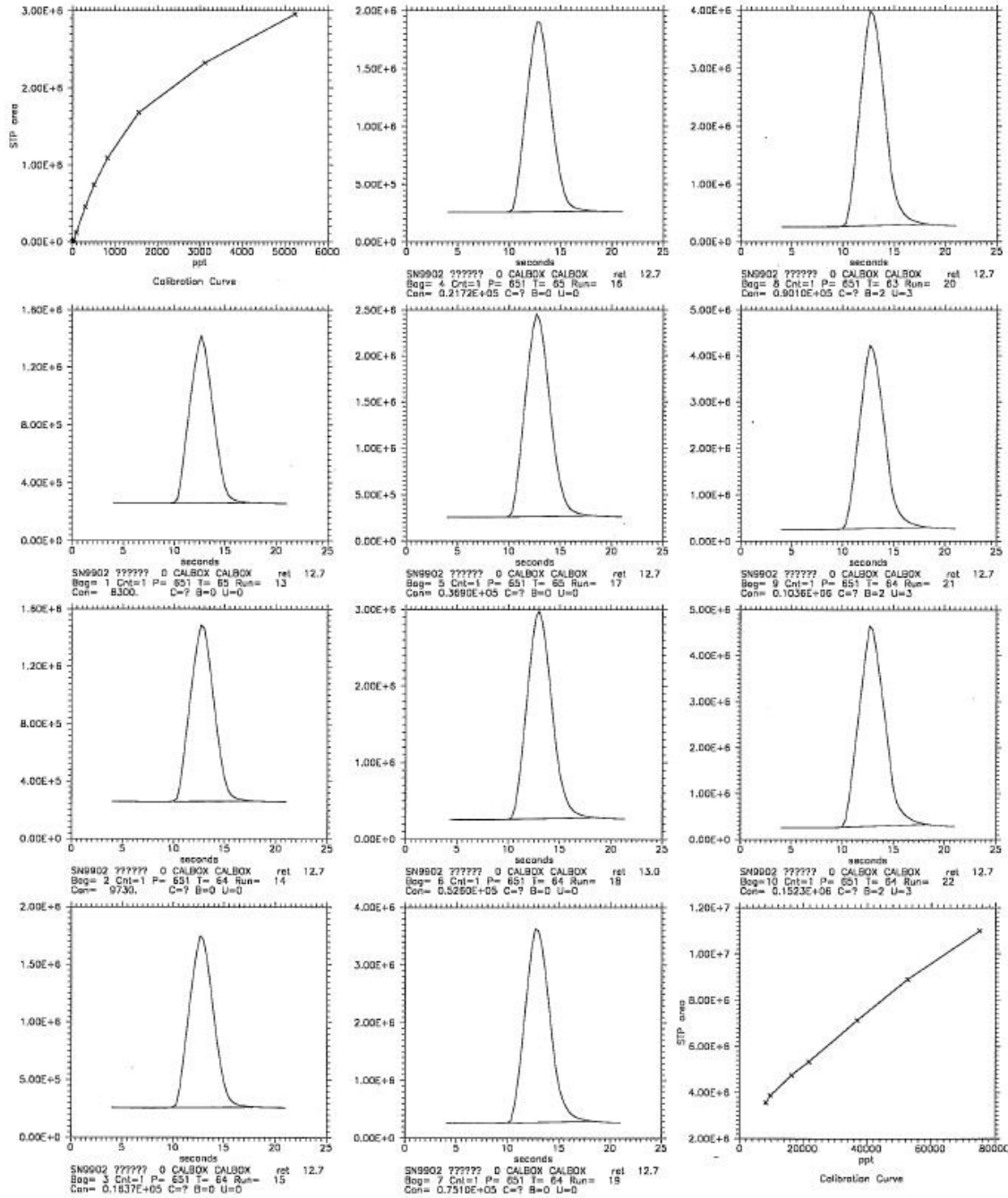


Figure 38. Example of chromatogram and calibration curve check sheet.

Quality Control Verification Sheet

Date: 23 Oct 2013
 Verifier: Roger Carter
 Data File: 61131016.P01
 Project: SAGEB

	YES	NO	NA
Data package contains complete and legible: Chromatograms Raw data Logbookcopy QC sheet	<input checked="" type="checkbox"/>	<input type="checkbox"/>	<input type="checkbox"/>
The same data fits is on the raw data sheet, logbook copy, QC sheet and chromatograms.	<input checked="" type="checkbox"/>	<input type="checkbox"/>	<input type="checkbox"/>
A complete set of calibration checks, that cover the range of sample concentrations, were analyzed at the end of the run.	<input checked="" type="checkbox"/>	<input type="checkbox"/>	<input type="checkbox"/>
All pressures are acceptable. Any low-pressure bags have been re-analyzed if not marked at flat.	<input checked="" type="checkbox"/>	<input type="checkbox"/>	<input type="checkbox"/>
The chromatograms show no anomalies.	<input checked="" type="checkbox"/>	<input type="checkbox"/>	<input type="checkbox"/>
The calibration curve shows no anomalies.	<input checked="" type="checkbox"/>	<input type="checkbox"/>	<input type="checkbox"/>
All flagged samples have been re-analyzed unless the sample is no longer usable.	<input checked="" type="checkbox"/>	<input type="checkbox"/>	<input type="checkbox"/>
All data that has "bad analysis flags" has been marked as unusable and re-analyzed if possible.	<input checked="" type="checkbox"/>	<input type="checkbox"/>	<input type="checkbox"/>
The background level was reported. The background level is greater than the lab blank indicating there is no leakage within the system.	<input checked="" type="checkbox"/>	<input type="checkbox"/>	<input type="checkbox"/>
All data greater than 10% higher than the highest calibration standard is flagged as an estimate and has been re-analyzed.	<input checked="" type="checkbox"/>	<input type="checkbox"/>	<input type="checkbox"/>
All data less than 10% lower than the lowest calibration standard is flagged as an estimate and has been re-analyzed.	<input checked="" type="checkbox"/>	<input type="checkbox"/>	<input type="checkbox"/>
All anomalies reported on the logbook copies are reported on the QC sheet and the data has been flagged appropriately.	<input checked="" type="checkbox"/>	<input type="checkbox"/>	<input type="checkbox"/>
All the data has been transferred correctly from the raw data to the QC sheet.	<input checked="" type="checkbox"/>	<input type="checkbox"/>	<input type="checkbox"/>
Calibration curve verification was within 7% of the true value. (12% for concentrations less than 50ppb) Any anomalies are noted.	<input checked="" type="checkbox"/>	<input type="checkbox"/>	<input type="checkbox"/>
Lab blanks were analyzed and were less than the lowest calibration standard.	<input checked="" type="checkbox"/>	<input type="checkbox"/>	<input type="checkbox"/>
Recoveries for the calibration checks were within ±10% (20% for concentrations less than 50ppb) or the instrument was re-calibrated and the samples within the invalid ranges were re-analyzed.	<input checked="" type="checkbox"/>	<input type="checkbox"/>	<input type="checkbox"/>
Duplicates were analyzed and were within ±10% RPD (20% for concentrations less than 50ppb). Those not meeting the acceptable range were re-analyzed.	<input checked="" type="checkbox"/>	<input type="checkbox"/>	<input type="checkbox"/>
The Min. and Max. even temperatures were within ± 2° C of the temperature set-point.	<input checked="" type="checkbox"/>	<input type="checkbox"/>	<input type="checkbox"/>
Date is usable as noted	<input checked="" type="checkbox"/>	<input type="checkbox"/>	<input type="checkbox"/>

SN4409 b.10 did not run
 SN1042 runs 491-495
 fig as est.

Verifier Comments: Data ok when noted run and flag sets complete.

Figure 40. Example of data package Data Verification sheet.

Analysis Summary for SAGE13 test 1 tracer:SF6
start year=2013 start month= 9
estimated results accepted as good.
12-NOV-13 17:16:39

Cartridges downloaded, but analysis NOT complete
SN0030 LC8061 2
SN4312 LC1020 5

Flat, damaged, or incorrectly connected bags that are NOT analyze
d

Locations downloaded but NOT listed as project locations

Project locations NOT downloaded

LC2004
LC2007
LC2010
LC2013
LC2016
LC2019
LC2022
LC2025
LC2028
LC2031
LC2034
LC2037
LC2040
LC2043
LC2046
LC2049
LC2052
LC2055
LC2058
LC2061
LC2064
LC2067
LC2070
LC2073
LC2076
LC2079
LC2082
LC2085
LC2116
LC2131
LC2155
LC2173

SN0030 10/2 Varsam
10/3 Check, Analyze (1) LLFSGGLGGGGG
10/10 Clean
10/18 Varsam
10/24 Check Analyze (3)

SN4312 10/2 Varsam
10/3 Check, Analyze (1) 5L, 11 I
10/8 Clean
10/11 Varsam
10/22 Check, Analyze (3)

clip was open
fig set
flat?

clip open
e purge
fig set
flat?

DF 11/14

Figure 41. Example of Analysis Summary sheet.

and the Analysis Summary report was re-run until all samples had been analyzed or a justifiable reason had been determined for a missing sample. Cartridges were not cleaned until all available samples had been analyzed.

19. Post-project determination of ILOD, ILOQ, MLOD, and MLOQ.

ILOD and ILOQ were previously defined in step 6 above of the quality control procedures. In that section a procedure was described for obtaining a preliminary pre-project estimate of the ILOD and ILOQ using a very low concentration calibration standard. These results were reported in Table 5. There are additional ways to estimate ILOD and ILOQ. These include the use of laboratory blanks and the low level laboratory control standards used for calibration and CCV. These alternative determinations together with a post-project repeat of the initial procedure are also shown in Table 5. With two exceptions, all of the various estimates for ILOD were consistently low and well below the stated MQO of 4 pptv. One exception was the ILOD for the lab blank result for GC3. As noted earlier, this is due to the sensitivity of GC3 to the effect of very small changes in baseline on the peak integration at very low level concentrations. The other exception was for the ILOD for the 3.11 pptv lab control for GC4. In this case, the exclusion of a single outlier decreased the ILOD from 6.12 to 1.26 pptv.

The method limit of detection (MLOD) and method limit of quantitation (MLOQ) are estimates of the lowest field concentration level that can be determined with some degree of certainty. Unlike ILOD and ILOQ, MLOD and MLOQ incorporate all the sources of variability and uncertainty introduced during each phase of the sampling, handling, and analysis. The MLOD is defined as the lowest field concentration measurement that can be determined to be statistically different from zero. It is based upon the method's ability to differentiate a low-level concentration standard from the combined effects of instrument and method noise. The MLOD and MLOQ are calculated exactly the same as ILOD and ILOQ except that method variability is factored into the determination by using results from samples that have been put through the rigors of field sampling. The MLOD is calculated as 3 times the standard deviation of a low level standard. The MLOQ is defined as the lowest concentration that can be determined within 30% of the actual concentration. The MLOQ is calculated as 10 times the standard deviation of the same low level standard.

There are several ways to attempt to estimate MLOD and MLOQ. These include field blanks, low concentration field controls, and field duplicates. Ambient background samples of all regular field samples can also be used to estimate MLOQ. However, these samples do not incorporate all sources of variability observed during experiments. Specifically, background samples, by definition, were not exposed to the higher level concentrations measured by many of the samplers that were strongly impacted by the tracer plume. Sampler cartridges located on parts of the grids that were heavily impacted by the tracer plume were seen to occasionally have their lower concentration bags affected. There is also the problem of setting a cutoff value separating truly background samples from those that were slightly influenced by the plume. For these reasons, the ambient background method was not calculated. Estimates of MLOQ were

made using each of the other methods. Table 13 summarizes the results of the analysis for the estimate of MLOQ.

Table 13. Estimates of MLOQ using field duplicates, field blanks, and field controls.

Field	IOP1		IOP2		IOP3		IOP4		IOP5		IOP Average	
Duplications												
	dup<10	dup<20	dup<10	dup<20								
count	87	113	36	50	91	106	46	61	65	75		
mean	-0.04	-0.19	-0.32	-0.54	-0.3	-0.09	-0.11	0.19	-0.42	-0.51		
s.d.	0.47	3.4	0.93	2.13	1.64	1.9	0.53	1.5	1.23	1.84		
mloq	4.73	33.98	9.32	21.34	16.37	19.01	5.27	15	12.32	18.37	9.6	21.54
Field Blanks											Combined	
count	36		35		36		36		36			
mean	0		-1.46		1.95		0.01		0		0.11	
s.d.	0		2.76		3.33		0.05		0		2.19	
mloq	0		27.61		33.3		0.5		0		21.93	
Field Controls (14.79 ppt)											Combined	
	14.8		14.8		14.5		15.5		15.1			
	14.8		15.5		14.4		15.6		15.7			
	14.9		14.9		14.2		16.1		15.2			
	14.7		14.7		17.7		15.7		15.4			
	14.8		14.8		16.9		15.9		15.4			
	15.2		14.9		16.2		15.5		15.2			
	15.7		14.4		14.2		16.1		15.2			
	15.2		14.2		15.2		16.2		15.4			
	15.8		14.2		17.3		15.7					
mean	15.1		14.71		15.62		15.81		15.33		15.31	
s.d.	0.41		0.41		1.42		0.27		0.19		0.78	
mloq	4.09		4.08		14.18		2.71		1.91		7.83	

Estimates of MLOQ using the field duplicates technique provided estimates ranging by IOP from 4.7 to 16.4 pptv for duplicate pairs less than 10 pptv with an overall IOP average of 9.6 pptv. For duplicate pairs less than 20 pptv estimates of MLOQ ranged from 15 to 34 pptv by IOP. Estimates of MLOQ using field blanks ranged from zero to 33 pptv. The higher estimates for IOPs 2 and 3 are due to the use of GC3 with its baseline sensitivity issues at low concentration (IOP2) and one cartridge that was clearly affected by high plume concentrations (IOP3). The highest concentrations measured during PSB1 were during IOP3. Estimates of MLOQ using the low concentration field control ranged from 1.9 to 14.2 pptv for all IOPs with only IOP3 having an MLOQ greater than 4.1 pptv. The MLOQ for the combined field control sample population was 7.8 pptv.

For reasons given earlier, it is preferable to use the lowest practicable concentrations for the calculation of MLOQ which would discount the estimates of MLOQ using duplicate pairs

<20 pptv and recommend the usage of duplicate pairs <10 pptv. While there is considerable disparity in the remaining estimates of MLOQ, a universal value of 9 pptv was adopted. The overall field duplicate estimate for pairs <10 pptv was 9.6 pptv. The combined estimate from the low concentration field control was 7.8 pptv. With the already noted exceptions of IOPs 2 and 3, the MLOQ given by the field blanks was zero. Even for the IOP3 case no affected field blank values were >10 pptv. While arguments could be made for a higher, somewhat more conservative value, the weight of evidence suggests that a reasonable universal value for PSB1 MLOQ is 9 pptv. For this reason, all values less than 9 pptv have been flagged as estimates in the final database.

20. Final data review.

All field data were verified to make sure there was a result for every location, cartridge, and sample bag and that all results were flagged appropriately. The following examples of verification plots and summaries were chosen to illustrate the diligence with which each data point is reviewed. Every quality control sheet (Figs. 35-37) for each data package was reviewed to ensure proper flagging of final data. Bubble/dot plots (Fig. 42) were created and reviewed to ensure all data were reasonable and consistent with respect to the overall concentration pattern

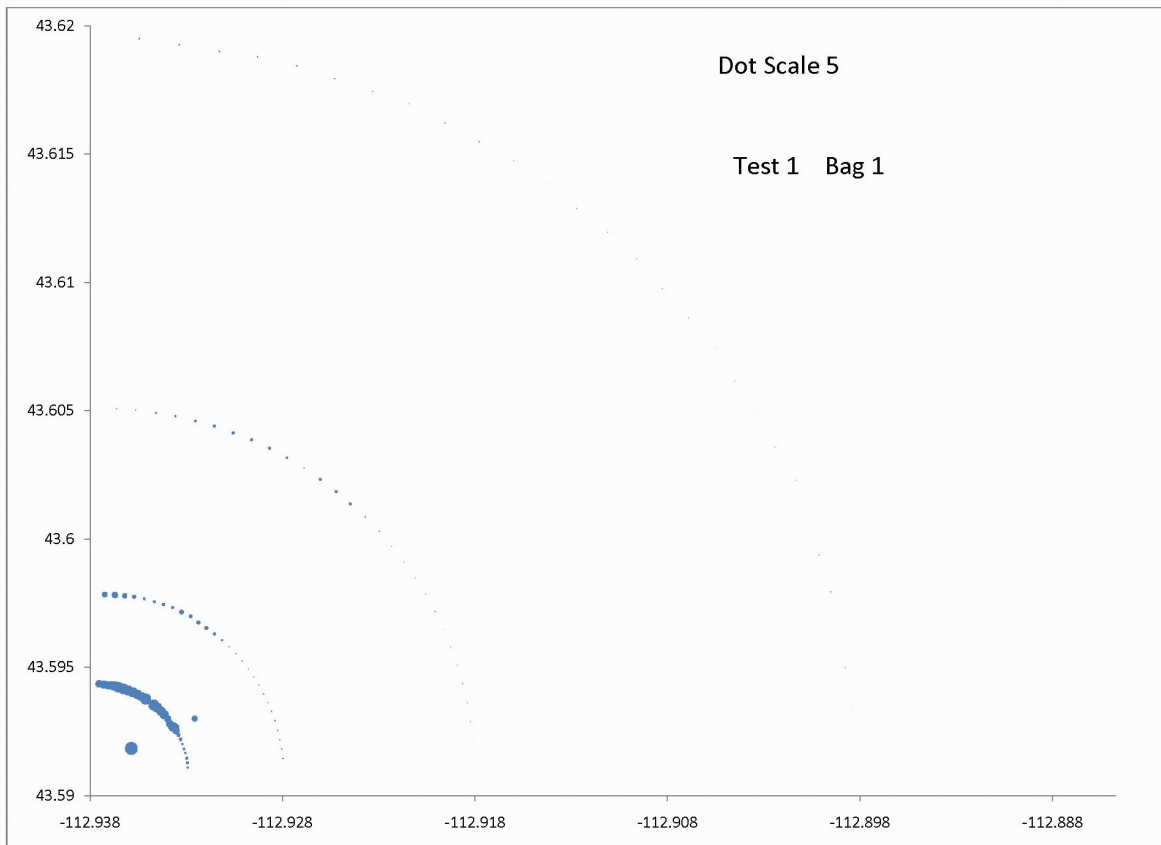


Figure 42. Example of bubble/dot plot for examining consistency of concentrations between neighboring locations and identifying suspicious values.

and the nearby neighbors of each bag sample. Any suspicious data point was traced back through the analysis and deployment records to determine if it was indeed a valid result. The sampler servicing records (Fig. 29), maintained by all field sampler deployment personnel for noting any problems, were used to check any outliers or anomalies in the data. Cartridge time

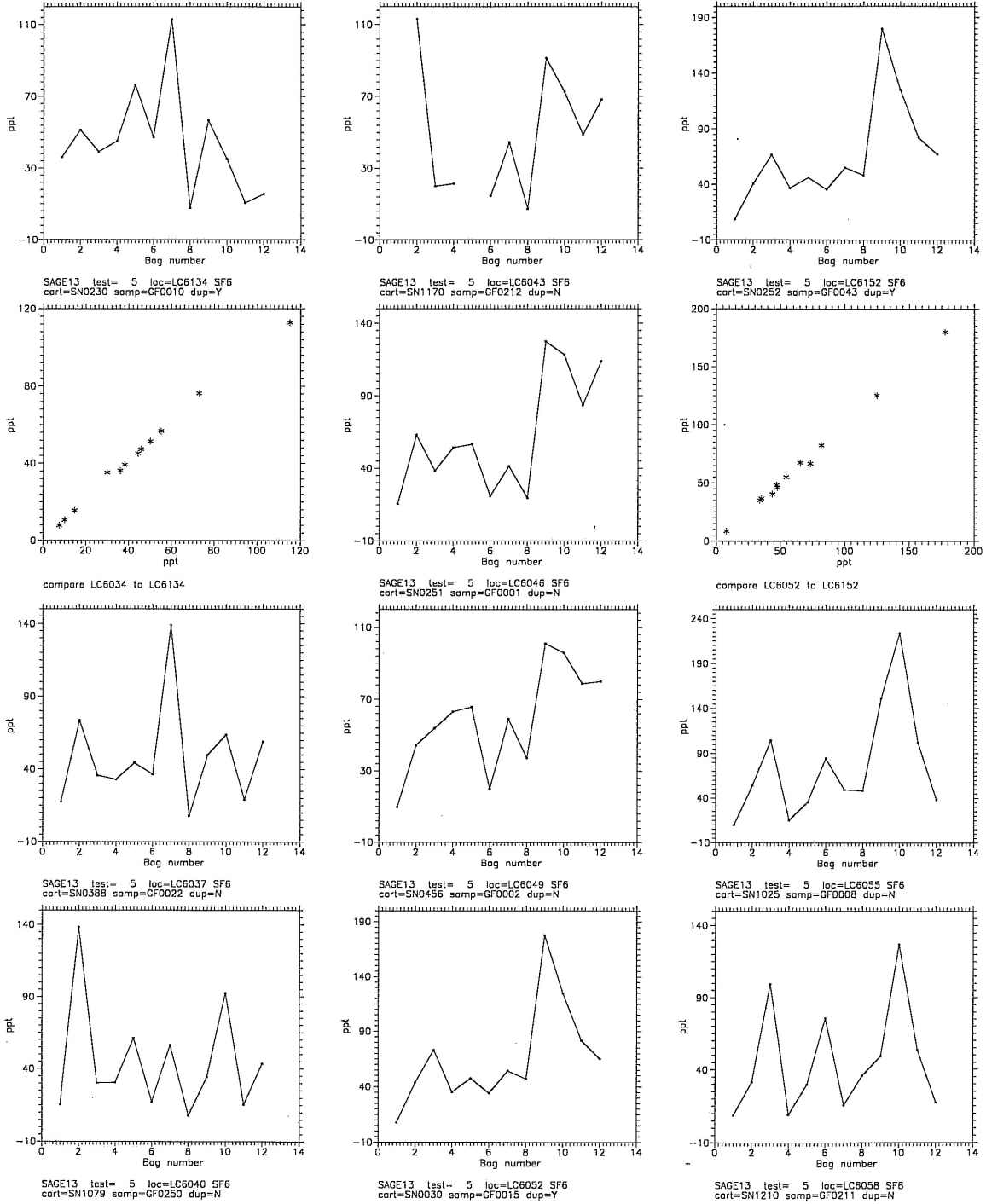


Figure 43. Example of cartridge time series plots used for identifying suspicious values.

history plots (Fig. 43) as well as individual chromatograms (Fig. 38) were also reviewed to determine any suspicious data points. Any suspicious data point was traced back through the analysis and deployment, sometimes with the aid of the master history file, to determine if it was indeed a valid result. All field QC was scrutinized. All suspicious data were appropriately flagged.

The finalized data set was then analyzed using a program used to determine if all flags were added correctly and if the sample results could possibly be QC results. Any results appearing on this sheet were verified and changes to the data base were made as necessary (Fig. 44).

```

Test3_1.Log
SBMAGIC version 1.5, 12-Dec-2013
Run on 13-Jan-2014 at 12:11
TEST = 3
Missing value on duplicate sampler 3 LC3055 2 - replace w. 3055 b2; reset flag
Missing value on duplicate sampler 3 LC3076 2 - replace w. 3176 b2; reset flag
Missing value on duplicate sampler 3 LC8025 1 - set as est. due to possibility clip not
closed during purge
NO CHECK IN FLAG. ASSUMED GOOD 3 LC8055 1
NO CHECK IN FLAG. ASSUMED GOOD 3 LC8055 2
NO CHECK IN FLAG. ASSUMED GOOD 3 LC8055 3
NO CHECK IN FLAG. ASSUMED GOOD 3 LC8055 4
NO CHECK IN FLAG. ASSUMED GOOD 3 LC8055 5
NO CHECK IN FLAG. ASSUMED GOOD 3 LC8055 6
NO CHECK IN FLAG. ASSUMED GOOD 3 LC8055 7
NO CHECK IN FLAG. ASSUMED GOOD 3 LC8055 8
NO CHECK IN FLAG. ASSUMED GOOD 3 LC8055 9
NO CHECK IN FLAG. ASSUMED GOOD 3 LC8055 10
NO CHECK IN FLAG. ASSUMED GOOD 3 LC8055 11
NO CHECK IN FLAG. ASSUMED GOOD 3 LC8055 12
Missing value on duplicate sampler 3 LC8085 7 - replace w. 8185 b7; reset flag
POSSIBLE CONTROL LC8046

----- SAMPLE COUNTS -----
Samples analyzed on GC1= 392
Samples analyzed on GC2= 297
Samples analyzed on GC3= 476
Samples analyzed on GC4= 371
Samples not analyzed = 0

Total samples= 1536
OK samples= 1486
Flag 3 samples= 23
Flag 4 samples= 24
Flag 5 samples= 3

```

Figure 44. Example of output from program used to assign flags to values in final data set and final check for possible errors.

21. Data handling.

All results were printed on hard copy as a backup in case of loss of the data files and to aid in the data verification process. The data packages were filed for future reference and to be readily available during the project for immediate review. Backup copies of the raw ATGAS data were made occasionally and at the end of the project to prevent total loss of data in the case of a computer failure. All final QC and sample results were printed on hard copy and placed in a binder to be stored with any reference materials in the project archive.

22. Summary of Data Completeness and Contribution by GC

Table 14 summarizes bag sampling data completeness for each test as well as for the entire project. The MQO of 90% (Table 4) was exceeded in every case. ‘Field Problems’ incorporates the complete range of possible field problems (e.g. clips found open, irregular random flat bags, entire cartridges with most or all bags flat, overfilled bags). In the worst case of cartridges with all bags flat, this represented a failure by the field operator to correctly download the sampling program into the sampler or a failure of the sampler itself. One of the more common ‘Lab Problem’ was clips being open during the GC purge cycle resulting in the bags being diluted with the nitrogen purge gas thus invalidating the sample. The 12 samples not analyzed for IOP4 was due to the fact that one cartridge was used for sampling in IOP3 and then redeployed again for IOP4 sampling without first being analyzed and cleaned in between. The results for this cartridge were flagged with having a field problem.

Table 14. Summary of data completeness by IOP with contribution to analyses by individual GC.

GC	IOP					Total
	1	2	3	4	5	
1	466	544	392	591	497	2490
2	347	263	297	298	415	1620
3	495	536	476	491	466	2464
4	228	193	371	144	157	1093
Total	1536	1536	1536	1536	1536	7680
Valid	1488	1495	1486	1467	1504	7440
Field Problems	39	19	23	65	19	165
Lab Problems	8	22	24	4	13	71
Estimate (lab prob.)	1	0	3	0	0	4
Not Analyzed	0	0	0	12	1	13
Completeness%	96.9	97.3	96.7	95.5	97.9	96.9

The numbers in Table 14 indicate that GCs 1 and 3 were the workhorses. GC1 provided the most consistently stable operation and required the fewest calibration checks and recalibrations. It did have a slight tendency for temperature drift that occasionally required

rerunning samples. GC3 had the widest analytical range available without resorting to sample loop changes, the shortest analytical cycle time, and usually provided consistently stable operation. The lower numbers for GC4 reflect a longer analytical cycle time, a strong tendency toward calibration drift, and a restricted analytical range as configured (Table 6). The lower numbers for GC2 mostly reflect the difficulties often experienced in achieving stable operation. Regardless of GC, however, data had to at a minimum satisfy the MQO to be acceptable.

Final Bag Sampler Data Files and Format

The final bag sample tracer data files provided with this report contain 12 columns:

1. test (IOP) number
2. bag number (1-12)
3. date (yyyymmdd)
4. start time (hhmmss)
5. sampling period (seconds)
6. dist (distance from release point in meters)
7. angle (angle in degrees along respective arc from north)
8. agl (meters, above ground level)
9. latitude (degrees, datum WGS-84)
10. longitude (degrees, datum WGS-84)
11. concentration (SF₆ pptv)
12. quality control flag

The files are in csv format with fixed width fields. The data files are named 'PSB1_IOP#_BagSampling_Final.csv' where '#' is the number of the Individual IOP test. The bag sampling Readme file accompanying this report summarizes the contents of this chapter on the bag sampling.

Final Data File Quality Control Flags

All of the data were flagged with one of six possible quality flags: These are:

- | | |
|---|--|
| 0 | > MLOQ; good data to be used without qualification. |
| 1 | < MLOD (4 pptv) |
| 2 | < MLOQ (9 pptv) and > MLOD (4 pptv). Treat as an estimate. |
| 3 | missing – field problem (check in was F, I, or B), also missing analyses are included here; data values set equal to -999. |
| 4 | missing – lab problem; data values set equal to -999. |
| 5 | estimate because of laboratory problem (don't use = 1 or 2) data values set equal to -999. |

Flag '1' applies primarily to anomalously low ambient samples. Ambient background samples were generally in the range from 6-8 pptv. Most values less than 5 pptv were

preemptively designated as estimates (Flag '2') since anything less than 5 pptv for an ambient sample is unlikely. However, a few samples were still flagged with '1'.

Flag '2' applies primarily to ambient background samples and those samples that were affected by the plume but still had concentrations below the MLOQ of 9 pptv. Flag '3' was applied to any data that was suspect due to field-related problems. This includes improperly connected bags, clips in the open position when they were checked in before laboratory analysis, flat bags, and overfilled bags. Flat bags were the most common problem in this category. The reasons for flat bags include the sampling program failed to download from the Timewand into the sampler or the sampler failed to function properly. In some cases it might be attributable to operator error. The bags remained flat because there was no program loaded to turn on the pumps to fill the bags. Flags '4' and '5' were applied to any data that was suspect due to problems with the laboratory analysis. An example of this was clips being open during the purge cycle of the analysis resulting in bag-filling and sample dilution.

This page is intentionally left blank

FAST RESPONSE TRACER ANALYZERS

Six fast response SF₆ analyzers were deployed for PSB1. Five were mounted in vehicles and were driven to points on the sampling grid where they remained stationary while measuring. One was mounted in an airplane during IOPs 1-3. The airplane flew a sampling pattern across the tracer plume and along the plume axis in the downwind direction at a number of altitudes. During IOPs 4 and 5, the airplane was not available so the sixth analyzer was deployed in an equipment shack located at 800 meters and 57 degrees on the sampling grid.

The analyzer output signal along with instrument temperatures and status were collected at the rate of 2 Hz and stored on a CompactFlash™ card. The airplane-mounted analyzer also recorded real-time GPS positions. The signal was simultaneously displayed on a hand held screen for operator interpretation and control. Using this display, operators performed real-time calculations of tracer concentrations and were able to communicate details of plume location, concentrations, and structure to the test director.

The data files provided with this report contain the 2 Hz analyzer signal converted to concentration, positions as latitude and longitude, and a quality flag. Specifically, each file contains six columns:

1. time (h Mountain Standard Time (MST))
2. latitude (degrees, datum WGS-84)
3. longitude (degrees, datum WGS-84)
4. altitude (m)
5. number of GPS satellites in use
6. HDOP (GPS quality indicator)
7. concentration (pptv)
8. quality flag

The files are named: FastR13_i_dist_an.csv where:

- i = IOP number
- dist = distance from release in meters
- an = angle east of north in degrees.

For example, FastR13_2_0800_31.csv contains measurements from an analyzer located 800 meters from the release and 31° from true north during IOP 2. The data files for the aircraft measurements have the same naming convention through FastR13_i_ but are followed by 'Plane'. Thus the aircraft measurements for IOP2 are in file FastR13_2_Plane.csv. More details about the files are in the README files included with the data files.

Quality Flags

The data quality flags included in the file were set as part of the quality control process which is discussed later. The flag values in the files are:

0. Good data.
1. Concentration less than MLOQ but greater than MLOD; treat as an estimate. (See note on dilution system below.)
2. Concentration less than MLOD; not statistically different than 0; treat as 0 or null value. (See note on dilution system below.)
3. Concentration is greater than 115% of the highest calibration; treat as an estimate.
4. Instrument over ranged its output; concentration is unusable.
5. Null values. Analyzer was in position and operating correctly and no SF₆ was found. Treating these concentrations as 0 is appropriate.
6. Analyzer was not in use. No measurements are available. Do NOT treat these as 0. Flag 6 indicates a human decision to not operate. For example: do calibrations, move to a new place, we don't need you this test, etc. This flag is used most frequently during calibrations and switching the dilution system on or off.
7. Analyzer was broken. No data available. Do NOT treat these as 0 values. Concentrations are unknown.
8. Analyzer was operating, but was experiencing problems. Treat all concentrations as estimates.
9. Concentrations are unusable because of instrument problems, but are included for qualitative indications only. In this case, the instrument was operating and collected data, but problems discovered later made it impossible to have any confidence in the concentrations. Since the concentrations were available they were included and may be useful for some purposes such as determining arrival times, etc. Calculations should not be done with these concentrations.
10. Concentrations unusable because of external problems. For example: fugitive sources, noise caused by trucks passing, etc.
11. Concentrations are estimates because of external problems. This flag indicates that something external to the analyzer had a small effect on the data, making it less certain but not totally unreliable. For example: a passing truck creating a small amount of noise during a high concentration peak.
12. Possible undershoot. These should be set to 0 when performing calculations.

Comments on QC flags

In most cases, concentrations flagged as unusable were set to -999 in the data files. In some cases, data were included with a flag that indicates missing or unusable data, the most common example being instrument over range (flag 4). In these cases, the data are provided for qualitative indications only and should not be used for calculations.

The undershoot flag (12) is required because of the analyzer's tendency to over respond to extremely rapid drops in concentration. The extremely high concentrations observed and the narrow plume widths resulting from the close proximity of the release resulted in extremely rapid concentration drops at times. In these cases, the instrument output would drop below the zero level and then recover. Flag 12 identifies the times when this was happening.

Note on dilution system use: When the dilution system was used, the incoming sample stream was mixed in equal parts with ultrapure air. This reduced the concentration to half the actual concentration in the sampled ambient air. The concentrations measured by the analyzer are doubled before reporting to reflect the actual air concentration. However, the MLOD and MLOQ levels reflect instrument operation and the flags must be set according to what the instrument was actually measuring, which was 50% of reported concentrations. While the dilution system was in use, the flag will be set to 1 as long as the instrument was seeing levels < MLOQ which means the reported concentrations will be < 2*MLOQ. Likewise, the flag will be set to 2 for reported concentrations < 2*MLOD.

Instrument Description

The FRD fast response SF₆ analyzers are based on a modified Precision Tracer Gas Analyzer (model TGA-4000) manufactured by Scientech Inc. of Pullman, Washington. Modifications include a modified plumbing system, a computer controlled calibration system, an integrated global positioning system (GPS), an automatic cleaning system, and a built in microcontroller with a CompactFlash™ card for data storage as shown in Fig. 45. The aircraft installation is shown in Fig. 46. The TGA-4000 measures atmospheric SF₆ concentrations with a response time of about 1-s (Benner and Lamb 1985). The rapid response time and mobile nature of the analyzers make them ideally suited for the determination of plume widths and structure. They have been utilized to determine both cross and along wind diffusion parameters commonly used in transport and dispersion models and Gaussian plume models (Clawson et al. 2004, Clawson et al. 2005).

The TGA-4000 uses a tritium based electron capture detector (ECD) to detect the SF₆. The ECD is very sensitive to halogenated compounds such as chloro-fluorocarbons and SF₆ as well as oxygen. Oxygen interferes with the ECD operation and is therefore removed from the sample prior to introducing it into the ECD. This is done by reacting the oxygen with hydrogen in a catalytic reactor and removing the resultant water through a semi-permeable membrane. The instrument limit of detection (ILOD) of the TGA-4000 is about 10 parts per trillion by volume (pptv) under optimal laboratory conditions. However, under field operations, the method limit of detection (MLOD) can be significantly higher. Calculations of MLODs and actual values for this experiment are discussed below.

The maximum concentration measurement capability is about 10,000 pptv, but can be doubled with the aid of a dilution system. The dilution system mixes the incoming sample air with an equal quantity of ultrapure air and reduces the concentration in the instrument to half



Figure 45. FRD mobile, fast response, tracer gas analyzer consisting of a data acquisition system, a TGA-4000 below the data acquisition system, and a calibration gas cartridge (foreground) installed in the passenger side seat.



Figure 46. Fast response tracer gas analyzer system installed in Piper Navajo aircraft.

what is in the sample air. However, using the dilution system also doubles the method limit of detection (MLOD) and method limit of quantitation (MLOQ) as was noted in the discussion of the data quality flags.

Calibration and Concentration Determination

Calibration of a fast response analyzer was accomplished by allowing it to sample calibration mixtures with known concentrations of SF_6 and recording the output corresponding to each concentration. SF_6 concentrations of sample air are then determined by linearly interpolating between the calibration concentrations whose output values bracket the sample

output. The calibration functions are all controlled by the built in microcontroller when initiated by the operator.

The SF₆ calibration standards were stored in Tedlar® bags identical to those used in the bag samplers which were described in a previous section of this report. The bags were connected to the analyzer sample stream by a series of electrically operated three-way valves. The computer switched the sample stream from outside air to a given calibration mixture by activating the corresponding valve. Eight calibration standards were used ranging in concentration from ultrapure air (0 pptv) to over 9,700 pptv SF₆. The calibration standards were manufactured by Scott-Marrin, Inc. of Riverside CA and had a manufacturer listed concentration uncertainty of ±5% and were NIST traceable. A full set of eight calibration standards were run on each analyzer both before the release began and after sampling was completed. Operators also ran calibration verification sets during the IOPs as needed.

All of the calibration standards were made by mixing small amounts of SF₆ with ultrapure air. Consequently, the analyzer response to any calibration concentration had to be calculated as a difference between the response to the calibration gas and the response to ultrapure air. This was done by running ultrapure air through the analyzer before and after the calibration gas. The automated calibration system ran the ultrapure air standard, then ran two or three calibration standards, then the ultrapure air standard, then two or three calibration standards, then the ultrapure air standard, etc. until all calibrations were completed. The ultrapure air signal corresponding to each calibration was then determined by linearly interpolating between the bracketing ultrapure air standards. This was subtracted from the response to the calibration standard to determine the analyzer response due to the SF₆ present in the standard.

Once the response to each calibration concentration was determined, the responses from multiple runs of the same calibration standard were averaged together. Sample concentrations were then determined by interpolating between these averages. In cases where sensitivity drift was a problem, concentrations were determined using only calibrations that were run close to the same time as the measurements.

MLOD/MLOQ

Two quantities that are useful for evaluating instrument performance are the method limit of detection (MLOD) and the method limit of quantitation (MLOQ). The MLOD is the lowest concentration level that can be determined to be statistically different from a blank or a 0 pptv SF₆ sample (Keith et. al. 1983). The MLOQ is typically defined to be the level at which the concentration may be determined with an accuracy of ±30%. The recommended values for these are 3σ for MLOD and 10σ for MLOQ, where σ is the standard deviation for measurements made on blanks or low concentration standards (Keith et. al. 1983). The MLOD differs from the instrument limit of detection (ILOD) in that it includes all variability introduced by the sampling method. MLOD/MLOQ are used in this report because they are calculated from the variability observed during actual sampling operations.

Since the analyzer was measuring continuously, every point may be viewed as a measurement of a blank so long as it was sampling clean air. The standard deviation of the baseline signal then defined σ . Ideally, this standard deviation should be calculated during actual sampling conditions; i.e. in the vehicle parked on the sampling grid or in the airplane as it is flying.

A second method of determining the MLOD and MLOQ is to calculate the standard deviation of the instrument's response to a calibration gas. This deviation may then be used as σ in the MLOD/MLOQ calculations.

Both methods were used for the real-time analyzers. After data collection for an IOP was completed, the data analyst followed a written procedure and calculated each instrument's MLOD and MLOQ from the baseline noise and from the variation of instrument response to each calibration gas used during the testing. The procedure called for comparing the MLOD from the lowest concentration calibration with a signal to noise ratio between 3 and 10 with the MLOD from the baseline calculation. The larger of these two values was generally selected as the instrument MLOD for that IOP. However, other factors such as the number of calibrations available for the calibration variation calculation, consistency of the calculated numbers from different calibration concentrations, and availability of good calibrations in the MLOD range were also considered. In some cases, adjustments were made or another value selected. Every effort was made to ensure that the selected MLOD accurately represented instrument performance or registered an error by being higher than necessary. Setting the MLOD too low allows some data to be flagged as valid when it should not be and is unacceptable by FRD quality standards. The MLOD/MLOQs for each instrument and each IOP are listed in Table 15.

Accuracy Verification Tests

In past years, a number of tests were conducted to determine the overall accuracy and precision of the fast response analyzer measurements. Calibrated analyzers were allowed to sample gas mixtures with known SF₆ concentrations. The percent recovery (i.e., 100% multiplied by the measured concentration divided by the actual concentration) for each test was recorded. The results are summarized in Table 16. The first 97 tests were made over a period of two months during the year 2000 on multiple analyzers. Most of these tests were made in the laboratory, but some were made with the analyzers mounted in minivans. The test conditions were designed to mimic the actual field operations as closely as possible. The calibration procedures were exactly the same as those used in the field and the times between calibration and test varied from a few minutes to several hours, just as they do in actual operations. Measurements were made both with and without the dilution system operating. The sampled mixtures were not the same as the calibration mixtures. A second set of 173 tests was conducted during the summer of 2004. The measurements were made the same way except all instruments were in the laboratory and no dilution system was used.

Table 15. Method Limit of Detection (MLOD) and Method Limit of Quantitation (MLOQ) for fast response analyzers during PSB1.

	IOP 1	IOP 2	IOP 3	IOP 4	IOP 5
analyzer 1, MLOD	7.8	11.1	9.5	5.5	9.9
analyzer 1, MLOQ	25.9	36.9	31.6	18.3	33.0
analyzer 4, MLOD	10.5	5.1	11.0	3.9	6.6
analyzer 4, MLOQ	35.0	17.1	37.3	13.1	22.2
analyzer 7, MLOD	10.4	14.4	17.3	16.1	10.3
analyzer 7, MLOQ	34.7	44.7	57.6	48.9	34.4
analyzer 9, MLOD	20.6	12.5	9.7	7.2	12.0
analyzer 9, MLOQ	55.0	41.3	32.3	23.9	39.0
analyzer 10, MLOD	10.8	5.4	13.7	10.2	10.8
analyzer 10, MLOQ	35.7	18.0	43.4	33.9	36.0
airplane, MLOD	36.5	45.4	23.4	13.3	5.4
airplane, MLOQ	121.7	151.2	178.0	47.5	18.0

Table 16. Percent recovery of SF₆ concentrations by real-time analyzers sampling known mixtures as unknowns.

SF ₆ Concentration (pptv)	Average Recovery (%)	Standard Deviation (%)	Number Of Trials
<u>year 2000</u>			
514	98	8.7	20
2065	110	4.1	17
2087	105	6.7	15
2065 and 2087 combined	107	5.9	32
4095	101	8.7	45
<u>year 2004</u>			
504	105	5.0	54
1593	105	7.3	46
8300	106	2.8	73

Since both the calibration mixtures and the sampled mixtures were listed by the manufacturer as $\pm 5\%$, it is reasonable to expect accuracy variations up to $\pm 10\%$. All of the

average recovery values are within this range. The standard deviations for all of the groups reported were less than 8.7%, which should be a reasonable estimate of instrument precision.

Quality Control (QC)

The quality control (QC) procedure for the real-time analyzers included 12 steps that ensure the real-time analyzer data was as reliable as possible. During field operations, operators were required to follow written checklists that included all QC steps. A written procedure was also followed during post-IOP processing. The QC steps were:

1. Pre-project preparation.
2. Monitoring of key operational parameters during the study.
3. Daily instrument calibrations.
4. Real-time monitoring of QC parameters during testing.
5. Operator logging of all measurements.
6. Post-IOP screening of calibrations.
7. Post-IOP determination of MLOD/MLOQ.
8. Post-IOP screening of data.
9. Verification of all calculations and data by a second analyst.
10. Identification of data problems and setting of QC flags.
11. Verification and conversion of position information.
12. Creation and review of final data files.

1. Pre-project preparation.

Before the experiment, each analyzer was thoroughly tested to be sure that all systems were in good working order. Any necessary repairs were made. The analyzers were then conditioned by running them for several weeks, which was required for optimum performance. During this period, each one was adjusted to provide the best response to the range of concentrations expected during the study.

Operator training occurred the week before field deployment. Dedicated binders were prepared for each analyzer that contained all procedures, phone numbers, safety and Nuclear Regulatory Commission (NRC) requirements. All operators had previous experience operating the analyzers and were trained on the operation of the analyzers, including troubleshooting and data handling. They were each required to complete hands-on training plus attend a training class at the FRD office in Idaho Falls, ID.

2. Monitoring of key operational parameters.

Analyzer operators were expected to follow a standard operating checklist (Fig. 47) which included operating and QC instructions. The checklist instructed them to fill out a

TGA-4000 Operating Checklist

Aug 27, 2013

- Initial Setup**
- Check gas and electrical connections
 - Remove caps from EX. 1 (Dryer-pump) & EX. 2 (Detector)
 - Remove cover from sample inlet AND make sure inlet is properly connected to the TGA.
 - Verify that the sample valve is in Nitrogen position
 - Turn on Nitrogen tank and record primary pressure on Settings Record
 - Turn Dryer Nitrogen on (yellow valve on back of TGA)
 - Use large flowmeter to verify that Nitrogen flows are within these ranges. If they are not, set Nitrogen flows by adjusting regulator pressure (**Do NOT exceed 40 psi!**)
 - EX. 1 (Dryer-Pump): >140 on large flowmeter (but NOT against the top stop)
 - EX. 2 (Detector): 15 to 60 on large flowmeter__ Record Nitrogen delivery pressure and flows on Settings Record
 - Disconnect flowmeter!
- Detector Cleaning** (If the detector was cleaned less than 18 hours ago AND it has been purged continuously with Nitrogen since the cleaning, skip cleaning)
- Verify that sample valve is in Nitrogen position and methanol bottle is not empty
 - Attach capture bottle to EX.2 (Detector) and note the level of methanol in the bottle
 - Turn black valve to METHANOL FLUSH (back of TGA)
 - Wait until 25 to 30cc of methanol flow into the capture bottle (about 2 minutes)
 - Turn black valve to NITROGEN SYSTEM
 - After 1 to 2 minutes, remove capture bottle and dispose of waste methanol
- Startup**
- Main power on
 - Dryer on
 - Pump on
 - Verify that the red Hydrogen valve is off
 - Turn on Hydrogen tank and record primary pressure on Settings Record
 - Wait for DTEMP to reach 80°C
 - Turn on the red Hydrogen valve and observe reactor temperature (RTEMP) increase
 - Record Hydrogen delivery pressure on Settings Record (**must be <40 psi**; usually 30-35 psi)
 - Insert Compact Flash card and power on data system
 - If GPS is not installed, check and set date and time.
 - Wait for RTEMP to reach operating levels (190-210°C) **DO NOT EXCEED 220°C!**
 - Wait for signal to stabilize
 - Switch sample valve to sample position
 - Wait for signal to stabilize
 - Determine O₂ break through by reducing H₂ controller SLOWLY. (instructions in binder)
 - Increase H₂ two units above break through; record sample and H₂ settings on Settings Record
 - Wait for signal to stabilize
 - Adjust signal to about 0 volts with the lower potentiometer and record zero, gain, period, and RTEMP on Settings Record
- Calibration (Dilution system must be OFF!)**
- Connect the cal module to a calibration box and verify that the bags are not empty
 - Check the connections on the cal module electrical cable
 - Wait for 2 minutes of stable base line
 - Use the Cal Bag switches to select desired bags (usually all), then press "Cal Start"
 - Verify that each bag runs properly - pressing "Cal Start" again will stop cals if there is a problem
 - Record calibration slope on Settings Record
 - Wait for baseline to stabilize, then press "Calculate LOD" on status screen and record LOD on the Settings Record
 - Record recoveries from status screen Cal List in notebook (skip for 1st cal set)
- Dilution Setup** (Skip this section if you do not have a dilution system)
- Turn on Ultrapur Air tank and record pressures on Settings Record (delivery should be <20psi; typically 10 psi)
 - Remove rain cup from the inlet and attach the small flowmeter
 - Carefully observe flow rate
 - Open dilution valve and adjust dilution controller until the flowmeter shows ½ of original flow rate. Be as accurate as possible!
 - Disconnect flowmeter and replace rain cup
 - Verify that the dilution light is on and the display indicates that dilution is on
 - Close dilution valve and record controller setting on Settings Record
- Operation Notes** During operation try to:
- Tape inlet on co-located sampler with rain cup near sampler inlets.
 - Keep vehicle temperature as constant as possible.
 - Do calibrations before and after each test and every few hours if test schedule permits.
 - Use the dilution system when needed. Check dilution flow rates every few hours if possible.
 - Switch to Nitrogen position while fueling vehicle, if you suspect outside air is heavily contaminated, or if there are any problems of any kind.
 - Turn Reactor on to stabilize RTEMP if it drifts out of allowable range.
 - Write everything in the notebook.
 - Mark all peaks on the display.
- Shutdown**
- Switch sample valve to Nitrogen position
 - Turn off the red Hydrogen valve and the Hydrogen tank
 - Reactor off
 - After about 1 minute, turn off data system. Compact Flash card may now be removed.
 - Record Nitrogen and Hydrogen pressures on Settings Record (Use a second line)
 - Turn off dilution valve and Ultrapur air tank
 - Wait until RTEMP is <100°C
 - Dryer off
 - Pump off
 - Main power off
 - Dryer Nitrogen off (yellow valve on back of TGA)
 - Cap EX. 1 (Dryer-Pump) and put inlet cover on sample inlet or plug TGA inlet
 - **Clean detector** (no exceptions!) (follow instructions for Detector Cleaning above)
 - If TGA will be used within 18 hours, leave Nitrogen flowing through the detector at a reduced rate of ¼ to ½ of normal to conserve Nitrogen.
 - If TGA will not be used within 18 hours, then turn off Nitrogen at tank and cap EX. 2
 - Give Compact Flash card and copies of notebook pages to data processor

Figure 47. Operating checklist for fast response analyzers.

Settings Record as they ran the real-time analyzers (Fig. 48). They recorded 17 instrument parameters at key times during the operation. These included gas pressures, flow rates, analyzer component temperatures, electrometer settings, etc. The Settings Record, constructed in table form, contained several days of entries. These sheets were reviewed for any large changes in the parameters that could indicate a problem with the analyzer. Any changes were investigated and the required maintenance was performed. Each analyzer operator also maintained a dedicated logbook during each IOP and recorded the location of the analyzer and any problems with the analyzer. Analyzers were run between IOPs to ensure optimum instrument performance.

TGA-4000 Settings Record

TGA number: 7 Cal Module: Sep. 2008

date	time	N ₂ primary	N ₂ delivery	EX.1 flow	EX.2 flow	H ₂ primary	H ₂ delivery	sample controller	H ₂ controller	zero	gain	period	RTEMP	cal slope	LOD	Air primary	Air delivery	dilution controller
9/27	9:25	1400	15	145	77	1590	38	142	67	173	8	0	195			1740	7	
		1210	15			1580												
9/30	10:50	1210	16			1570	36	144	66	172	8	0	199					
	12:50	1150				1510	21											
10/2	8:30	1100	16					145	75									
10/3	12:53	1100	15	145	73	1500	35	144	66	172	8	0	193	1422	11ppt	1600	12	49.5
10/3	18:00	900	14			1450	35											
10/4	11:00	800	14	143	66	1320	35	140	65.5	176	8	0	202					
	15:30	650	14			1300	37											
10/5	9:07	1800	16	145	75	1300	35	140	67	177	8	0	207	1288	8ppt	1740	14	51
10/5	16:27	1600	16			1100	35											
10/7/13	11:39	1490	14	145	75	1080	36	140	66	176	8	0	205	1397	11ppt	1600	10	48.5
10-5-12	10:23	1100	14	142	63	870	36	138	67	168	8	0	195					
	13:50	Adjusted Sample back to 1400. RTEMP had dropped to 190																
	14:43	920				870												

Figure 48. An example of a fast response analyzer Settings Record.

3. Daily instrument calibrations.

All analyzers were calibrated at the beginning and end of each IOP and periodically during IOPs. If time permitted, multiple calibrations were run before the IOP started. These helped identify response drift and were used in MLOD/MLOQ calculations.

4. Real-time monitoring of QC parameters during testing.

After the first set of calibrations was completed, the calibration curve was checked every time additional calibrations were performed. This was done by treating the new calibrations as unknowns and calculating their concentration based on the calibration curve generated from the

first set of calibrations. When the calculated concentrations were more than 20% different than the actual concentrations, the operator ensured that a complete set of calibrations was run and then immediately continued with sampling. Appropriate calibrations for each measurement period were selected later during the post-IOP screening of calibrations. The analyzer also calculated and displayed an MLOD from the baseline noise. Operators were required to display and record this value after every set of calibrations. If large variations were observed, the cause was investigated and corrected.

5. Operator logging of all measurements.

To help ensure that noise spikes, analyzer adjustments, and extraneous features were not reported as valid measurements, operators were required to mark all SF₆ peaks on the computer using the software marking function. They also recorded details of each peak, e.g., time, concentration, location, together with other pertinent observations in a notebook. Any signals that could be mistaken for SF₆ were also recorded in the notebooks.

6. Post-IOP screening of calibrations.

After an IOP was completed, the analyzer operators delivered their logbook and a CompactFlash™ card containing all data for the IOP to the data analyst. The entire data file including the calibrations was then carefully reviewed by the data analyst. To ensure that concentration calculations were as accurate as possible, any calibration points with problems such as significant baseline drift, contamination, accidental instrument adjustments, etc., were identified and eliminated. The recovery for each calibration was calculated and examined. This was done by treating the calibration as an unknown and calculating the concentration using the calibration curve. The recovery was defined as the calculated concentration divided by the actual concentration converted to a percent. The recoveries for all calibrations above the MLOQ were expected to be between 80% and 120%. If they were not, they were re-examined for problems and the logbook entries were reviewed. In cases where the calibrations showed evidence of significant sensitivity drift during the IOP, the calibrations could be divided into several groups, typically an “early” group and a “late” group. Each group was used to calculate concentrations for peaks within the time frame they encompassed. If the calibrations still failed to meet the recovery limits, all data in the concentration ranges that were out of limits were flagged as estimates.

7. Post-IOP determination of MLOD/MLOQ.

The MLOD and MLOQ were determined for each analyzer for each day’s operation. These values define the lower limit of valid measurements. Concentrations below these levels are flagged with appropriate QC flags so users of the data are aware of its limitations. The MLOD and MLOQ were calculated by two methods: calculations based on the baseline noise and calculations based on the variation in response to calibrations of the same concentration. The data analyst then compared these two calculations and selected the instrument MLOD/MLOQ following the guidelines in a written FRD procedure. Typically, the value calculated

from the lowest concentration calibration with a signal to noise ratio in the 3 to 10 range was compared to the value calculated from the baseline noise and the larger of the two selected. However, other factors such as number of calibrations available, instrument problems, behavior on other calibration levels, etc. were considered in the selection. A more complete discussion of this calculation was included in a previous section of this chapter.

8. Post-IOP screening of data.

After an IOP, the data analyst reviewed the peaks marked by the operators and compared them with the notebook log to ensure that marked peaks were above the MLOD and that they were not false peaks caused by extraneous factors such as altitude changes, bumps, interfering chemicals in the air, etc. The peaks were checked for correct identification of instrument baseline on leading and trailing sides of each peak. The entire data set was examined for possible peaks that may have been missed. Once necessary corrections were made, the peaks were converted to concentrations, plotted and reviewed.

9. Verification of all calculations and data by a second analyst.

During steps 5 through 8, the data analyst generated a QC sheet (Fig. 49), plots of the calibrations curves, results from the MLOD/MLOQ calculations, and plots of all peaks. The QC sheet was annotated with notes explaining problems that were identified, corrective actions taken, and justification for all data processing decisions that were made by the analyst. A second person familiar with the data processing procedures reviewed and verified this entire data package. If any errors were discovered or if the verifier did not agree with the decisions made, the problems were discussed with the data analyst and a resolution agreed on and implemented.

10. Identification of data problems and setting of QC flags.

The operator logbooks and concentration plots were carefully reviewed for any anomalies that required QC flags to be set. The review focused specifically on instrument over range, dilution system usage that was not detected, and starting or stopping of the dilution system during a peak. Any other problems were also noted. From this review, a list of flags that needed to be set was generated. These were combined with the data during the generation of final data files.

11. Verification and conversion of position information.

During testing, the analyzers were collocated with a bag sampler. The location numbers of this bag sampler was recorded by the operator and also in the operation center's notes. The known distance, angle, latitude, and longitude of the sampler location were used to generate the final file name and insert the latitude and longitude in the file. In the case of the airplane mounted analyzer, the GPS latitude and longitude recorded during the flight were used without modification.

Try 1, Final

NOAA ARLFRD TGA-4000 Quality Control Sheet

version: v07-2.1
file: .\T0091310.05A
TGA: 9
start time = 5-Oct-13 09:02:06

operator: S. Beard

data analyst: R. Carter

verified by: D. Finn

analysis date: 30 Oct 2013

verify date: 7 Mar 2014

	analyst	verifier
All calibration recoveries are within +/-20%	<input checked="" type="checkbox"/> yes <input type="checkbox"/> no	<input checked="" type="checkbox"/> yes <input type="checkbox"/> no
LOQ < 150 ppt	<input checked="" type="checkbox"/> yes <input type="checkbox"/> no	<input checked="" type="checkbox"/> yes <input type="checkbox"/> no
RMS error (as percent of range center) < 10%	<input checked="" type="checkbox"/> yes <input type="checkbox"/> no	<input checked="" type="checkbox"/> yes <input type="checkbox"/> no
Data is usable as is	<input checked="" type="checkbox"/> yes <input type="checkbox"/> no	<input checked="" type="checkbox"/> yes <input type="checkbox"/> no
IF data is not usable as is, it could be usable with corrective actions noted below	yes no	yes no

*All < 41.3 should be Flagged.
Center ocal should be Flagged.*

limit of detection (LOD) = 12.5 ppt
limit of quantitation (LOQ) = 41.3 ppt
(LOD/LOQ calculated from baseline variations.)

Calibrations recalculated as unknowns:

(UHP air (0.0) results are "change since previous 0.0")

cal #	true value	result using 1st cal set	%recovery using 1st cal set	result using all calcs ave.	%recovery using all calcs ave.
0	0.0	-0.0		-0.0	
1	35.1	35.1	100.0	34.7	98.9
2	504.0	504.0	100.0	515.2	102.2
3	0.0	-16.7		-16.5	
4	1550.0	1550.0	100.0	1594.7	102.9
5	3110.0	3110.0	100.0	3198.1	102.8
6	0.0	-81.1		-80.3	
7	5220.0	5220.0	100.0	5404.4	103.5
8	8300.0	8300.0	100.0	8293.0	99.9
9	9730.0	9730.0	100.0	9584.8	98.5
10	0.0	-276.3		-273.3	
11	0.0	-103.4		-102.2	
12	0.0	-9.8		-9.7	
13	35.1	35.8	102.0	35.5	101.0
14	504.0	482.9	95.8	493.2	97.9
15	0.0	5.7		5.7	
16	1550.0	1467.8	94.7	1507.7	97.3
17	3110.0	2899.7	93.2	3000.5	96.5
18	0.0	-55.9		-55.3	
19	5220.0	5001.1	95.8	5109.4	97.9
20	8300.0	8324.1	100.3	8310.9	100.1
21	9730.0	10050.4	103.3	9875.2	101.5
22	0.0	-192.7		-190.6	

Calibration curve errors (for all calibrations averaged):

	RMS error	percent of range center
all calcs	96.75 ppt	2.0%
< 2330	31.77 ppt	2.7%
> 2330	134.35 ppt	2.2%

comments/corrective actions:

Figure 49. Example of a fast response analyzer QC sheet.

12. Creation and review of final data files.

Final data files were generated in a three step process. First, the software used to review the data and generate the QC sheets was used to create a data file for each analyzer on each IOP. This software automatically adds most of the quality flags. Then, additional flags identified in step 10 were added to these files. Finally, a custom computer program was used to re-format the files into their final form.

After the final data files were created, they were carefully reviewed for any problems. Each of the data files were read into a spreadsheet and the concentration and flags plotted versus time. The concentrations were compared to the earlier peak plots to verify that all the peaks were included at the correct time. The QC flags were checked visually by plotting and by computer programs that listed start and stop times for each flag and the range of concentrations for each flag. These lists were then compared with the lists generated earlier in the QC process. Any problems were fixed and the files regenerated using the updated information. The process was repeated until no discrepancies were found.

This page is intentionally left blank

METEOROLOGICAL MEASUREMENTS

An extensive array of meteorological instrumentation was used to measure the boundary layer in the Project Sagebrush study area during PSB1. Most of it was provided by ARLFRD but the measurements on the Grid 3 tall tower (GRI) were made in collaboration with WSULAR. GRI is 62.3 m in height. Other site designations are:

- COC – 100 foot command center meteorological tower located within the tracer sampling array
- TOW – 10 m meteorological tower on 3200 m arc
- ASC – permanent Atmospheric Systems Corp. sodar on the 800 m arc
- ART – mobile Atmospheric Research & Technology sodar near TOW on 3200 m arc
- PRO – permanent radar wind profiler plus RASS on the 800 m arc
- G1 – NOAA sonic anemometer at 4 m on GRI
- G2 – NOAA sonic anemometer at 30 m on GRI
- R1 – NOAA sonic anemometer at 45 m on GRI
- R2 – NOAA sonic anemometer at 3.2 m near TOW on 3200 m arc
- R3 – NOAA sonic anemometer at 3.2 m near north end of 3200 m arc
- R4 – NOAA sonic anemometer at 3.2 m near south end of 3200 m arc
- FLX – NOAA flux station, within tracer sampling array about 900 m NE of release point

Table 17 provides a listing of the meteorological instruments used during PSB1. The locations of the instrumentation are shown on Figs. 2, 4, and 5. Data from the NOAA/INL Mesonet stations are included in the PSB1 database in addition to measurements from the instrumentation listed in Table 17. Quality control procedures are described for each instrument as well as the formats of their respective data files.

Table 17. Meteorological instrumentation used during PSB1.

Type	Instrument		Location		
	Make	Model	Arc Distance	Arc Angle	Height (m)
<u>Grid 3 Tower (GRI) [43.5897N, 112.939933W]</u>			200 m	235 deg	62.3 m
Wind Speed	Met One Inc.	010C			2, 9.96, 15.31, 45.1, 60.05 m
Wind Direction	Met One Inc.	020C			2, 9.96, 15.31, 45.1, 60.05 m
Air Temperature	Vaisala	HMP45C			1.5 m
Air Temperature Aspirated					10.7, 14.9, 45, 59.6 m
Solar Radiation	LI-COR	LI200X			60.35 m
Barometric Pressure	Setra Systems	270			1.75 m
Rain Gauge	Friez Engineering	7405H			1 m
Data Logger (x2)	Campbell Scientific	CR23X			
3d Sonic Anemometer (Acumen G1)	Gill	Solent 1210R3A			4 m
3d Sonic Anemometer (Acumen G2)	Gill	Windmaster Pro			30 m
3d Sonic Anemometer (Acumen R1)	R.M. Young	Ultrasonic 81000			45 m
3d Sonic Anemometer	Campbell Scientific	CSAT3			2, 8, 16, 60 m
IRGA (closed path)	LI-COR	LI7200			2 m
IRGA (open path)	LI-COR	LI7500A			8, 16, 60 m
Net Radiometer	Kipp & Zonen	CNR2			30, 60 m
Air Temperature/RH (x8)	Vaisala	HMP45C			2, 12, 20, 25, 30, 45, 52, 60 m
Air Temperature/RH (x5)	Rotronic	HC2S3			4, 8, 16, 35, 40 m
Barometric Pressure (x2)	Vaisala	CS106			2, 60 m
Soil Heat Flux Plates (x2)	Hukseflux	HFP01			6, 12 cm
Soil Heat Flux Plates, self-calibrating (x2)	Hukseflux	HFP01SC			6, 12 cm
Soil Moisture/ Temperature	Stevens	Hydra Probe II			5, 10, 20, 50, 100 cm
Infrared Radiometer	Apogee	SI-111			30 m
2d Sonic Anemometer (x6)	Campbell Scientific				12, 20, 25, 35, 40, 52 m
Data Logger (x4)	Campbell Scientific	CR5000			
Data Logger (x2)	Campbell Scientific	CR1000			
<u>100 Foot Tower (COC) [43.593N, 112.933W]</u>			499	60	
Wind Speed	Met One Inc.	010C			2, 10, 30 m
Wind Direction	Met One Inc.	020C			2, 10, 30 m
Data Logger	Campbell Scientific	CR23X			
<u>3200 m Arc (TOW)</u>					
3d Sonic Anemometer (Acumen R2)	R.M. Young	Ultrasonic 81000	3200	44.5	3.2 m
Wind Speed	Met One Inc.	010C	3200	44.5	2, 10 m
Wind Direction	Met One Inc.	020C	3200	44.5	2, 10 m
Data Logger	Campbell Scientific	CR23X			

Table 17 continued. Meteorological instrumentation used during PSB1.

Type	Instrument		Location		
	Make	Model	Arc Distance	Arc Angle	Height (m)
3200 m Arc (near TOW)					
SoDAR (ART)	ART	VT-1	3200	44.5	
Solar Panel Array			3200	44.5	
3200 m Arc (R3)					
3d Sonic Anemometer (Acumen R3)	R.M. Young	Ultrasonic 81000	3200	7	3.2 m
3200 m Arc (R4)					
3d Sonic Anemometer (Acumen R4)	R.M. Young	Ultrasonic 81000	3200	82	3.2 m
Permanent Remote Sensors					
Radar Wind Profiler (PRO) [43.59473N, 112.9293W]	Radian	LAP-3000	828	~56	
RASS [43.59473N, 112.9293W]	Radian	LAP-3000	828	~56	
SoDAR (ASC) [43.59443N, 112.9292W]	ASC	4000	816	~57	
Flux Station (FLX) [43.59586N, 112.9288W]			916	51	
Net Radiometer	Kipp & Zonen	NR-LITE-L			2.5 m
Air Temperature/RH	Visalia	HMP45C			1.5 m
Barometric Pressure	Visalia	PTB101B			1 m
Solar Radiation	LI-COR	LI200X-L			2.5 m
3d Sonic Anemometer	Gill	1210R3			3.2 m
IRGA (open path)	LI-COR	LI7500			2.54 m
Soil Temperature	Campbell Scientific	TCAV-L			2, 6 cm
Soil Moisture	Campbell Scientific	CS616			2.5 cm
Soil Heat Flux Plates (x4)	Hukseflux	HFP01SC			8 cm

Grid 3 Tower (GRI)

GRI was of particular significance due to its close proximity to the tracer dispersion grid and the extensive suite of meteorological measurements that were made there (Table 17). This tower is located approximately 200 m southwest of the test area release location (Figs. 2 and 5). Figure 50 is a schematic representation of the instrumentation on the Grid 3 tower. The GRI tower (Figs. 4, 50) has been collecting data since 1957. The tower provided important data about the overall meteorological conditions during the project. Of particular importance are the vertical profiles of wind, temperature, and turbulence it afforded. The permanent ARLFRD mesonet cup anemometer and wind vane measurements and the temperature measurements were mounted on booms extending at 155 degrees from GRI. The array of sonic anemometers deployed by WSULAR and ARLFRD during PSB1 were mounted on booms extending at 335 degrees from GRI.

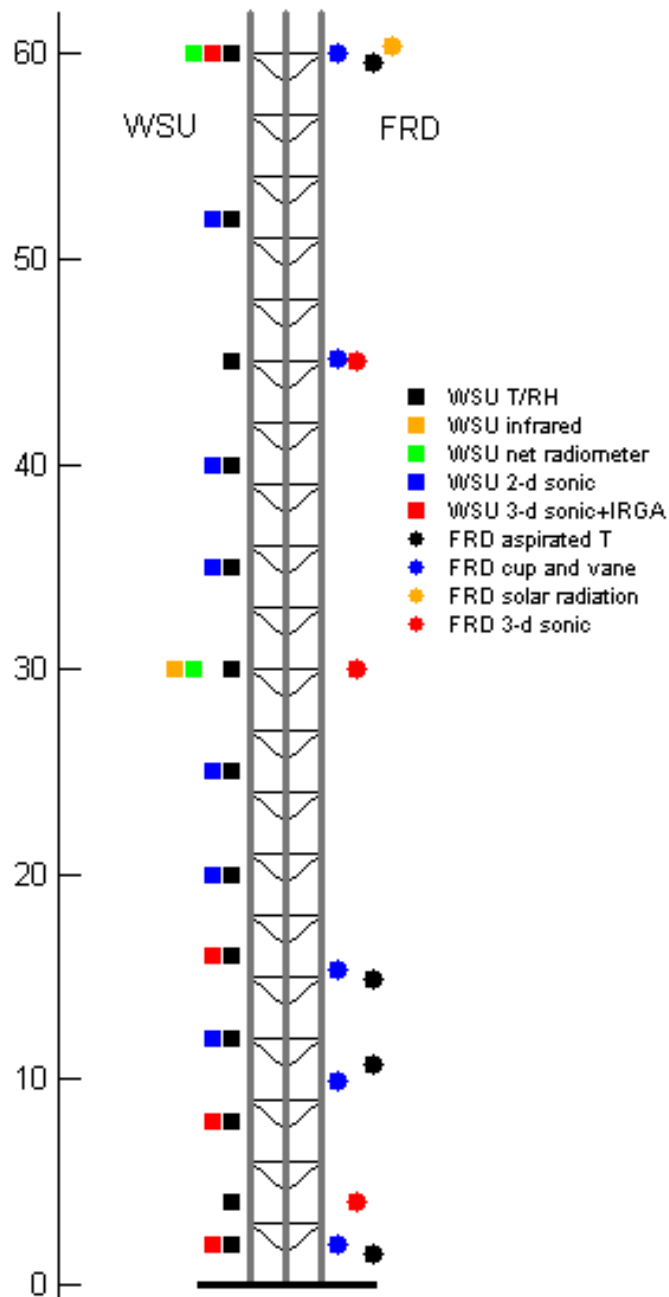


Figure 50. Schematic representation of the 62 m Grid 3 tower instrumentation. All anemometers mounted transverse to the prevailing wind direction on booms extending from the tower. Barometric pressure, rain gauge, and soil heat flux not shown.

NOAA ARLFRD

Sonic Anemometers

Experimental Setup

Sonic anemometers were deployed during the study to measure the turbulence field driving the tracer dispersion in the horizontal and vertical. The sonics measured the turbulence by taking high frequency (10 Hz) measurements of the 3-d wind field and temperature (u, v, w, t). A 3-d sonic anemometer “sample” consisted of transmitting sound back and forth across the measurement volume of the anemometer. The delay between transmission and receipt of a sound pulse in both directions along the 3 axes of the anemometer yields wind speed and direction in 3 dimensions. Virtual temperature was also derived from the speed of sound across the sonic sampling volume.

For measurements of the vertical turbulence profile on GRI, ARLFRD deployed three 3-d sonic anemometers during the study. One Gill Model Solent 1210R3A sonic anemometer (G1) was installed at 4 m height on a tripod adjacent to GRI. One Gill Windmaster Pro sonic anemometer (G2) was installed on the tower at 30 m height. One R. M. Young Model 81000 Ultrasonic Anemometer (R1) was installed on the tower at 45 m height. A close up picture of a Windmaster Pro and an 81000 sonic anemometer can be seen in Fig. 51. These were complemented by four 3-d Campbell Scientific CSAT3 sonic anemometers at 2, 8, 16, and 60 m heights installed by WSULAR. Power was supplied to the sonics and all other instrumentation on GRI by gel cell batteries. The batteries on GRI were continuously charged by AC line power.

The ARLFRD sonic data were continuously recorded for the duration of the experimental period at 10 Hz on a compact flash card inserted into an Acumen Serial Data Collection Bridge (Fig. 52). The data bridge was configured manually with a laptop computer with the sonic designation at the start of its filename (e.g., R1, G1). A GPS unit was also used to verify, and synchronize if needed, the correct time in the data bridge. The sonic



Figure 51. A closeup picture of an R. M. Young Ultrasonic 81000 (left) and a Gill Windmaster Pro (right) used during PSB1.

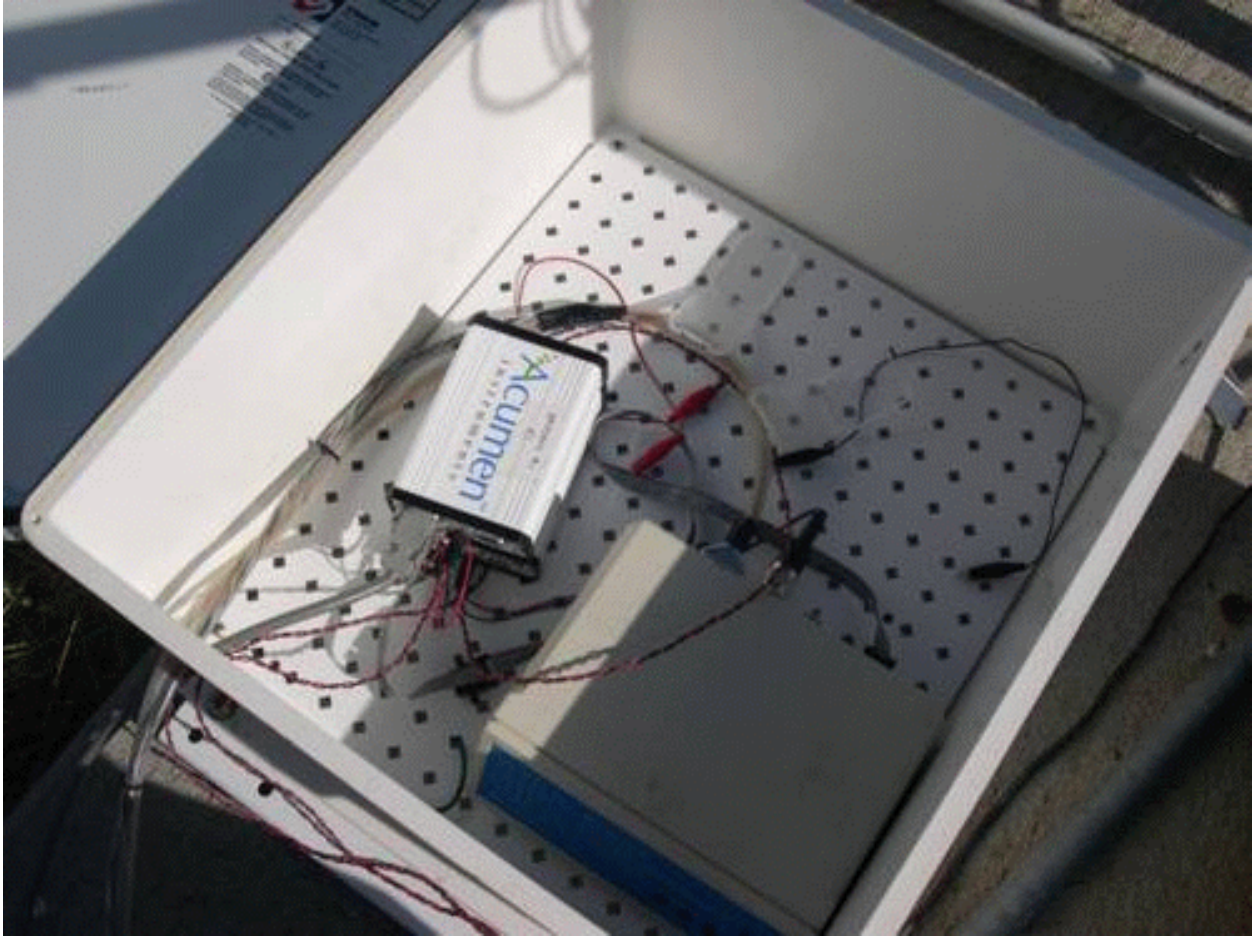


Figure 52. An Acumen data collection bridge (white device inside box) is used to collect data from the sonic anemometers.

data were recorded in an ASCII text file. The compact flash cards were gathered and returned to ARLFRD for processing and data archival at regular intervals during the testing period.

Quality Control

It is common practice to use the factory calibration of sonic anemometers without additional QC steps. However, ARLFRD considered it necessary to perform some tests of all of the sonics to verify that they were functioning properly before deployment. The ARLFRD R.M. Young sonic anemometers were tested at the time of purchase when they were new and factory calibrated with a set of collocated experiments between sonics. These tests and the results are described in Clawson et al. (2009). There was good agreement between all of the anemometers at that time and they had operated reliably in other deployments in the interim. An additional comparison test was made between a little used Gill Solent Model 1210R3A anemometer acquired by ARLFRD in the months prior to PSB1 with another R. M. Young 3-d sonic anemometer in ARLFRD's inventory. This test also found good agreement between sonics (see file G1R5TestFRD.xlsx in project database).

Once the flash cards were returned to ARLFRD, the data was uploaded onto the network for processing. The 10 Hz data was parsed into both 10-minute and 30-minute files containing roughly 6000 and 18,000 observations, respectively, for the entire PSB1 experimental period. Means, variances, covariances, and other calculations were made on these 10 and 30-minute data files. On average, one record was dropped every 26 seconds in R.M. Young data records. As a result, a normal 30-minute R.M. Young data file only had about 17930 records.

The 10-minute averaging time was selected to match with the 10-minute averaging period of the SF₆ tracer sampling period. The longer 30-minute averaging period better accounts for nonstationarity effects in the flow and provides a more robust statistical measurement of the turbulent fluxes. If necessary, the data was rotated into the correct meteorological coordinate system prior to processing (60 degrees, Gill sonic anemometers only).

Data collected from the three ARLFRD sonic anemometers were subjected to a comprehensive quality control and processing software package based upon the schemes detailed in Vickers and Mahrt (1997). That package included spike detection, coordinate rotations to zero out the mean vertical and crosswind wind speeds and calculate the streamwise mean wind, range checks, amplitude resolution tests, dropout tests, Haar transform stationarity (discontinuity) tests, checks for excessive skewness and kurtosis, tests for relative systematic flux sampling error (RSET), tests for random flux sampling error (RFET), tests for flux variations associated with mesoscale motions (RNT), and tests for alongwind relative nonstationarity (RNU), crosswind relative nonstationarity (RNV), and vector wind relative nonstationarity (RNS).

The most common problem with sonic anemometer measurements was spiking in which large, random, very brief, and infrequent electronic signal noise is recorded. Spikes were detected based upon the criteria of Vickers and Mahrt (1997), with slight modification. This entailed identifying 3 or less consecutive points exceeding the mean \pm a multiple of the standard deviation for a 5-minute (3000 point) moving average. The thresholds used were 4.0 standard deviations for u, v, w, and t. For w, the standard deviation threshold was adjusted to 4.5 if it was nighttime with temperatures below freezing. This was done to account for nocturnal periods often characterized by low and very intermittent turbulence. This did not affect any of the data for the IOPs since they were all conducted during the daytime but some nighttime results are included in the project database. Spikes were replaced recursively by the mean of the nearest non-spike values on either side of the spike. The spike replacement routine was repeated for up to 11 passes through the record or until no spikes were detected. The threshold increased by 0.1 with each pass. The quality control data files provide information on both the total number of passes through the record and the cumulative number of spikes detected in all passes. If the total number of spikes detected for any channel exceeded 0.5% of the total record on any pass, the record was flagged accordingly. Final calculations were done using the despiked output files. These calculations included both the uncorrected and corrected mean and flux quantities as well as a suite of quality control parameters.

The resulting despiked sonic anemometer data sets were plotted and reviewed by the data analyst for consistency and accuracy by comparing results with other measurements for the

duration of each IOP plus one hour before and after each IOP. This included the following comparisons:

- All wind speed and direction measurements in the study area, where available, at 2 m; at 10 m; at 30 m; at 45 m; and at 60 m. These comparisons included the sonic anemometers, cup anemometer and wind vanes at GRI and COC, the 10 m meteorological tower on the 3200 m arc (TOW), and the ASC and ART sodars. In some cases heights were compared if they were close. For example, 2 m cup and vane results at GRI and COC were compared with sonic results at 3 m (R2, R3, and R4) and 4 m (G1) and 40 m sonic results for ASC and ART were compared to 45 m anemometer results at GRI.
- Vertical comparisons of sonic anemometer at 4, 30, and 45 m with cup and vane anemometer results at 2, 10, 15, 45, and 60 m on GRI.

The cup anemometers and wind vanes on GRI were calibrated to rigorous standards. Like the other meteorological towers in the NOAA/INL Mesonet, a detailed and comprehensive data quality assurance program is performed on GRI on a routine basis. The instrumentation, quality control, calibration, and maintenance procedures at GRI meet the generally accepted requirements and guidelines set out in DOE (2004, 2005), ANSI/ANS-3.11 (2005), and ANSI/ANS-3.2 (2006). To help follow these guidelines, the quality assurance program uses an excellent set of software tools to display trended meteorological data. This enhances the data quality evaluations and makes them more efficient. The quality control program consisted of both manual and automated processes. Every 5-minute period for each parameter was plotted for missing or spiked data. Data were also screened for electronic noise, non-working aspirators that affect air temperature and relative humidity values, orientation errors in the wind direction, stalled wind sensors, rime icing that degrade wind speeds, and other erroneous values caused by maintenance, bird droppings, etc. Plotting the data allowed the meteorologist to identify and flag any of the problems in the database and, if needed, a technician is notified to quickly fix the problem. Calibrations of all instrumentation are completed on a semi-annual basis.

The results for these comparisons are included in sets of graphs in each IOP summary (see Summary of Individual IOPs section).

The plots of the new data sets were reviewed and verified by a second analyst. If any problems or errors were discovered, the two analysts had to agree upon and implement a resolution. The initial review process discovered a one-hour clock offset error in sonics G1 and G2. The data were adjusted accordingly and then there was good agreement with other anemometer data on GRI. Wind speeds at the 2, 10, and 30 m heights for COC were also found to be anomalously high in the initial review for IOP4. It was found that the maximum 5-minute gusts instead of the mean 5-minute wind speeds had been incorporated into the review plots for that IOP. This was corrected and then good agreement was found. Wind speeds for PRO were anomalously low at the 159 m height relative to the ASC and ART sodars at 160 m. No other problems or errors were discovered in the measurements of wind speed and direction in any of

the anemometer data sets. The processes in the data set below were derived from Vickers and Marht (1997).

Data File Formats

There are 12 ARLFRD files containing processed data for the G1, G2, and R1 sonic anemometers on GRI. This includes one data file and one quality control file for the 10-minute averaging period and one data and quality control file for the 30-minute averaging period for each sonic. Similarly, there are 12 ARLFRD data and quality control files containing the processed data for the R2, R3, and R4 sonic anemometers located on the 3200 m arc.

The data files for each period are summaries of the measurements and calculated quantities during the period. Each file is in CSV format. The files contain data for the month of October, when available. The data filenames are specified as 'XX_PSB1data_##min_October.csv' where 'XX' is the identity of the sonic anemometer specified in Table 17 (i.e., G1, G2, R1, R2, R3, R4) and '##' is the averaging period (10 or 30 minutes). The corresponding quality control filenames are specified as 'XX_PSB1qc_##min_October.csv'. The quality control files contain a listing of quality control parameter values and flags for each period. These files encompass the testing period of the IOPs with the exceptions already noted (R1).

Some data have been automatically flagged out with '-9999' due to flags set in the 'qc' files, columns 4-7 and 24-27. These are for excessive number of spikes or min/max values exceeding certain thresholds, respectively. Temporal gaps with missing data are also flagged '-9999'. The corresponding 'data' and 'qc' files contain matching records by row. The temperatures reported are virtual sonic temperatures.

The column header designations for the data summary files are:

1. XXMMDDYYHRMN, 'XX' is the identity of the sonic anemometer, 'MM' is the month, 'DD' is the day, 'YY' is the year, and 'HRMN' is the starting hour and minute of the 10 or 30 minute averaging period for that row
2. KNT, Data points in interval
3. VECWD, Vector Wind Direction (despiked), [degrees azimuth]
4. SCALWS, Mean Scalar Wind Speed (despiked), [m s^{-1}]
5. SCALWSr, Mean Scalar Wind Speed (raw), [m s^{-1}]
6. VECWS, Mean Vector Wind Speed (despiked), [m s^{-1}]
7. USPD_rot, Mean Vector Wind Speed (despiked, rotated/streamwise), [m s^{-1}]
8. VN, Mean north vector, [m s^{-1}]
9. VE, Mean east vector, [m s^{-1}]
10. UVAR, U Variance (despike,detrend,unrotated), [$\text{m}^2 \text{s}^{-2}$]
11. VVAR, V Variance (despike,detrend,unrotated), [$\text{m}^2 \text{s}^{-2}$]
12. WVAR, W Variance (despike,detrend,unrotated), [$\text{m}^2 \text{s}^{-2}$]
13. UVAR_rot, U Variance (despike,detrend,rotated), [$\text{m}^2 \text{s}^{-2}$]

14. VVAR_rot, V Variance (despike,detrend,rotated), [$\text{m}^2 \text{s}^{-2}$]
15. WVAR_rot, W Variance (despike,detrend,rotated), [$\text{m}^2 \text{s}^{-2}$]
16. SIGMAT, Sigma (theta), horizontal, [radians]
17. SIGMAP, Sigma (phi), vertical, [radians]
18. UV_rot, u'v' momentum flux (despike,detrend,rotated), [$\text{m}^2 \text{s}^{-2}$]
19. UW_rot, u'w' momentum flux (despike,detrend,rotated), [$\text{m}^2 \text{s}^{-2}$]
20. VW_rot, v'w' momentum flux (despike,detrend,rotated), [$\text{m}^2 \text{s}^{-2}$]
21. WTBAR_rot, w'T' sensible heat flux (despike,detrend,rotated), [m K s^{-1}]
22. USTR_rot, u* (despike,detrend,rotated), [m s^{-1}]
23. OLEN_rot, Obukhov Length (despike,detrend,rotated), [m^{-1}]
24. TAVG, Mean Virtual Sonic Temperature (despiked), [C]
25. TSDEV, Standard deviation temperature (despike,detrend), [C]
26. UAVGr, Mean U Component Wind Speed (raw), [m s^{-1}]
27. VAVGr, Mean V Component Wind Speed (raw), [m s^{-1}]
28. WAVGr, Mean W Component Wind Speed (raw), [m s^{-1}]
29. USDEVr, Standard Deviation U (raw), [m s^{-1}]
30. VSDEVr, Standard Deviation V (raw), [m s^{-1}]
31. WSDEVr, Standard Deviation W (raw), [m s^{-1}]
32. USTR, u* (despike,detrend,unrotated), [m s^{-1}]
33. UV, u'v' momentum flux (despike,detrend,unrotated), [$\text{m}^2 \text{s}^{-2}$]
34. UW, u'w' momentum flux (despike,detrend,unrotated), [$\text{m}^2 \text{s}^{-2}$]
35. VW, v'w' momentum flux (despike,detrend,unrotated), [$\text{m}^2 \text{s}^{-2}$]
36. WTBAR, w'T' sensible heat flux (despike,detrend), [m K s^{-1}]
37. UT, u'T' advective heat flux (despike,detrend), [m K s^{-1}]
38. OLEN, Obukhov Length (despike,detrend), [m^{-1}]
39. UAVG, Mean U Component Wind Speed (despiked), [m s^{-1}]
40. VAVG, Mean V Component Wind Speed (despiked), [m s^{-1}]
41. WAVG, Mean W Component Wind Speed (despiked), [m s^{-1}]
42. TAVGr, Mean Virtual Sonic Temperature (raw), [C]
43. TSDEVr, Standard deviation temperature (raw), [C]
44. skwU, Skewness U
45. skwV, Skewness V
46. skwW, Skewness W
47. skwT, Skewness T
48. kurU, Kurtosis U
49. kurV, Kurtosis V
50. kurW, Kurtosis W
51. kurT, Kurtosis T

In the description below, a cycle refers to a single pass through a single record for the specified variable during the despiking process. The column headers for the quality control parameter file are:

1. XXMMDDYYHRMN, 'XX' is the identity of the sonic anemometer, 'MM' is the month, 'DD' is the day, 'YY' is the year, and 'HRMN' is the starting hour and minute of the 10 or 30 minute averaging period for that row
2. Number of observations in the averaging period
3. Flag=1 if number of observations is more than 100 outside of nominal 10 Hz value for the averaging period (10-minutes, 5900-6100; 30-minutes, 17900-18100)
4. Flag=1 if number of spikes in u is greater than 0.5% of observations for any single cycle
5. Flag=1 if number of spikes in v is greater than 0.5% of observations for any single cycle
6. Flag=1 if number of spikes in w is greater than 0.5% of observations for any single cycle
7. Flag=1 if number of spikes in T is greater than 0.5% of observations for any single cycle
8. Total (cumulative) number of spikes detected in u after 'lpknt_U' cycles through record
9. Total (cumulative) number of spikes detected in v after 'lpknt_V' cycles through record
10. Total (cumulative) number of spikes detected in w after 'lpknt_W' cycles through record
11. Total (cumulative) number of spikes detected in T after 'lpknt_T' cycles through record
12. lpknt_U, number of cycles through u record to eliminate all spikes. The maximum number of cycles allowed is 11.
13. lpknt_V, number of cycles through v record to eliminate all spikes.
14. lpknt_W, number of cycles through w record to eliminate all spikes.
15. lpknt_T, number of cycles through T record to eliminate all spikes.
16. flgRES_U, number of times >70% of bins in 1000 point moving window amplitude resolution test are empty for u
17. flgRES_V, number of times >70% of bins in 1000 point moving window amplitude resolution test are empty for v
18. flgRES_W, number of times >70% of bins in 1000 point moving window amplitude resolution test are empty for w
19. flgRES_T, number of times >70% of bins in 1000 point moving window amplitude resolution test re empty for T
20. flgDRP_U, number of times >15% of points in u record fall in same bin for 1000 point moving window
21. flgDRP_V, number of times >15% of points in v record fall in same bin for 1000 point moving window
22. flgDRP_W, number of times >15% of points in w record fall in same bin for 1000 point moving window
23. flgDRP_T number of times >15% of points in T record fall in same bin for 1000 point moving \ window
24. flgABS_U, number of points in u record > 30 m s⁻¹ (check after despiking)

25. flgABS_V, the number of points in v record $> 30 \text{ m s}^{-1}$ (check after despiking)
26. flgABS_W, number of points in w record $> |5 \text{ m s}^{-1}|$ (check after despiking)
27. flgABS_T, number of points in T record, $T > 45\text{C}$ or $T < -30\text{C}$ (check after despiking)
28. flgHT1_U, number of “soft” Haar transform threshold exceedances for mean u (2x threshold)
29. flgHT1_V, number of “soft” Haar transform threshold exceedances for mean v (2x threshold)
30. flgHT1_W, number of “soft” Haar transform threshold exceedances for mean w (2x threshold)
31. flgHT1_T, number of “soft” Haar transform threshold exceedances for mean T (2x threshold)
32. flgHT2_U, number of “soft” Haar transform threshold exceedances for standard deviation u (2x threshold)
33. flgHT2_V, number of “soft” Haar transform threshold exceedances for standard deviation v (2x threshold)
34. flgHT2_W, number of “soft” Haar transform threshold exceedances for standard deviation w (2x threshold)
35. flgHT2_T, number of “soft” Haar transform threshold exceedances for standard deviation T (2x threshold)
36. flgHT3_U, number of “hard” Haar transform threshold exceedances for mean u (3x threshold)
37. flgHT3_V, number of “hard” Haar transform threshold exceedances for mean v (3x threshold)
38. flgHT3_W, number of “hard” Haar transform threshold exceedances for mean w (3x threshold)
39. flgHT3_T, number of “hard” Haar transform threshold exceedances for mean T (3x threshold)
40. flgHT4_U, number of “hard” Haar transform threshold exceedances for standard deviation u (3x threshold)
41. flgHT4_V, number of “hard” Haar transform threshold exceedances for standard deviation v (3x threshold)
42. flgHT4_W, number of “hard” Haar transform threshold exceedances for standard deviation w (3x threshold)
43. flgHT4_T, number of “hard” Haar transform threshold exceedances for standard deviation T (3x threshold)
44. flgSKW_U, flag=1 for $|u \text{ skewness}| > 1$; flag=2 for $|u \text{ skewness}| > 2$
45. flgSKW_V, flag=1 for $|v \text{ skewness}| > 1$; flag=2 for $|v \text{ skewness}| > 2$
46. flgSKW_W, flag=1 for $|w \text{ skewness}| > 1$; flag=2 for $|w \text{ skewness}| > 2$
47. flgSKW_T, flag=1 for $|T \text{ skewness}| > 1$; flag=2 for $|T \text{ skewness}| > 2$
48. flgKUR_U, flag=1 for u kurtosis < -1 or u kurtosis > 2 ; flag=2 for u kurtosis < -2 or u kurtosis > 5
49. flgKUR_V, flag=1 for v kurtosis < -1 or v kurtosis > 2 ; flag=2 for v kurtosis < -2 or v kurtosis > 5

50. flgKUR_W, flag=1 for w kurtosis < -1 or w kurtosis > 2; flag=2 for w kurtosis < -2 or w kurtosis > 5
51. flgKUR_T, flag=1 for T kurtosis < -1 or T kurtosis > 2; flag=2 for T kurtosis < -2 or T kurtosis > 5
52. flgRNU, RN alongwind relative nonstationarity test for u; flag=1 for RNU > 0.5
53. flgRNV, RN crosswind relative nonstationarity test for v; flag=1 for RNV > 0.5
54. flgRNS, RN vector wind relative nonstationarity test for wind speed; flag=1 for RNS > 0.5
55. flgRSET, flag=1 for relative systematic flux sampling error test (RSE) > 0.5
56. RSET, value for RSE
57. flgRFET, flag=1 for random flux sampling error (RFET) test value > 0.25
58. flgRNT, flag=1 for flux trends associated mesoscale motions (RNT) value > 0.25
59. RFET, value for RFET
60. RNT, value for RNT

Finally, there is a group of text files containing the despiked data for the sonic anemometer measurements. They are reported in a series of data records each 30 minutes in length. The 8 half-hour data records covering the two hours during each IOP plus one hour before and after are included in the final data set for the project. The filename convention for the flux station sonic tower files is XXMMDDYYHRMN.DSP where the 'XX' specifies the anemometer (e.g., G1, R1), 'MM' specifies the month, 'DD' specifies the day, 'YY' specifies the year, 'HRMN' specifies the hour and minute starting time of the half-hour period, and 'DSP' is the extension for the despiked files. These files contain 10 Hz data and have the following columns:

1. U, wind component, [m s⁻¹]
2. V, wind component, [m s⁻¹]
3. W, wind component, [m s⁻¹]
4. T, [deg C]

Other Measurements

Configuration

In addition to the three 3-d sonic anemometers listed above, ARLFRD also made measurements with the permanently installed instrumentation on GRI that relates to its function as a Mesonet station. These other measurements include wind speed and wind direction at 2, 10, 15.3, 45.1, and 60 m heights using Met One cup anemometers (Model 010C) and vanes (Model 020C); aspirated air temperature at heights of 1.5, 10.7, 14.9, 45, and 59.6 m; and measurements of solar radiation, relative humidity, precipitation, atmospheric pressure, and soil temperatures and moisture at five levels (5, 10, 20, 50, 100 cm depths) (Table 17).

In addition to the obvious importance of wind speed and direction, the wind speed, temperature gradient (ΔT), and net radiation measurements permitted the determination of the

Pasquill stability class using the Solar Radiation Delta-T (SRDT) method described in EPA (2000c).

Quality Control

As noted earlier, a detailed and comprehensive data quality assurance program is performed at GRI and the other meteorological towers in the NOAA/INL Mesonet on a routine basis (see above).

The GRI wind speed and direction data sets were plotted and reviewed by the data analyst for consistency and accuracy by comparing results with other measurements for the duration of each IOP plus one hour before and after each test. This includes the same comparisons described in detail above for the despiked sonic anemometer data. The results for these comparisons are included in sets of graphs for each IOP in the Summary of Individual IOPs chapter.

Data File Formats

There are five NOAA/INL Mesonet files for GRI in PSB1 that provide the non-sonic anemometer data. Each covers the 24-hour day encompassing the IOP test days (October 2, 5, 7, 11, and 18). The filenames are 'PSB1_GRI_IOP#.csv' where '#' specifies the number of the IOP. The time listed for each record is the end time for the 5-minute period. All times are MST. Missing values are indicated by '-999'. The column headers are:

- 1: year
- 2: month
- 3: day
- 4: hour, [MST, end time of the 5-minute interval]
- 5: minute, (end time of the 5-minute interval)
- 6: 2m, Wind Speed, [m s^{-1}]
- 7: 2m, Wind Direction, [deg]
- 8: 2SD, standard deviation wind direction at 2m, [deg]
- 9: 10m, Wind Speed, [m s^{-1}]
- 10: 10m, Wind Direction, [deg]
- 11: 10SD, standard deviation wind direction at 10m, [deg]
- 12: 15m, Wind Speed, [m s^{-1}]
- 13: 15m, Wind Direction, [deg]
- 14: 15SD, standard deviation wind direction at 15m, [deg]
- 15: 45m, Wind Speed, [m s^{-1}]
- 16: 45m, Wind Direction, [deg]

- 17: 45SD, standard deviation wind direction at 45m, [deg]
- 18: Top Wind Speed, wind speed at 60m, [m s⁻¹]
- 19: Top Wind Direction, wind direction at 60m, [deg]
- 20: TopSD, standard deviation wind direction at 60m, [deg]
- 21: 2m Temp, air temperature at 1.5 m, [deg C]
- 22: 10m Temp, air temperature at 10.7 m, [deg C]
- 23: 15m Temp, air temperature at 14.9 m, [deg C]
- 24: 45m Temp, air temperature at 45.0 m, [deg C]
- 25: TopT, air temperature at 59.6 m, [deg C]
- 26: 2m RH%, relative humidity at 2 m, [%]
- 27: Solar Rad, solar radiation, [W m⁻²]
- 28: BP, barometric pressure, [in. Hg]
- 29: Rain, [inches]
- 30. 5cm, Soil Moisture, [fractional]
- 31. 10cm Soil Moisture, [fractional]
- 32. 20cm Soil Moisture, [fractional]
- 33. 50cm Soil Moisture, [fractional]
- 34. 100cm Soil Moisture, [fractional]
- 35. 5cm Soil Temperature, [deg C]
- 36. 10cm Soil Temperature, [deg C]
- 37. 20cm Soil Temperature, [deg C]
- 38. 50cm Soil Temperature, [deg C]
- 39. 100cm Soil Temperature, [deg C]

WSULAR

Sonic Anemometers

Experimental Setup

WSULAR installed four 3-d Campbell Scientific CSAT3 sonic anemometers at 2, 8, 16, and 60 m heights on GRI for the measurement of fluxes and the vertical turbulence profile. These were complemented by NOAA ARLFRD 3-d sonic anemometers at 4, 30, and 45 m. The anemometer at 2 m height was installed on a tripod near GRI. The CSAT3 anemometers were collocated with IRGAs for the measurement of the fluxes of sensible heat, water vapor, and carbon dioxide. The IRGA at 2 m was a closed path LICOR Model LI7200. The other IRGAs were open path LICOR Model LI7500A. WSU deployed an additional six 2-d sonic anemometers on GRI at 12, 20, 25, 35, 40, and 52 m heights.

The WSULAR 3-d sonic data were continuously recorded for the duration of the experimental period at 10 Hz on a compact flash card installed in Campbell Scientific CR5000 data loggers, one for each 3-d sonic and IRGA pair. Data from the WSU 2-d sonic anemometers was archived on CR1000 data loggers. Some of the data from these anemometers was lost during the experimental period due to a wiring problem.

The wind directions and standard deviation in the crosswind direction (v) measured by the 3-d sonics at 2, 8, 16, and 60 m heights exhibited some differences relative to the ARLFRD sonic anemometers and wind vanes on GRI. These four sonics often had a wider range of wind directions and somewhat larger turbulence intensities (σ_v/U) relative to adjacent ARLFRD anemometers. It is conjectured that this might be due to the collocated IRGAs creating local flow distortions and increasing wind direction variability. However, the differences in make of sonic might also be a factor.

Quality Control

The WSULAR 3-d sonic data and LI-COR data were processed following two steps: 1) preprocessing with the algorithms described in Vickers and Mahrt (1997) including quality control tests (e.g. spike detection, amplitude resolution tests, dropout tests, Haar transform stationarity (discontinuity) tests, checks for excessive skewness and kurtosis, time lag tests and tests for alongwind relative nonstationarity (RNU), crosswind relative nonstationarity (RNV), and vector wind relative nonstationarity (RNS)), mean, standard deviation, and covariance calculations for both 10 minute and 30 minutes, and pre-flux computations; 2) flux computation, including flux corrections (SND-correction (Schotanus et al. 1983) and WPL-correction (Webb et al. 1980)), and quality control (steady state test and developed turbulence test, detailed in Foken et al., (2012), Chapter 4).

Data File Formats

There are 4 files containing processed data per pair of CSAT3 sonic anemometer and LI-COR's Infrared Gas Analyzer. This includes one preprocessed data file and one corrected and quality controlled flux data file for both the 10-minute and 30-minute averaging periods. The 2 data files for each period are summaries of the measurements and calculated quantities during the period. Each file is in CSV format. The preprocessed data filenames are specified as 'Preprocessing_INL_XXM_###min.csv' where 'XX' is the identity of the sonic anemometer specified at different heights (i.e., 2, 8, 16, 60) and '###' is the averaging period (10 or 30 minutes). The quality controlled flux data filenames are specified as

‘EC_Flux_CR_QC_INL_XXM_###min.csv’. Missing values are indicated by ‘-9999’. The column header designations for the preprocessed data summary files are:

- 1: date, yyyy is the year, mm is the month, dd is the day, [yyyymmdd]
- 2: time, hh:mm is the middle of the 10 or 30 minute averaging period, e.g. 00:00-00:30
-> 00:15, [hh:mm]
- 3: decimal_day, decimal day of year, [#]
- 4: u_unrot, Mean unrotated u, [m s⁻¹]
- 5: v_unrot, Mean unrotated v, [m s⁻¹]
- 6: w_unrot, Mean unrotated w, [m s⁻¹]
- 7: u_rot, Mean rotated u, [m s⁻¹]
- 8: v_rot, Mean rotated v, [m s⁻¹]
- 9: w_rot, Mean rotated w, [m s⁻¹]
- 10: Ts_avg, Mean sonic temperature, [K]
- 11: c_avg, Mean CO₂ concentration, [mg m⁻³]
- 12: q_avg, Mean H₂O concentration, [g m⁻³]
- 13: p_avg, Mean pressure from LiCor, [kPa]
- 14: Pre_Hs, Pre-calculated Sensible heat flux, [W m⁻²]
- 15: Pre_LE, Pre-calculated Latent heat flux, [W m⁻²]
- 16: Pre_Fq, Pre-calculated water vapor flux, [mmol s⁻¹ m⁻²]
- 17: Pre_Fc, Pre-calculated CO₂ flux, [umol s⁻¹ m⁻²]
- 18: Pre_tau, Pre-calculated momentum flux, [kg s⁻¹ m⁻²]
- 19: Pre_ustar, Pre-calculated friction velocity, [m s⁻¹]
- 20: Pre_zL, Pre-calculated stability parameter, [#]
- 21: rho_a, Wet air density, [kg m⁻³]
- 22: rho_d, Dry air density, [kg m⁻³]
- 23: e, Water vapor partial pressure, [hPa]
- 24: es, Saturated water vapor pressure, [hPa]
- 25: RH, Relative humidity, [%]
- 26: VPD, Vapor pressure deficit, [hPa]
- 27: Td, Dew-point temperature, [C]
- 28: dir_cp, Compass wind direction, [deg]
- 29: sonic_wd, Sonic wind direction, [deg]
- 30: u_unrot_SD, Standard deviation of unrotated u, [m s⁻¹]
- 31: v_unrot_SD, Standard deviation of unrotated v, [m s⁻¹]
- 32: w_unrot_SD, Standard deviation of unrotated w, [m s⁻¹]
- 33: u_SD, Standard deviation of rotated u, [m s⁻¹]
- 34: v_SD, Standard deviation of rotated v, [m s⁻¹]

- 35: w_SD , Standard deviation of rotated w , [$m\ s^{-1}$]
- 36: Ts_SD , Standard deviation of sonic temperature, [K]
- 37: c_SD , Standard deviation of Co_2 concentration, [$mg\ m^{-3}$]
- 38: q_SD , Standard deviation of H_2O concentration, [$g\ m^{-3}$]
- 39: P_SD , Standard deviation of air pressure, [kPa]
- 40: uv_unrot , Covariance of unrotated u and v , [$m^2\ s^{-2}$]
- 41: uw_unrot , Covariance of unrotated u and w , [$m^2\ s^{-2}$]
- 42: uTs_unrot , Covariance of unrotated u and sonic temperature, [$K\ m\ s^{-1}$]
- 43: uc_unrot , Covariance of unrotated u and Co_2 concentration, [$mg\ m^{-2}\ s^{-1}$]
- 44: uq_unrot , Covariance of unrotated u and H_2O concentration, [$g\ m^{-2}\ s^{-1}$]
- 45: uP_unrot , Covariance of unrotated u and air pressure, [$kPa\ m\ s^{-1}$]
- 46: vw_unrot , Covariance of unrotated v and w , [$m^2\ s^{-2}$]
- 47: vTs_unrot , Covariance of unrotated v and sonic temperature, [$K\ m\ s^{-1}$]
- 48: vc_unrot , Covariance of unrotated v and Co_2 concentration, [$mg\ m^{-2}\ s^{-1}$]
- 49: vq_unrot , Covariance of unrotated v and H_2O concentration, [$g\ m^{-2}\ s^{-1}$]
- 50: vP_unrot , Covariance of unrotated v and air pressure, [$kPa\ m\ s^{-1}$]
- 51: wTs_unrot , Covariance of unrotated w and sonic temperature, [$K\ m\ s^{-1}$]
- 52: wc_unrot , Covariance of unrotated w and Co_2 concentration, [$mg\ m^{-2}\ s^{-1}$]
- 53: wq_unrot , Covariance of unrotated w and H_2O concentration, [$g\ m^{-2}\ s^{-1}$]
- 54: wP_unrot , Covariance of unrotated w and air pressure, [$kPa\ m\ s^{-1}$]
- 55: uv , Covariance of rotated u and v , [$m^2\ s^{-2}$]
- 56: uw , Covariance of rotated u and w , [$m^2\ s^{-2}$]
- 57: uTs , Covariance of rotated u and sonic temperature, [$K\ m\ s^{-1}$]
- 58: uc , Covariance of rotated u and Co_2 concentration, [$mg\ m^{-2}\ s^{-1}$]
- 59: uq , Covariance of rotated u and H_2O concentration, [$g\ m^{-2}\ s^{-1}$]
- 60: uP , Covariance of rotated u and air pressure, [$kPa\ m\ s^{-1}$]
- 61: vw , Covariance of rotated v and w , [$m^2\ s^{-2}$]
- 62: vTs , Covariance of rotated v and sonic temperature, [$K\ m\ s^{-1}$]
- 63: vc , Covariance of rotated v and Co_2 concentration, [$mg\ m^{-2}\ s^{-1}$]
- 64: vq , Covariance of rotated v and H_2O concentration, [$g\ m^{-2}\ s^{-1}$]
- 65: vP , Covariance of rotated v and air pressure, [$kPa\ m\ s^{-1}$]
- 66: wTs , Covariance of rotated w and sonic temperature, [$K\ m\ s^{-1}$]
- 67: wc , Covariance of rotated w and Co_2 concentration, [$mg\ m^{-2}\ s^{-1}$]
- 68: wq , Covariance of rotated w and H_2O concentration, [$g\ m^{-2}\ s^{-1}$]
- 69: wP , Covariance of rotated w and air pressure, [$kPa\ m\ s^{-1}$]
- 70: cTs , Covariance of Co_2 concentration and sonic temperature, [$K\ m\ s^{-3}$]
- 71: qTs , Covariance of H_2O concentration and sonic temperature, [$K\ m\ s^{-3}$]
- 72: Pts , Covariance of air pressure and sonic temperature, [$kPa\ m\ s^{-1}$]

- 73: cq, Covariance of Co₂ concentration and HO₂ concentration, [g m⁻³ mg m⁻³]
- 74: Pc, Covariance of Co₂ concentration and air pressure, [kPa m s⁻³]
- 75: Pq, Covariance of H₂O concentration and air pressure, [kPa m s⁻³]
- 76: Ruv, Correlation coefficient of rotated u and v, [#]
- 77: Ruw, Correlation coefficient of rotated u and w, [#]
- 78: RuTs, Correlation coefficient of rotated u and sonic temperature, [#]
- 79: Ruc, Correlation coefficient of rotated u and Co₂ concentration, [#]
- 80: Ruq, Correlation coefficient of rotated u and H₂O concentration, [#]
- 81: RuP, Correlation coefficient of rotated u and air pressure, [#]
- 82: Rvw, Correlation coefficient of rotated v and w, [#]
- 83: RvTs, Correlation coefficient of rotated v and sonic temperature, [#]
- 84: Rvc, Correlation coefficient of rotated v and Co₂ concentration, [#]
- 85: Rvq, Correlation coefficient of rotated v and H₂O concentration, [#]
- 86: RvP, Correlation coefficient of rotated v and air pressure, [#]
- 87: RwTs, Correlation coefficient of rotated w and sonic temperature, [#]
- 88: Rwc, Correlation coefficient of rotated w and Co₂ concentration, [#]
- 89: Rwq, Correlation coefficient of rotated w and H₂O concentration, [#]
- 90: RwP, Correlation coefficient of rotated w and air pressure, [#]
- 91: RcTs, Correlation coefficient of Co₂ concentration and sonic temperature, [#]
- 92: RqTs, Correlation coefficient of H₂O concentration and sonic temperature, [#]
- 93: RPTs, Correlation coefficient of air pressure and sonic temperature, [#]
- 94: Rcq, Correlation coefficient of Co₂ concentration and HO₂ concentration, [#]
- 95: Rpc, Correlation coefficient of Co₂ concentration and air pressure, [#]
- 96: Rpq, Correlation coefficient of H₂O concentration and air pressure, [#]
- 97: spike_u, Number of spikes detected and points exceeding absolute limits in u (± 50 m/s), [#]
- 98: spike_v, Number of spikes detected and points exceeding absolute limits in v (± 50 m/s), [#]
- 99: spike_w, Number of spikes detected and points exceeding absolute limits in w (± 10 m/s), [#]
- 100: spike_Ts, Number of spikes detected and points exceeding absolute limits in sonic temperature (-20 ~ 50 C), [#]
- 101: spike_c, Number of spikes detected and points exceeding absolute limits in Co₂ concentration (200 ~ 1000 mg / m³), [s]
- 102: spike_q, Number of spikes detected and points exceeding absolute limits in H₂O concentration (0 ~ 30 g / m³), [s]
- 103: spike_P, Number of spikes detected and points exceeding absolute limits in air pressure (80 ~ 110 kPa), [#]

- 104: n_missing, Number of missing values for sonic anemometer (CSAT diagnostic code > 63), [#]
- 105: Skw_u_unrot, Skewness of unrotated u, [#]
- 106: Skw_v_unrot, Skewness of unrotated v, [#]
- 107: Skw_w_unrot, Skewness of unrotated w, [#]
- 108: Skw_u, Skewness of rotated u, [#]
- 109: Skw_v, Skewness of rotated v, [#]
- 110: Skw_w, Skewness of rotated w, [#]
- 111: Skw_Ts, Skewness of sonic temperature, [#]
- 112: Skw_c, Skewness of CO₂ concentration, [#]
- 113: Skw_q, Skewness of H₂O concentration, [#]
- 114: Skw_P, Skewness of air pressure from LiCor, [#]
- 115: Kur_u_unrot, Kurtosis of unrotated u, [#]
- 116: Kur_v_unrot, Kurtosis of unrotated v, [#]
- 117: Kur_w_unrot, Kurtosis of unrotated w, [#]
- 118: Kur_u, Kurtosis of rotated u, [#]
- 119: Kur_v, Kurtosis of rotated v, [#]
- 120: Kur_w, Kurtosis of rotated w, [#]
- 121: Kur_Ts, Kurtosis of sonic temperature, [#]
- 122: Kur_c, Kurtosis of CO₂ concentration, [#]
- 123: Kur_q, Kurtosis of H₂O concentration, [#]
- 124: Kur_P, Kurtosis of air pressure from LiCor, [#]
- 125: HF_sr, Hard Flag for spike detection: Flag = 91111111 if number of total spikes in all variables (u, v, w, Ts, CO₂, H₂O, and P) is greater than 1% of observations (4.5x threshold, increasing 0.1 each time up to 10 passes, [#]
- 126: HF_ar, Hard Flag for amplitude resolution: Flag = 91111111 if number of times >70% f bins in 1000 point moving window amplitude resolution test are empty for all variables, [#]
- 127: HF_dt, Hard Flag for dropouts: Flag = 91111111 if number of times >10% of points in all variables fall in same bin for 1000 point moving window, [#]
- 128: HF_al, Hard Flag for absolute limits: Flag = 91111111 if number of points exceeding absolute limits is greater than 1 for all variables, [#]
- 129: HF_sk, Hard Flag for skewness and kurtosis: Flag=91111111 for |skewness in all variables| > 2, or kurtosis in all variables < 1.0 or > 8.0, [#]
- 130: SF_sk, Soft Flag for skewness and kurtosis: Flag=91111111 for |skewness in all variables| > 1, or kurtosis in all variables < 2.0 or > 5.0, [#]

- 131: HF_ds, Hard Flag for discontinuities: Flag=91111111 if Haar transform threshold exceedances for mean u, v (4x threshold), w (2x threshold), Ts, Co₂, H₂O and P (4x threshold), or for standard deviation (3x threshold), [#]
- 132: SF_ds, Soft Flag for discontinuities: Flag=91111111 if Haar transform threshold exceedances for mean u, v (2x threshold), w (1x threshold), Ts, Co₂, H₂O and P (4x threshold), or for standard deviation (2x threshold), [#]
- 133: HF_tl, Hard Flag for time lag: Flag = 911 if the ratio (Rmax-R0)/R0 exceeds 20% for Co₂ and H₂O, where Rmax is the absolute value maximum correlation coefficient at any lag up to plus or minus 2s, and R0 is the absolute correlation at zero lag, [#]
- 134: SF_tl, Sort Flag for time lag: Flag = 911 if the ratio (Rmax-R0)/R0 exceeds 10% for Co₂ and H₂O, where Rmax is the absolute value maximum correlation coefficient at any lag up to plus or minus 2s, and R0 is the absolute correlation at zero lag, [#]
- 135: HF_ns, Hard Flag for nonstationarity test; Flag = 1 when RNS > 0.5, RNU > 0.5, or RNV > 0.5, [#]

The column header designations for the corrected and quality controlled data summary files are:

- 1: date, 'yyyy' is the year, mm is the month, dd is the day", [yyyymmdd]
- 2: time, 'hh:mm' is the middle of the 10 or 30 minute averaging period, e.g. 00:00-00:30 -> 00:15", [hh:mm]
- 3: decimal_day, decimal day of year, [#]
- 4: FC, Uncorrected Co₂ flux, [$\mu\text{mol m}^{-2} \text{s}^{-1}$]
- 5: FCR, Corrected Co₂ flux, [$\mu\text{mol m}^{-2} \text{s}^{-1}$]
- 6: E, Uncorrected latent heat flux, [W m^{-2}]
- 7: ER, Corrected latent heat flux, [W m^{-2}]
- 8: HS, Uncorrected sensible heat flux, [W m^{-2}]
- 9: HSR, Corrected sensible heat flux, [W m^{-2}]
- 10: Bowen, Bowen ratio, [#]
- 11: TKE, Turbulence kinetic energy, [$\text{m}^2 \text{s}^{-2}$]
- 12: tau, Momentum flux, [$\text{kg m}^{-1} \text{s}^{-2}$]
- 13: U_star, Friction velocity, [m s^{-1}]
- 14: T_star, Scale temperature, [K]
- 15: Q_star, Scale Humidity, [g m^{-3}]
- 16: zL, Stability parameter, [#]
- 17: L, Monin-Obukhov length, [m]
- 18: wu, Covariance of u and w, [$\text{m}^2 \text{s}^{-2}$]
- 19: wv, Covariance of v and w, [$\text{m}^2 \text{s}^{-2}$]

- 20: wq, Corrected covariance of w and H₂O concentration, [g m⁻² s⁻¹]
- 21: wT, Corrected covariance of w and sonic temperature, [K m s⁻¹]
- 22: wc, Corrected covariance of w and CO₂ concentration, [mg m⁻² s⁻¹]
- 23: WS, Wind speed, [m s⁻¹]
- 24: WD, Wind direction, [deg]
- 25: Temp_air, Air temperature, [K]
- 26: Rho_air, Wet air density, [kg m⁻³]
- 27: Rho_w, Water vapor density, [kg m⁻³]
- 28: Pres_air, Air pressure, [Pa]
- 29: U_std, Standard deviation of u, [m s⁻¹]
- 30: V_std, Standard deviation of v, [m s⁻¹]
- 31: W_std, Standard deviation of w, [m s⁻¹]
- 32: q_std, Standard deviation of q, [g m⁻³]
- 33: T_std, Standard deviation of T, [K]
- 34: C_std, Standard deviation of CO₂ concentration, [mg m⁻³]
- 35: STFlag_wc, Steady state test flag in wc, [#]
- 36: STFlag_wq, Steady state test flag in wq, [#]
- 37: STFlag_wT, Steady state test flag in wT, [#]
- 38: STFlag_wu, Steady state test flag in wu, [#]
- 39: DTFlag_u, Developed turbulence test flag in u, [#]
- 40: DTFlag_w, Developed turbulence test flag in w, [#]
- 41: DTFlag_T, Developed turbulence test flag in T, [#]
- 42: QCFlag_c, Overall quality flag for CO₂ flux, [#]
- 43: QCFlag_e, Overall quality flag for latent heat flux, [#]
- 44: QCFlag_h, Overall quality flag for sensible heat flux, [#]
- 45: QCFlag_t, Overall quality flag for momentum flux, [#]

Other Measurements

Experimental Setup

In addition to the four 3-d sonic anemometers, four IRGAs, and six 2-3 sonic anemometers listed above, WSULAR also made measurements of non-aspirated air temperature and relative humidity at 2, 12, 20, 25, 30, 45, 52, and 60 m heights using Vaisala HMP45C sensors and at 4, 8, 16, 35, and 40 m heights using Rotronic HC2S3 sensors. Measurements of net radiation (30 and 60 m), atmospheric pressure (2 and 60 m), surface temperature by infrared thermometer (30 m), and soil heat flux (6 and 12 cm) were also made. The slow-response

sensors were sampled at 1 Hz, and 5 and 30-minute averages were automatically calculated and stored in separate files on the CR5000s.

Quality Control

The air temperature, relative humidity, wind speed and direction, net radiation, air pressure, and soil heat flux data sets were plotted and reviewed by the data analyst for consistency and accuracy by comparing results with other measurements for the duration of each test plus one hour before and after each test.

Data File Formats

There are two files that provide the non-sonic anemometer data (10 min and 30 min). The filenames are 'RM_###min.csv' where '###' specifies the averaging period (10 or 30 min). Missing values are indicated by '-999'. The column headers, description, and units are:

- 1: TimeStamp, End time for the averaging period (10min or 30 min)
e.g. 00:00-00:30 -> 00:30, yyyy/mm/dd hh:mm
- 2: Rn_30m, Net radiation at 30 m height, [W m⁻²]
- 3: Rn_60m, Net radiation at 60 m height, [W m⁻²]
- 4: T_surf, Surface temperature for infrared radiometer at 30 m, [deg C]
- 5: T_2m, Air temperature at 2 m, [deg C]
- 6: T_4m, Air temperature at 4 m, [deg C]
- 7: T_8m, Air temperature at 8 m, [deg C]
- 8: T_12m, Air temperature at 12 m, [deg C]
- 9: T_16m, Air temperature at 16 m, [deg C]
- 10: T_20m, Air temperature at 20 m, [deg C]
- 11: T_25m, Air temperature at 25 m, [deg C]
- 12: T_30m, Air temperature at 30 m, [deg C]
- 13: T_35m, Air temperature at 35 m, [deg C]
- 14: T_40m, Air temperature at 40 m, [deg C]
- 15: T_45m, Air temperature at 45 m, [deg C]
- 16: T_52m, Air temperature at 52 m, [deg C]
- 17: T_60m, Air temperature at 60 m, [deg C]
- 18: RH_2m, Relative humidity at 2 m, [%]
- 19: RH_4m, Relative humidity at 4 m, [%]
- 20: RH_8m, Relative humidity at 8 m, [%]
- 21: RH_12m, Relative humidity at 12 m, [%]

- 22: RH_16m, Relative humidity at 16 m, [%]
- 23: RH_20m, Relative humidity at 20 m, [%]
- 24: RH_25m, Relative humidity at 25 m, [%]
- 25: RH_30m, Relative humidity at 30 m, [%]
- 26: RH_35m, Relative humidity at 35 m, [%]
- 27: RH_40m, Relative humidity at 40 m, [%]
- 28: RH_45m, Relative humidity at 45 m, [%]
- 29: RH_52m, Relative humidity at 52 m, [%]
- 30: RH_60m, Relative humidity at 60 m, [%]
- 31: WS_12m, Wind speed at 12 m from 2D sonic, [m s^{-1}]
- 32: WD_12m, Wind direction at 12 m from 2D sonic, [deg]
- 33: WS_20m, Wind speed at 20 m from 2D sonic, [m s^{-1}]
- 34: WD_20m, Wind direction at 20 m from 2D sonic, [deg]
- 35: WS_25m, Wind speed at 25 m from 2D sonic, [m s^{-1}]
- 36: WD_25m, Wind direction at 25 m from 2D sonic, [deg]
- 37: WS_35m, Wind speed at 35 m from 2D sonic, [m s^{-1}]
- 38: WD_35m, Wind direction at 35 m from 2D sonic, [deg]
- 39: WS_40m, Wind speed at 40 m from 2D sonic, [m s^{-1}]
- 40: WD_40m, Wind direction at 40 m from 2D sonic, [deg]
- 41: WS_52m, Wind speed at 52 m from 2D sonic, [m s^{-1}]
- 42: WD_52m, Wind direction at 52 m from 2D sonic, [deg]
- 43: Pres_surf, Surface air pressure, [kPa]
- 44: Pres_30m, Air pressure at about 30 m, [kPa]
- 45: Gs_6cm, Soil heat flux at 6 cm under surface, [W m^{-2}]
- 46: Gs_12cm, Soil heat flux at 12 cm under surface, [W m^{-2}]

Meteorological Towers on Sampling Grid

Experimental Setup

A 30 m open lattice aluminum meteorological tower purchased from Triex (model T-15) was located at approximately 499 m arc distance and 60 degrees arc angle during PSB1. This was the ‘100 foot’ meteorological tower linked to the command center (COC). Met One Instruments Inc. cup anemometers (Model 010C) and wind vanes (Model 020C) were used to measure the wind speed and direction at 2, 10, and 30 m heights. A picture of this tower is shown in Fig. 53.



Figure 53. 30 m command center meteorological and tracer sampling tower (COC).

A 10 m open lattice aluminum meteorological tower was located near the center of the 3200 m arc at about 44.5 degrees arc angle (TOW). Met One Instruments Inc. cup anemometers (Model 010C) and wind vanes (Model 020C) were used to measure the wind speed and direction at 2 and 10 m heights. This tower was collocated with the R2 sonic and the ART VT-1 sodar. Power was supplied to the batteries servicing the R2 sonic, the ART VT-1 sodar, and TOW using a large trailer-mounted solar panel array. This solar array experienced problems in providing adequate charge to the batteries during the experimental period and had largely failed by the end of the experiment resulting in data loss for IOPs 4 and 5 at TOW.

Data from the towers was collected on a Campbell Scientific CR23X data logger and recorded in 5-minute averages. One-second averages from the 100 foot tower were transferred by direct line back to the command center during tests where the project manager was able to monitor the current winds from a graphical display on a computer. This information was used to advise the TGA operators where to expect the tracer along the grid sampling arcs and to assist with positioning. The one-second data were not saved for use in this archive.

Quality Control

The cup anemometers and wind vanes on COC and TOW were calibrated to rigorous standards. The instrumentation selection criteria, quality control, calibration, and maintenance procedures at COC and TOW were the same as those at GRI and met the generally accepted requirements and guidelines set out in DOE (2004, 2005), ANSI/ANS-3.11 (2005), and ANSI/ANS-3.2 (2006).

The wind speed and direction data sets for the COC and TOW towers were plotted and reviewed by the data analyst for consistency and accuracy by comparing results with other measurements for the duration of each test plus one hour before and after each test. This included the following comparisons:

- All wind speed and direction measurements in the horizontal at 2, 10, and 30 m, where available. These comparisons included the sonic anemometers and cup anemometers and wind vanes at GRI, and the ASC and ART sodars. In some cases heights were compared if they were close. For example, 2 m cup and vane results at GRI, COC, and TOW were compared with sonic results at 3 m (R2, R3, and R4) and 4 m (G1).

The results for these comparisons are included in the Summary of Individual IOPs chapter.

Data File Formats

There are five COC files in the final PSB1 project database. Each covers the 24-hour day encompassing the IOP test days (October 2, 5, 7, 11, and 18). The filenames are 'PSB1_COC_IOP#.csv' where '#' specifies the number of the IOP. The time listed for each record is the end time for the 5-minute period. All times are MST. Missing values are indicated by '-999'. The column headers are:

- 1: Date and Time (MST) [MM/DD/YYYY HR:MN] where HR:MN is hour and minute at the end of the 5-minute period
- 2: Sequential record number
- 3: Battery voltage minimum
- 4: Battery voltage maximum
- 5: Wind speed at 2 m, [m s⁻¹]
- 6: Wind direction at 2 m, [degrees]
- 7: Wind direction at 2 m, standard deviation [degrees]
- 8: Wind speed at 10 m, [m s⁻¹]
- 9: Wind direction at 10 m, [degrees]
- 10: Wind direction at 10 m, standard deviation [degrees]
- 11: Wind speed at 30 m, [m s⁻¹]
- 12: Wind direction at 30 m, [degrees]
- 13: Wind direction at 30 m, standard deviation [degrees]
- 14: Wind speed gust at 2 m, 3-sec maximum [m s⁻¹]
- 15: Wind speed gust at 10 m, 3-sec maximum [m s⁻¹]
- 16: Wind speed gust at 30 m, 3-sec maximum [m s⁻¹]

There are three TOW files in the final PSB1 project database. Each covers the 24-hour day encompassing IOP test days (October 2, 5, and 7). The filenames are 'PSB1_TOW_IOP#.csv' where '#' specifies the number of the IOP. The time listed for each record is the end time for the 5-minute period. All times are MST. Missing values are indicated by '-999'. The column headers are:

- 1: Date and Time (MST) [MM/DD/YYYY HR:MN] where HR:MN is hour and minute at the end of the 5-minute period
- 2: Sequential record number
- 3: Battery voltage minimum
- 4: Battery voltage maximum
- 5: Wind speed at 2 m, [m s⁻¹]
- 6: Wind direction at 2 m, [degrees]
- 7: Wind direction at 2 m, standard deviation, [degrees]
- 8: Wind speed at 10 m, [m s⁻¹]
- 9: Wind direction at 10 m, [degrees]
- 10: Wind direction at 10 m, standard deviation, [degrees]
- 11: Wind speed gust at 2 m, 3-sec maximum, [m s⁻¹]
- 12: Wind speed gust at 10 m, 3-sec maximum, [m s⁻¹]

Sonic Anemometers on Sampling Grid

Experimental Setup

ARLFRD deployed an additional three 3-d sonic anemometers on the 3200 m arc to evaluate the horizontal homogeneity in the turbulence field in conjunction with the measurement of turbulence on GRI. All were at 3.2 m height on tripod mounts. One anemometer was located near the north end of the 3200 m arc (R3), one near the south end of the 3200 m arc (R4), and one near the 10 m meteorological tower and ART sodar near the center of the 3200 m arc (R2) at TOW. The locations of the R2, R3, and R4 3-d sonic anemometers are shown in Fig. 5.

Power was supplied to the batteries servicing the sonic anemometer, ART VT-1 sodar, and 10 m tower (TOW) at the center of the 3200 m arc using a large trailer-mounted solar panel array. This solar array experienced problems in providing adequate charge to the batteries during the experimental period and had largely failed by the end of the experiment. This affected data recovery at TOW and the ART but data recovery at R2 was unaffected. The R3 and R4 sonics near the north and south ends of the 3200 m arc were each supplied with power by their own solar panel and battery. Batteries could provide power for at least a week without being recharged.

Quality Control

Data collected from the three ARLFRD sonic anemometers on the 3200 m arc were subjected to the same comprehensive quality control and processing software package, based upon the schemes detailed in Vickers and Mahrt (1997), that was used for the ARLFRD sonic anemometers on GRI (see NOAA ARLFRD, Sonic Anemometers, Quality Control section for details).

The wind speed and direction data sets for R2, R3, and R4 were plotted and reviewed by the data analyst for consistency and accuracy by comparing results with other measurements for the duration of each test plus one hour before and after each test. This included the following comparisons:

- All wind speed and direction measurements in the horizontal at about 3 m, where available. These comparisons included the sonic anemometer G1 at 4 m and the cup and vane anemometers at 2 m on GRI, COC, and TOW.

The results for these comparisons are included for each IOP in the Summary of Individual IOPs chapter.

Data File Formats

The data file formats and filename convention for sonics R2, R3, and R4 on the 3200 m arc are the same as those described above for sonics G1, G2, and R1 on GRI.

Sodars

Experimental Setup

A minisodar is a remote sensing device that measures vertical profiles of wind speed and direction in the lowest levels of the atmosphere. It has a vertical range of as low as 15 m up to 200 m maximum with a height resolution of as small as 5 m. The height range and resolution during PSB1 were set at 30 to 200 m and at 10 m, respectively. Two sodars were deployed on the tracer dispersion grid during PSB1.

An Atmospheric Systems Corporation ASC4000 minisodar was located at a permanent site at about 800 m arc distance, 57 degrees arc angle (Figs. 2 and 5). A picture of this sodar can be seen in Fig. 54. Another minisodar, an Atmospheric Research & Technology (ART) model VT-1, was deployed during PSB1. It was located at about 3200 m from the source at a 44.5 degrees arc angle near TOW. Data from the ASC4000 was averaged at 10-minute intervals and transmitted by radio link back to the ARLFRD office. Data from the VT-1 was averaged at 10-minute intervals and stored on both primary and backup drives on site. Computer times on the minisodars were regularly checked and synched to the official internet time.

Power was supplied to the batteries servicing the sonic anemometer



Figure 54. Photo of the ASC sodar, collocated with radar wind profiler at PRO.

(R2), ART VT-1 sodar, and 10 m tower (TOW) near the center of the 3200 m arc using a large trailer-mounted solar panel array. As noted previously, this solar array experienced problems in providing adequate charge to the batteries and had largely failed by the end of the experiment. These power problems occurred mostly overnight into later morning, and the ART-1 was always operational during the actual IOPs. There was data loss at TOW during IOPs 4 and 5. Power to the ASC4000 was supplied by AC line power.

Quality Control

Data was automatically screened for acceptance or rejection by internal algorithms using criteria based primarily on signal-to-noise ratio and number of acceptable values during the averaging period. Rejected data were specified as missing values. The ASC data screening algorithm was proprietary while the ART screening algorithm could be configured. ARLFRD used the software program called SodarView for the ASC and the software program Data Manager for the ART for data review, analysis, and display.

The wind speed and direction data sets for the ASC and ART sodars were plotted and reviewed by the data analyst for consistency and accuracy by comparing results with other measurements for the duration of each test plus one hour before and after each test. This included the following comparisons:

- All wind speed and direction measurements in the horizontal at 30 m (sonic G1 on GRI, COC at 30 m), 40 m (45 m on GRI, sonic G2 on GRI), 60 m (GRI), and 160 m (PRO), where available.

The results for these comparisons are included for each IOP in the Summary of Individual IOPs chapter. All of the comparisons were good with the exception of PRO at 160 m which appeared to have a low wind speed bias relative to the sodar results.

Data File Formats

Five files for the ASC4000 sodar are included in the PSB1 project database, one for each of the IOP test days. Each file contains 10-minute averages covering the 24-hour period of the data record. The files are designated 'Grid3sodar_PSB1_IOP#_Oct**.csv' where '#' specifies the IOP test number and '**' specifies the date in October. The times listed are MST (hh:mm:ss) for the start time of the 10-minute averaging period. The notation in the column headers follows: ws = wind speed, wd = wind direction, w = mean vertical wind speed, sdw = standard deviation in w, sdu = standard deviation in u, sdv = standard deviation in v, tempC = temperature in degrees C. Wind speeds and standard deviations are in units of m s^{-1} and the wind direction is in

degrees. The number following (30, 40, ...) is the height of the measurement in meters. Missing values are designated by '9999' for wind direction and '99.99' for everything else. The sodar's internal algorithms determined which points were missing. No further processing was done.

Five files for the ART VT-1 sodar are included in the PSB1 database, one for each of the IOP test days. While there were power supply problems for the ART VT-1, these did not occur during any of the actual IOPs. The files are named 'Arc3200sodar_PSB1_IOP#_Oct**'.csv' where '#' specifies the IOP test number and '**' specifies the date in October. The times listed are MST for the start time of the 10-minute averaging periods. The notation in the column headers follows: WS = wind speed, WD = wind direction, WSPD = mean vertical wind speed (w), WSD = standard deviation in w , VSD = standard deviation in v , and USD = standard deviation in u . Wind speeds and standard deviations are in units of m s^{-1} and the wind direction is in degrees. The number following (30, 40, ...) is the height of the measurement in meters. Missing values are designated by '999' for wind direction, '-99.9' for u and v wind speeds, '-9.99' for w wind speed, and '99.9' for the standard deviations. Standard deviations are zero if wind speed data is missing.

Radar Wind Profiler and RASS

Experimental Setup

A 500 W, 915 MHz radar wind profiler (PRO) with Radio Acoustic Sounding System (RASS) measured boundary layer wind and air temperature profiles during PSB1. This system has operated continuously at its location on the tracer dispersion grid at about 800 m arc distance and 56 degrees arc angle since 1992 (Figs. 2 and 6). The radar wind profiler with RASS (Fig. 55) provides highly-resolved round-the-clock data for mixing layer characteristics above the sounding site. The radar wind profiler was configured to take measurements at 28 levels covering a vertical range from 159 to 2895 m with a vertical resolution set at 101 m. Remotely-sensed measurements include wind speed and direction. The RASS was configured to take measurements of temperature with a vertical resolution of 105 m covering the range 165 to 1633 m AGL.



Figure 55. Photo of the radar wind profiler and RASS.

Quality Control

The wind profiler data were retrieved and stored in the ARLFRD database similarly to the Mesonet data. The system has a built-in automatic quality control algorithm from the manufacturer. Data was flagged as -950 for any data points identified as suspect.

Some of the data from the wind speed profiler is suspect. As noted above, the PRO wind directions were roughly consistent with wind direction measurements made by other instruments at similar heights. However, the PRO wind speed measurements were characterized by a low wind speed bias relative to other instruments when wind speeds were below 5 m s^{-1} .

Data File Formats

The data for the wind profiler are archived in CSV format for the month of October in the file 'GRIprofiler_PSB1_October.csv'. Wind data were collected for 25 minute intervals twice each hour at 5 to 30 minutes past the hour and at 35 to 60 minutes past the hour. The 'hrmn' listed in

the file are the hour and minute starting times in MST for the 25 minute sampling period. Wind speed (m s^{-1}) is specified with 'wsxxx' and wind direction (degrees) is specified with 'wdxxx', where 'xxx' represents the AGL (m) height level of the measurement. Missing values are designated by '-950'.

The data for the RASS are archived in their original text file format (extension T2B). There are 5 files, one for each full day that included a test release during PSB1. The five files are GRI31002, GRI31005, GRI31007, GRI31011, and GRI31018. The temperature data were collected for 5 minute intervals twice each hour from zero to 5 minutes past the hour and from 30 to 35 minutes past the hour. The files contain a data block representing each half-hour record designated by starting time (MST) in HHMM format. Within each individual half-hour data block the first 3 columns are QC code, height (m, agl), and temperature (T_v , deg C). The QC code '0' indicates valid data and temperature records with '-950' represent failed consensus. The data codes are listed in the header text of each file along with date, location, Julian day, and other information. Data recovery for the RASS was often poor.

Flux Station

Experimental Setup

The energy flux station is a permanent installation designed to measure how the shrub-steppe habitat of the INL interacts with the global energy cycle. It has been operational since 2000. For PSB1 it provided an additional site for the evaluation of horizontal homogeneity as well as a means of determining energy balance.

A suite of measurements were made on two separate towers at the flux station (Fig. 56) and in the soil subsurface. Measurements of net radiation, air temperature, relative humidity, barometric pressure, and solar radiation are made on one tripod tower. A Gill Model 1210R3 sonic anemometer and an open path LI-7500 infrared gas analyzer (IRGA) are mounted on the other tripod tower. This tower is used to measure the fluxes of momentum, sensible heat, latent heat and carbon dioxide. The anemometer and IRGA are mounted at heights of 3.2 and 2.54 m, respectively. The subsurface sensors make measurements of soil temperature (2 and 6 cm), soil moisture (2.5 cm), and soil heat flux (8 cm). The soil heat flux plates represent varying degrees of vegetation cover. Additional measurements include net radiation, air temperature/RH, solar radiation, and barometric pressure. The energy flux station is located approximately 500 m NE of the command center (about 900 m NE of the release location). Full details on instrumentation are provided in Table 17.



Figure 56. Photo of the flux station.

Quality Control

The data from the energy flux station is being provided on an as is basis and caution is advised in use of the data. However, a similar set of quality assurance calculations as those described for the other ARLFRD sonic anemometers in PSB1 (NOAA ARLFRD, Sonic Anemometers, Quality Control) were done for the Gill sonic anemometer and LI-COR IRGA data. These were based on Vickers and Mahrt (1997), Aubinet et al. (2000), and Burba et. al (2008). The calculations were done for 30-minute records only. The calculated quality control parameters for the anemometer and IRGA are included in the processed data file below for reference although they have not been carefully reviewed. In particular, it is noted that the calculated number of “drops” is considered to be excessively high and might not be an accurate representation. In any case, the quality control parameters provided should be sufficient to screen the data for any obvious problems. No quality control review was performed on the soil temperature and heat flux measurements. Turbulent fluxes measured at the flux station (FLX) sonic anemometer were compared with other sonic anemometer measurements in the study area (see Summary of Individual IOPs).

Data File Formats

Data from the energy flux station is provided in two files.

The first file includes all of the measurements made on the first (non-sonic) tower and in the soil subsurface. This data file is in comma separated variable (CSV) format with fixed length fields. The data record covers the month of October and provides 5-minute averages. The filename is 'FluxStationPSB1_Tower1_October.CSV'. The columns in the file are:

- 1: Year
- 2: Month
- 3: Day
- 4: Hour (MST)
- 5: Minute
- 6: Battery Voltage
- 7: Air Temperature at 2 m, [deg C]
- 8: Relative Humidity at 2 m, [%]
- 9: Solar Radiation, [W m^{-2}]
- 10: Soil Temperature Location A at 2 cm, [deg C]
- 11: Pressure, [mb]
- 12: Net Radiation, [W m^{-2}]
- 13: Soil Moisture, 2.5 cm, [% by volume]
- 14: Soil Heat Flux, Plate 1, 8 cm, [W m^{-2}]
- 15: Soil Heat Flux, Plate 2, 8 cm, [W m^{-2}]
- 16: Soil Temperature Location B at 6 cm, [deg C]
- 17: Soil Heat Flux, Plate 3, 8 cm, [W m^{-2}]
- 18: Soil Heat Flux, Plate 4, 8 cm, [W m^{-2}]

The second file (FluxStationPSB1_Tower2_October.csv) contains data processed from the sonic anemometer and LI-7500 IRGA and the associated calculated quality control parameters for 30-minute records for the month of October. Missing values are indicated by '-9999'. In the description below, a cycle refers to a single pass through a single record for the specified variable during the despiking process. The column headers are:

1. Record – 'Gjjjhmm' where jjj = Julian day and hhmm is the start time of the 30-minute record
2. Sensible heat flux, with rotation, [$\text{J m}^{-2} \text{s}^{-1}$]
3. Kinematic heat flux, with rotation, [m K s^{-1}]
4. Sensible heat flux, 10% correction for non-orthogonal sonic axes, [$\text{J m}^{-2} \text{s}^{-1}$]
5. Kinematic heat flux, 10% correction for non-orthogonal sonic axes, [$\text{J m}^{-2} \text{s}^{-1}$]
6. Sensible heat flux, 10% correction for non-orthogonal sonic axes and sensor heating, [$\text{J m}^{-2} \text{s}^{-1}$]
7. Latent heat flux, with rotation, [$\text{J m}^{-2} \text{s}^{-1}$]
8. Latent heat flux, with rotation, [$\text{mmol m}^{-2} \text{s}^{-1}$]

9. Latent heat flux, 10% correction for non-orthogonal sonic axes and frequency loss, [$\text{J m}^{-2} \text{s}^{-1}$]
10. Latent heat flux, 10% correction for non-orthogonal sonic axes and frequency loss, [$\text{mmol m}^{-2} \text{s}^{-1}$]
11. Latent heat flux, 10% correction for non-orthogonal sonic axes, frequency loss, and sensor heating
12. Friction velocity u^* , uncorrected, [m s^{-1}]
13. Friction velocity u^* , with rotation, [m s^{-1}]
14. Friction velocity u^* , corrected for non-orthogonal sonic axes, [m s^{-1}]
15. Friction velocity u^* , rotated corrected for non-orthogonal sonic axes, [m s^{-1}]
16. z/L
17. z/L with rotation
18. U variance, uncorrected, [$\text{m}^2 \text{s}^{-2}$]
19. V variance, uncorrected, [$\text{m}^2 \text{s}^{-2}$]
20. W variance, uncorrected, [$\text{m}^2 \text{s}^{-2}$]
21. U variance, with rotation, [$\text{m}^2 \text{s}^{-2}$]
22. V variance, with rotation, [$\text{m}^2 \text{s}^{-2}$]
23. W variance, with rotation, [$\text{m}^2 \text{s}^{-2}$]
24. itS_flag1, stationarity flag for sensible heat flux
25. itS_flag2, stationarity flag for sensible heat flux
26. itS_flag3, stationarity flag for sensible heat flux
27. itL_flag1, stationarity flag for latent heat flux
28. itL_flag2, stationarity flag for latent heat flux
29. itL_flag3, stationarity flag for latent heat flux
30. itt_U, integral turbulence flag for wind
31. itt_T, integral turbulence flag for temperature
32. H₂O conc, water vapor concentration, [mmol m^{-3}]
33. Count, number of data points in half hour record
34. Flg_count, ('0' if $17900 < \text{count} < 18100$, otherwise '1')
35. Flgspk_w, ('0' if fraction of spikes in $w < 0.5\%$ for any single cycle, otherwise '1')
36. Flgspk_u, ('0' if fraction of spikes in $u < 0.5\%$ for any single cycle, otherwise '1')
37. Flgspk_v, ('0' if fraction of spikes in $v < 0.5\%$ for any single cycle, otherwise '1')
38. Flgspk_t, ('0' if fraction of spikes in $t < 0.5\%$ for any single cycle, otherwise '1')
39. Flgspk_H₂O, ('0' if fraction of spikes in H₂O $< 0.5\%$ for any single cycle, otherwise '1')
40. Flgspk_CO₂, ('0' if fraction of spikes in CO₂ $< 0.5\%$ for any single cycle, otherwise '1')
41. Spkcnt_w, cumulative number of spikes detected in w in 'Loop_w' cycles
42. Spkcnt_u, cumulative number of spikes detected in u in 'Loop_u' cycles
43. Spkcnt_v, cumulative number of spikes detected in v in 'Loop_v' cycles
44. Spkcnt_t, cumulative number of spikes detected in t in 'Loop_t' cycles
45. Spkcnt_H₂O, cumulative number of spikes detected in H₂O in 'Loop_H₂O' cycles

46. Spkcnt_CO₂, cumulative number of spikes detected in CO₂ in 'Loop_CO₂' cycles
47. Loop_w, number of cycles through record to despiking w (max=11)
48. Loop_u, number of cycles through record to despiking u (max=11)
49. Loop_v, number of cycles through record to despiking v (max=11)
50. Loop_t, number of cycles through record to despiking t (max=11)
51. Loop_H₂O, number of cycles through record to despiking H₂O (max=11)
52. Loop_CO₂, number of cycles through record to despiking CO₂ (max=11)
53. W_skw, skewness in w
54. U_skw, skewness in U
55. V_skw, skewness in V
56. T_skw, skewness in T
57. H₂O_skw, skewness in H₂O
58. CO₂_skw, skewness in CO₂
59. W_kur, kurtosis in w
60. U_kur, kurtosis in U
61. V_kur, kurtosis in V
62. T_kur, kurtosis in T
63. H₂O_kur, kurtosis in H₂O
64. CO₂_kur, kurtosis in CO₂
65. Ampres_w, amplitude resolution test w
66. Ampres_u, amplitude resolution test u
67. Ampres_v, amplitude resolution test v
68. Ampres_t, amplitude resolution test t
69. Ampres_H₂O, amplitude resolution test H₂O
70. Ampres_CO₂, amplitude resolution test CO₂
71. Drops_w, drop test w
72. Drops_u, drop test u
73. Drops_v, drop test v
74. Drops_t, drop test t
75. Drops_H₂O, drop test H₂O
76. Drops_CO₂, drop test CO₂
77. W_mean_hts, haar transform test (soft flag) for mean w
78. U_mean_hts, haar transform test (soft flag) for mean u
79. V_mean_hts, haar transform test (soft flag) for mean v
80. T_mean_hts, haar transform test (soft flag) for mean T
81. H₂O_mean_hts, haar transform test (soft flag) for mean H₂O
82. CO₂_mean_hts, haar transform test (soft flag) for mean CO₂
83. W_sd_hts, haar transform test (soft flag) for standard deviation w
84. U_sd_hts, haar transform test (soft flag) for standard deviation u
85. V_sd_hts, haar transform test (soft flag) for standard deviation v
86. T_sd_hts, haar transform test (soft flag) for standard deviation T
87. H₂O_sd_hts, haar transform test (soft flag) for standard deviation H₂O
88. CO₂_sd_hts, haar transform test (soft flag) for standard deviation CO₂
89. W_mean_hth, haar transform test (hard flag) for mean w

90. U_mean_hth, haar transform test (hard flag) for mean u
91. V_mean_hth, haar transform test (hard flag) for mean v
92. T_mean_hth, haar transform test (hard flag) for mean T
93. H₂O_mean_hth, haar transform test (hard flag) for mean H₂O
94. CO₂_mean_hth, haar transform test (hard flag) for mean CO₂
95. W_sd_hth, haar transform test (hard flag) for standard deviation w
96. U_sd_hth, haar transform test (hard flag) for standard deviation u
97. V_sd_hth, haar transform test (hard flag) for standard deviation v
98. T_sd_hth, haar transform test (hard flag) for standard deviation T
99. H₂O_sd_hth, haar transform test (hard flag) for standard deviation H₂O
100. CO₂_sd_hth, haar transform test (hard flag) for standard deviation CO₂
101. W_abs, range test flag for w
102. U_abs, range test flag for u
103. V_abs, range test flag for v
104. T_abs, range test flag for t
105. H₂O_abs, range test flag for H₂O
106. CO₂_abs, range test flag for CO₂
107. RSE_t, relative systematic flux sampling error test value for t
108. RSE_H₂O, relative systematic flux sampling error test value for H₂O
109. RSE_CO₂, relative systematic flux sampling error test value for CO₂
110. RSE_tflg, relative systematic flux sampling error test flag for t ('0' = pass, '1'=fail at test=0.25)
111. RSE_H₂Oflg, relative systematic flux sampling error test flag for H₂O
112. RSE_CO₂flg, relative systematic flux sampling error test flag for CO₂
113. RFE_t, relative random flux sampling error test value for t
114. RFE_H₂O, relative random flux sampling error test value for H₂O
115. RFE_CO₂, relative random flux sampling error test value for CO₂
116. RFE_tflg, relative random flux sampling error test flag for t ('0' = pass, '1'=fail at test=0.25)
117. RFE_H₂Oflg, relative random flux sampling error test flag for H₂O
118. RFE_CO₂flg, relative random flux sampling error test flag for CO₂
119. RN_t, mesoscale flux trends test value for t
120. RN_H₂O, mesoscale flux trends test value for H₂O
121. RN_CO₂, mesoscale flux trends test value for CO₂
122. RN_tflg, flux trends test flag for t ('0' = pass, '1'=fail at test=0.25)
123. RN_H₂Oflg, flux trends test flag for H₂O
124. RN_CO₂flg, flux trends test flag for CO₂
125. RNU_flg, alongwind relative nonstationarity test flag ('0'=pass, '1'=fail at test=0.5)
126. RNV_flg, crosswind relative nonstationarity test flag
127. RNS_flg, vector wind relative nonstationarity test flag

Radiosondes

Experimental Procedures

Radiosonde launches (Fig. 57) were performed before and after each test period from near the command center. The first balloon of a test period was launched approximately 15 minutes before the samplers were set to begin sampling the tracer plume. The second balloon was launched approximately 15 minutes after the end of the sampling period. A summary of the radiosonde launches is given in Table 18. Data from all launches were recorded during ascent through balloon burst and continued through descent until the signal could no longer be acquired, except for the second launch of IOP5. During this launch, the battery failed in the base station signal receiving radio during balloon ascent and this problem was not discovered until it was too late to reacquire the radiosonde signal. The longest flight was 2 hours, 18 minutes, while the shortest flight was 56 minutes. The average flight length was 1 hour and 38 minutes.



Figure 57. Photo of releasing the radiosonde.

Table 18. Summary of radiosonde launch dates, times, durations and calculated variables.

Test #	Date	Launch #	Launch		Duration HH:MM	LCL hPa	CCL hPa	LI	SI	K- index	S- index	TT- index	Ko- index	Freezing			Highest			Average		
			Time MDT	End Time MDT										Level hPa	hPa	m	Tropopause hPa	Point hPa	m	Rate m.s ⁻¹	Ascent	Pot. Temp
1	10/2/2013	1	15:03	16:46	1:43	698.2	628.2	2	3	21	41	47	9	737.7	2.693	237	10.878	27.4	23.186	4.2	1233	1550
1	10/2/2013	2	17:41	19:59	2:18	NA	NA	NA	NA	NA	NA	NA	NA	706.5	2.970	230	10.978	20.4	24.992	3.4	997	1337
2	10/5/2013	1	13:50	15:30	1:40	740.0	530.0	14	17	0	11	22	11	682.4	3.456	185	12.720	31.6	22.255	4.3	1066	1041
2	10/5/2013	2	16:07	17:45	1:38	706.2	512.2	13	14	6	17	26	3	658.8	3.744	178	12.943	39.8	20.765	4.4	1208	1132
3	10/7/2013	1	13:38	15:14	1:36	631.8	520.8	8	NA	NA	NA	NA	NA	609.6	4.424	186	12.550	49.0	19.348	4.3	979	588
3	10/7/2013	2	16:18	17:50	1:32	544.5	456.5	6	NA	NA	NA	NA	NA	640.2	3.814	218	11.526	36.4	21.194	4.7	922	971
4	10/11/2013	1	14:45	16:19	1:34	NA	NA	NA	NA	NA	NA	NA	NA	734.7	2.585	196	12.009	36.9	21.161	4.4	2107	1980
4	10/11/2013	2	17:08	18:41	1:33	649.8	593.8	5	NA	NA	NA	NA	NA	737.6	2.652	190	12.233	40.8	20.534	4.6	2154	1880
5	10/18/2013	1	13:42	15:34	1:52	680.1	533.6	12	12	2	7	31	4	774.4	2.325	218	11.458	29.3	22.512	4.1	1135	1176
5	10/18/2013	2	16:02	16:58	0:56	645.3	520.4	9	11	3	16	32	1	707.9	3.039	229	11.140	105.4	14.531	4.3	1122	1171

The radiosonde system used was the GRAW model GS-H ground station (GRAW Radiosondes GmbH & Co. KG, Nuernberg, Germany) with GRAWMET software version 5.9.2.4, in conjunction with the GRAW digital radiosonde model DFM-09. A 200-gram balloon supplied the lift. The balloons were intentionally under-inflated to slow the balloon ascent in order to maximize the number of measurements in the boundary layer during balloon ascent. A target ascent rate of 4 m s^{-1} was selected. An average ascent rate of 4.3 m s^{-1} was achieved, which is only slightly less than the minimum ascent rate of 4.6 m s^{-1} requested by the National Weather Service (NWS).

Quality Control

The data are provided on an as is basis. The only data available for any kind of comparison are the wind speed and direction data from PRO and temperature data from the RASS and that comparison is limited. As noted previously, the wind speed from PRO exhibited a low bias below 5 m s^{-1} .

Data Files and Results

A summary table of various calculated atmospheric variables for each radiosonde ascent is provided in Table 18. It contains the lifted index, freezing level, convective condensation level, lifting condensation level, tropopause height, characteristics of the maximum wind speed including the direction and height of occurrence, and the height of the mixed layer based on potential temperature and specific humidity. The latter two parameters were calculated based on the initial height of the most rapid change in potential temperature or specific humidity. The results using the two methods were comparable. Mixed layer heights ranged from less than 1 km in IOP3 to approximately 2 km in IOP4.

Summary graphs of the radiosonde data were produced for each ascent. These graphs are: 1) profile data diagram, 2) thermodynamic (Stueve) diagram, 3) tephigram, 4) skew-T diagram, 5) emagram, 6) altitude diagram, 7) balloon track, and 8) hodograph. Each of these graphs are described below.

An example of the profile data diagram is shown in Fig. 58. It contains traces of wind speed, air temperature, relative humidity, air pressure, balloon altitude, and balloon rise speed plotted against time since balloon launch. The graph contains data from both the ascent and descent of the sonde.

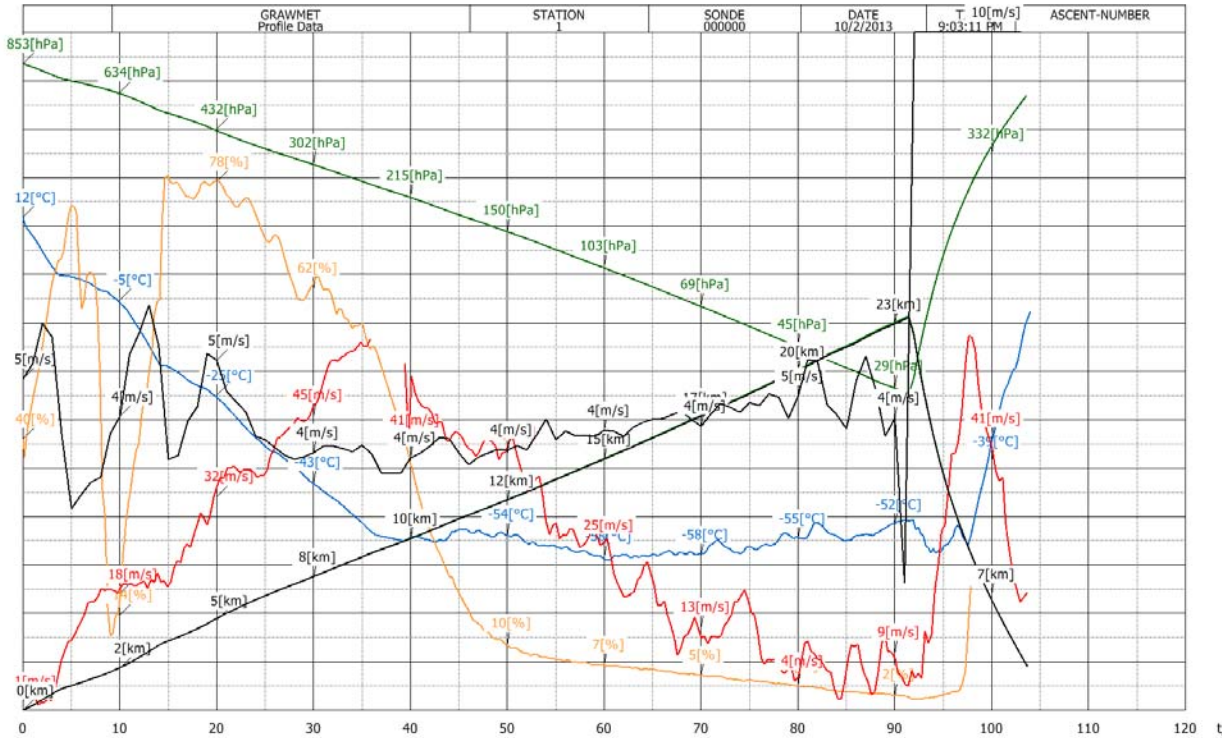


Figure 58. Example balloon profile data diagram from IOP1, Launch 1, with atmospheric pressure (green), relative humidity (orange), air temperature (blue), balloon ascent rate (black), wind speed (red), and radiosonde height AGL (black) plotted as a function of time after launch. The time stamp is the start of the ascent in UTC.

An example of the thermodynamic or Stueve diagram is shown in Fig. 59. It contains traces of wind speed, wind direction, air temperature, and relative humidity plotted as a function of geopotential height. An air temperature curve steeper than the dry adiabatic curve indicates a stable layer, while an air temperature curve that equals the dry adiabatic curve indicates a layer of neutral stability.

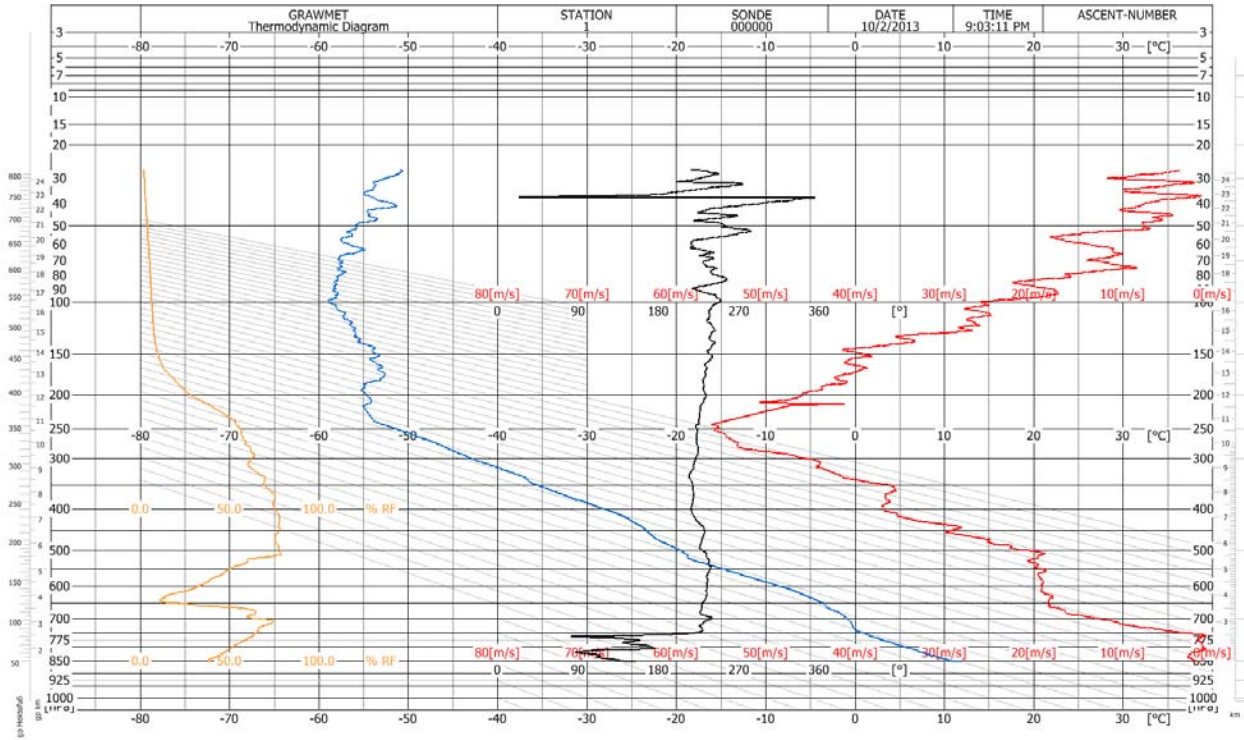


Figure 59. Example thermodynamic (Stueve) diagram from IOP1, Launch 1, with relative humidity (orange), air temperature (blue), wind direction (black), and wind speed (red) plotted as a function of geopotential height MSL. The time stamp is the start of the ascent in UTC.

An example tephigram is shown in Fig. 60. It contains traces of air temperature, dew point temperature, and wet bulb temperature on a temperature-potential temperature graph. This graph is used to estimate the thermal stability of the atmosphere.

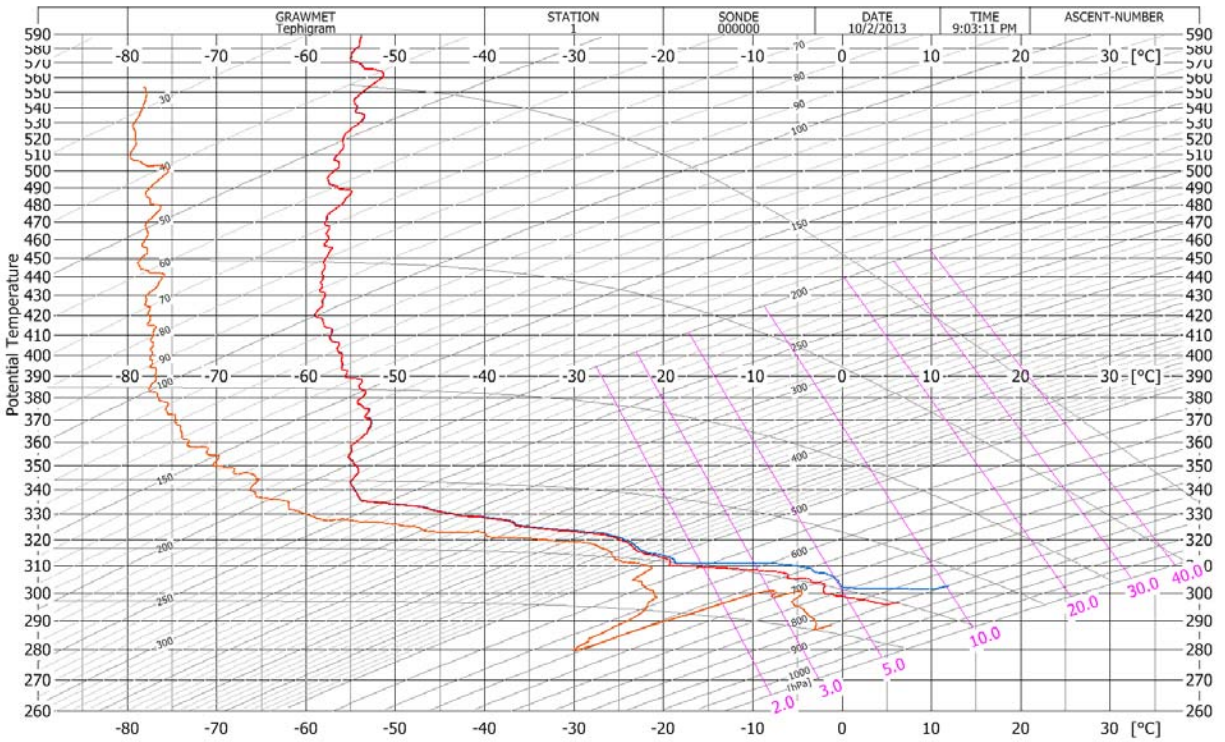


Figure 60. Example tephigram from IOP1, Launch 1, with air temperature (blue), wet bulb temperature (red) and dew point temperature (orange) plotted on a temperature/potential temperature graph. The time stamp is the start of the ascent in UTC.

The Skew-T diagram example is shown in Fig. 61. It shows traces of air temperature and dew point temperature on a temperature-pressure graph. This graph produces a perpendicular angle between isotherms and dry adiabats.

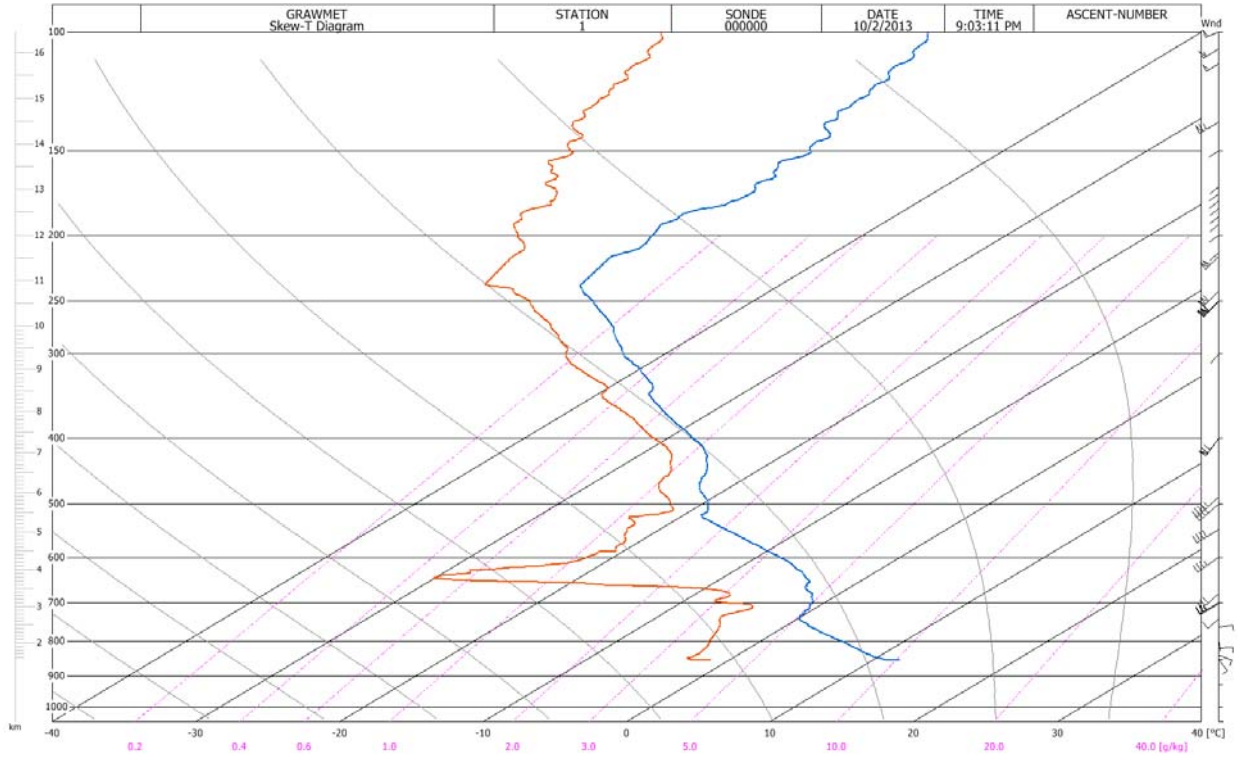


Figure 61. Example Skew-T diagram from IOP1, Launch 1, with air temperature (blue) and dew point temperature (orange) plotted on a temperature/pressure graph. The time stamp is the start of the ascent in UTC.

An example emagram is shown in Fig. 62, and shows traces of air temperature and dew point temperature on a temperature-pressure (logarithmic scale) graph. It is a vertical representation of temperature and humidity.

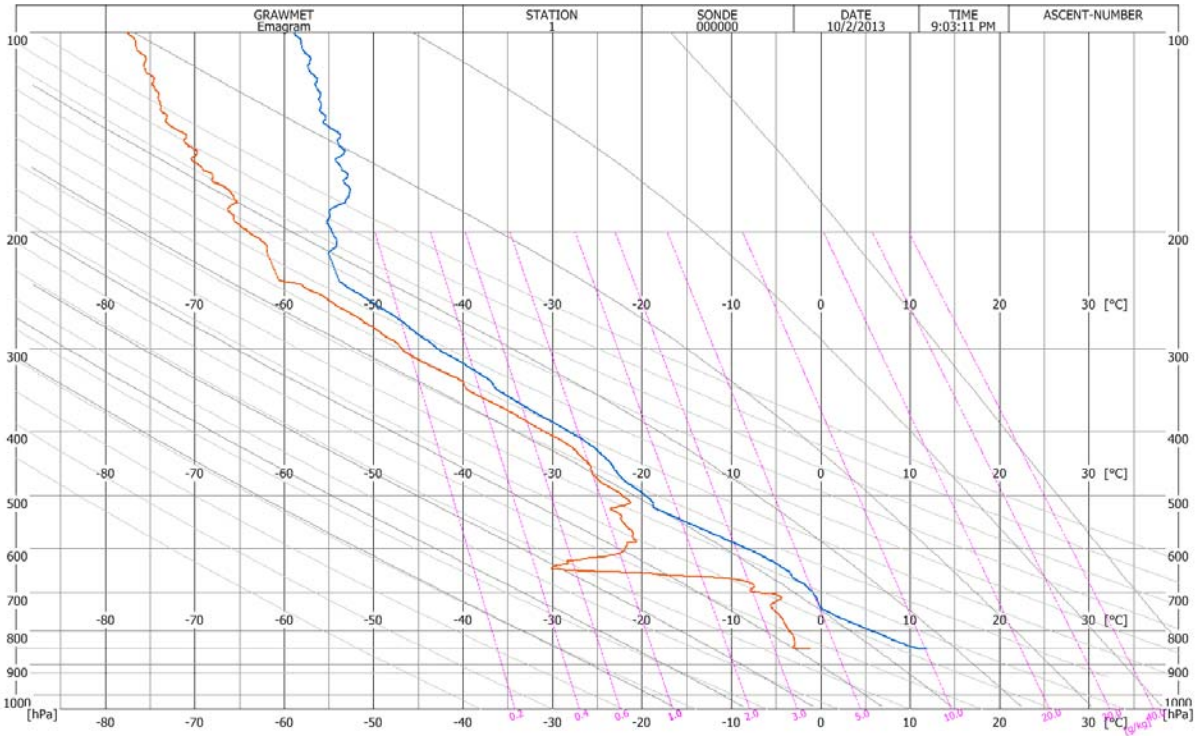


Figure 62. Example emagram from IOP1, Launch 1, with air temperature (blue) and dew point temperature (orange) plotted on a temperature/pressure graph. The time stamp is the start of the ascent in UTC.

An example altitude diagram is shown in Fig. 63 and shows wind speed, wind direction, air temperature, relative humidity and pressure as a function of altitude.

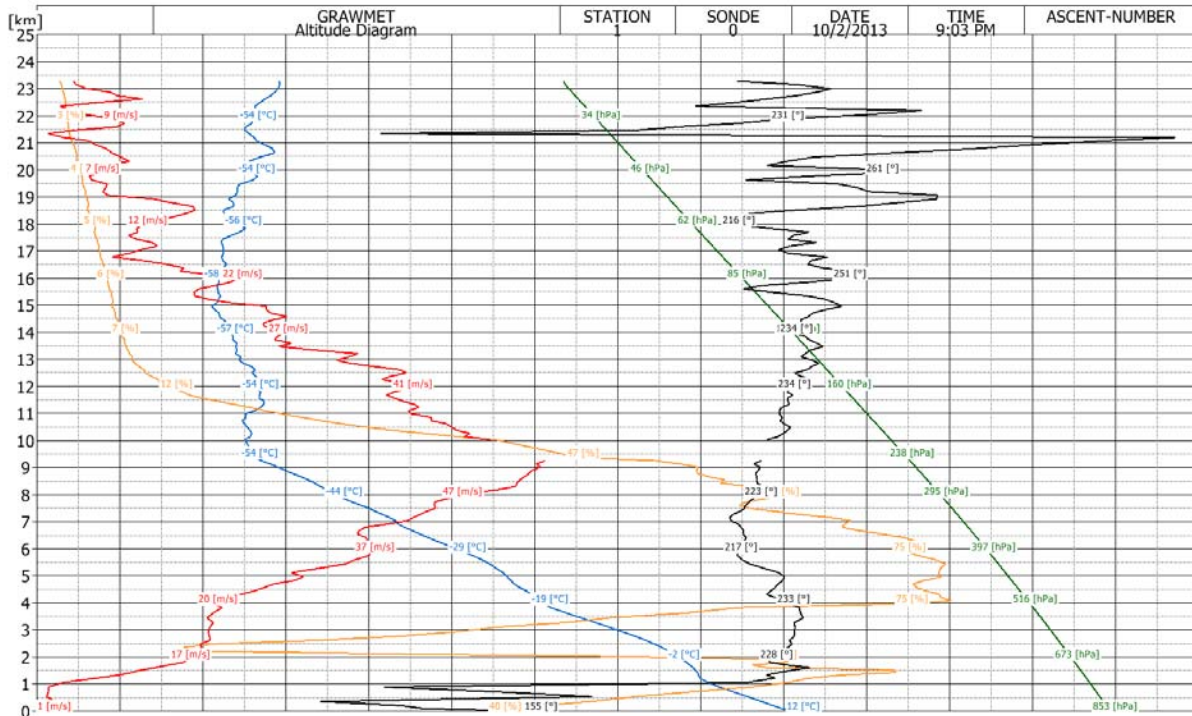


Figure 63. Example altitude diagram from IOP1, Launch 1, with wind speed (red), relative humidity (orange), temperature (blue), and wind direction (black) plotted as a function of height. The time stamp is the start of the ascent in UTC.

The balloon track (example not provided) shows the distance and direction of the balloon over the earth's surface. It also contains wind barbs plotted in two-minute intervals. Each stroke is 10 knots, while each ½ stroke is 5 knots wind speed. The plot contains data from both the ascent and descent of the sonde. The hodograph (example not provided) shows the vector representation of wind motion. A new vector is plotted every 1,000 geopotential meters. Wind barbs are also plotted on the right-hand side of the graph in two-minute intervals in units of knots.

Various reports were automatically generated by the GRAWMET software at the completion of each radiosonde flight. These reports included: 1) 20,000 ft., 2) altitude, 3) forecast, 4) RTS, 5) SHR, 6) significant levels (according to WMO specifications), 7) standard levels, 8) summary, 9) upper air data table report, 10) wind report, 11) TEMP messages, 12) PILOT messages, 13) BUFR messages, and 14) ballistic messages. These reports were generated in ASCII text and PDF formats.

Four other reports that may be of additional interest were manually generated and saved in ASCII format. These files are called: 1) AverageLayerWinds.txt, 2) Overradiabats.txt, 3) ProfileData.txt, and 4) RTS.txt. The AverageLayerWinds file contains averaged radiosonde output in approximately 100 m altitude increments for comparison with output from the 915 MHz wind profiling radar. The data included in this file are: 1) height AGL, 2) time after launch, 3) pressure, 4) air temperature, 5) virtual temperature, 6) relative humidity, 7) absolute humidity, 8) dew point temperature, 9) wind direction, and 10) wind speed. The Overradiabats file contains the altitudes at which the GRAWMET software calculated overadiabatic conditions during ascent of the radiosonde. The data included in this file are: 1) altitude range both AGL and MSL, 2) air temperature difference, 3) average temperature gradient, and 4) maximum temperature gradient. ProfileData.txt provides a number of measured and calculated variables in one second time steps. The data include: 1) pressure, 2) air temperature, 3) relative humidity, 4) wind speed, 5) wind direction, 6) latitude, 7) longitude, 8) altitude, 9) geopotential height, 10) dew point temperature, 11) virtual temperature, and 12) balloon ascent rate. The RTS file contains similar information as the ProfileData file.

The entire collection of graphs and reports described above is provided in the radiosonde directory in the data archive CD for the project. The header information in each file explains the contents. The data are provided as is, without the application of any additional quality controls. All time stamps are UTC (7 hours ahead of MST).

NOAA/INL Mesonet

Configuration

ARLFRD has maintained a large network of (presently) 34 meteorological stations or towers across the Eastern Snake River Plain that includes the INL and the local test area at Grid 3. This network provided a complete historical archive of wind speed, wind direction, air temperature, and other data. This database served as the source for graphical wind rose analyses by month of the year and hour of the day. These analyses have guided the optimization of the experimental field configuration to maximize the frequency of winds across the tracer sampling grid from the appropriate direction.

The Mesonet data were collected in Campbell Scientific CR23X data loggers and recorded as averages, totals, or extremes for 5-minute periods. Wind speed, wind direction, air temperature, relative humidity, and solar radiation were measured every 1-second and averaged over the 5-minute periods. Precipitation was totaled for the same 5-minute interval. The maximum and minimum 1-minute averages were used as the maximum and minimum air temperatures for each 5-minute period. A 3-second average wind gust is selected as the maximum of a 3-second running average of wind speed. Data was collected and transmitted every 5-minutes by a radio link back to the FRD office and eventually onto the Internet. The project manager was able to access the Mesonet data in the command center during the test via Internet connection.

Quality Control

The cup anemometers and wind vanes on COC and TOW were calibrated to the rigorous standards of the NOAA/INL Mesonet described previously.

Data File Formats

Files in this section contain subsets of data from the NOAA/INL Mesonet towers near the location of PSB1. The Mesonet data files are broken up into two rings based on the distance to the Grid 3 area. The inner ring consists of Mesonet stations that are within 10 miles of the Grid 3 study area. The outer ring consists of Mesonet stations that are between 10-20 miles of the Grid 3 study area. These are designated 'MesoRing1PSB1_Oct#.csv' for the inner and outer rings, respectively, and '#' denotes day of month. All files are archived in csv format. The first of these records in each file is a header record. The first four columns in each header record are the year, month, day of month, and time in hhmm format for the end of the five minute period for the data record. Times are Mountain Standard Time (MST).

The following columns in the header record describe the location, height, description of the measurement, and the units of the measurement. The general format of these column headers is 'NNN ##M MMMM Units' or 'NNN ##M FFFF' where 'NNN' is a 3-character site identifier (tower code), '##' is the height of the measurement (AGL, m), 'MMMM' is a description of the measurement, 'FFFF' is a quality flag code, and 'Units' specifies the units of the measurement. The measurement and flag fields are always paired in successive columns.

The remaining records in each data file contain 5-minute average data values for each measurement or its paired quality flag value. The flags are assigned during quality assurance procedures which are executed after the data have been collected. The flag values which appear in these files consist of the following:

Flag Value	Interpretation
0	Data OK
5	Data affected by maintenance
10	Data values too small
30	Data value constant or changes too slowly
72	Instrument (including rain gage) affected by ice/snow
73	Very low wind speed - excessively high threshold value
75	Temperature or relative humidity values inaccurate due to inoperative aspirator
78	Values too high
79	Bad data due to unknown cause
80	Orientation error in wind direction
121	Suspect data

Mesonet data files with Ring1 in their names contain data from nine towers located closest to the experiment location. These towers are:

Tower Code	Latitude (deg N)	Longitude (deg W)	Elevation (ft MSL)	Facility or Location Name
690	43.532598	112.947757	4950	Central Facilities (building 690)
BAS	43.677557	113.006053	4900	Base of Howe Peak
DEA	43.624868	113.059840	5108	Dead Man Canyon
GRI	43.589718	112.939855	4897	INTEC/Grid 3
LOS	43.548538	113.008460	4983	Lost River Rest Area
NRF	43.647887	112.911193	4847	Naval Reactors Facility
PBF	43.547477	112.869697	4910	Critical Infrastructure Complex (formerly PBF)
RWM	43.503362	113.046030	5025	Radioactive Waste Management Complex
TRA	43.584612	112.968653	4937	Reactor Technologies Complex (formerly TRA)

Mesonet data files with Ring2 in their names contain data from ten other towers. These towers are:

Tower Code	Latitude (deg N)	Longitude (deg W)	Elevation (ft MSL)	Facility or Location Name
ARC	43.624522	113.297087	5290	Arco
ATO	43.443700	112.812400	5058	Atomic City
BIG	43.294095	113.181607	5200	Cox's Well (formerly Big Southern)
EBR	43.594138	112.651713	5143	Materials Fuels Complex (formerly EBR II)
HOW	43.784113	112.977358	4815	Howe
LOF	43.859793	112.730253	4790	Specific Manufacturing Capability (formerly LOFT)
ROV	43.720590	112.529560	5008	Rover
SAN	43.779632	112.758165	4820	Sand Dunes
SUM	43.396300	113.021800	7576	Big Southern Summit
TAB	43.318700	112.691875	4730	Taber

Summary of Individual IOPs

Introduction

The map presentations of the bag sampling results for the individual IOPs shows markers for each ground-based 1 m AGL sampling location colored in accordance with the measured SF₆ concentration in parts per trillion by volume (ppt). The same maps also show colored contour lines representing concentrations normalized by the SF₆ release rate for the respective IOP (ppt s g⁻¹). These contour lines are shown to provide the reader with a means to compare normalized concentrations between IOPs. The color code for the markers is:

Gray	< 10 ppt
Purple	10-100 ppt
Blue	100-500 ppt
Green	500-1,000 ppt
Olive	1,000-5,000 ppt
Orange	5,000-10,000 ppt
Red	> 10,000 ppt

The color code for the normalized concentration contours is:

Purple	> 10 ppt s g ⁻¹
Blue	> 100 ppt s g ⁻¹
Green	> 500 ppt s g ⁻¹
Yellow	> 1,000 ppt s g ⁻¹
Orange	> 5,000 ppt s g ⁻¹
Red	> 10,000 ppt s g ⁻¹

Similarly, the aircraft maps show color-coded concentrations along the flight paths. The color code for the aircraft flight paths is:

Gray	< 10 ppt
Purple	10-100 ppt
Blue	100-300 ppt
Green	300-500 ppt
Olive	500-700 ppt
Orange	700-1,000 ppt
Red	> 1,000 ppt

For IOPs 1-3, several of the plots showing vertical concentration profiles at the towers at 201, 408, and 499 m also indicate a concentration with a round black marker. These were calculated by averaging concentrations along flight paths that intersected a restricted area around the arc sampling array in the approximate vicinity of the sampling towers. The average

concentration is assigned to the bag coinciding with the time of the flight path through the specified area. The estimated AGL height is shown directly on the plot and was derived from the onboard GPS. The mean latitude and longitude of each averaging interval is denoted on the zoomed in aircraft flight path maps by a symbol for each bag. The downwind distance indicated in the legends of the tower vertical concentration profiles was estimated from the location of these symbols on the aircraft maps. This aircraft data is included with the tower profiles to provide a crude estimate of the concentrations aloft corresponding to the tower profiles.

IOP1

Date/Time and General Description

IOP 1 was conducted on 02 October from 1430-1630 MST (1530-1730 MDT). Winds were very light and variable throughout IOP1 with mostly sunny conditions but filtered through patchy cirrostratus. Estimates of stability exhibit large uncertainty with respect to traditional Pasquill-Gifford (P-G) schemes. Overall conditions were highly non-stationary and the adverse wind directions made for generally poor tracer sampling. A summary of the meteorological conditions during IOP1 are shown in Table 19. The SF₆ release rate was 10.18 g s⁻¹ (Tables 1 and 2). The fast response analyzers were located on the 400 m arc at 25 and 55 degrees, on the 800 m arc at 25 and 55 degrees, on the 1600 m arc at 55 degrees, and on the airplane.

Table 19. Meteorological conditions during IOP1. Wind speeds, directions, σ_θ , and P-G stability class determinations (EPC, 200c) are from COC at 10 m. Solar radiation measurements are from FLX. R3 and R4 indicate sonic anemometer data from their respective locations.

Bag	Wind Speed (m s ⁻¹)	Wind Direction (deg)	Solar Radiation (W m ⁻²)	R3 u* (m s ⁻¹)	R4 u* (m s ⁻¹)	R3 z/L	R4 z/L	σ_θ (deg)	P-G SRDT	P-G σ_λ
1	1.8	115.5	146.0	0.19	0.22	-0.21	-0.18	22.0	D	B
2	1.8	160.3	155.0	0.10	0.17	-1.20	-0.40	21.4	D	B
3	1.5	165.8	174.0	0.10	0.12	-1.46	-0.70	16.8	D	C
4	1.2	94.3	175.0	0.17	0.11	-0.45	-0.82	52.9	B	A
5	1.1	235.2	170.0	0.07	0.14	-3.27	-0.43	63.0	D	A
6	1.0	162.2	154.0	0.20	0.05	-0.27	-12.60	67.4	D	A
7	1.0	301.7	137.0	0.14	0.11	-0.45	-0.68	29.0	D	A
8	1.1	240.6	119.5	0.04	0.10	-10.04	-1.17	22.1	D	B
9	1.2	71.3	122.0	0.07	0.11	-3.22	-0.76	31.1	D	A
10	1.5	103.7	121.5	0.08	0.13	-1.27	-0.33	26.7	D	A
11	1.6	82.7	116.5	0.12	0.16	-0.68	-0.21	17.7	D	B
12	1.0	84.2	151.0	0.11	0.14	-0.81	-0.38	40.3	D	A

Winds and Quality Assurance

Figure 64 shows wind speed and direction comparisons for ARLFRD data in the vertical at the GRI and COC towers for IOP1. Data for R1 was not available for this IOP due to data card failure. There was generally good agreement in wind speed and direction. The occasional slight shift of peak maxima/minima in the sonics (G1, G2) relative to the other GRI measurements is likely due largely to the comparison between plotting the end time of 5-minute averaging periods and the start time of 10-minute averaging periods. Wind speeds were light before, during, and after the tracer release period and were very low between about 1500-1530 h. All of the major deviations in wind direction with height occurred during very low wind periods. The periods with the lightest winds were associated with very large σ_{θ} (Fig. 65).

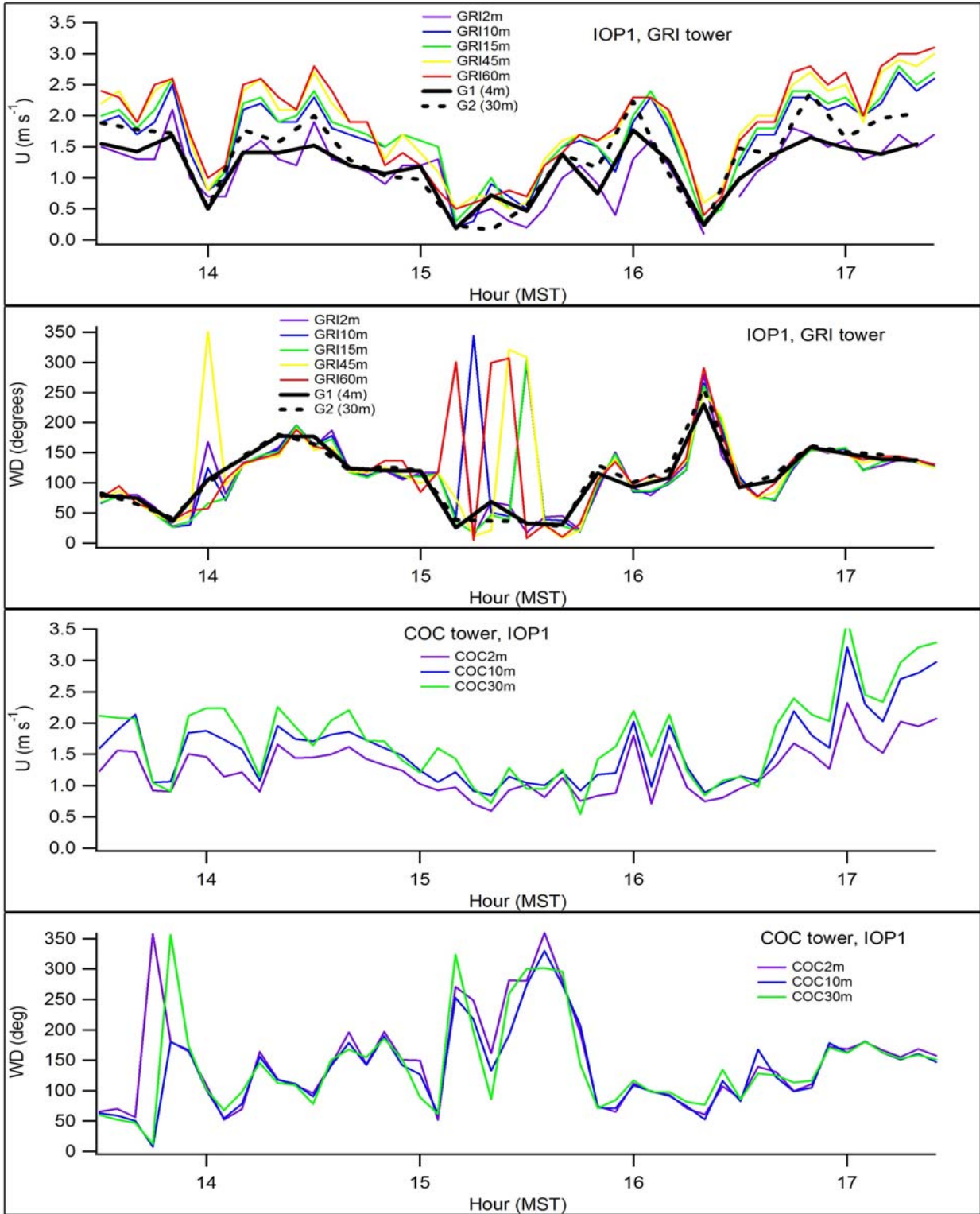


Figure 64. ARLFRD wind speed and direction comparisons in the vertical at GRI and COC for IOP1.

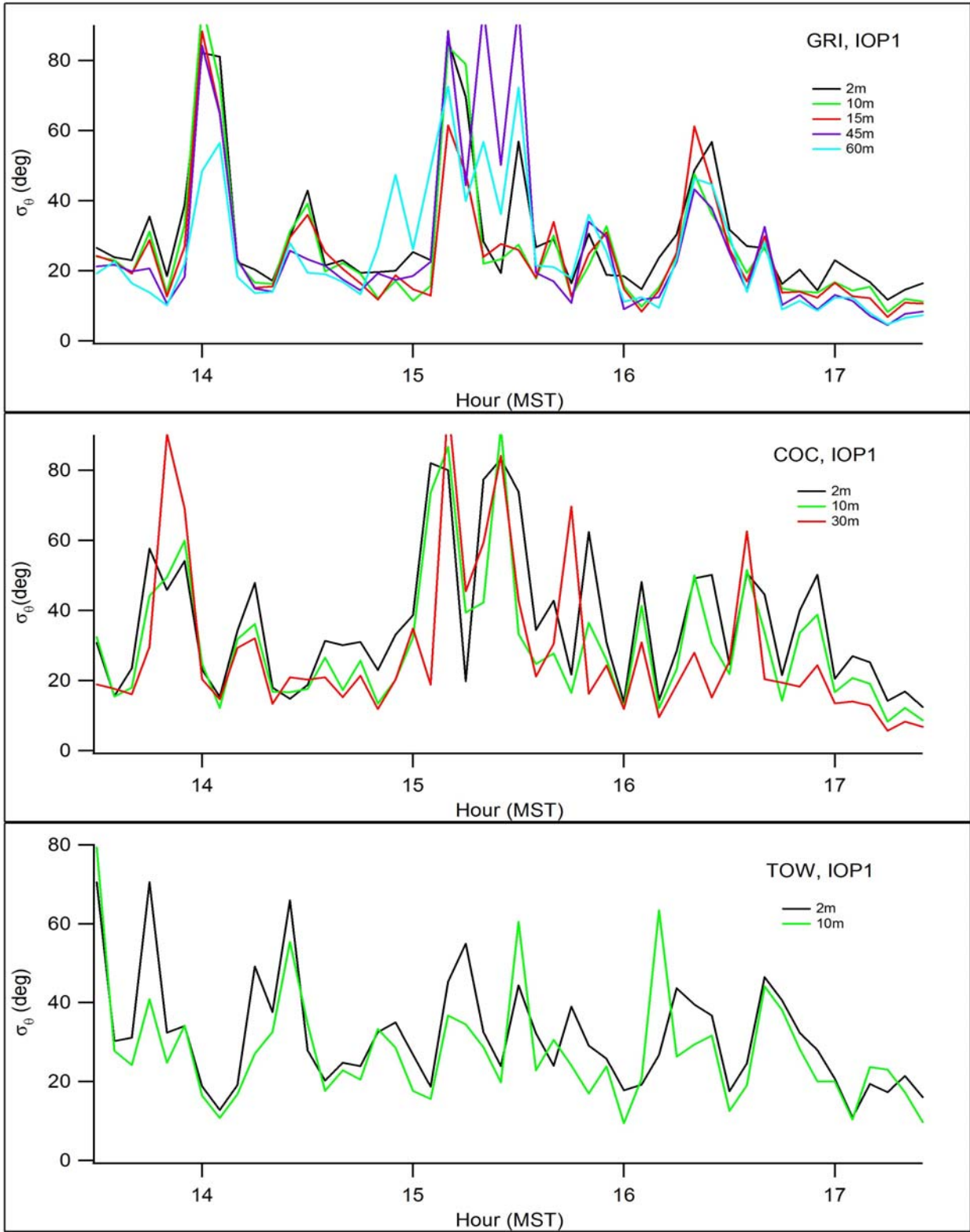


Figure 65. Standard deviation in wind direction σ_θ (σ_A) using the wind vanes at GRI, COC, and TOW for IOP1.

Figures 66-68 show wind speed and direction comparisons in the horizontal across the study area at 2 m, 10 m, 30 m, 45 m, 60 m, and 160 m from the data available. These comparisons included the sonic anemometers; cup anemometers and wind vanes at GRI, COC and TOW; the ASC and ART sodars; and the PRO wind profiler. In some cases heights were compared if they were close. For example, 2 m cup and vane results at GRI and COC were compared with sonic results at 3 m (R2, R3, and R4) and 4 m (G1) and 40 m sonic results for ASC and ART were compared to 45 m anemometer results at GRI. The ASC sodar did not have any data recovery at the 160 m level during the test. Measurements were largely consistent with each other at all heights with few exceptions. These include wind direction variation with height in very low wind speed conditions and a distinct low bias in PRO wind speeds at 160 m. With the possible exception of the latter point, there is little evidence for a problem with the measurements.

It is apparent that the wind directions were very poor for the sampling of the tracer across the bag sampling array. Winds were E and SE for much of the tracer release period (1430-1630 h). There were periods between about 1500-1540 h during which the wind direction was a little more optimal but varied erratically from S through WNW at different sites across the study area. Again, this variation was mostly associated with the periods having the lightest wind speeds. In no way was the variation in wind direction uniform as the flow displayed temporal and spatial inhomogeneities in both the vertical and horizontal across the study area. During IOP1 only two sampling periods (bags 5 and 8) had average wind directions appropriate for advecting the tracer across the ground sampling array, as measured at the COC 10 m level. Other wind sampling locations did not indicate agreement.

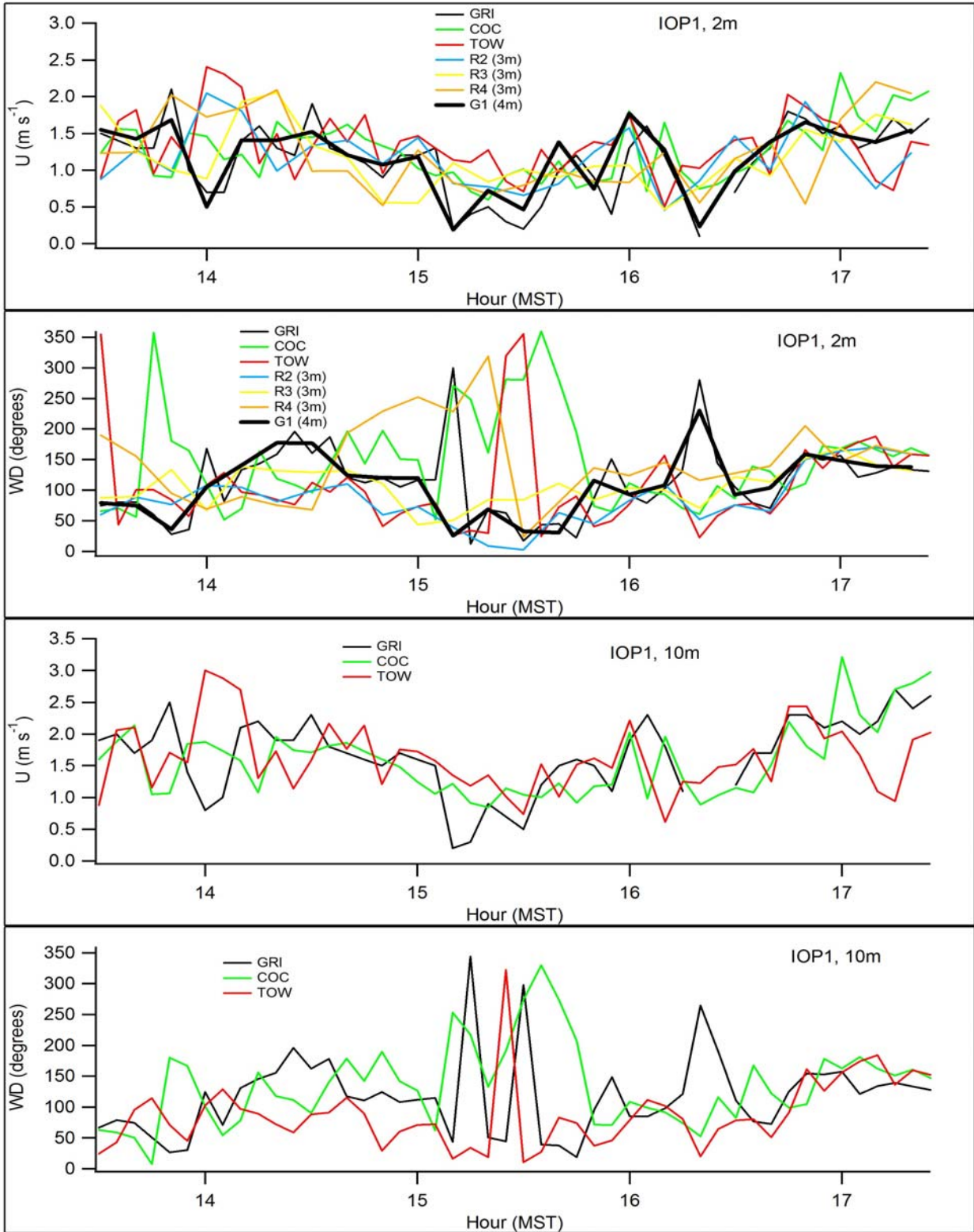


Figure 66. ARLFRD wind speed and direction comparisons in the horizontal at 2 and 10 m during IOP1.

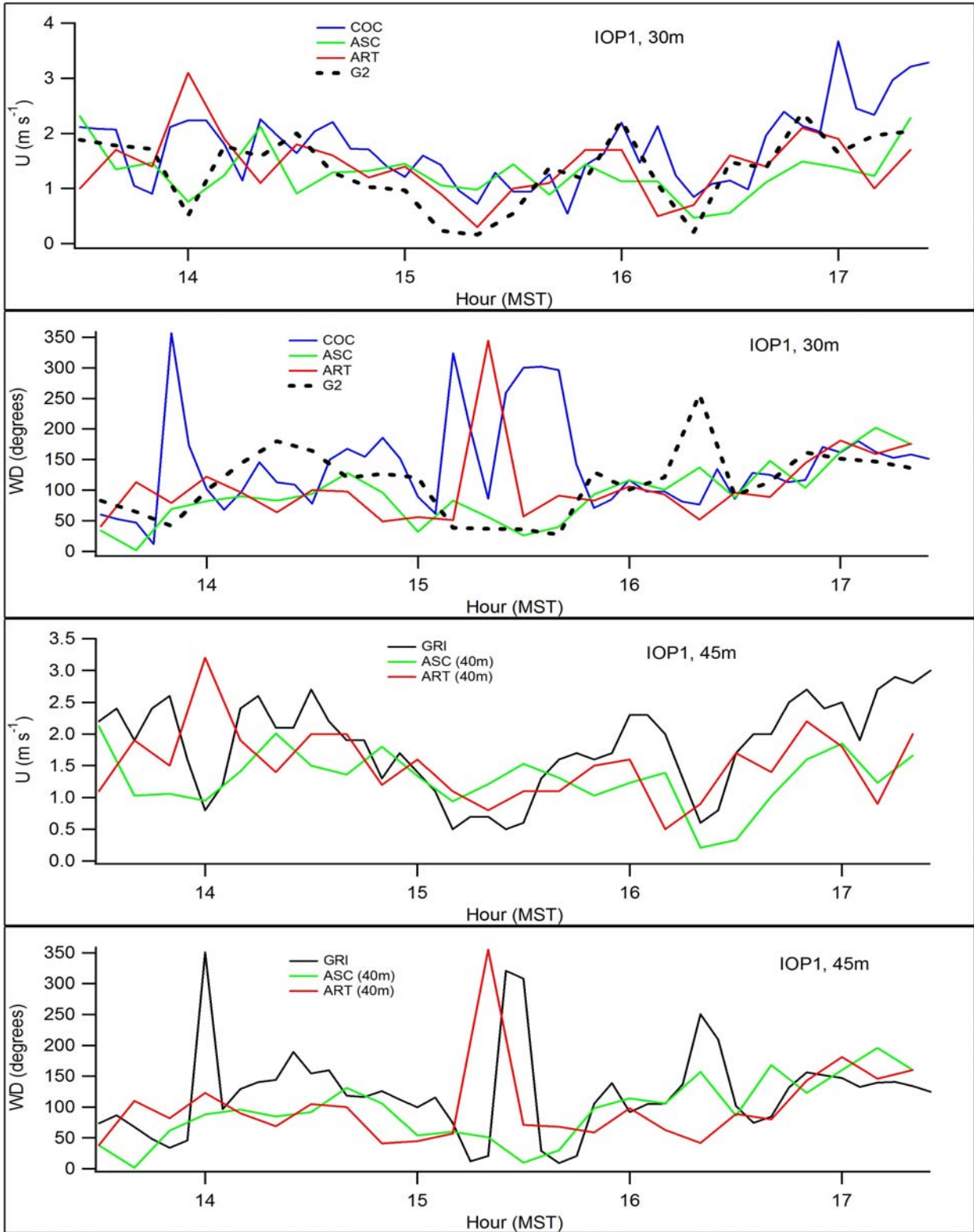


Figure 67. ARLFRD wind speed and direction comparisons in the horizontal at 30 and 45 m during IOP1.

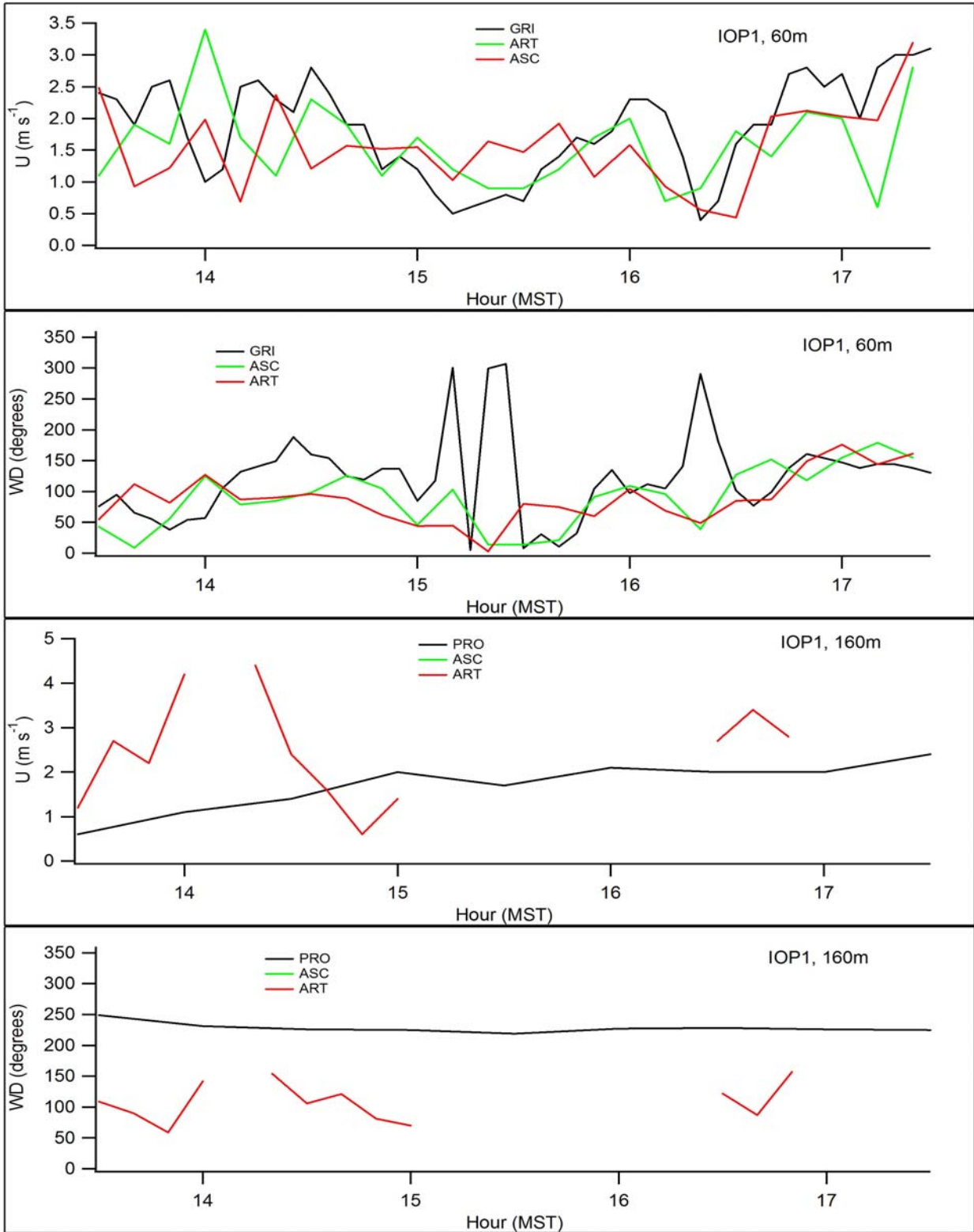


Figure 68. ARLFRD wind speed and direction comparisons in the horizontal at 60 and 160 m during IOP1.

Figures 69-71 show time-height cross-sections for wind speed and direction for the ASC sodar, ART sodar, and PRO wind profiler, respectively. All of these measurements are consistent with other measurements of low wind speeds in the lower atmosphere. The PRO measurements suggest the presence of a prominent wind shear layer at about 1.2-1.4 km height although data recovery was sparse for the layer just above that height. In any case, the PRO wind speeds below 5 m s^{-1} are suspect.

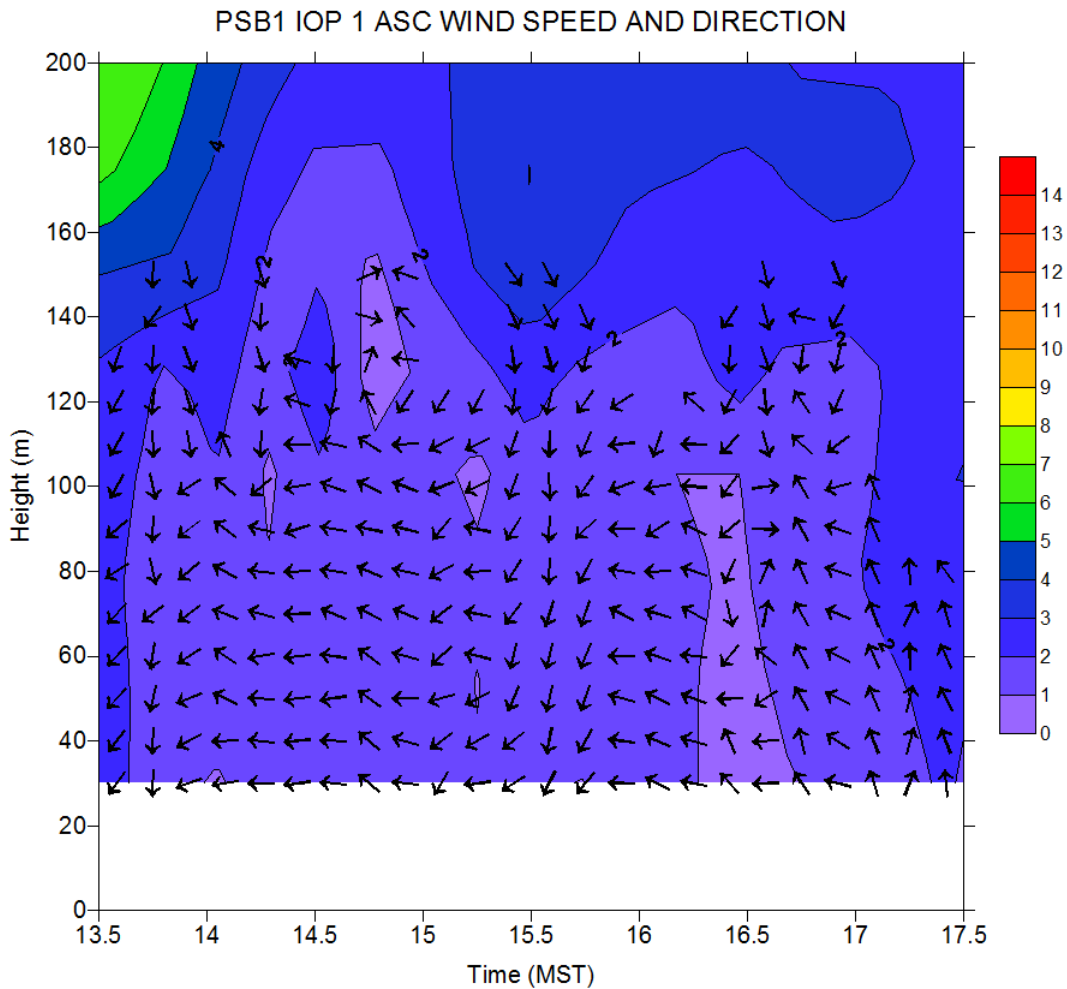


Figure 69. Time-height cross-section of wind speed and direction at ASC sodar during IOP1.

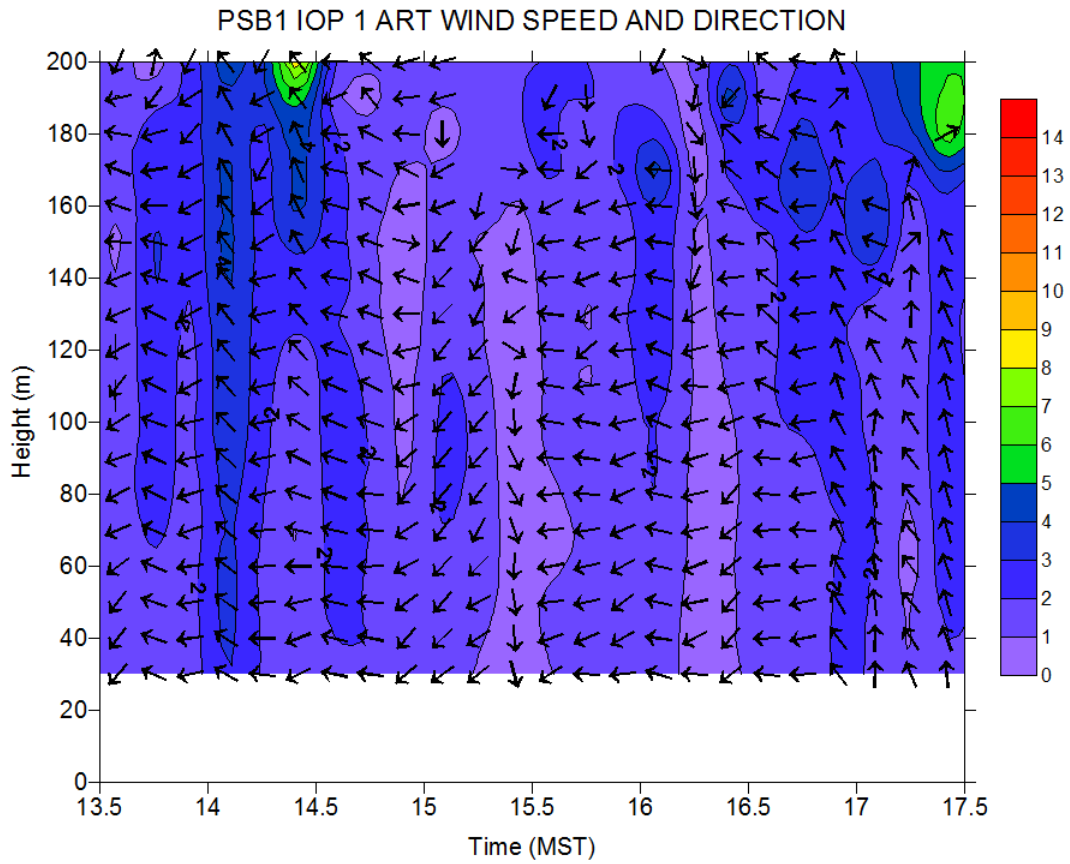


Figure 70. Time-height cross-section of wind speed and direction at ART sodar during IOP1.

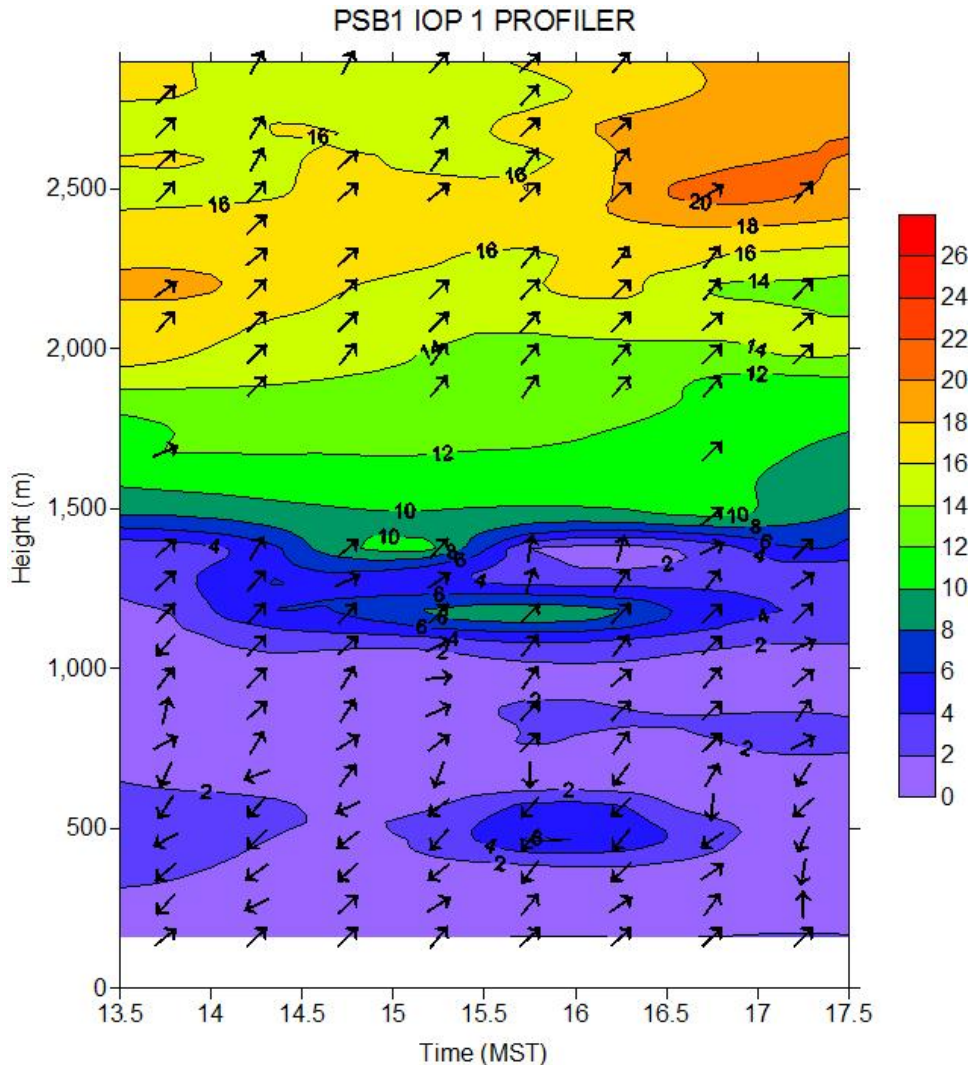


Figure 71. Time-height cross-section of wind speed and direction at wind profiler (PRO) during IOP1.

Turbulence

Figures 72 and 73 show time series of the turbulence measurements for 10 and 30-minute averaging periods, respectively, for σ_w , turbulent kinetic energy (TKE), u^* , kinematic heat flux $\langle w'T \rangle$, and $1/L$ where L = Obukhov length. The 30-minute periods more correctly account for nonstationarity effects and should provide more reliable estimates than the 10-minuted averaging periods. The very low wind speed periods were associated with some very low values for TKE and u^* . Measurements were largely consistent with each other and there no apparent evidence for a problem with them. The high values of σ_w at G2 are due to the fact these represent measurements at 30 m whereas all the other measurements are between 3-4 m height.

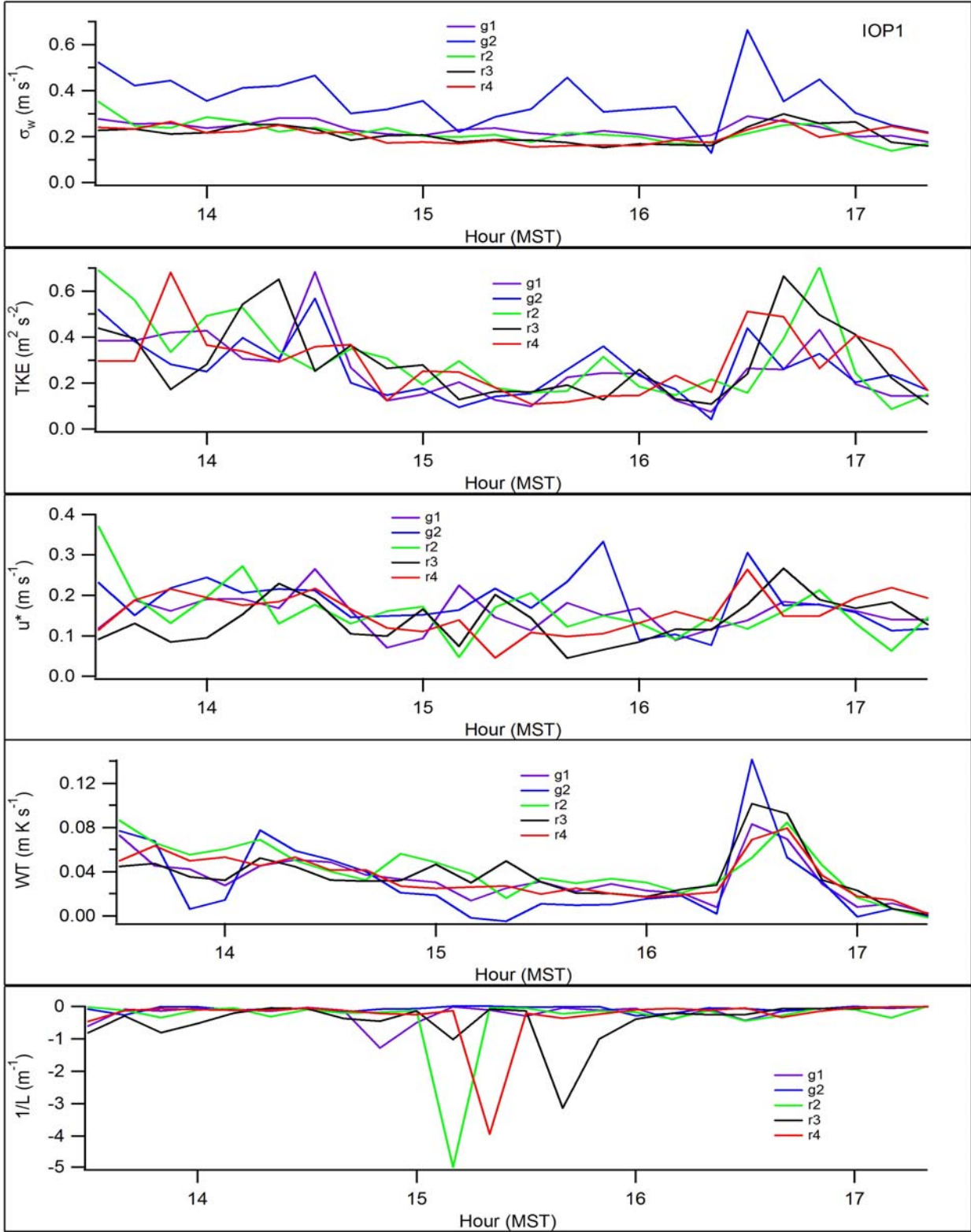


Figure 72. ARLFRD sonic anemometer 10-minute averages for σ_w , TKE, u^* , kinematic heat flux, and $1/L$ during IOP1 (G1, G2, R2, R3, and R4).

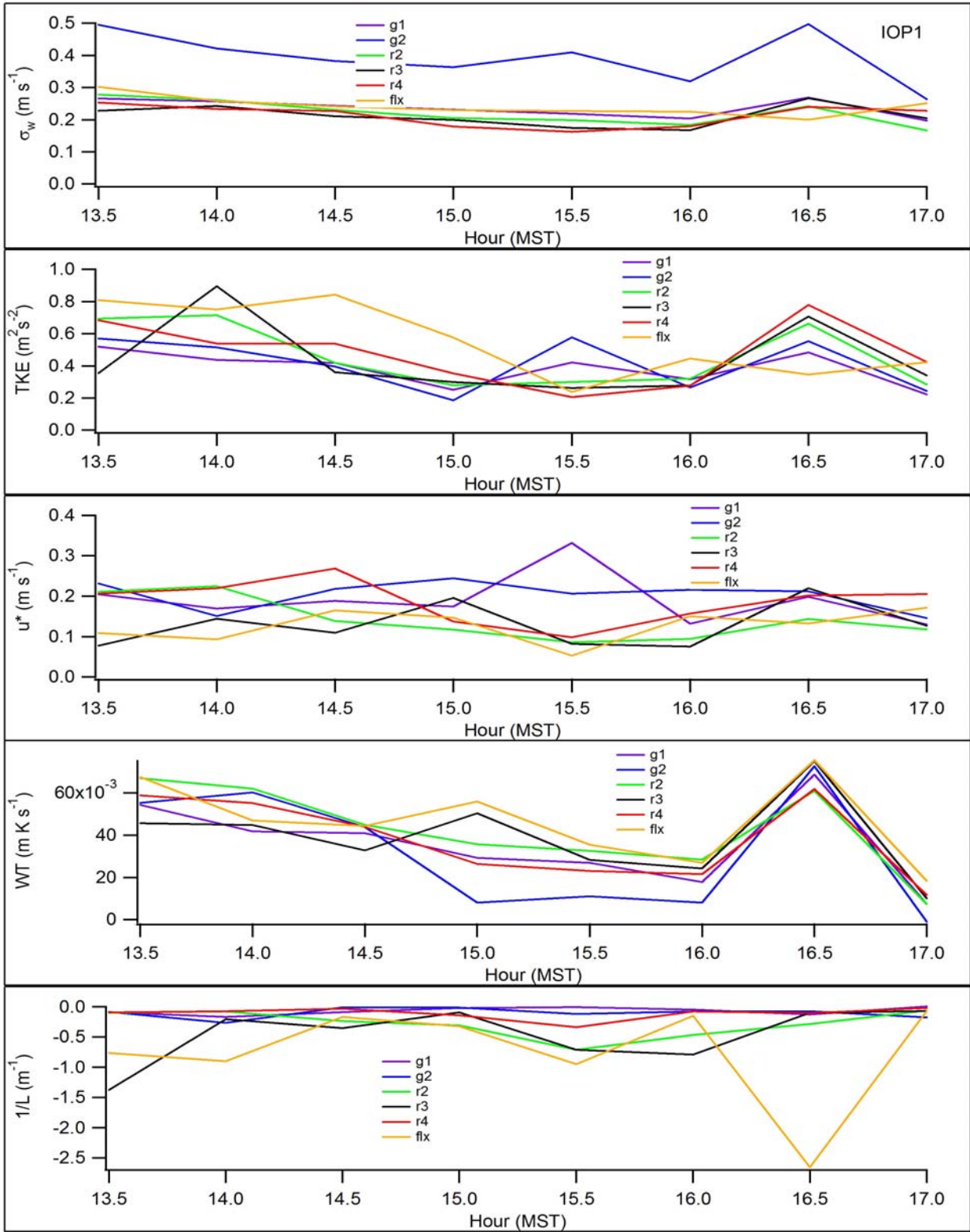


Figure 73. ARLFRD sonic anemometer 30-minute averages for σ_w , TKE, u^* , kinematic heat flux, and $1/L$ during IOP1 (G1, G2, R2, R3, R4, and FLX).

Figures 74 and 75 show time-height cross-sections for σ_w and TKE for the ASC sodar. Figures 76 and 77 show time-height cross-sections for σ_w and TKE for the ART sodar. The absolute magnitudes of TKE and σ_w shown for the ART and ASC sodars should not be assumed to be comparable between the two sodars nor with the same measurements at the sonic anemometers. The magnitudes of σ_w at ASC and ART are usually similar but the values of TKE at the ART were typically about an order of magnitude greater than the ASC. Restricting the comparison to the relative magnitudes of TKE and σ_w for each sodar, within an IOP or across IOPs, should be valid.

The σ_w and TKE values for both the ASC and ART during IOP1 were the lowest of all the IOPs. The minima in turbulence at ART and ASC are roughly consistent in time with those measured at the sonic anemometers and the period when the tracer plume was most consistently over the sampling array. Figure 78 shows a time-height cross-section for temperature from the RASS.

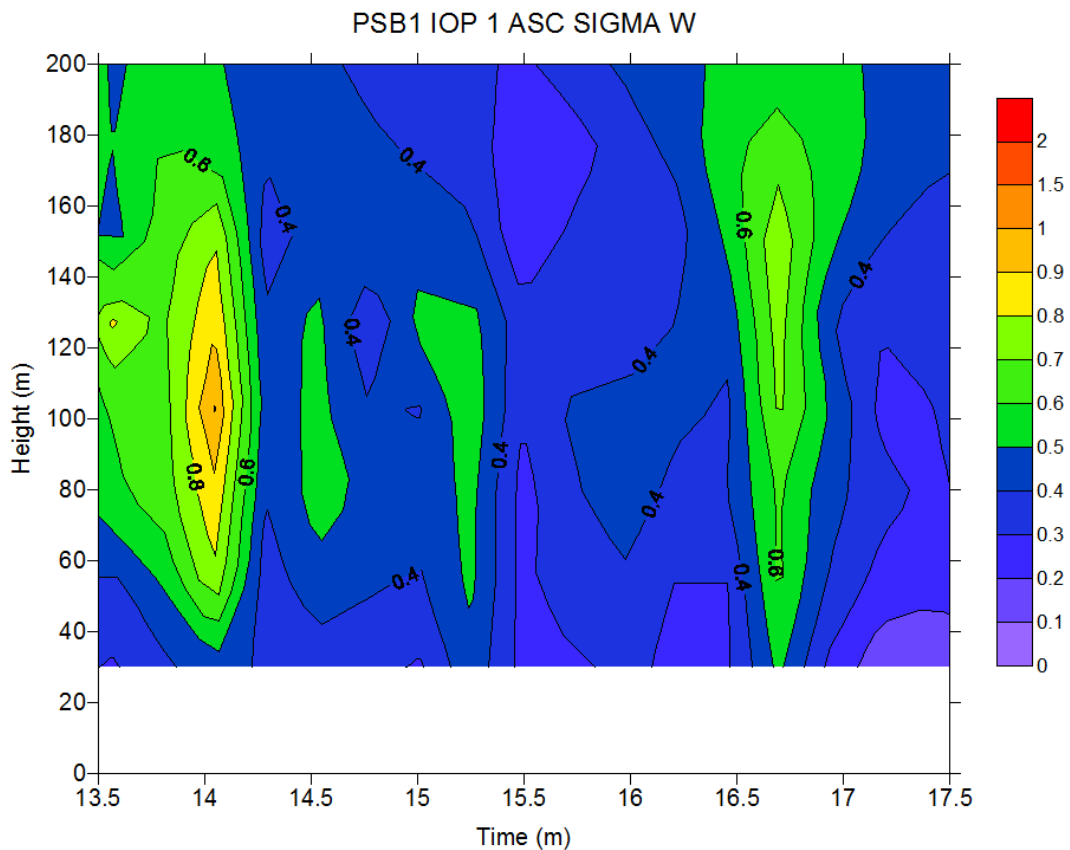


Figure 74. Time-height cross-section of σ_w at ASC sodar during IOP1.

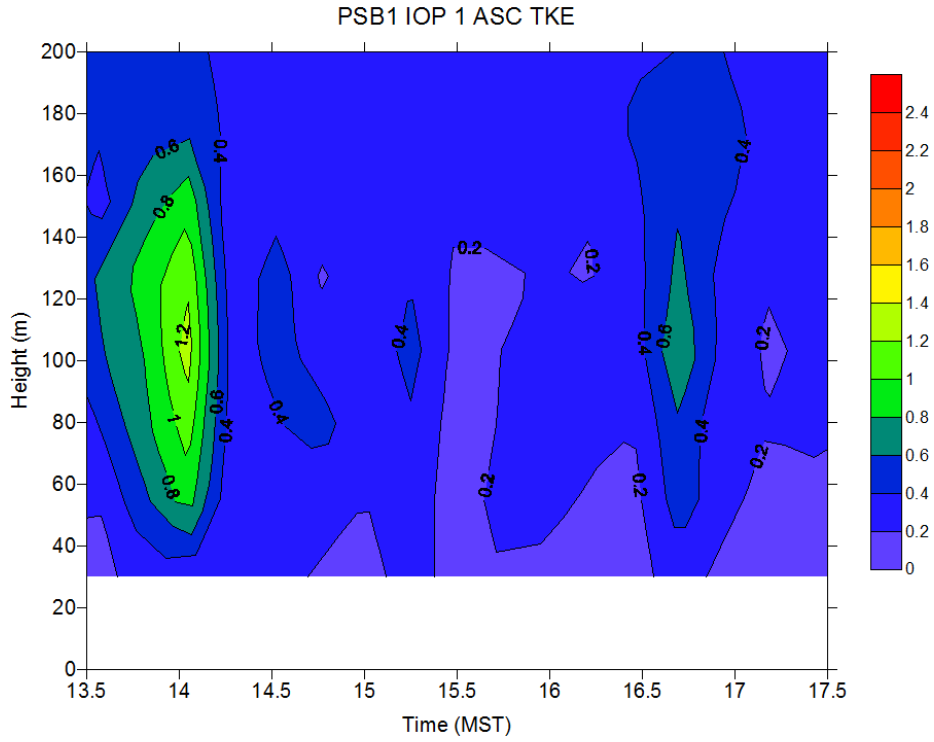


Figure 75. Time-height cross-section of TKE at ASC sodar during IOP1.

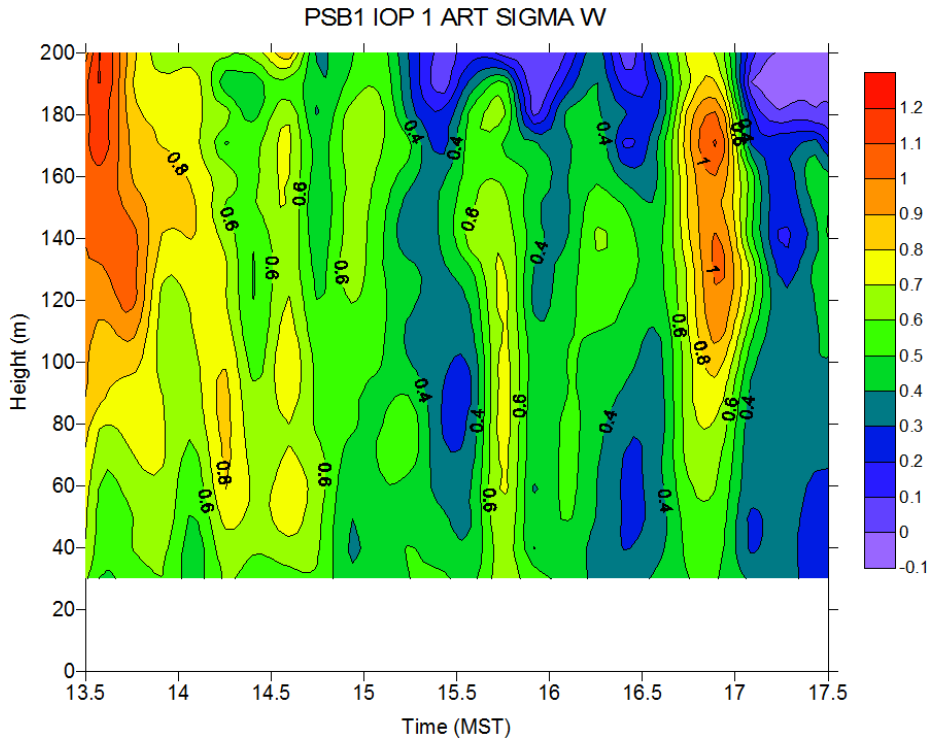


Figure 76. Time-height cross-section of σ_w at ART sodar during IOP1.

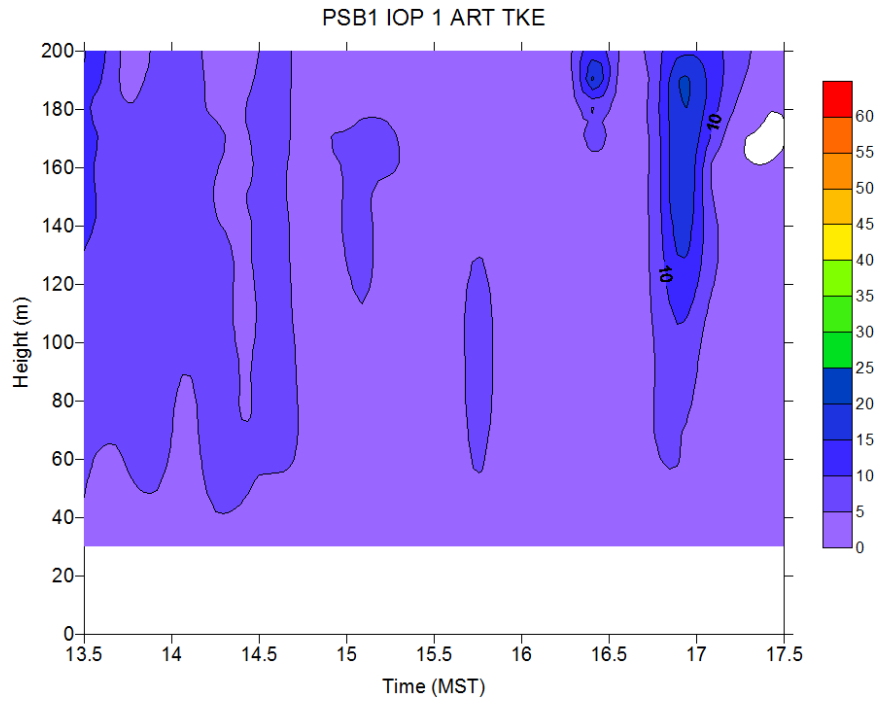


Figure 77. Time-height cross-section of TKE at ART sodar during IOP1.

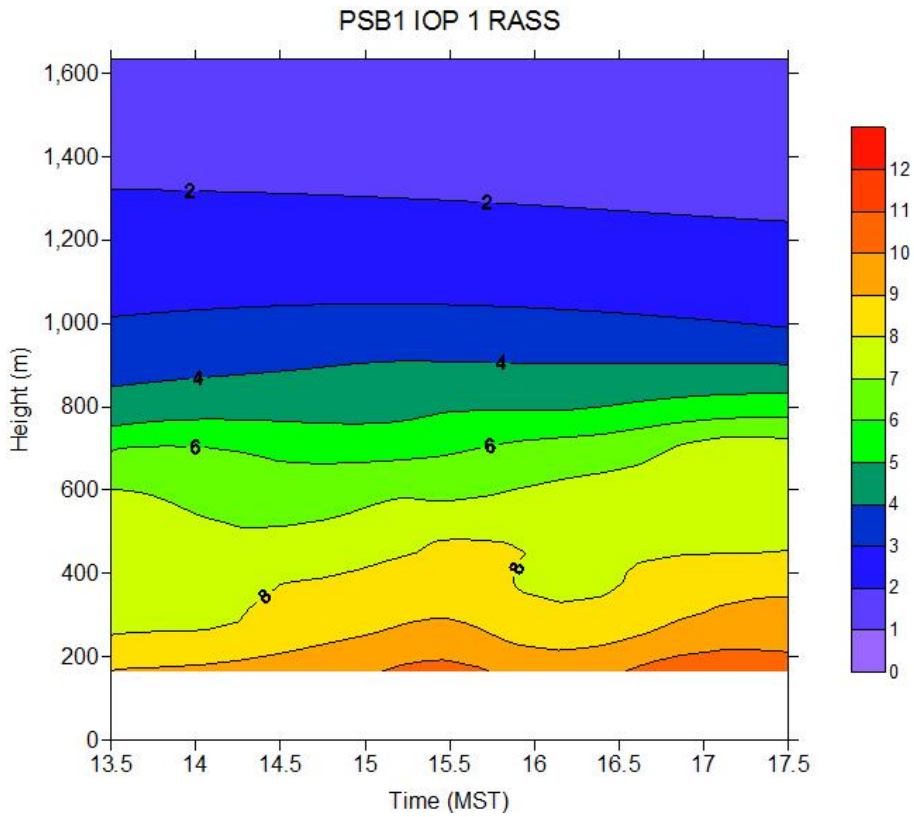


Figure 78. Time-height cross-section of virtual temperature at the RASS during IOP1. Temperatures are in degrees C.

Vertical profiles of wind speed, wind direction, and calculated turbulence parameters from sonic anemometer measurements at GRI during IOP1 are shown in Figs. 79-81. Vertical profiles of wind speed, wind direction, and σ_θ from cup anemometers and wind vanes plus aspirated air temperature during IOP1 are shown in Figs. 82 and 83. Turbulence intensities were large (σ_v/U for sonic anemometers (Slade, 1968) or σ_θ in radians for cup anemometers with wind vanes). The wind speed measurements at the 8 m sonic appear to be sometimes biased low. Wind speeds and turbulence intensities measured by sonic anemometers and wind vanes (σ_θ) anemometers were mostly consistent in spite of the very light winds.

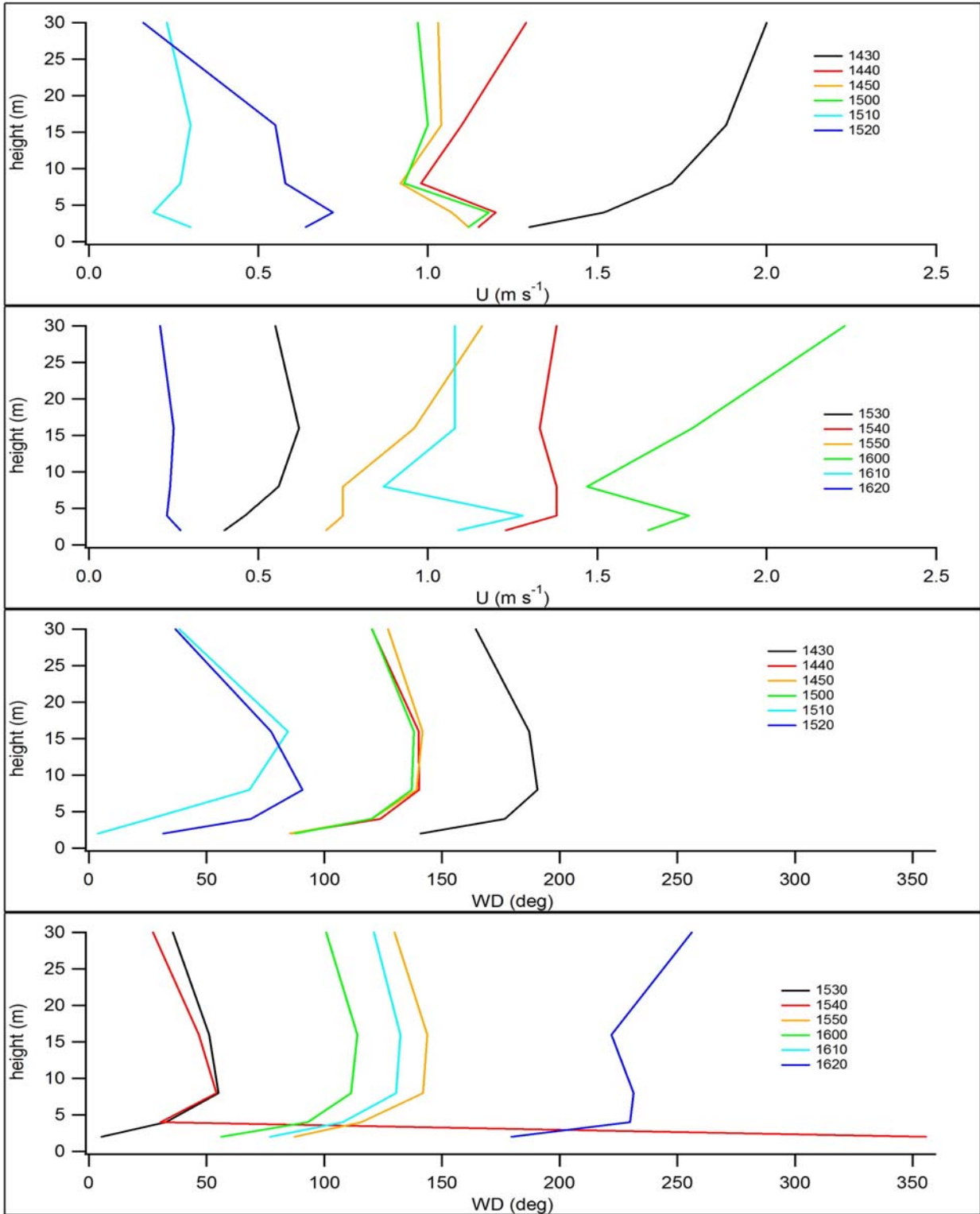


Figure 79. Vertical profiles of wind speed and direction from sonic anemometer measurements at GRI during IOP1. ARLFRD instruments were at 4 and 30 m; WSULAR instruments were at 2, 8, and 16 m. Times in legend are start times for the 10 minute interval (hhmm MST).

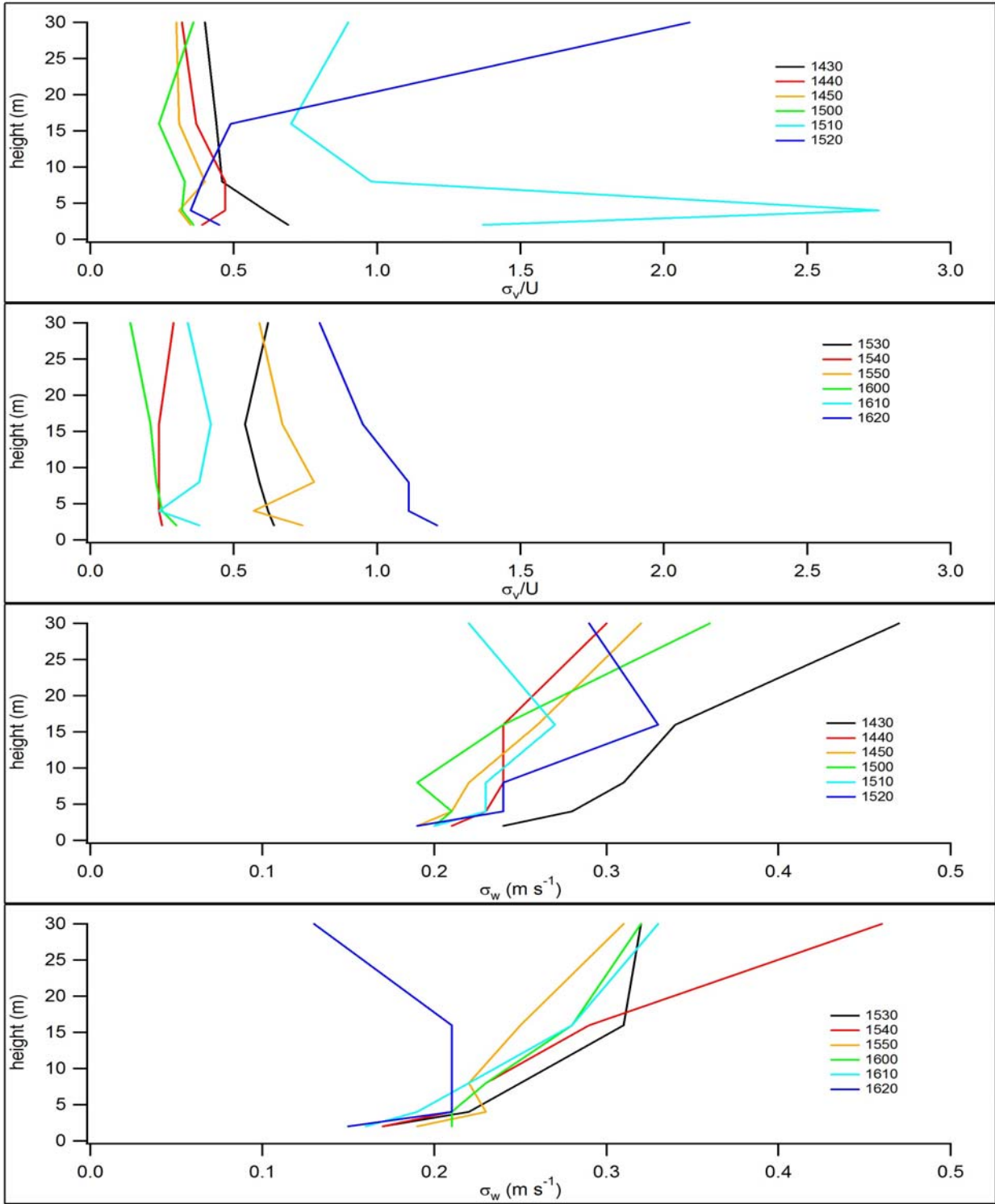


Figure 80. Vertical profiles of turbulence intensity and σ_w from sonic anemometer measurements at GRI during IOP1. ARLFRD instruments were at 4 and 30 m; WSULAR instruments were at 2, 8, and 16 m. Times in legend are start times for the 10 minute interval (hhmm MST).

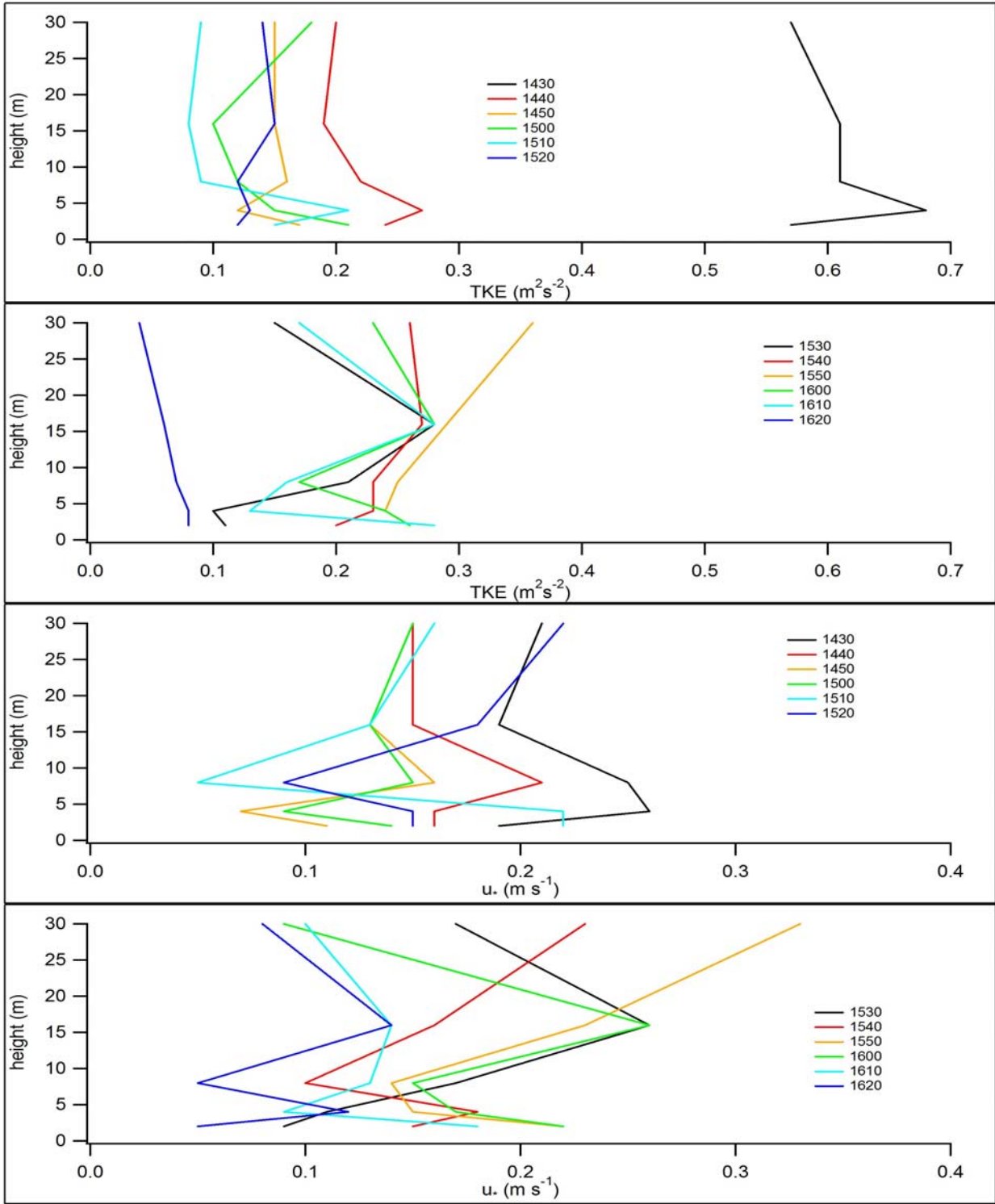


Figure 81. Vertical profiles of turbulent kinetic energy (TKE) and u^* from sonic anemometer measurements at GRI during IOP1. ARLFRD instruments were at 4 and 30 m; WSULAR instruments were at 2, 8, and 16 m. Times in legend are start times for the 10 minute interval (hhmm MST).

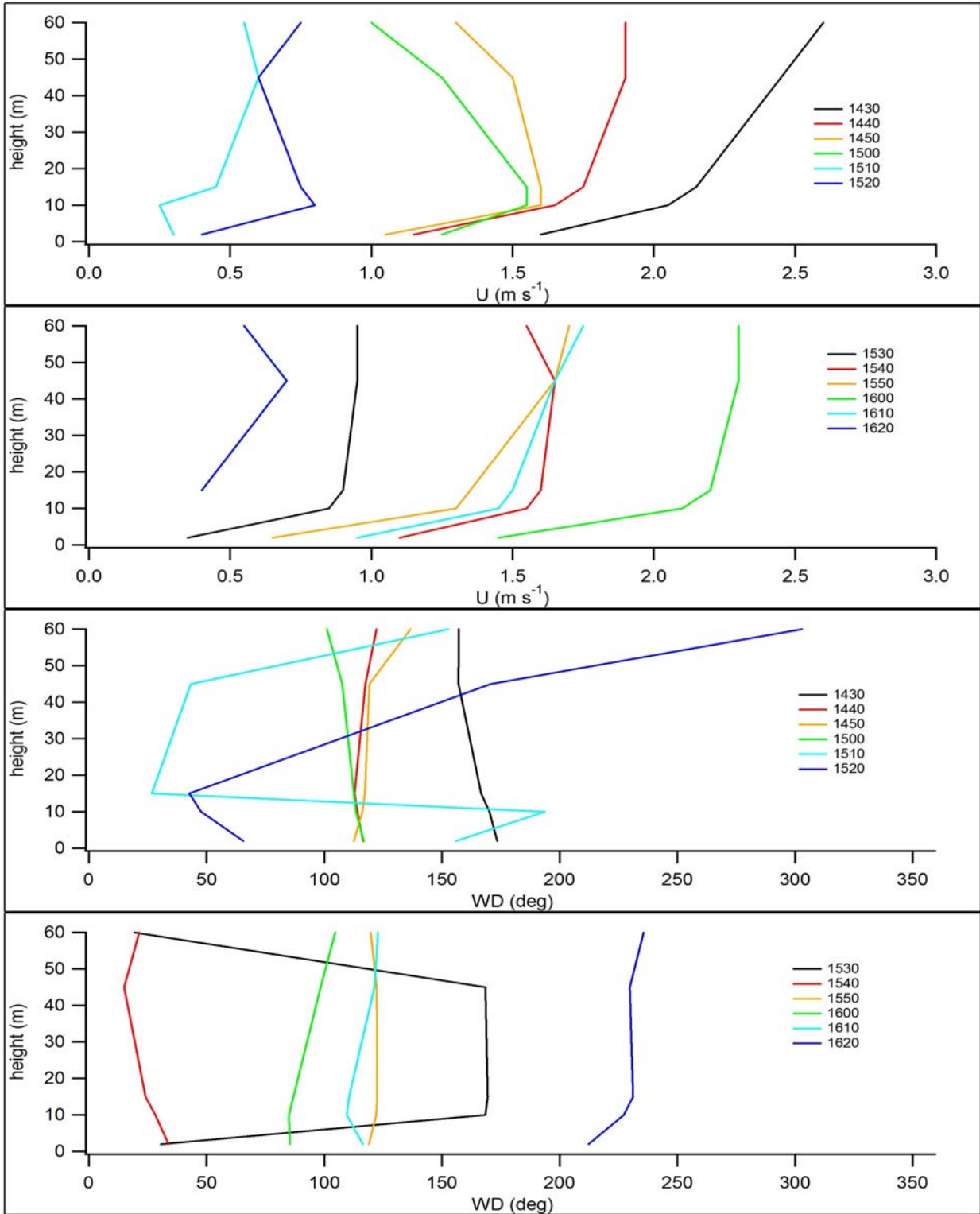


Figure 82. Vertical profiles of wind speed and direction from cup anemometer and wind vane measurements at GRI during IOP1. Times in legend are start times for the 10 minute interval (hhmm MST).

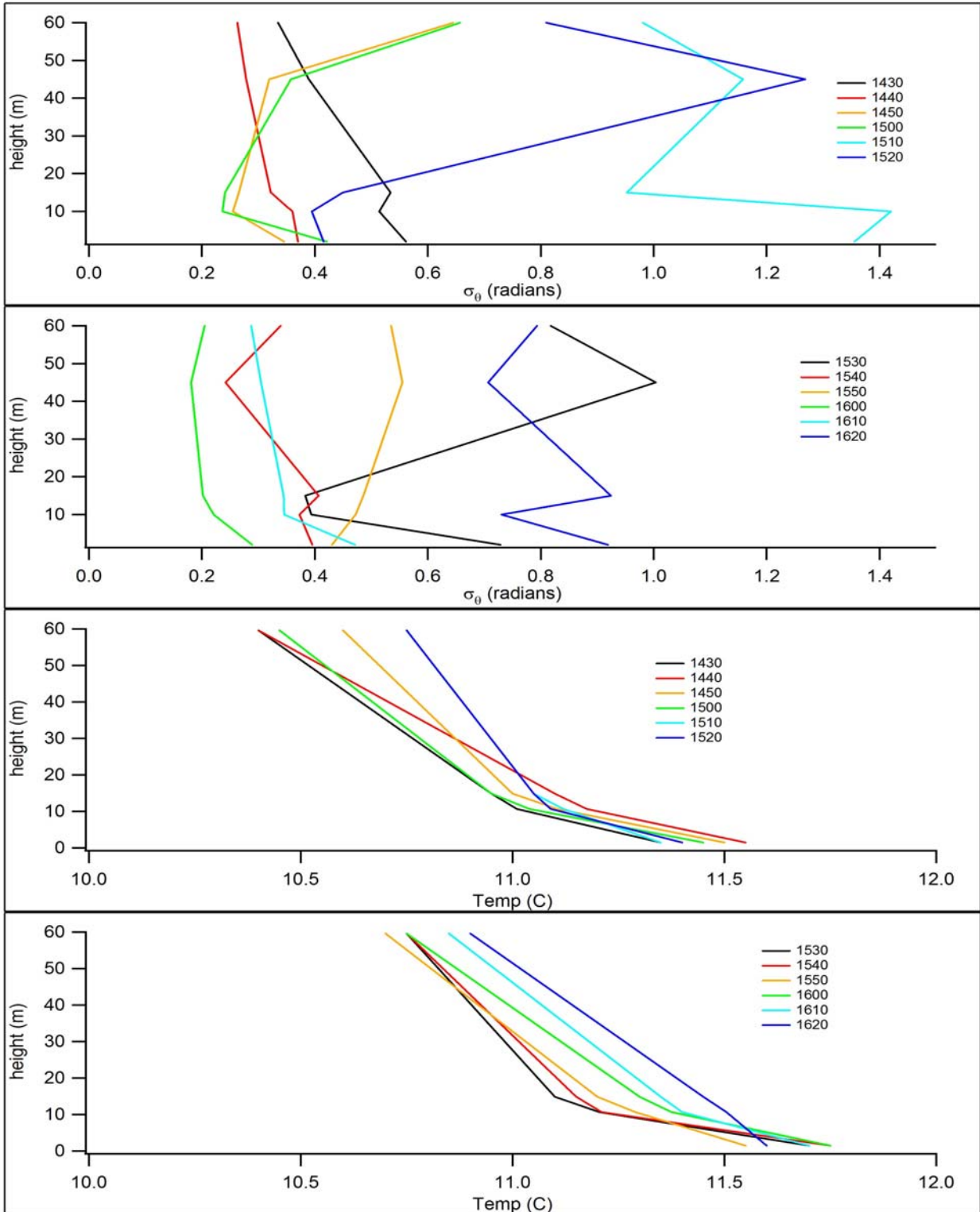


Figure 83. Vertical profiles of σ_θ (from cup and vane) and aspirated air temperature measurements at GRI during IOP1. Times in legend are start times for the 10 minute interval (hhmm MST).

Stability

The Pasquill-Gifford (P-G) stability category was determined using the Solar Radiation Delta-T (SRDT) and σ_θ (also denoted σ_A) methods (EPA, 2000c). The two methods gave very different results for stability category (Table 19). The SRDT method yielded almost all category D and the σ_A method yielded almost all categories A and B. The former method utilizes solar radiation in combination with wind speed in while the latter utilizes σ_θ in combination with wind speed. The relatively large magnitude negative z/L stability parameter values are more consistent with the σ_A method results while the relatively low solar radiation values would be more consistent with the SRDT method results.

Radiosonde Results

Figures 84 and 85 show potential temperature and specific humidity profiles from radiosonde measurements pre and post IOP1. The mixing depths estimated from these plots are given in Table 18.

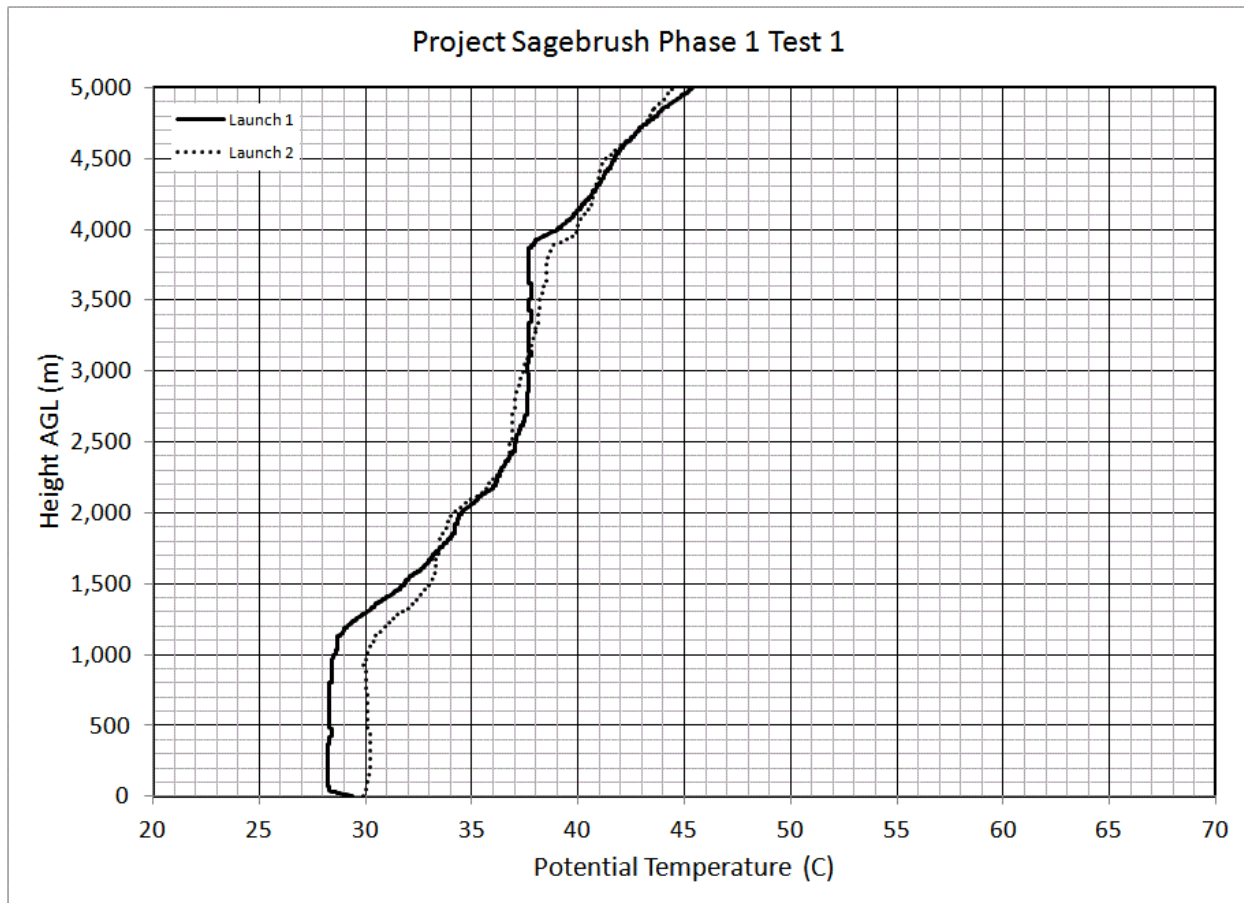


Figure 84. Pre and post IOP radiosonde potential temperature profiles for IOP1.

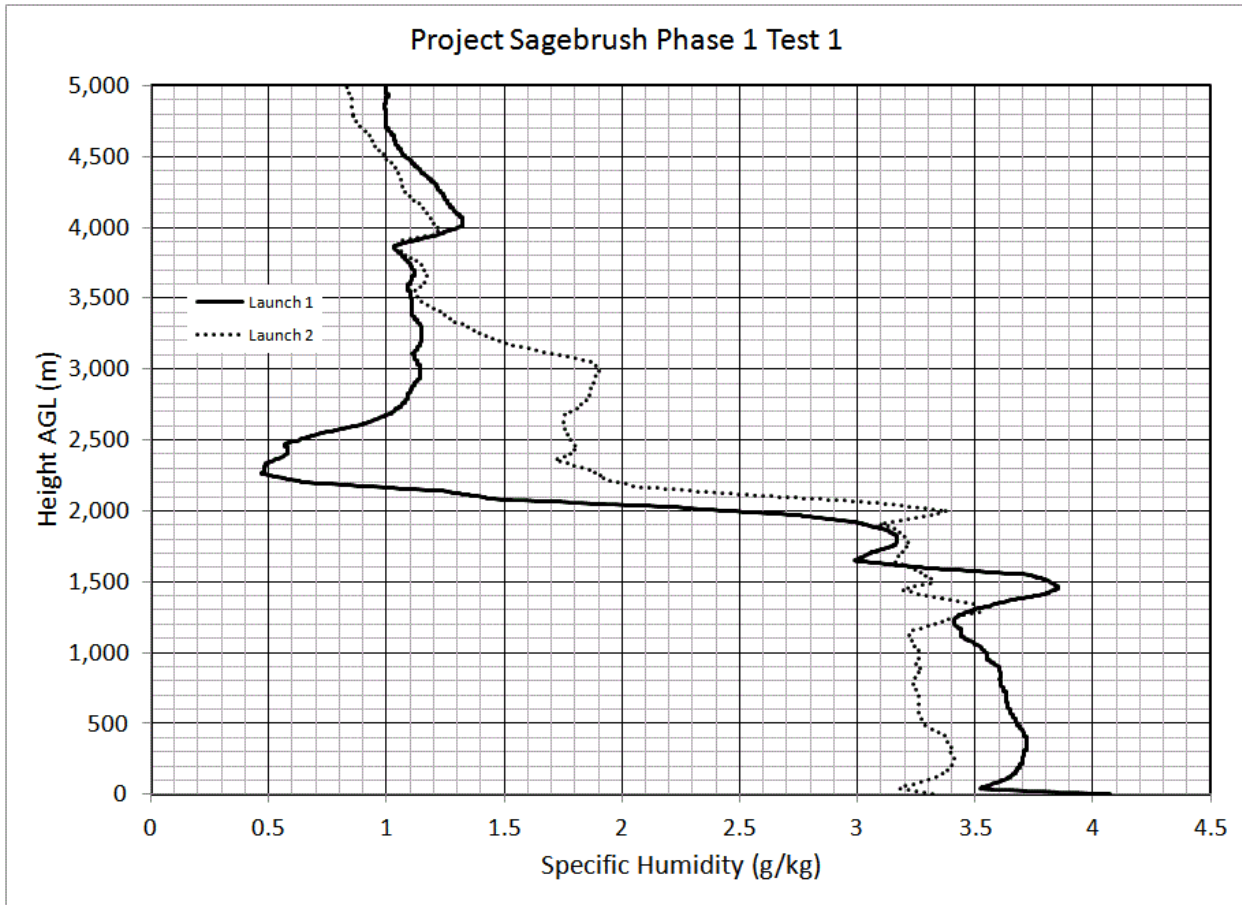


Figure 85. Pre and post IOP radiosonde specific humidity profiles for IOP1.

Concentration Results and Analysis

Figures 86 a-l show the bag sampling results for IOP1. As noted above, wind directions were adverse for most of IOP1 and this is reflected in the large number of bag samplers that only measured background concentrations (gray). The plume was marginally on the grid for only bags 5-9 (1510-1600 MST) and both measured and normalized concentrations were generally low throughout the IOP.

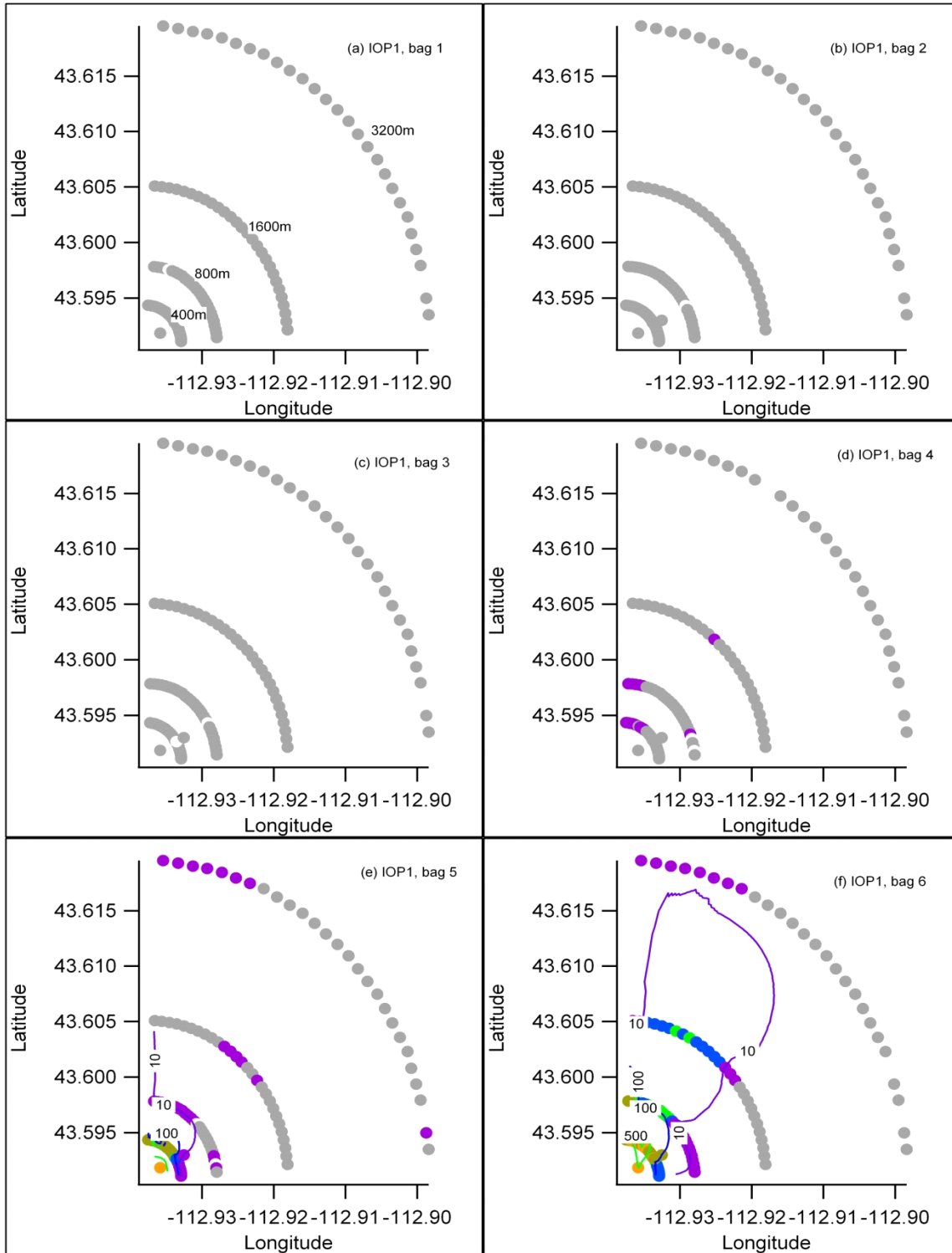


Figure 86. Bag sampling results (a-f, bags 1-6) for IOP1 with color-coded concentration markers for each 1 m AGL bag sampling location and contour lines of normalized concentration. The color scheme for the markers and contours is described in the Introduction to this section.

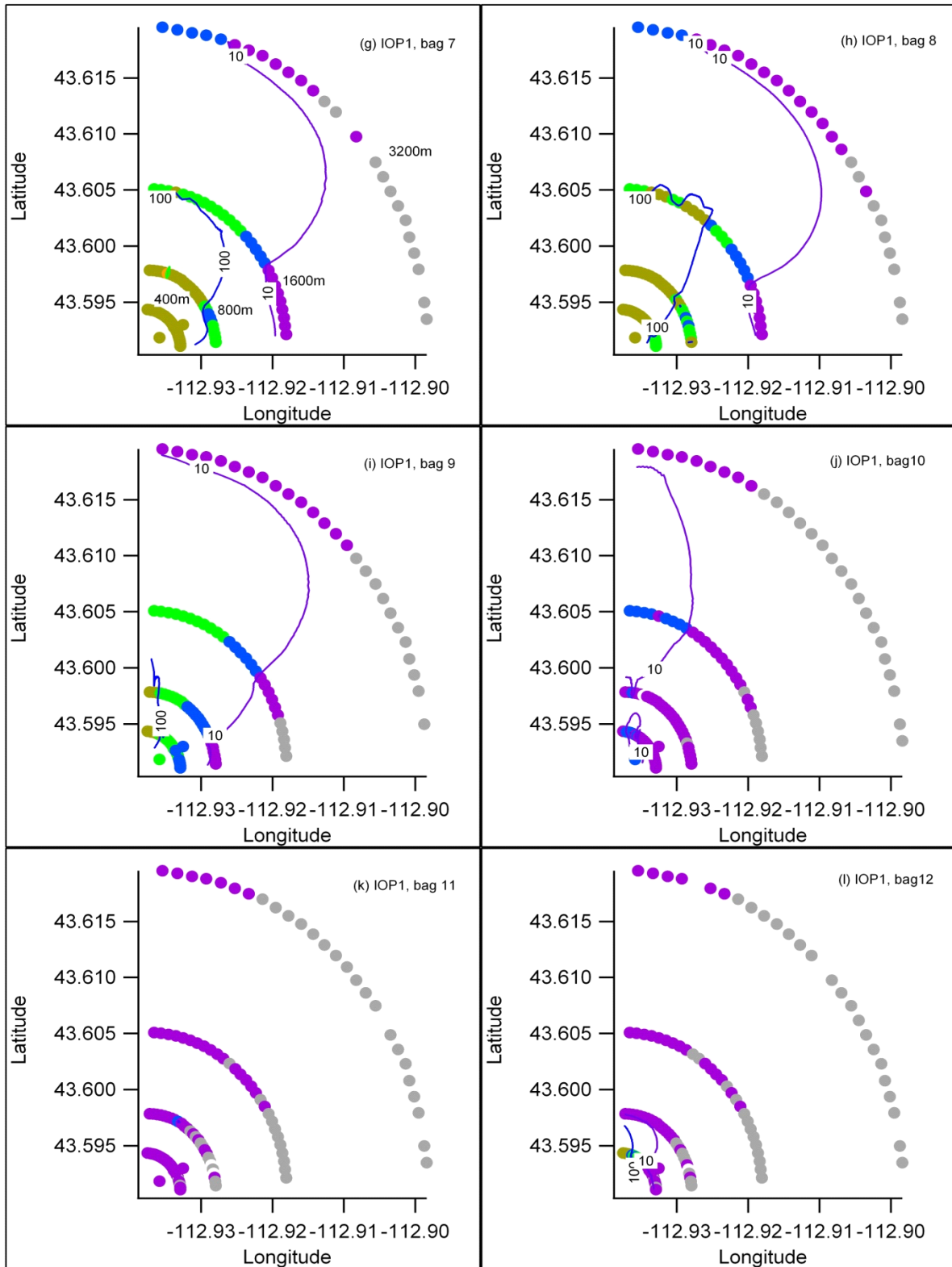


Figure 86 continued (g-l, bags 7-12).

Figures 87 a-l show cross-sections of tracer concentration along each arc for each 10-minute bag sampling period during IOP1. It is apparent that the plume, when present on the sampling array during IOP1, tended to be very broad. Several profiles were truncated at the edge of the sampling array. The broadness of the plume is consistent with the large observed values of σ_θ (Table 19). That result would also tend to be more consistent with the z/L values and the P-G σ_A method result than the P-G SRDT method result for stability.

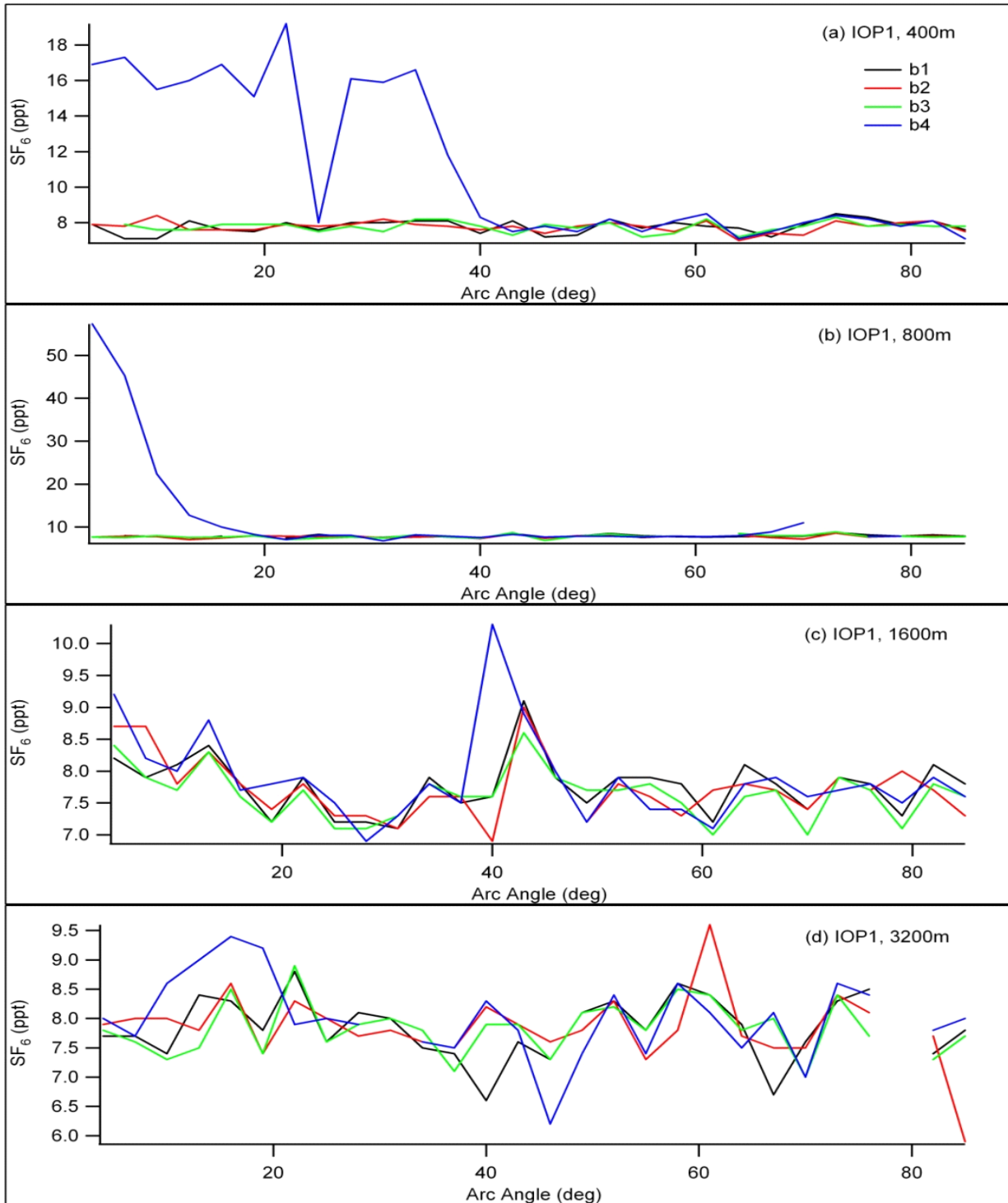


Figure 87. Cross-sections of concentration along each arc for each 10-minute bag sampling period during IOP1. The individual plume cross-section layouts are arranged to illustrate the variation in time, across 40 minutes per layout (bags 1-4), and the simultaneous variation with distance across all four arcs.

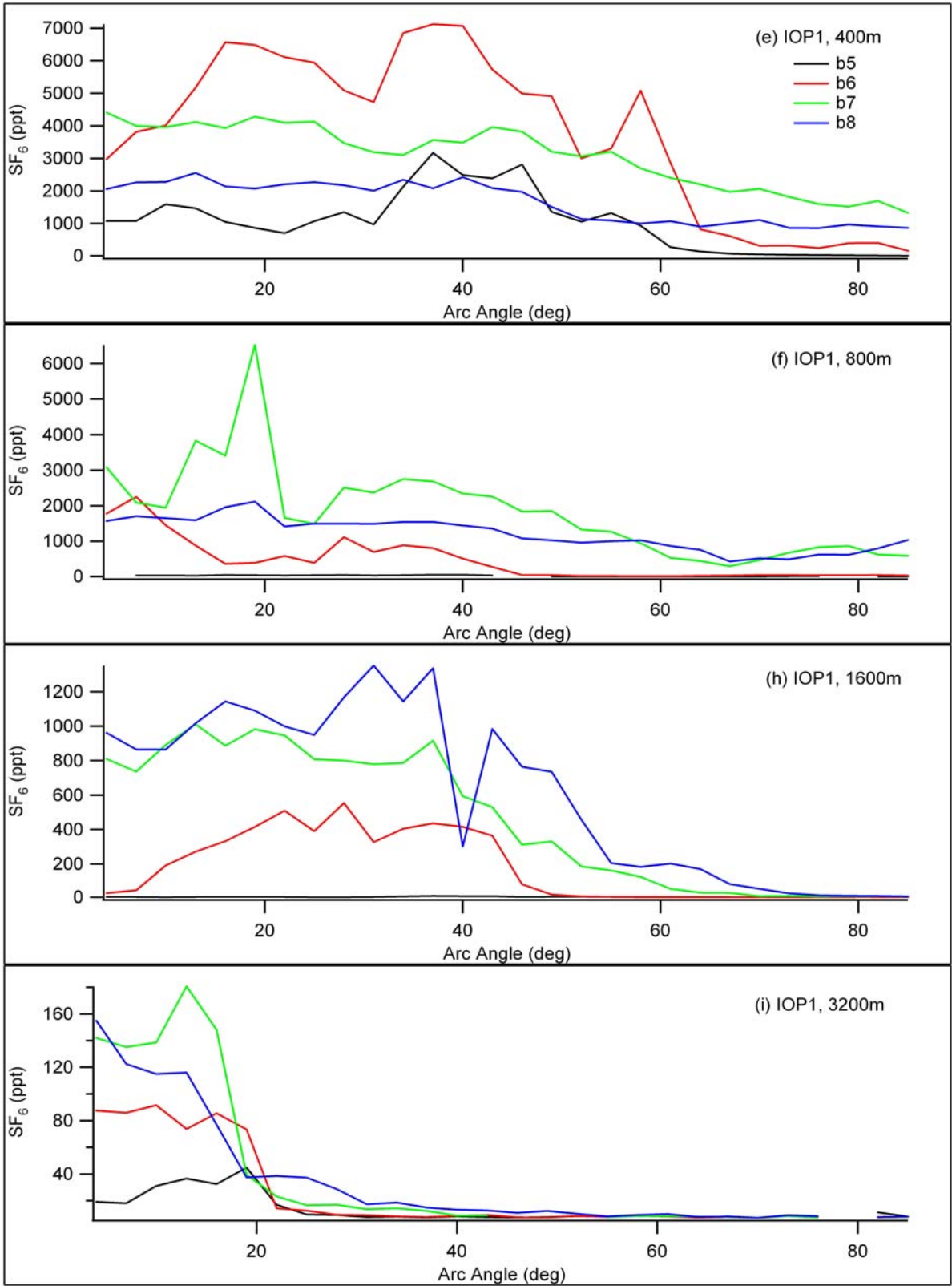


Figure 87 continued (e-h, bags 5-8).

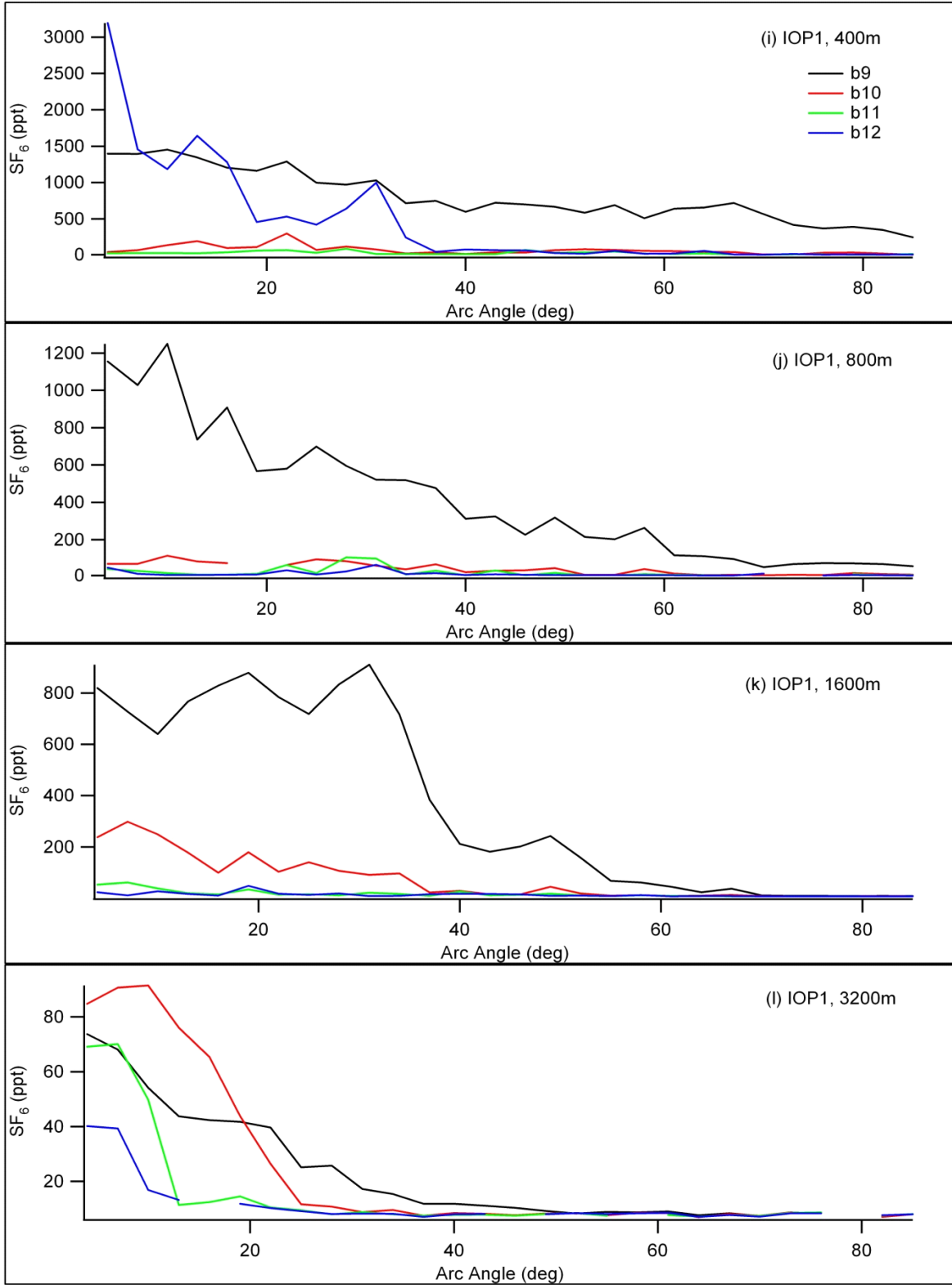


Figure 87 continued (i-l, bags 9-12).

Figures 88 a-l show vertical tracer concentration profiles at the towers at 201, 408, and 499 m downwind for all 10-minute bag sampling intervals for IOP1. Round black markers also show the average tracer concentration obtained from aircraft measurements at the height and downwind distance indicated as described in the Introduction to this section. Some of the profiles suggest lift off from the surface of the vertical plume centerline.

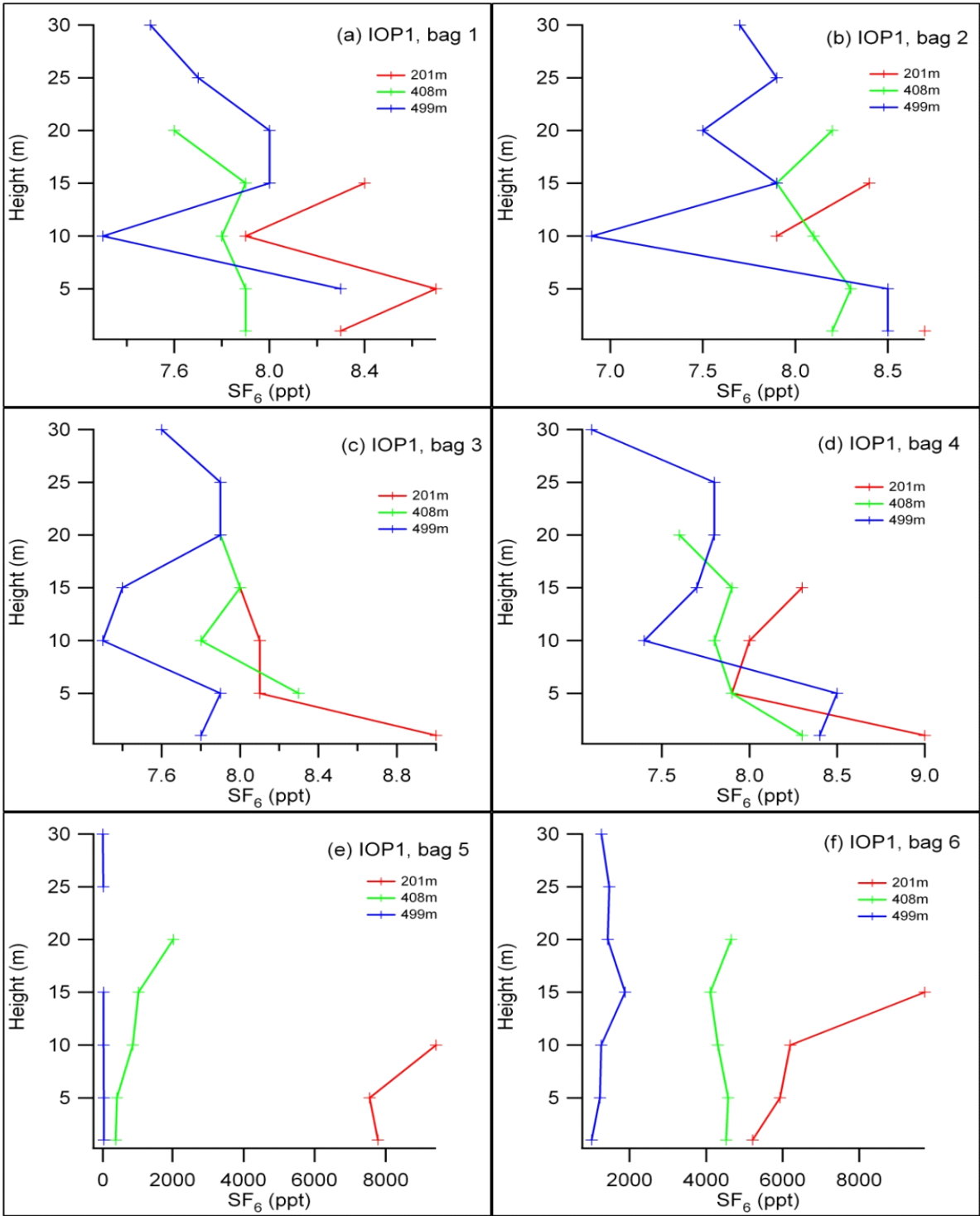


Figure 88. Vertical concentration profiles (a-f, bags 1-6) at the towers at 201, 408, and 499 m downwind for all 10-minute bag sampling intervals for IOP1. Round black markers show the average concentration obtained from aircraft measurements at the plotted height. The approximate downwind distance of the aircraft measurement is indicated in the legend.

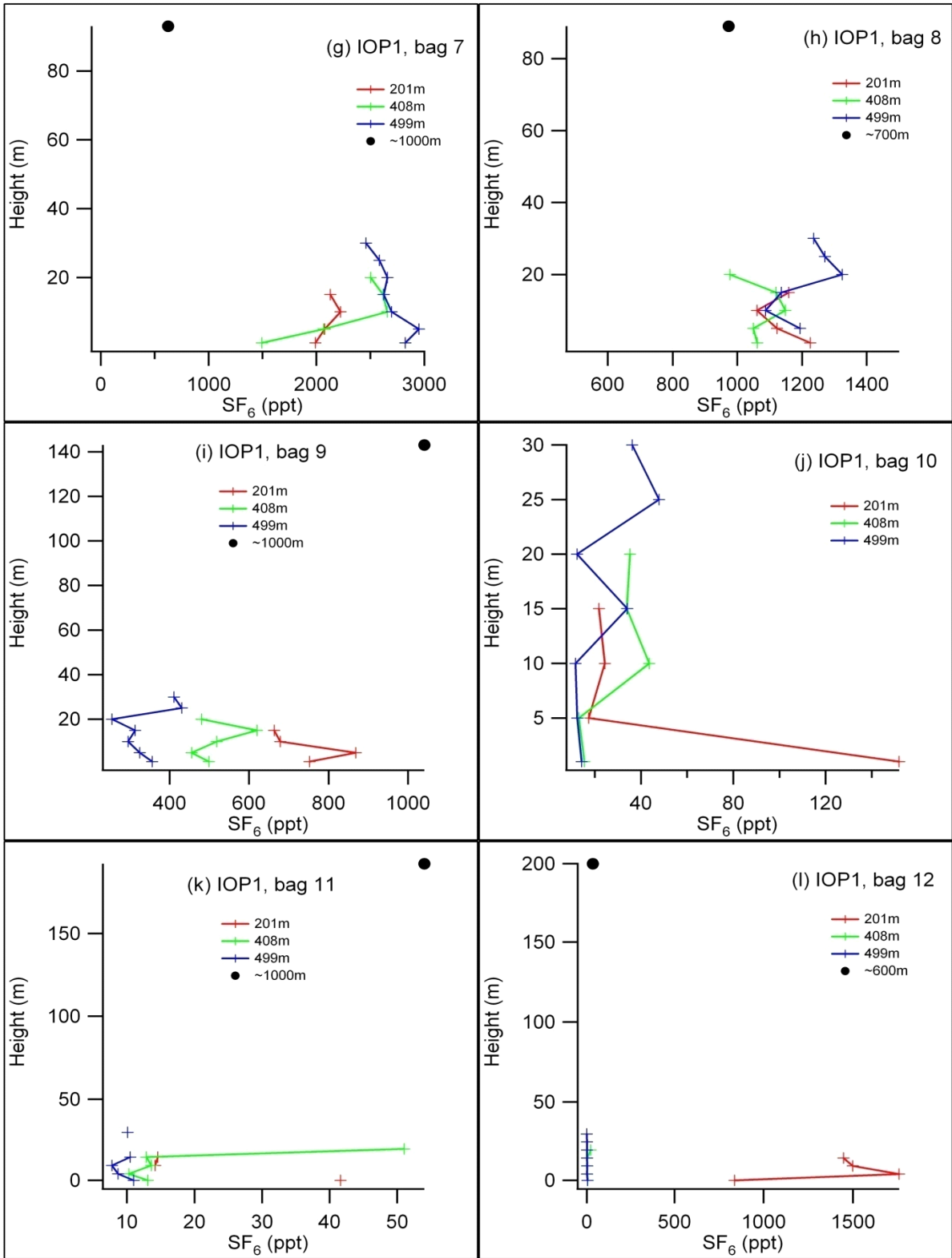


Figure 88 continued (g-l, bags 7-12).

Figure 89 shows time series of SF₆ concentrations measured by the fast response analyzers at the specified arc and arc angle location during IOP1. The series of small peaks after the main peak on the 1600 m arc suggest a periodicity of approximately 12-15 minutes.

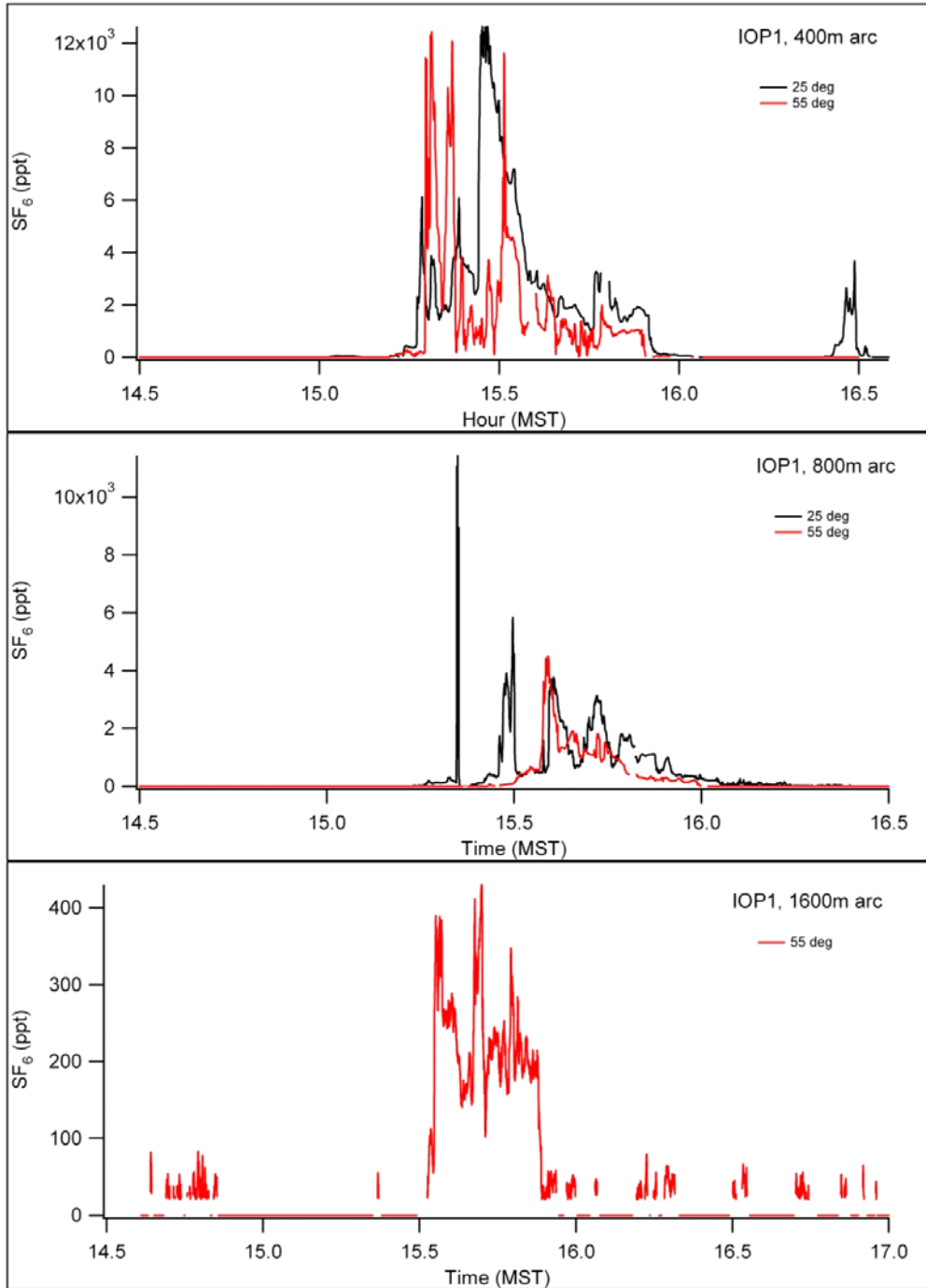


Figure 89. Time series of SF₆ concentrations measured by the fast response analyzers at the specified arc and arc angle location during IOP1.

Figure 90 shows a time series of aircraft height and SF₆ concentrations measured by the onboard fast response analyzer during IOP1. The highest concentrations were measured at the 100 m AGL flight level with a lesser set of peaks at 200 m AGL. Figure 91a shows color-coded concentrations along the aircraft flight path during IOP1. It is clear from this plot that transport of the tracer plume was toward the NNW for much of the experiment. Figure 91b is the same as Fig. 91a except zoomed in over the bag sampling array. The plume patterns seen in the aircraft data were consistent with plume patterns observed in the bag sampling data. All of the flight paths with higher concentrations over the sampling array were near the 800 m arc. Very little tracer was detected over the sampling array beyond 1600 m. The color scheme and significance of the black markers are described in the Introduction to this section.

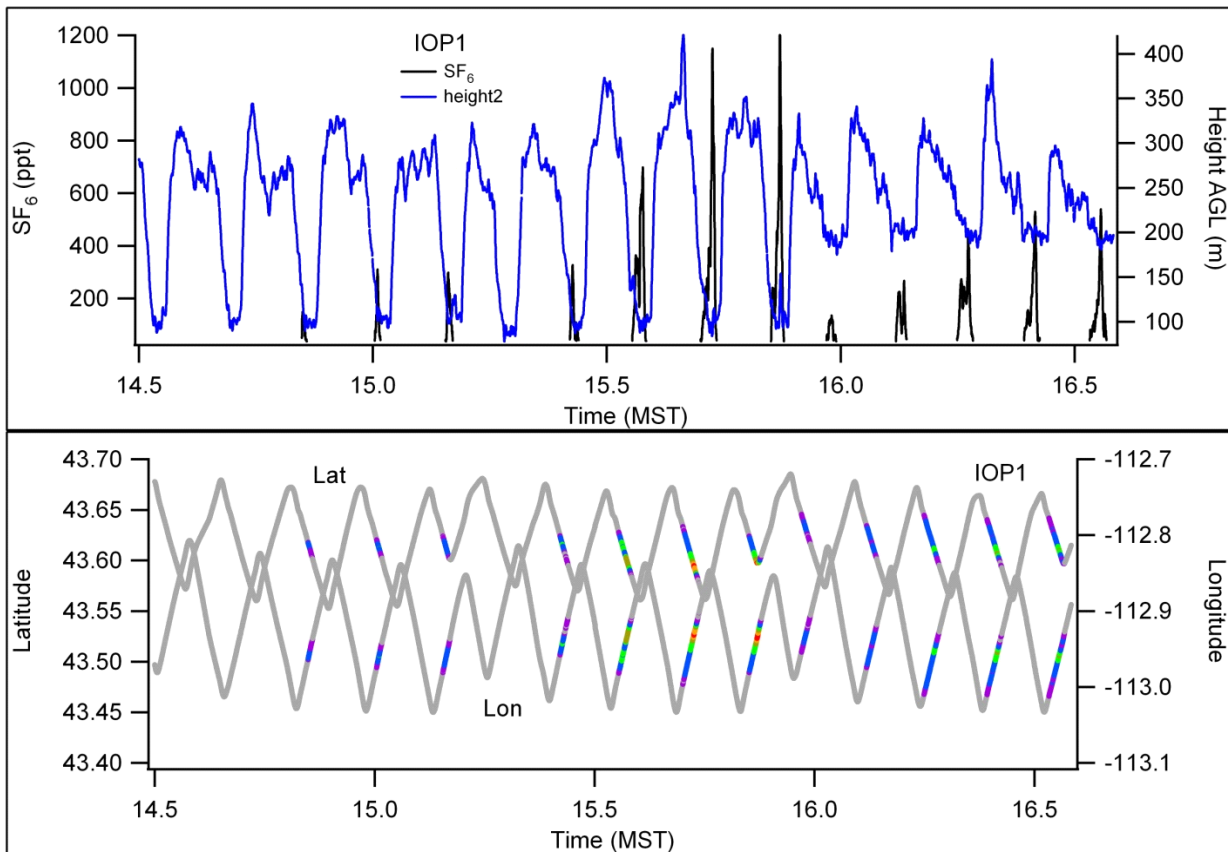


Figure 90. Time series of aircraft height and SF₆ concentrations measured by the onboard fast response analyzer during IOP1. Heights are approximate AGL calculated by subtracting the elevation at the release from the aircraft altitude.

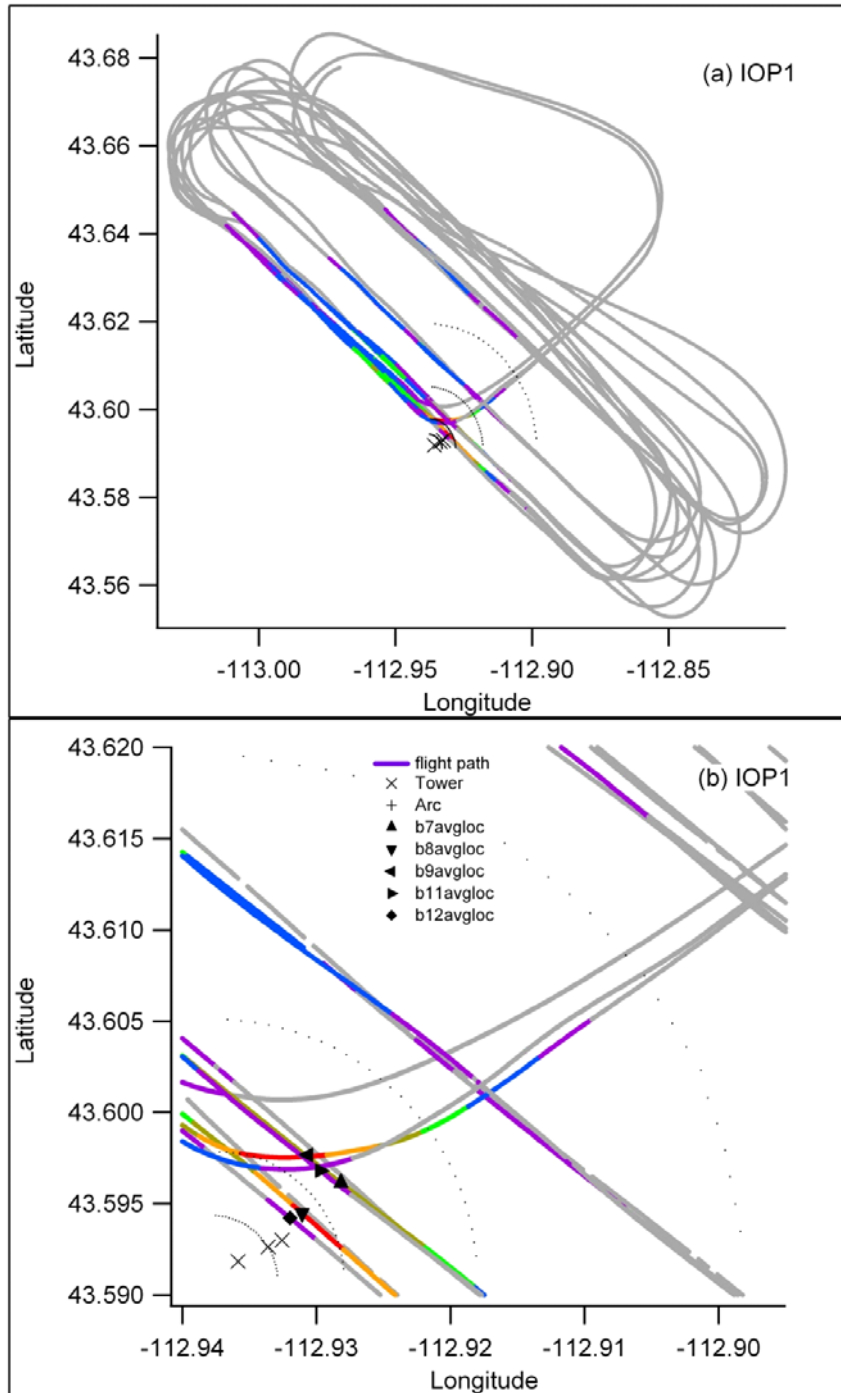


Figure 91. Color-coded concentrations along the aircraft flight path during IOP1 for (a) the overall flight path and (b) zoomed in over the bag sampling array. The color scheme and significance of the black markers are described in the Introduction to this section. They are linked to the black markers in Fig. 88 where b# is bag number and avgloc is average location.

IOP2

Date/Time and General Description

IOP2 was conducted on 05 October from 1300-1500 MST (1400-1600 MDT). It was mostly sunny. Winds were generally relatively light and under 3 m s^{-1} during the first half of the IOP, increasing somewhat over the second half of the IOP. Wind directions varied but were consistently southwesterly with few exceptions. Estimates of stability exhibit large uncertainty with respect to traditional P-G classification schemes although less so than IOP1. Overall conditions were relatively stationary although there is evidence of a shift toward some non-stationarity midway through the experiment. Overall, the wind directions and other conditions were much more favorable for advecting the tracer over the sampling array than IOP1 although the variations in flow made it slightly less than ideal. A summary of the meteorological conditions during IOP2 is given in Table 20. The SF_6 release rate was 9.99 g s^{-1} (Tables 1 and 2). The fast response analyzers were located on the 400 m arc at 31 and 61 degrees, on the 800 m arc at 31 and 61 degrees, on the 1600 m arc at 61 degrees, and on the airplane.

Table 20. Meteorological conditions during IOP2. Wind speeds, directions, σ_θ , and P-G stability class determinations (EPA, 200c) are from COC at 10 m. Solar radiation measurements are from FLX. R3 and R4 indicate sonic anemometer data from their respective locations.

Bag	Wind Speed (m s^{-1})	Wind Direction (deg)	Solar Radiation (W m^{-2})	R3 u^* (m s^{-1})	R4 u^* (m s^{-1})	R3 z/L	R4 z/L	σ_θ (deg)	P-G SRDT	P-G σ_θ
1	3.0	249.5	575.0	0.18	0.22	-1.39	-0.90	29.9	C	A
2	2.7	266.6	532.0	0.24	0.18	-0.55	-1.08	40.0	C	A
3	2.6	186.4	561.5	0.26	0.25	-0.37	-0.49	46.8	C	A
4	2.7	236.4	514.0	0.28	0.17	-0.41	-1.52	20.9	C	B
5	2.6	240.3	479.0	0.23	0.18	-0.55	-0.82	35.2	C	A
6	2.4	278.5	390.5	0.13	0.14	-3.27	-2.46	64.2	C	A
7	3.2	195.7	500.5	0.21	0.19	-0.63	-1.05	15.9	C	C
8	3.8	240.0	546.0	0.23	0.33	-0.73	-0.22	26.6	C	B
9	4.1	206.0	457.0	0.27	0.24	-0.36	-0.60	20.4	C	C
10	3.4	190.7	291.0	0.26	0.28	-0.26	-0.27	16.3	C	C
11	3.2	202.5	239.0	0.27	0.28	-0.19	-0.16	15.8	C	C
12	4.8	186.8	391.0	0.26	0.24	-0.34	-0.29	10.0	C	D

Winds and Quality Assurance

Figure 92 shows wind speed and direction comparisons for ARLFRD data in the vertical at the GRI and COC towers for IOP2. There was generally good agreement in wind speed and direction. Spatial and temporal homogeneity and stationarity in the flow were much better than during IOP1 and it was a much more optimal scenario for tracer dispersion across the sampling array. The most apparent deviation from stationarity occurred midway through the tracer release

period, just before 1400 h. At that time wind speeds increased moderately and wind directions shifted slightly from generally WSW to more SW and SSW. Some large deviations in σ_θ occurred just prior to this, mainly at the GRI and COC towers (Fig. 93). The increase in σ_θ was not seen at TOW at this time even though the increase in wind speed was observed. The occasional slight shift of peak wind speed maxima/minima in the sonic anemometers (G1, G2) relative to the other GRI measurements is likely due largely to the comparison between 5 and 10 minute averaging periods.

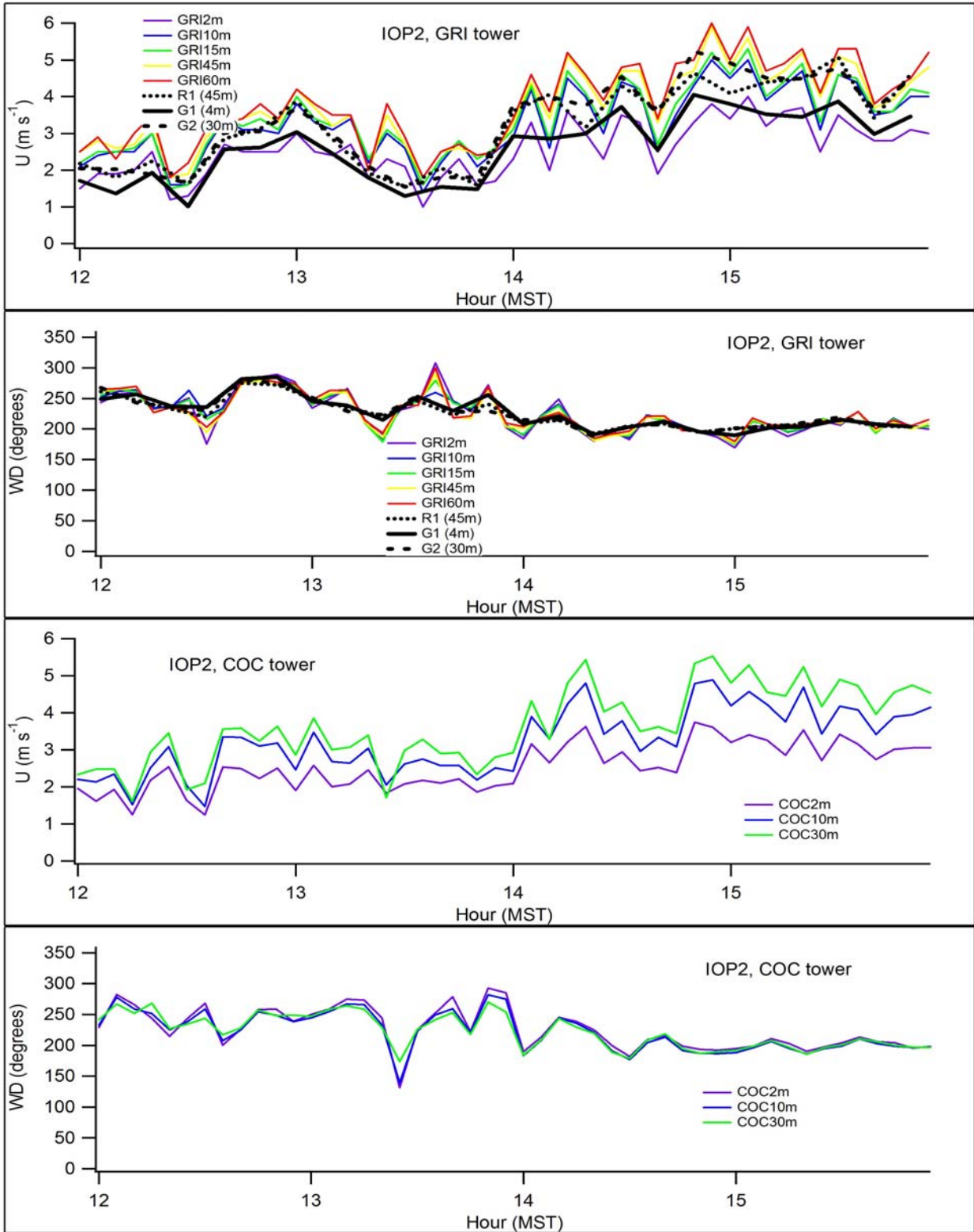


Figure 92. ARLFRD wind speed and direction comparisons in the vertical at GRI and COC for IOP2.

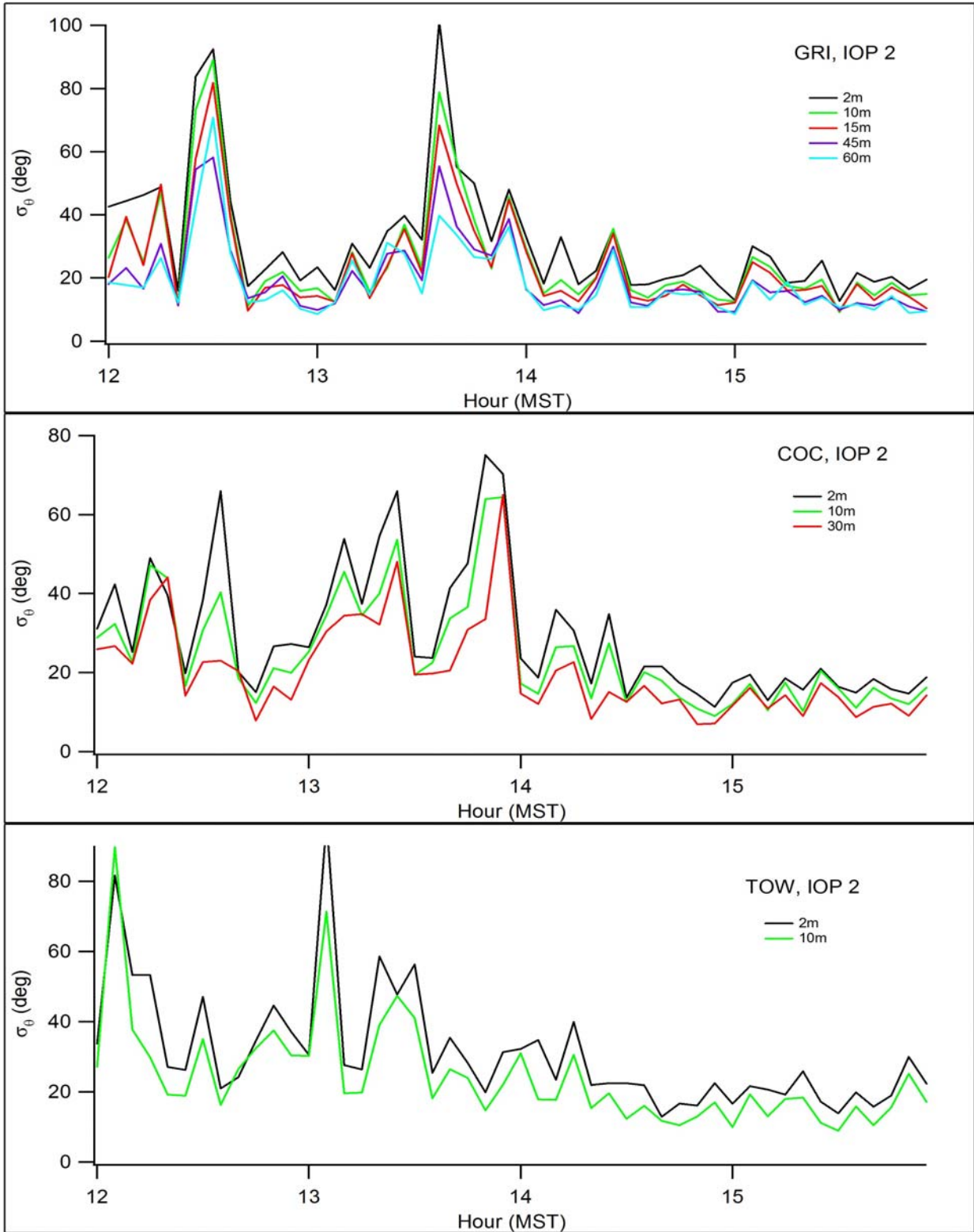


Figure 93. Standard deviation in wind direction σ_θ (σ_A) using wind vanes at GRI, COC, and TOW for IOP2.

Figures 94-96 show wind speed and direction comparisons in the horizontal across the study area at 2 m, 10 m, 30 m, 45 m, 60 m, and 160 m from the data available. The comparisons are the same as those described for IOP1. Measurements were largely consistent with each other. The most notable inconsistency was the wind speed measurements at 160 m for the ASC and ART sodars and PRO. The PRO wind speeds appear to have a distinct low bias. Wind directions are consistent in all cases. The ASC sodar did not have any data recovery at the 160 m level during the second half of the test. With the exception noted, there is little evidence for a problem with the measurements.

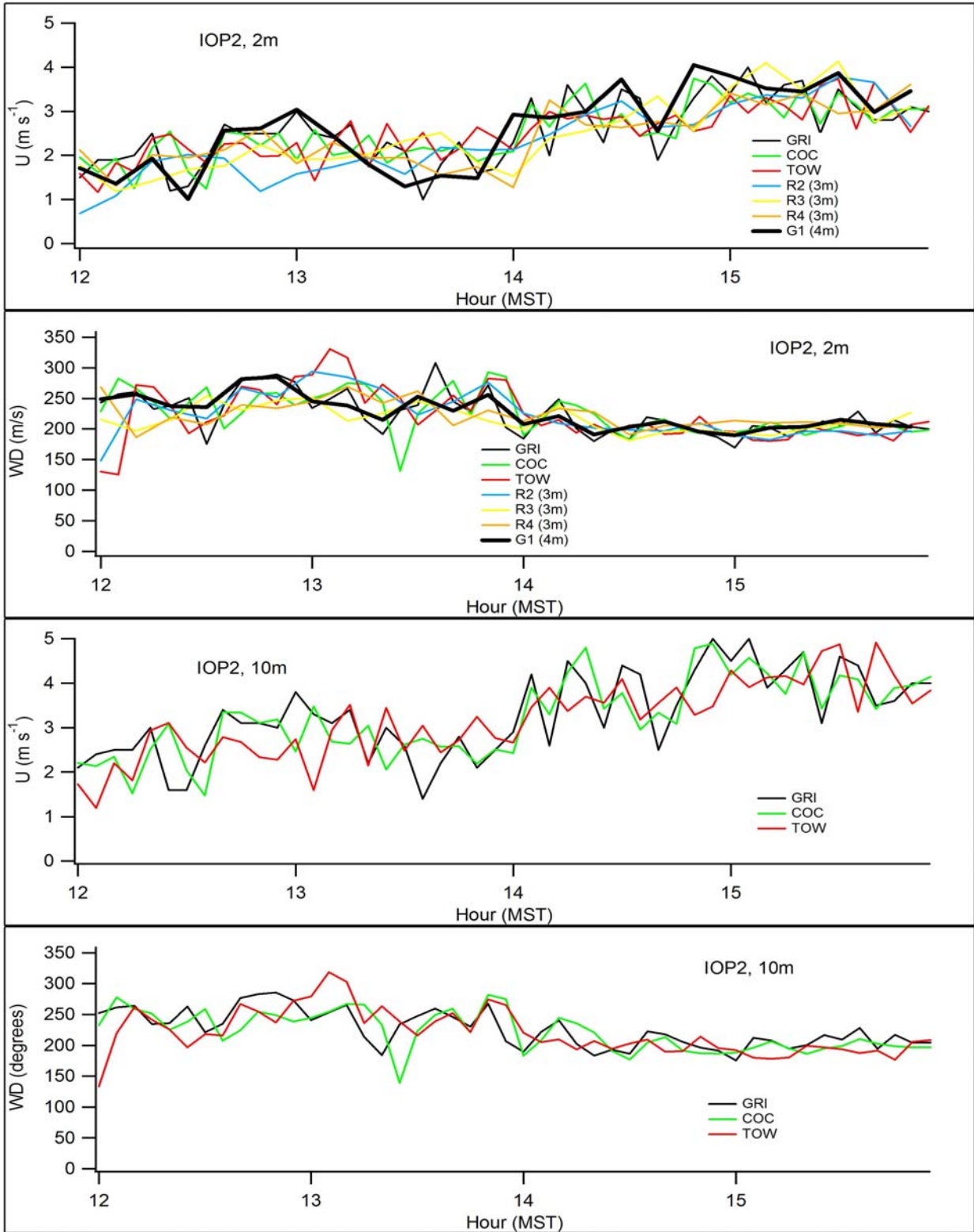


Figure 94. ARLFRD wind speed and direction comparisons in the horizontal at 2 and 10 m during IOP2.

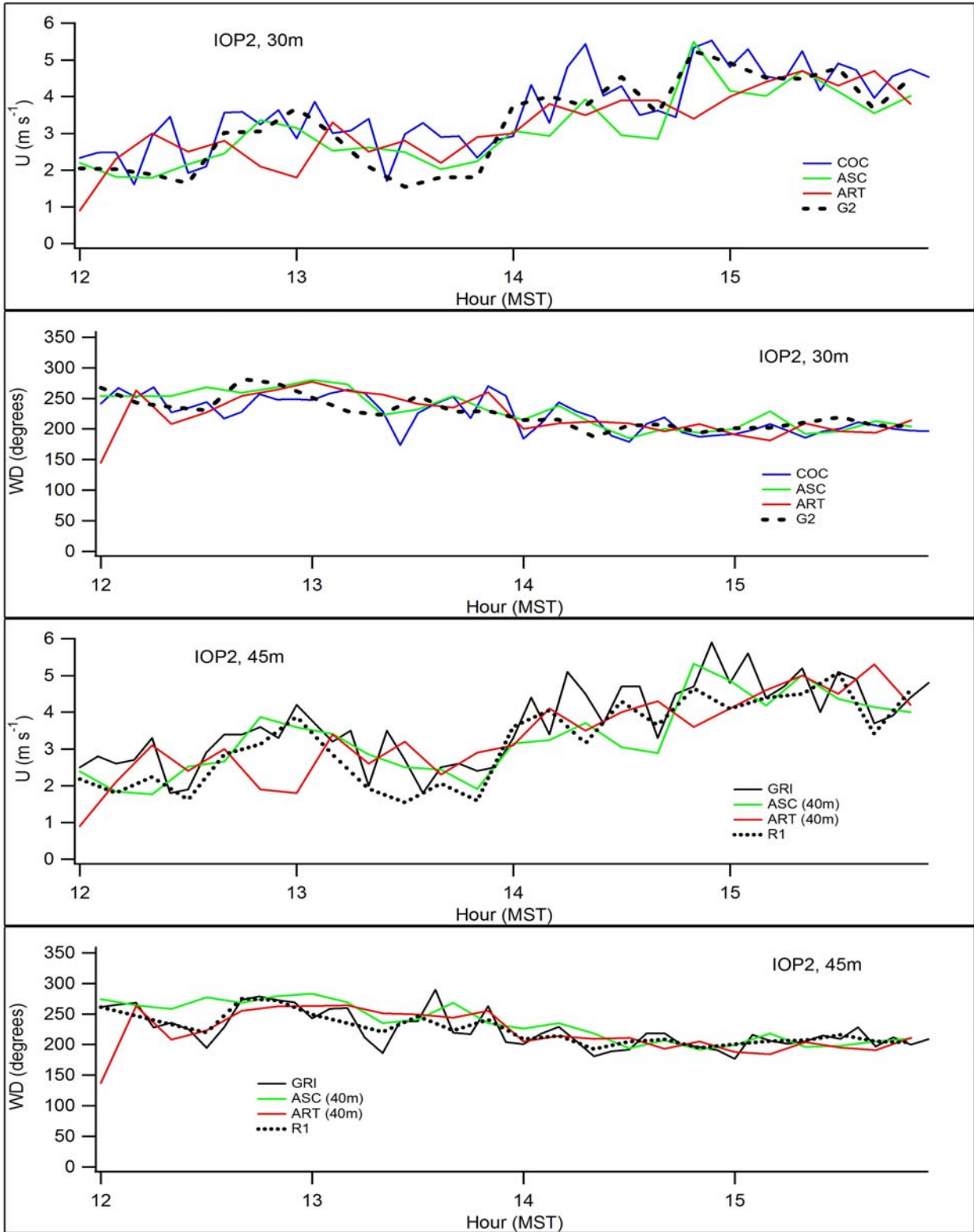


Figure 95. ARLFRD wind speed and direction comparisons in the horizontal at 30 and 45 m during IOP2.

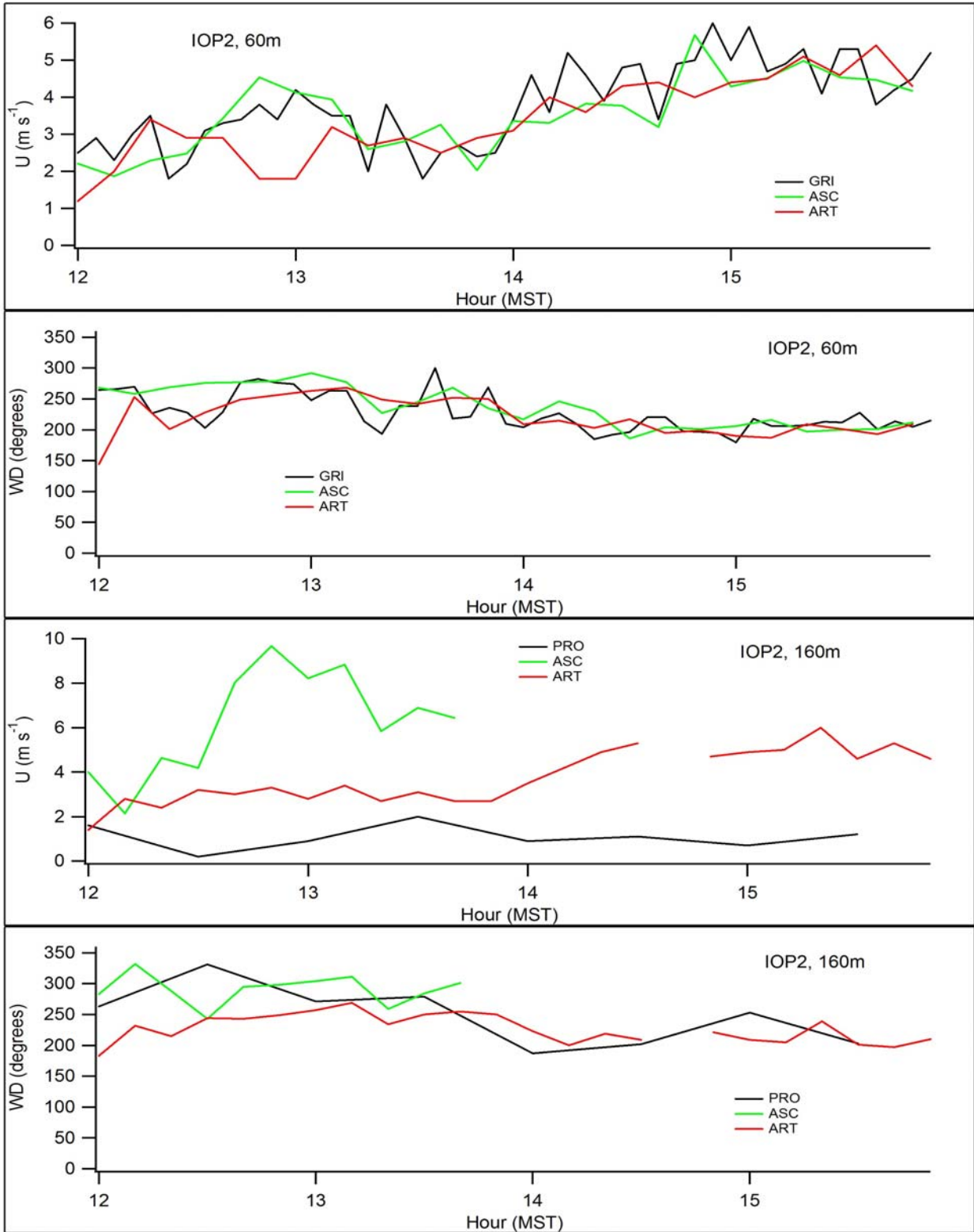


Figure 96. ARLFRD wind speed and direction comparisons in the horizontal at 60 and 160 m during IOP2.

Figures 97-99 show time-height cross-sections for wind speed and direction for the ASC sodar, ART sodar, and PRO wind profiler, respectively. Both the ART and ASC measured relatively low wind speeds out of the WSW until about 1400 h and then measured a moderate increase in wind speeds and shift to SSW wind directions. That is consistent with results at the Grid 3 tower (Figs. 95, 96). The PRO results also showed low wind speeds but with poorly organized wind directions. An increase in wind speed was not observed at about 1400 h. The data again suggest that there was a prominent shear layer at about 1.4 km height although data is relatively sparse above that.

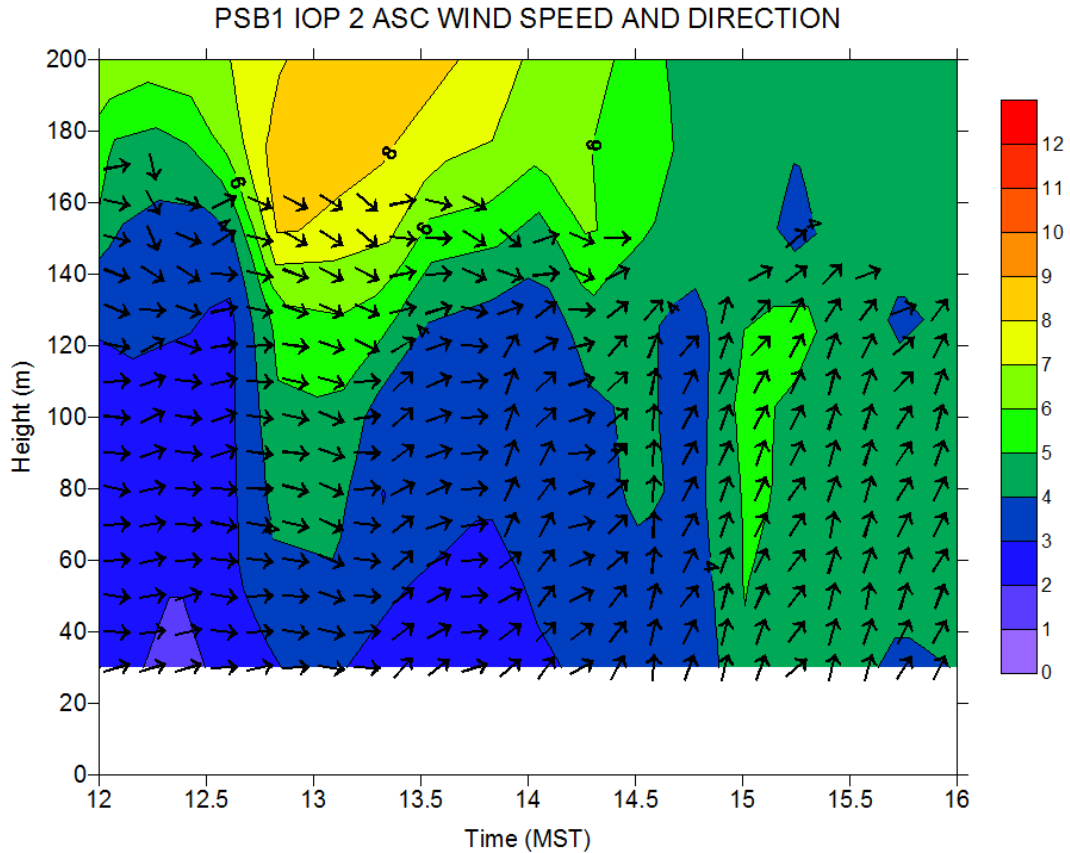


Figure 97. Time-height cross-section of wind speed and direction at ASC sodar during IOP2.

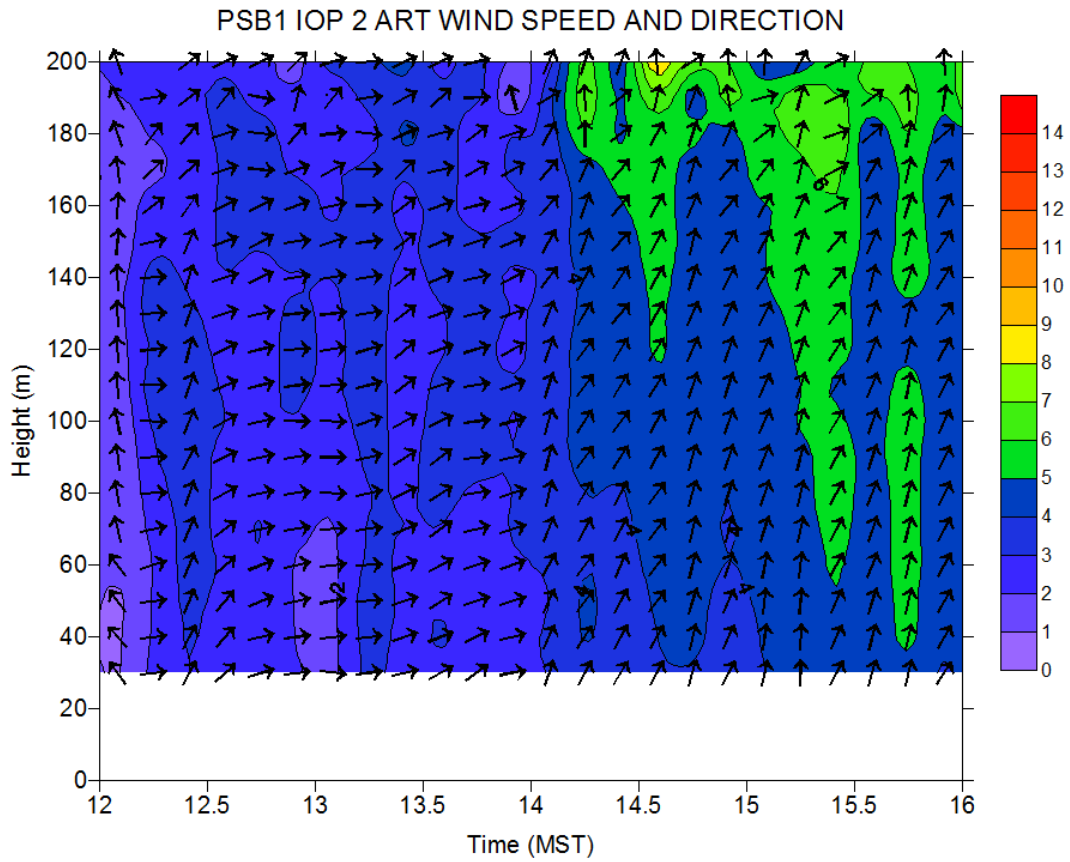


Figure 98. Time-height cross-section of wind speed and direction at ART sodar during IOP2.

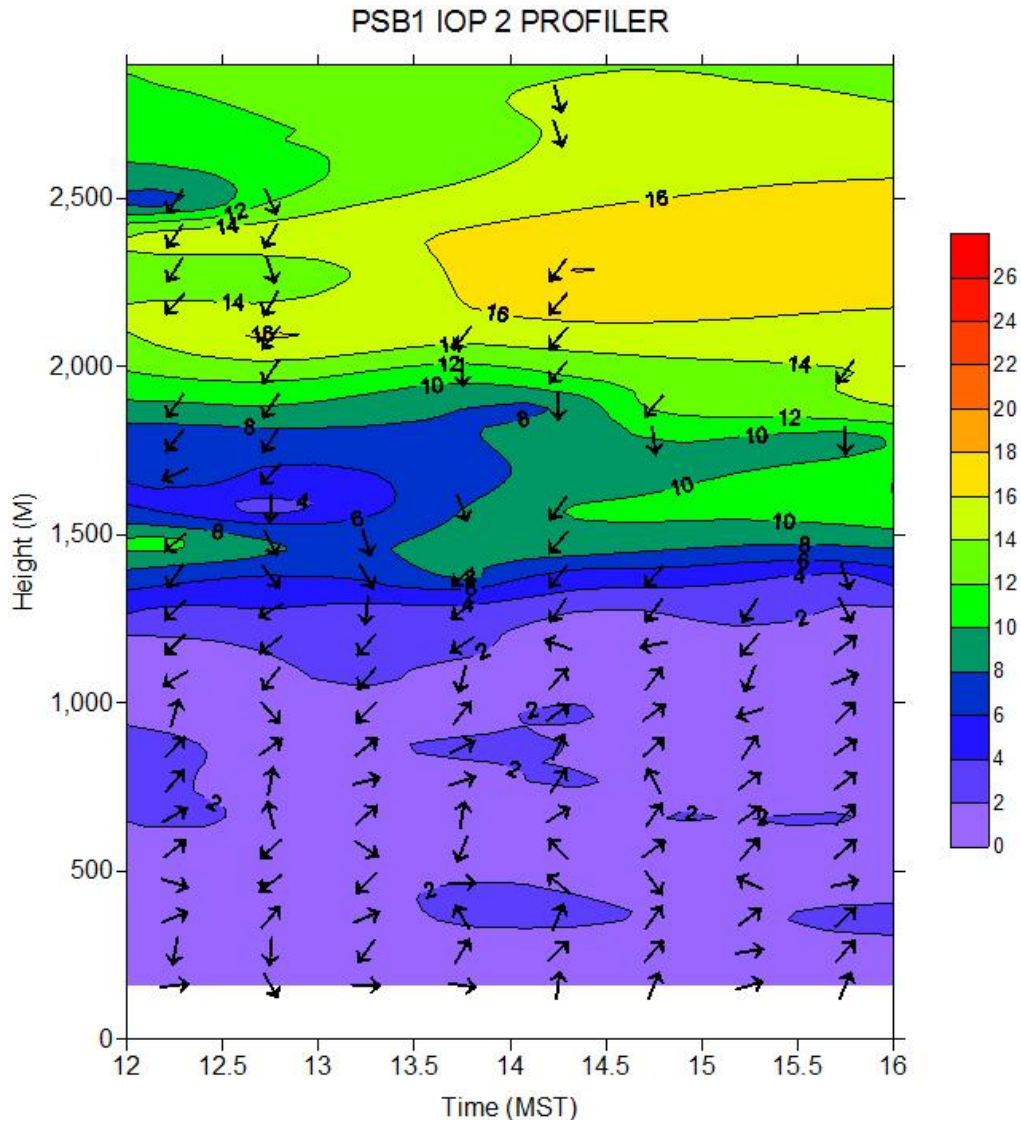


Figure 99. Time-height cross-section of wind speed and direction at wind profiler (PRO) during IOP2.

Turbulence

Figures 100 and 101 show time series of the turbulence measurements for 10 and 30-minute averaging periods, respectively, for σ_w , turbulent kinetic energy (TKE), u_* , kinematic heat flux $\langle w'T' \rangle$, and $1/L$ where L = Obukhov length. The 30-minute periods more correctly account for nonstationarity effects and should provide more reliable estimates than the 10-minute averaging periods. Measurements were largely consistent with each other and there was no apparent evidence for a problem with them. The high values of σ_w at G2 are due to the fact these represent measurements at 30 m whereas all the other measurements are between 3-4 m height.

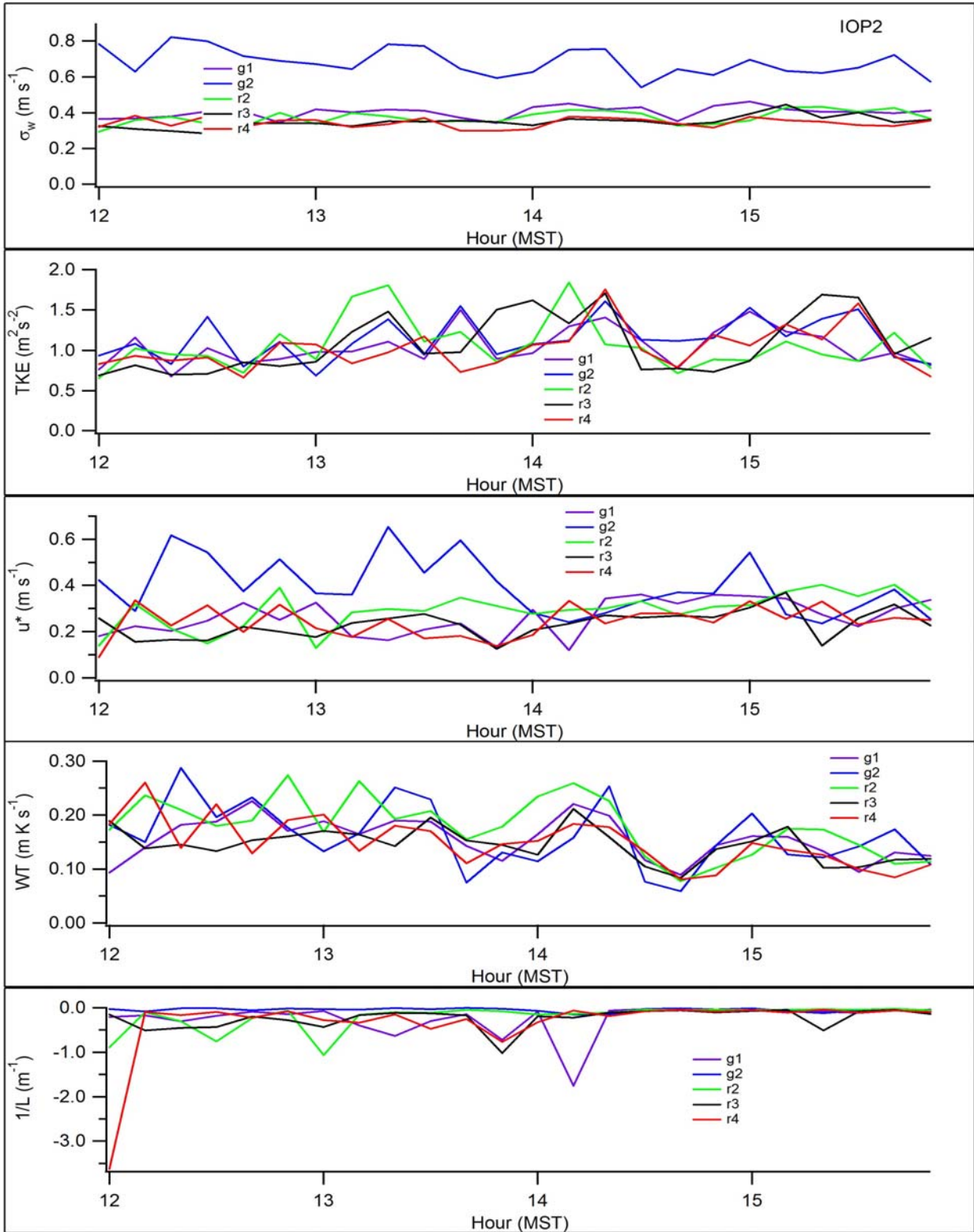


Figure 100. ARLFRD sonic anemometer 10-minute averages for σ_w , TKE, u_* , kinematic heat flux, and $1/L$ during IOP2 (G1, G2, R2, R3, and R4)

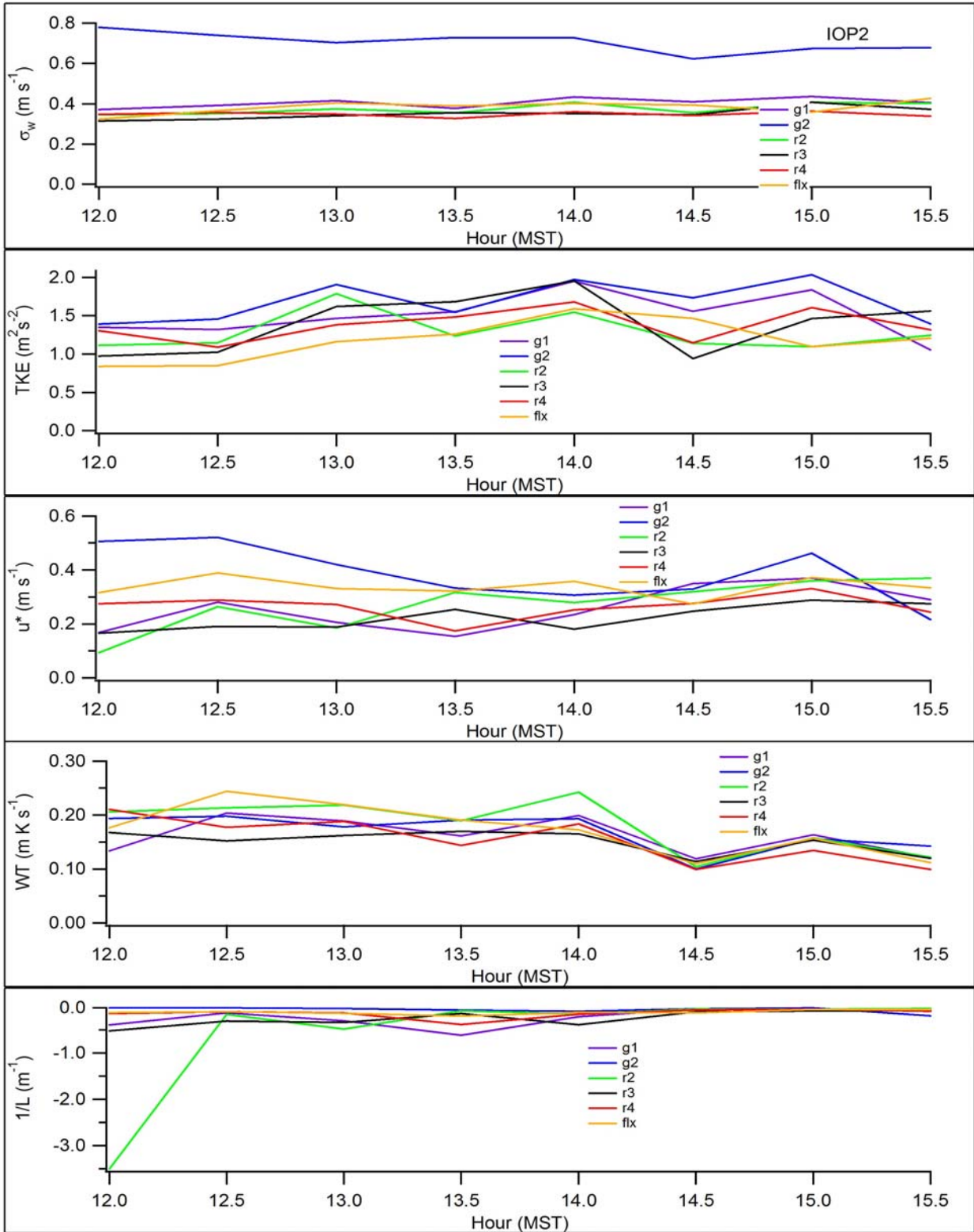


Figure 101. ARLFRD sonic anemometer 30-minute averages for σ_w , TKE, u_* , kinematic heat flux, and $1/L$ during IOP2 (G1, G2, R2, R3, and R4).

The results for L indicate that the stability conditions shifted subtly from weakly unstable during the first half of the IOP to near neutral during the second half. That shift occurred at the same time as the observed moderate increase in wind speed.

Figures 102 and 103 show time-height cross-sections for σ_w and TKE for the ASC sodar. Figures 104 and 105 show time-height cross-sections for σ_w and TKE for the ART sodar. The absolute magnitudes of TKE and σ_w shown for the ART and ASC sodars should not be assumed to be comparable between the two sodars nor with the same measurements by the sonic anemometers. The magnitudes of σ_w at ASC and ART are usually similar but the values of TKE at the ART were typically about an order of magnitude greater than the ASC. Restricting the comparison to the relative magnitudes of TKE and σ_w for each sodar, within an IOP or across IOPs, should be valid.

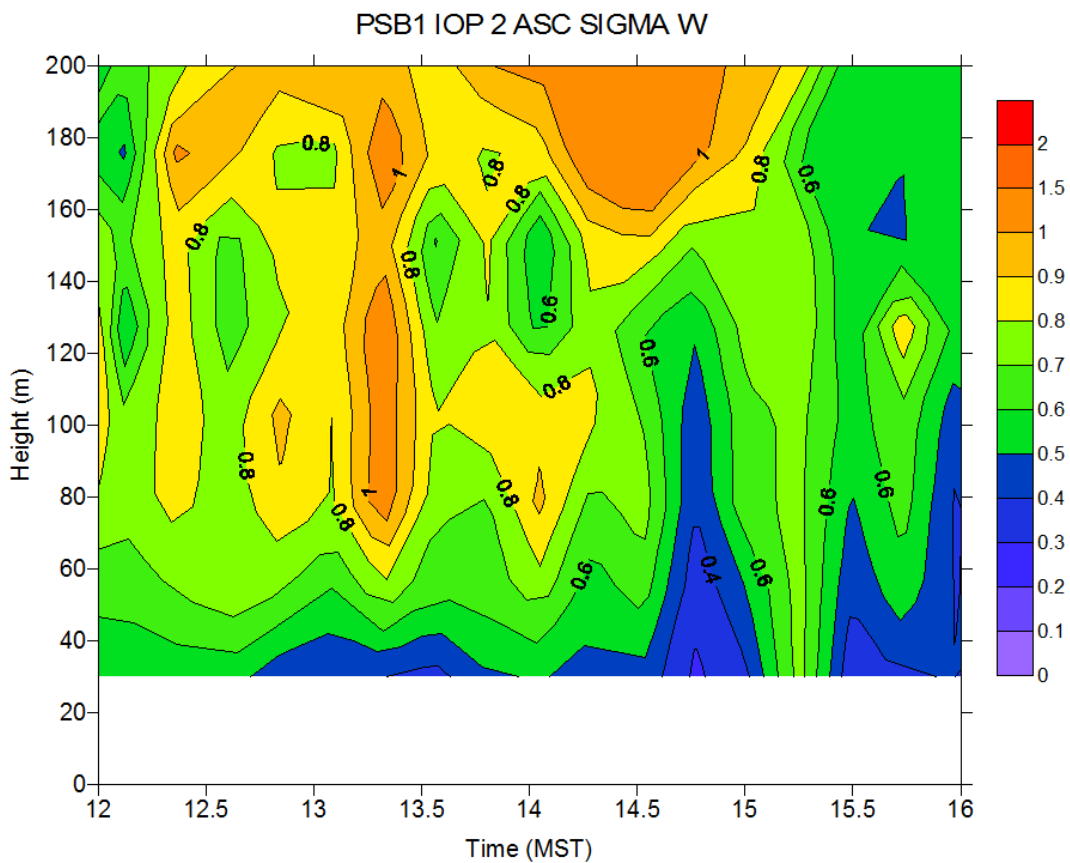


Figure 102. Time-height cross-section of σ_w at ASC sodar during IOP2.

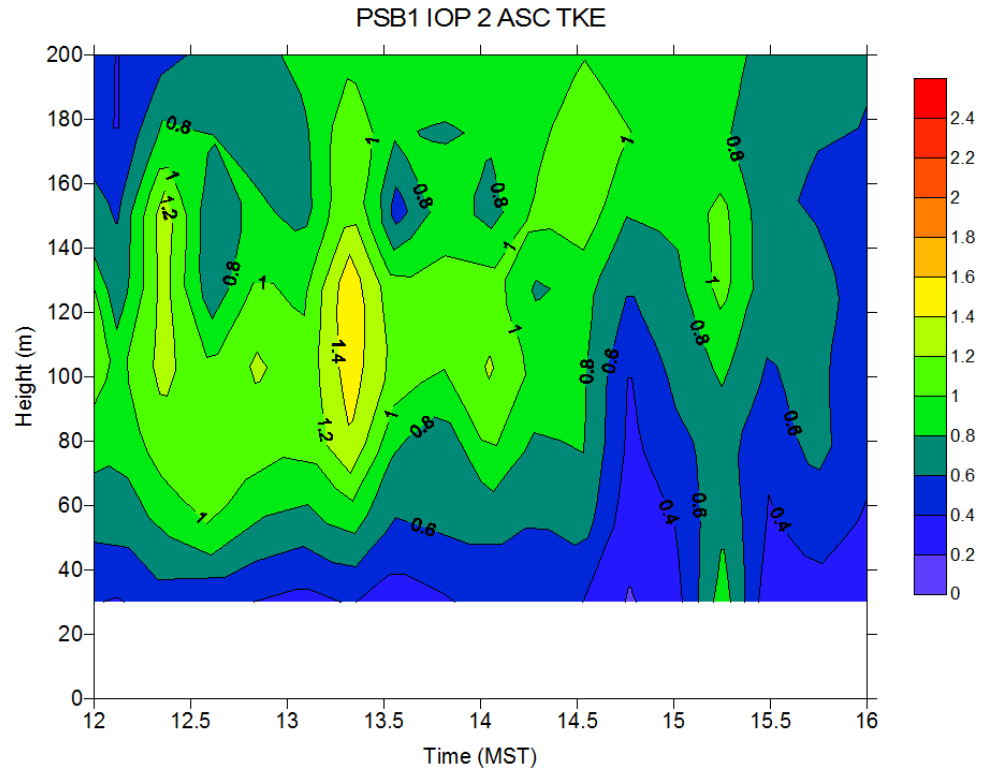


Figure 103. Time-height cross-section of TKE at ASC sodar during IOP2.

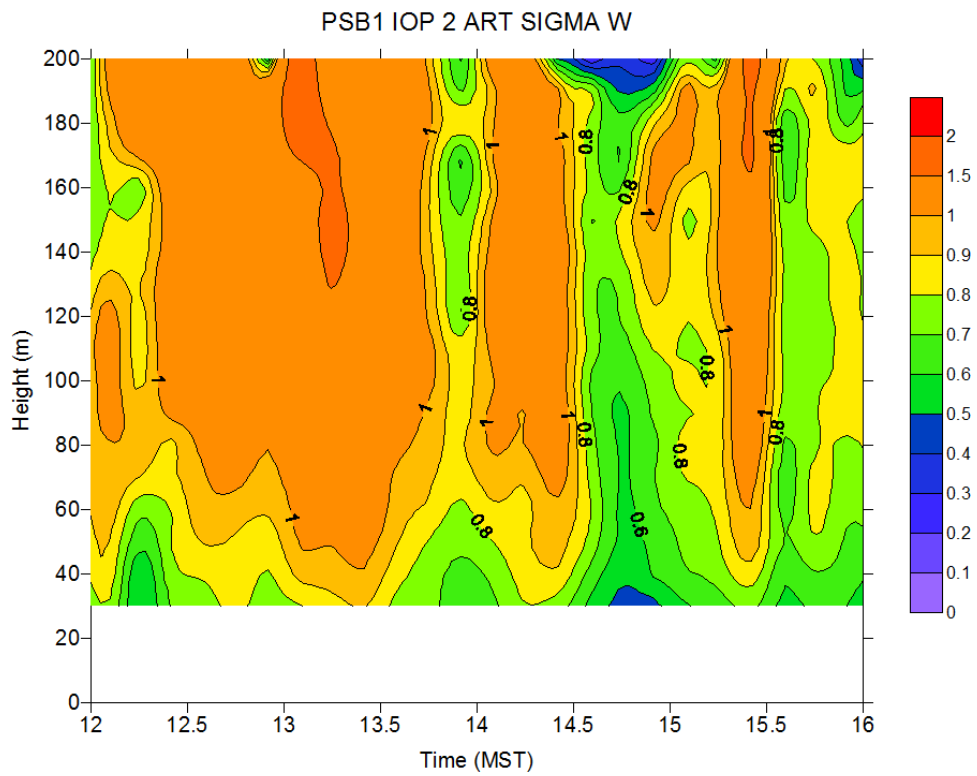


Figure 104. Time-height cross-section of σ_w at ART sodar during IOP2.

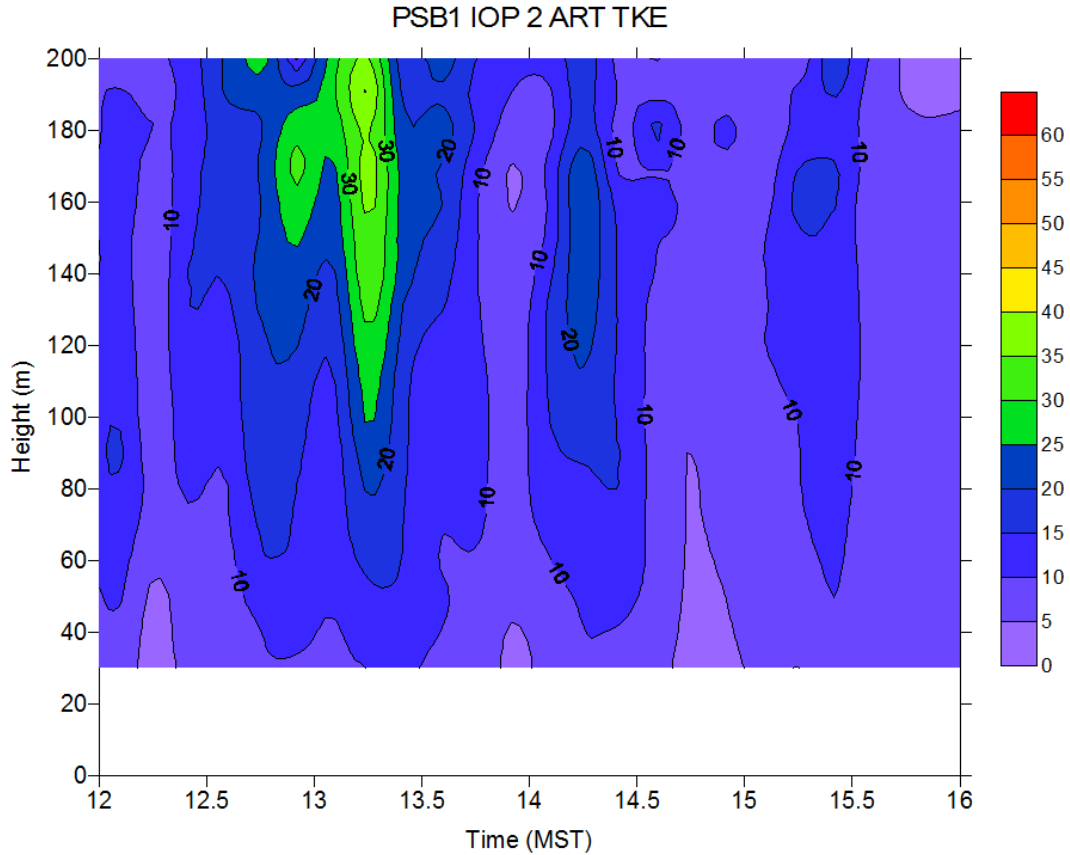


Figure 105. Time-height cross-section of TKE at ART sodar during IOP2.

The ART TKE and σ_w was greater than that observed during IOPs 1 but similar to other IOPs. The ASC TKE was much greater than IOP1 but similar in magnitude to the other IOPs. ASC σ_w was much greater than IOP1, greater than IOP 3, and similar to IOPs 4 and 5. The range of values for σ_w and TKE at the ASC were roughly comparable in magnitude to those observed at the sonic anemometers.

Figure 106 shows a time-height cross-section for temperature from the RASS.

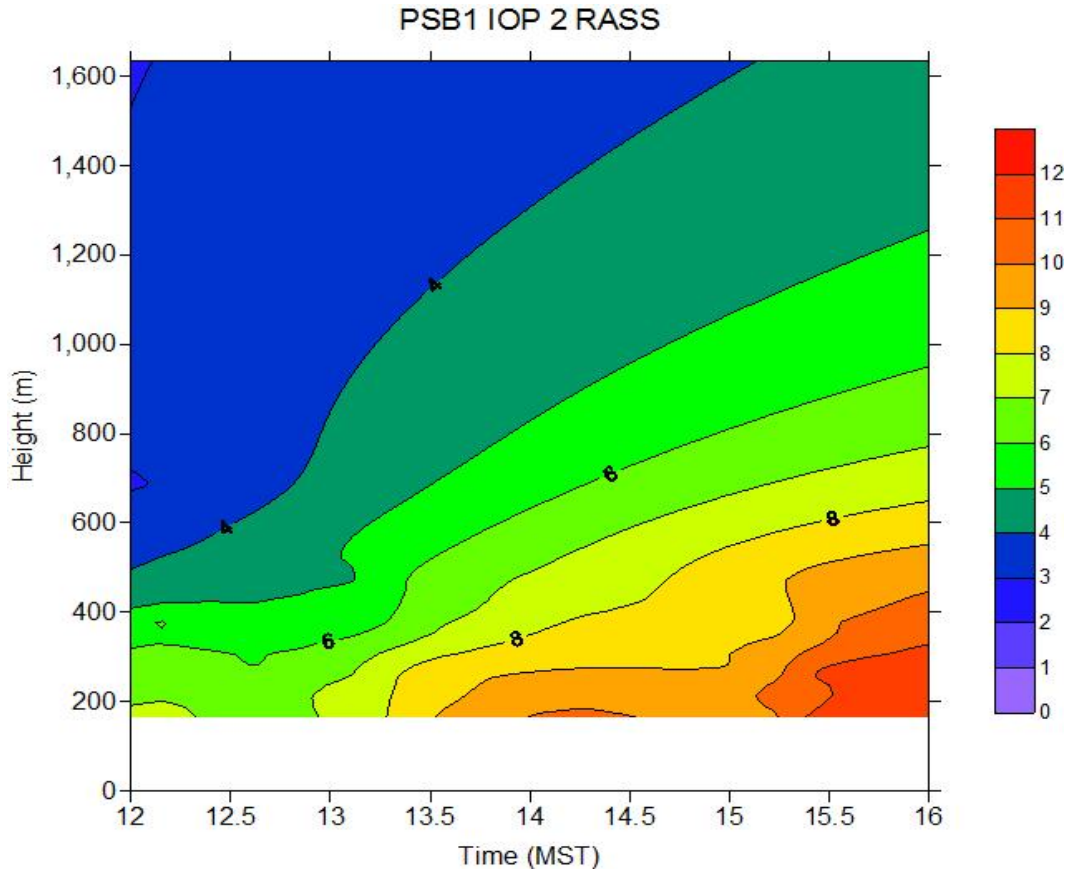


Figure 106. Time-height cross-section of virtual temperature at the RASS during IOP2. Temperatures are in degrees C.

Vertical profiles of wind speed, wind direction, and calculated turbulence parameters from sonic anemometer measurements at GRI during IOP2 are shown in Figs. 107-109. Vertical profiles of wind speed, wind direction, and σ_θ from cup anemometers and wind vanes plus aspirated air temperature during IOP2 are shown in Figs. 110 and 111. Turbulence intensities (σ_v/U) were mostly large and there was general consistency between the sonic and cup and vane (σ_θ) results. There appears to be some discrepancies in turbulent intensity profiles at the 4, 30, and 45 m sonic levels relative to the other sonic levels but it is not consistently present (Fig. 108). These 3 levels correspond to the ARLFRD sonics while the other 4 levels are WSULAR sonics. There appears to be somewhat better agreement between the turbulent intensities measured by the ARLFRD sonics (Fig. 108) and those measured by the cup anemometers and wind vanes (Fig. 111) although this is not conclusive. A similar pattern of TKE sonic profile discrepancies was observed (Fig. 109). There was mostly good agreement between wind speed and direction measurements made by the sonic anemometers and cup anemometers and wind vanes although there are some inconsistencies between the ARLFRD and WSULAR sonics.

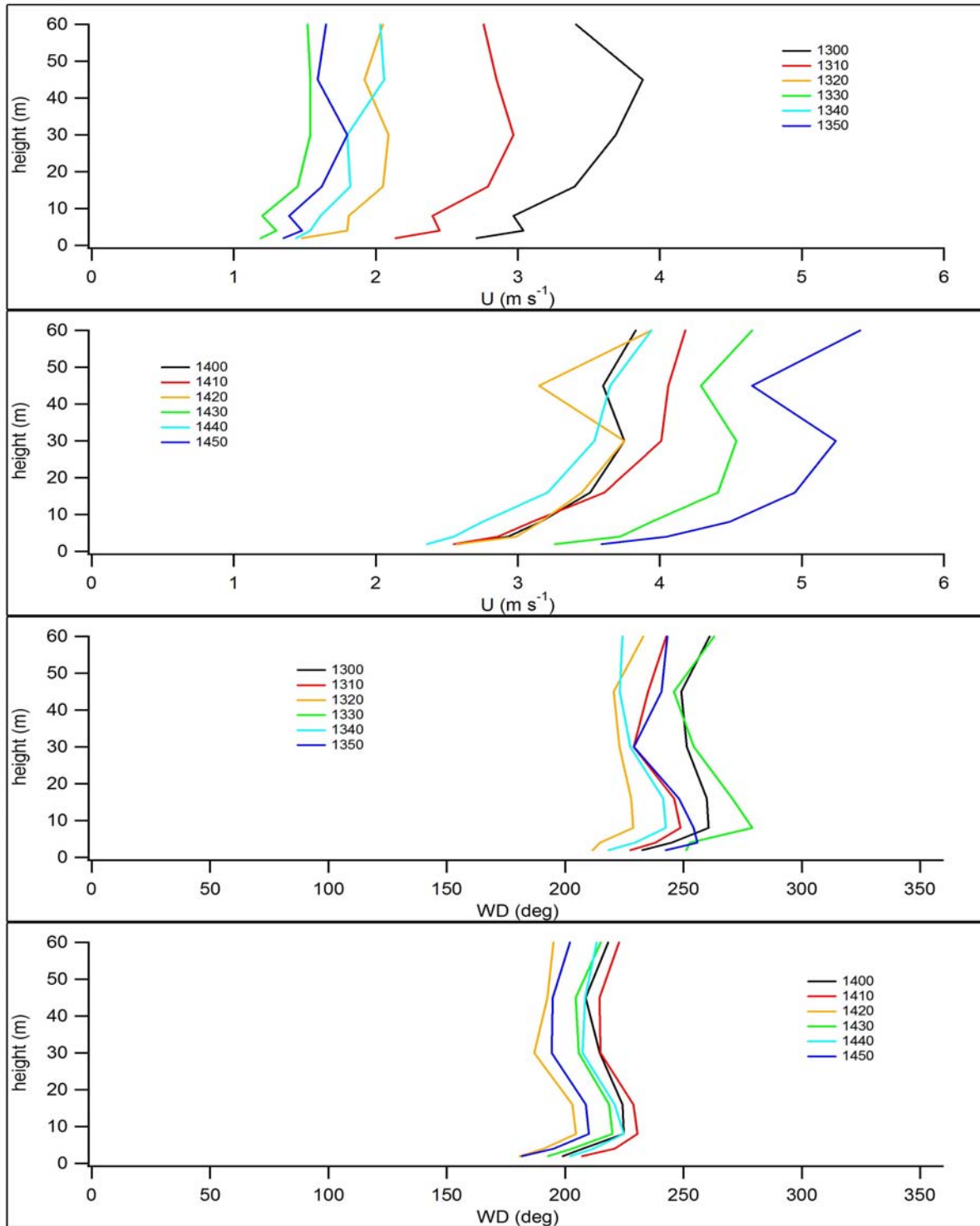


Figure 107. Vertical profiles of wind speed and direction from sonic anemometer measurements at GRI during IOP2. ARLFRD instruments were at 4, 30, and 45 m; WSULAR instruments were at 2, 8, 16, and 60 m. Times in legend are start times for the 10 minute interval (hhmm MST).

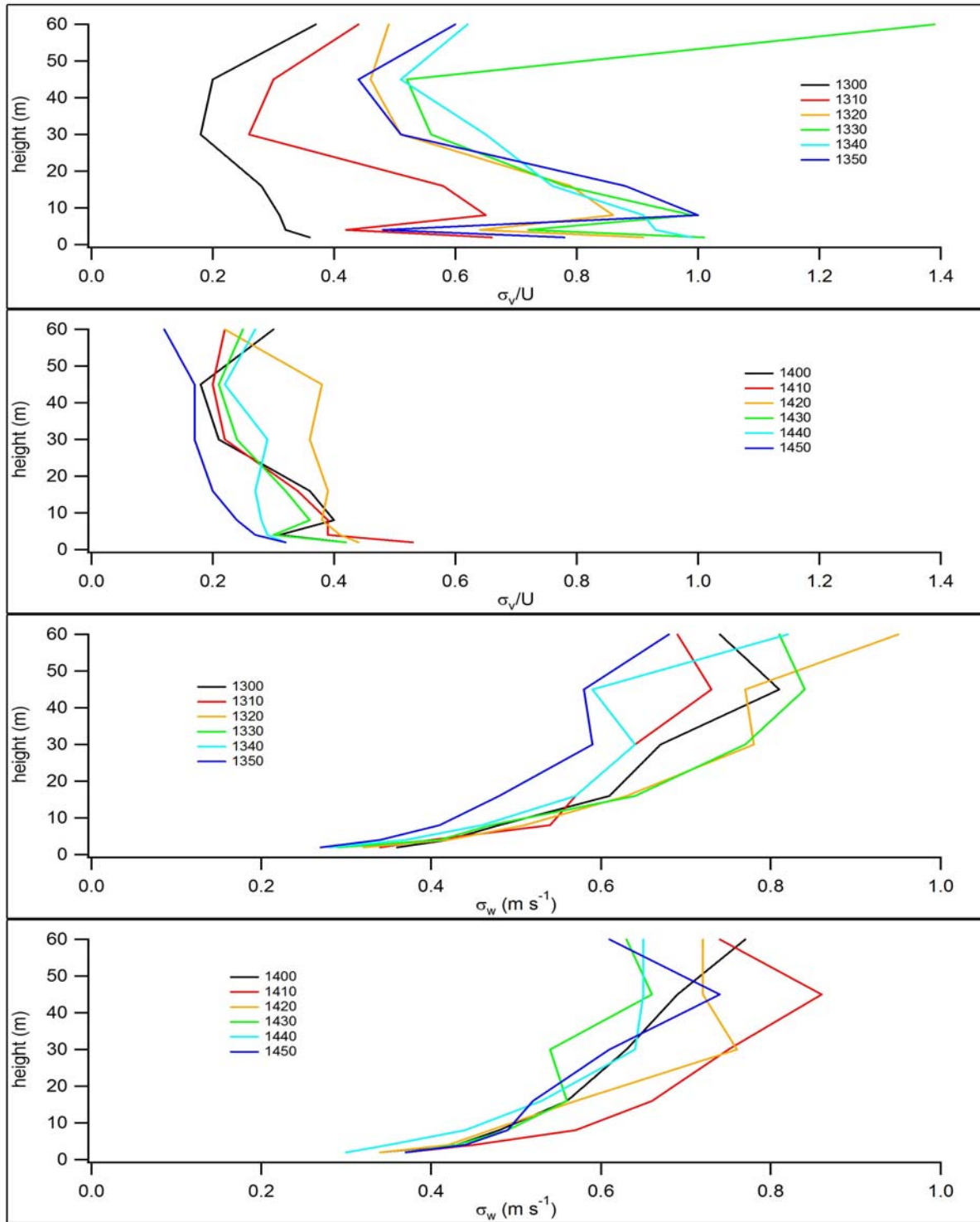


Figure 108. Vertical profiles of turbulence intensity and σ_w from sonic anemometer measurements at GRI during IOP2. ARLFRD instruments were at 4, 30, and 45 m; WSULAR instruments were at 2, 8, 16, and 60 m. Times in legend are start times for the 10 minute interval (hhmm MST).

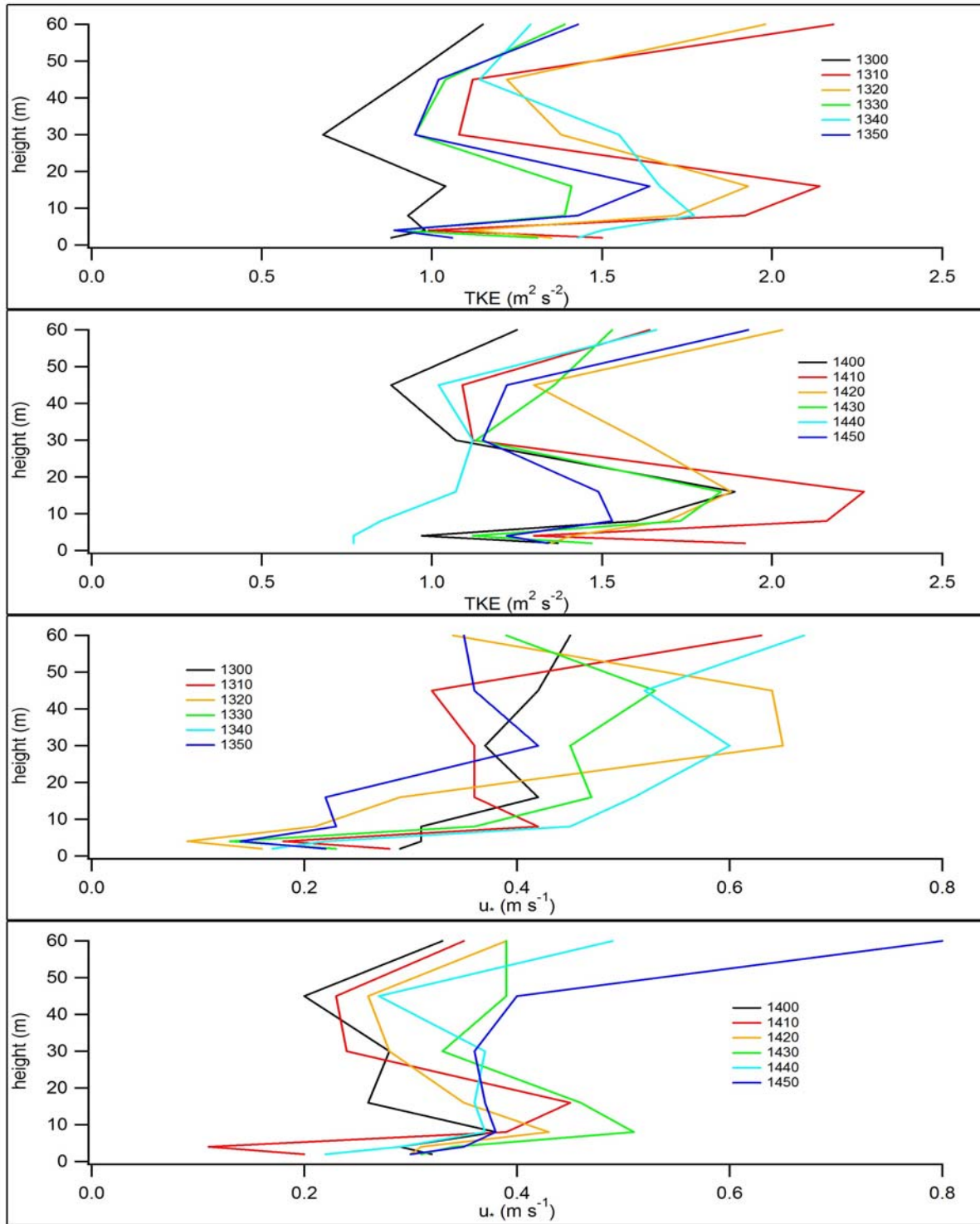


Figure 109. Vertical profiles of turbulent kinetic energy (TKE) and u_* from sonic anemometer measurements at GRI during IOP2. ARLFRD instruments were at 4, 30, and 45 m; WSULAR instruments were at 2, 8, 16, and 60 m. Times in legend are start times for the 10 minute interval (hhmm MST).

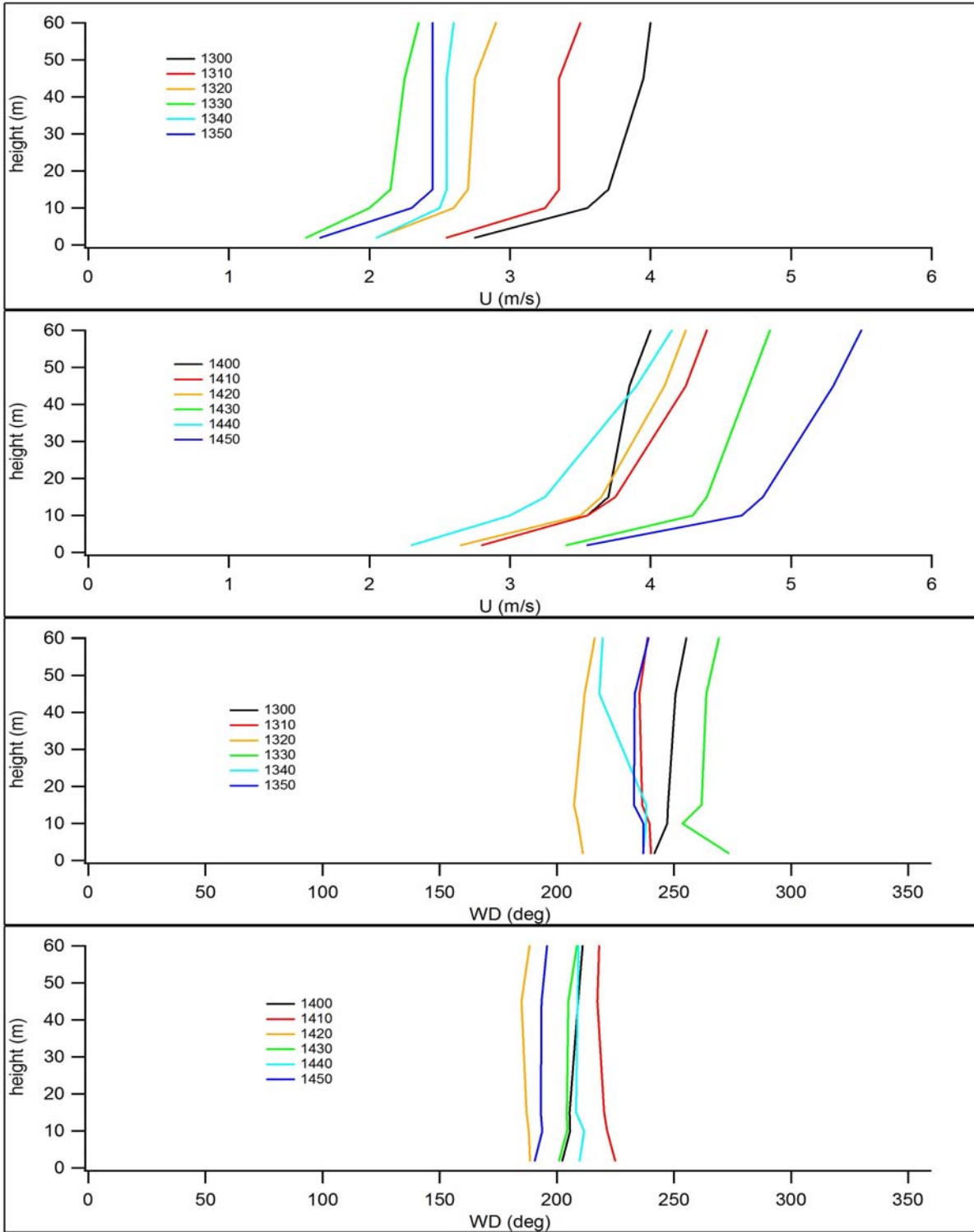


Figure 110. Vertical profiles of wind speed and direction from cup anemometer and wind vane measurements at GRI during IOP2. Times in legend are start times for the 10 minute interval (hhmm MST).

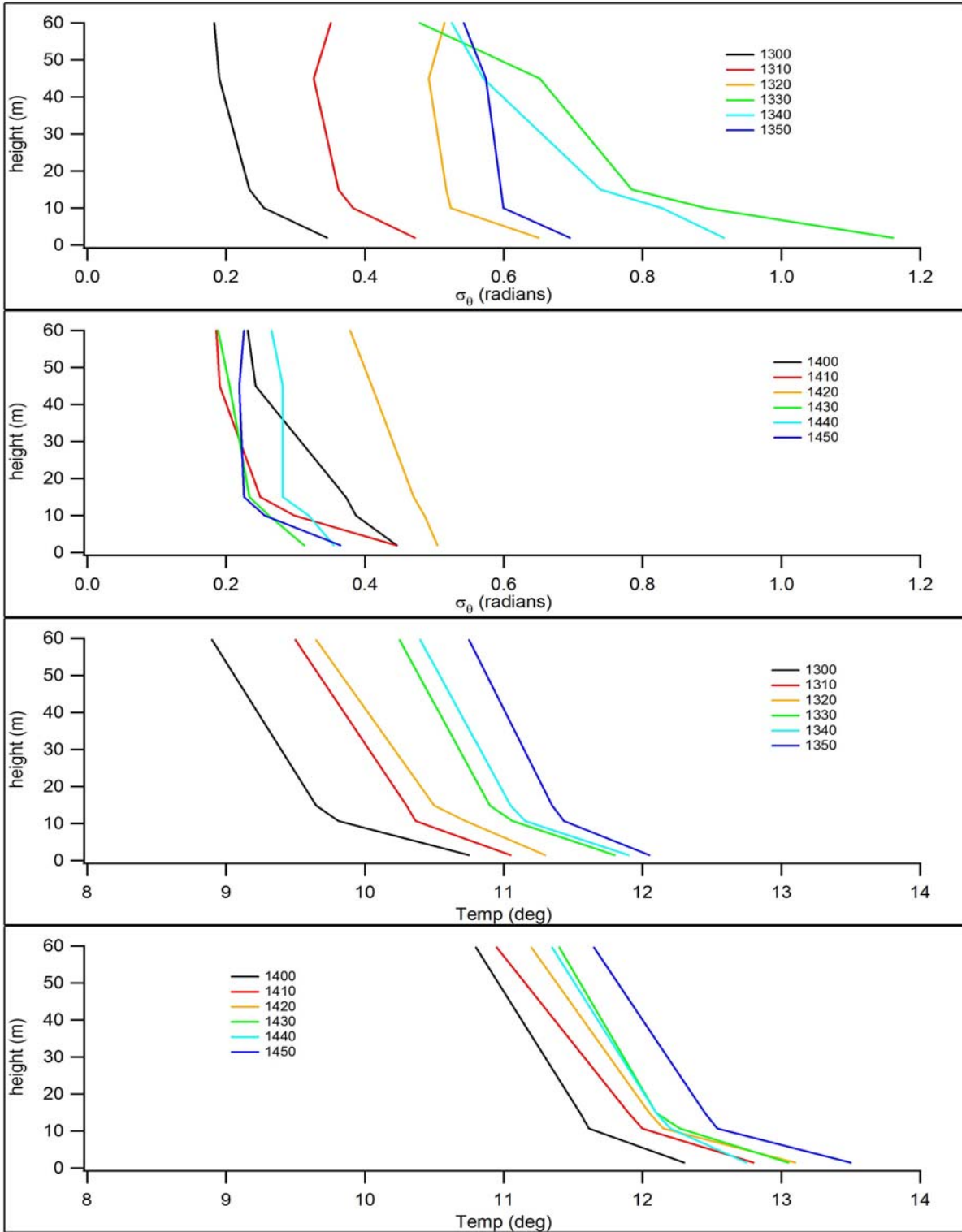


Figure 111. Vertical profiles of σ_θ (from cup anemometers and wind vanes) and aspirated air temperature measurements at GRI during IOP2. Times in legend are start times for the 10 minute interval (hhmm MST).

Stability

Like IOP1, the SRDT-Delta T and σ_A methods gave very different results for (P-G) stability category although the differences were somewhat less severe and occurred mainly during the first hour. The SRDT method yielded all category C while the σ_A method yielded a mix of categories A, B, and C. The magnitudes and sign of the z/L stability parameter values are generally consistent with moderately unstable conditions. The decreasing magnitudes of z/L and the shift from mostly category A during the first half of the IOP to mostly category C during the second half of the IOP are consistent with the other observations of non-stationarity.

Radiosonde Results

Figures 112 and 113 show potential temperature and specific humidity profiles from radiosonde measurements pre and post IOP2. The mixing depths estimated from these plots are given in Table 18.

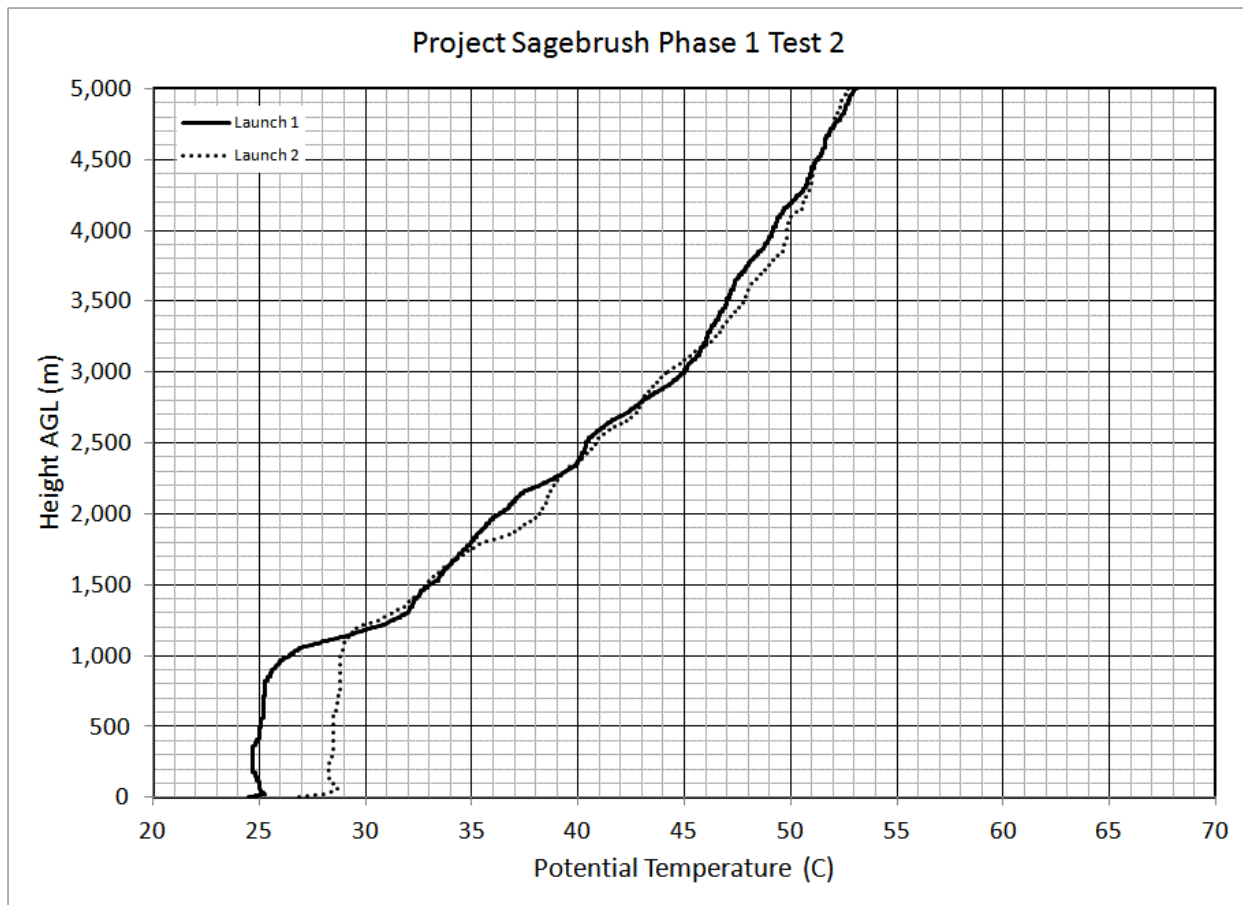


Figure 112. Pre and post IOP radiosonde potential temperature profiles for IOP2.

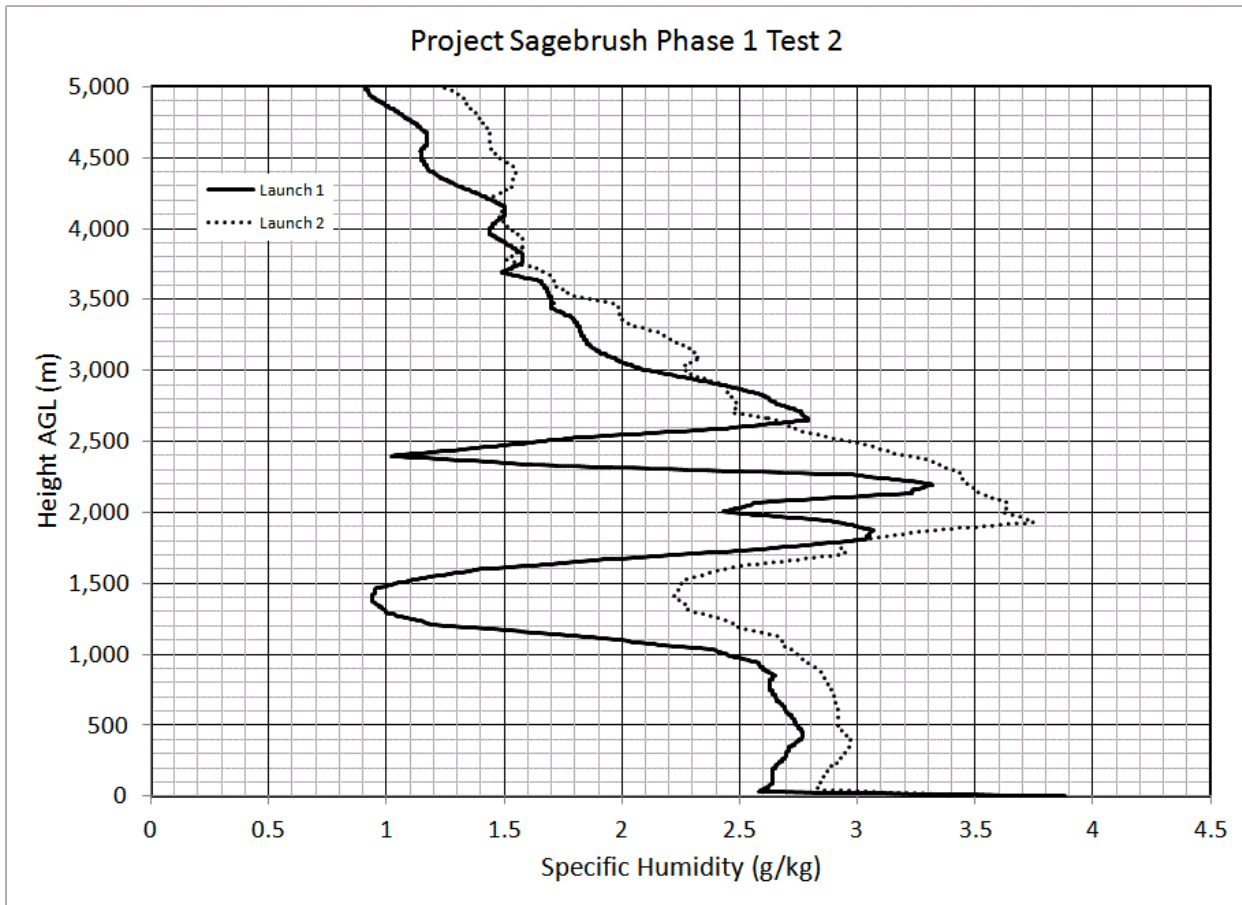


Figure 113. Pre and post IOP radiosonde specific humidity profiles for IOP2.

Concentration Results and Analysis

Figures 114 a-l show the bag sampling results for IOP2. Unlike IOP1, wind directions were such that the plume was mostly present on the sampling array during IOP2 and both measured and normalized concentrations were much higher than IOP1.

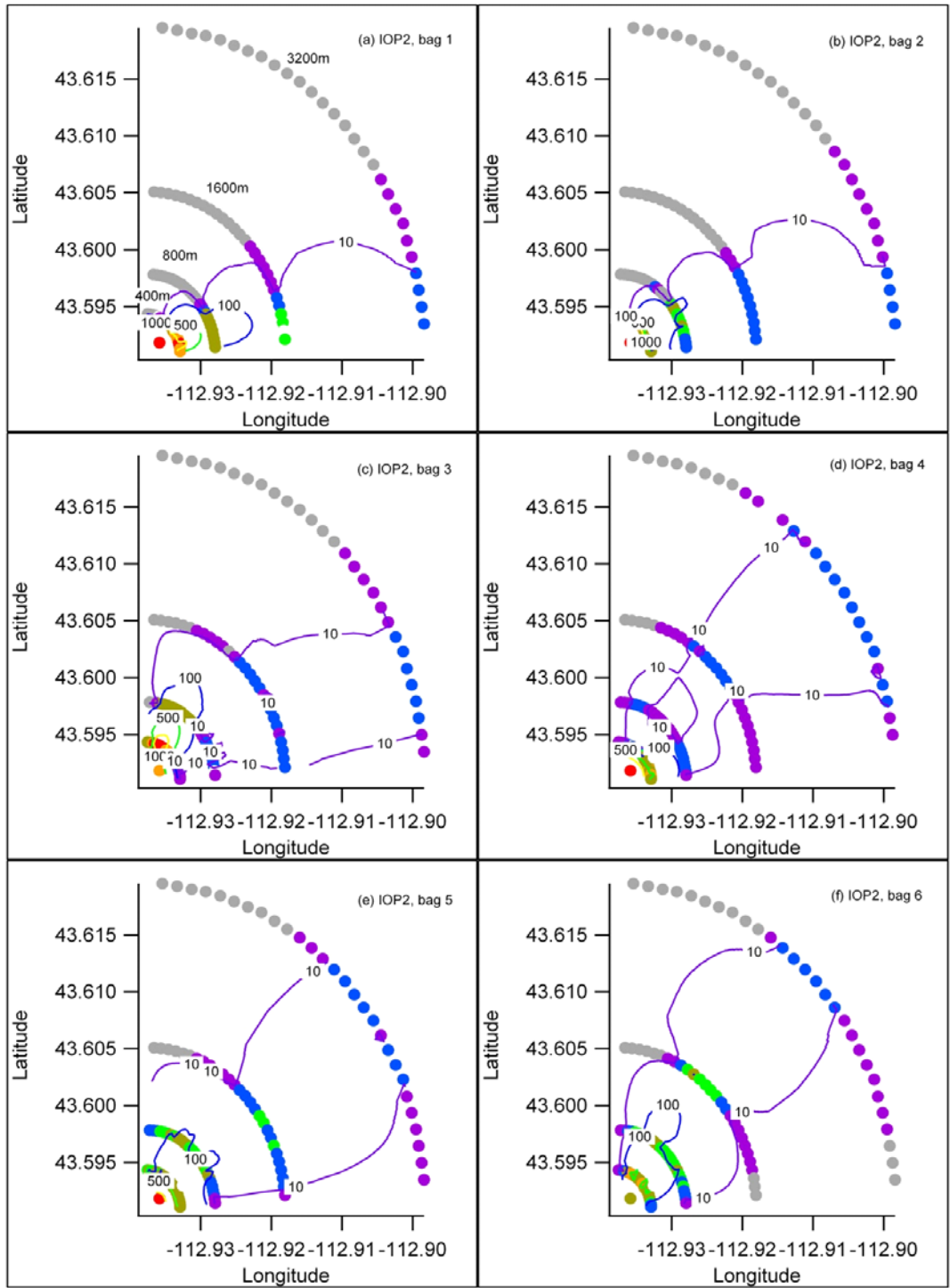


Figure 114. Bag sampling results (a-f, bags 1-6) for IOP2 with color-coded concentration markers for each 1 m AGL bag sampling location and contour lines of normalized concentration. The color scheme for the markers and contours is described in the Introduction to this section.

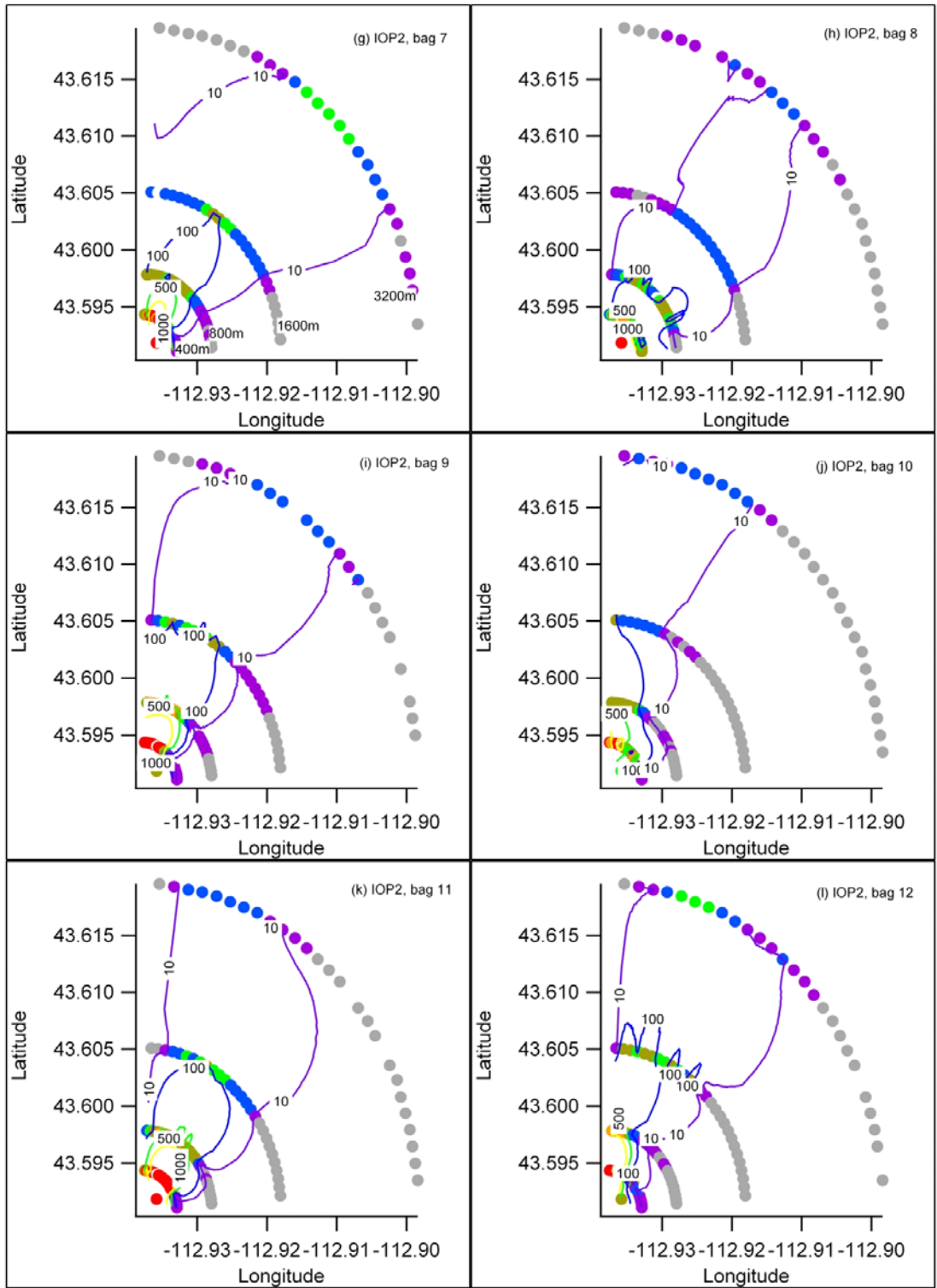


Figure 114 continued (g-l, bags 7-12).

Figures 115 a-l show cross-sections of tracer concentration along each arc for each 10-minute bag sampling period during IOP2. Like IOP1, the plumes were often very broad, a result that is consistent with the relatively large σ_{θ} values observed during most of the IOP (Table 20). Furthermore, individual arc concentration cross-sections often exhibited a non-ideal Gaussian form with profiles having asymmetries about their maxima and/or very irregular concentration profiles. Many cross-section profiles were contained within the sampling array but numerous profiles exhibit truncation at the edge of the sampling array.

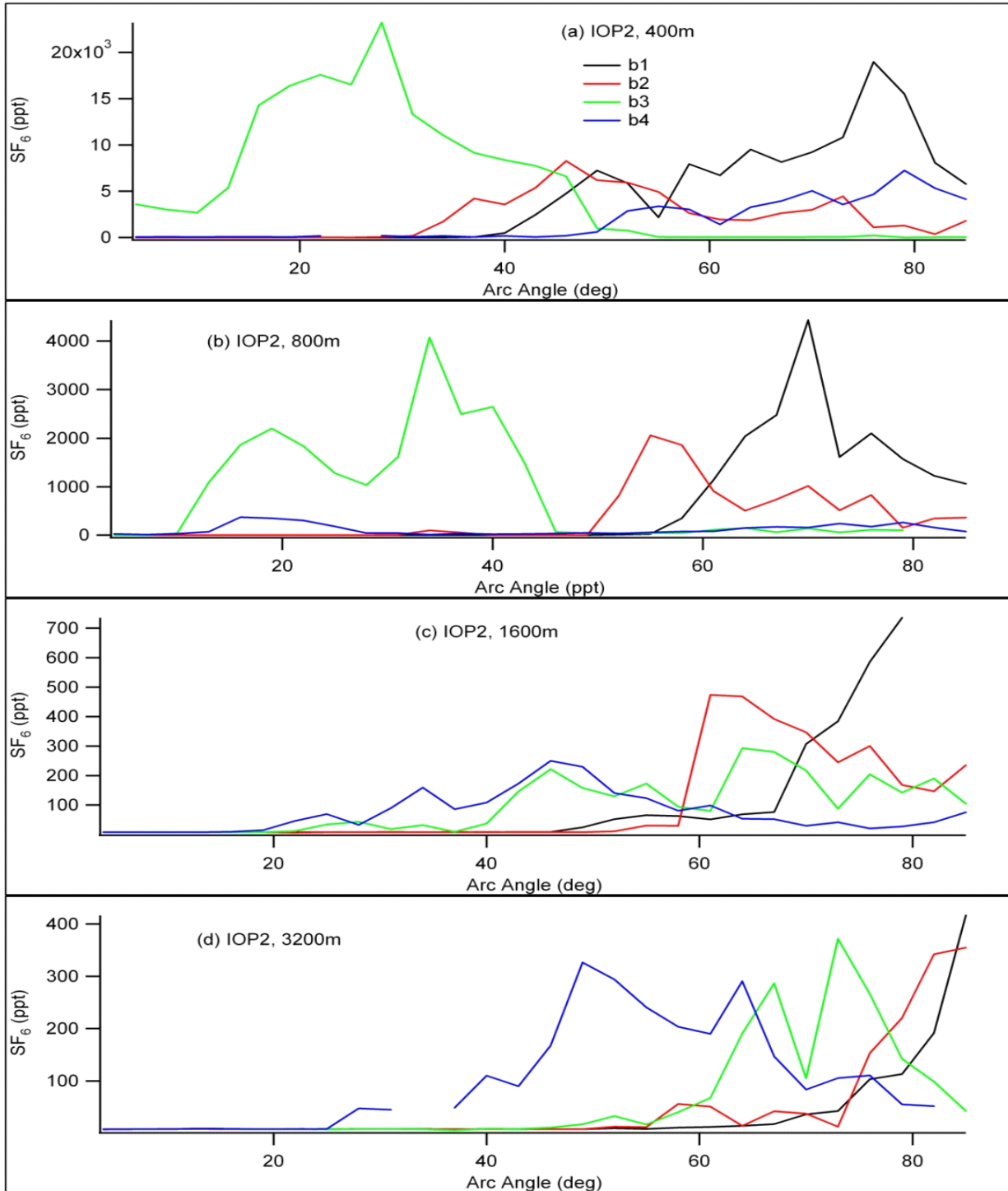


Figure 115. Cross-sections of concentration along each arc for each 10-minute bag sampling period during IOP2. The individual plume cross-section layouts are arranged to illustrate the variation in time, across 40 minutes per layout (a-d, bags 1-4), and the simultaneous variation with distance across all four arcs.

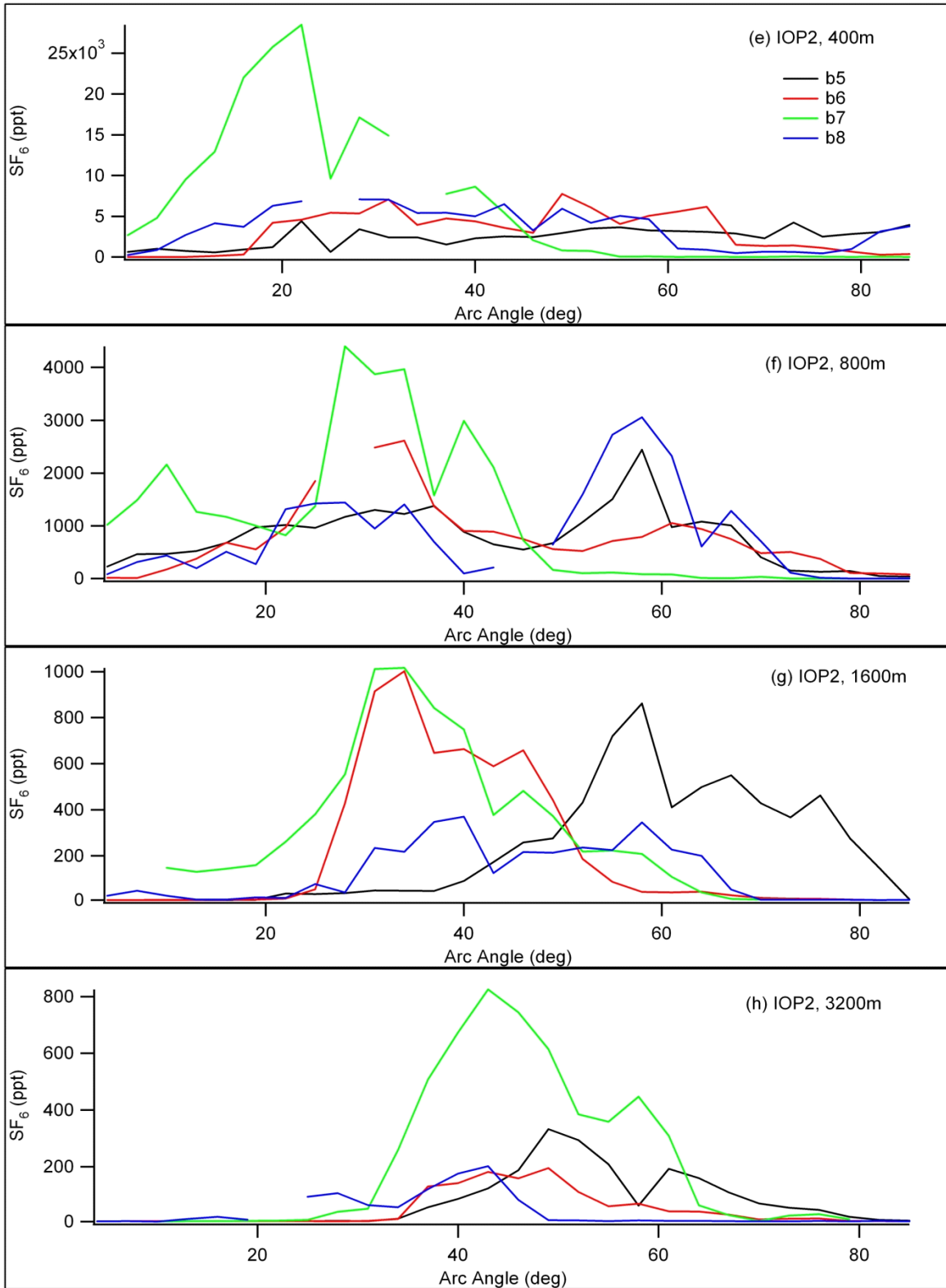


Figure 115 continued (e-h, bags 5-8).

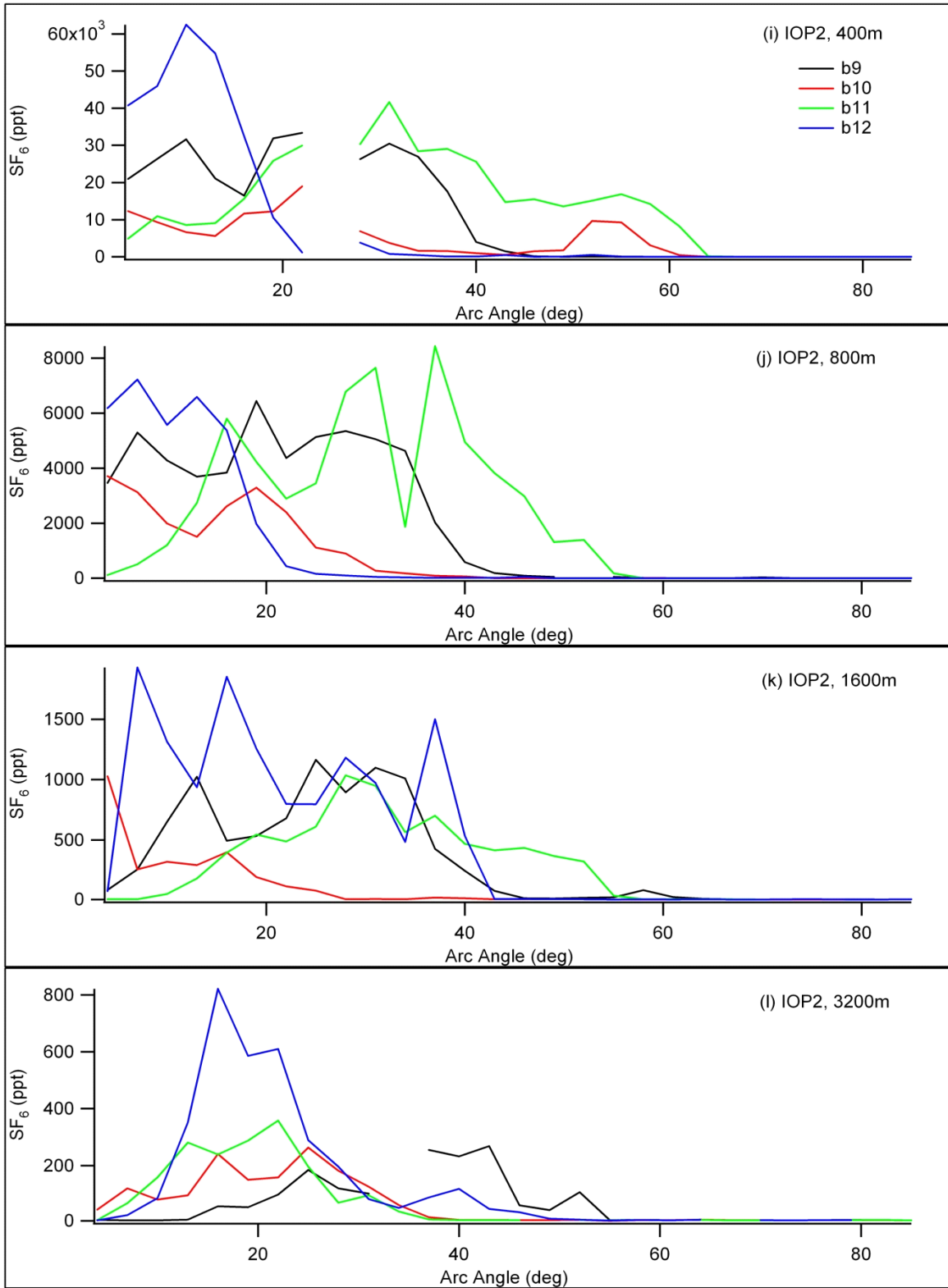


Figure 115 continued (i-l, bags 9-12).

Figures 116 a-l show vertical tracer concentration profiles at the towers at 201, 408, and 499 m downwind for all 10-minute bag sampling intervals for IOP2. Round black markers also show the average tracer concentration obtained from aircraft measurements at the height and downwind distance indicated as described in the Introduction to this section. Several of the vertical profiles suggest evidence of lift off from the surface of the vertical plume centerline.

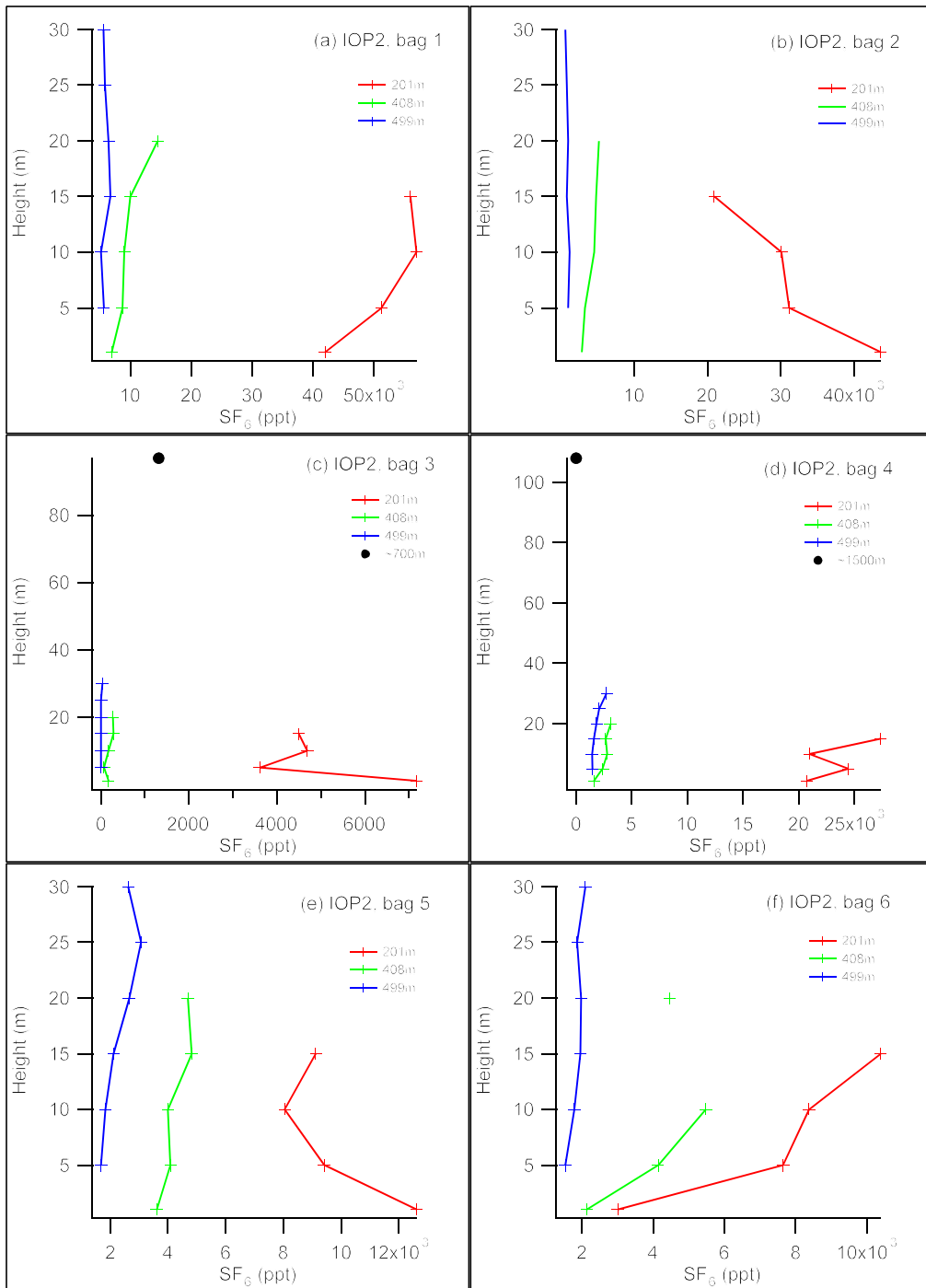


Figure 116. Vertical concentration profiles (bags 1-6) at the towers at 201, 408, and 499 m downwind for all 10-minute bag sampling intervals for IOP2. Round black markers show the average concentration obtained from aircraft measurements at the plotted height. The approximate downwind distance indicated of the aircraft measurement is indicated in the legend.

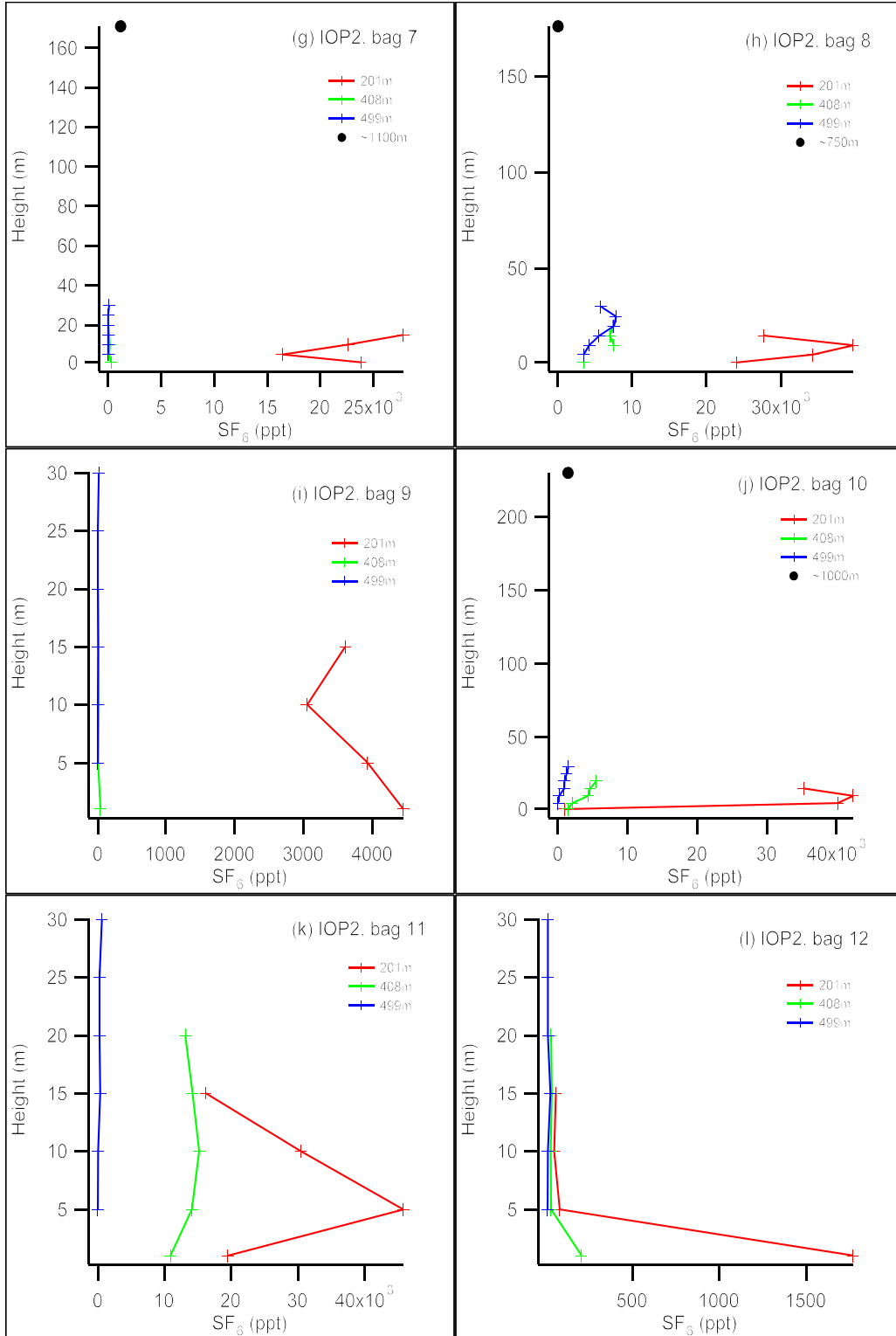


Figure 116 continued (g-l, bags 7-12).

Figure 117 shows time series of SF₆ concentrations measured by the fast response analyzers at the specified arc and arc angle location during IOP2. The plume arrival times on the 1600 m arc appear to have a periodicity of approximately 15 minutes.

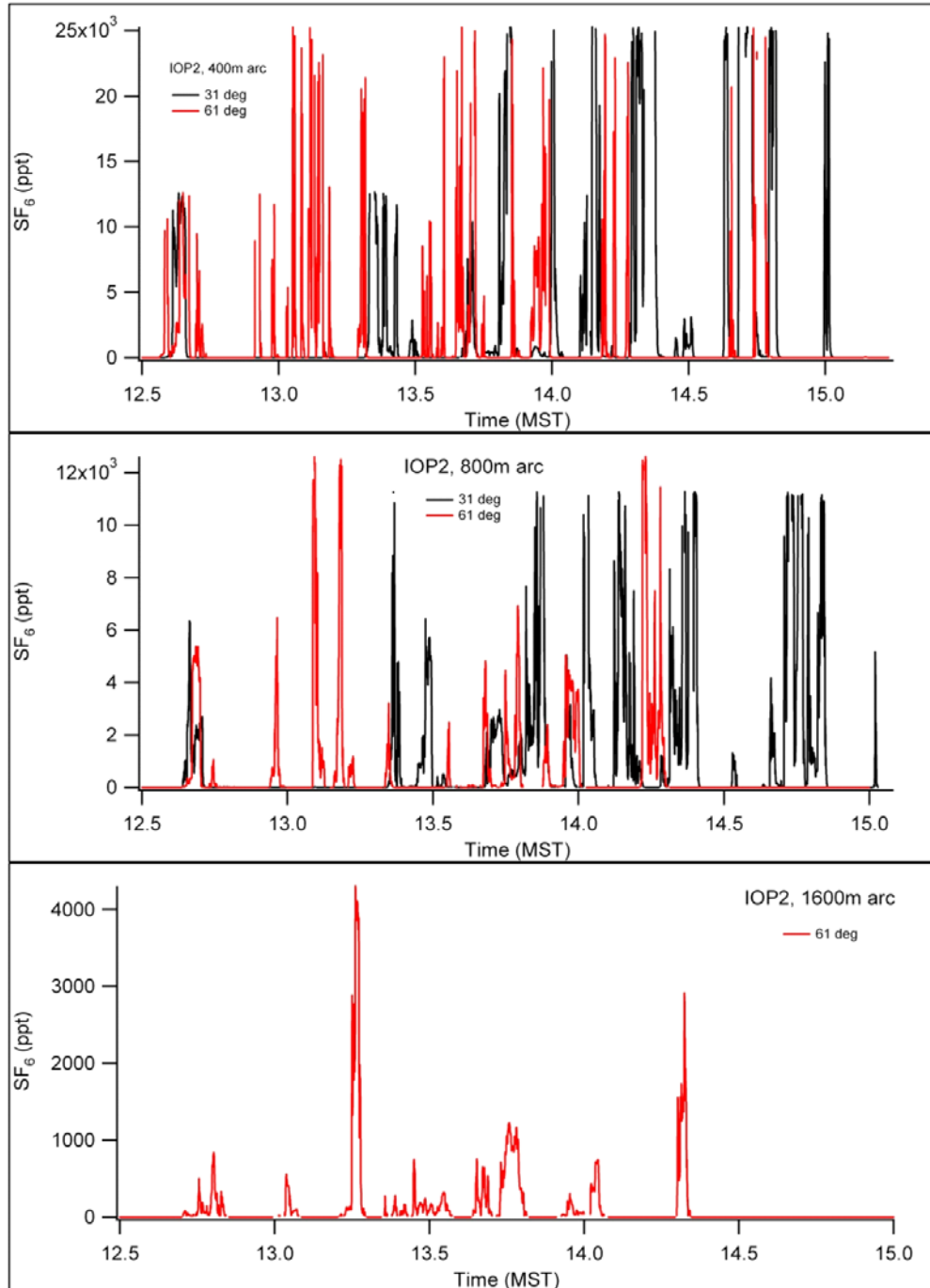


Figure 117. Time series of SF₆ concentrations measured by the fast response analyzers at the specified arc and arc angle location during IOP2.

Figure 118 shows a time series of aircraft height and SF₆ concentrations measured by the onboard fast response analyzer during IOP2. Four high concentration peaks were detected, one at about 100 m AGL one at about 200 m AGL and two at higher levels. There is an interesting peak pattern, best developed between 1300 and 1330 MST, with a relatively higher concentration peak at the 100 m level followed by lower concentration peaks a short time later of about 300 ppt at approximately 300 m height. Figure 119a shows color-coded concentrations along the aircraft flight path during IOP2. Figure 119b is the same except zoomed in over the bag sampling array. The aircraft flew through high SF₆ concentrations over the sampling array, mostly near 800 m downwind and lower concentrations along traverses well beyond 1600 m. The plume patterns seen in the aircraft data were consistent with plume patterns observed in the bag sampling data. Like IOP1, the plume was sometimes off the sampling array and not all of the high concentrations were observed over the array. In comparing the aircraft and tower sampling results for IOPs 1-3, IOP2 clearly has the best developed vertical dispersion over the sampling array. The color scheme and significance of the black markers are described in the Introduction to this section.

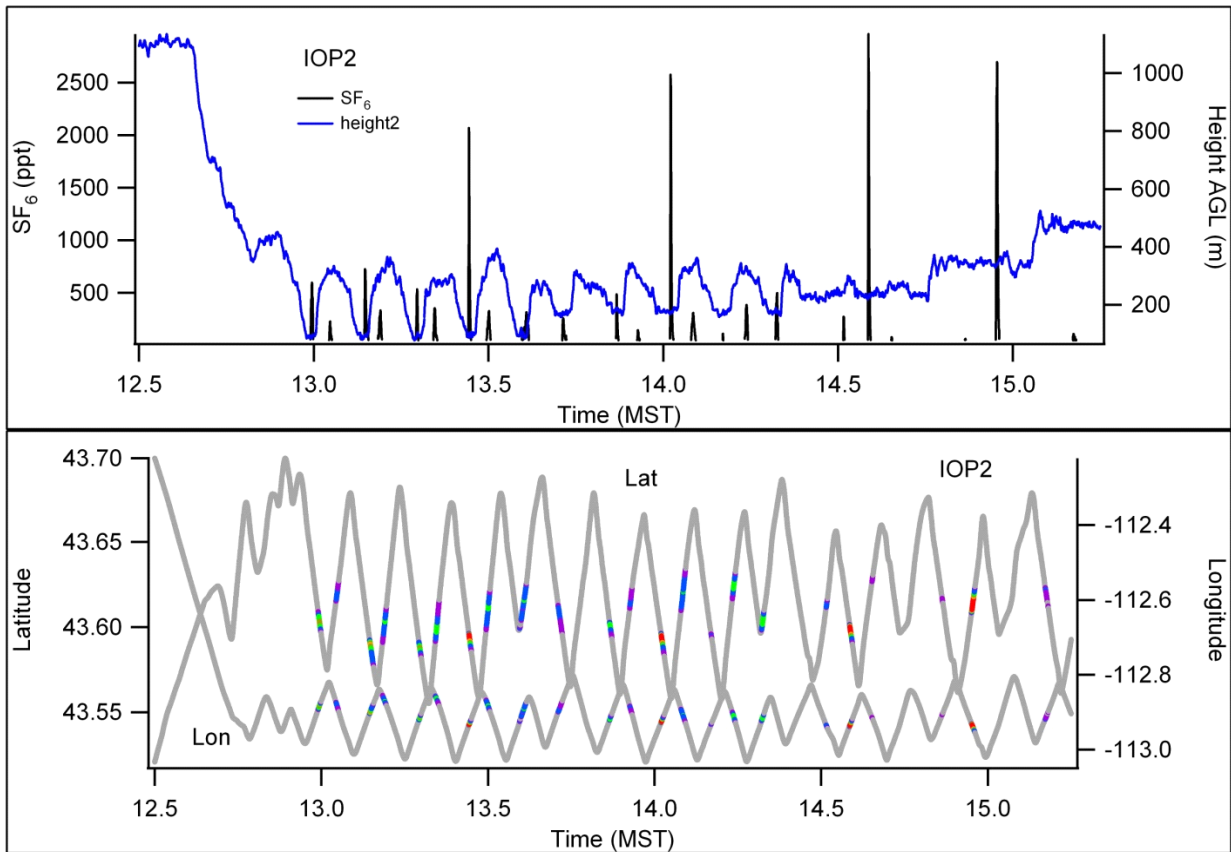


Figure 118. Time series of aircraft height and SF₆ concentrations measured by the onboard fast response analyzer during IOP2. Heights are approximate AGL calculated by subtracting the elevation at the release from the aircraft altitude.

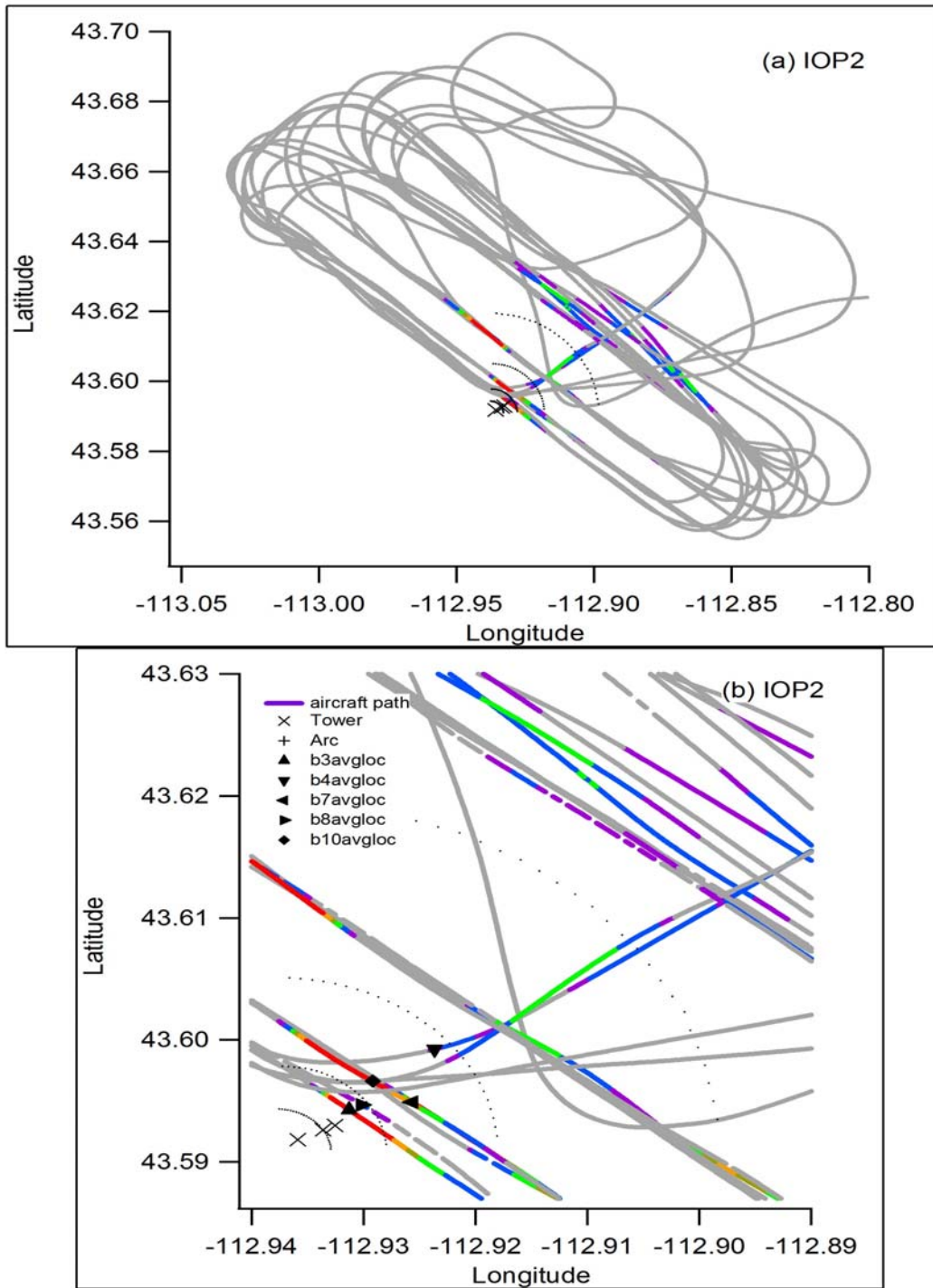


Figure 119. Color-coded concentrations along the aircraft flight path during IOP2 for (a) the overall flight path and (b) zoomed in over the bag sampling array. The color scheme and significance of the black markers are described in the Introduction to this section. They are linked to the black markers in Fig.116 where b# is bag number and avgloc is average location.

IOP3

Date/Time and General Description

IOP3 was conducted on 07 October from 1300-1500 MST (1400-1600 MDT). It was mostly sunny. Winds were consistently moderate to strong in excess of 7 m s^{-1} throughout the IOP under generally clear skies and wind directions were consistently southwesterly and showed minimal variation. All estimates of stability indicate near-neutral conditions. Flows exhibited a high degree of spatial and temporal homogeneity and stationarity. The stationarity in combination with the favorable wind direction made for nearly ideal conditions for advection of the tracer across the sampling array. A summary of the meteorological conditions during IOP3 is shown in Table 21. The SF_6 release rate was 9.93 g s^{-1} (Tables 1 and 2). The fast response analyzers were located on the 400 m arc at 55 degrees, on the 800 m arc at 13, 16, 22, 34, 43, 46, 55, and 76 degrees, on the 1600 m arc at 16, 22, 25, 34, and 55 degrees, and on the airplane. The extra fast response analyzer locations were utilized because of the narrowness of the plume and the high concentrations within the plume. Operators attempted to locate their analyzers to make measurements of the plume while avoiding railing. These efforts were not always successful with the consequence that SF_6 concentrations were often zero or railed.

Table 21. Meteorological conditions during IOP3. Wind speeds, directions, σ_θ , and P-G stability class determinations (EPA, 2000c) are from COC at 10 m. Solar radiation measurements are from FLX. R3 and R4 indicate sonic anemometer data from their respective locations.

Bag	Wind Speed (m s^{-1})	Wind Direction (deg)	Solar Radiation (W m^{-2})	R3 u^* (m s^{-1})	R4 u^* (m s^{-1})	R3 z/L	R4 z/L	σ_θ (deg)	P-G SRDT	P-G σ_A
1	7.5	202.3	412.0	0.39	0.40	-0.11	-0.10	11.0	D	D
2	7.2	212.3	563.0	0.50	0.45	-0.07	-0.07	9.5	D	D
3	7.3	215.5	593.5	0.52	0.45	-0.09	-0.10	11.5	D	D
4	7.8	211.5	582.5	0.55	0.51	-0.06	-0.07	11.2	D	D
5	8.0	214.7	557.5	0.58	0.49	-0.05	-0.08	11.0	D	D
6	8.4	211.1	418.0	0.54	0.57	-0.04	-0.04	8.9	D	D
7	8.9	205.9	450.0	0.64	0.64	-0.03	-0.03	8.5	D	D
8	9.5	211.6	383.5	0.56	0.63	-0.04	-0.02	8.3	D	D
9	10.0	213.1	370.5	0.73	0.56	-0.02	-0.03	7.8	D	D
10	9.7	215.4	334.5	0.66	0.60	-0.02	-0.03	8.2	D	D
11	9.3	219.6	281.0	0.62	0.67	-0.02	-0.02	8.2	D	D
12	9.3	220.0	196.0	0.65	0.62	-0.01	-0.01	8.3	D	D

Winds and Quality Assurance

Figure 120 shows wind speed and direction comparisons for ARLFRD data in the vertical at the GRI and COC towers for IOP3. There was excellent agreement in wind speed and

direction. Flows during IOP3 exhibited strong spatial and temporal homogeneity and stationarity. Fluctuations in wind direction were very small (Fig. 121).

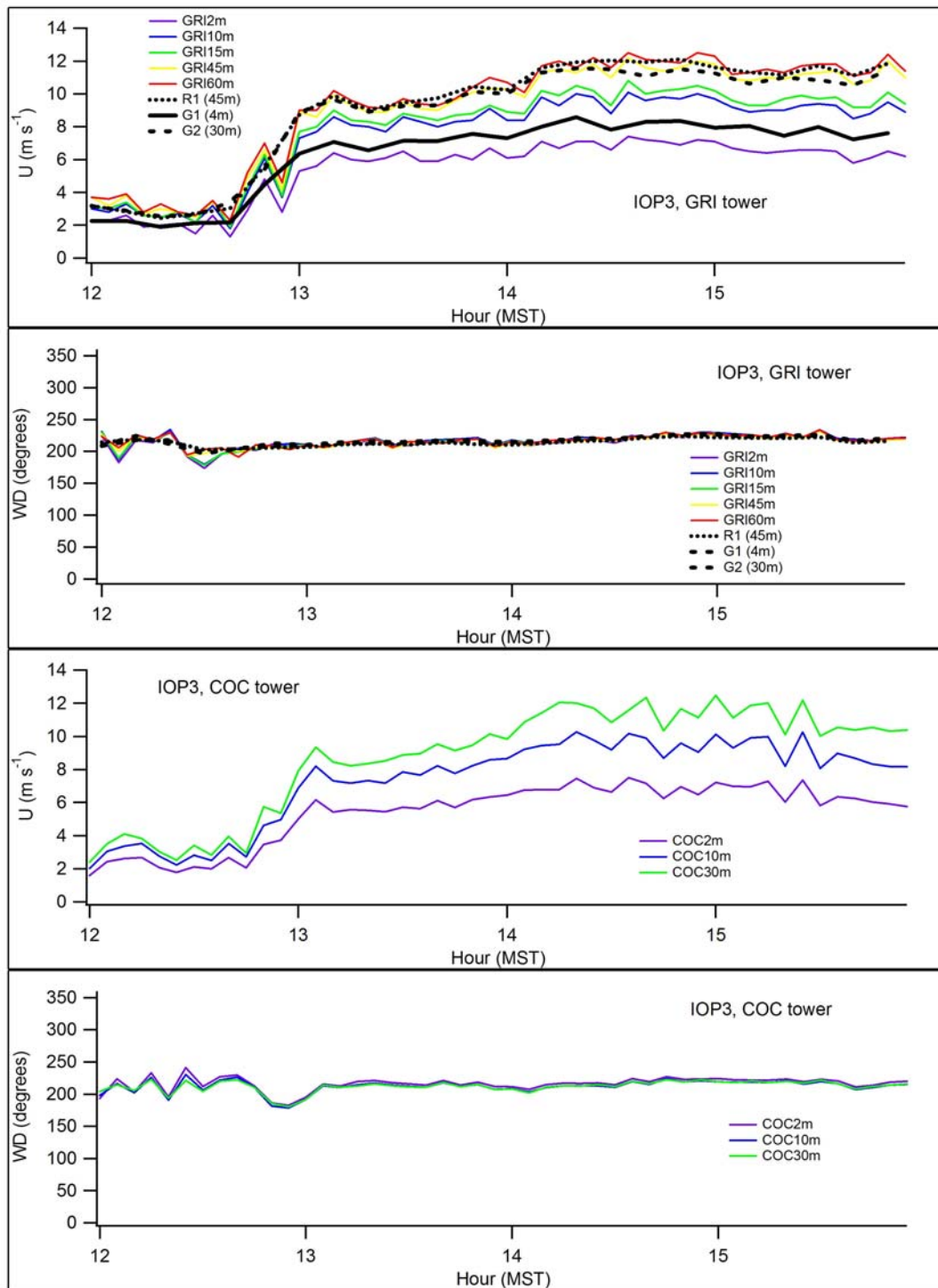


Figure 120. ARLFRD wind speed and direction comparisons in the vertical at GRI and COC for IOP3.

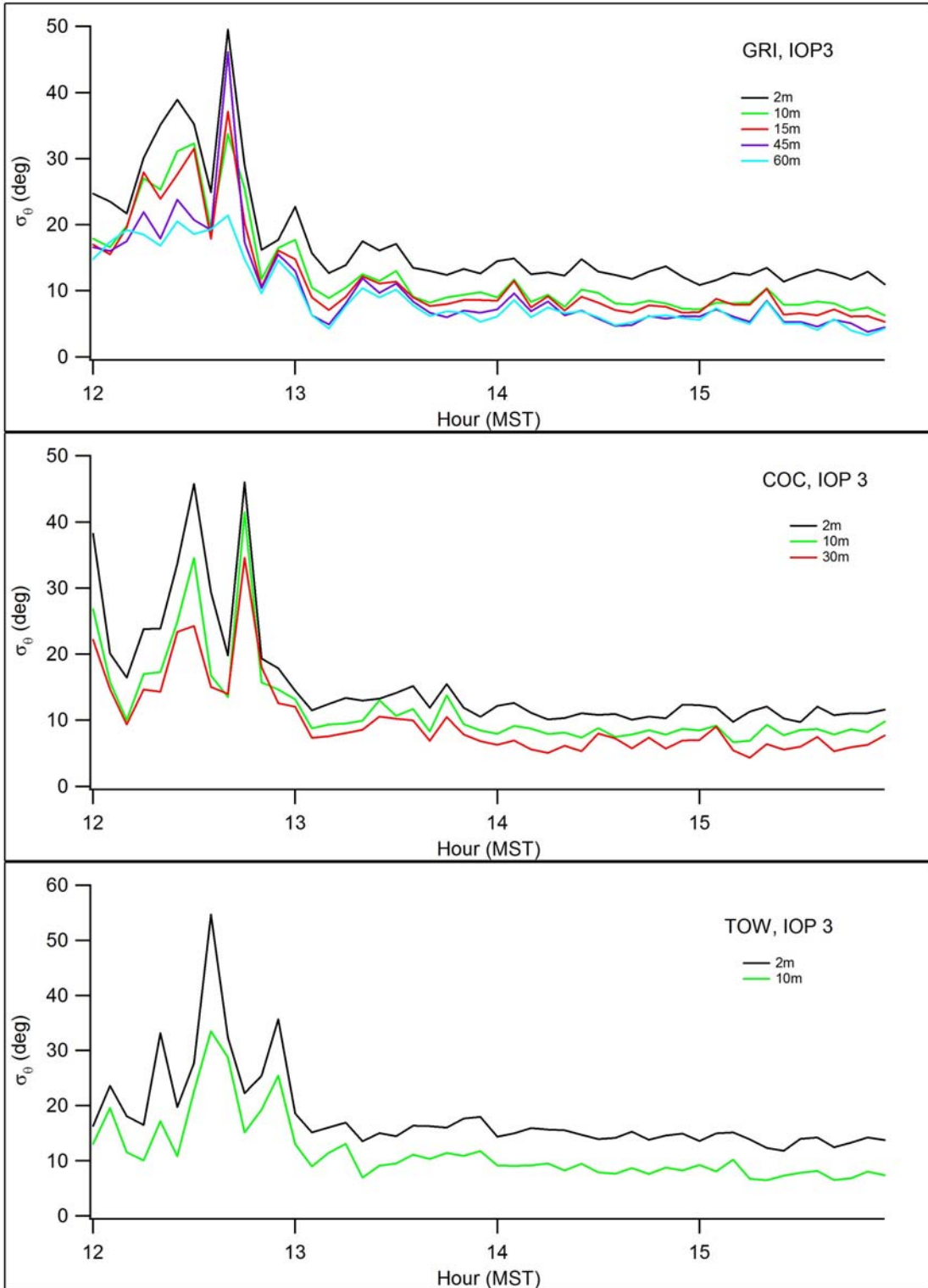


Figure 121. Standard deviation in wind direction σ_θ (σ_A) using wind vanes at GRI, COC, and TOW for IOP3.

Figures 122-124 show wind speed and direction comparisons in the horizontal across the study area at 2 m, 10 m, 30 m, 45 m, 60 m, and 160 m from the data available. The comparisons are the same as those described for IOP1. Observations showed good agreement between sites and measurement type across the study area. The available ART and ASC sodar data show some consistency with the PRO wind profiler observations although there was little data recovery by the sodars for comparison. There is little evidence for a problem with the measurements. Plume advection was across the sampling array throughout the sampling period.

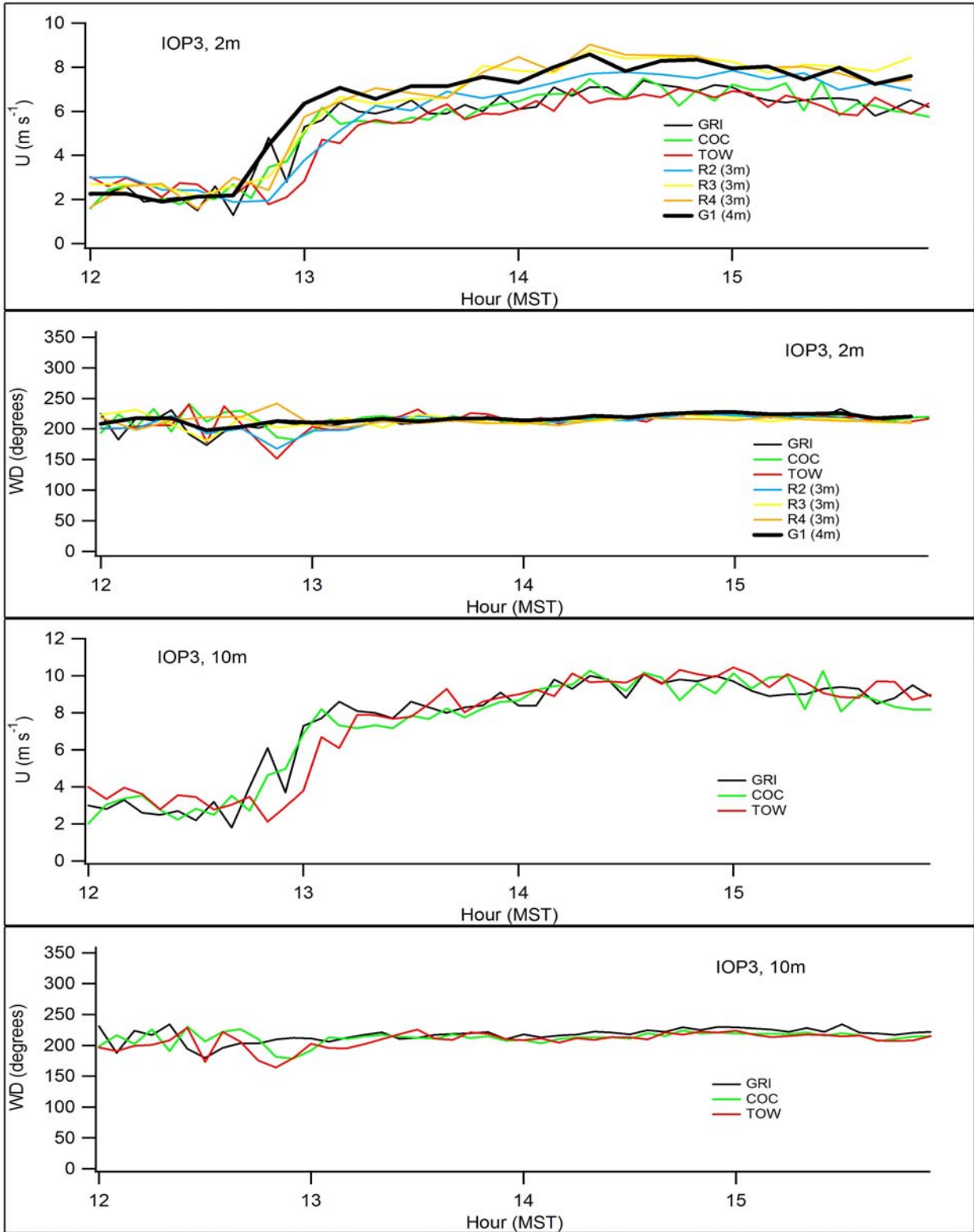


Figure 122. ARLFRD wind speed and direction comparisons in the horizontal at 2 and 10 m during IOP3.

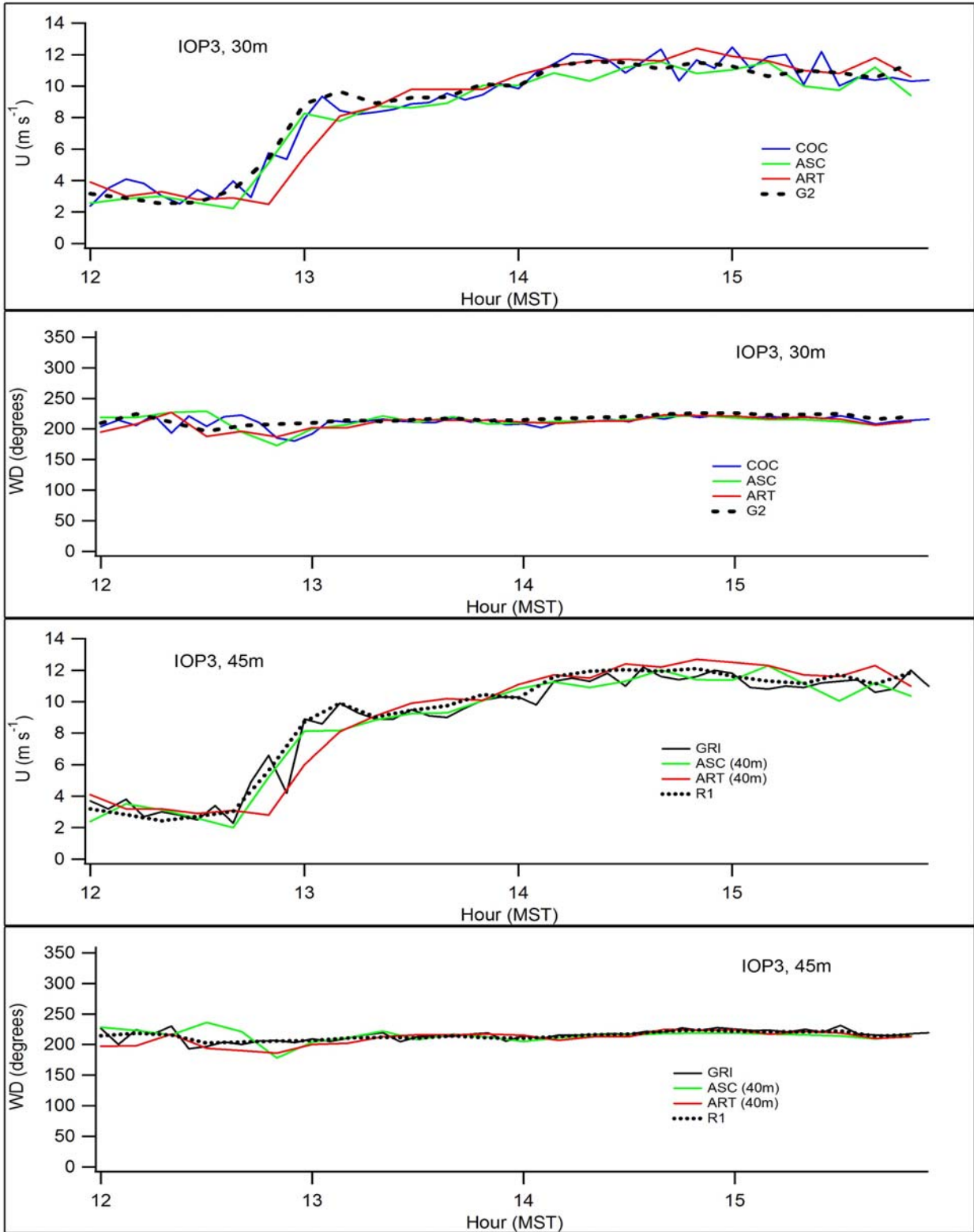


Figure 123. ARLFRD wind speed and direction comparisons in the horizontal at 30 and 45 m during IOP3.

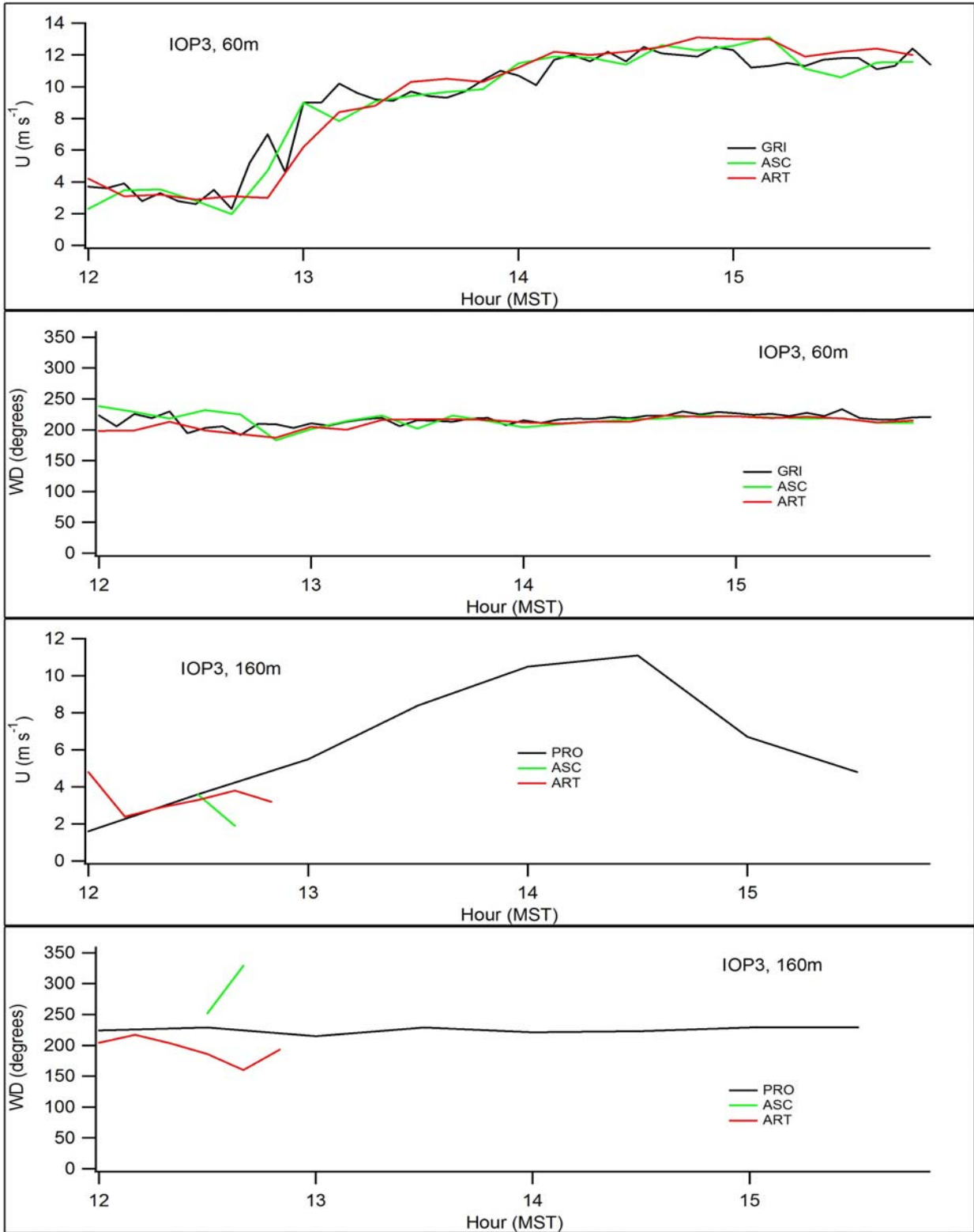


Figure 124. ARLFRD wind speed and direction comparisons in the horizontal at 60 and 160 m during IOP3.

Figures 125-127 show time-height cross-sections for wind speed and direction for the ASC sodar, ART sodar, and PRO wind profiler, respectively. The wind speeds and directions measured at ASC, ART, and PRO were consistent with the measurements at the Grid 3 tower and sonic anemometers. There is little or no evidence of an upper level shear layer in the PRO data like that observed for IOPs 1 and 2.

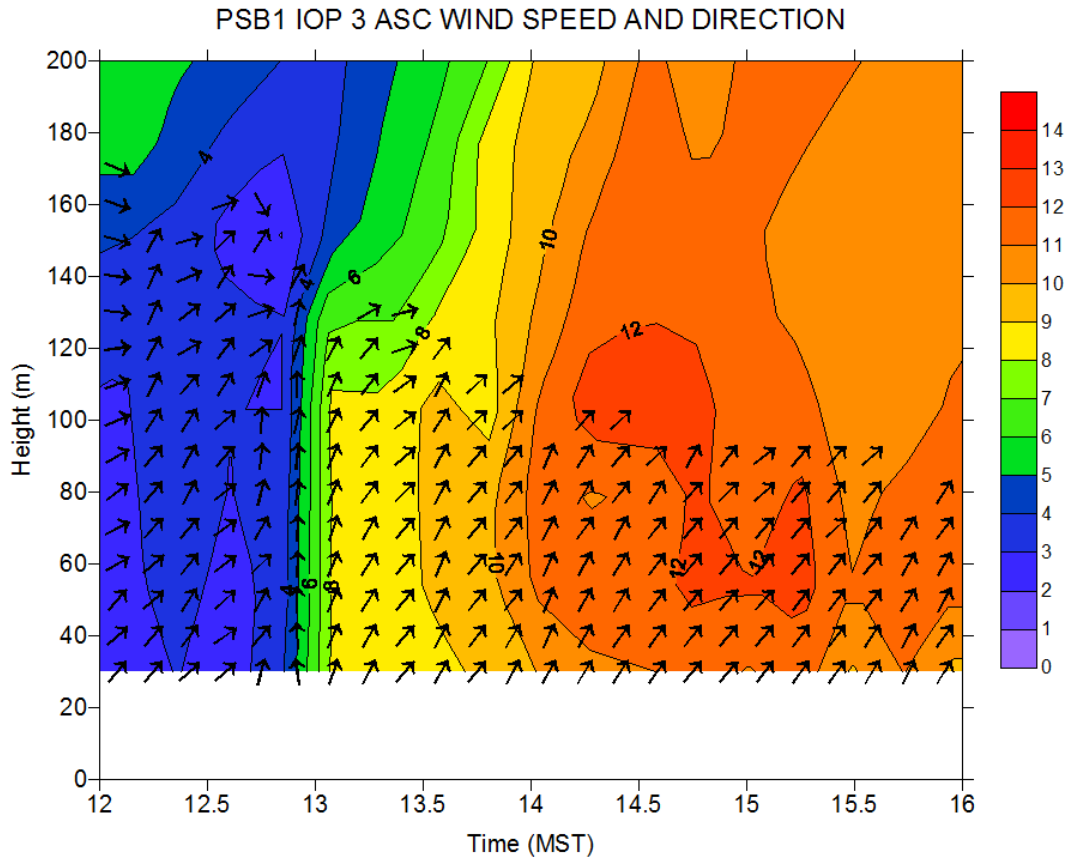


Figure 125. Time-height cross-section of wind speed and direction at ASC sodar during IOP3.

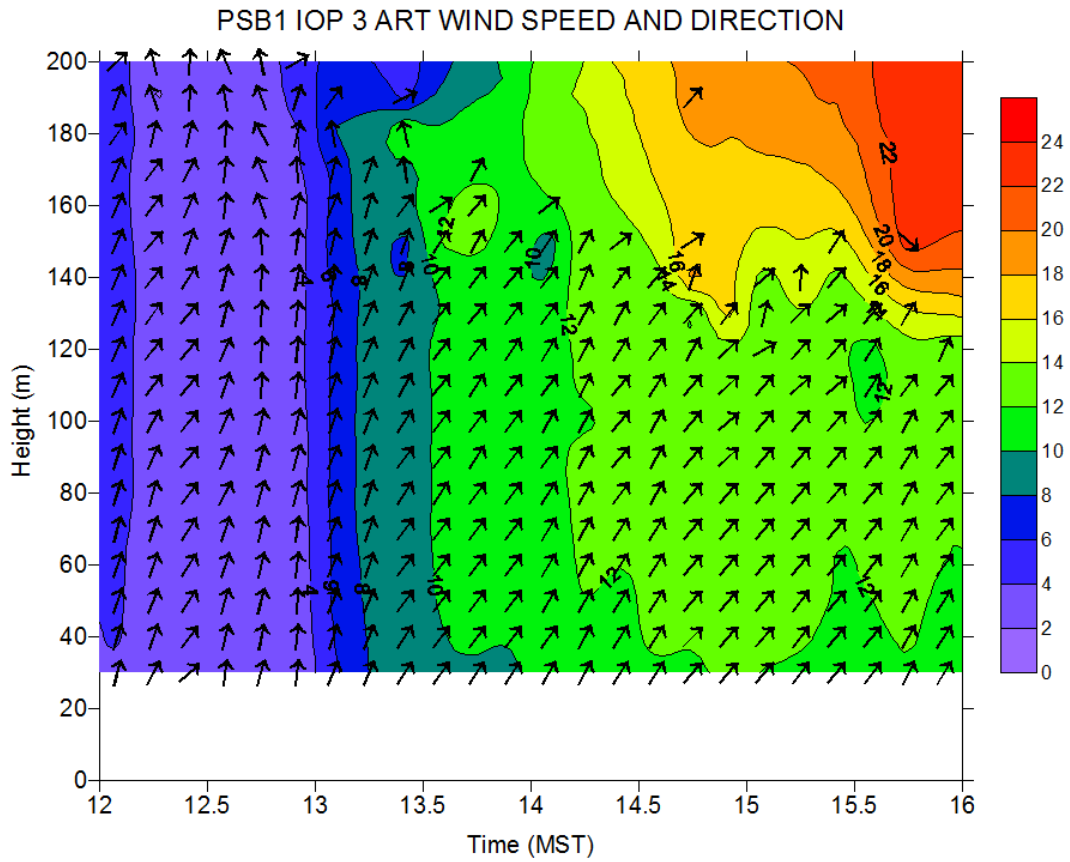


Figure 126. Time-height cross-section of wind speed and direction at ART sodar during IOP3.

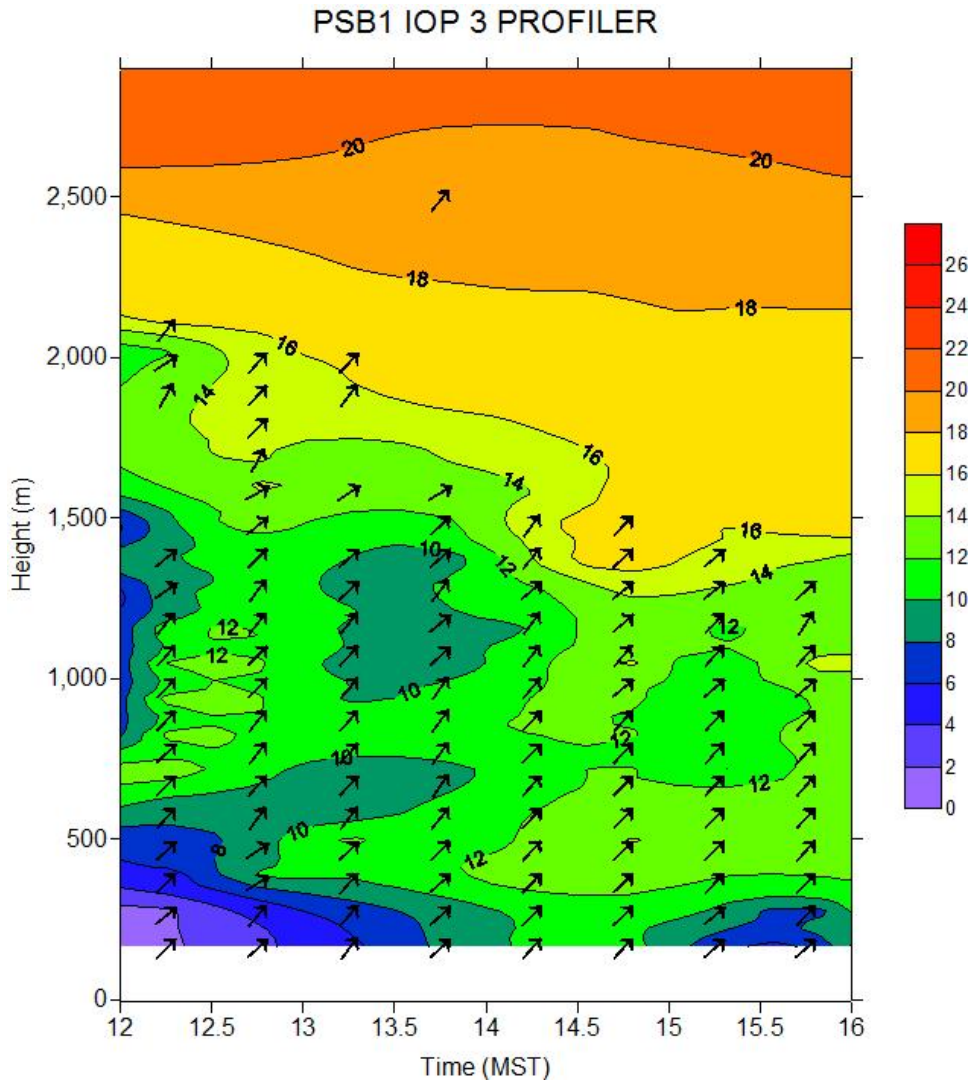


Figure 127. Time-height cross-section of wind speed and direction at wind profiler (PRO) during IOP3.

Turbulence

Figures 128 and 129 show time series of the turbulence measurements for 10 and 30-minute averaging periods, respectively, for σ_w , turbulent kinetic energy (TKE), u_* , kinematic heat flux $\langle w'T' \rangle$, and $1/L$ where L = Obukhov length. The 30-minute periods more correctly account nonstationarity affects and should provide more reliable estimates than the 10-minute averaging periods. Observations showed good agreement between sites across the study area. The high values of σ_w at G2 are due to the fact these represent measurements at 30 m whereas all the other measurements are between 3-4 m height. The results for L indicate that the stability conditions were consistently near neutral throughout the experiment due to the high wind speeds. Conditions were more unstable in the hour prior to the start of tracer measurements at 1300 h.

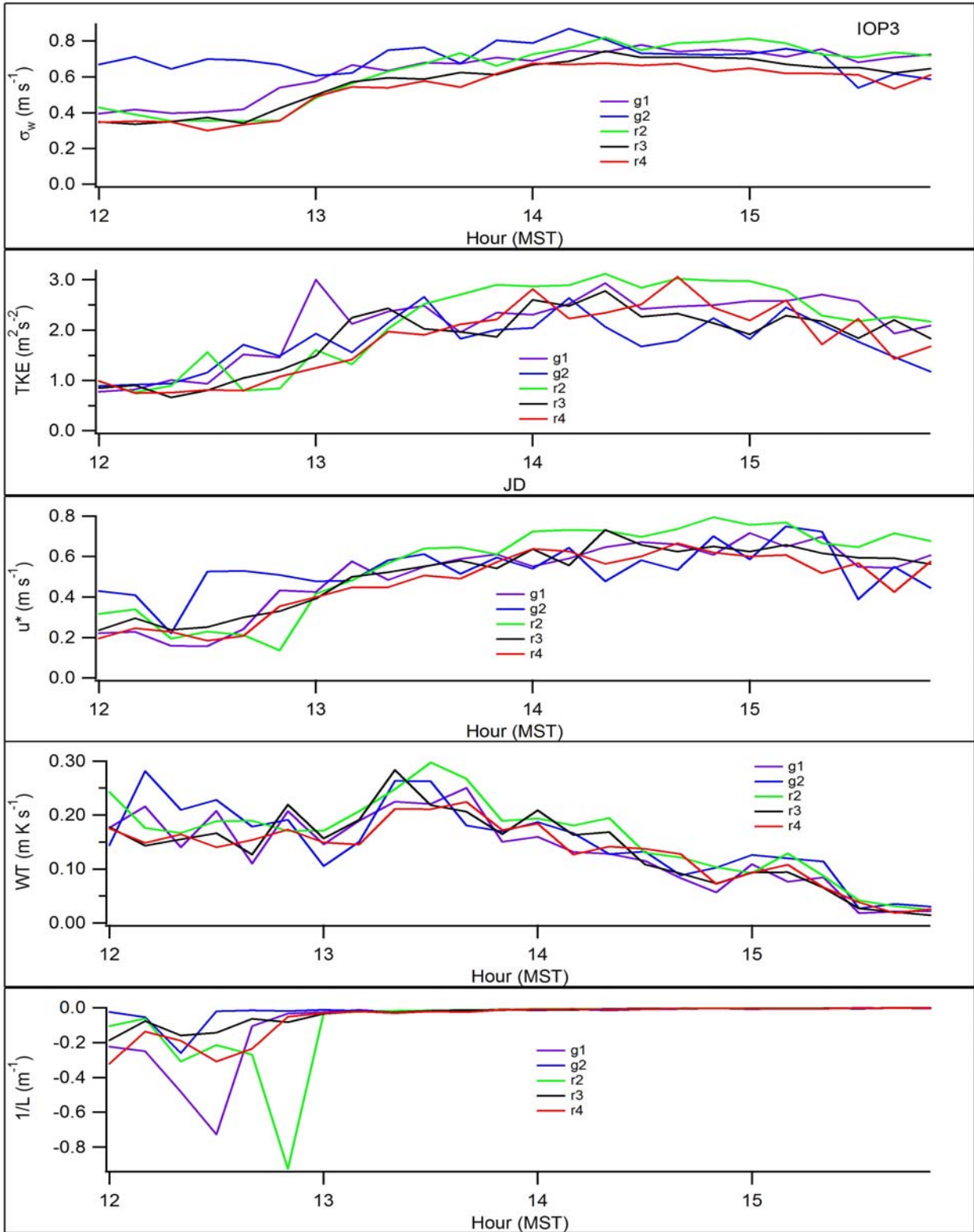


Figure 128. ARLFRD sonic anemometer 10-minute averages for σ_w , TKE, u_* , kinematic heat flux, and $1/L$ during IOP3 (G1, G2, R2, R3, and R4).

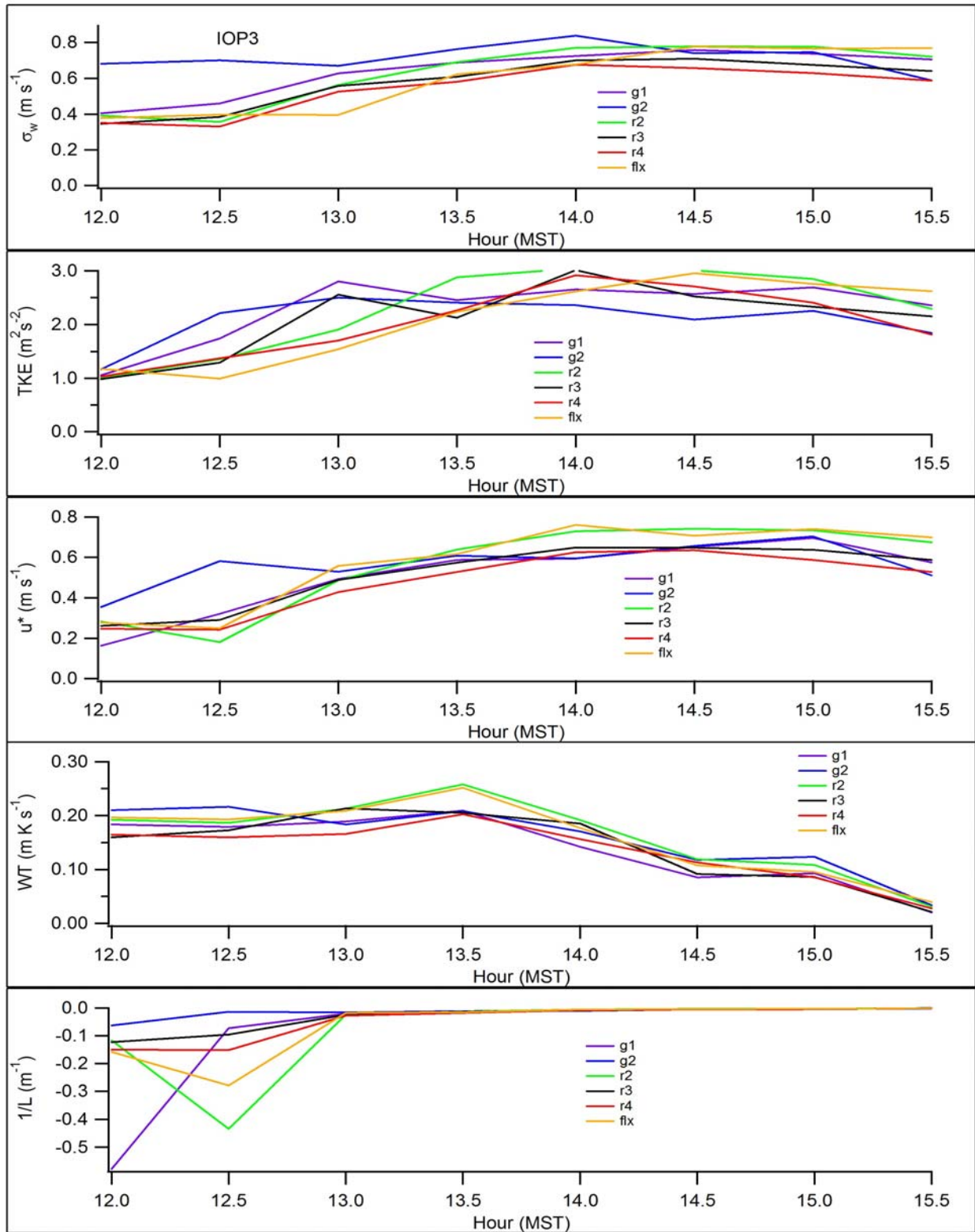


Figure 129. ARLFRD sonic anemometer 30-minute averages for σ_w , TKE, u_* , kinematic heat flux, and $1/L$ during IOP3 (G1, G2, R2, R3, and R4).

Figures 130 and 131 show time-height cross-sections for σ_w and TKE for the ASC sodar. Figures 132 and 133 show time-height cross-sections for σ_w and TKE for the ART sodar. The absolute magnitudes of TKE and σ_w shown for the ART and ASC sodars should not be assumed to be comparable between the two sodars nor with the same measurements at the sonic anemometers. The magnitudes of σ_w at ASC and ART are usually similar but the values of TKE at the ART were typically about an order of magnitude greater than the ASC. Restricting the comparison to the relative magnitudes of TKE and σ_w for each sodar, within an IOP or across IOPs, should be valid. The σ_w measured at the ASC and ART were similar in magnitude to those measured at the sonic anemometers with ASC and ART being a little lower/higher, respectively (Fig. 128). The TKE measured at ASC and ART were less/more, respectively, than at the sonic anemometers. Figure 134 shows a time-height cross-section for temperature from the RASS.

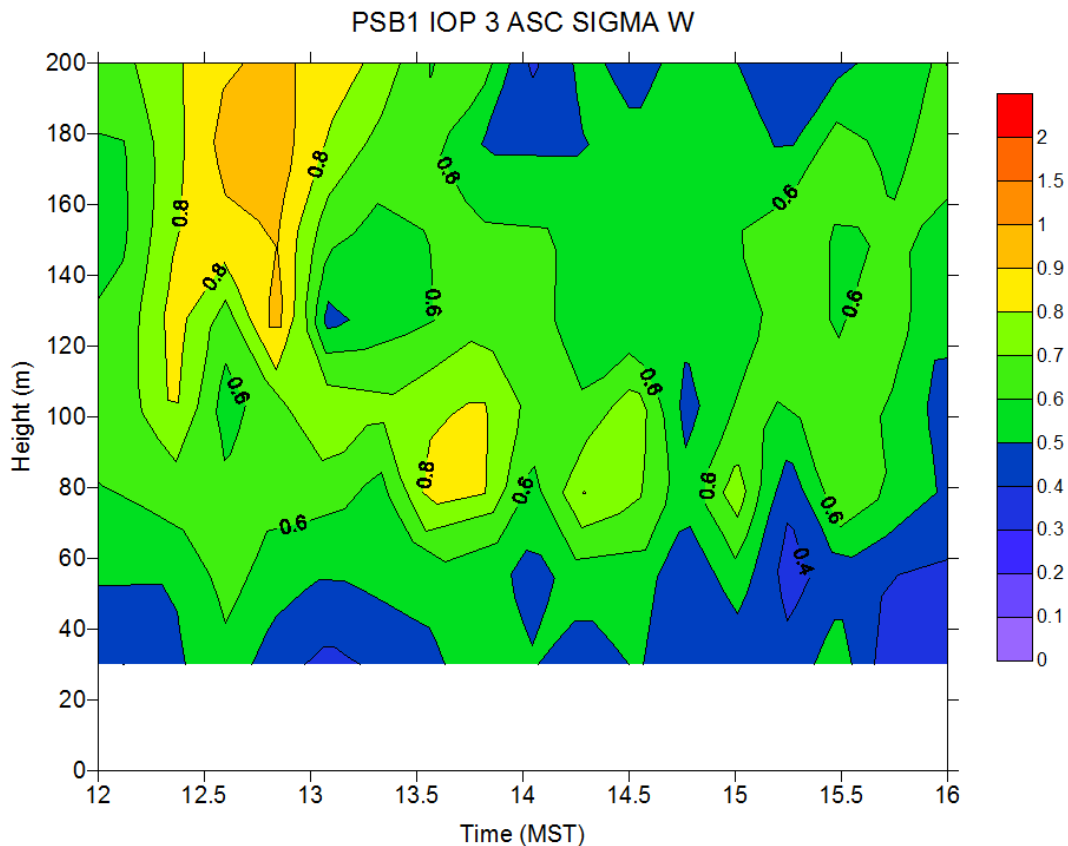


Figure 130. Time-height cross-section of σ_w at ASC sodar during IOP3.

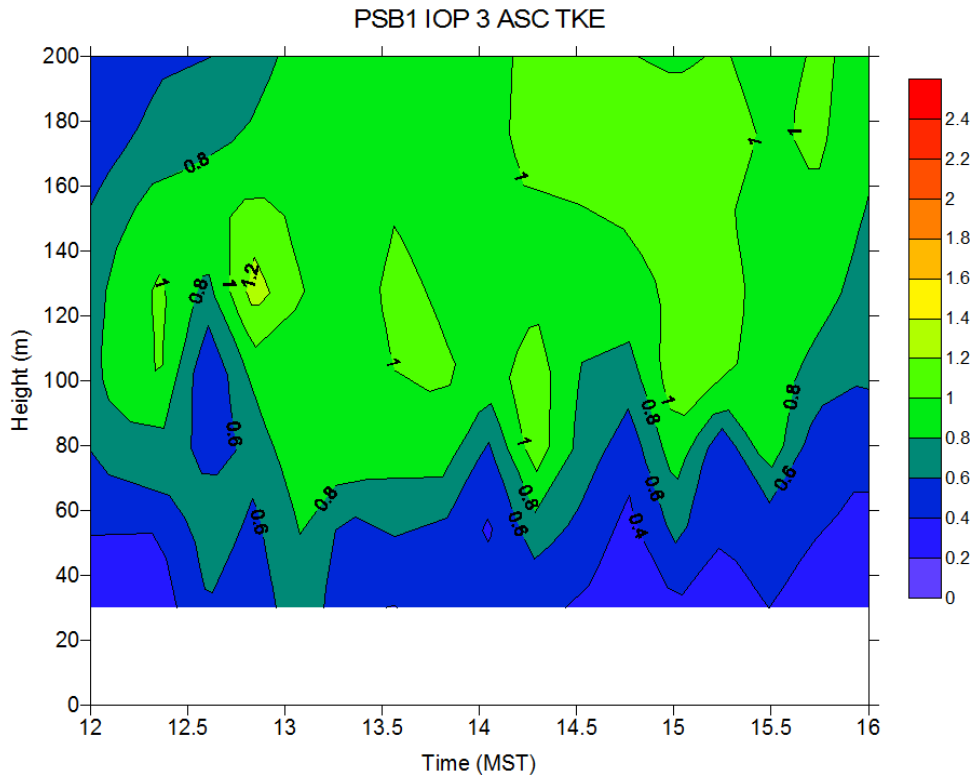


Figure 131. Time-height cross-section of TKE at ASC sodar during IOP3.

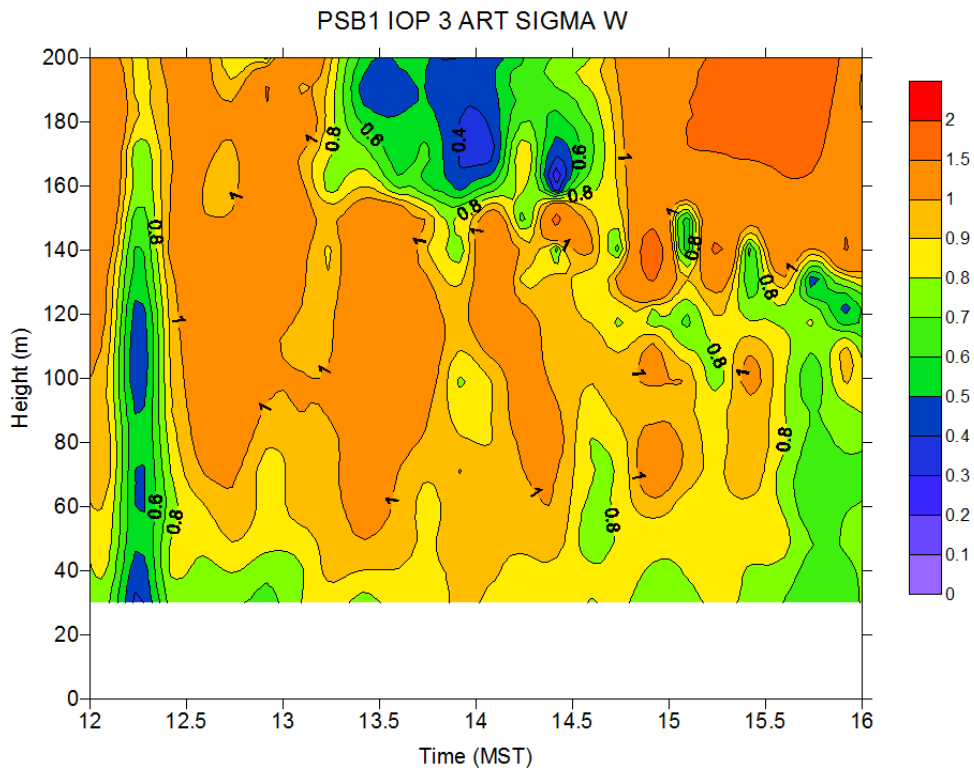


Figure 132. Time-height cross-section of σ_w at ART sodar during IOP3.

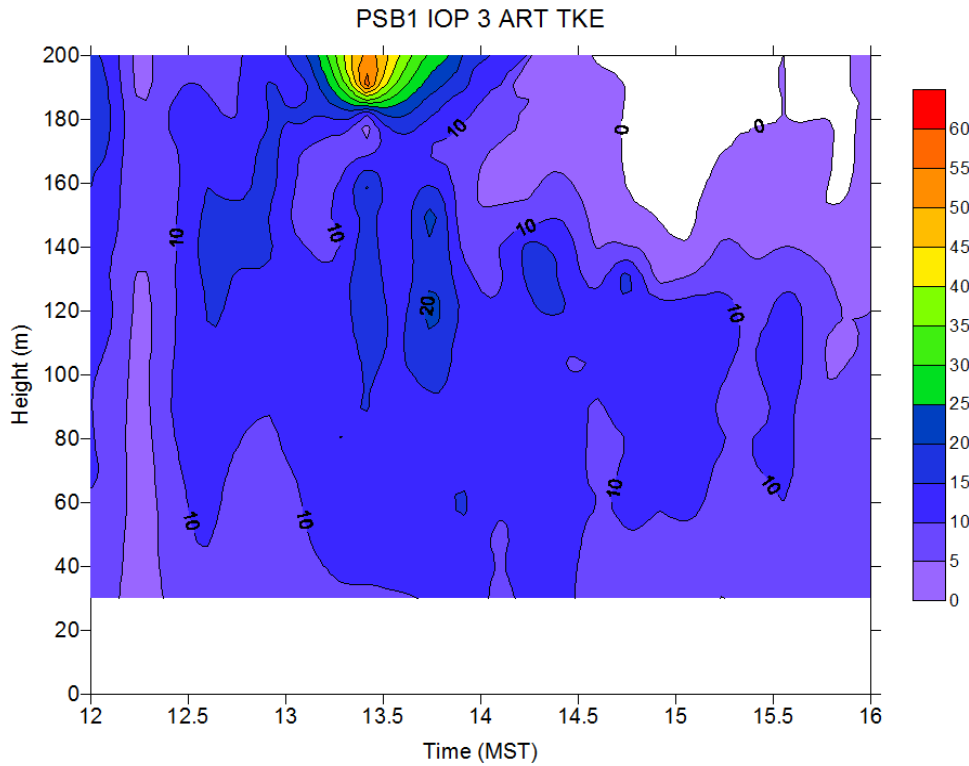


Figure 133. Time-height cross-section of TKE at ART sodar during IOP3.

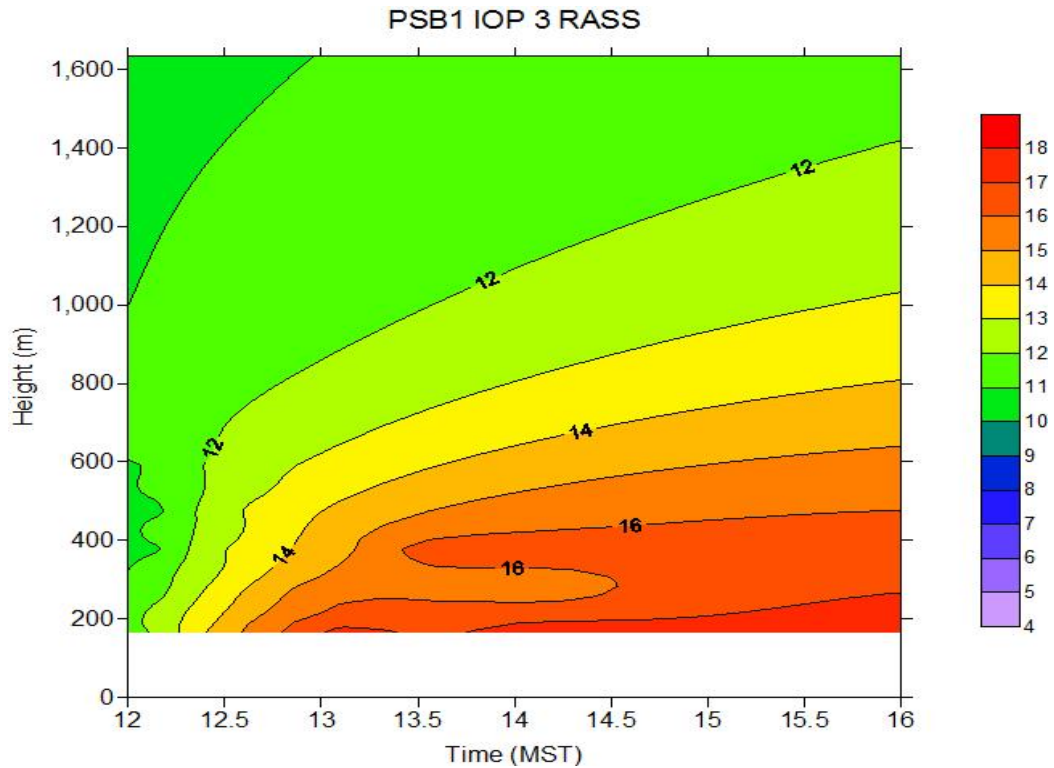


Figure 134. Time-height cross-section of virtual temperature at the RASS during IOP3. Temperatures are in degrees C.

Vertical profiles of wind speed, wind direction, and calculated turbulence parameters from sonic anemometer measurements at GRI during IOP3 are shown in Figs. 135-137. Vertical profiles of wind speed, wind direction, and turbulence intensity (σ_θ) from cup anemometers and wind vanes plus aspirated air temperature during IOP3 are shown in Figs. 138 and 139. Turbulence intensities (σ_v/U) were much smaller than in IOPs 1 and 2 and there was general consistency between the sonic and cup and vane (σ_θ) results. There were again some discrepancies in turbulent intensity profiles at the 4, 30, and 45 m sonic levels relative to the other sonic levels but they were not consistently present (Fig. 136). These 3 levels correspond to the ARLFRD sonics while the other 4 levels are WSULAR sonics. There does not appear to be a clear pattern of better agreement between the turbulent intensities measured by the ARLFRD or WSULAR sonics compared to those measured by the cup anemometers and wind vanes (Fig. 139). A similar pattern of TKE sonic profile discrepancies was also observed (Fig. 137). There was good agreement between wind speed measurements made by the sonic anemometers and cupanemometers and wind vanes. There were some inconsistencies in wind direction between the ARLFRD and WSULAR sonics with the ARLFRD sonics showing somewhat better consistency with the cup and vane results.

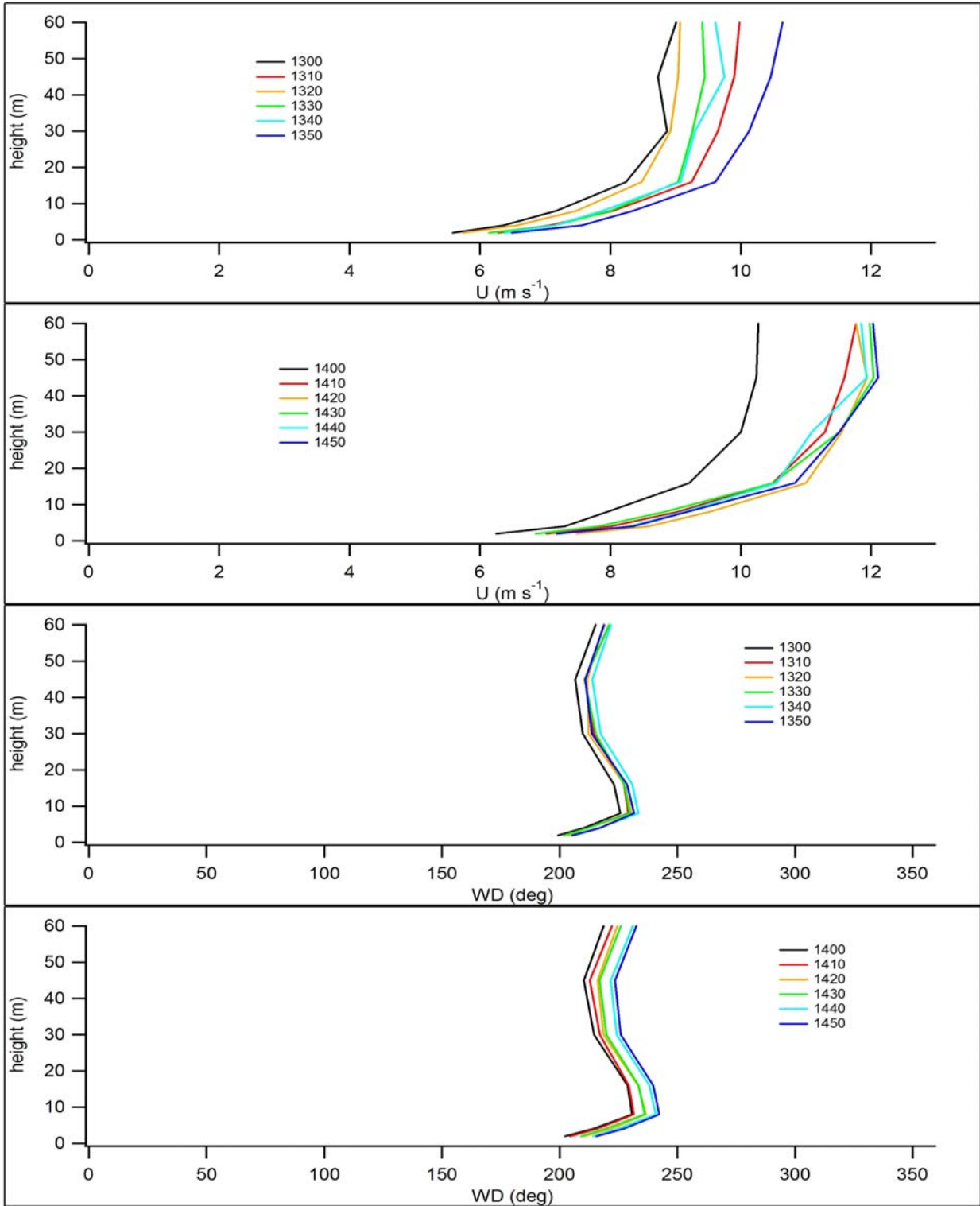


Figure 135. Vertical profiles of wind speed and direction from sonic anemometer measurements at GRI during IOP3. ARLFRD instruments were at 4, 30, and 45 m; WSULAR instruments were at 2, 8, 16, and 60 m. Times in legend are start times for the 10 minute interval (hhmm MST).

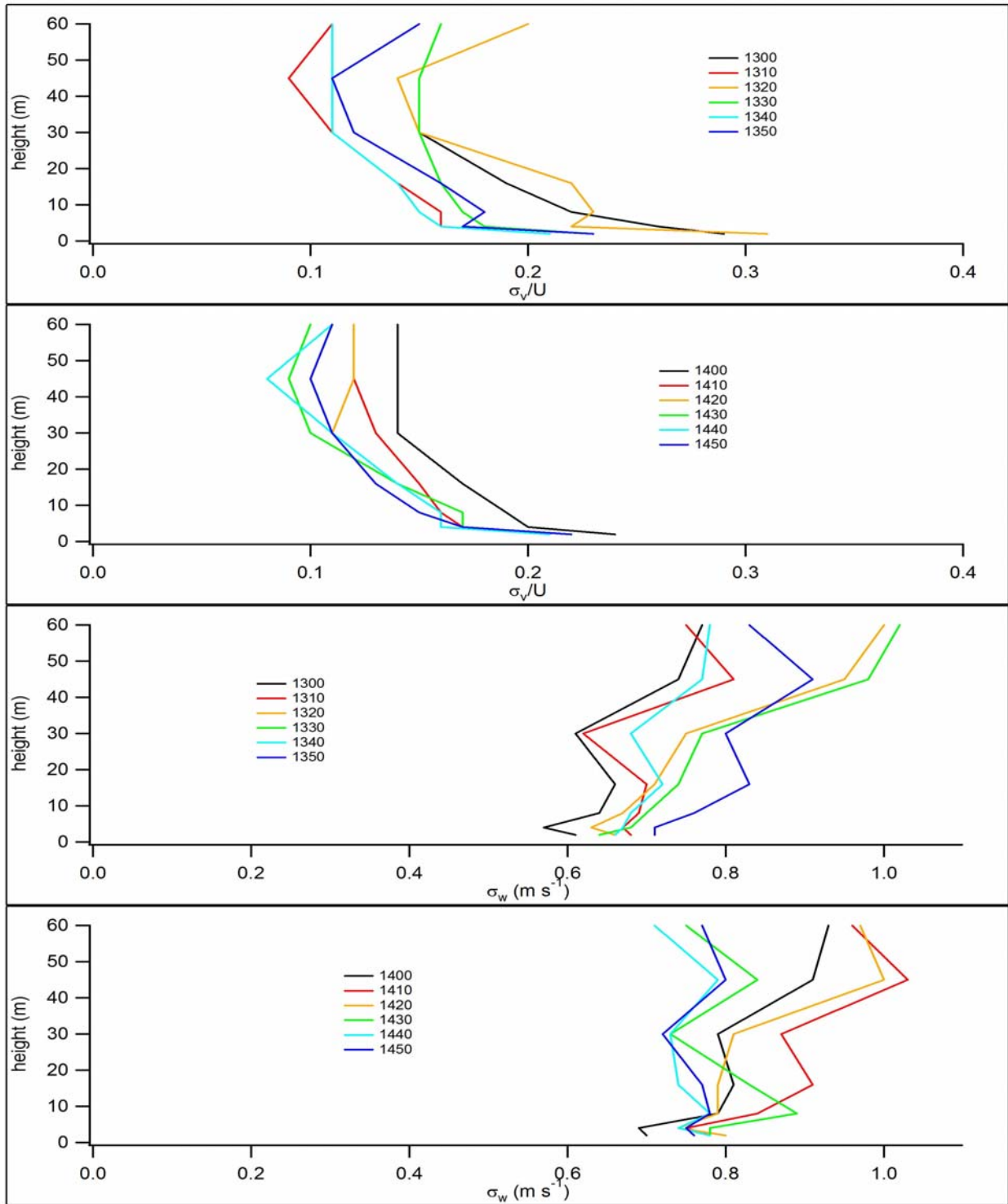


Figure 136. Vertical profiles of turbulence intensity and σ_w from sonic anemometer measurements at GRI during IOP3. ARLFRD instruments were at 4, 30, and 45 m; WSULAR instruments were at 2, 8, 16, and 60 m. Times in legend are start times for the 10 minute interval (hhmm MST).

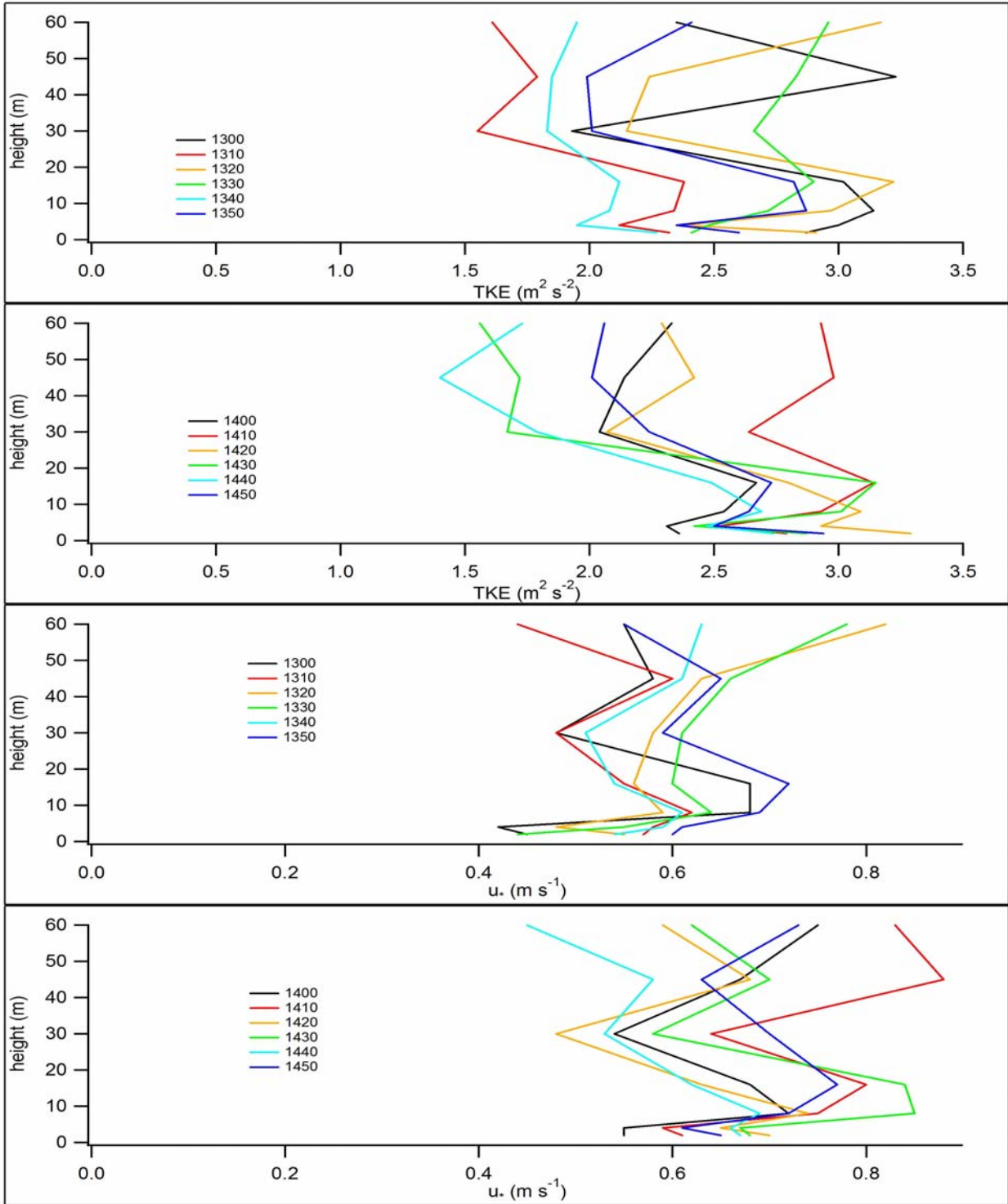


Figure 137. Vertical profiles of turbulent kinetic energy (TKE) and u_* from sonic anemometer measurements at GRI during IOP3. ARLFRD instruments were at 4, 30, and 45 m; WSULAR instruments were at 2, 8, 16, and 60 m. Times in legend are start times for the 10 minute interval (hhmm MST).

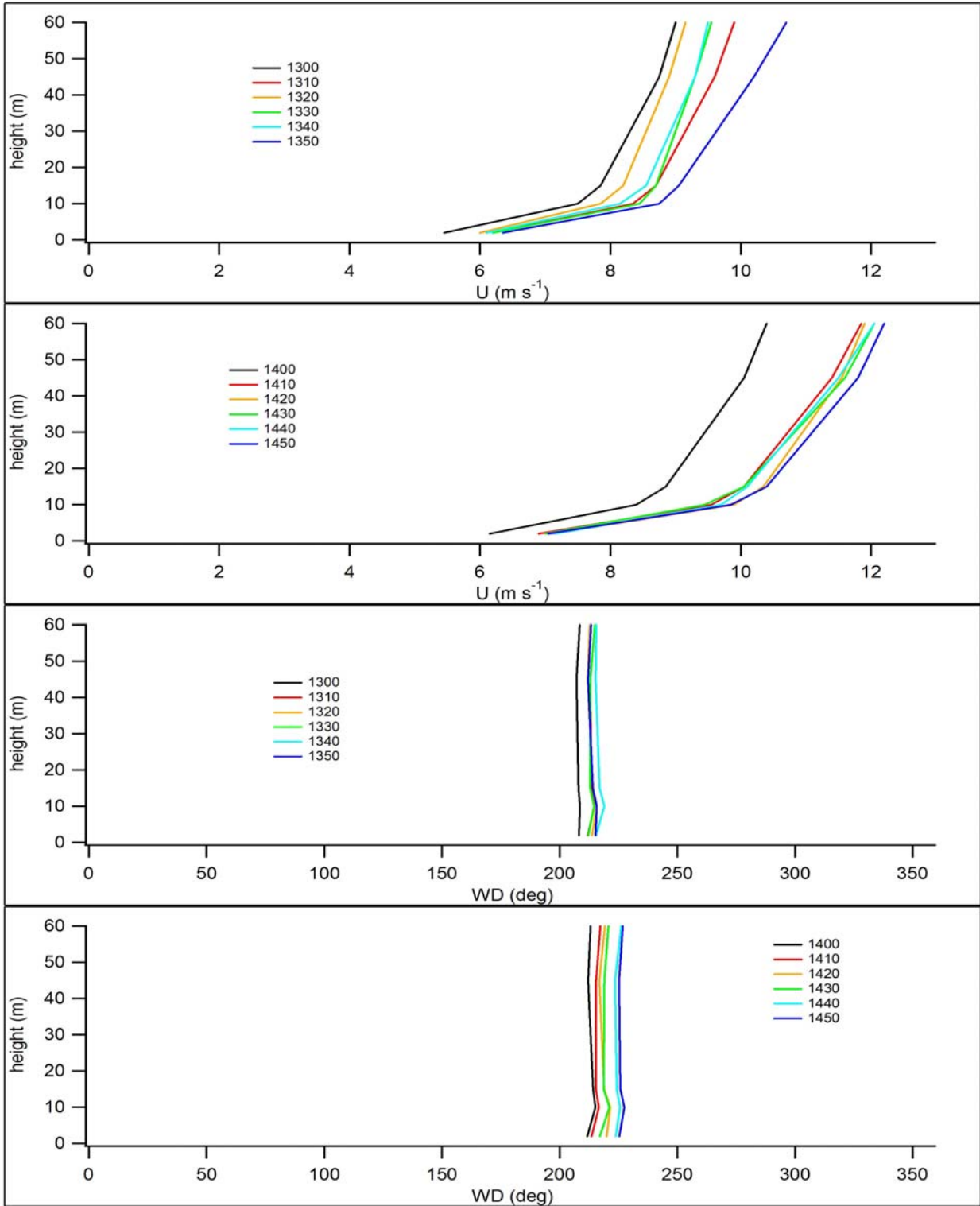


Figure 138. Vertical profiles of wind speed and direction from cup anemometer and wind vane measurements at GRI during IOP3. Times in legend are start times for the 10 minute interval (hhmm MST).

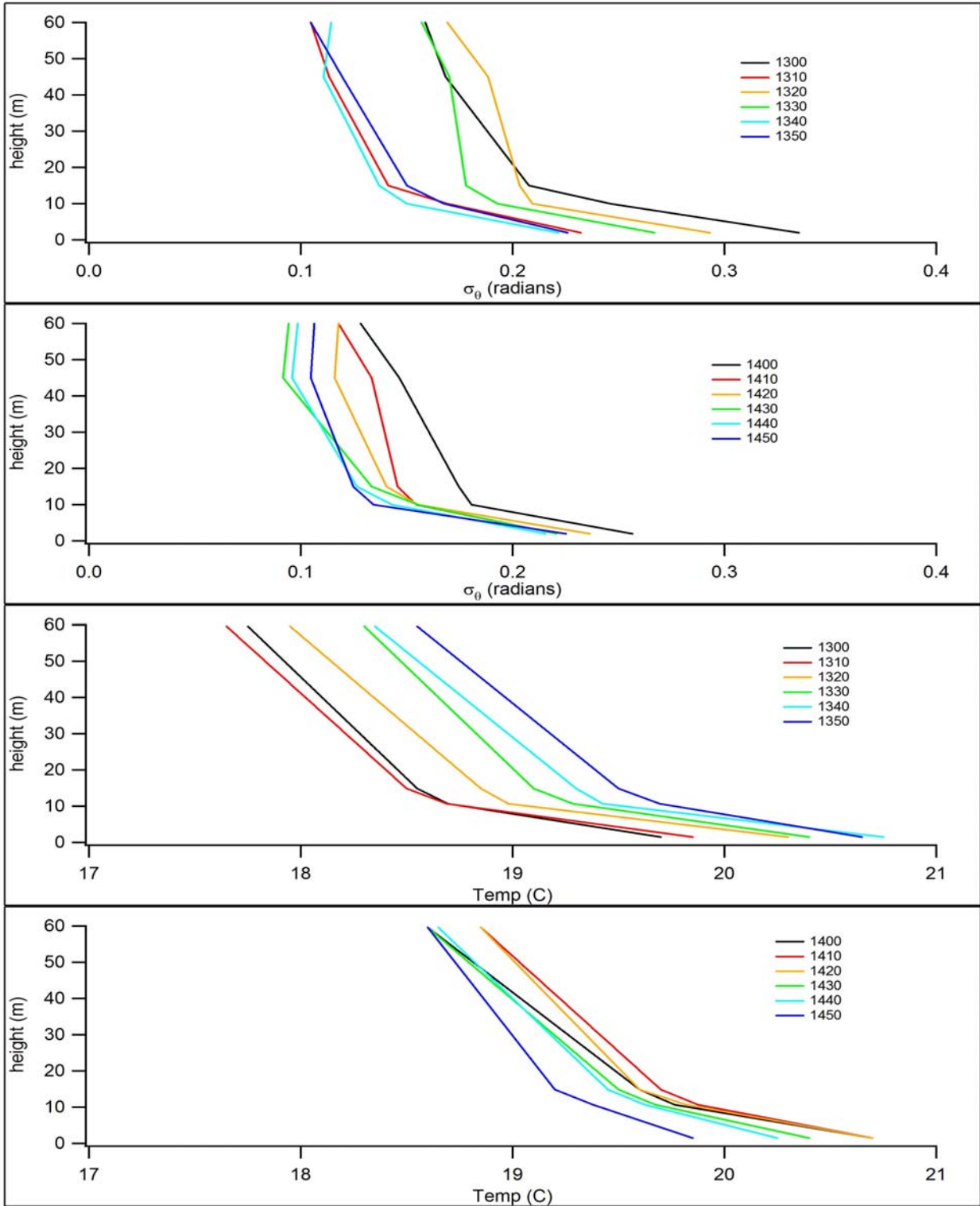


Figure 139. Vertical profiles of σ_θ (from cup and vane) and aspirated air temperature measurements at GRI during IOP3. Times in legend are start times for the 10 minute interval (hhmm MST).

Stability

The SRDT-Delta T and σ_A methods gave identical results for (P-G) stability category (all D). The magnitudes and sign of the z/L stability parameter values are generally consistent with near neutral, weakly unstable conditions and the category D classification.

Radiosonde Results

Figures 140 and 141 show potential temperature and specific humidity profiles from radiosonde measurements pre and post IOP3. The mixing depths estimated from these plots are given in Table 18.

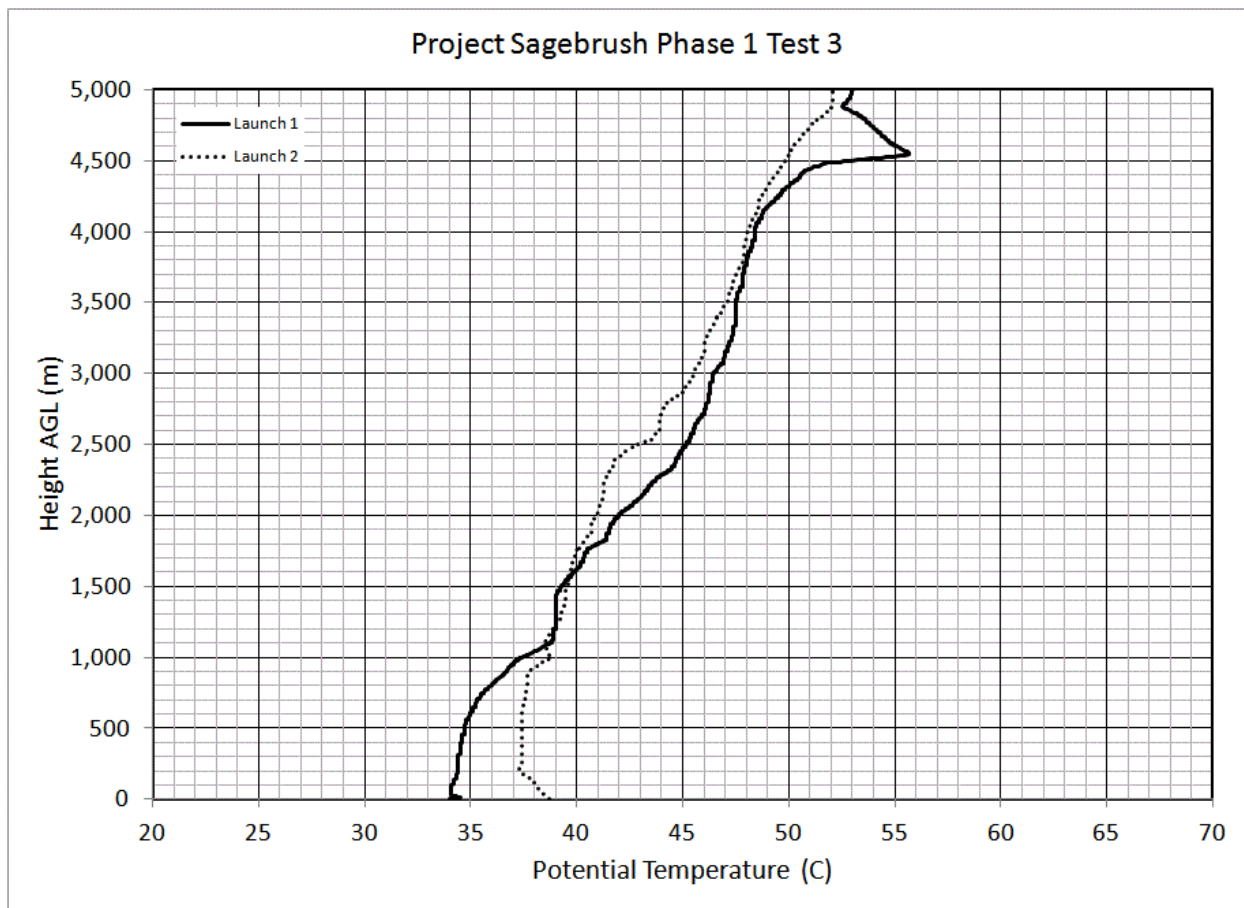


Figure 140. Pre and post IOP radiosonde potential temperature profiles for IOP3.

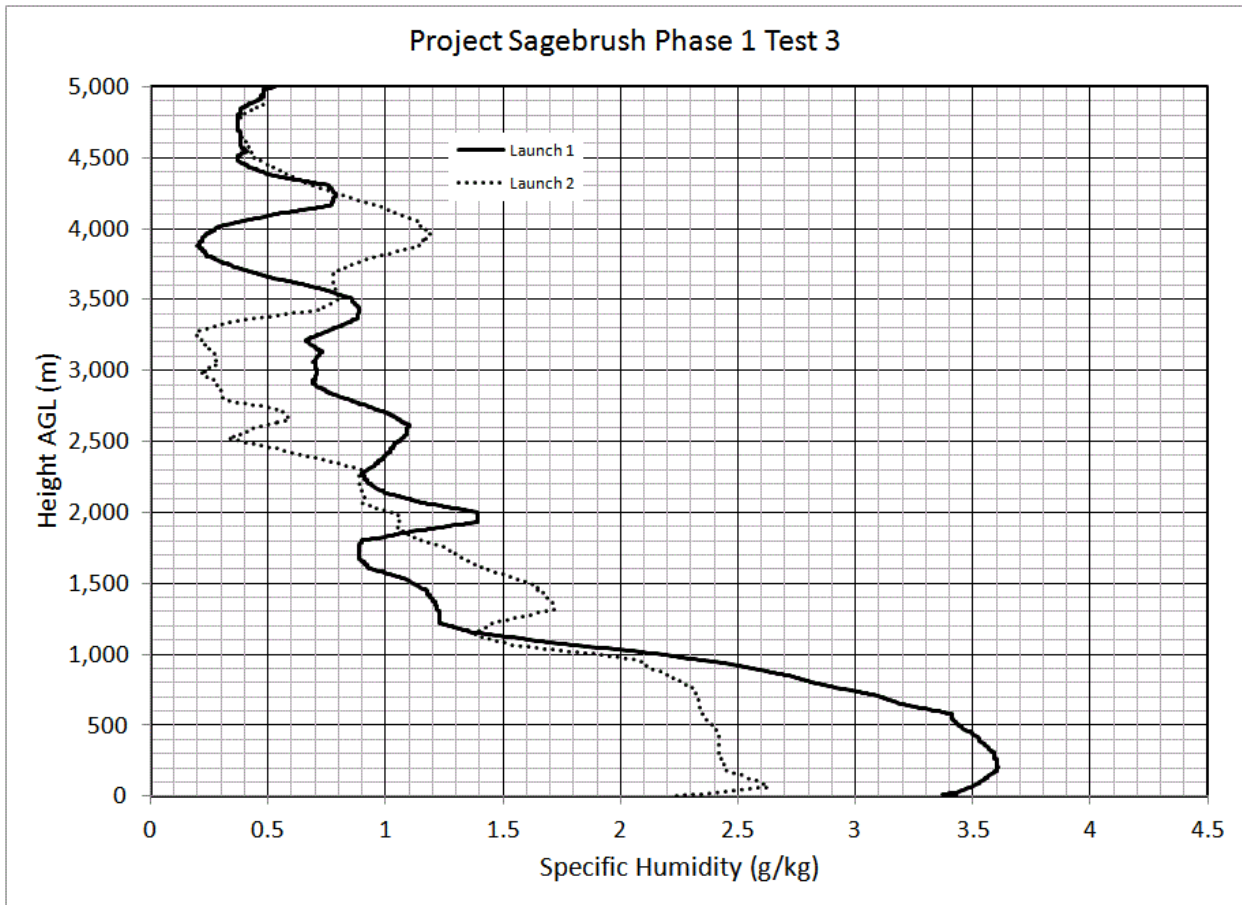


Figure 141. Pre and post IOP radiosonde specific humidity profiles for IOP3.

Concentration Results and Analysis

Figures 142 a-l show the bag sampling results for IOP3. Unlike IOP1, wind directions were such that the plume was present on the sampling array throughout IOP3 and both measured and normalized concentrations were higher than IOPs 1 or 2.

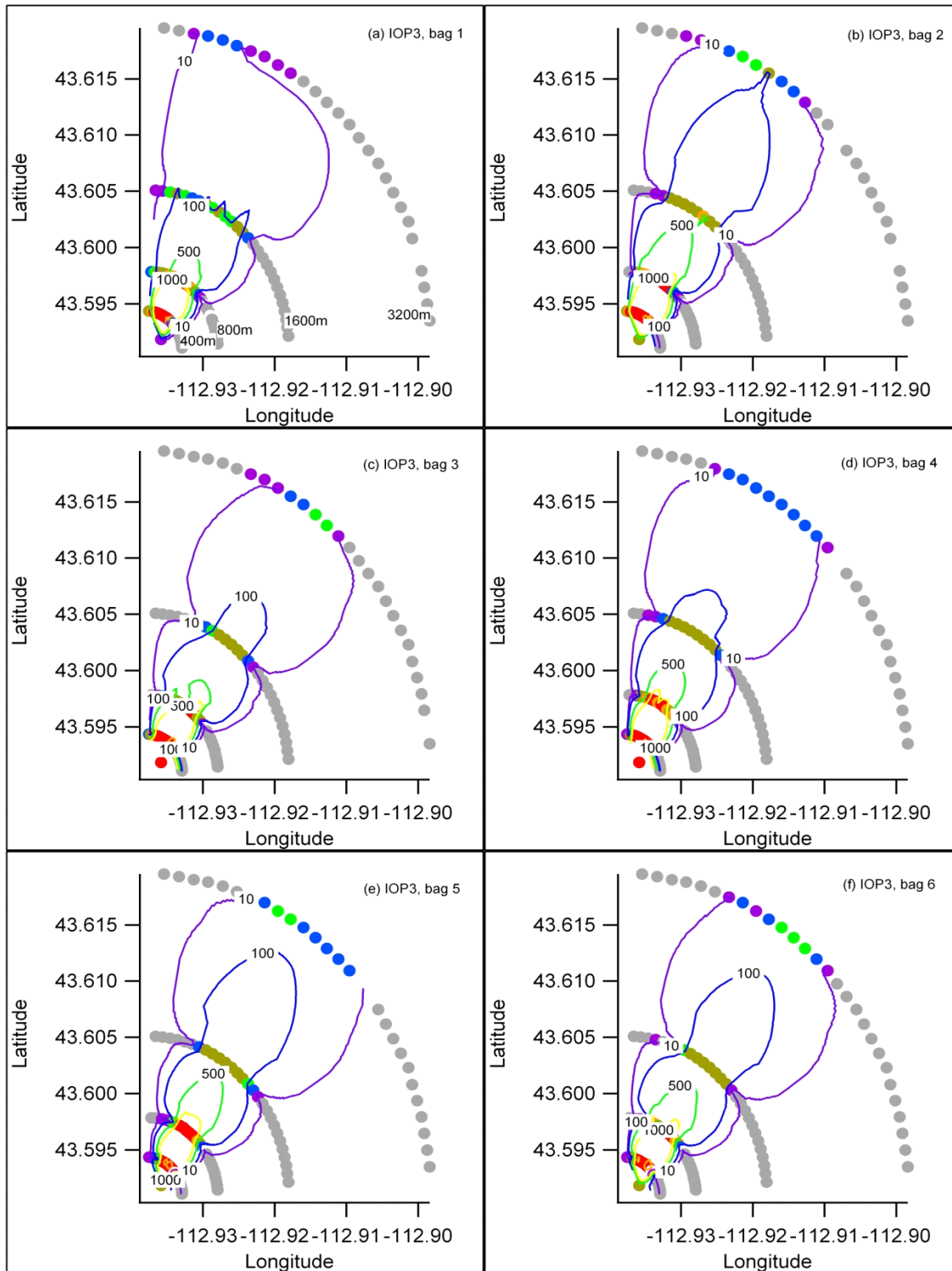


Figure 142. Bag sampling results (a-f, bags 1-6) for IOP3 with color-coded concentration markers for each 1 m AGL bag sampling location and contour lines of normalized concentration. The color scheme for the markers and contours is described in the Introduction to this section.

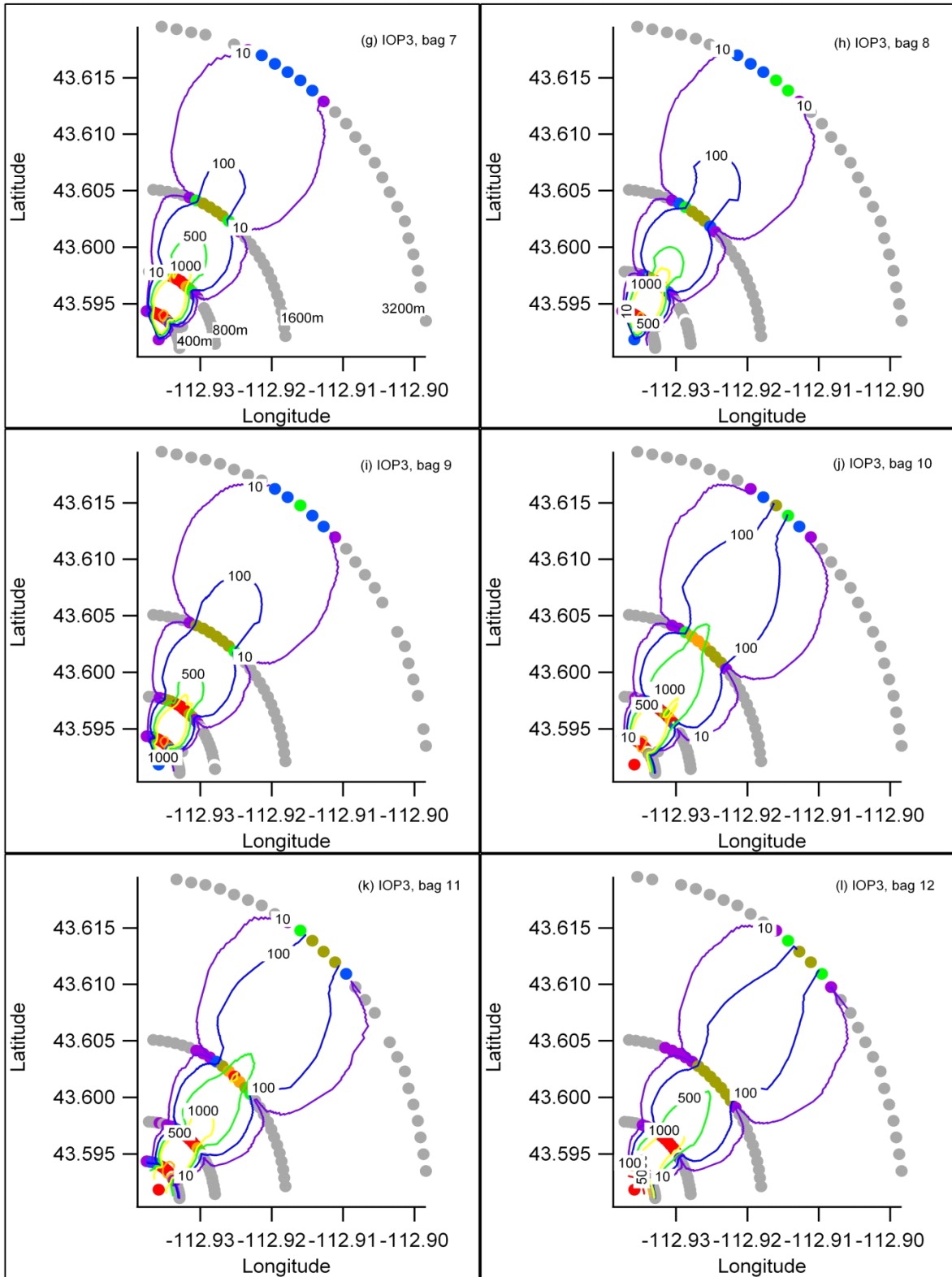


Figure 142 continued (g-l, bags 7-12).

Figures 143 a-l show cross-sections of tracer concentration along each arc for each 10-minute bag sampling period during IOP3. Plumes were generally much narrower with much higher concentrations than IOPs 1 and 2. The narrowness of the plumes is consistent with the small σ_0 values observed during the IOP (Table 21). While some profile asymmetries and irregularities were still seen, most of the profiles exhibited quasi-Gaussian form. There was no plume truncation at the edges of the sampling array.

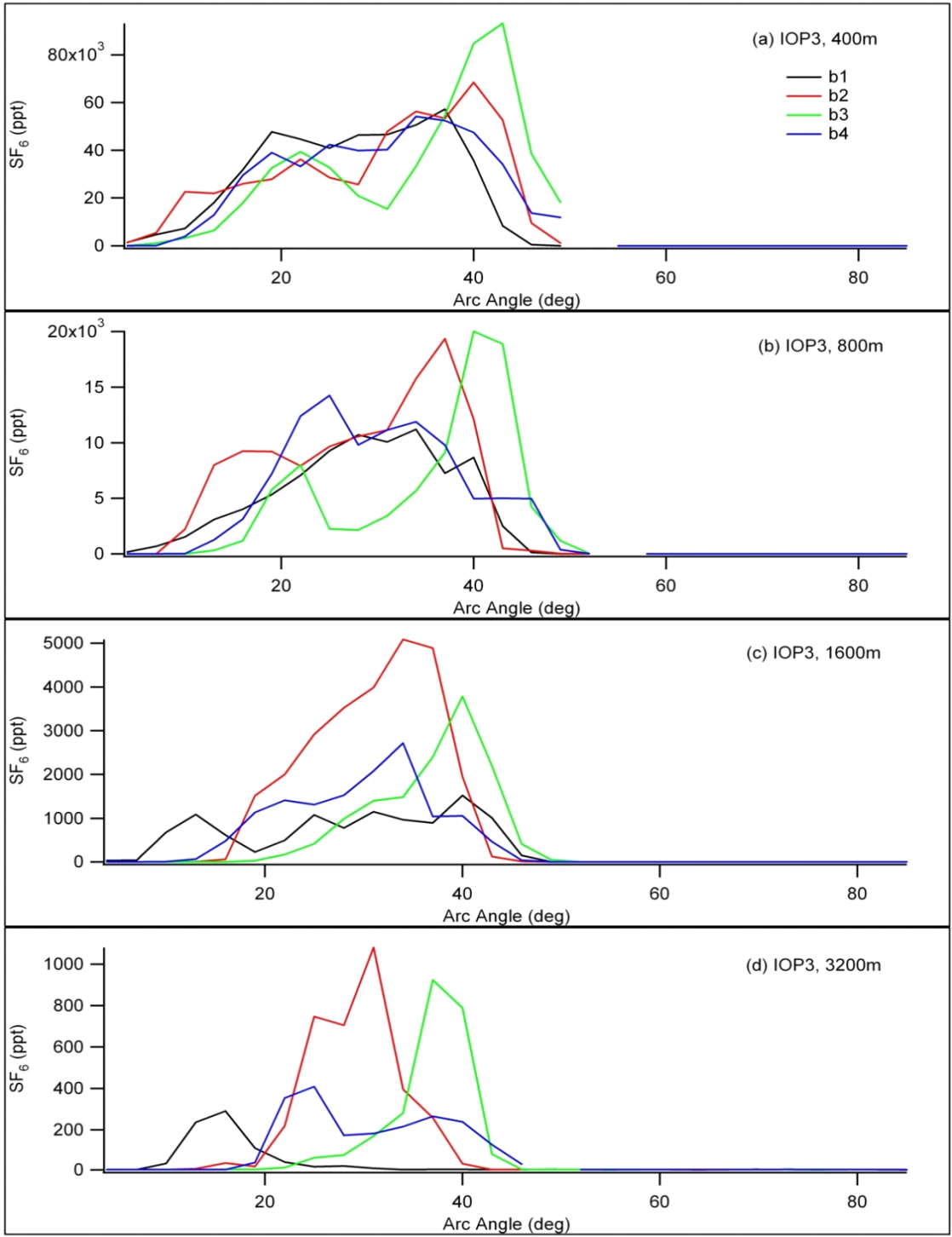


Figure 143. Cross-sections of concentration along each arc for each 10-minute bag sampling period during IOP3. The individual plume cross-section layouts are arranged to illustrate the variation in time, across 40 minutes per layout (a-d, bags 1-4), and the simultaneous variation with distance across all four arcs.

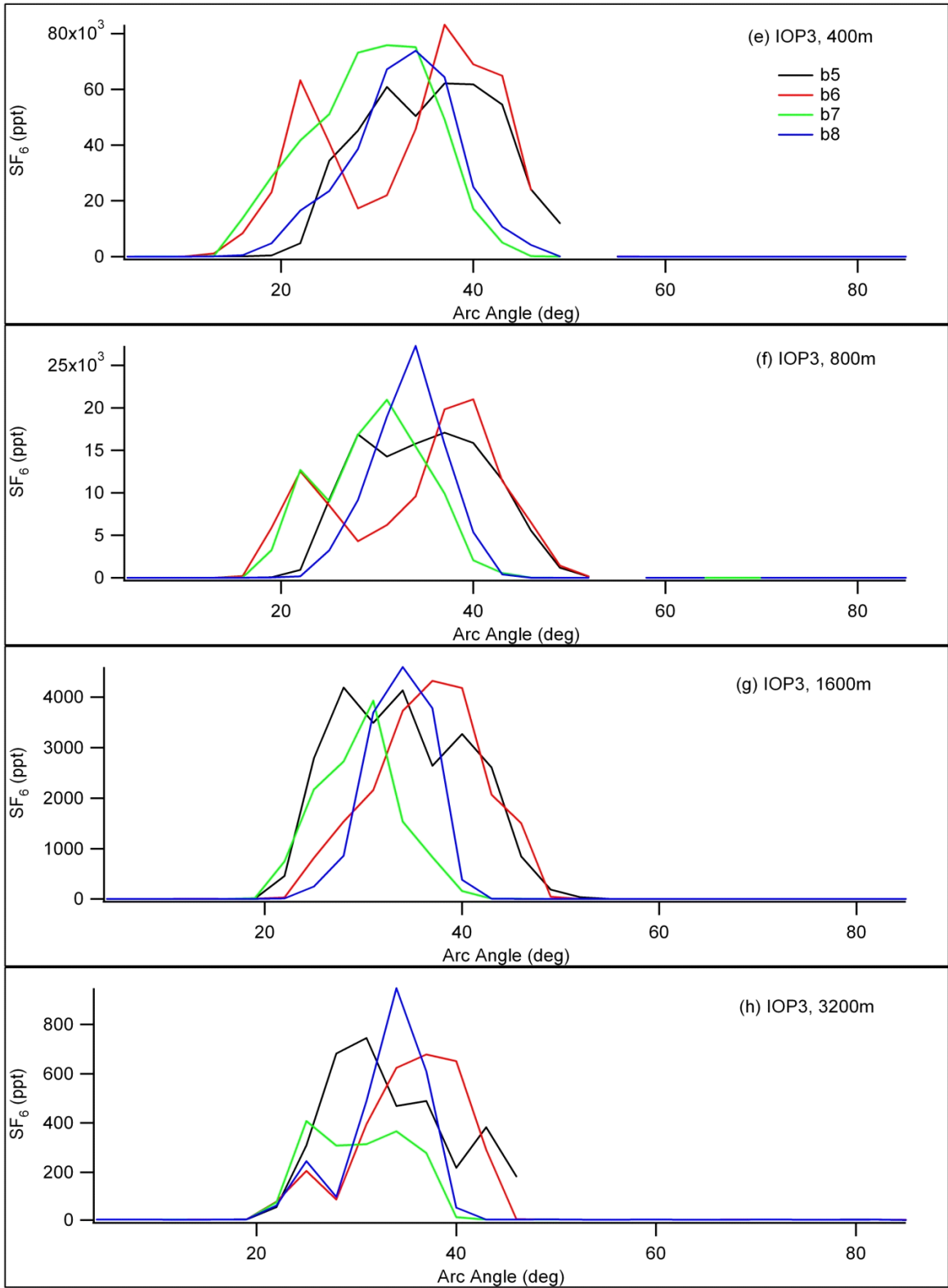


Figure 143 continued (e-h, bags 5-8).

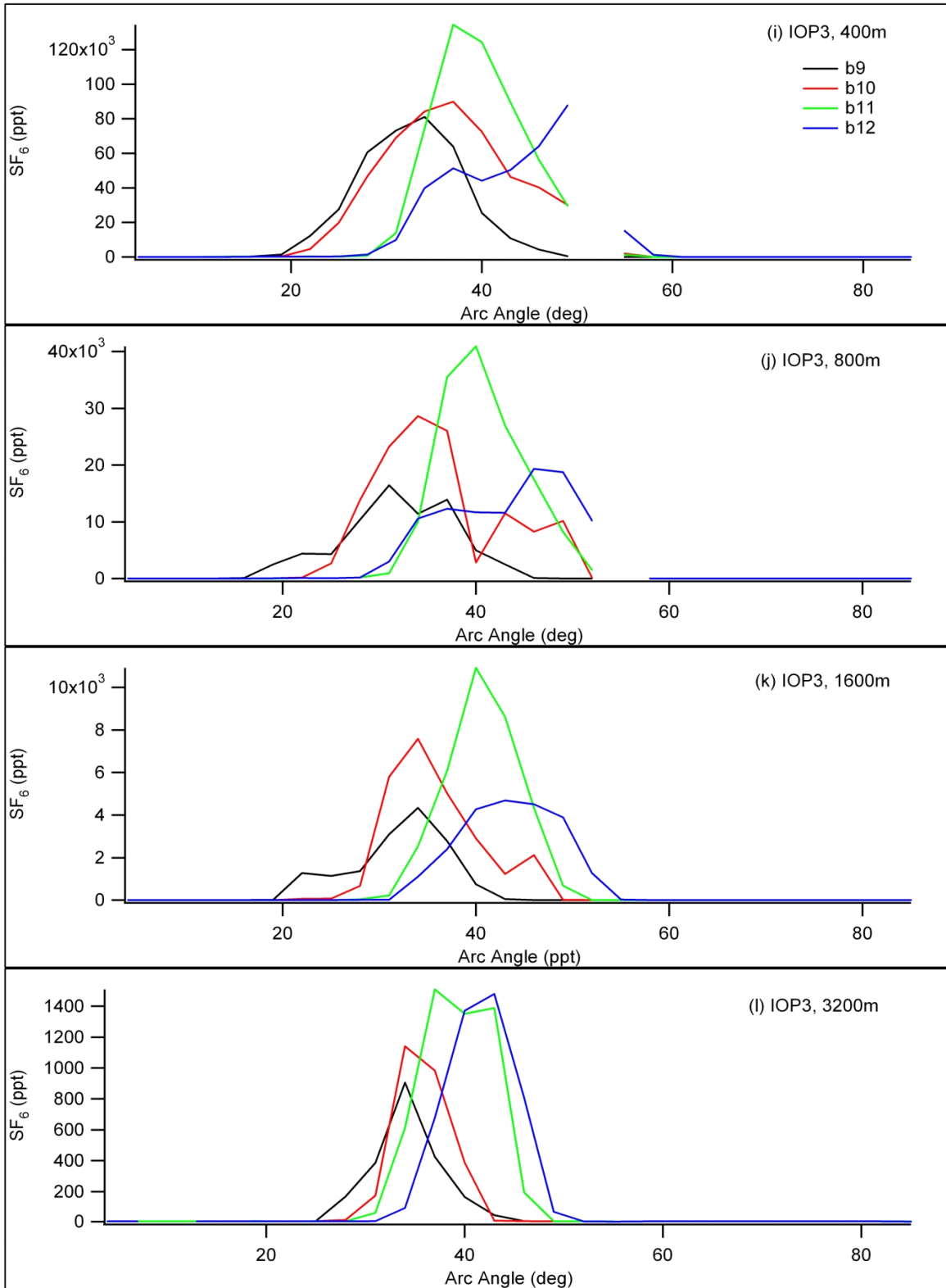


Figure 143 continued (i-l, bags 9-12).

Figures 144 a-l show vertical tracer concentration profiles at the towers at 201, 408, and 499 m downwind for all 10-minute bag sampling intervals for IOP3. Due to the wind direction and narrowness of the plumes during IOP3, no tracer was detected on the 408 or 499 m towers. Significant quantities of SF₆ were measured on the 201 m tower. Some profiles there suggest increasing concentrations with height while others suggest decreasing concentrations with height. Round black markers show the average concentration obtained from aircraft measurements at the height and downwind distance indicated as described in the Introduction to this section.

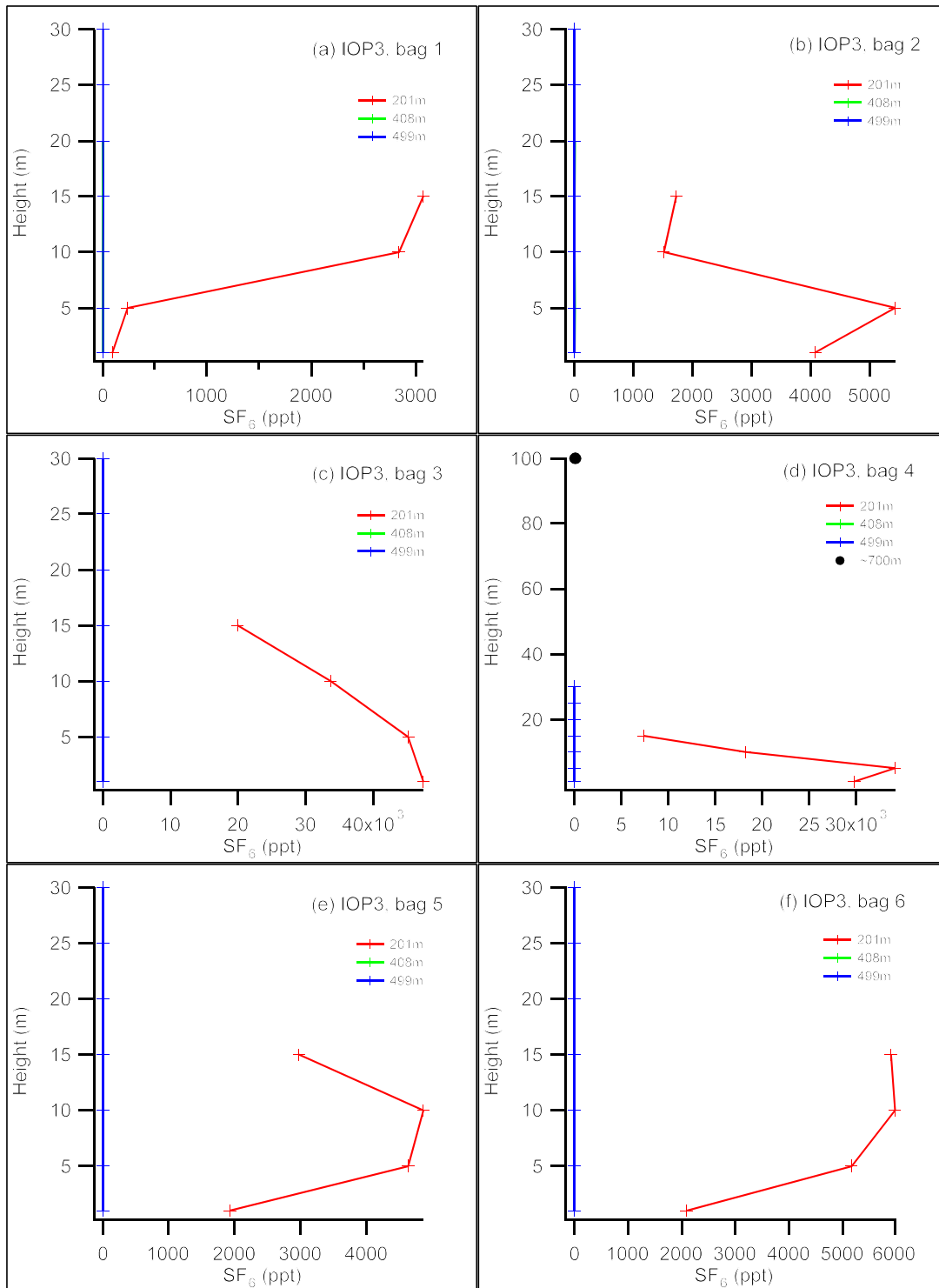


Figure 144. Vertical concentration profiles (a-f, bags 1-6) at the towers at 201, 408, and 499 m downwind for all 10-minute bag sampling intervals for IOP3. Round black markers show the average concentration obtained from aircraft measurements at the plotted height. The approximate downwind distance of the aircraft measurements is indicated in the legend.

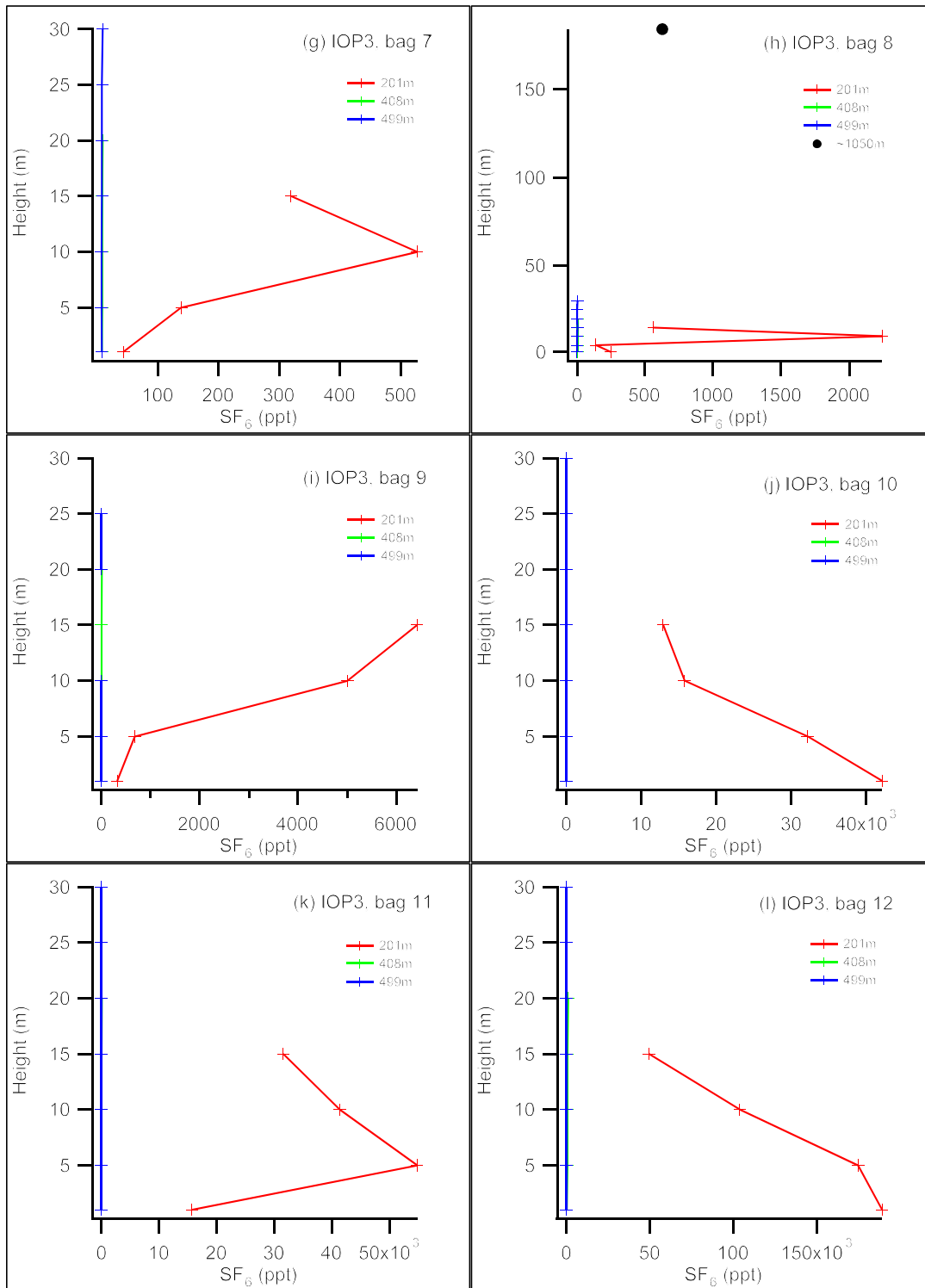


Figure 144 continued (g-l, bags 7-12).

Figure 145 shows time series of SF_6 concentrations measured by the fast response analyzers at the specified arc and arc angle location during IOP3. The high concentrations

present across the sampling array resulted in difficulties in making the fast response measurements during IOP3. The high concentrations often resulted in railing of the detectors. This was true for some analyzers both with and without dilution systems installed. Examples of this can be seen at the 400 m arc in Fig. 145 where data has been flagged out and is missing through many of the higher concentration peaks at about 12.55 and 12.57 hours MST. In other cases, where a dilution system was not available, the combination of the narrowness of the plume and high concentrations was problematic. This resulted in situations where the analyzer was outside the plume and not detecting any SF₆ or, with a slight shift in location, encountered frequent railing. The best example of this can be seen in data from the 1600 m arc.

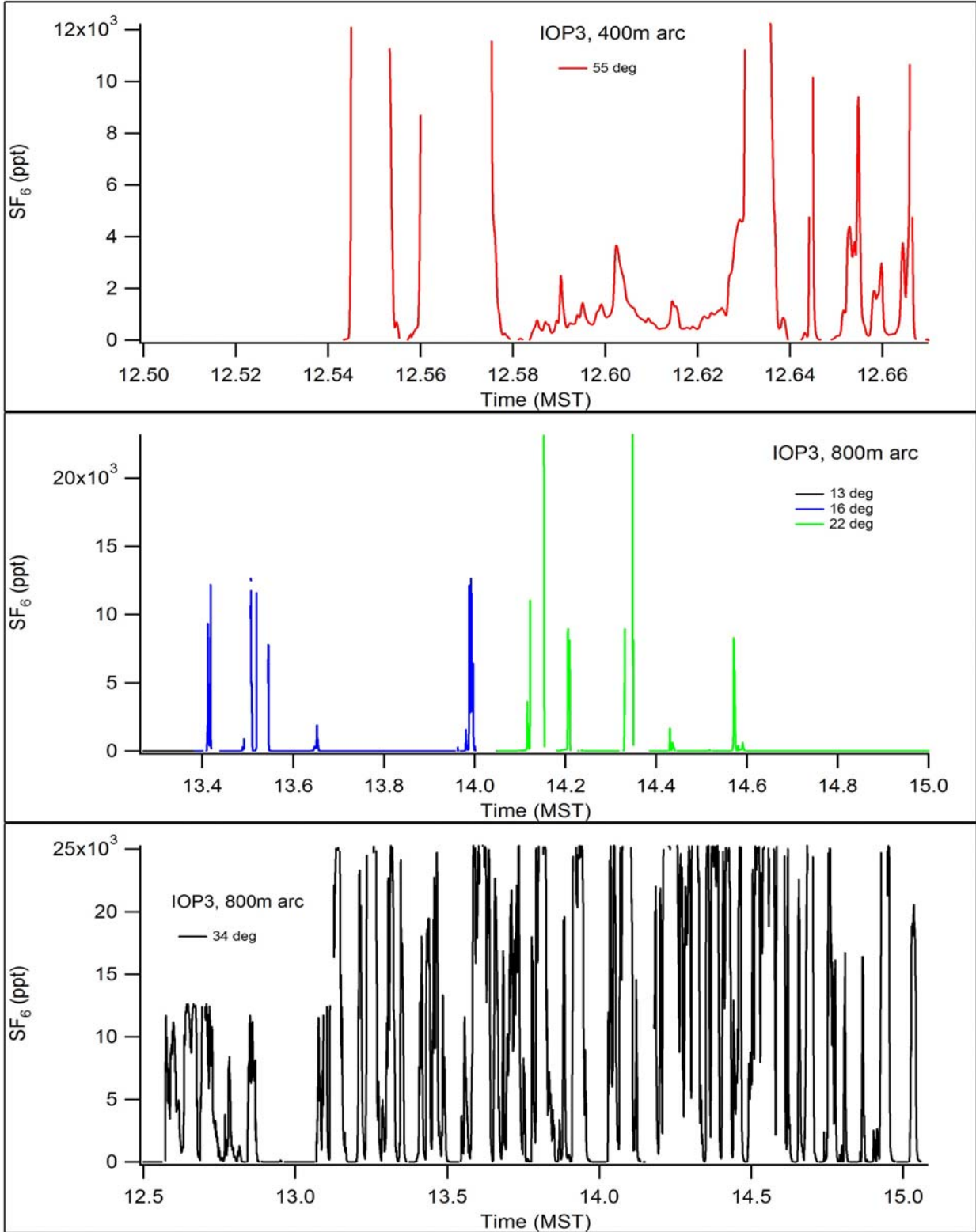


Figure 145. Time series of SF₆ concentrations measured by the fast response analyzers at the specified arc and arc angle location during IOP3.

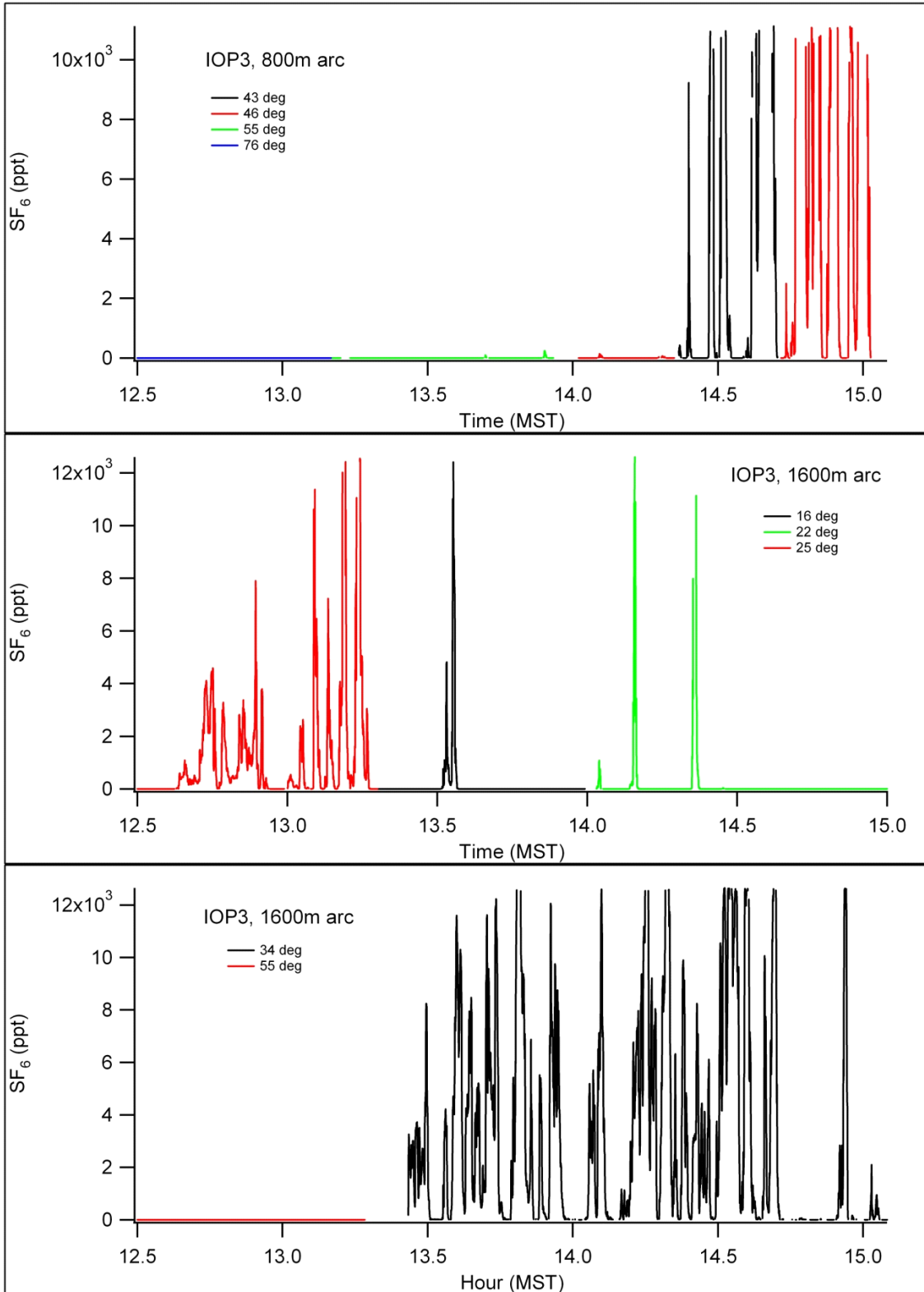


Figure 145 continued..

Figure 146 shows a time series of aircraft height and SF₆ concentrations measured by the onboard fast response analyzer during IOP3. Figure 147a shows color-coded concentrations along the aircraft flight path during IOP3. Figure 147b is the same except zoomed in over the bag sampling array. The plume patterns seen in the aircraft data were consistent with plume patterns observed in the bag sampling data. The color scheme and significance of the black markers are described in the Introduction to this section. The aircraft data suggest that plume rise was suppressed during IOP3 and that, for the most part, the plume failed to reach the aircraft sampling level until it was well beyond the sampling array. There was only one major peak measured over the sampling array (near 1100 m downwind) and little besides that. Most measured peaks were beyond 3200 m downwind.

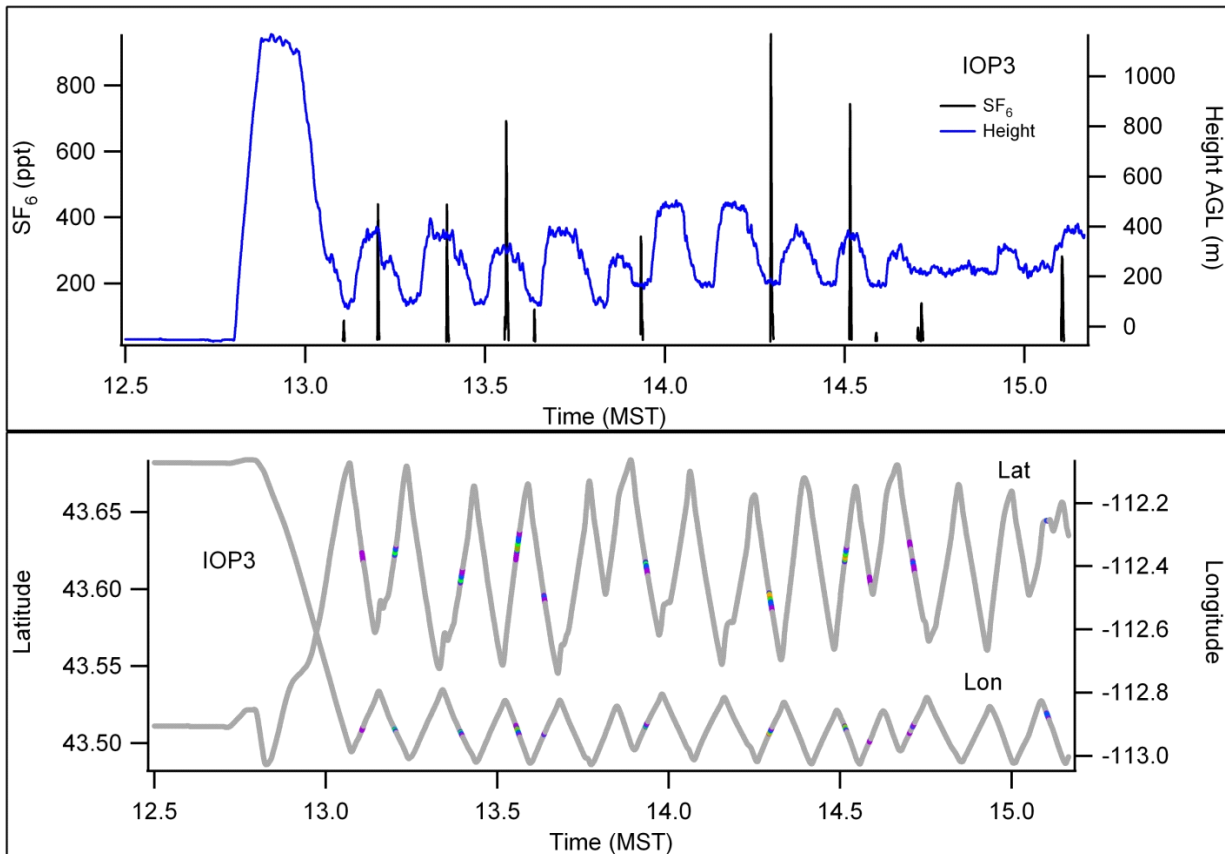


Figure 146. Time series of aircraft height and SF₆ concentrations measured by the onboard fast response analyzer during IOP3. Heights are approximate AGL calculated by subtracting the elevation at the release from the aircraft altitude.

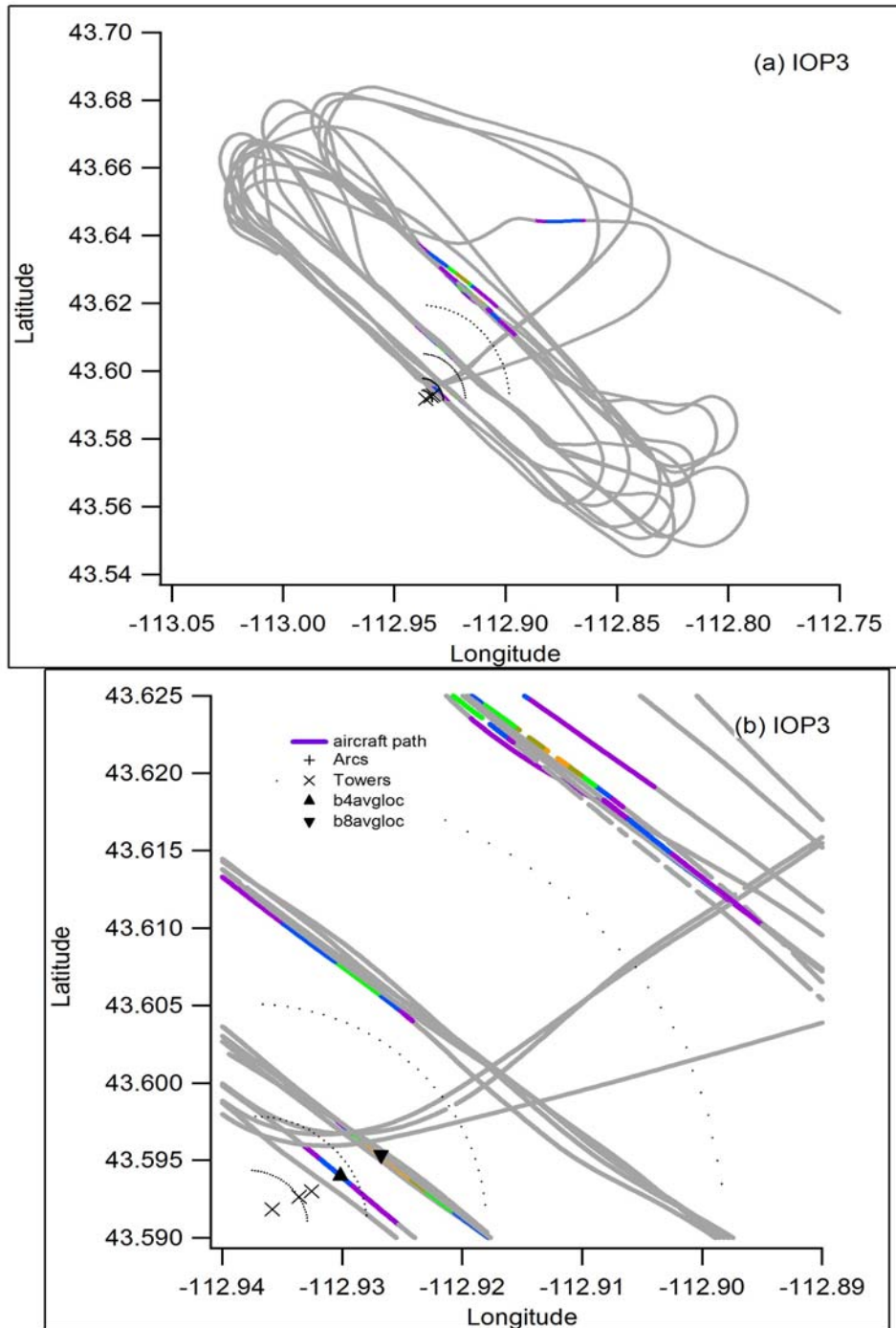


Figure 147. Color-coded concentrations along the aircraft flight path during IOP3 for (a) the overall flight path and (b) zoomed in over the bag sampling array. The color scheme and significance of the black markers are described in the Introduction to this section. They are linked to the black markers in Fig. 144 where b# is bag number and avgloc is average location.

IOP4

Date/Time and General Description

IOP4 was conducted on 11 October from 1400-1600 MST (1500-1700 MDT). It was mostly sunny. Conditions during IOP4 resembled those during IOP3 with some differences. Wind speeds and turbulence were generally less and there was a somewhat greater variation in wind direction. Wind speeds were commonly in the 3-7 m s⁻¹ range, depending upon height. All estimates of stability point to weakly unstable conditions. Overall, there was good stationarity in the flow during IOP4. The stationarity, in combination with the generally favorable southwesterly wind directions, made for good conditions for tracer advection across the sampling array. A summary of the meteorological conditions during IOP4 are shown in Table 22. The SF₆ release rate was 1.043 g s⁻¹ (Tables 1 and 2), roughly the previous IOPs due to the absence of the UTSI aircraft. The fast response analyzers were located on the 400 m arc at 31 and 55 degrees, on the 800 m arc at 31 and 57 degrees, and on the 1600 m arc at 31 and 55 degrees.

Table 22. Meteorological conditions during IOP4. Wind speeds, directions, σ_θ , and P-G stability class determinations (EPA, 2000c) are from COC at 10 m. Solar radiation measurements are from FLX. R3 and R4 indicate sonic anemometer data from their respective locations.

Bag	Wind Speed (m s ⁻¹)	Wind Direction (deg)	Solar Radiation (W m ⁻²)	R3 u* (m s ⁻¹)	R4 u* (m s ⁻¹)	R3 z/L	R4 z/L	σ_θ (deg)	P-G SRDT	P-G σ_λ
1	5.4	216.5	496.5	0.37	0.18	-0.18	-1.08	16.1	D	D
2	4.3	235.3	486.0	0.36	0.35	-0.15	-0.23	19.9	C	C
3	4.7	216.4	458.0	0.35	0.28	-0.22	-0.34	14.3	C	C
4	4.3	206.1	434.0	0.39	0.33	-0.14	-0.26	17.9	C	C
5	4.8	223.7	419.5	0.33	0.27	-0.19	-0.33	12.3	C	D
6	5.3	204.0	401.0	0.42	0.31	-0.11	-0.27	12.1	D	D
7	4.6	229.8	380.5	0.33	0.20	-0.17	-0.56	14.0	C	C
8	4.6	195.6	360.0	0.32	0.36	-0.19	-0.14	16.6	C	C
9	5.8	208.1	338.5	0.40	0.29	-0.12	-0.25	14.6	D	C
10	4.9	216.2	315.0	0.39	0.40	-0.10	-0.09	17.0	C	C
11	5.5	202.6	291.0	0.31	0.38	-0.14	-0.09	11.7	D	D
12	5.9	206.7	264.0	0.45	0.35	-0.04	-0.11	9.5	D	D

Winds and Quality Assurance

Figure 148 shows wind speed and direction comparisons for ARLFRD data in the vertical at the GRI and COC towers for IOP4. There was excellent agreement in wind speed and direction. Flows during IOP4 exhibited good spatial and temporal homogeneity and stationarity although less so than IOP3. Fluctuations in wind direction were moderate and decreased with time (Fig. 149).

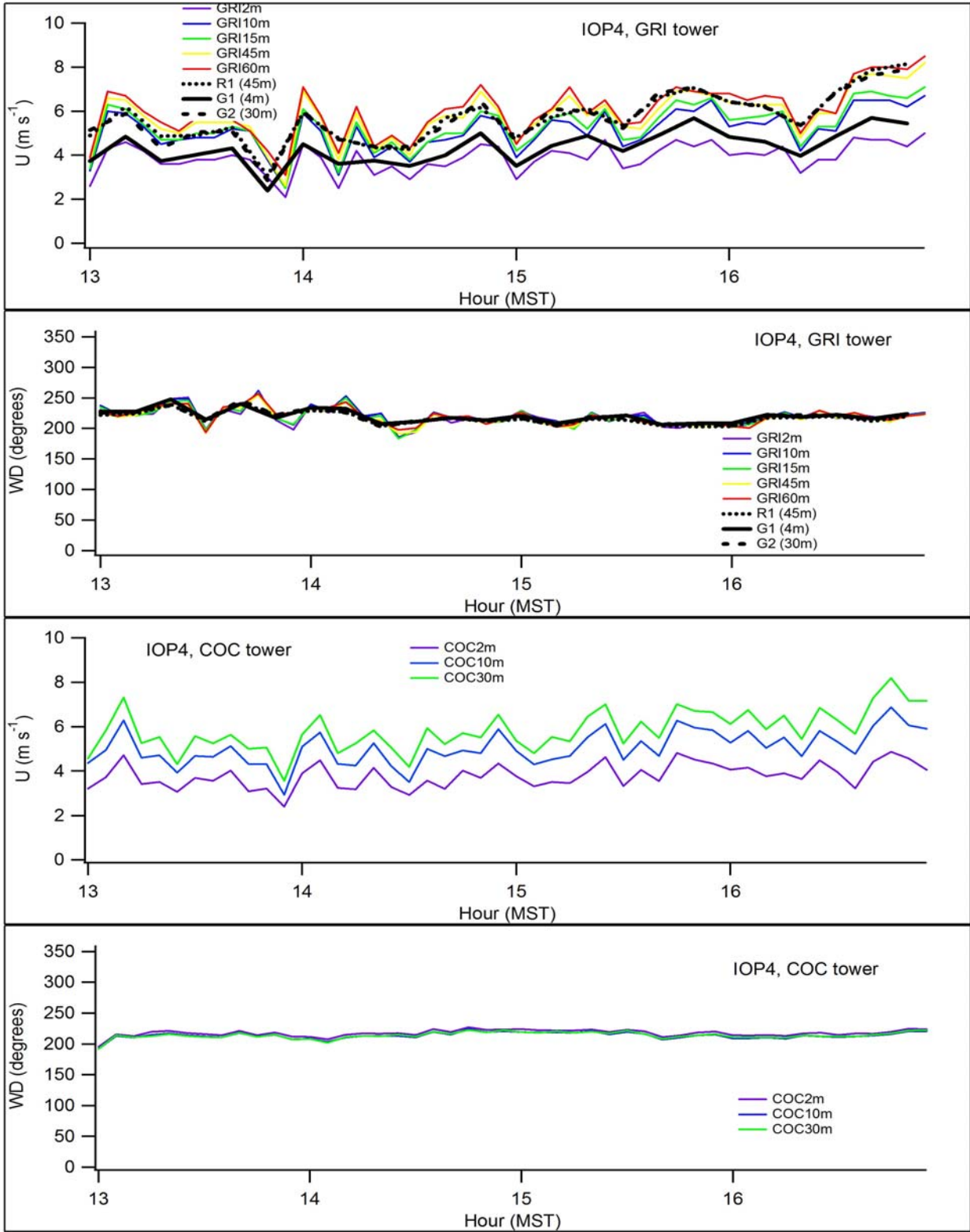


Figure 148. ARLFRD wind speed and direction comparisons in the vertical at GRI and COC for IOP4.

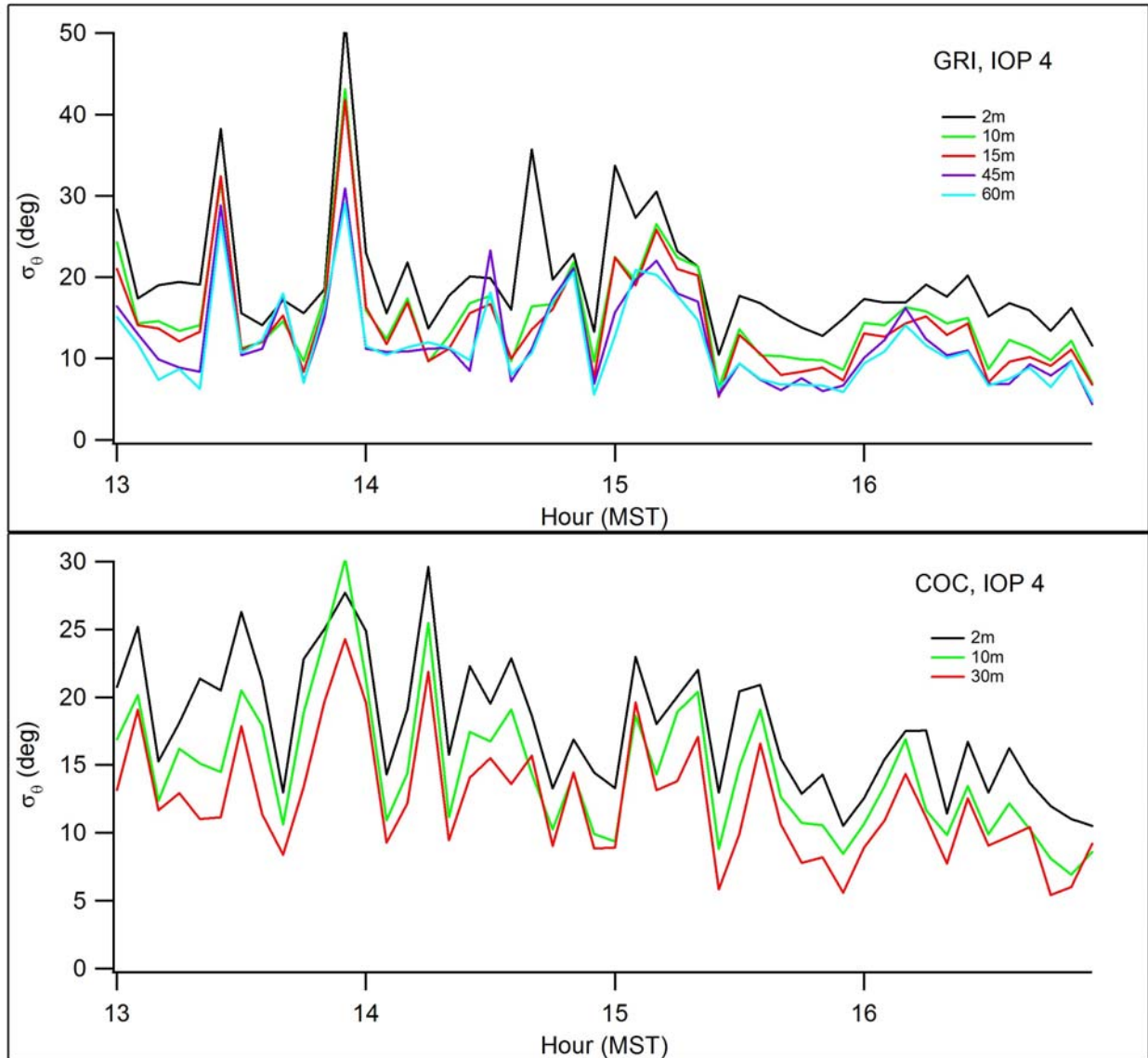


Figure 149. Standard deviation in wind direction σ_θ (σ_A) using wind vanes at GRI and COC for IOP4.

Figures 150-152 show wind speed and direction comparisons in the horizontal across the study area at 2 m, 10 m, 30 m, 45 m, 60 m, and 160 m from the data available. The comparisons are the same as those described for IOP1 except that data were not available from TOW due to power supply problems. Observations showed good agreement between sites and measurement type across the study area. All of the available data are generally consistent and show good agreement with the exception of a low wind speed bias at PRO. With the exception of the low wind speed bias at PRO, there is little evidence for a problem with the measurements.

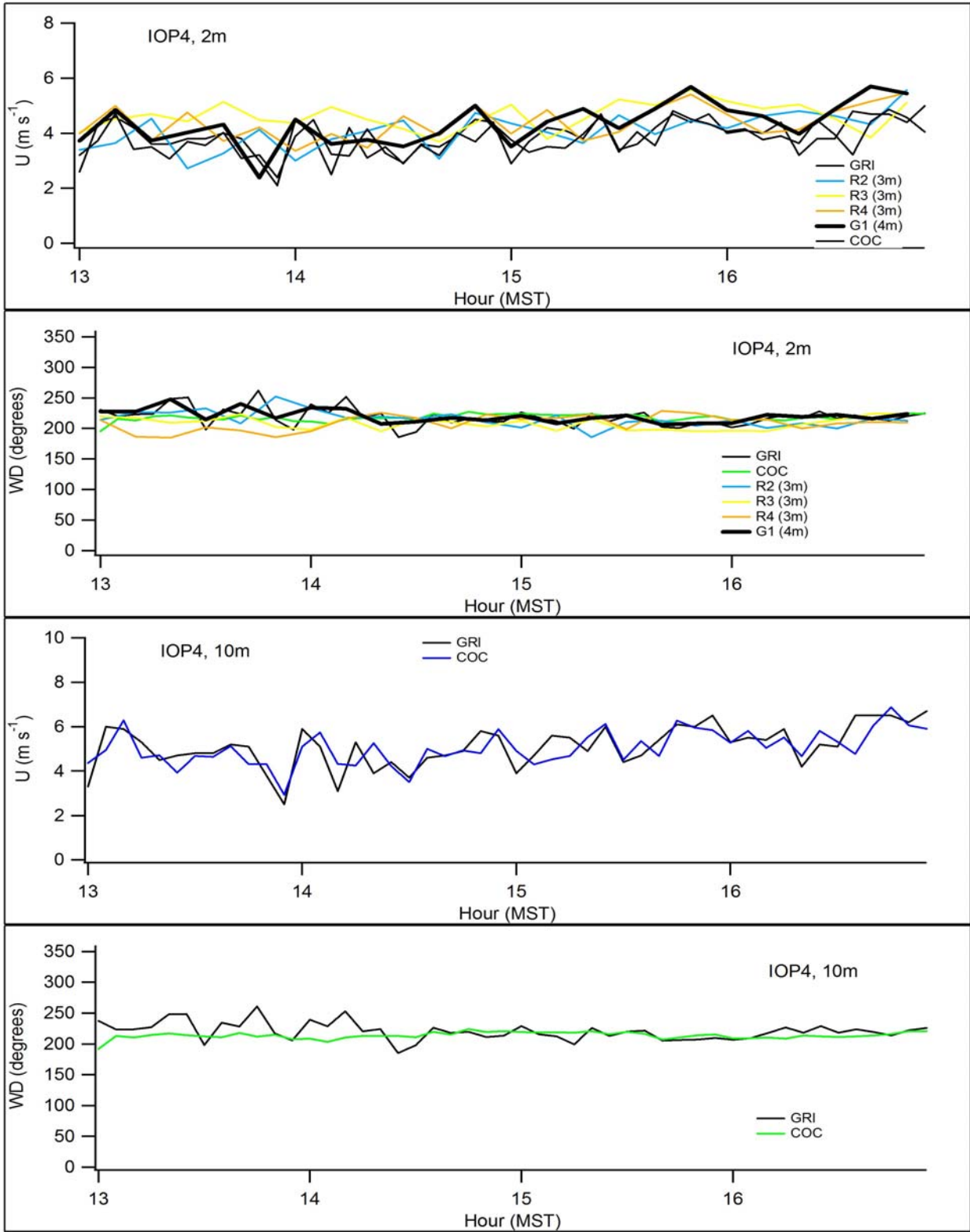


Figure 150. ARLFRD wind speed and direction comparisons in the horizontal at 2 and 10 m during IOP4.

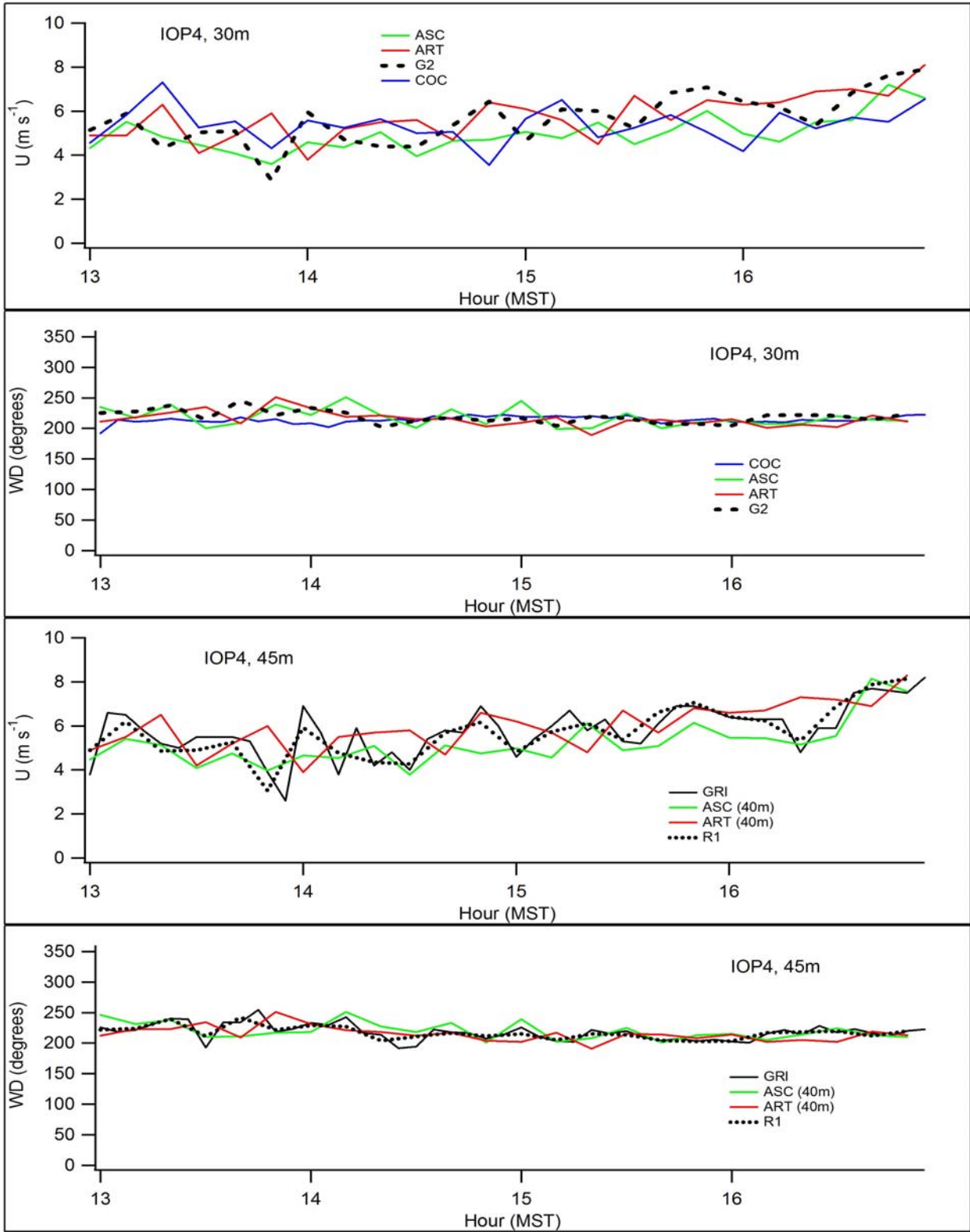


Figure 151. ARLFRD wind speed and direction comparisons in the horizontal at 30 and 45 m during IOP4.

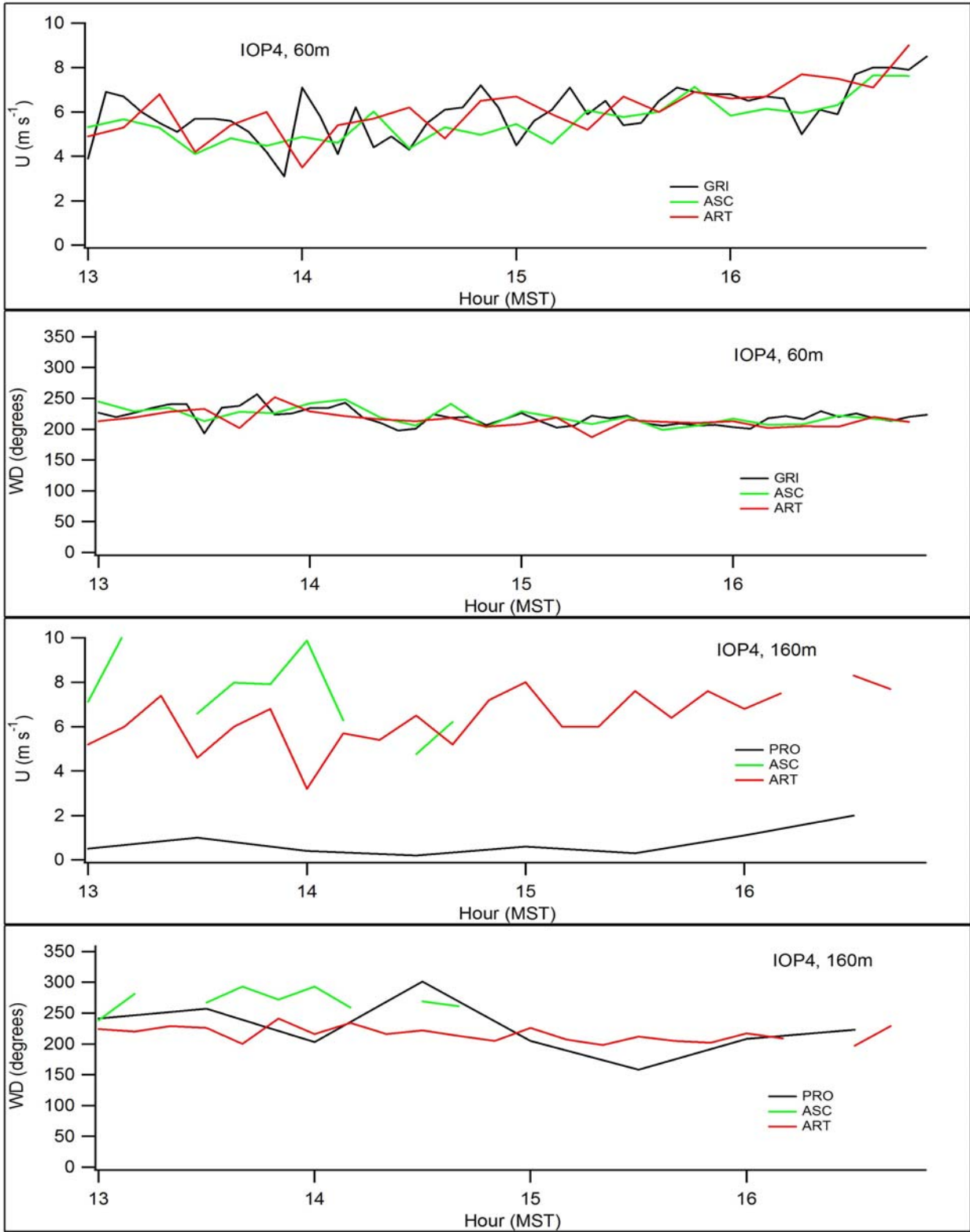


Figure 152. ARLFRD wind speed and direction comparisons in the horizontal at 60 and 160 m during IOP4.

Figures 153-155 show time-height cross-sections for wind speed and direction for the ASC sodar, ART sodar, and PRO wind profiler, respectively. The wind speeds and directions observed at ASC and ART were consistent with those observed elsewhere including the increase in wind speeds at about 1500 h (Figs. 151, 152). The wind speeds and directions observed at PRO were biased low relative to other measurements, at least at lower levels.

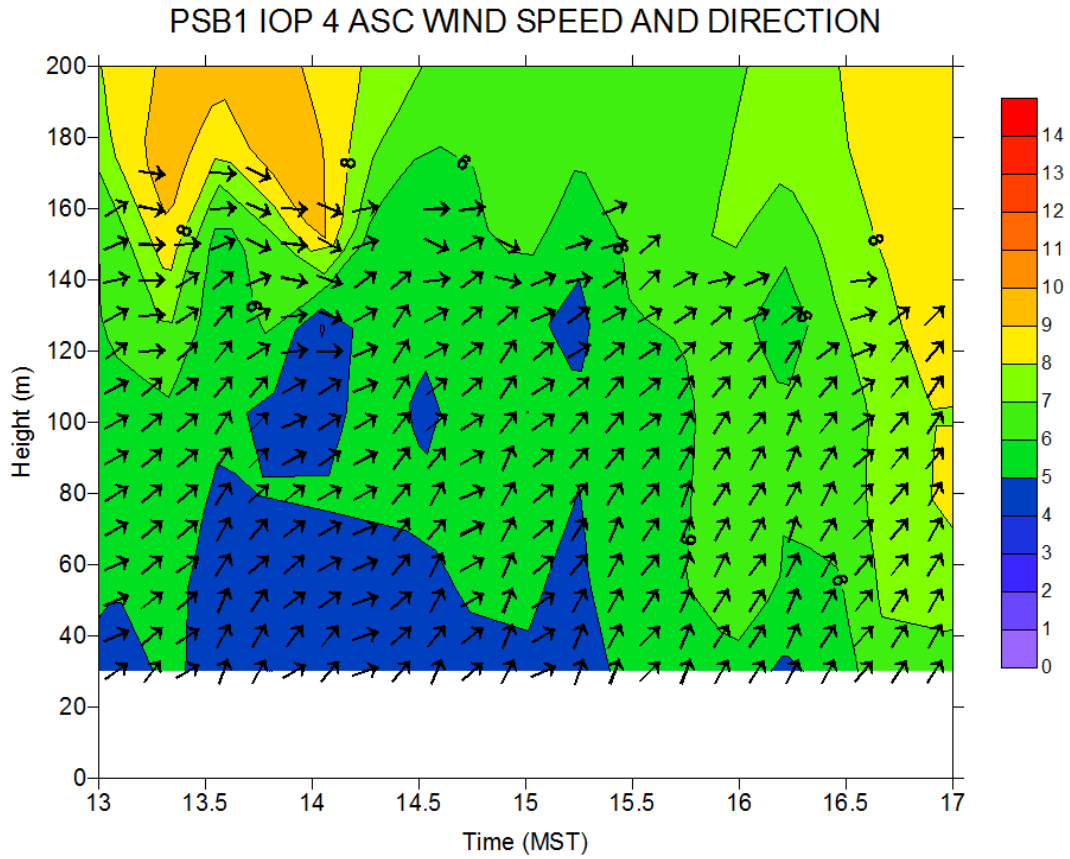


Figure 153. Time-height cross-section of wind speed and direction at ASC sodar during IOP4.

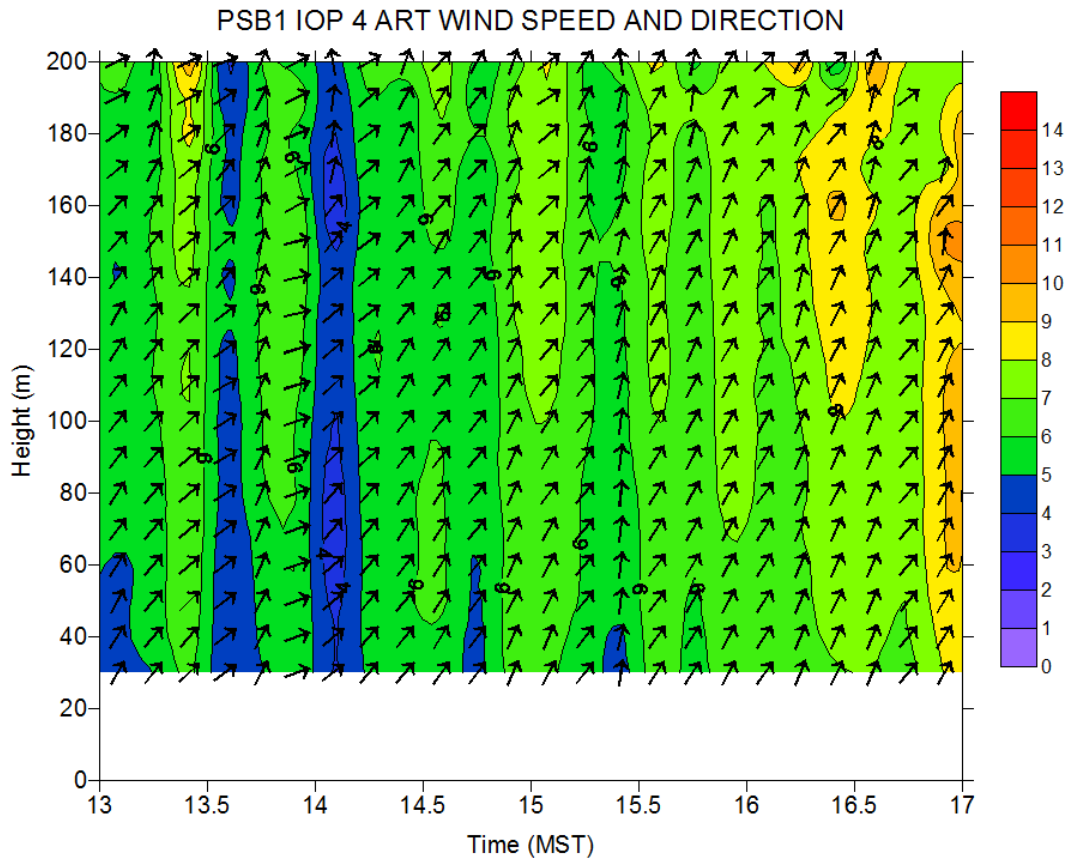


Figure 154. Time-height cross-section of wind speed and direction at ART sodar during IOP4.

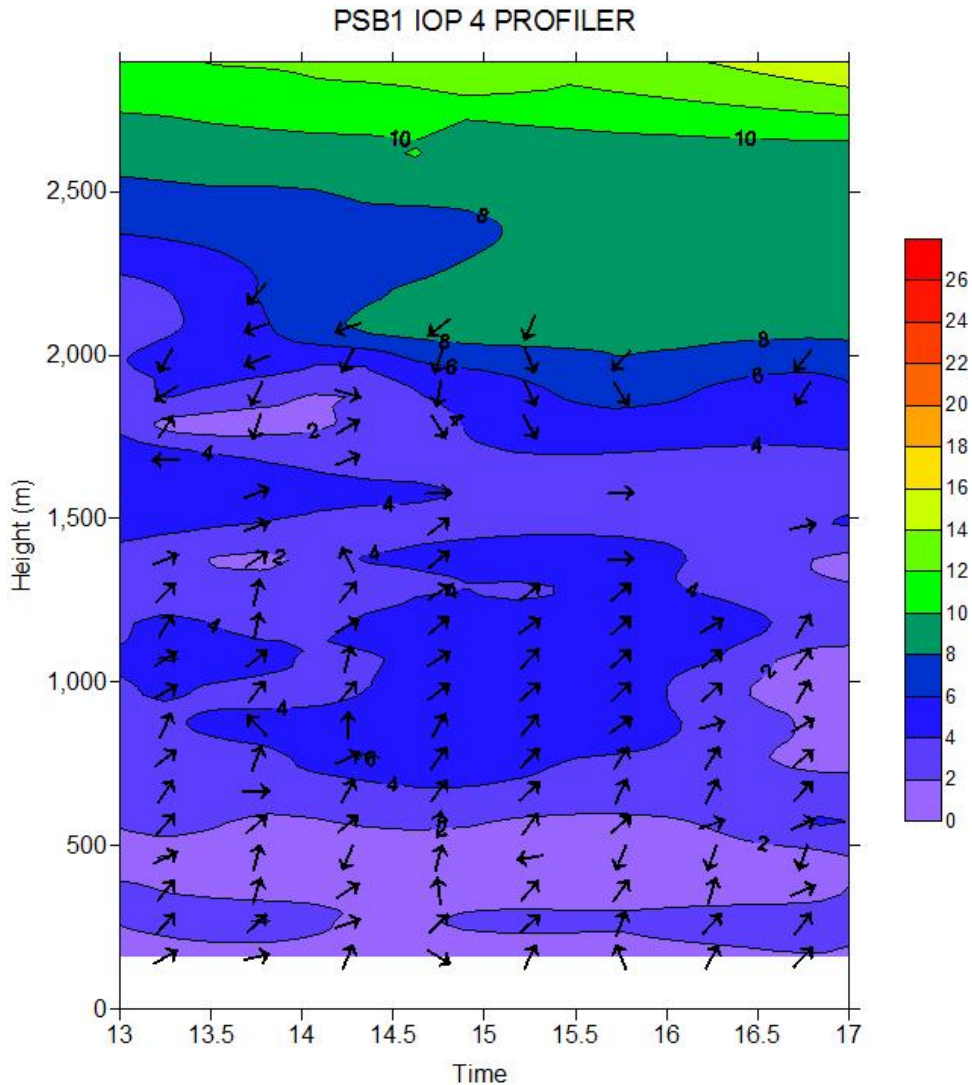


Figure 155. Time-height cross-section of wind speed and direction at wind profiler (PRO) during IOP4.

Turbulence

Figures 156 and 157 show time series of the turbulence measurements for 10 and 30-minute averaging periods, respectively, for σ_w , turbulent kinetic energy (TKE), u^* , kinematic heat flux $\langle w'T' \rangle$, and $1/L$ where L = Obukhov length. The 30-minute periods more accurately account for nonstationarity affects and should provide more reliable estimates than the 10-minute averaging periods. Observations showed good agreement between sites across the study area. The high values of σ_w at G2 are due to the fact these represent measurements at 30 m whereas all the other measurements are between 3-4 m height. The results for L indicate that the stability conditions were weakly unstable throughout the experiment. The kinematic heat flux trended downward throughout the test.

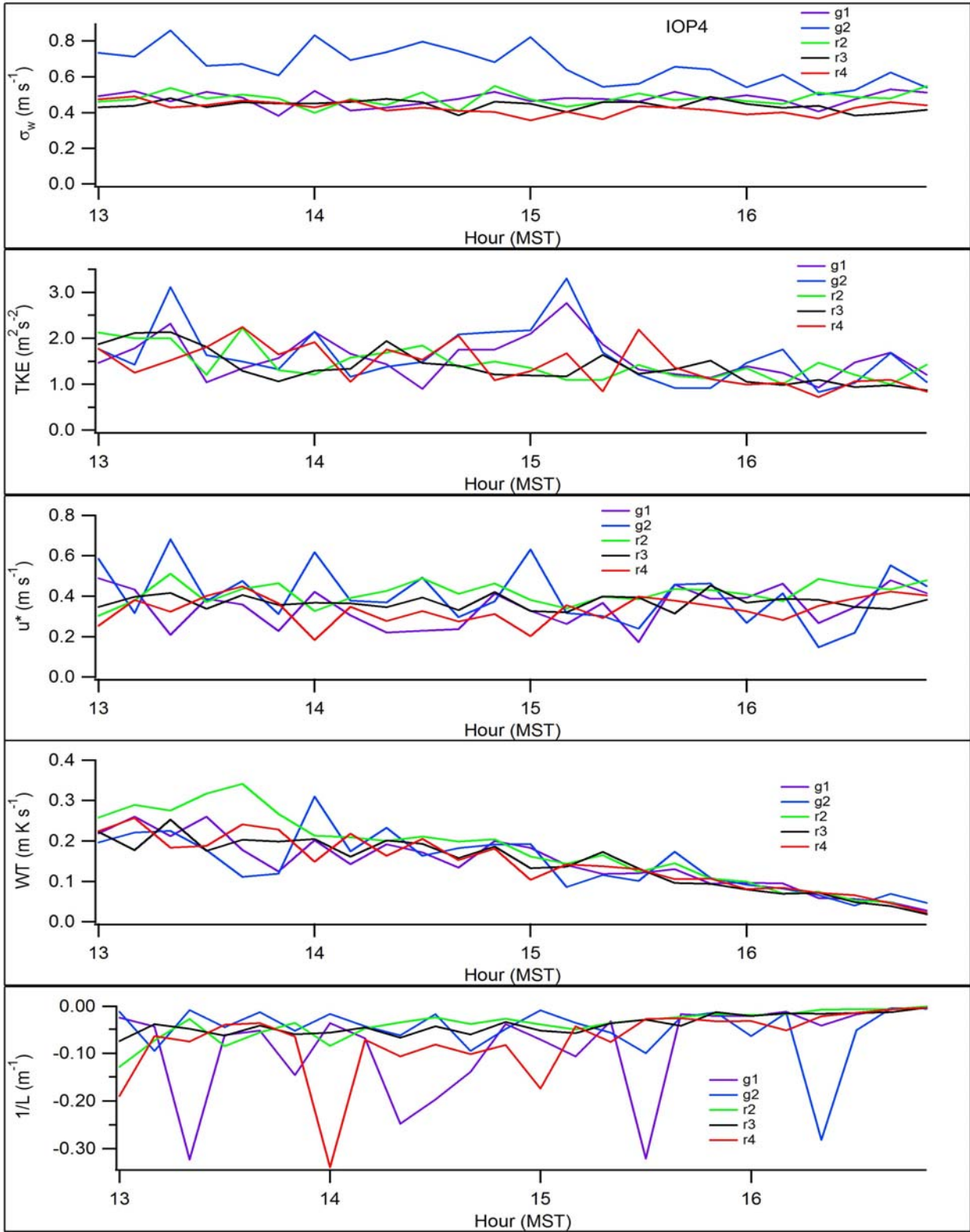


Figure 156. ARLFRD sonic anemometer 10-minute averages for σ_w , TKE, u^* , kinematic heat flux, and $1/L$ during IOP4 (G1, G2, R2, R3, and R4).

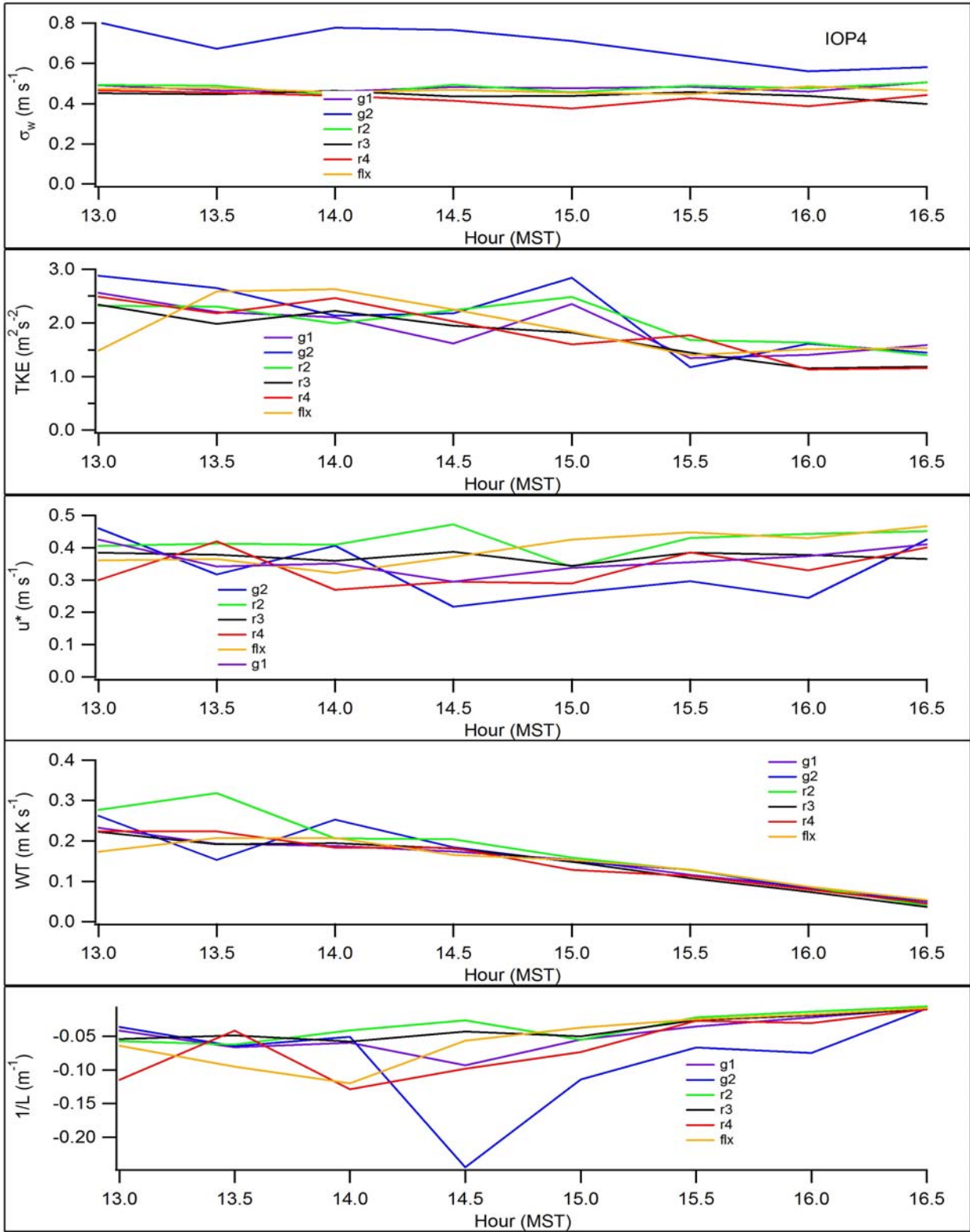


Figure 157. ARLFRD sonic anemometer 30-minute averages for σ_w , TKE, u^* , kinematic heat flux, and $1/L$ during IOP4 (G1, G2, R2, R3, and R4).

Figures 158 and 159 show time-height cross-sections for σ_w and TKE for the ASC sodar. Figures 160 and 161 show time-height cross-sections for σ_w and TKE for the ART sodar. The absolute magnitudes of TKE and σ_w shown for the ART and ASC sodars should not be assumed to be comparable between the two sodars nor with the same measurements at the sonic anemometers. The magnitudes of σ_w at ASC and ART are usually similar but the values of TKE at the ART were typically about an order of magnitude greater than the ASC. Restricting the comparison to the relative magnitudes of TKE and σ_w for each sodar, within an IOP or across IOPs, should be valid.

The magnitudes of σ_w observed at ASC and ART were similar to those measured at the sonic anemometers (Figs. 156, 157) including a trend toward decreasing values midway through the IOP. The ASC σ_w and TKE observed during IOP4 were much greater than IOP1 and similar to the rest of the IOPs. The magnitudes of ASC TKE were about half of those reported by the sonic anemometers but they do exhibit a trend toward decreasing values in the latter part of the experiment. The ART σ_w and TKE observed during IOP4 was greater than IOPs 1 and similar to the rest of the IOPs. Figure 162 shows a time-height cross-section for temperature from the RASS.

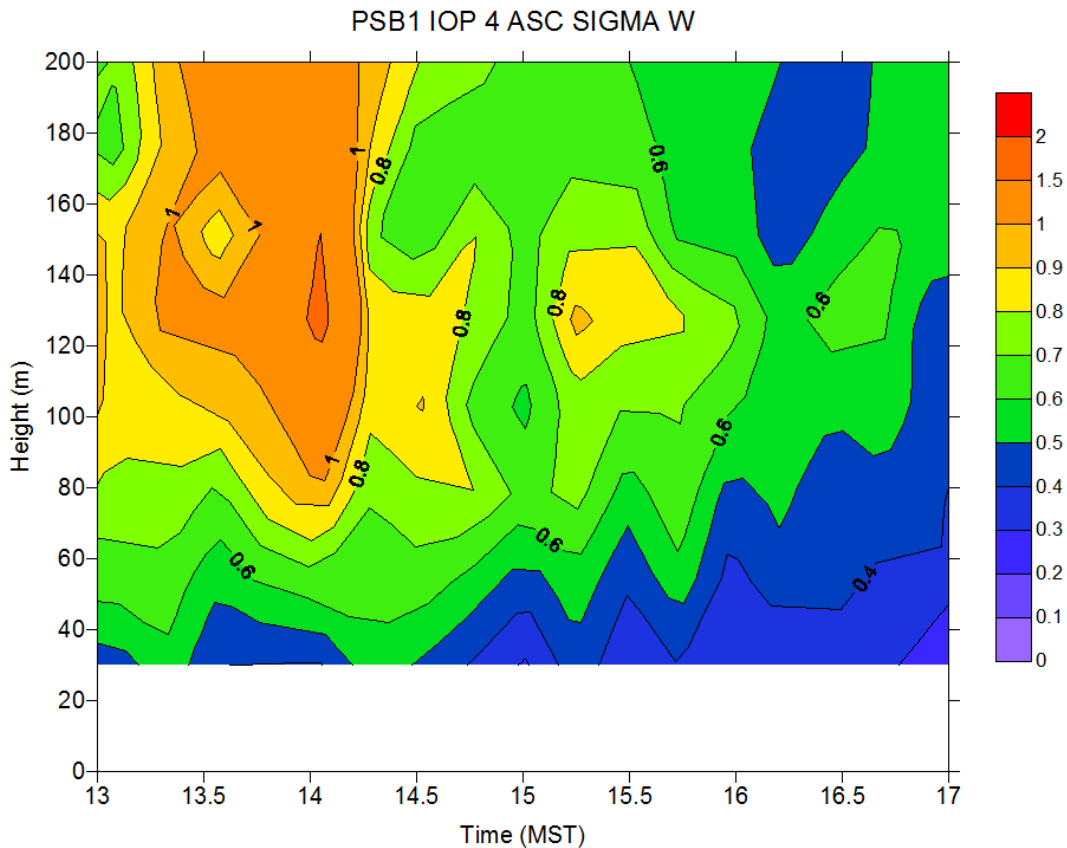


Figure 158. Time-height cross-section of σ_w at ASC sodar during IOP4.

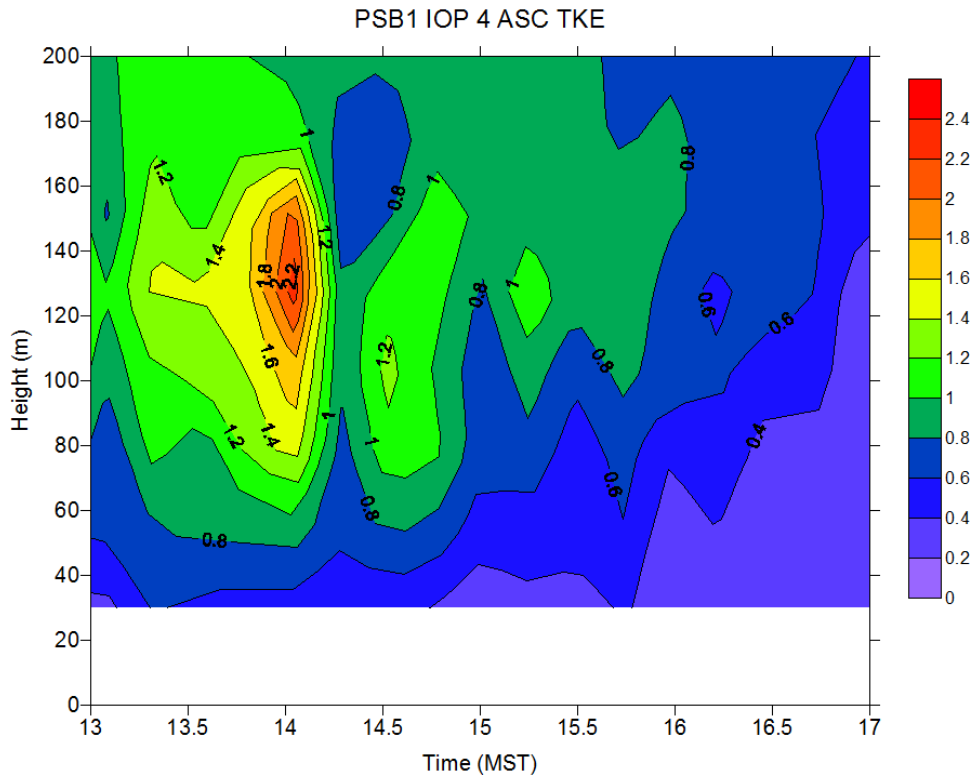


Figure 159. Time-height cross-section of TKE at ASC sodar during IOP4.

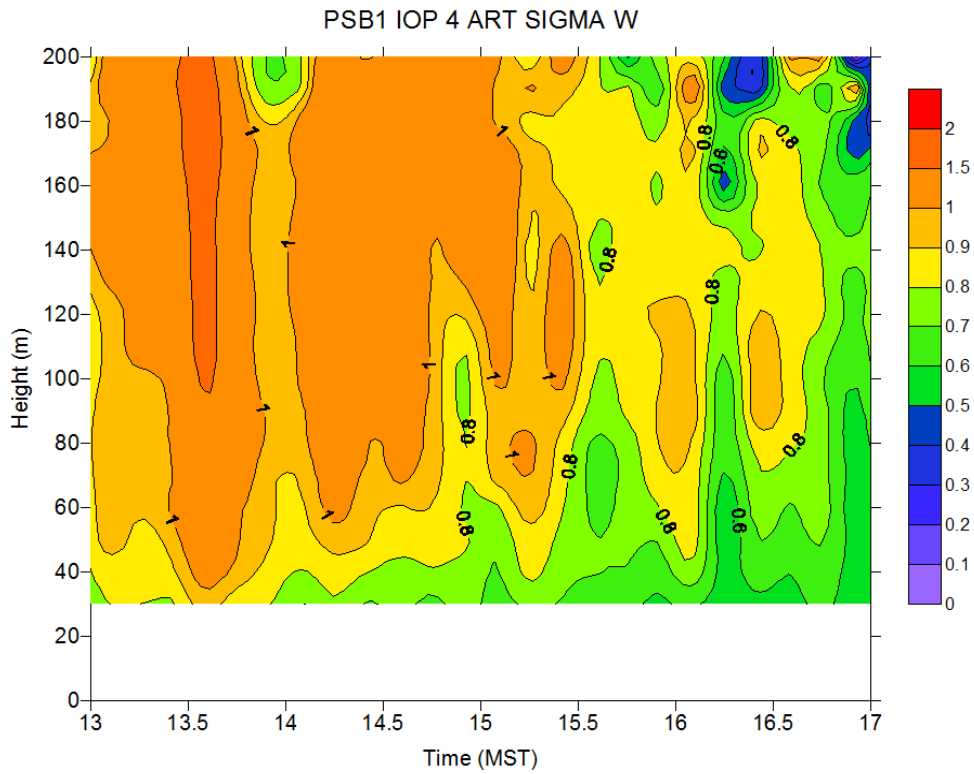


Figure 160. Time-height cross-section of σ_w at ART sodar during IOP4.

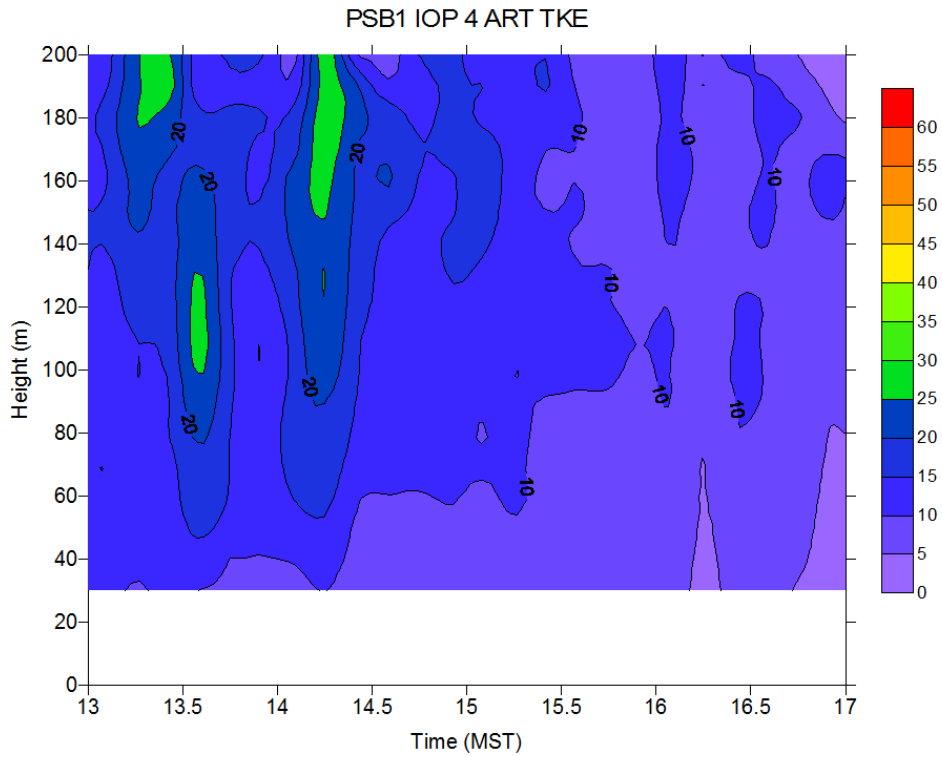


Figure 161. Time-height cross-section of TKE at ART sodar during IOP4.

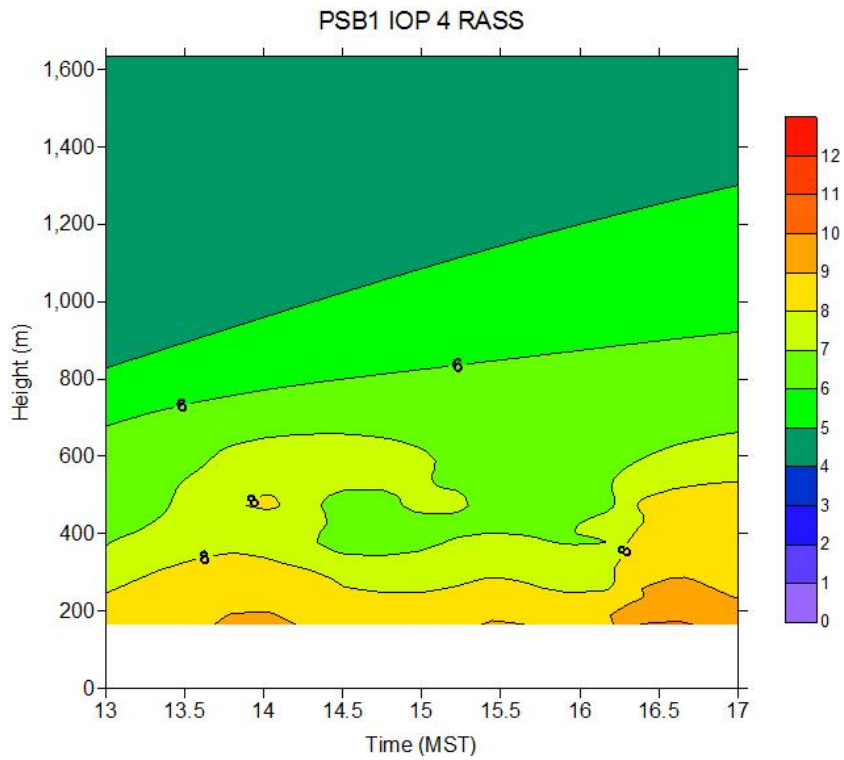


Figure 162. Time-height cross-section of virtual temperature at the RASS during IOP4. Temperatures are in degrees C.

Vertical profiles of wind speed, wind direction, and calculated turbulence parameters from the ARLFRD and WSULAR sonic anemometer measurements at GRI during IOP4 are shown in Figs. 163-165. Vertical profiles of wind speed, wind direction, and turbulence intensity (σ_θ) from cup anemometers and wind vanes plus aspirated air temperature during IOP4 are shown in Figs. 166 and 167. Turbulence intensities at the sonic anemometers (σ_w/U) were less than during IOPs 1 and 2 but greater than IOP3. There was general consistency between the sonic and cup and vane (σ_θ) results but there were some exceptions, mainly in the first hour of the IOP. The 45 m (ARLFRD) intensities were sometimes low while the 8, 12, and 60 m (WSULAR) intensities were sometimes high during that time (Figs. 164, 167). A similar pattern of TKE sonic profile discrepancies was also observed (Fig. 165). There was mostly good agreement between wind speed measurements made by the sonic anemometers and cup anemometers. The wind speed from the sonic anemometer at the 45 m level was often inconsistent relative to the other sonic anemometers in the wind speed profiles. There were some inconsistencies in wind direction between the ARLFRD and the WSULAR sonic anemometers with the ARLFRD sonics showing better consistency with the cup and vane results.

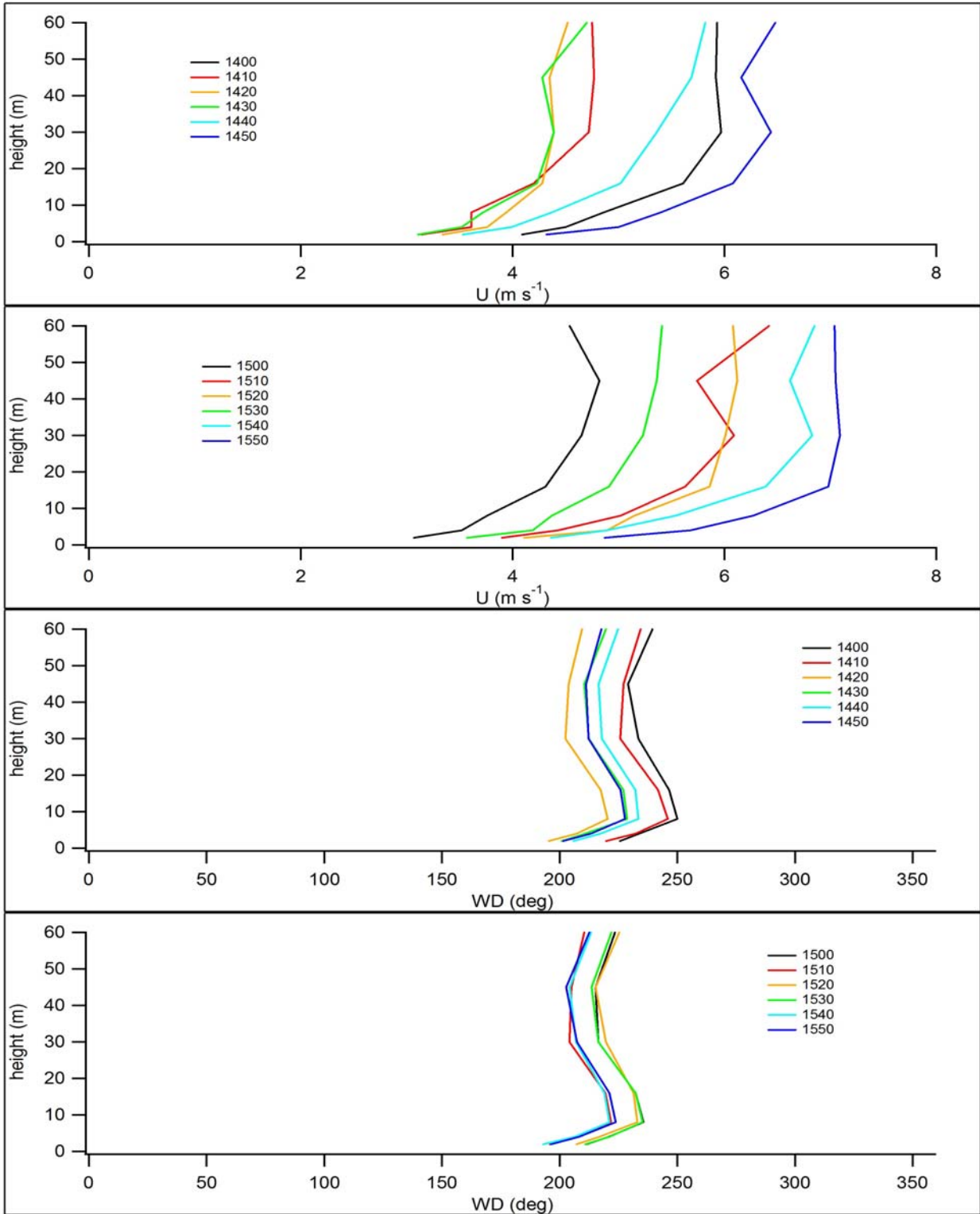


Figure 163. Vertical profiles of wind speed and direction from sonic anemometer measurements at GRI during IOP4. ARLFRD instruments were at 4, 30, and 45 m; WSULAR instruments were at 2, 8, 16, and 60 m. Times in legend are start times for the 10 minute interval (hhmm MST).

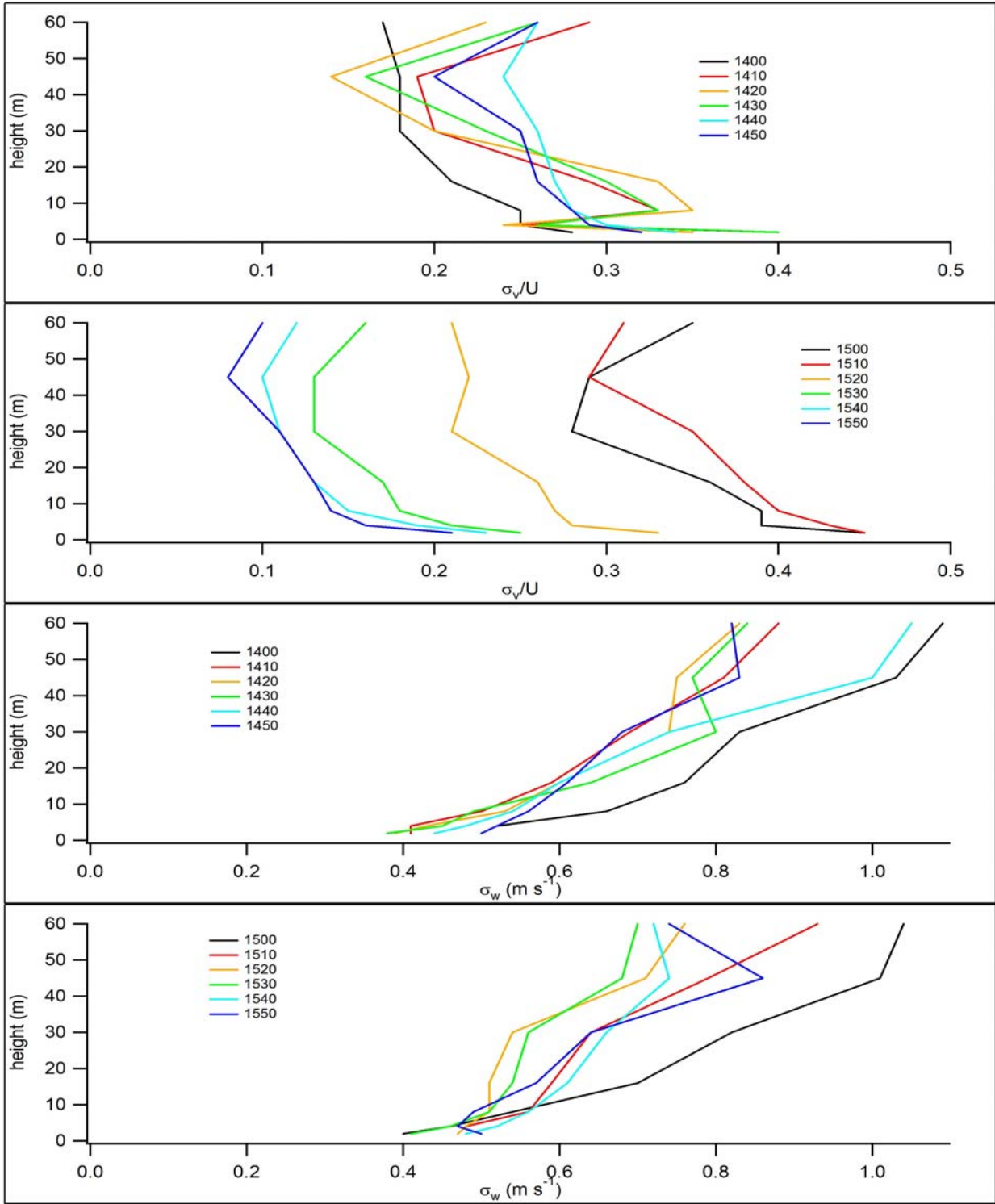


Figure 164. Vertical profiles of turbulence intensity and σ_w from sonic anemometer measurements at GRI during IOP4. ARLFRD instruments were at 4, 30, and 45 m; WSULAR instruments were at 2, 8, 16, and 60 m. Times in legend are start times for the 10 minute interval (hhmm MST).

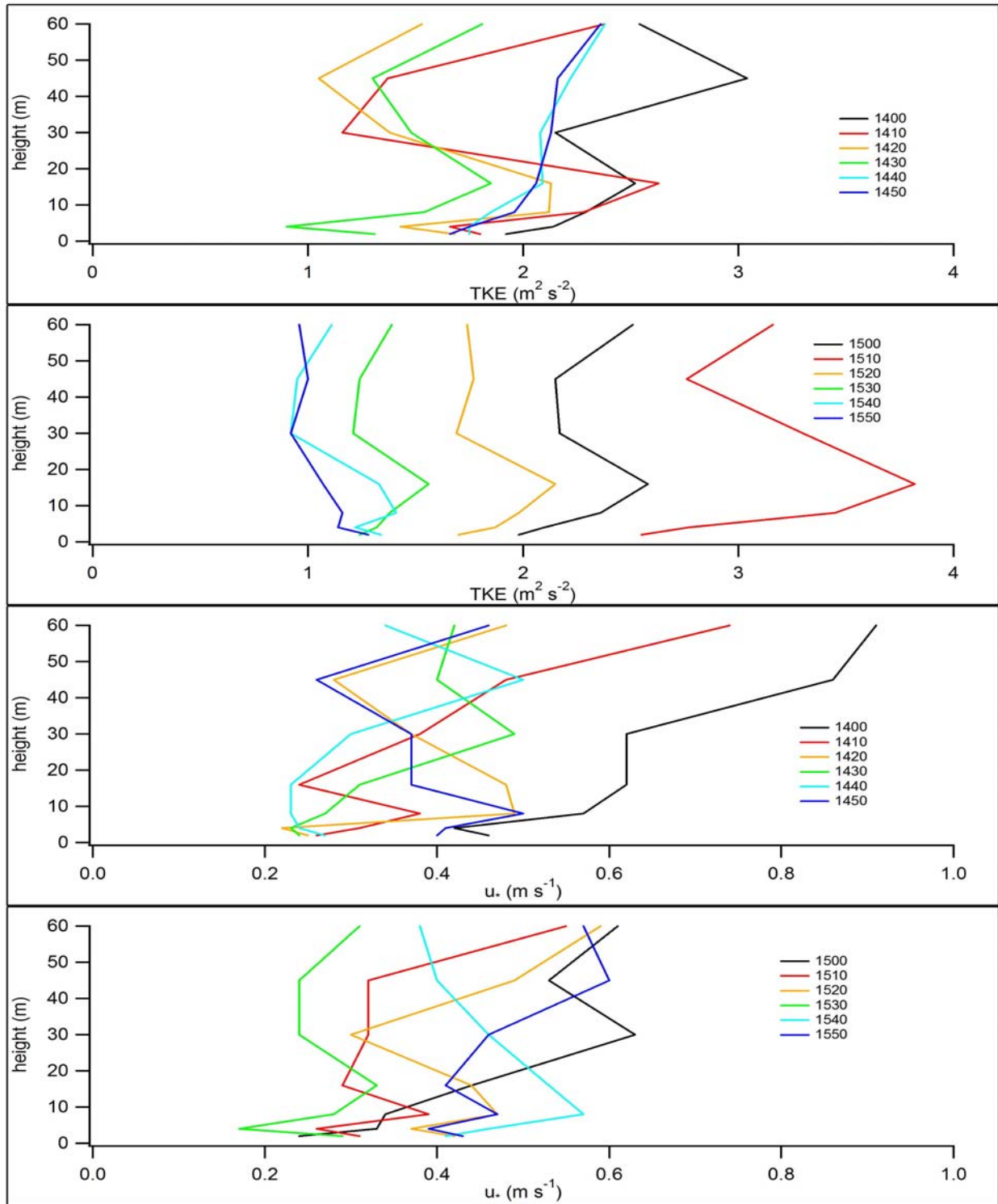


Figure 165. Vertical profiles of turbulent kinetic energy (TKE) and u_* from sonic anemometer measurements at GRI during IOP4. ARLFRD instruments were at 4, 30, and 45 m; WSULAR instruments were at 2, 8, 16, and 60m. Times in legend are start times for the 10 minute interval (hhmm MST).

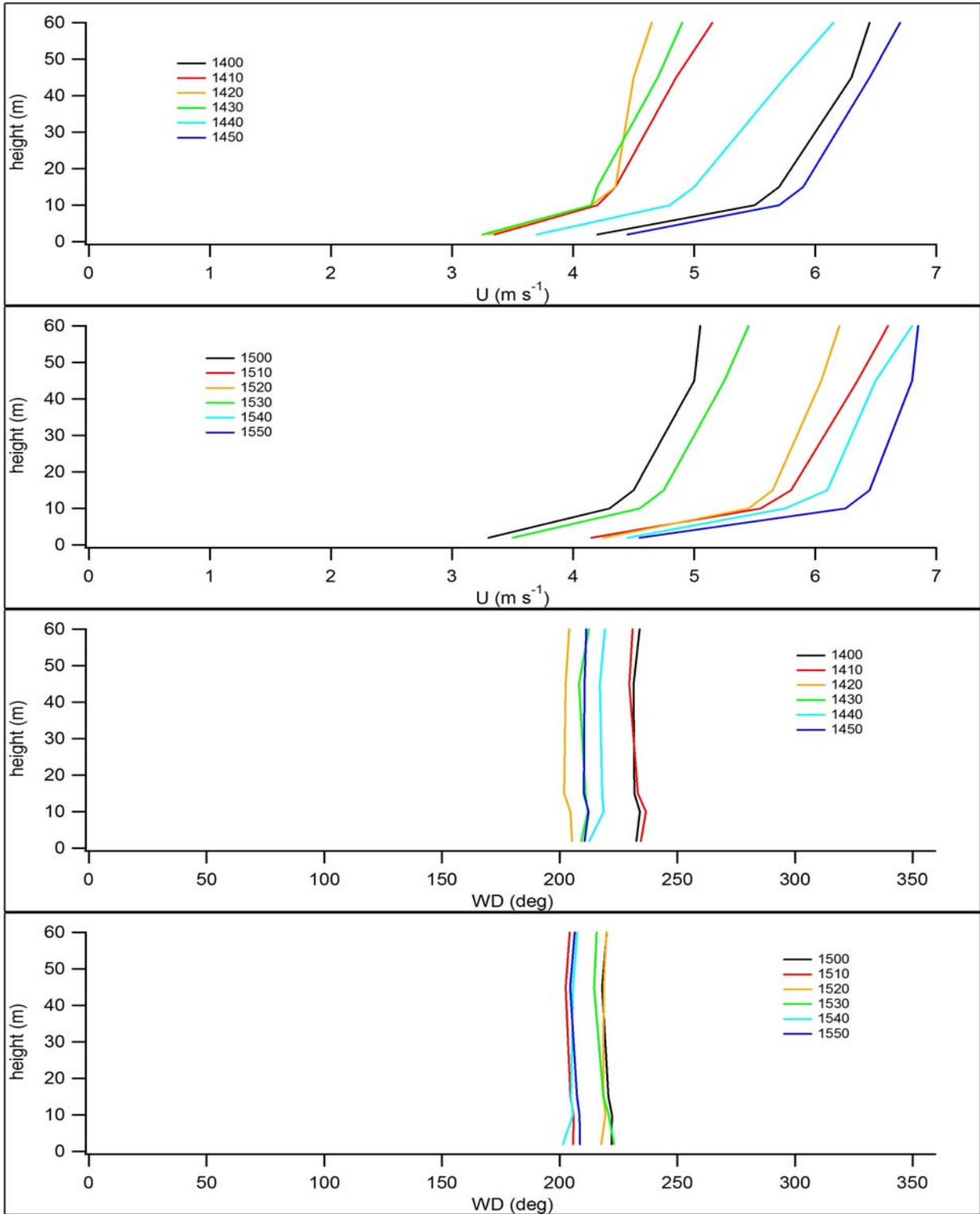


Figure 166. Vertical profiles of wind speed and direction from cup anemometer and wind vane measurements at GRI during IOP4. Times in legend are start times for the 10 minute interval (hhmm MST).

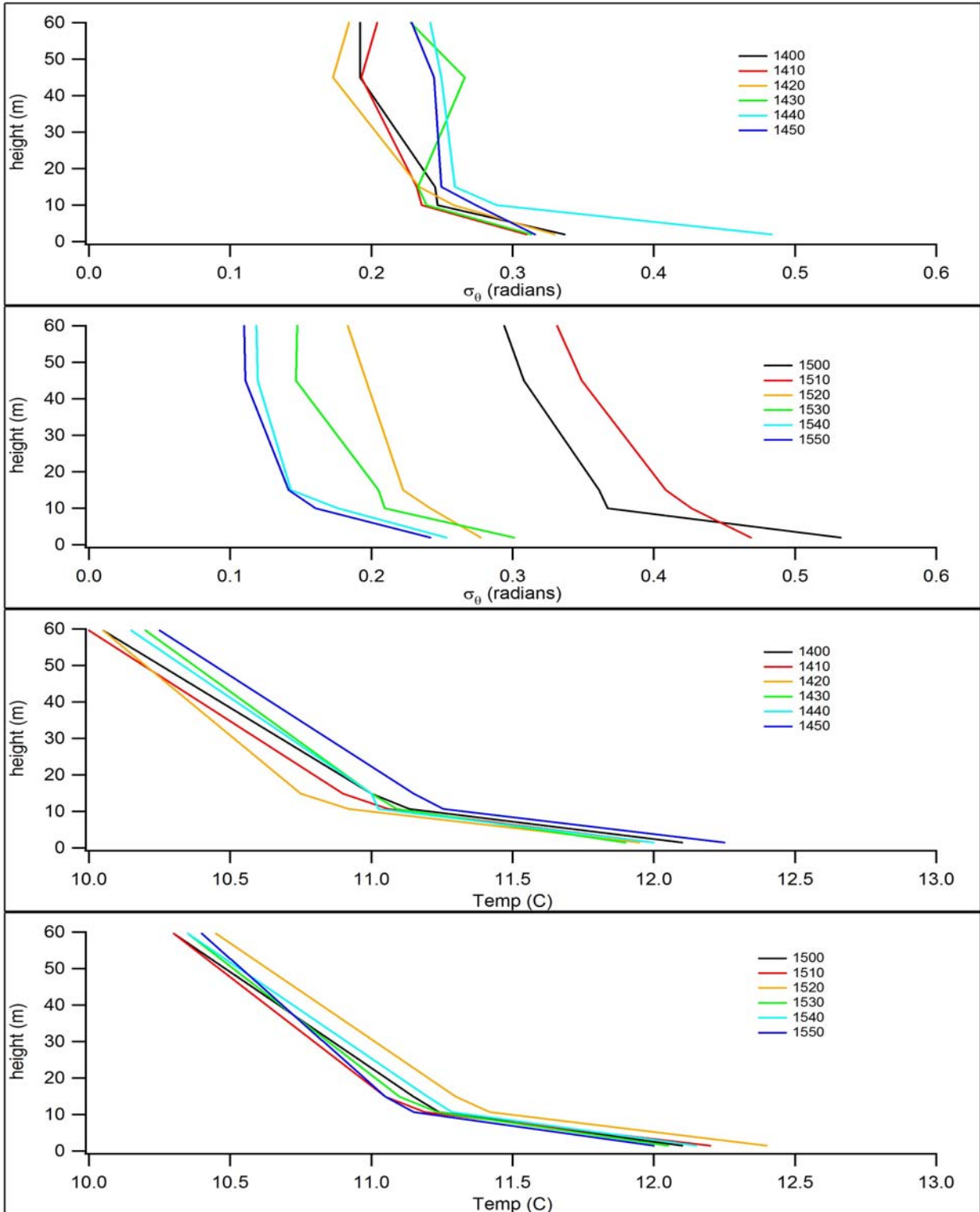


Figure 167. Vertical profiles of σ_θ (from cup and vane) and aspirated air temperature measurements at GRI during IOP4. Times in legend are start times for the 10 minute interval (hhmm MST).

Stability

The SRDT-Delta T and σ_A methods gave similar results for (P-G) stability category determinations. All results were categories C or D and in most cases there was agreement between the methods. The magnitudes and signs of the z/L stability parameter values are generally consistent with weakly unstable conditions and the category C and D classifications.

Radiosonde Results

Figures 168 and 169 show potential temperature and specific humidity profiles from radiosonde measurements pre and post IOP4. The mixing depths estimated from these plots are given in Table 18.

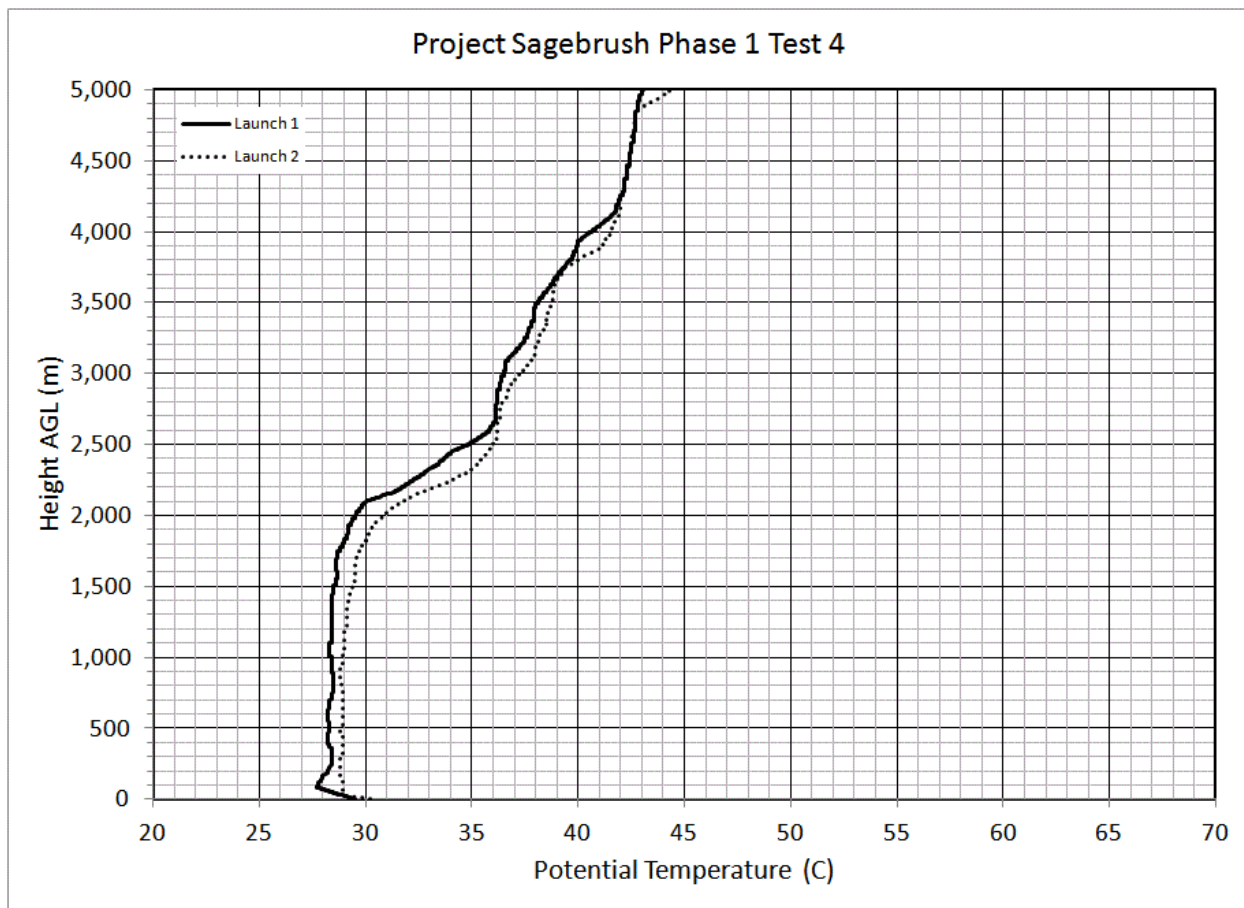


Figure 168. Pre and post IOP radiosonde potential temperature profiles for IOP4.

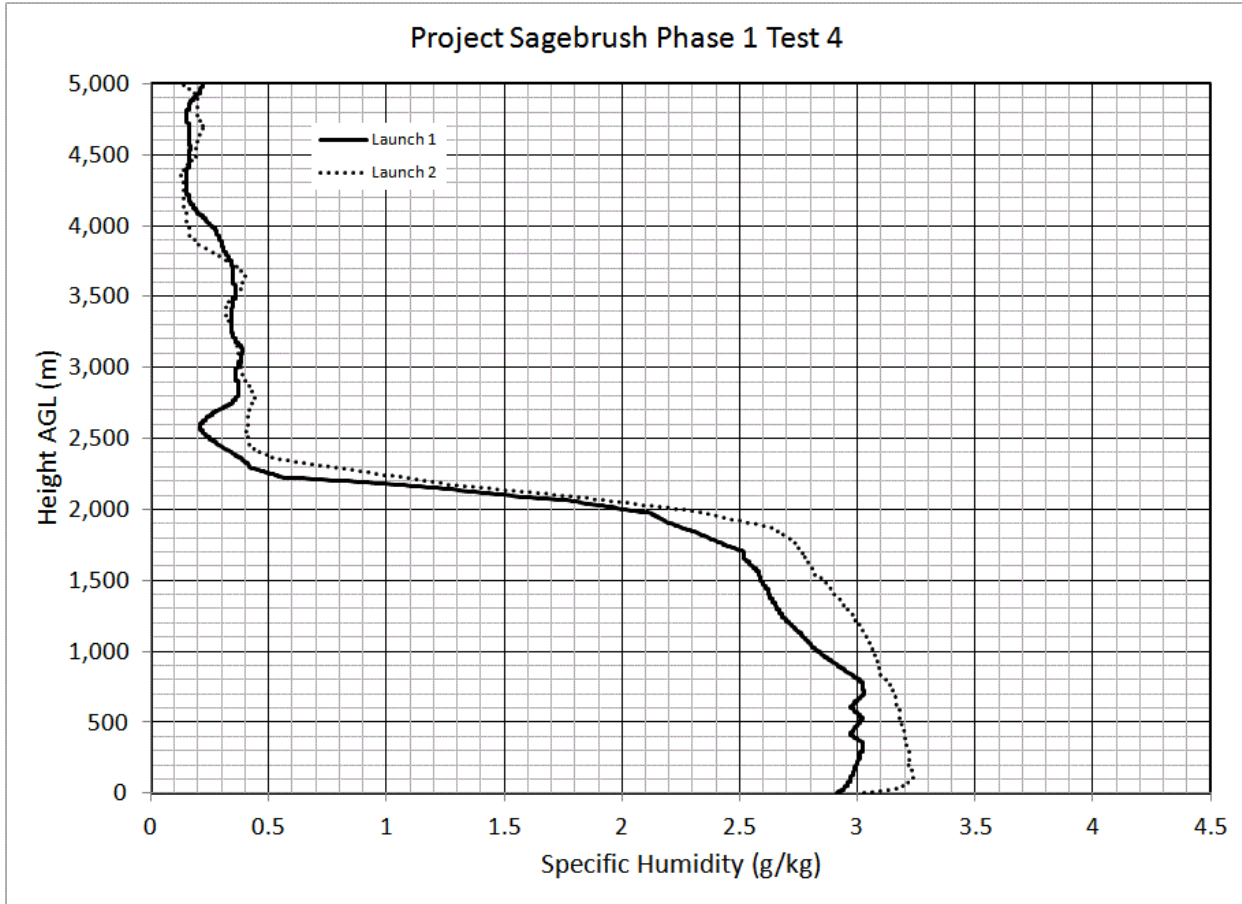


Figure 169. Pre and post IOP radiosonde specific humidity profiles for IOP4.

Concentration Results and Analysis

Figure 170 shows the bag sampling results for IOP4. While measured concentrations during IOP4 were much less than those during IOP3, the normalized concentrations tended to be somewhat higher based on a comparison between the extents of the normalized contours (compare Fig. 142). Wind directions were such that the plume was present on the sampling array throughout IOP4.

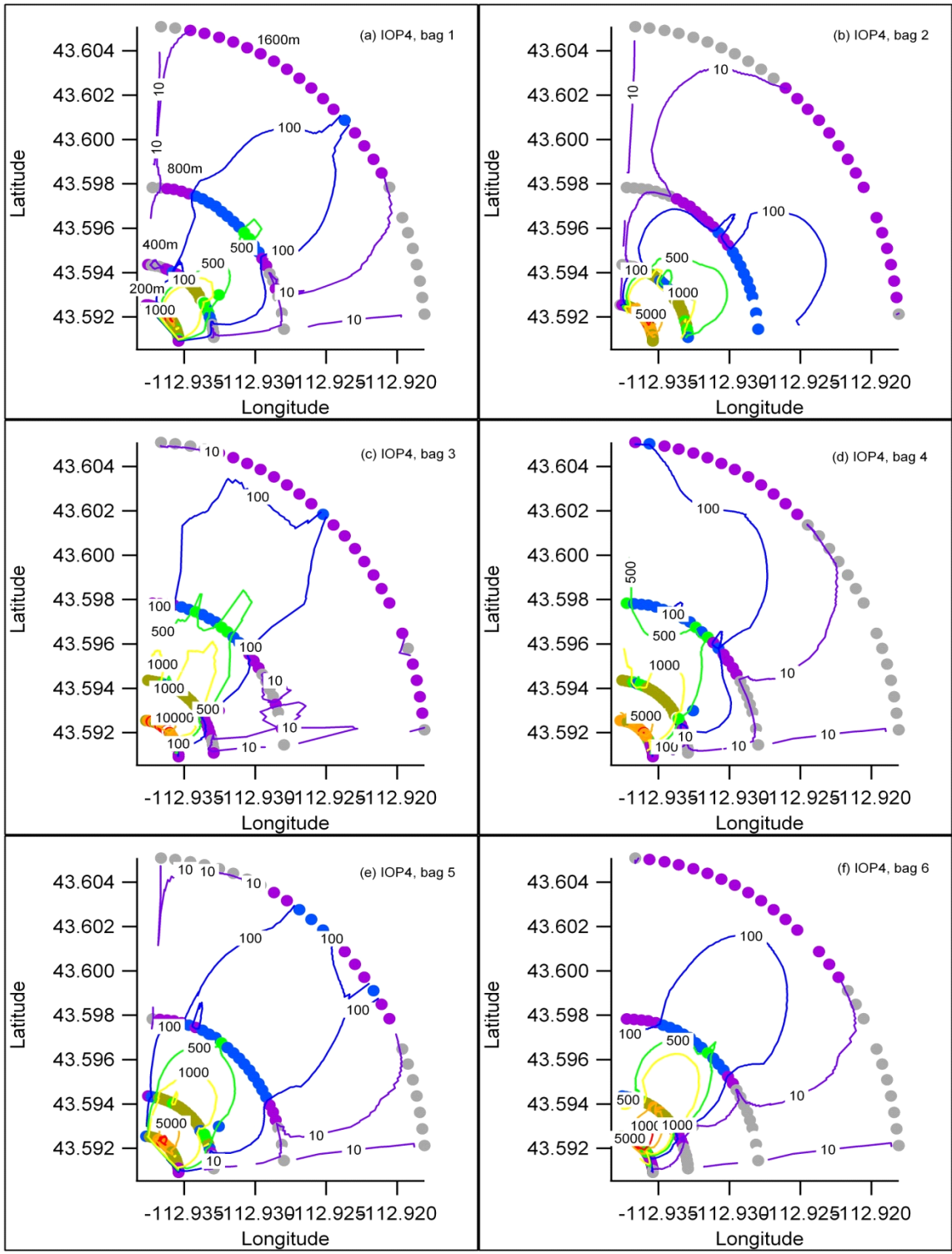


Figure 170. Bag sampling results (a-f, bags 1-6) for IOP4 with color-coded concentration markers for each 1 m AGL bag sampling location and contour lines of normalized concentration. The color scheme for the markers and contours is described in the Introduction to this section.

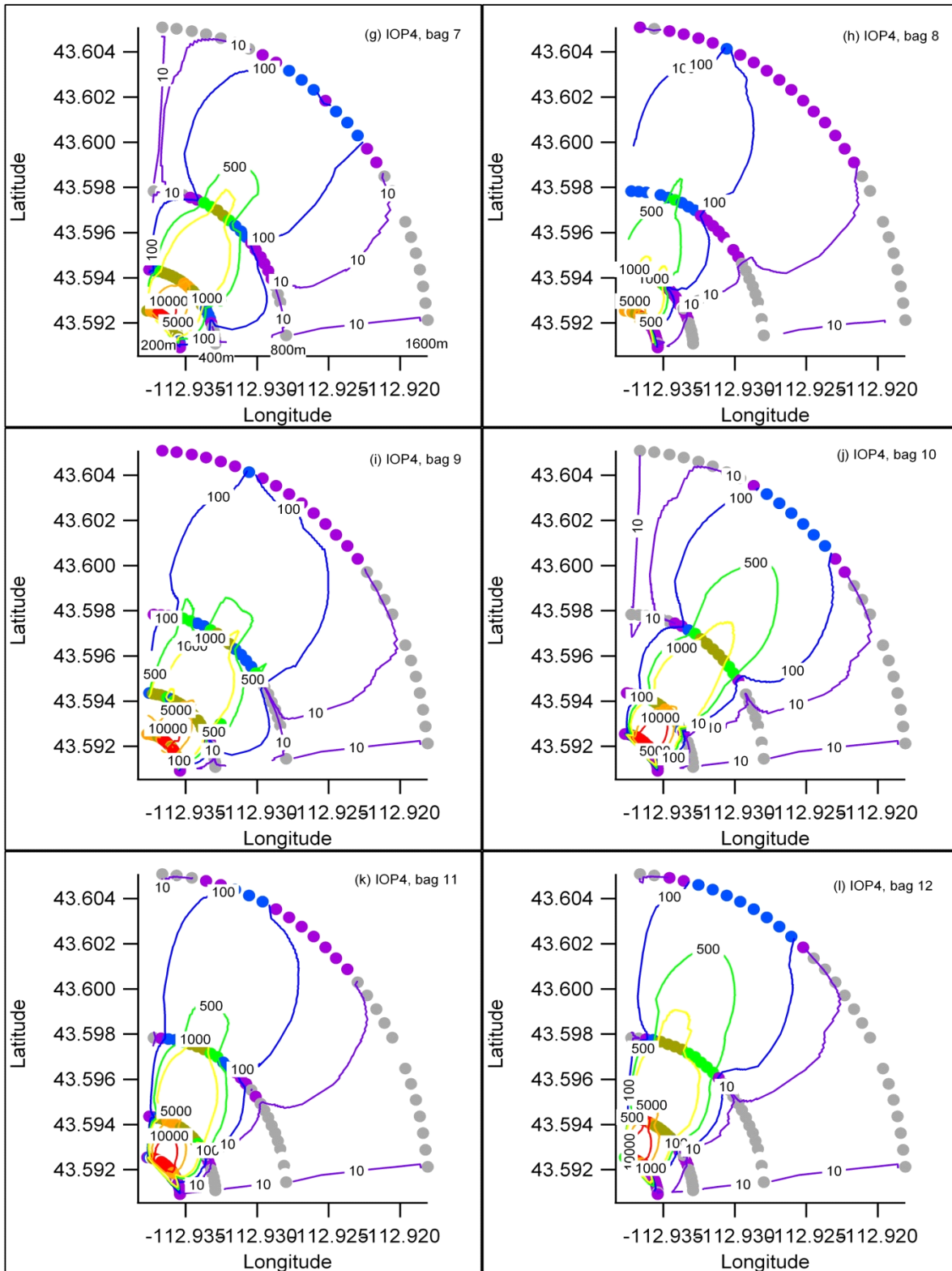


Figure 170 continued (g-l, bags 7-12).

Figure 171 shows cross-sections of tracer concentration along each arc for each 10-minute bag sampling period during IOP4. Plumes were sometimes broad, less so than IOPs 1 and 2 but more so than IOP3. That result is consistent with the intermediate values, comparatively speaking, of σ_0 observed during most of the IOP (Table 22). Individual arc concentration cross-sections often exhibited a non-ideal Gaussian form with profiles having asymmetries about their maxima and/or very irregular concentration profiles. This was less prevalent compared to IOPs 1 and 2 (Figs. 87, 115) but more common than in IOP3 (Fig. 143). Plumes were largely confined to the sampling array but truncation of some cross-section profiles at the edge of the sampling array is evident.

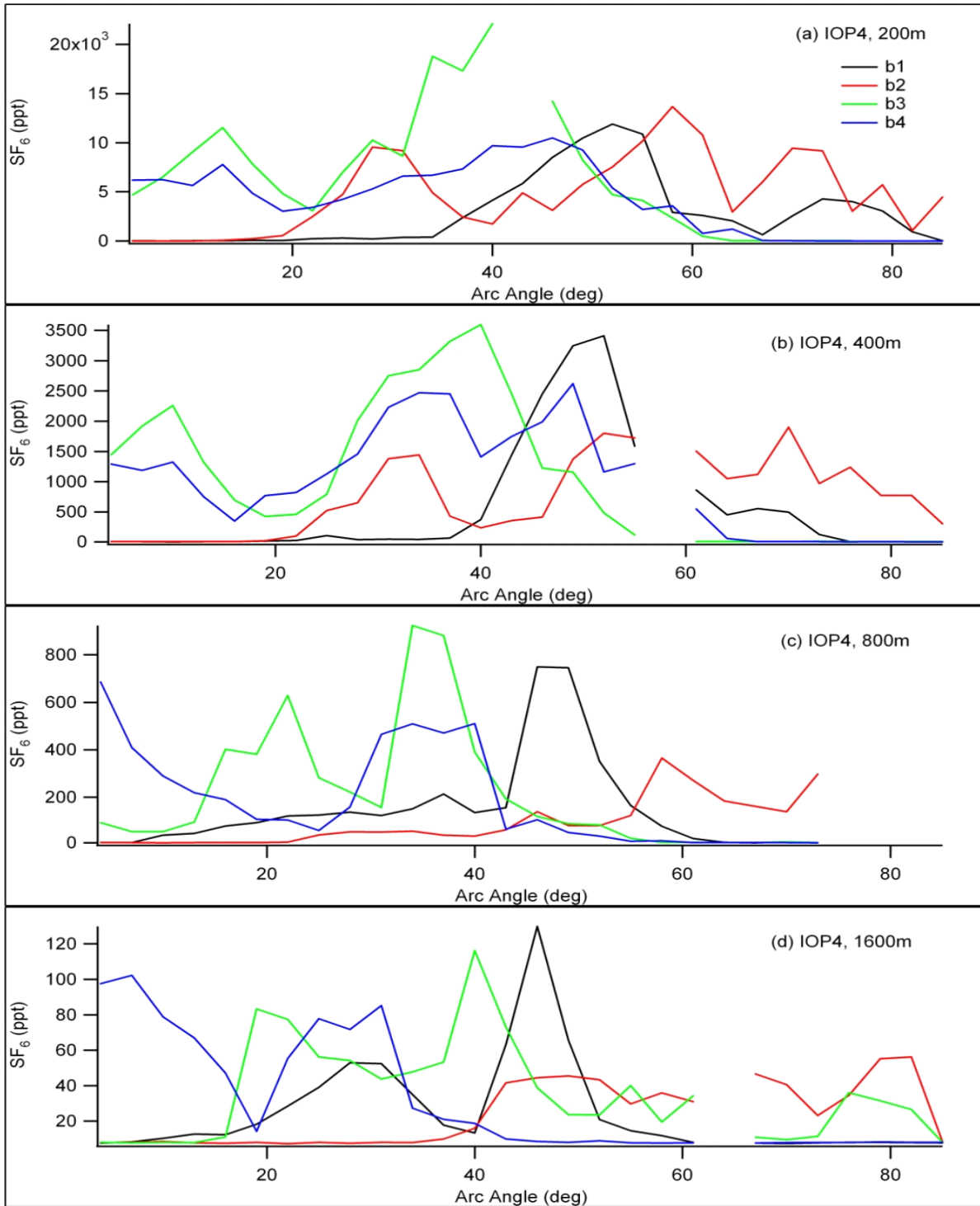


Figure 171. Cross-sections of concentration along each arc for each 10-minute bag sampling period during IOP4. The individual plume cross-section layouts are arranged to illustrate the variation in time, across 40 minutes per layout (a-d, bags 1-4), and the simultaneous variation with distance across all four arcs.

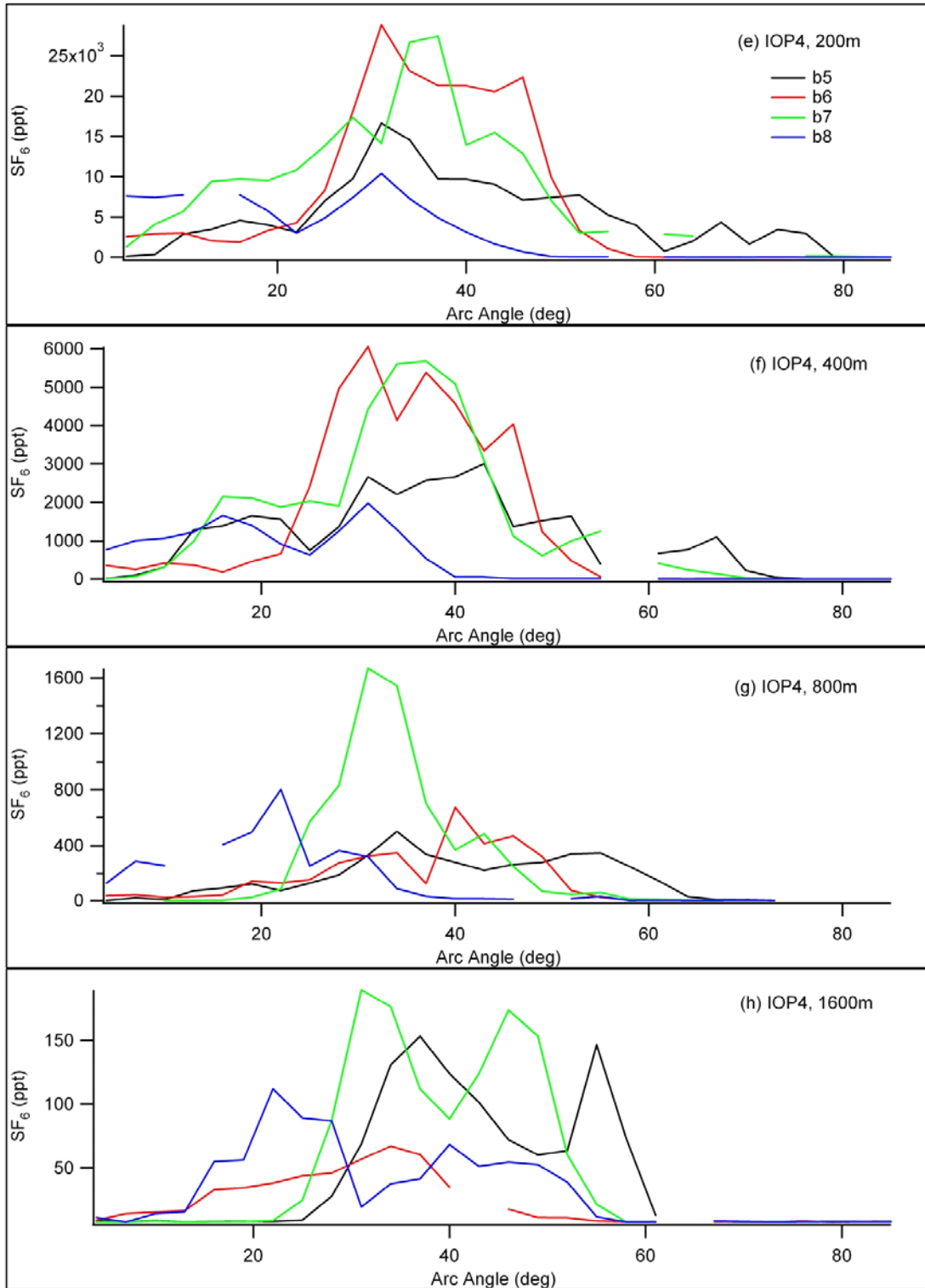


Figure 171 continued (e-h, bags 5-8).

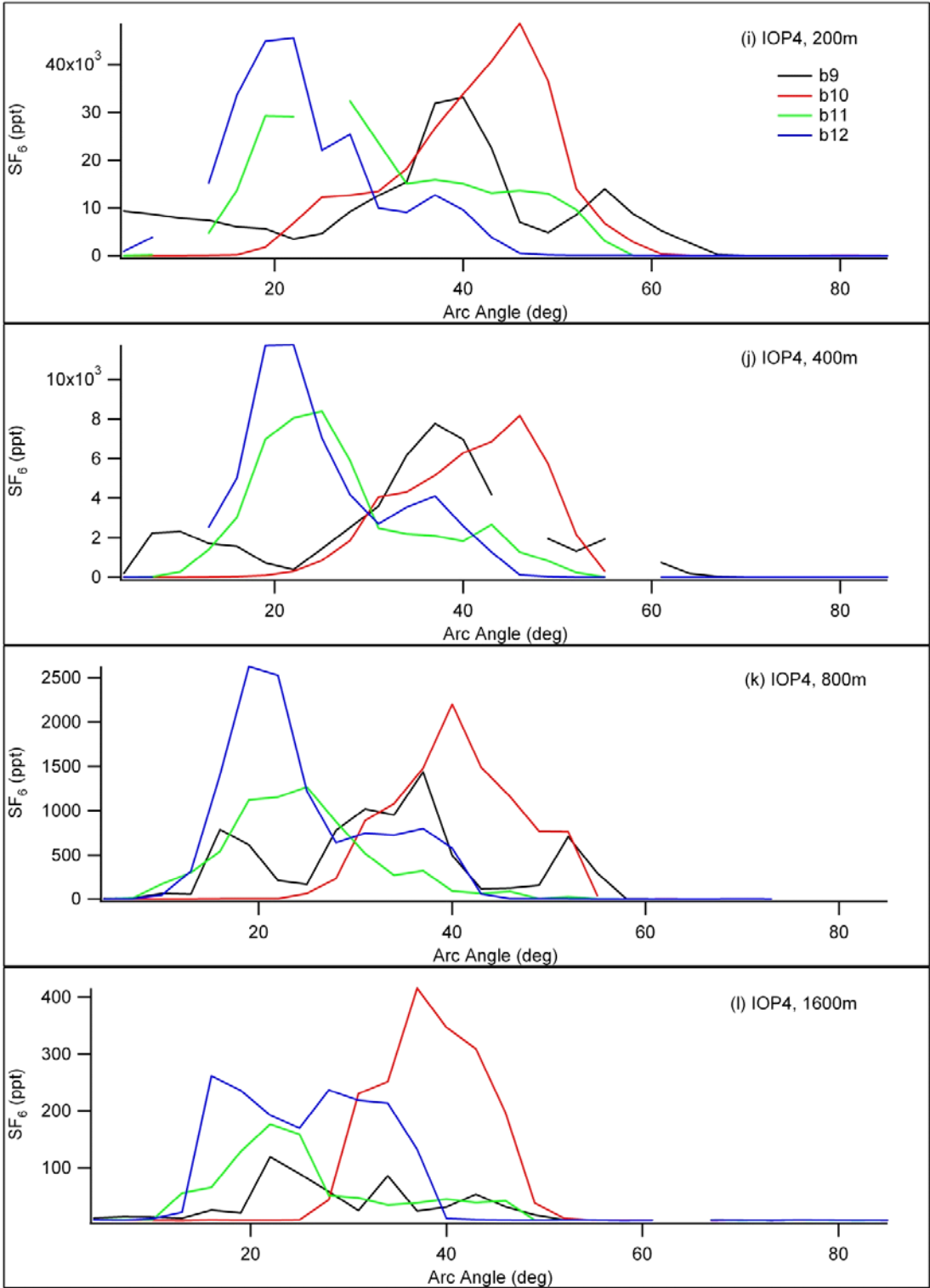


Figure 171 continued (i-l, bags 9-12).

Figure 172 shows vertical tracer concentration profiles at the towers at 201, 408, and 499 m downwind for all 10-minute bag sampling intervals for IOP4. Any evidence for liftoff of the vertical plume centerline is inconclusive.

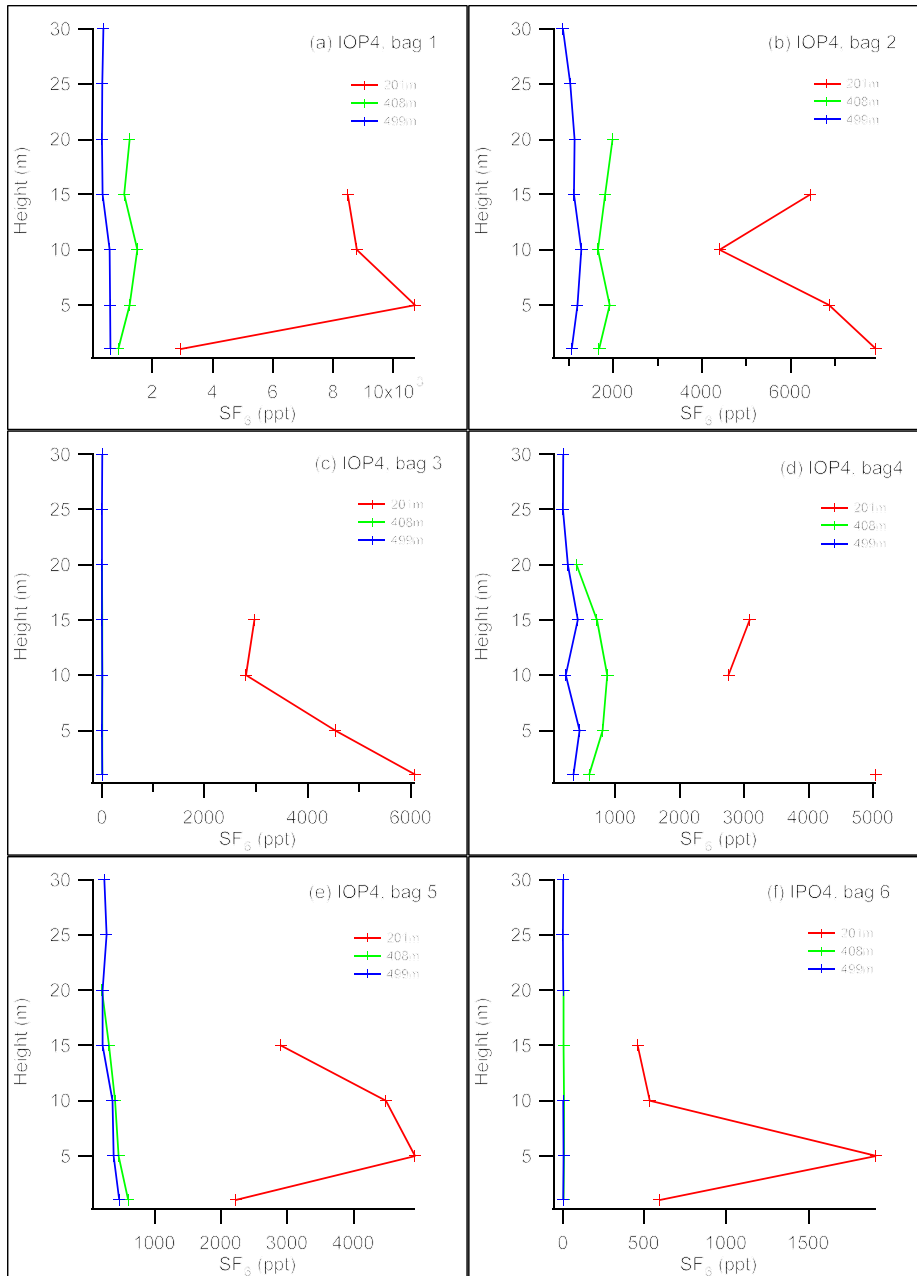


Figure 172. Vertical concentration profiles (a-f, bags 1-6) at the towers at 201, 408, and 499 m downwind for all 10-minute bag sampling intervals for IOP4. No aircraft measurements were available.

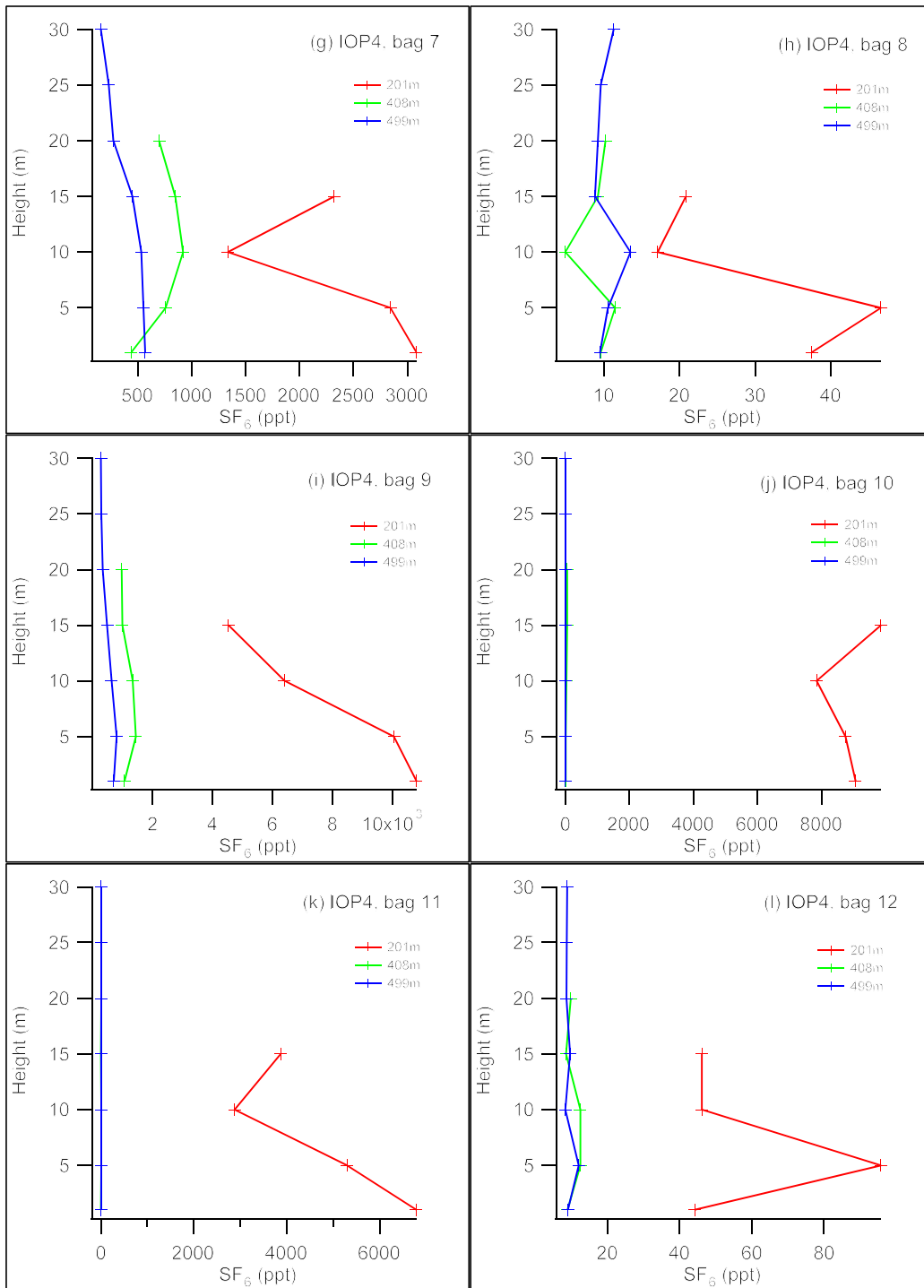


Figure 172 continued (g-l, bags 7-12).

Figure 173 shows time series of SF₆ concentrations measured by the fast response analyzers at the specified arc and arc angle location during IOP4. Due to the lower release rate and concentrations over the sampling array, there were fewer problems with analyzer railing than

during IOP3. Nevertheless, this did occur in some instances. Peaks with missing data due to railing can be seen in Fig. 173 for the 400 m arc at both the 31 and 55 degrees locations. Various periodicities are suggested by the data. One example would be about 25-30 minutes at the 800 and 1600 m arcs.

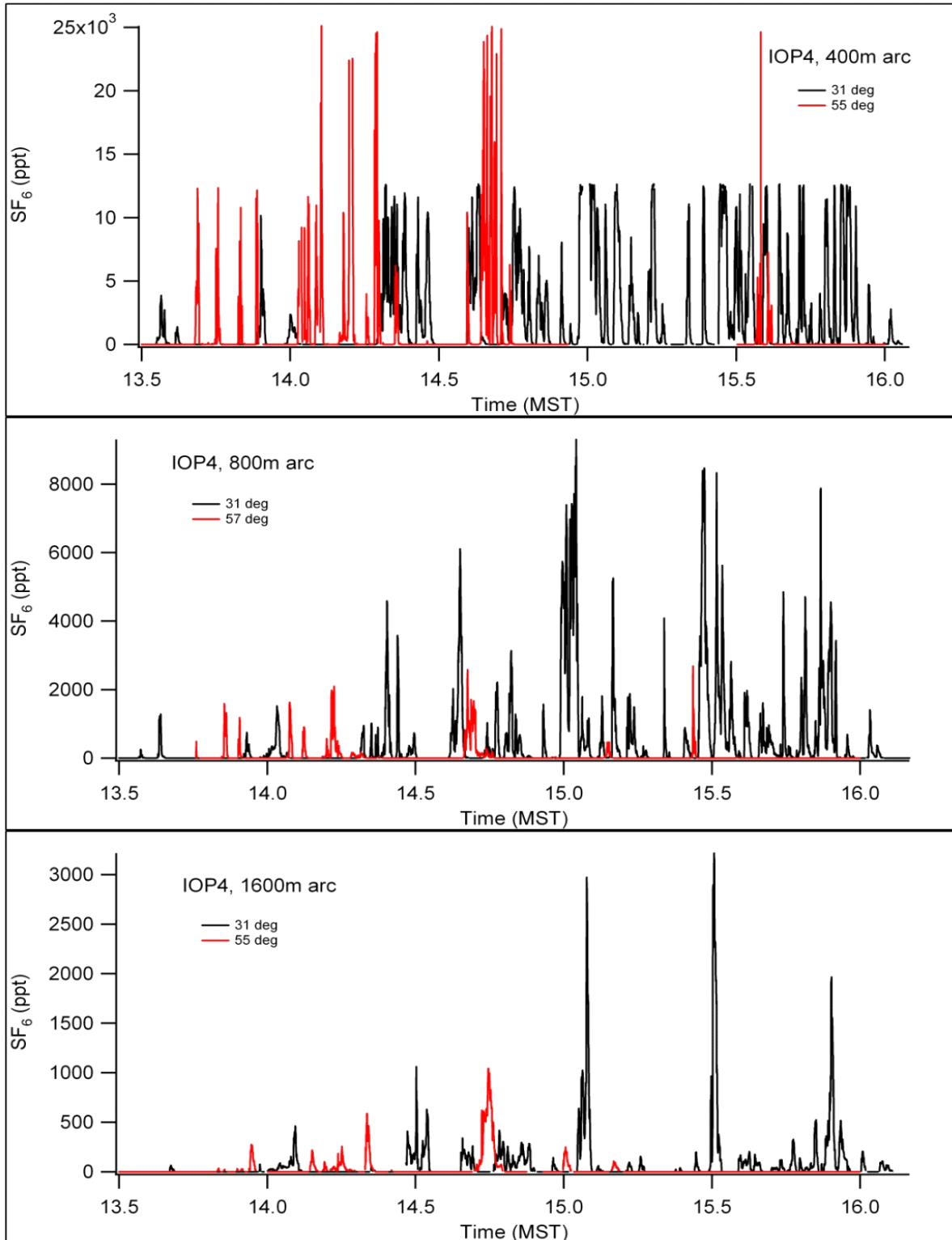


Figure 173. Time series of SF₆ concentrations measured by the fast response analyzers at the specified arc and arc angle location during IOP4.

IOP5

Date/Time and General Description

IOP5 was conducted on 18 October from 1300-1500 MST (1400-1600 MDT). It was mostly sunny. Conditions during IOP5 resembled those during IOP4 with some differences. Wind speeds exhibited an upward trend over the course of the test. Depending on height, wind speeds increased from about 3-4 m s⁻¹ at the start of the tracer sampling period (1300 h) to 3-6 m s⁻¹ at the end (1500 h). Overall turbulence levels and wind direction variation were similar to that observed during IOP4. All estimates of stability point to weakly unstable conditions. Overall, there was good stationarity in the flow during IOP5. Flows were relatively stationary during IOP5 although the trend in wind speeds indicates some degree of non-stationarity. The relative stationarity, in combination with the generally favorable southwesterly wind directions, made for good experimental conditions across the tracer sampling array. A summary of the meteorological conditions during IOP5 are shown in Table 23. The SF₆ release rate was 1.030 g s⁻¹ (Tables 1 and 2). Like IOP4, the UTSI aircraft was not present for IOP5. The fast response analyzers were located on the 400 m arc at 25 and 55 degrees, on the 800 m arc at 25 and 57 degrees, and on the 1600 m arc at 25 and 55 degrees.

Table 23. Meteorological conditions during IOP5. Wind speeds, directions, σ_θ , and P-G stability class determinations (EPA, 2000c) are from COC at 10 m. Solar radiation measurements are from FLX. R3 and R4 indicate sonic anemometer data from their respective locations.

Bag	Wind Speed (m s ⁻¹)	Wind Direction (deg)	Solar Radiation (W m ⁻²)	R3 u* (m s ⁻¹)	R4 u* (m s ⁻¹)	R3 z/L	R4 z/L	σ_θ (deg)	P-G SRDT	P-G σ_λ
1	4.0	210.2	512.0	0.40	0.29	-0.15	-0.29	15.7	C	C
2	3.6	225.6	504.5	0.34	0.34	-0.25	-0.24	22.1	C	B
3	4.1	196.4	495.5	0.41	0.33	-0.11	-0.21	18.7	C	C
4	3.8	213.5	486.0	0.43	0.26	-0.10	-0.35	15.9	C	C
5	3.6	226.1	475.5	0.32	0.29	-0.25	-0.31	18.0	C	B
6	4.6	201.3	464.0	0.42	0.28	-0.12	-0.31	14.2	C	C
7	4.6	234.7	449.5	0.27	0.34	-0.36	-0.20	12.6	C	C
8	5.0	235.3	435.5	0.35	0.38	-0.19	-0.14	16.4	C	C
9	4.3	220.8	420.0	0.29	0.30	-0.21	-0.19	15.1	C	C
10	4.9	233.9	402.5	0.41	0.36	-0.09	-0.13	11.1	C	D
11	4.6	227.6	384.5	0.42	0.32	-0.08	-0.18	12.7	C	C
12	4.9	226.0	365.5	0.36	0.36	-0.13	-0.13	12.3	C	D

Winds and Quality Assurance

Figure 174 shows wind speed and direction comparisons for ARLFRD cup anemometer and wind vane data in the vertical at the GRI and COC towers for IOP5. There was excellent

agreement in wind speed and direction. Flows during IOP5 exhibited good spatial homogeneity although the gradual increase in wind speed indicates temporal non-stationarity. Fluctuations in wind direction (σ_θ) were moderate and decreased with time as the wind speeds increased (Fig. 175).

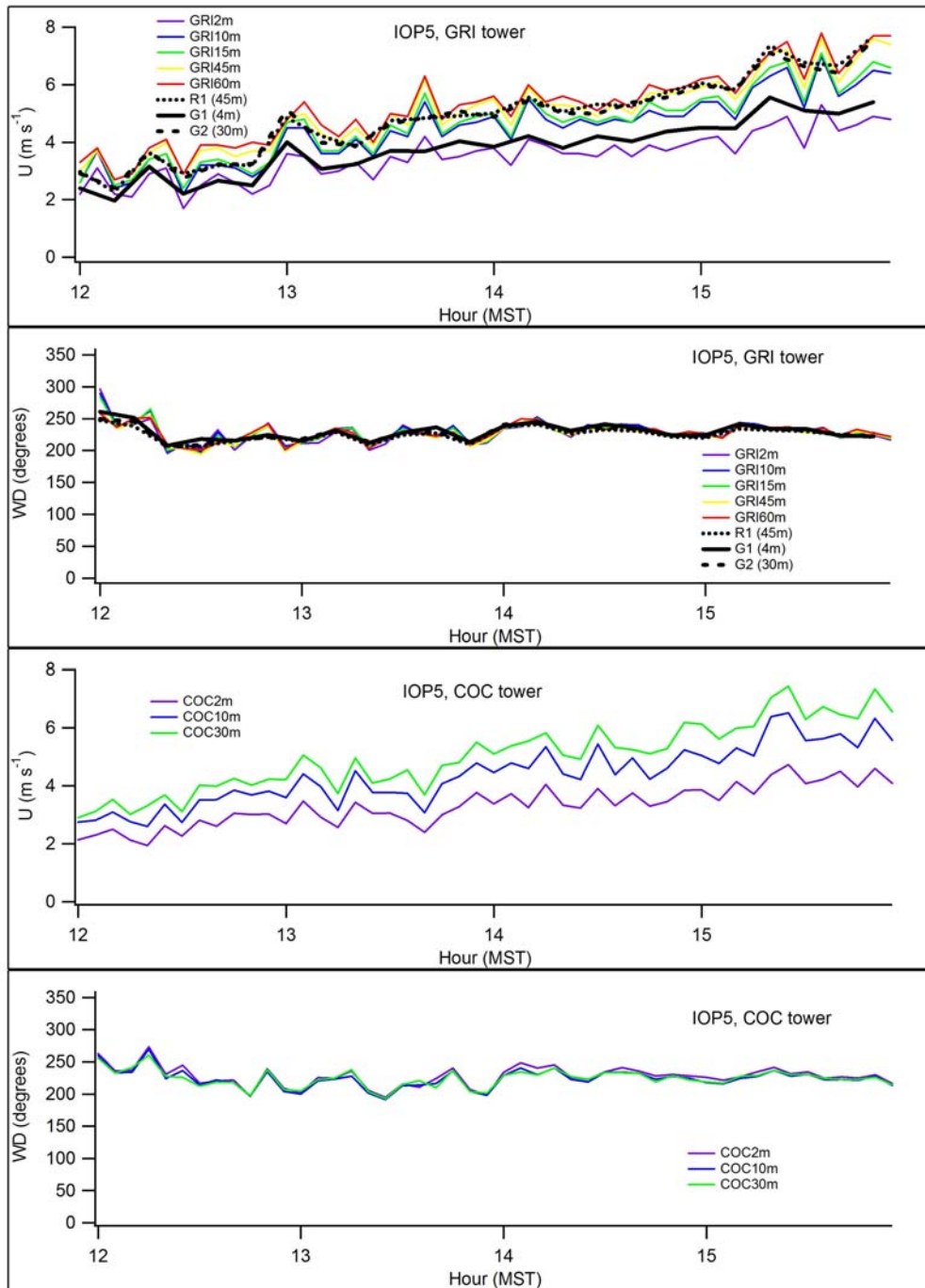


Figure 174. ARLFRD wind speed and direction comparisons in the vertical at GRI and COC for IOP5.

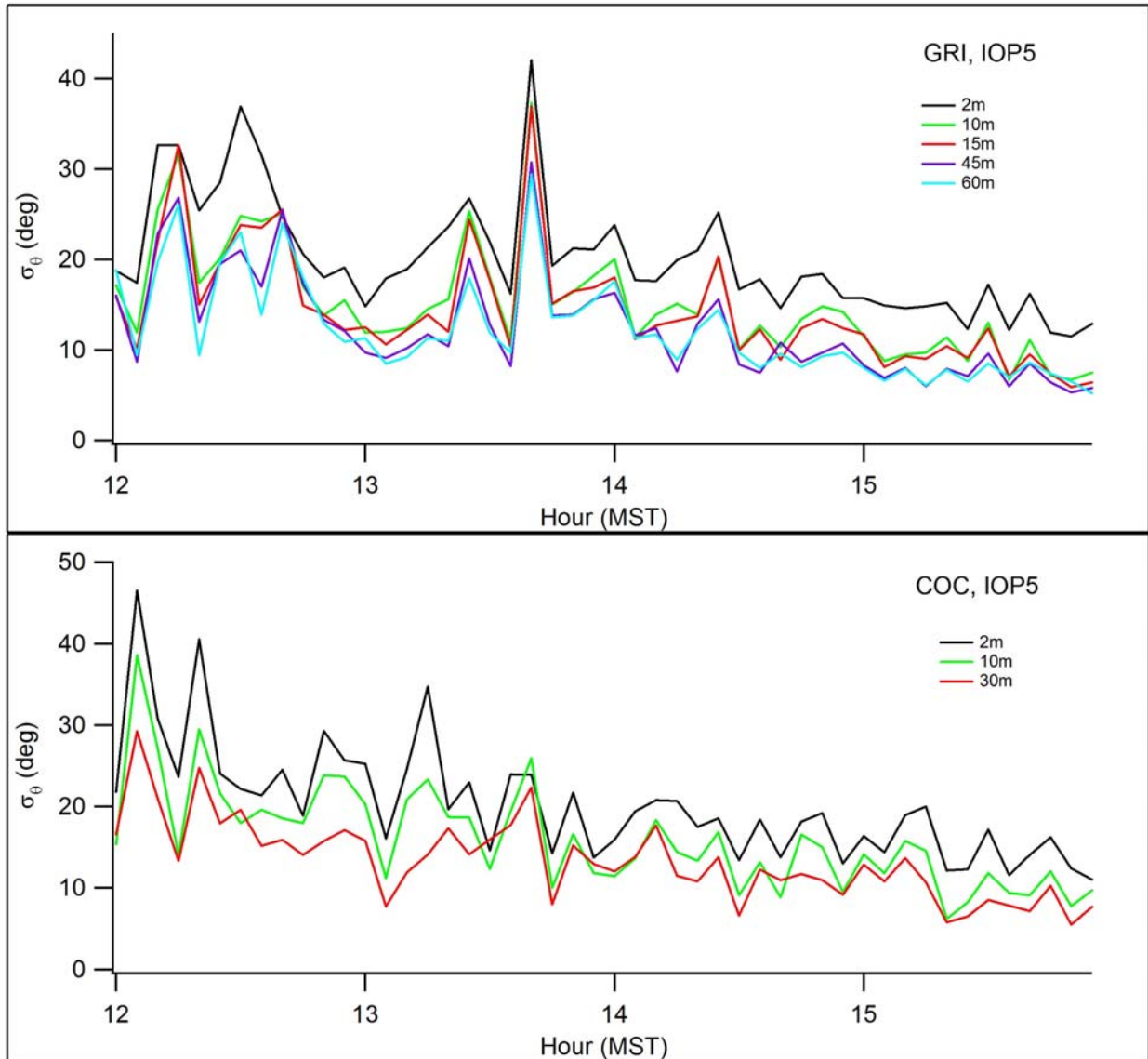


Figure 175. Standard deviation in wind direction σ_θ (σ_A) using wind vanes at GRI and COC for IOP5.

Figures 176-178 show wind speed and direction comparisons in the horizontal across the study area at 2 m, 10 m, 30 m, 45 m, 60 m, and 160 m from the data available. The comparisons are the same as those described for IOP1 except that data was not available from TOW due to power supply problems. Observations showed good agreement between sites and measurement type across the study area. All of the available data are generally consistent and show good agreement with the exception of a low wind speed bias at PRO. This is based upon limited data from the ASC at 160 m. With the exception of the low wind speed bias at PRO, there is little evidence for a problem with the measurements.

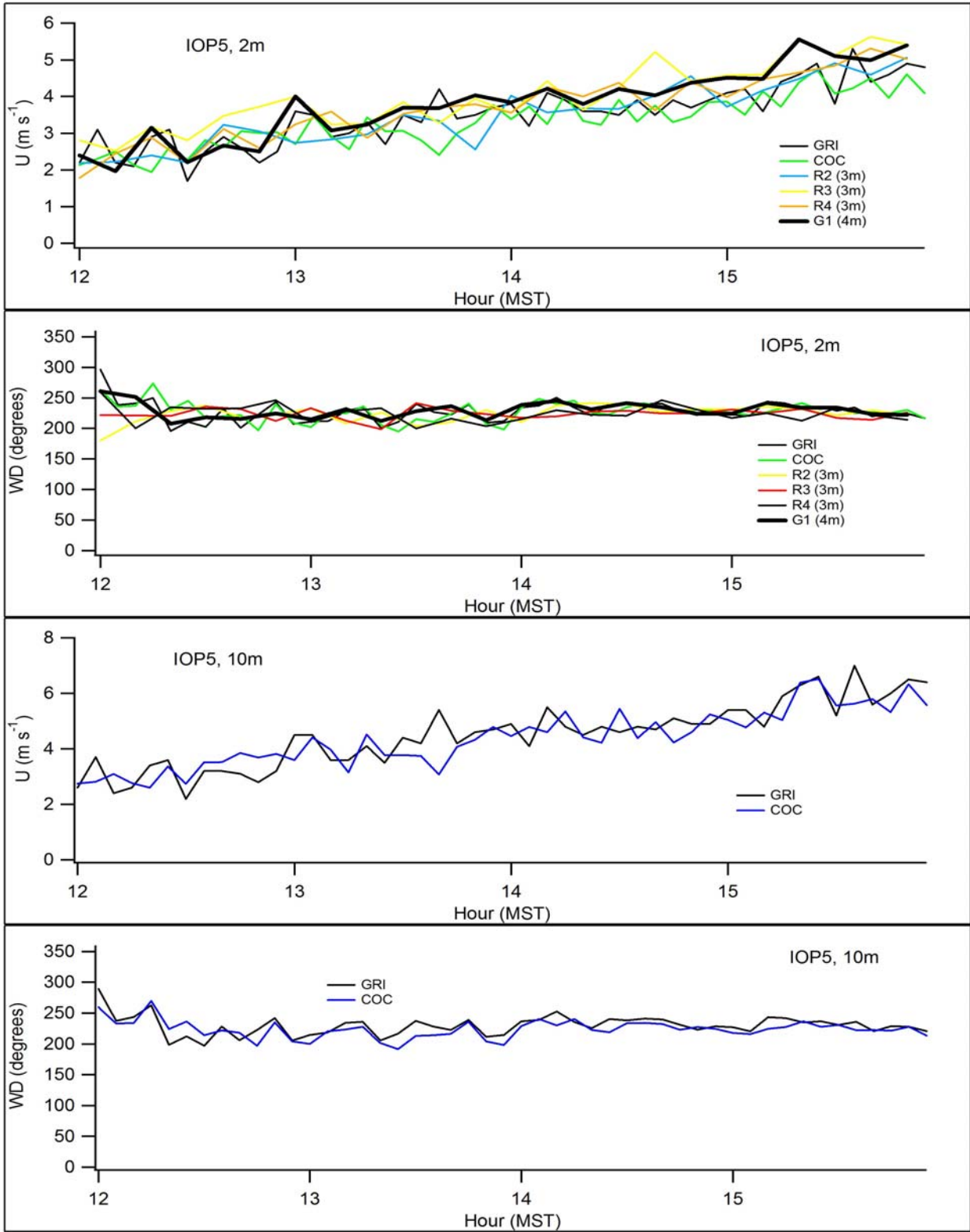


Figure 176. ARLFRD wind speed and direction comparisons in the horizontal at 2 and 10 m during IOP5.

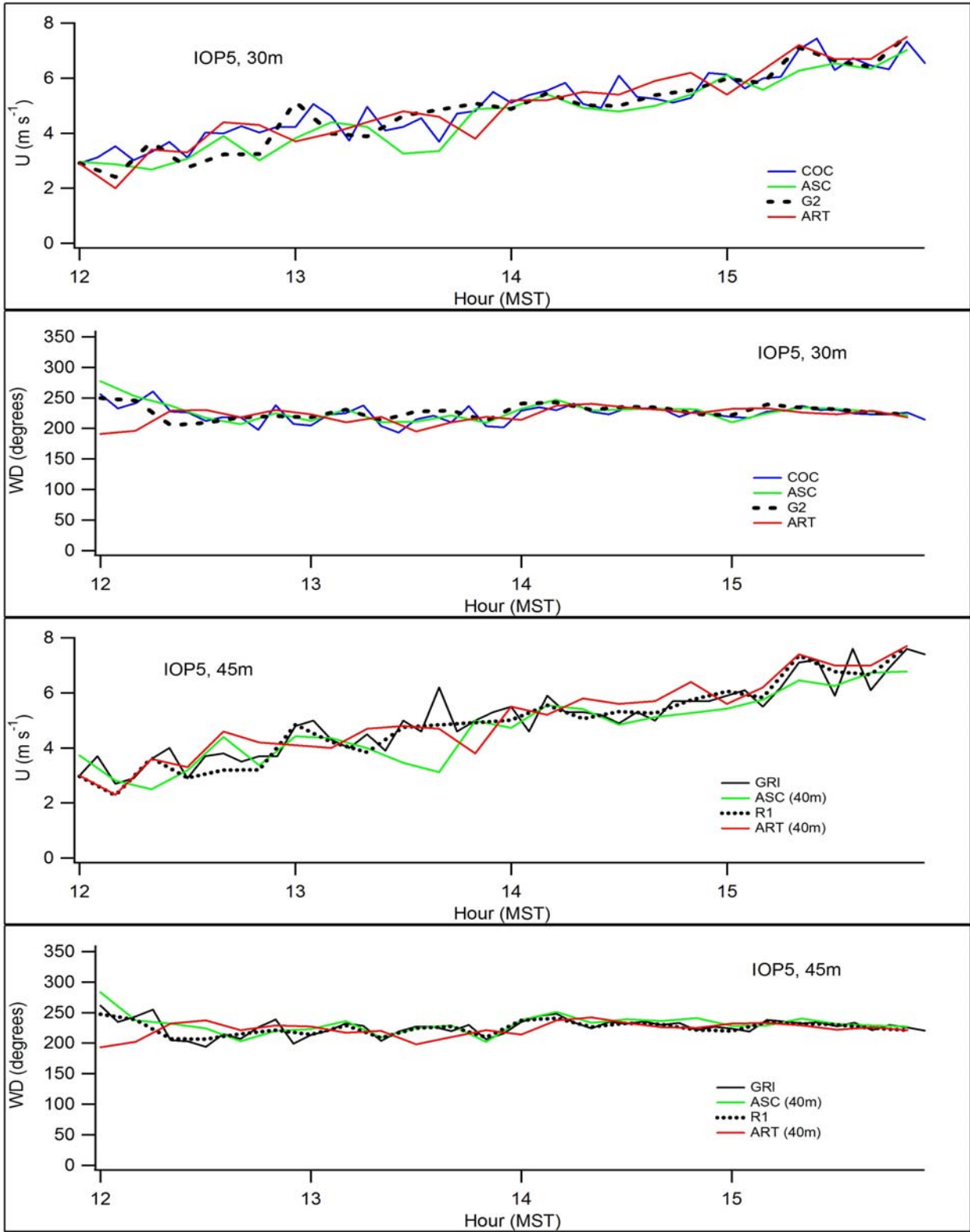


Figure 177. ARLFRD wind speed and direction comparisons in the horizontal at 30 and 45 m during IOP5.

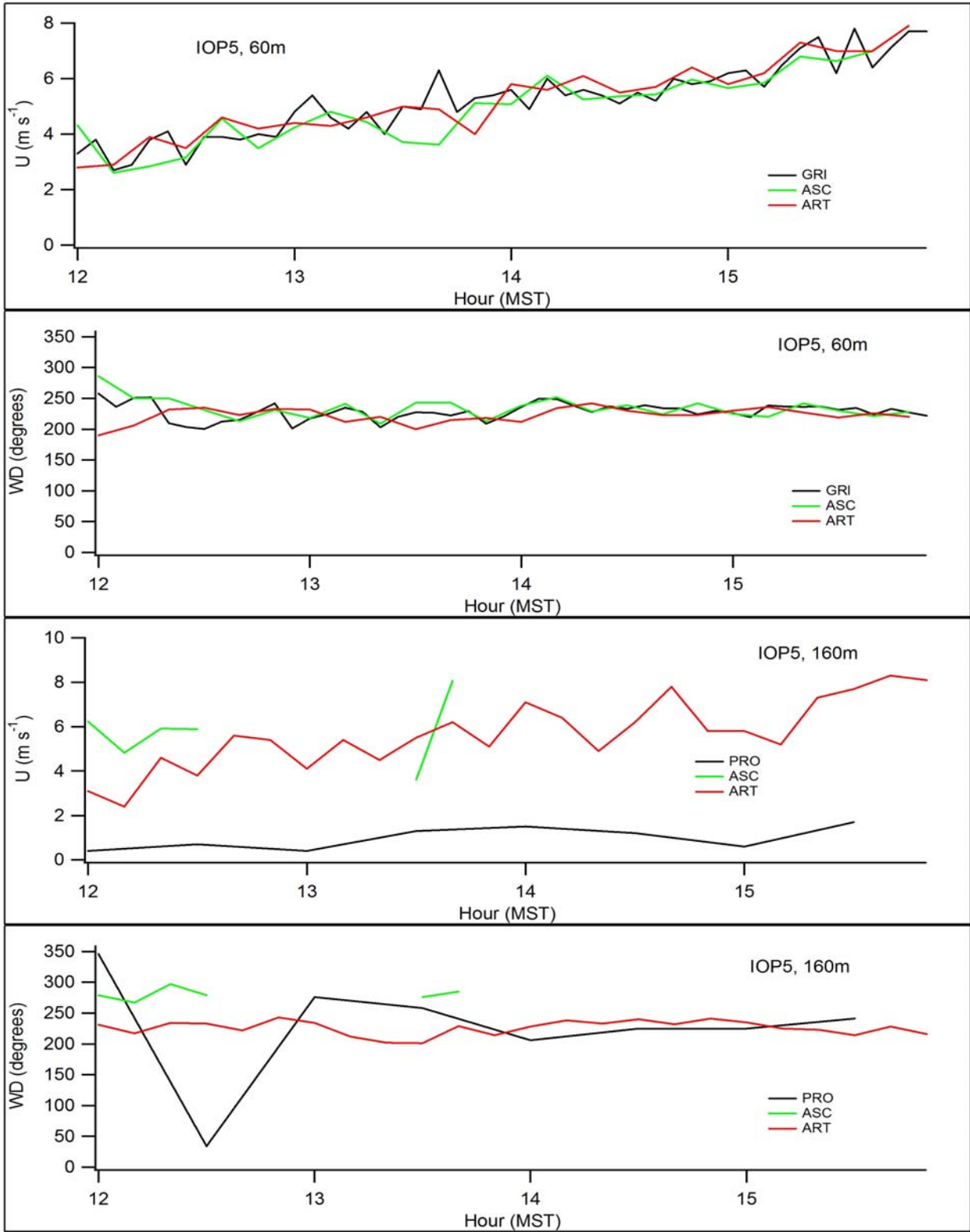


Figure 178. ARLFRD wind speed and direction comparisons in the horizontal at 60 and 160 m during IOP5.

Figures 179-181 show time-height cross-sections for wind speed and direction for the ASC sodar, ART sodar, and PRO wind profiler, respectively. The wind speeds and directions at ASC and ART are consistent with each other and with measurements of wind speed and direction on the Grid 3 tower (Figs. 177, 178). That includes the increase in wind speed seen in the sodar data beginning about 1400 h. Similar to IOPs 1, 2, and 4, the wind speeds at PRO were biased low. There was also some evidence for a sharp wind shear layer at about 1.3-1.4 km height like that seen in IOPs 1 and 2.

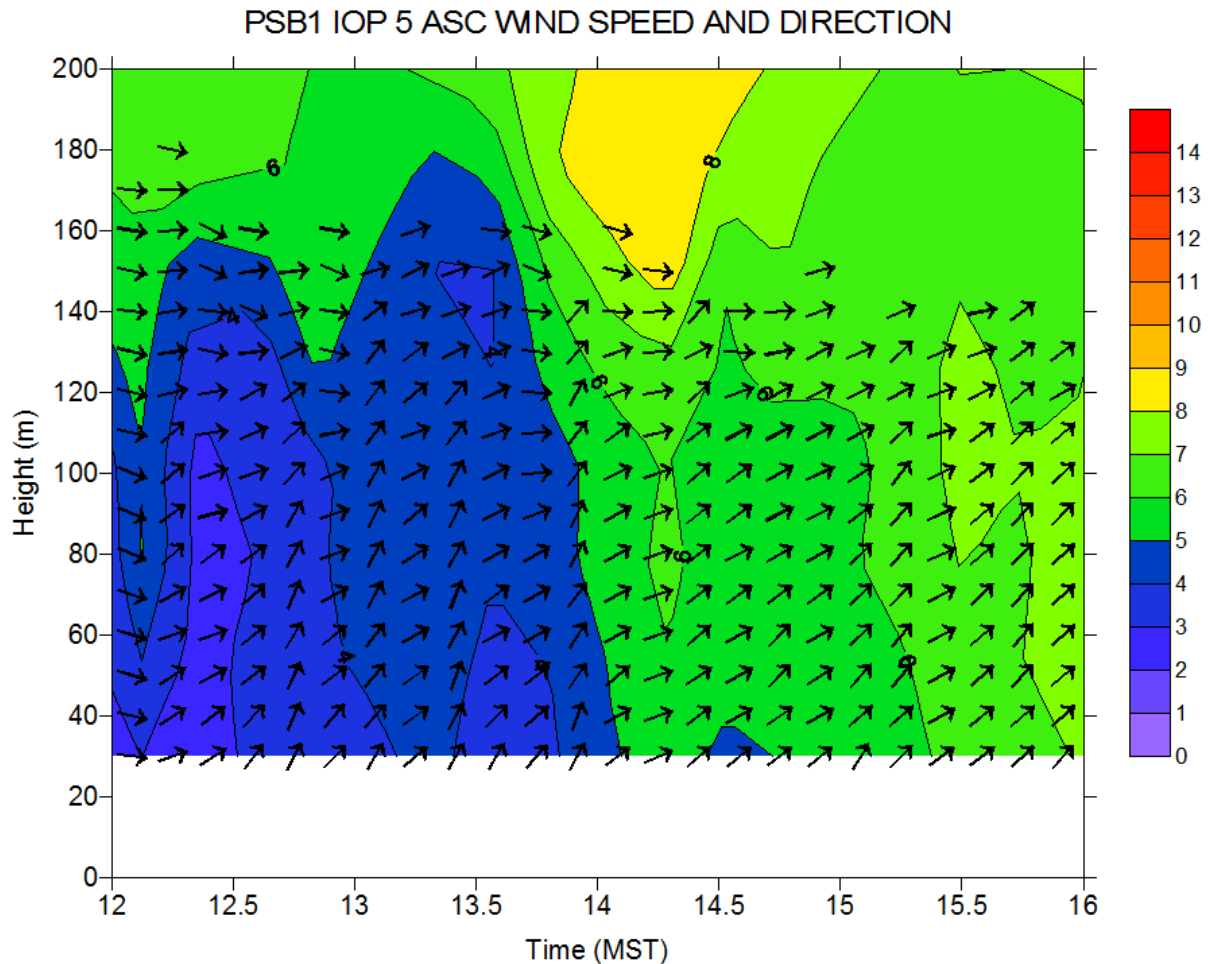


Figure 179. Time-height cross-section of wind speed and direction at ASC sodar during IOP5.

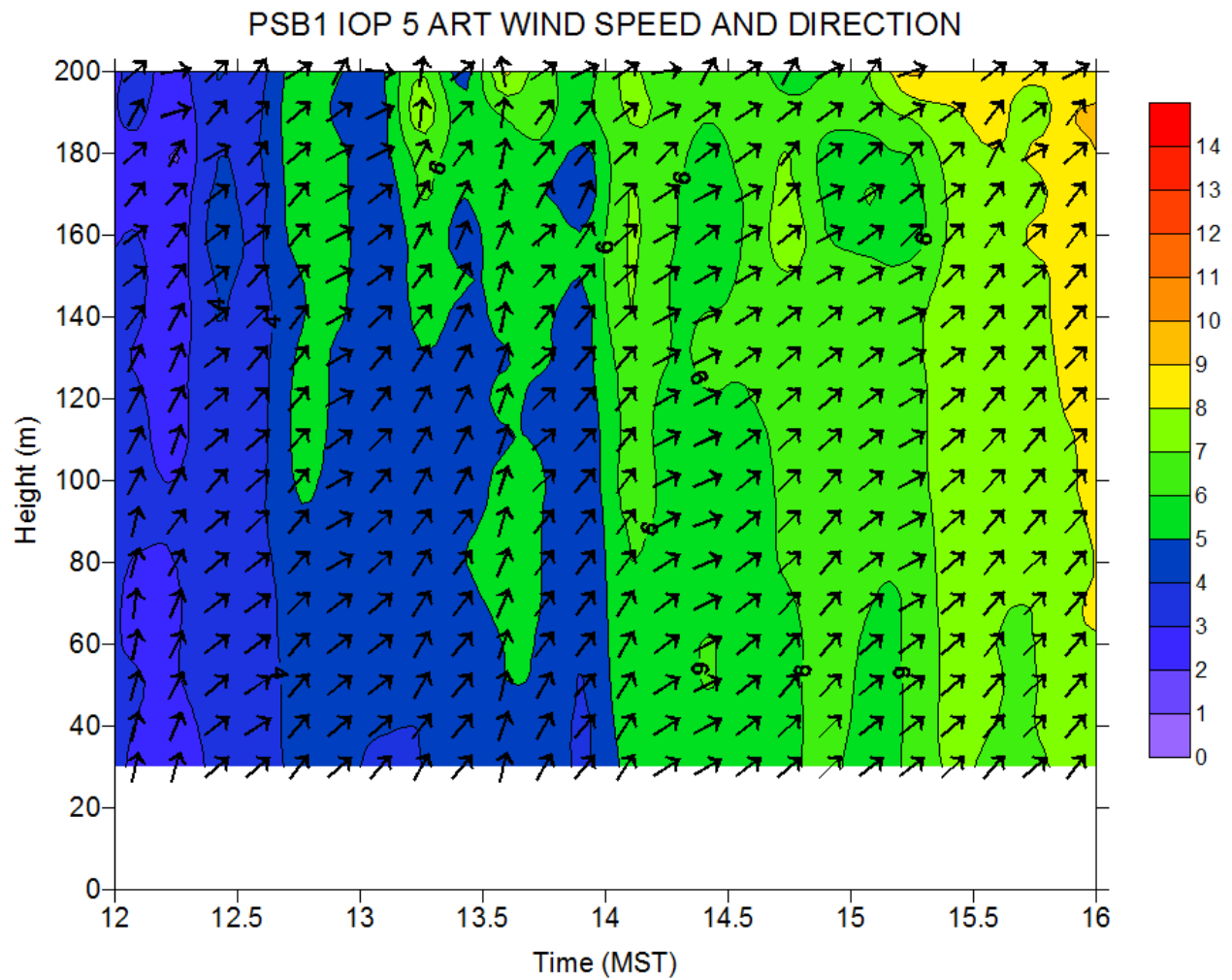


Figure 180. Time-height cross-section of wind speed and direction at ART sodar during IOP5.

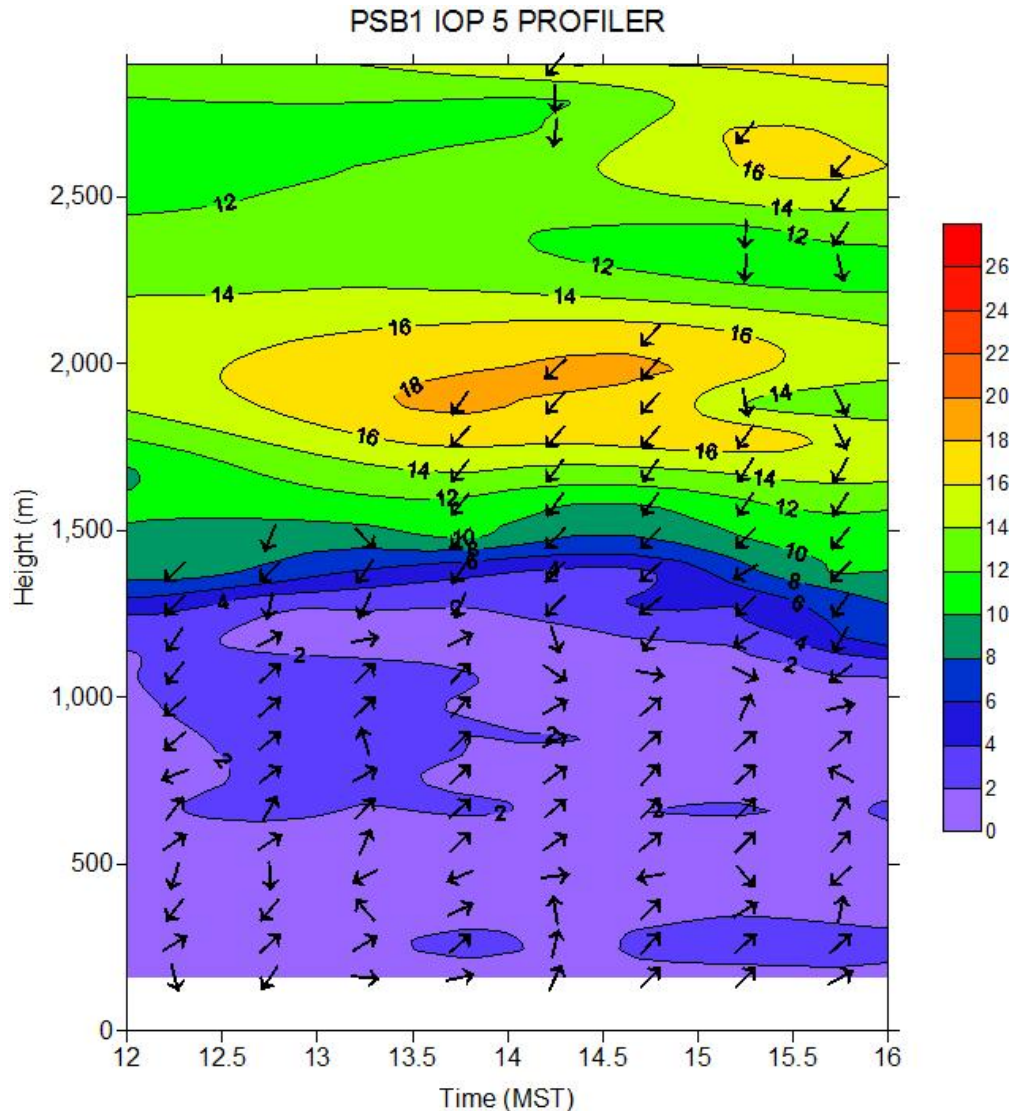


Figure 181. Time-height cross-section of wind speed and direction at wind profiler (PRO) during IOP5.

Turbulence

Figures 182 and 183 show time series of the turbulence measurements for 10 and 30-minute averaging periods, respectively, for σ_w , turbulent kinetic energy (TKE), u^* , kinematic heat flux $\langle w'T' \rangle$, and $1/L$ where L = Obukhov length. The 30-minute periods more correctly account for nonstationarity affects and should provide more reliable estimates than the 10-minute averaging periods. Observations showed good agreement between sites across the study area. The high values of σ_w at G2 are due to the fact these represent measurements at 30 m whereas all the other measurements are between 3-4 m height. The results for L indicate that the stability conditions were weakly unstable throughout the experiment. The kinematic heat flux trended downward throughout the test while u^* trended slightly upward.

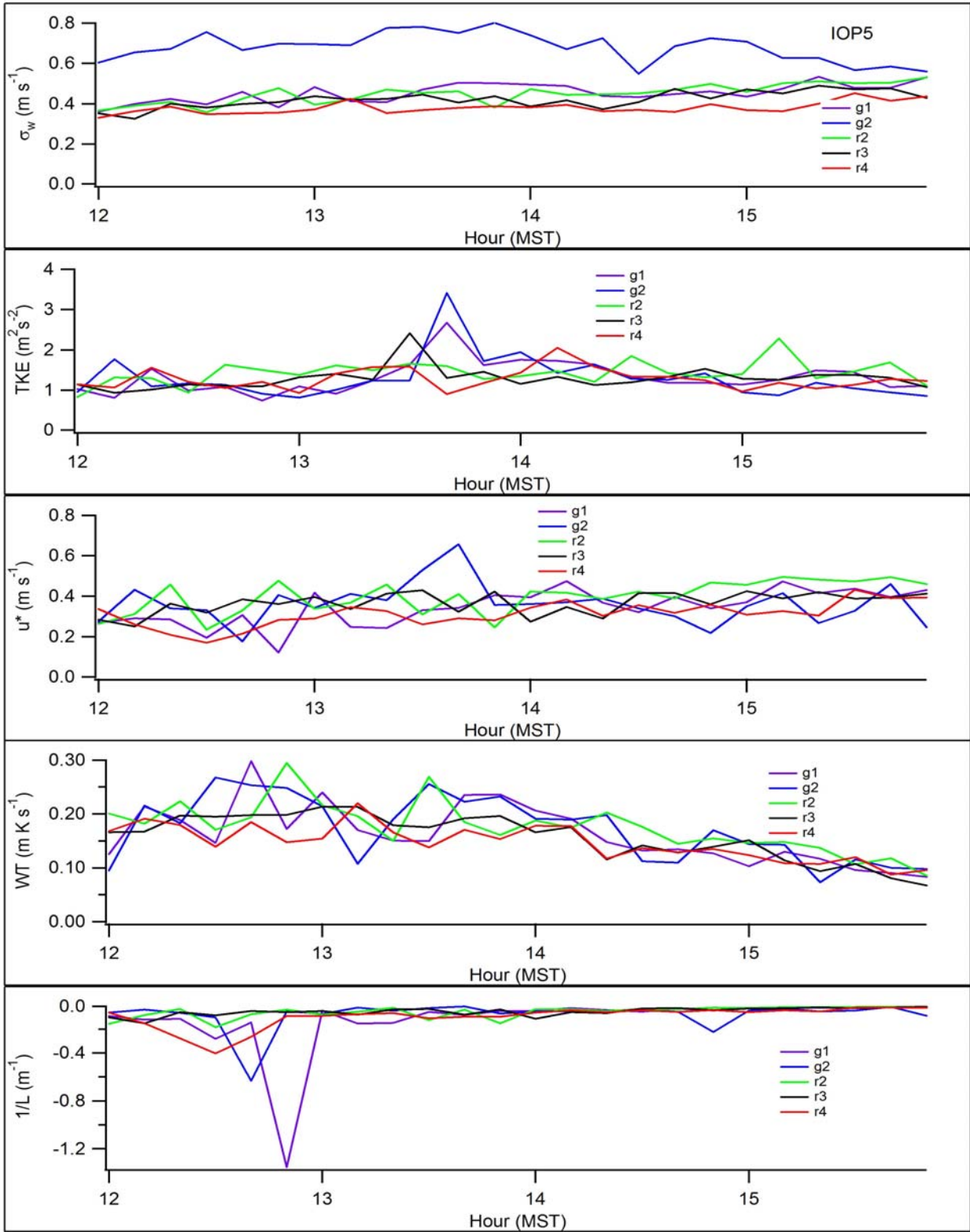


Figure 182. ARLFRD sonic anemometer 10-minute averages for σ_w , TKE, u^* , kinematic heat flux, and $1/L$ during IOP5 (G1, G2, R2, R3, and R4).

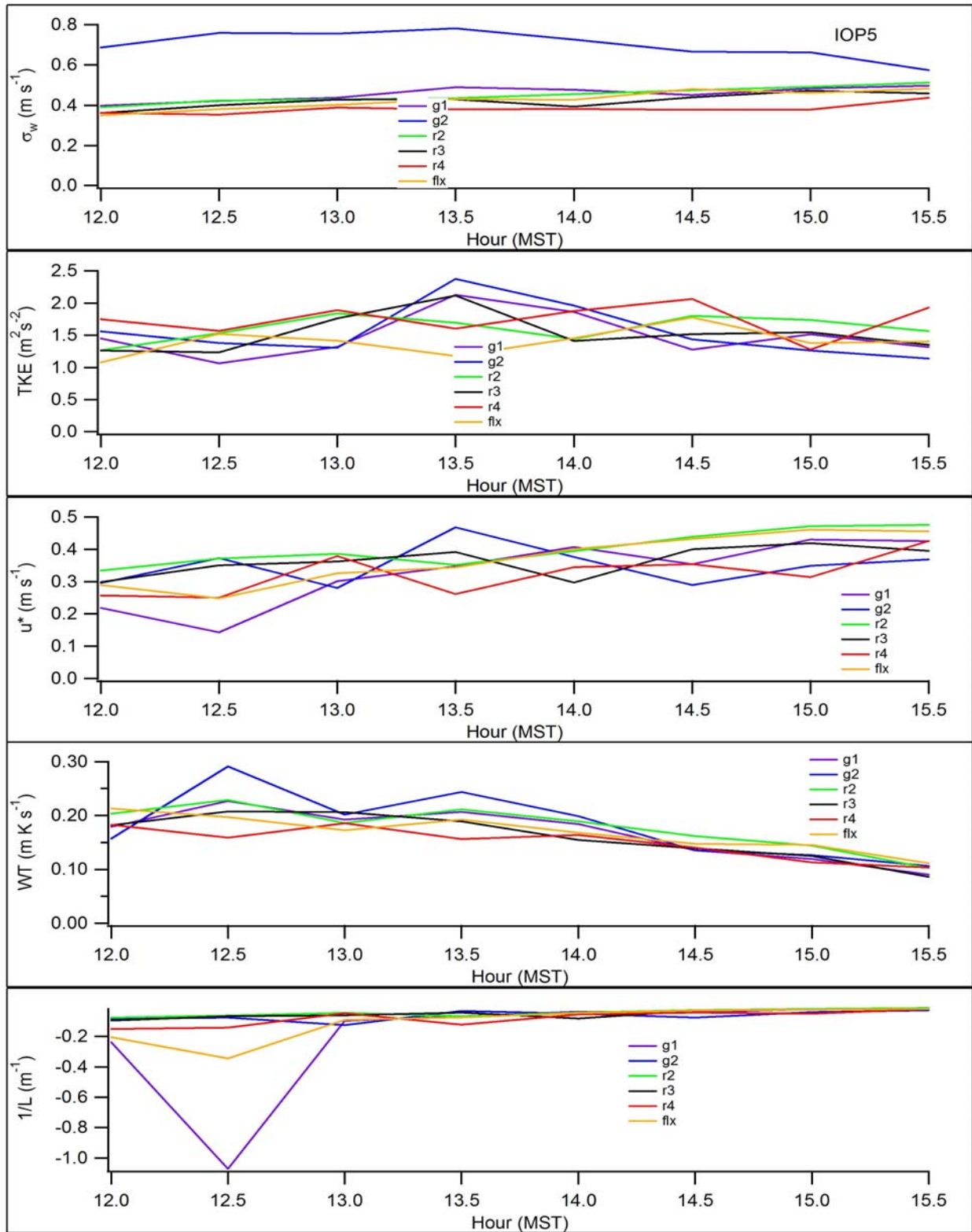


Figure 183. ARLFRD sonic anemometer 30-minute averages for σ_w , TKE, u^* , kinematic heat flux, and $1/L$ during IOP5 (G1, G2, R2, R3, and R4).

Figures 184 and 185 show time-height cross-sections for σ_w and TKE for the ASC sodar. Figures 186 and 187 show time-height cross-sections for σ_w and TKE for the ART sodar. The absolute magnitudes of TKE and σ_w shown for the ART and ASC sodars should not be assumed to be comparable between the two sodars nor with the same measurements at the sonic anemometers. The magnitudes of σ_w at ASC and ART are usually similar but the values of TKE at the ART were typically about an order of magnitude greater than the ASC. Restricting the comparison to the relative magnitudes of TKE and σ_w for each sodar, within an IOP or across IOPs, should be valid.

The magnitudes of σ_w observed at ASC and ART were consistent with those measured at the sonic anemometers (Figs. 182, 183). The ASC σ_w were more consistent with the sonic measurements at low heights while the ART σ_w were more consistent with the G2 sonic measurement at 30 m height (matching the lowest sonic level). The ASC σ_w and TKE observed during IOP5 were much greater than IOP1 and similar to those observed during the other IOPs. The ART σ_w and TKE observed during IOP5 were greater than IOP1 and similar to the other IOPs. Figure 188 shows a time-height cross-section for temperature from the RASS.

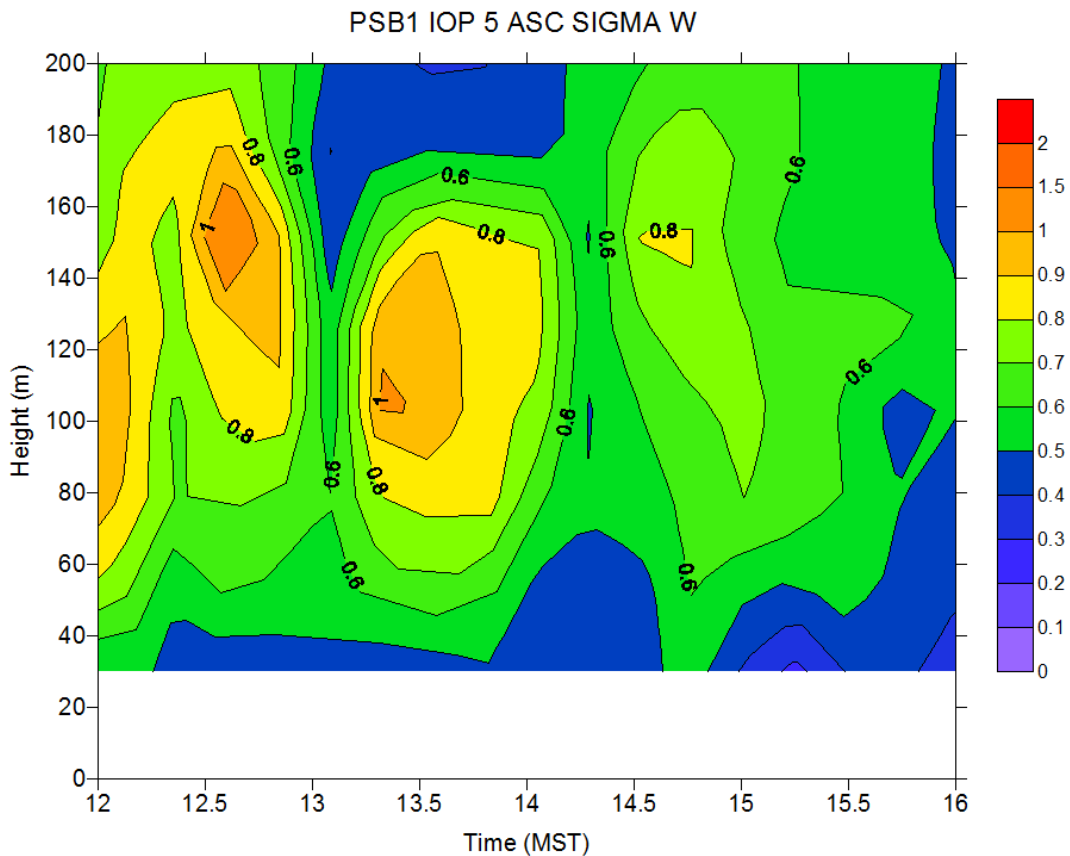


Figure 184. Time-height cross-section of σ_w at ASC sodar during IOP5.

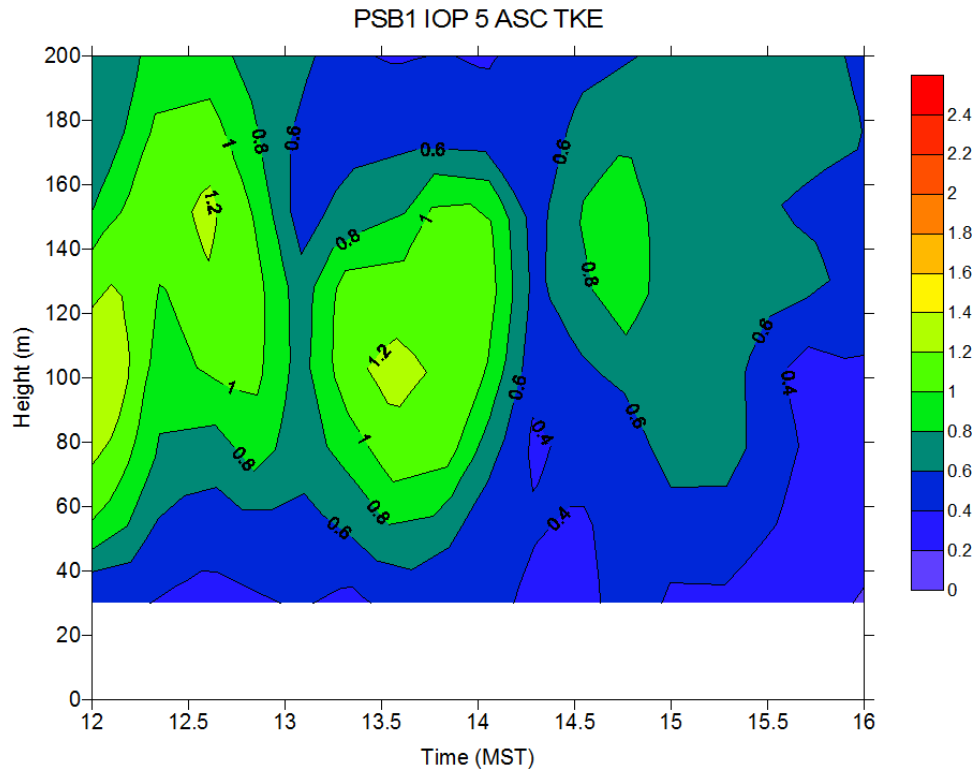


Figure 185. Time-height cross-section of TKE at ASC sodar during IOP5.

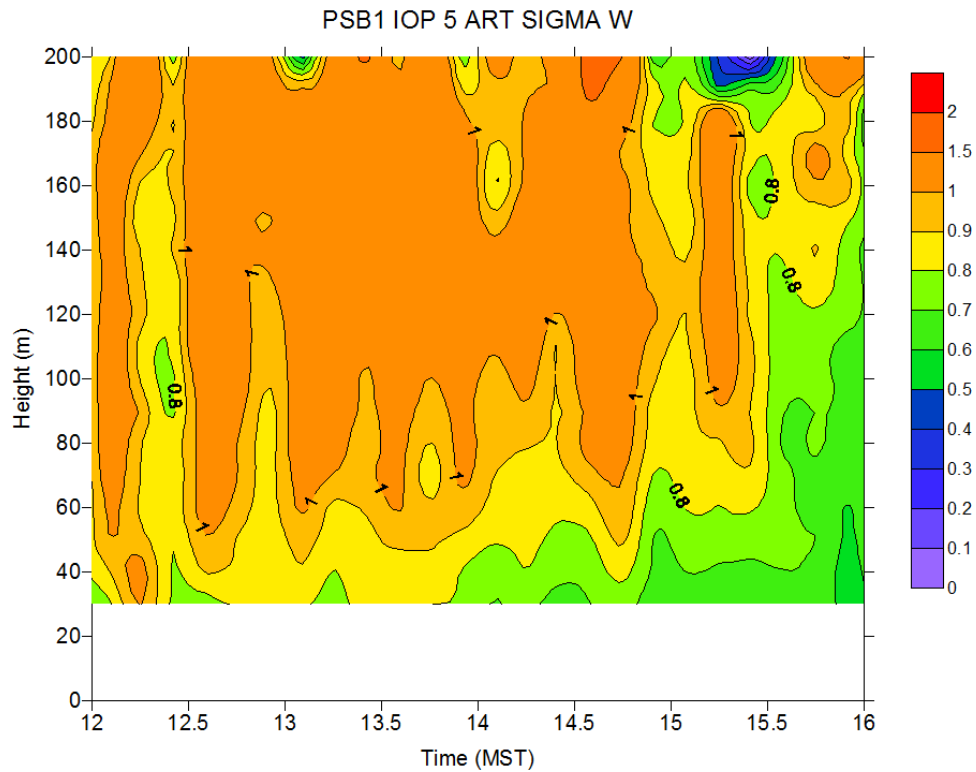


Figure 186. Time-height cross-section of σ_w at ART sodar during IOP5.

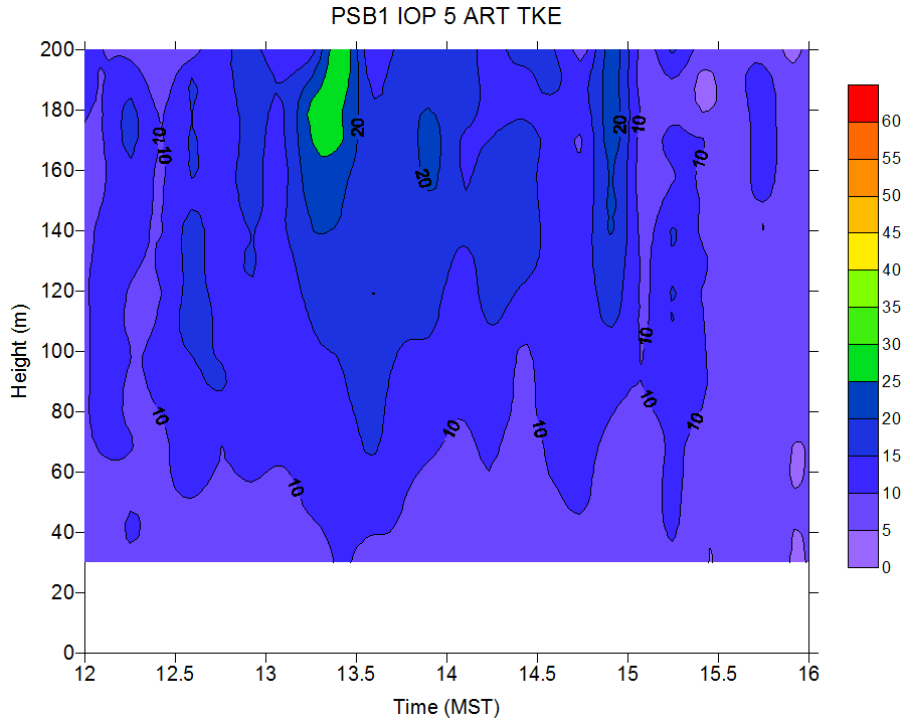


Figure 187. Time-height cross-section of TKE at ART sodar during IOP5.

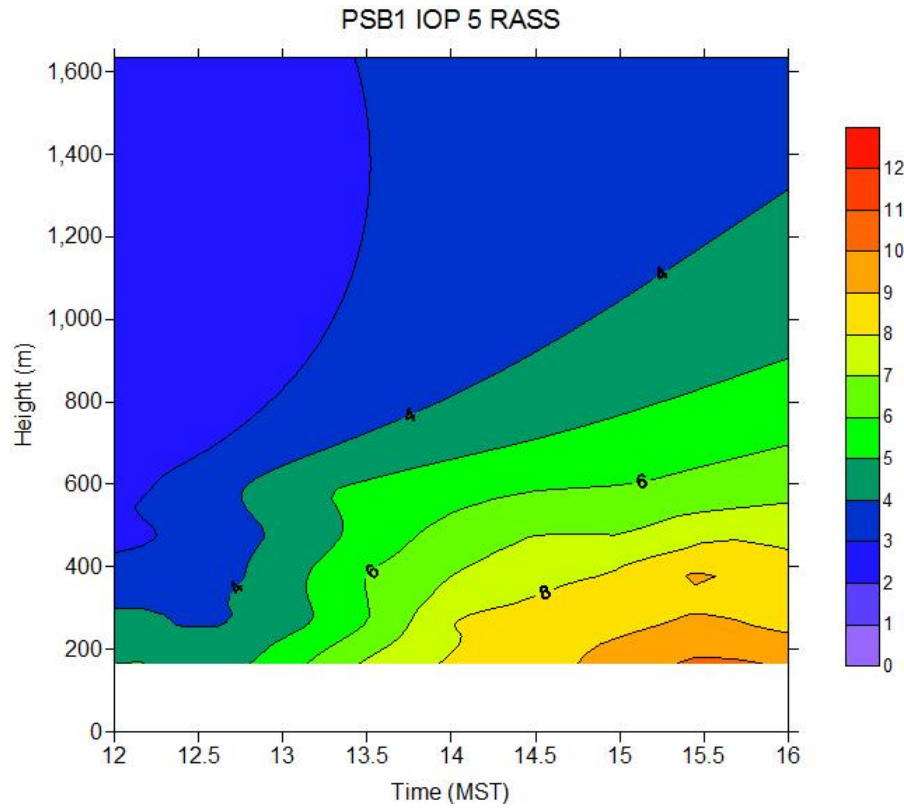


Figure 188. Time-height cross-section of virtual temperature at the RASS during IOP5. Temperatures are in degrees C.

Vertical profiles of wind speed, wind direction, and calculated turbulence parameters from the ARLFRD and WSULAR sonic anemometer measurements at GRI during IOP5 are shown in Figs. 189-191. Vertical profiles of wind speed, wind direction, and turbulence intensity (σ_θ) from cup anemometers and wind vanes plus aspirated air temperature during IOP5 are shown in Figs. 192 and 193. Turbulence intensities measured by the sonic anemometers (σ_v/U) were less than during IOPs 1 and 2, slightly greater than IOP4, and much larger than IOP3. There was general consistency in the profiles of turbulence intensity (sonic- (σ_v/U) and wind vane- (σ_θ)) and σ_w . However, there were some inconsistencies relative to other data, mainly in the first hour and at upper levels of the profiles (e.g., compare Figs. 190, 193). Profiles of TKE were generally ragged with the irregularities often related to transitions between ARLFRD and WSULAR sonics (Fig. 191). There was mostly good agreement between wind speed measurements made by the sonic anemometers and cup anemometers. Unlike the cup anemometer wind speeds, the sonic anemometer wind speeds decreased at upper levels, mainly at 60 m.

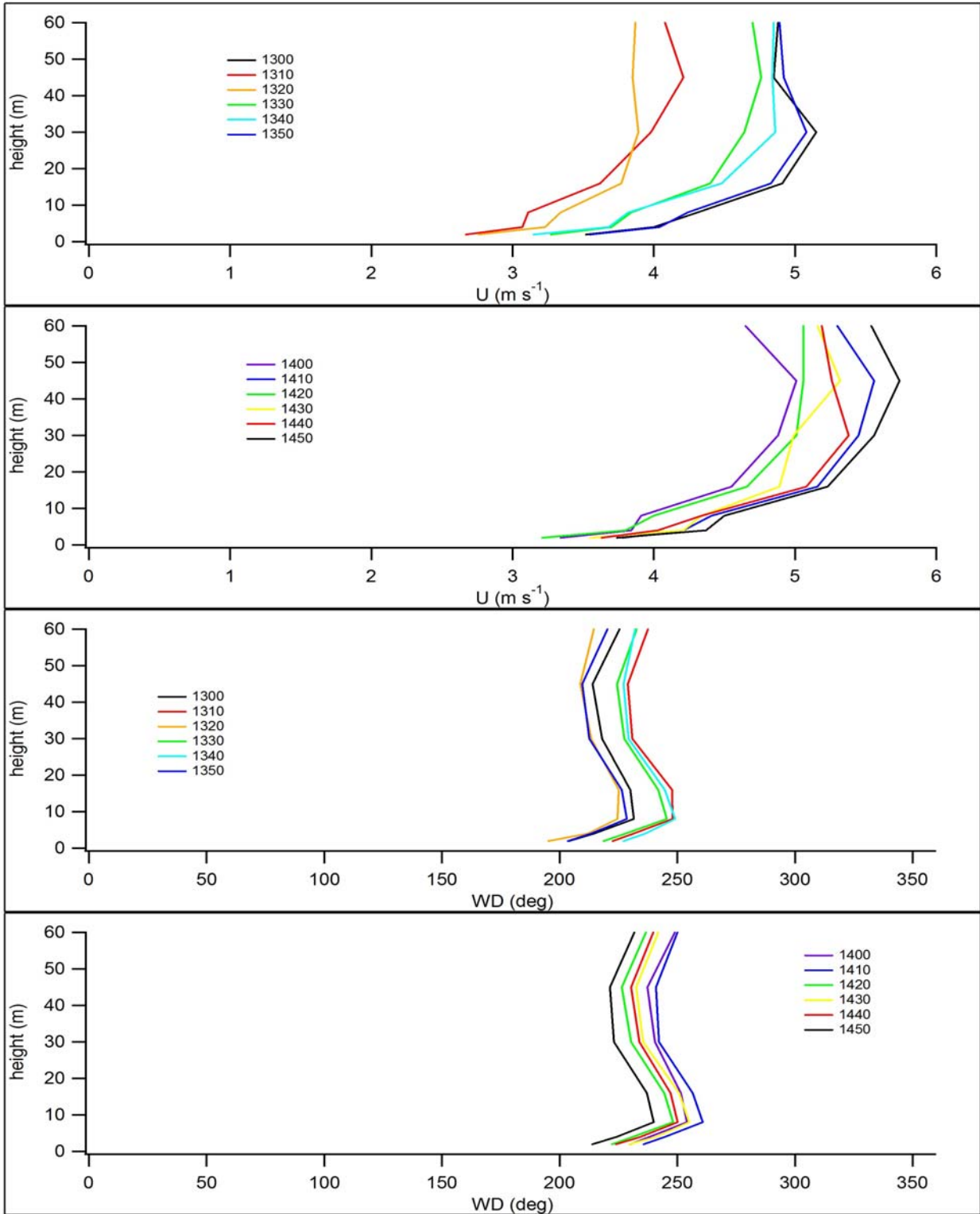


Figure 189. Vertical profiles of wind speed and direction from sonic anemometer measurements at GRI during IOP5. ARLFRD instruments were at 4, 30, and 45 m; WSULAR instruments were at 2, 8, 16, and 60 m. Times in legend are start times for the 10 minute interval (hhmm MST).

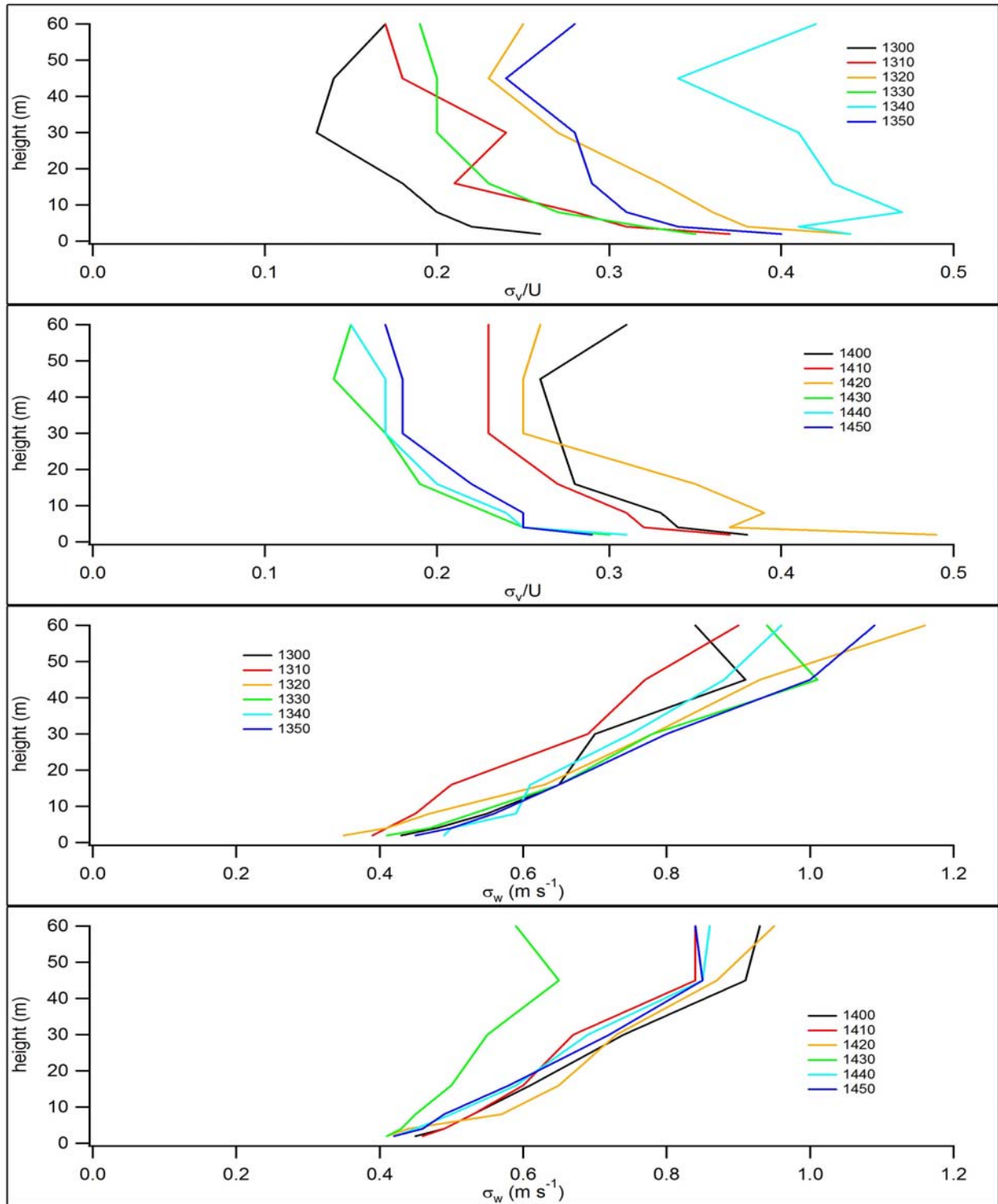


Figure 190. Vertical profiles of turbulence intensity and σ_w from sonic anemometer measurements at GRI during IOP5. ARLFRD instruments were at 4, 30, and 45 m; WSULAR instruments were at 2, 8, 16, and 60 m. Times in legend are start times for the 10 minute interval (hhmm MST).

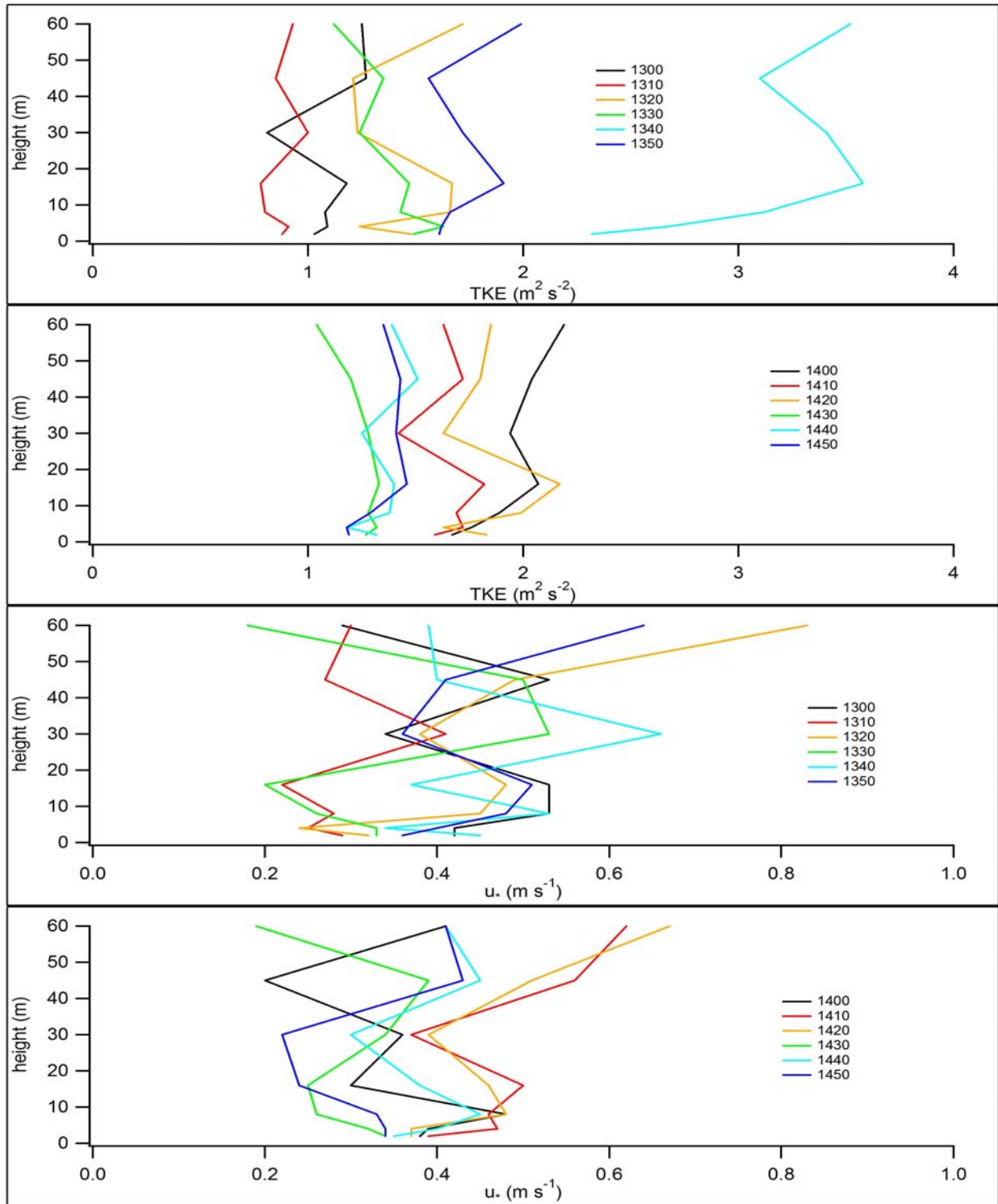


Figure 191. Vertical profiles of turbulent kinetic energy (TKE) and u_* from sonic anemometer measurements at GRI during IOP5. ARLFRD instruments were at 4, 30, and 45 m; WSULAR instruments were at 2, 8, 16, and 60 m. Times in legend are start times for the 10 minute interval (hhmm MST).

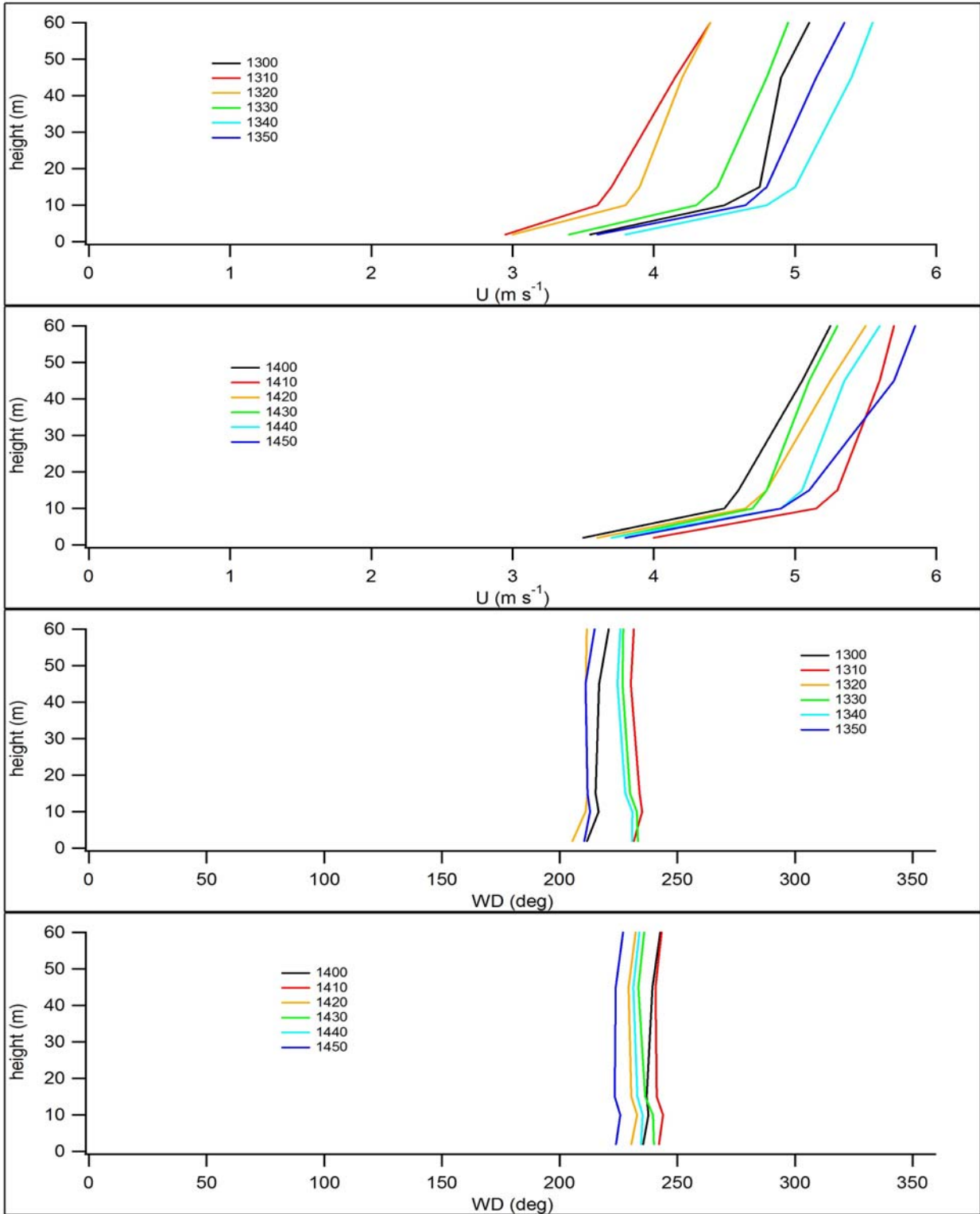


Figure 192. Vertical profiles of wind speed and direction from cup anemometer and wind vane measurements at GRI during IOP5. Times in legend are start times for the 10 minute interval (hhmm MST).

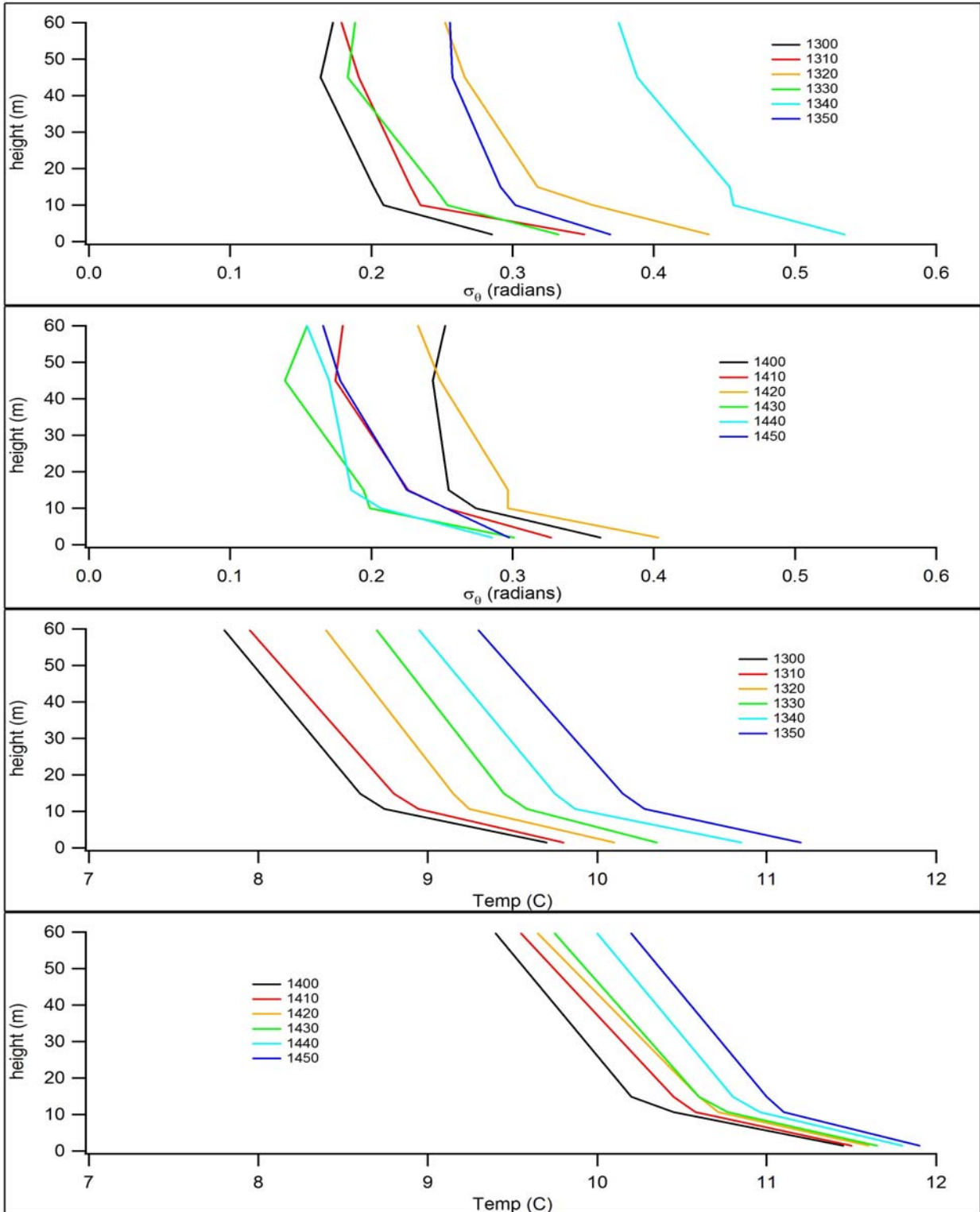


Figure 193. Vertical profiles of σ_θ (from cup and vane) and aspirated air temperature measurements at GRI during IOP5. Times in legend are start times for the 10 minute interval (hhmm MST).

Stability

The SRDT-Delta T and σ_A methods for determining P-G stability category gave similar results although the σ_A method showed more variability. All SRDT method results were category C. All the σ_A method results were category C with the exception of 2 category B in the first hour and 2 category D in the second hour of the test. The magnitudes and sign of the z/L stability parameter values are generally consistent with weakly unstable conditions and the P-G classifications.

Radiosonde Results

Figures 194 and 195 show potential temperature and specific humidity profiles from radiosonde measurements pre and post IOP5. The mixing depths estimated from these plots are given in Table 18.

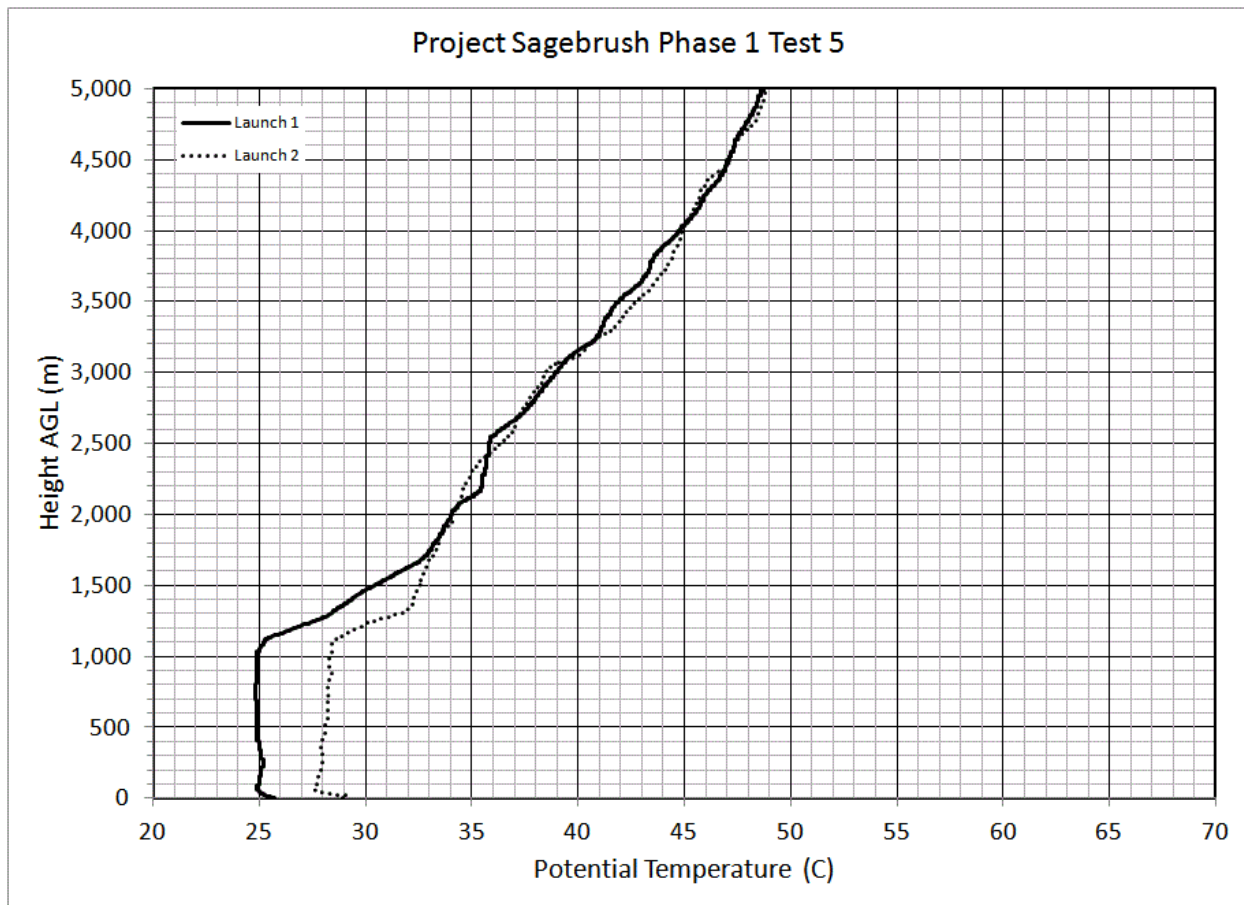


Figure 194. Pre and post IOP radiosonde potential temperature profiles for IOP5.

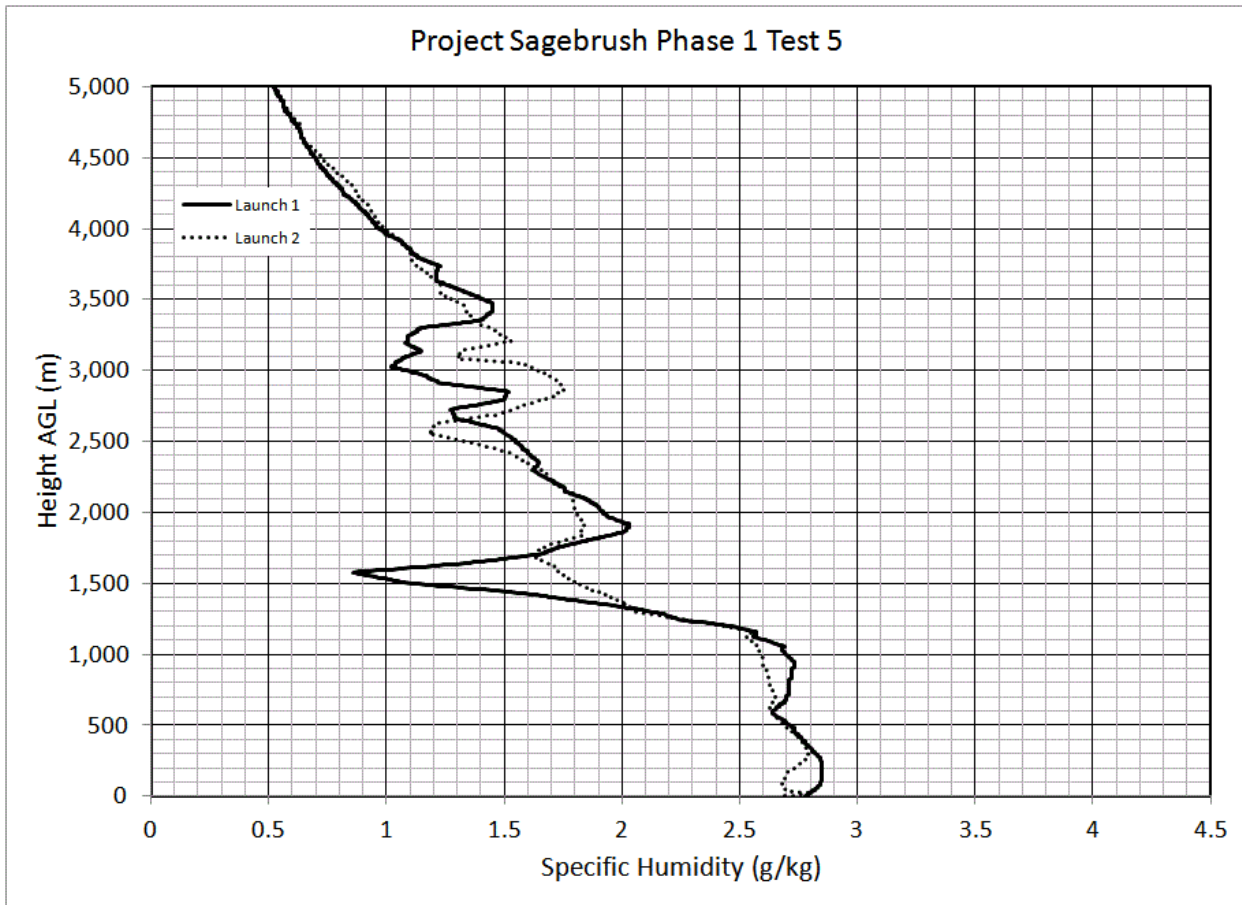


Figure 195. Pre and post IOP radiosonde specific humidity profiles for IOP5.

Concentration Results and Analysis

Figure 196 shows the bag sampling results for IOP5. Measured concentrations during IOP5 were similar to IOP4 and both IOPs 4 and 5 were much lower than IOP3. Nevertheless, the normalized concentrations during IOPs 4 and 5 tended to be similar to or somewhat higher than IOP3 based on a comparison between the extents of the normalized contours (compare Figs. 142, 170, 196). Wind directions were such that the plume was largely confined to the sampling array throughout IOP5.

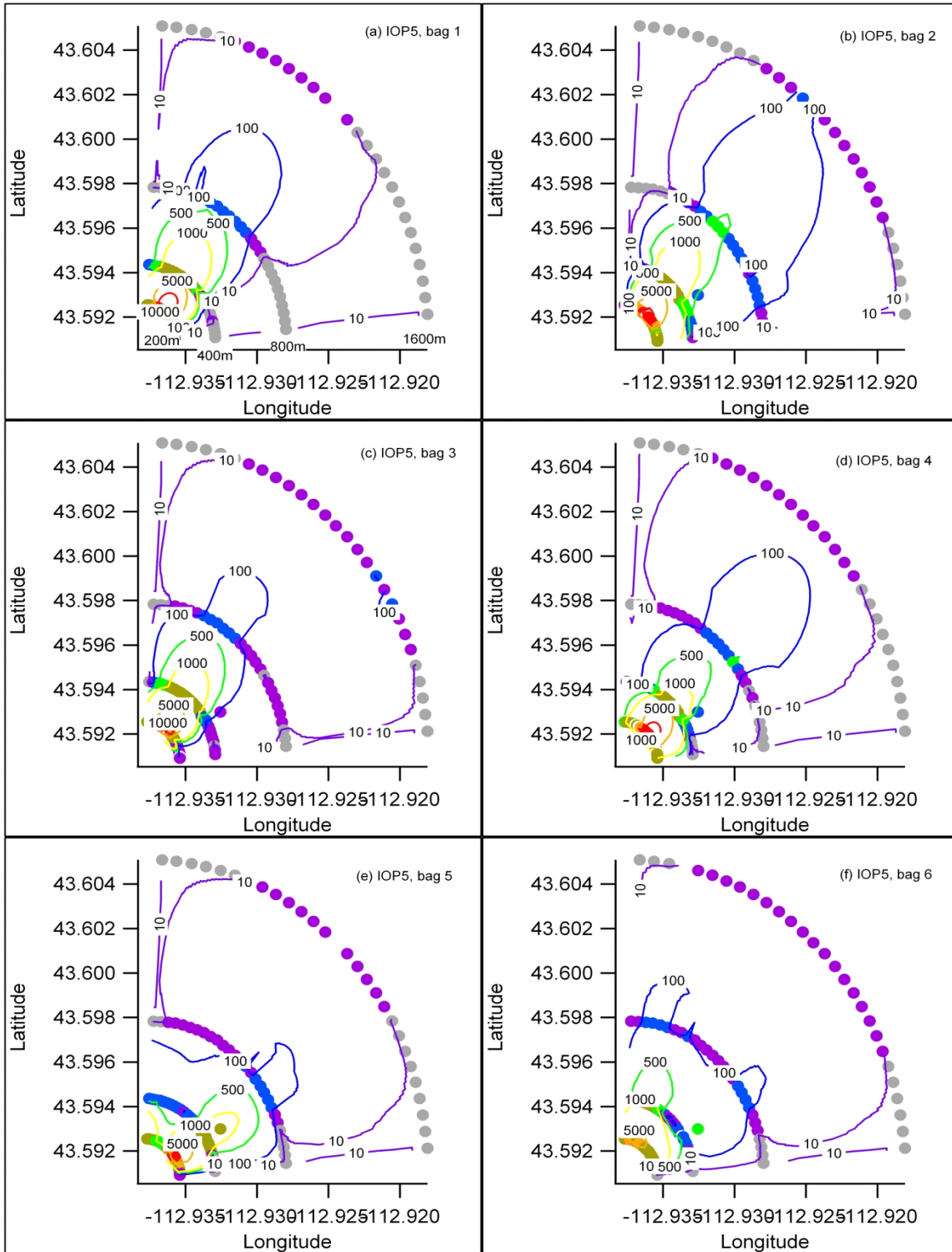


Figure 196. Bag sampling results (a-f, bags 1-6) for IOP5 with color-coded concentration markers for each 1 m AGL bag sampling location and contour lines of normalized concentration. The color scheme for the markers and contours is described in the Introduction to this section.

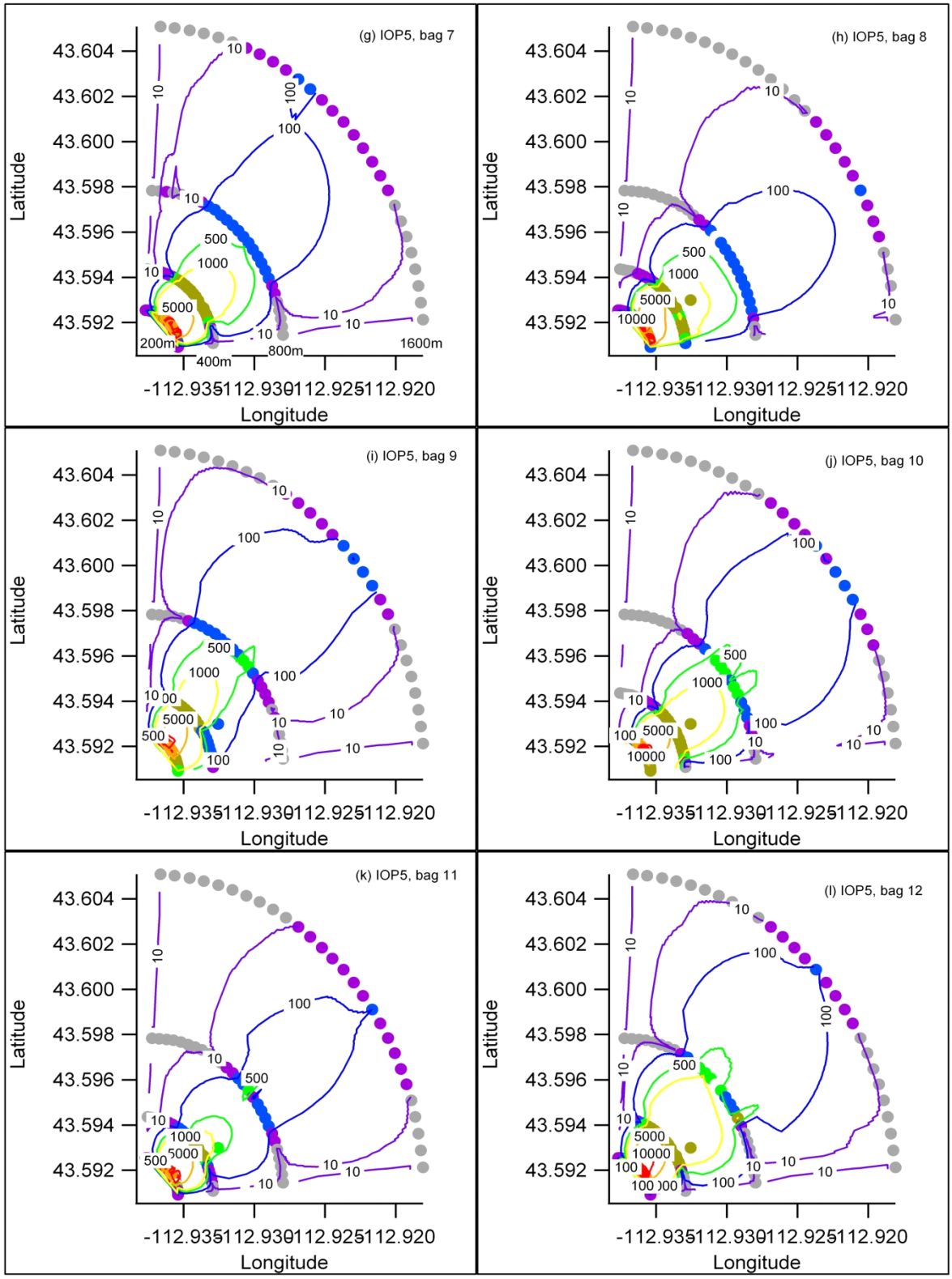


Figure 196 continued (g-l, bags 7-12).

Figure 197 shows cross-sections of tracer concentration along each arc for each 10-minute bag sampling period during IOP5. Plumes were sometimes broad, less so than IOPs 1 and 2, more so than IOP3, and similar to IOP4. That result is consistent with the values of σ_{θ} observed during most of the IOP (Table 23). Individual arc concentration cross-sections often exhibited non-ideal Gaussian forms with profiles having asymmetries about their maxima and/or very irregular concentration profiles. This was less prevalent compared to IOPs 1 and 2 (Figs. 87, 115), more common than in IOP3 (Fig. 143), and similar to that during IOP4 (Fig. 171). Truncation of plume cross-section profiles at the edge of the sampling array was present but minimal.

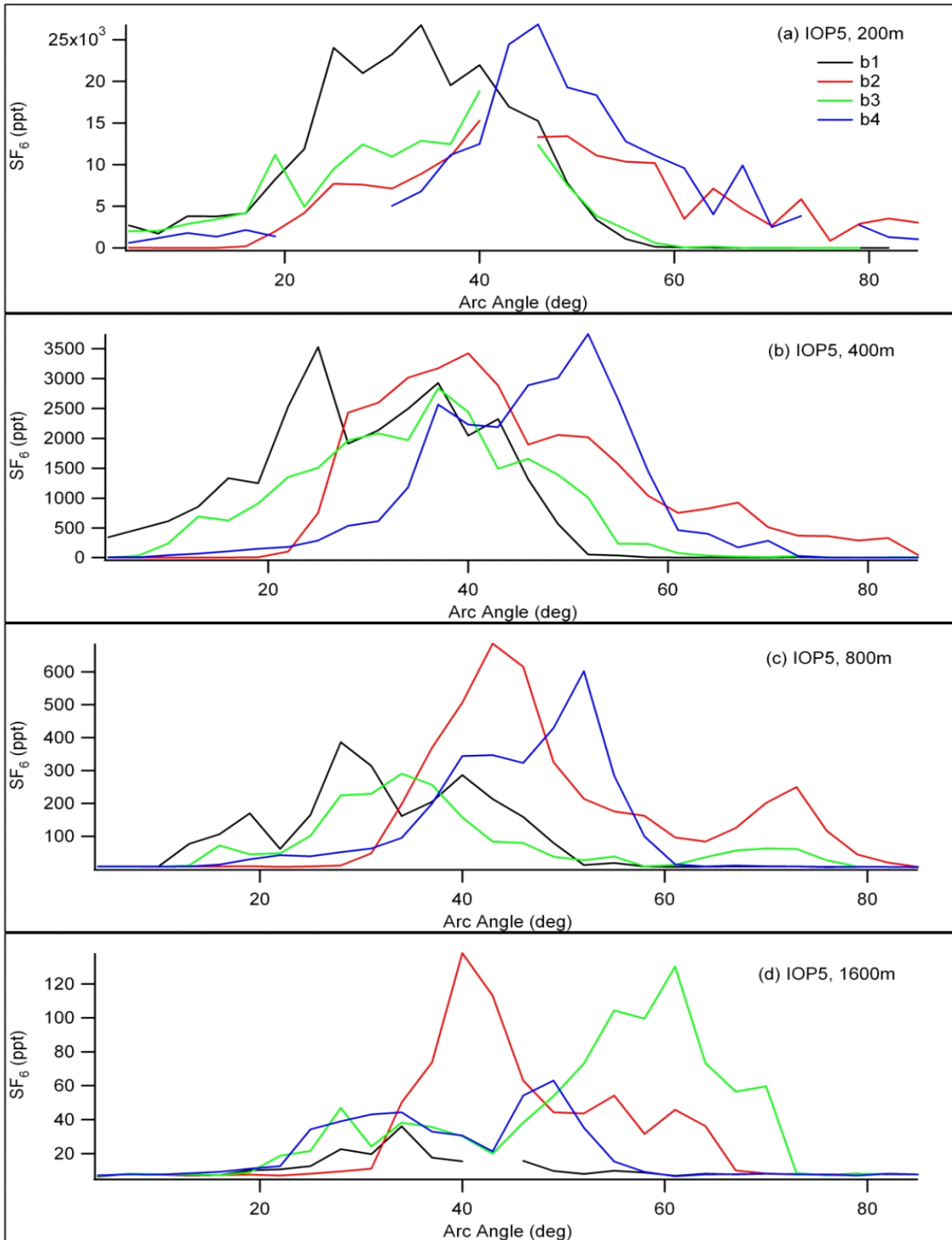


Figure 197. Cross-sections of concentration along each arc for each 10-minute bag sampling period during IOP5. The individual plume cross-section layouts are arranged to illustrate the variation in time, across 40 minutes per layout (a-d, bags 1-4), and the simultaneous variation with distance across all four arcs.

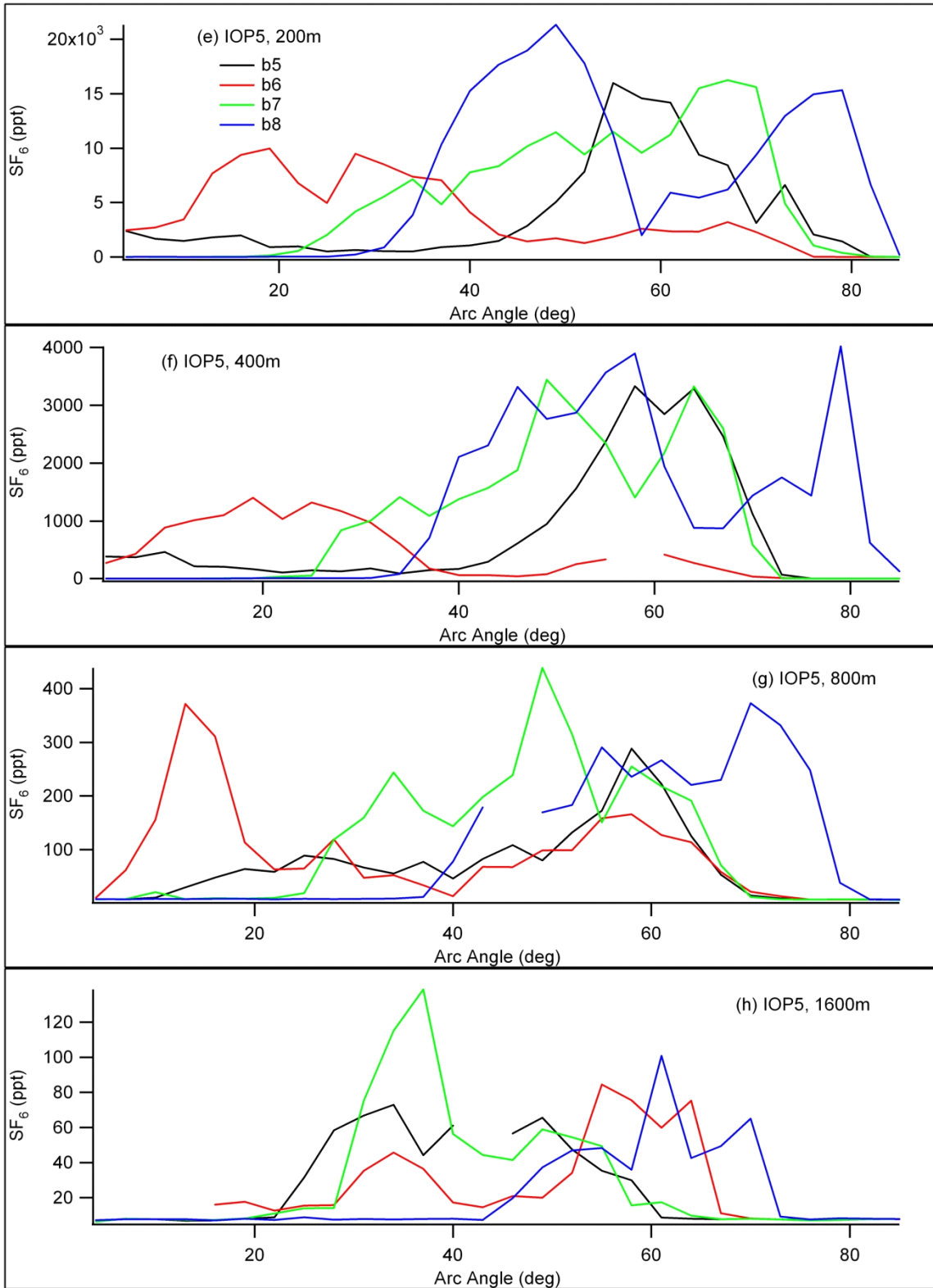


Figure 197 continued (e-h, bags 5-8).

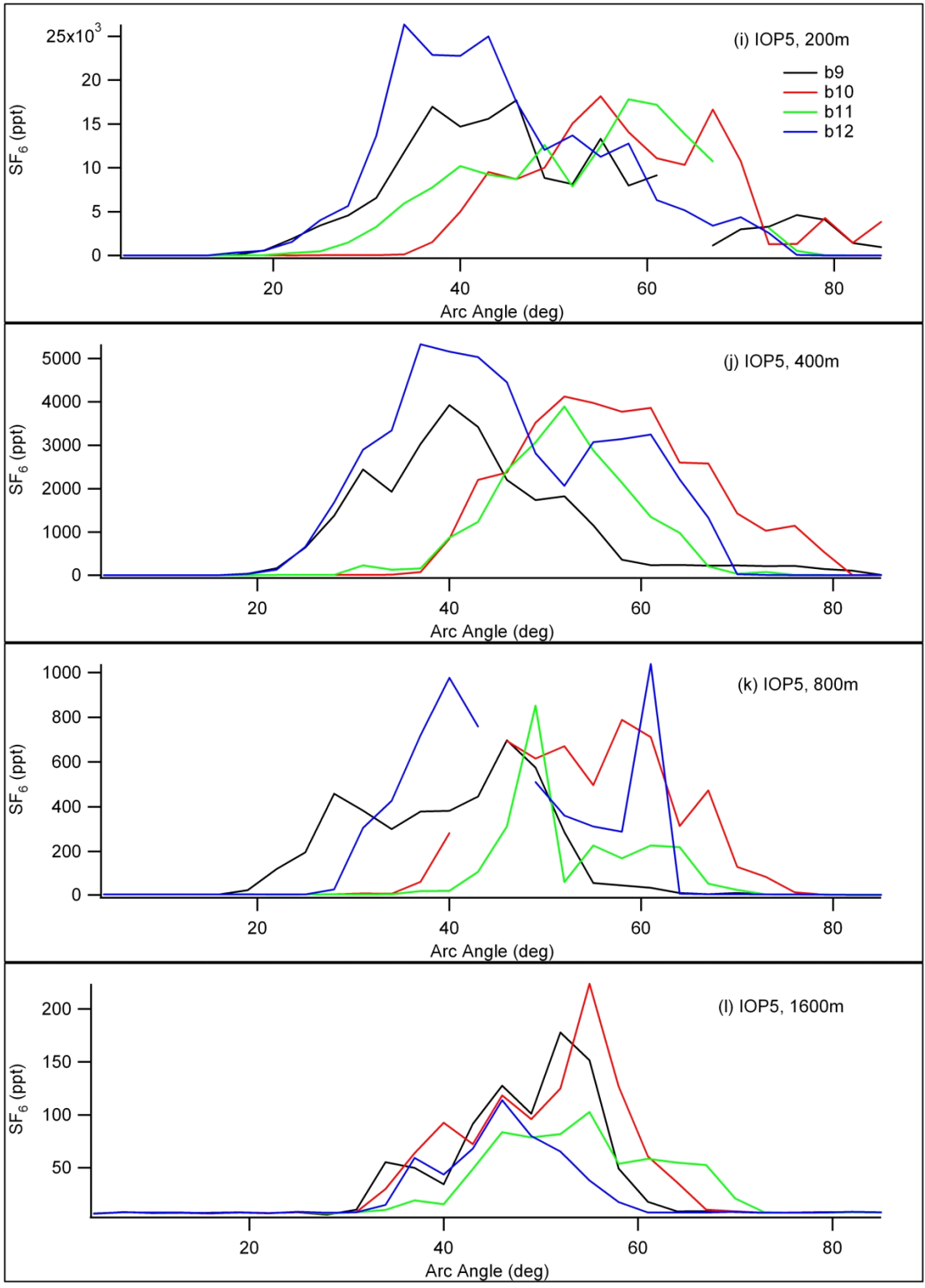


Figure 197 continued (i-l, bags 9-12).

Figure 198 shows vertical concentration profiles at the towers at 201, 408, and 499 m downwind for all 10-minute bag sampling intervals for IOP5. Any evidence for liftoff of the vertical plume centerline is inconclusive.

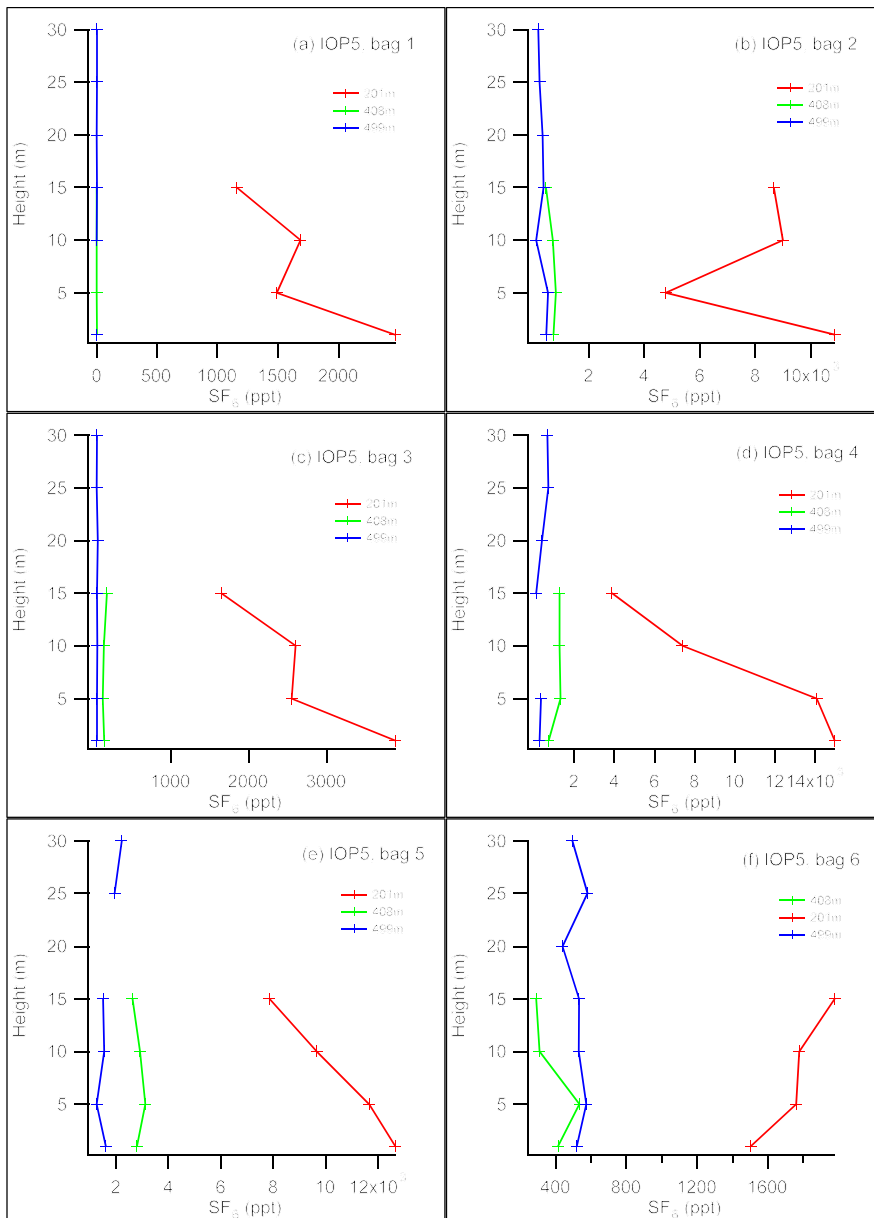


Figure 198. Vertical concentration profiles (a-f, bags 1-6) at the towers at 201, 408, and 499 m downwind for all 10-minute bag sampling intervals for IOP5. No aircraft measurements were available.

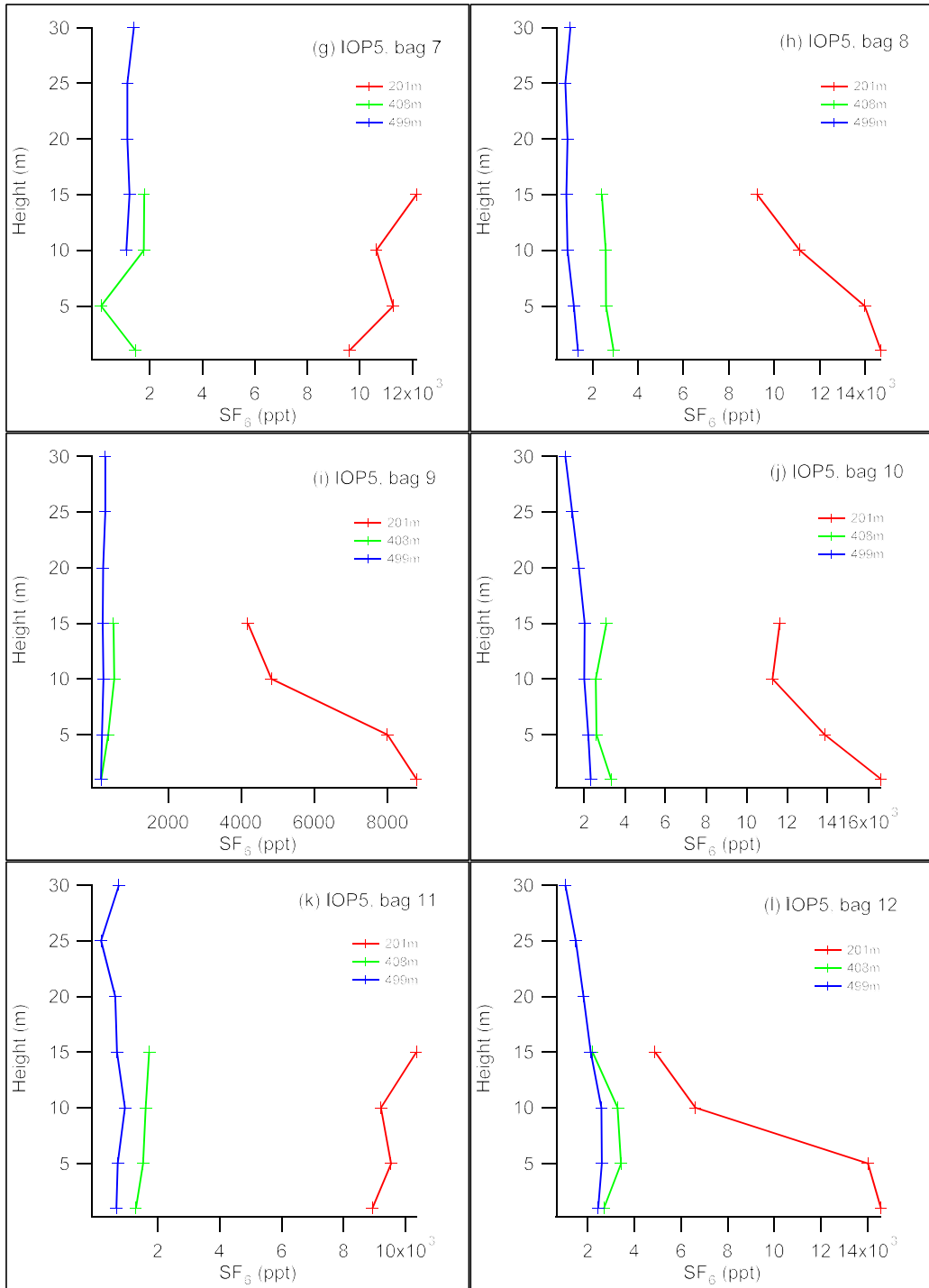


Figure 198 continued (g-l, bags 7-12).

Figure 199 shows time series of SF₆ concentrations measured by the fast response analyzers at the specified arc and arc angle location during IOP5. Problems with analyzer railing were negligible during IOP5. Various periodicities are suggested by the data. One example would be about 20-30 minutes.

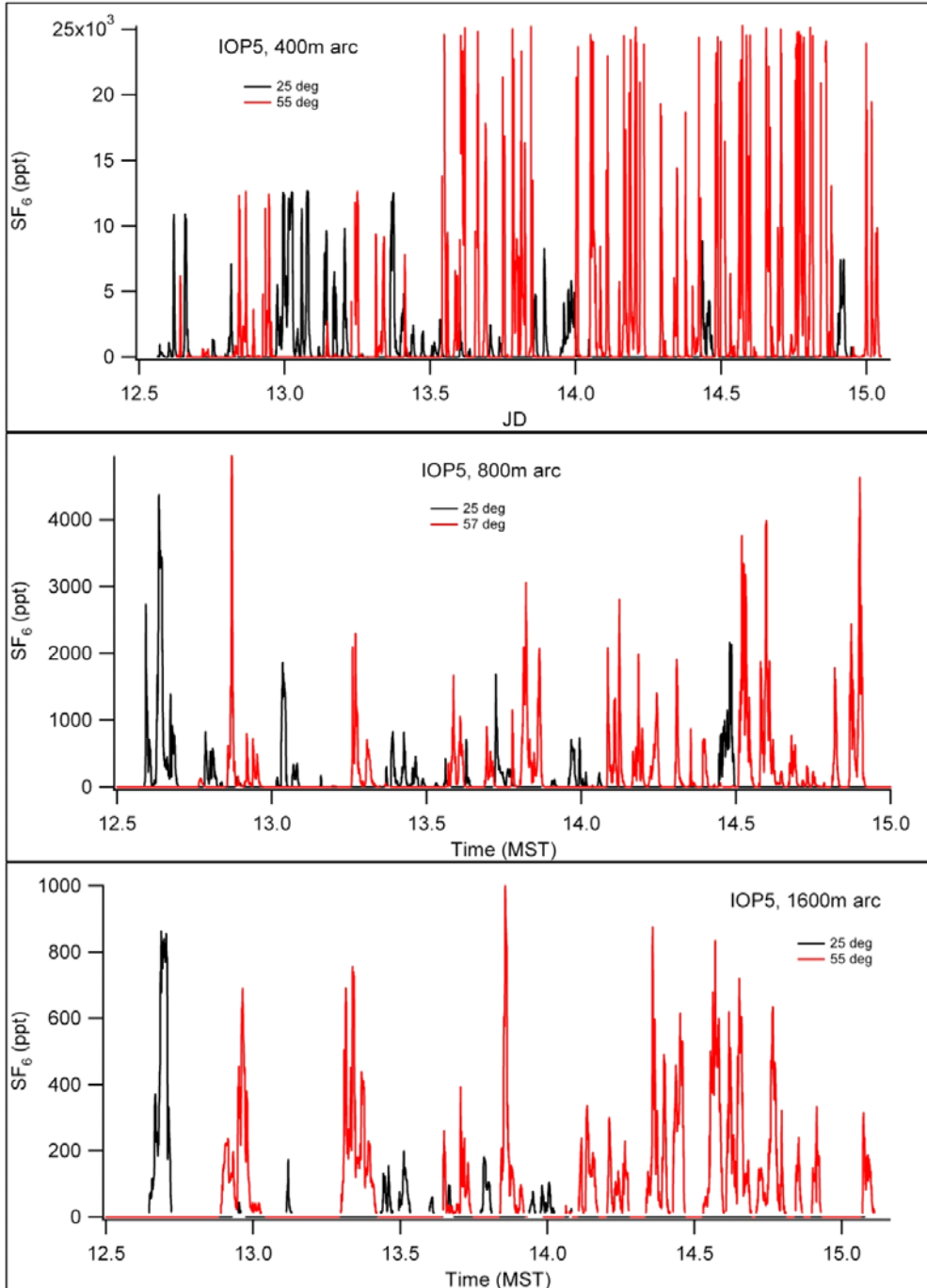


Figure 199. Time series of SF₆ concentrations measured by the fast response analyzers at the specified arc and arc angle location during IOP5.

This page is intentionally left blank.

PRELIMINARY ANALYSIS

DETERMINATION OF σ_y

Methods for Determining σ_y

Preliminary efforts were made at estimation of the horizontal plume spread parameter σ_y using PSB1 data. Three methods were utilized. The first was based on crosswind integration along the sampling arc to determine the second moment about the mean of the data. The plume width was estimated by calculating the second moment about the mean of the data

$$\langle Y \rangle^2 = \frac{1}{A} \int_{-\infty}^{\infty} (Y - Y_o)^2 C dy \quad (1)$$

where Y is the cross-plume coordinate in meters, C is the concentration (ppt) as a function of cross-plume distance, Y_o is the weighted plume centerline, and A is the integrated concentration:

$$(2) \quad Y_o = \frac{1}{A} \int_{-\infty}^{\infty} Y C dy$$

and

$$(3) \quad A = \int_{-\infty}^{\infty} C dy$$

σ_y was then calculated as the square root of $\langle Y \rangle^2$.

A second method used Gifford's (1961) relationship

$$\sigma_y = x \tan\left(\frac{W}{2}\right) / 2.15 \quad (4)$$

where x is the downwind distance in meters and W is the plume width in radians at the points where the concentration values decrease to 10% of their centerline magnitude. This assumes a Gaussian distribution of the plume.

The third method was based on the basic relationship $\sigma_y = x \sigma_\theta$ in which the horizontal plume spread is proportional to the standard deviation in wind direction, σ_θ , in radians (Pasquill, 1961; 1976). An exponent for the downwind distance x , commonly ranging in value from 0.85 to 0.894 (Cramer, 1964; Martin, 1976; Eckman, 1994), is often used to account for the increase in wind speed with height ($\sigma_y = x^b \sigma_\theta$). The value of b can vary lower depending on the value of σ_θ (Cramer, 1964; Slade, 1968).

Comparison of σ_y Results by the Three Methods

As seen in Figs. 87, 115, 143, 171, and 197, PSB1 plume cross-sections tended to exhibit complex internal structure with significant variability, at least on the 10-minute averaging basis. Cross-sections deviated significantly from an idealized Gaussian form with few exceptions, mostly during IOP3. Large, irregular concentration variations, distinct outlier peaks separate from the main plume, and skewed asymmetry of concentrations around the peak concentration for individual cross-sections were all very common. Furthermore, many of the cross-sections exhibited truncated profiles at the edge of the sampling array. These observations introduced complications and significant uncertainties with respect to the use of the first two methods described above due to the implied assumptions of Gaussian behavior. Determination of the plume centerlines and maximum concentrations was particularly uncertain. Furthermore, neither the second moment nor Gifford methods were suited to handle plume truncation at the edge of the sampling array.

To partially account for the non-Gaussian behavior with 10-minute averaging and plume meander, the individual profiles for IOPs 2-5 were shifted such that the approximate centroid of each cross-section were aligned and then averaged. The approximate centroid for each plume cross-section was determined mathematically by Y_0 using the second moment method. While this exercise involved the potential merging of plume sampling intervals with different stability categories, it generated plumes that, in general, came much closer to the idealized Gaussian form. This was not done for IOP1 due to the very large plume spread and limited time when the plume was over the sampling array. A comparison between the three methods is shown in Fig. 200. The value of b was set to 1.0 and 0.894 in this comparison. The results for the third method are strongly sensitive to the value of b . Most of the curves lie near the 1:1 line showing good agreement between the methods. There are discrepancies for IOP3 where the second moment method provides larger estimates of σ_y except for $b = 1.0$. The estimates of σ_y determined by the $x^b \sigma_0$ method are biased low in IOP5 and high in IOP2 depending on the value of b

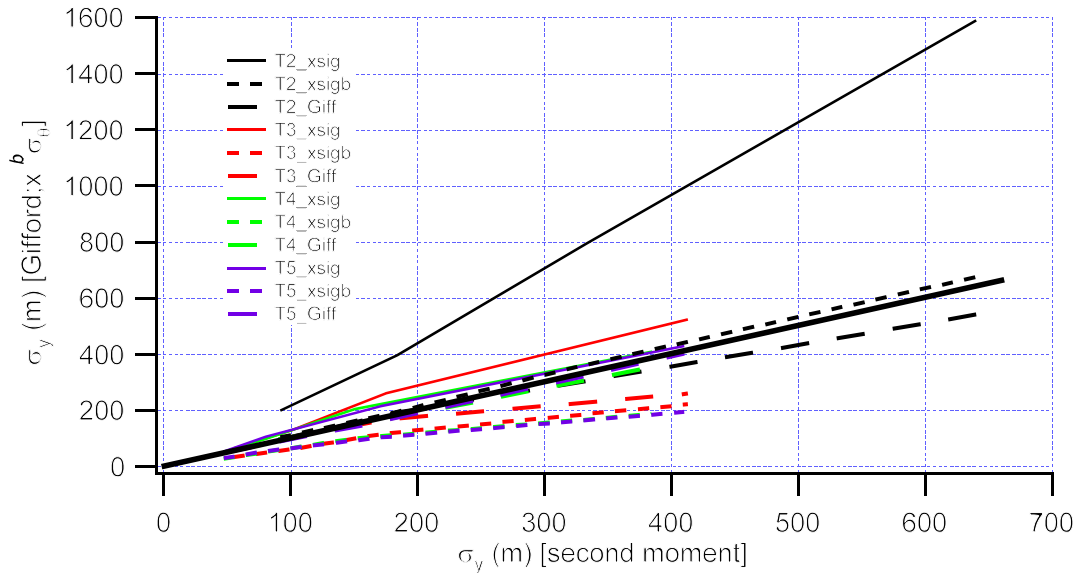


Figure 200. Comparison between σ_y calculated by the three methods using shifted, aligned, and combined plume cross-sections for IOPs (T) 2, 3, 4, and 5. For ‘xsig’ the value of $b=1.0$; for ‘xsigb’ the value of $b=0.894$. The bold line is a 1:1 reference.

A more detailed comparison between the $x^b\sigma_\theta$ method and second moment methods is shown in Fig. 201. This shows individual 10-minute average periods for all IOPs with the x exponent b equal to (a) 1.0, (b) 0.894, and (c) 0.85 and includes some potentially truncated cross-sections in the analysis. While there is a bias toward higher values of σ_y by the $x^b\sigma_\theta$ method for IOPs 3 and 4 with $b = 1.0$, the bias with respect to the second moment method is minimal and the relationship is approaching 1:1. The bias is greater for IOP5. The bias is very large for IOPs 1 and 2. Some of that discrepancy can be explained by the inclusion of some truncated cross-sections in the analysis. However, nearly all of the values for IOPs 1 and 2 were biased high including many cases representing non-truncated plumes. IOPs 1 and 2 also had the largest σ_θ values. This suggests that the basic relationship $\sigma_y = x\sigma_\theta$ overestimates the plume spread observed for large σ_θ during PSB1 but provides better estimates for smaller σ_θ .

The bias is largely eliminated with $b = 0.894$ for IOPs 1, 2, and 5. For IOPs 3 and 4 there is overcompensation and a bias in the other direction. The use of $b = 0.85$ imposes a strong bias with suppression of σ_y estimates from $\sigma_y = x^b\sigma_\theta$ for all IOPs. Allowing for the considerable scatter, the IOPs (1 and 2) with the largest σ_θ exhibited the least bias for $b = 0.85$.

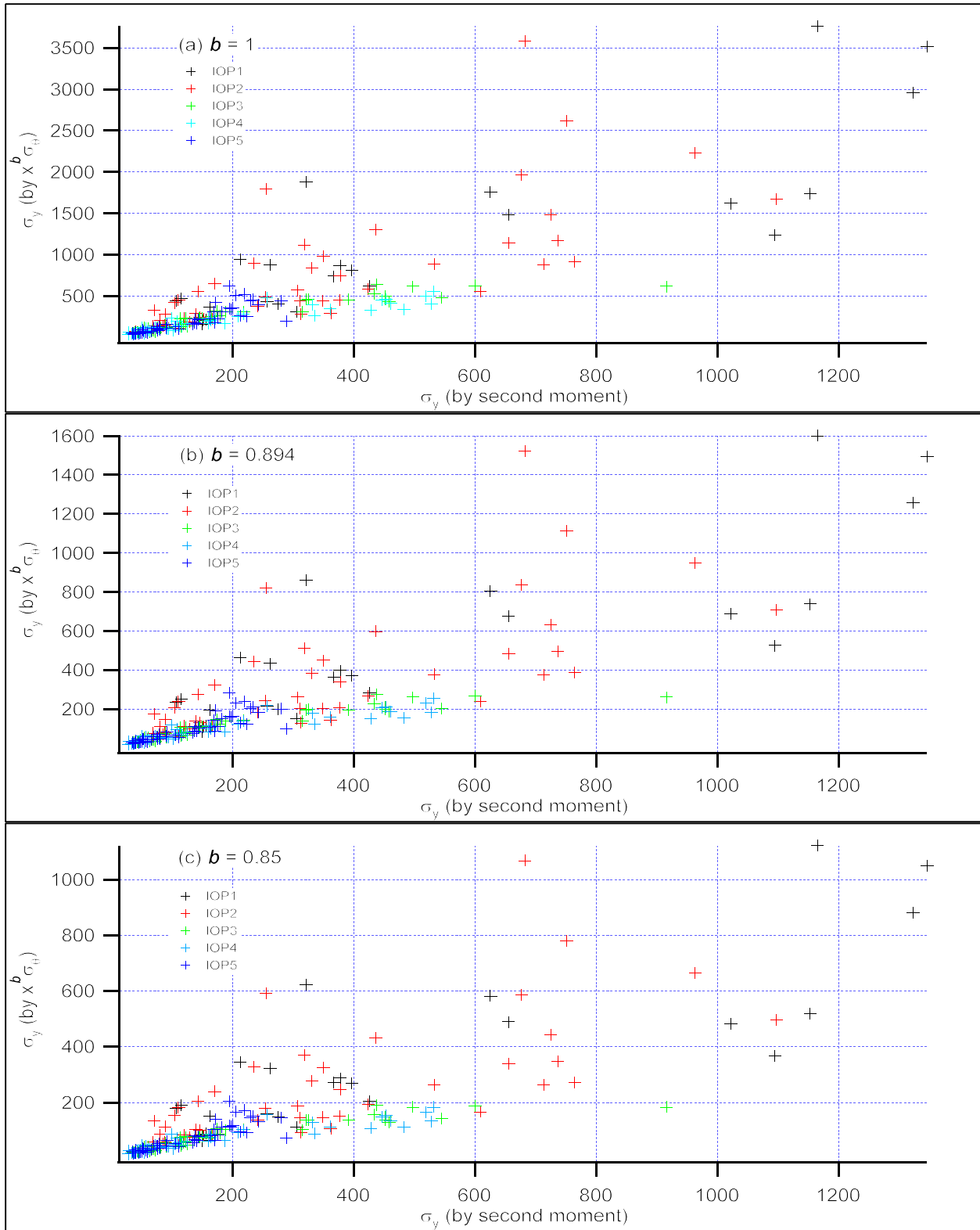


Figure 201. σ_y calculated using the $x^b \sigma_0$ and second moment methods for b equal to (a) 1.0, (b) 0.894, and (c) 0.85.

σ_y Comparisons Between PSB1 and Previous Work

Figure 202 examines the relationship between σ_y observed during PSB1 and estimates of σ_y obtained using traditional Pasquill-Gifford (P-G) curve methods. The PSB1 second moment σ_y results are plotted as functions of downwind distance after classification of P-G stability as determined from the EPA σ_θ method (EPA, 2000c). The P-G curves shown are taken from the scheme systematized by Turner (1969, 1970) using equations developed by Martin (1976) to fit the P-G curves for σ_y . The PSB1 results are greater than the P-G curves by about a factor of two. The differences in magnitude of σ_y observed during PSB1 and the P-G curves are diminished somewhat if the comparison is made using σ_y from the combined IOP cross-sections but they are still significant. Some possible explanations for the discrepancies in σ_y include:

1. Differences in site and meteorological conditions between PSB1 and previous work that affected measured concentrations used for the estimation of σ_y .
2. Possible differences arising from the P-G method used for determining stability classification. That is, different methods could determine different stability categories due to the meteorological criteria used. As described in the Summary of Individual IOPs chapter, the SRDT and σ_θ methods often provided much different stability classifications during PSB1.
3. Both the classical Prairie Grass (Barad, 1958) and PSB1 studies used continuous releases. However, for Prairie Grass, these consisted of individual release periods 10 minutes in duration, separated by at least two hours to assure that the SO_2 tracer was flushed from the area. For PSB1, there was one continuous release period covering the entire period of the 10-minute average tracer measurements plus a preliminary equilibration period for developing a quasi-steady state concentration field.

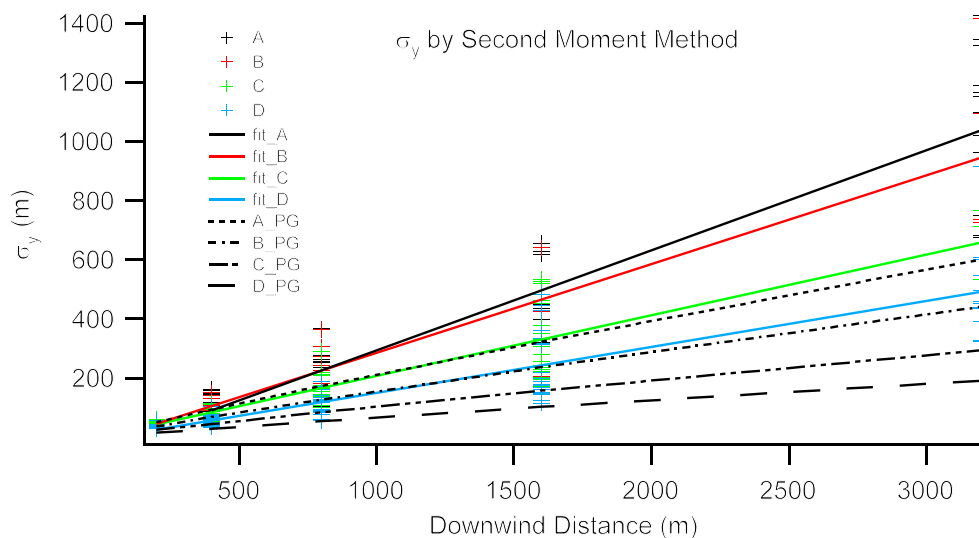


Figure 202. σ_y calculated using second moment method with individual PSB1 10-minute intervals classified by σ_A P-G stability class (EPA 2000c) with linear fit compared to σ_y P-G curves calculated from Turner (1969, 1970).

4. Differences in the assumed magnitudes of σ_θ used in different P-G methods for each stability category.
5. The use of some truncated profiles in this analysis. However, this would tend to make the calculated σ_y smaller, not larger.

Regarding (3), Prairie Grass investigated the dispersion of 10-minute plume segments rather than a true continuous plume. There was less chance for plume meander and turbulence to shred the segment in the time available, leaving a greater chance for the tracer to cross an arc at a specified distance as a more or less coherent cloud. In contrast, sampling during PSB1 used successive 10-minute sampling intervals within a plume released continuously over more than two hours. Each fixed 10-minute sampling period had greater potential to be affected by plume segments of greater than 10-minute release duration. Portions of the tracer plume could have been pulled away from the main plume by turbulence, redirected by plume meander, and slowed down or sped up with respect to the main plume due to turbulence. This would more likely result in tracer-bearing parcels with more complex and different histories arriving at a specified arc distance within a given 10-minute sampling period. The Prairie Grass parcels would be likely to have had less complex histories. These differences would, for a given 10-minute sampling period, make it more likely to produce the broader, often multimodal plumes of PSB1, than the narrower, generally unimodal plumes of Project Prairie Grass.

The data were reanalyzed with any concentration cross-sections that exhibited evidence of truncation being excluded. Ideally plumes were bounded by background level concentrations of about 8 ppt SF₆ on both ends of an arc. Since this was commonly not the case, truncated concentration profiles, in which the concentration at an end arc position was greater than 10% of the maximum concentration along the arc, were excluded from the σ_y second moment calculation.

The effects of sampling time were examined using non-truncated cross-sections. Simple averages of the 10-minute bag sample concentrations were averaged over 20, 30, 40, and 60 minute periods for successive periods without interruption by truncated cross-sections. The averaging was done by arc position with no plume realignment. The σ_y were determined for each qualifying arc profile and averaging period using the second moment method. The 5-minute average wind speeds at 10 m AGL on COC were similarly averaged to create 10, 20, 30, 40, and 60 minute averages. The corresponding mean σ_θ for each of the qualifying averaging periods were determined using a calculation adapted from the EPA (2000c)

$$\sigma_\theta = \left[\left(\sum_n \sigma_{\theta_n}^2 \right) / n \right]^{1/2} \quad (5)$$

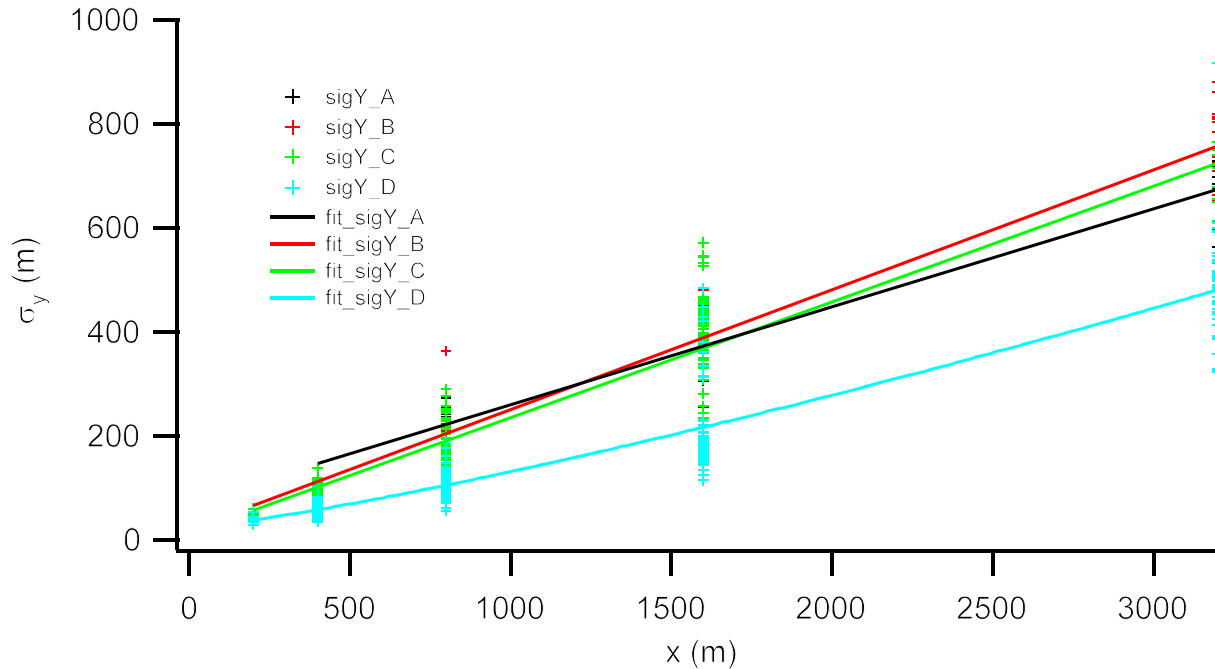


Figure 203. Calculated σ_y with best-fit lines for stability classes A, B, C, and D including all averaging periods for each class. Truncated profiles excluded.

where n is the number of 10-minute samples in the averaging period. The resulting wind speeds and σ_θ for each of the qualifying averaging periods were used to determine the stability class with the EPA σ_θ method.

The results for all of the qualifying data were combined and binned by stability class and averaging period. The mean wind speeds and mean σ_θ for each averaging period were used to determine the P-G stability class. There was large variability in the data about the best-fit lines for σ_y (Fig. 203). This was due, at least in part, to some of the factors already discussed.

A more detailed look at the σ_y results by stability class and averaging period is shown in Fig. 204 together with comparisons to P-G (Turner, 1969, 1970; Martin, 1976), Markee (Sagendorf and Carter, 1999; Start and Wendell, 1974; Fuquay et al., 1964), and Briggs (Briggs, 1974; Gifford, 1976) dispersion curves. Three features are worth noting. One is that the calculated PSB1 σ_y results are, with the exception of class A, consistently high relative to the published dispersion curves shown. Two, the PSB1 results also trend higher than the Project Prairie Grass (PPG) results. The discrepancies increase with increasing downwind distance in both cases. Finally, the averaging time makes relatively little difference in the values of σ_y .

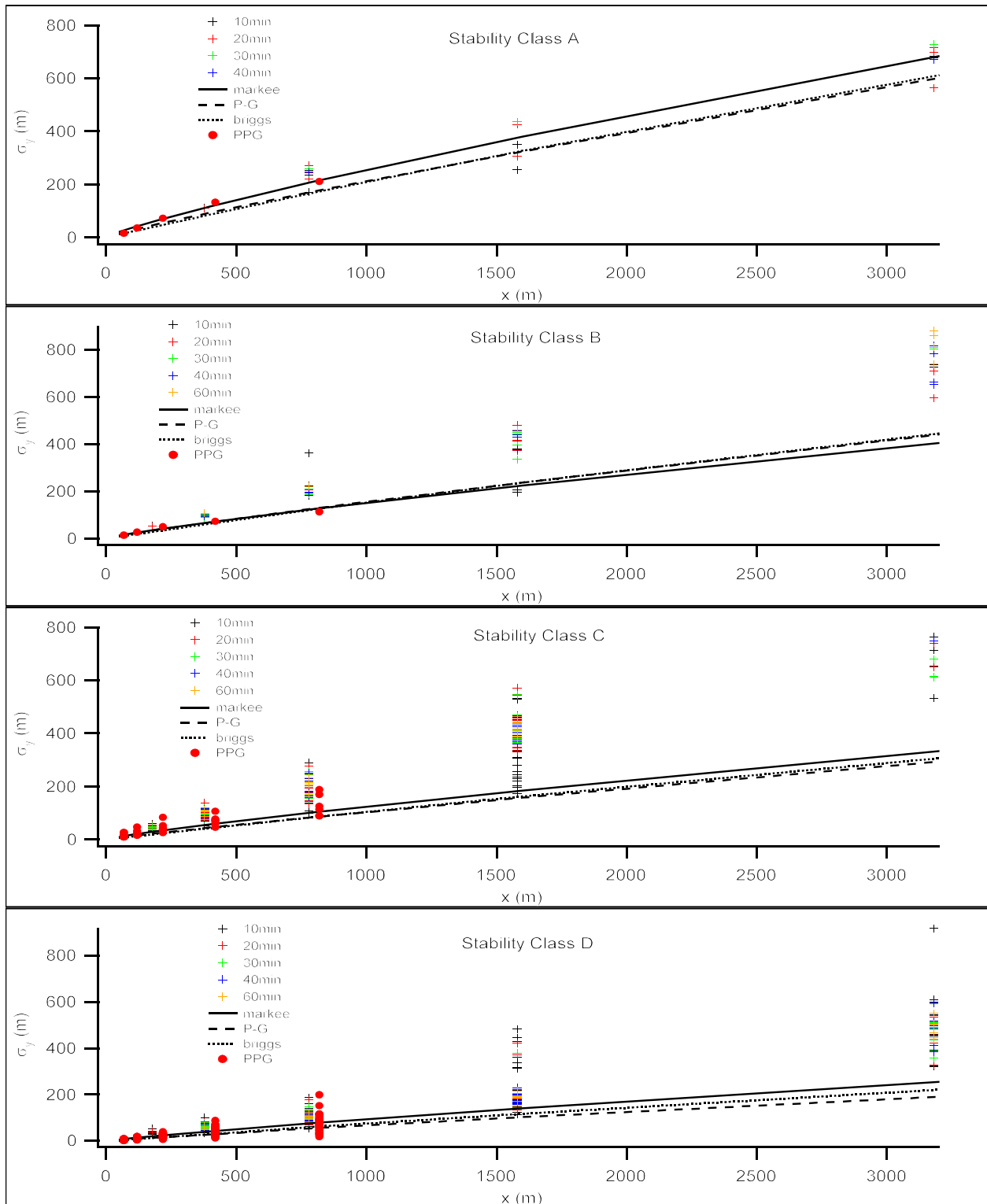


Figure 204. Plots of PSB1 σ_y results for qualifying profiles binned by stability class (A, B, C, D) and averaging period (10, 20, 30, 40, 60 minutes). Project Prairie Grass (PPG) results and the dispersion model curves for Markee, P-G, and Briggs are shown for comparison.

This last point is obscure but is more readily seen with the aid of the best fit lines in Fig. 205. Discounting the very large scatter about the best fit lines, there is a suggestion of a trend toward higher values of σ_y as averaging time increases but the effect appears to be small. Larger values of σ_y would be anticipated for longer averaging times as the effects of lower frequency wind meander are more fully incorporated into longer averaging periods. Some previous work has found that σ_θ was a function of sampling time and surface roughness and increased by a factor of two for 1 h averaging compared to 3 min averaging (Pasquill 1975, 1976). However, the PSB1 data indicates it appears to be a relatively small effect. The explanation for the relatively small differences might be due to the PSB1 continuous release establishing a quasi-steady state concentration field as opposed to shorter, discrete continuous release time periods. It is possible that many of the effects of lower frequency wind meander were incorporated into shorter averaging periods due to the steady state concentration field and the factors discussed above. Recall from the fast response data that periodicities were commonly on the order of 12-15 minutes or less.

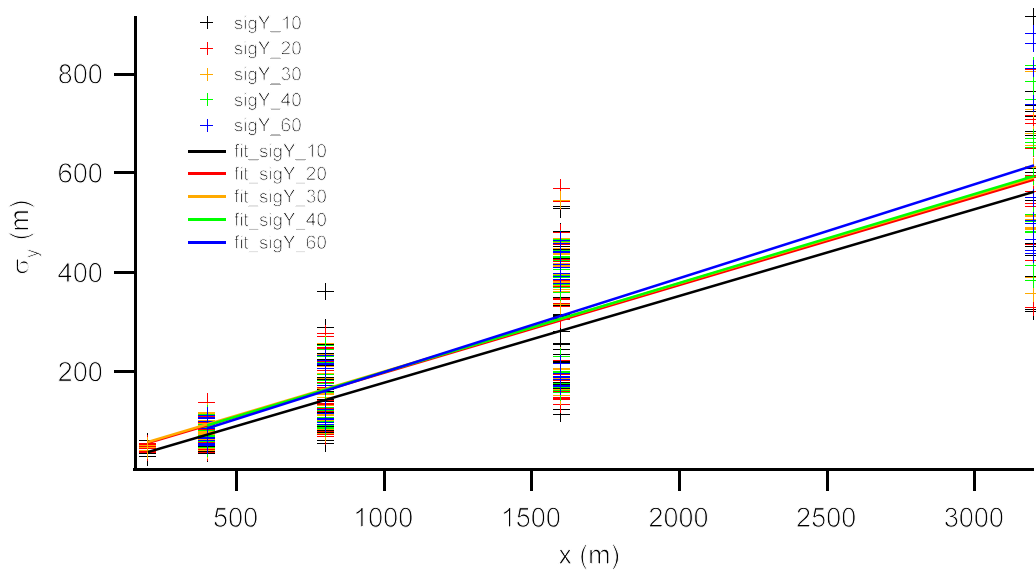


Figure 205. Calculated PSB1 σ_y results for qualifying profiles binned by averaging period (10, 20, 30, 40, and 60 minutes).

Further confirmation of the significantly greater plume spread observed during PSB1 was seen by following a line of analysis suggested by Taylor diffusion theory (Taylor, 1921) and the relationship $\sigma_y = \sigma_v t$. The σ_v for each 10 minute period for each IOP was determined after detrending and rotation into the mean wind direction. The travel times t were calculated by dividing the arc distances by the mean streamwise wind speed for each 10 minute period. The G1, G2, R2, R3, and R4 sonics were all used. The results for IOPs 2-5 are shown in Figs. 206a-d, respectively. In all cases the distribution of σ_y values mostly falls outside the range bracketed by the class A to class D stabilities determined from the Markee, PG, and Briggs curves. The best fit was found in IOP3 which had the best behaved, most Gaussian-like plumes. IOP1, not shown, had the worst fit. The values of σ_y determined by this approach tend to be somewhat

greater than those determined from the analysis of the σ_θ and tracer data. However, there is clearly greater consistency between those three approaches than there is to the established curves.

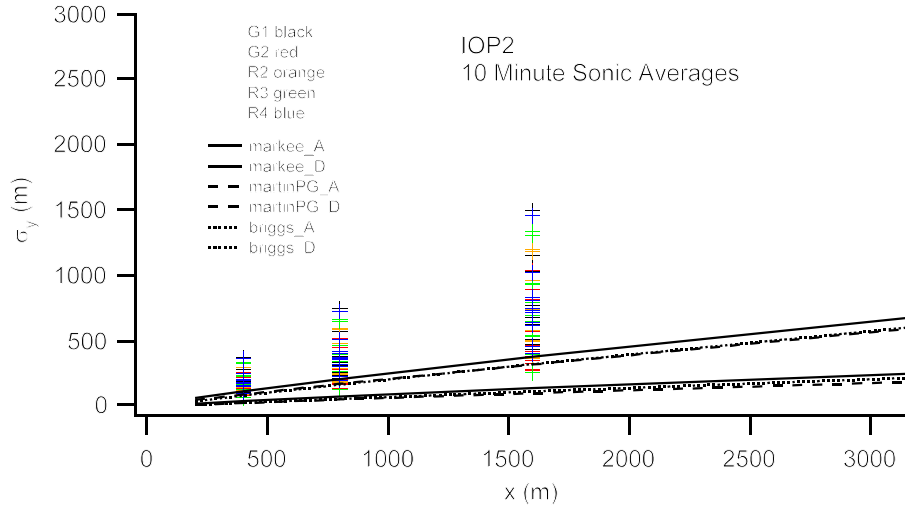


Figure 206. Comparison between σ_y calculated from the Taylor theory relationship $\sigma_y = \sigma_y t$ for sonics G1, G2, R2, R3, and R4 to the class A and D stability class dispersion curves from Markee, P-G, and Briggs.

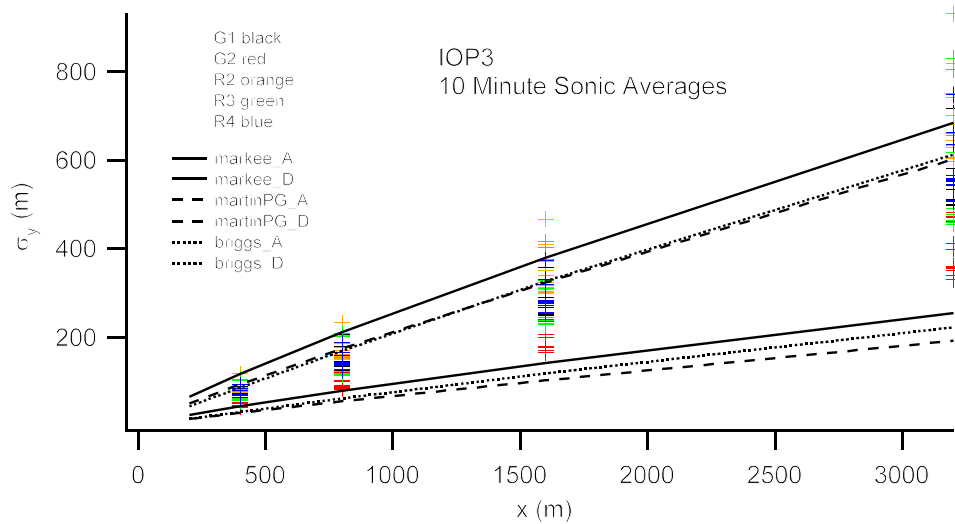


Figure 206b.

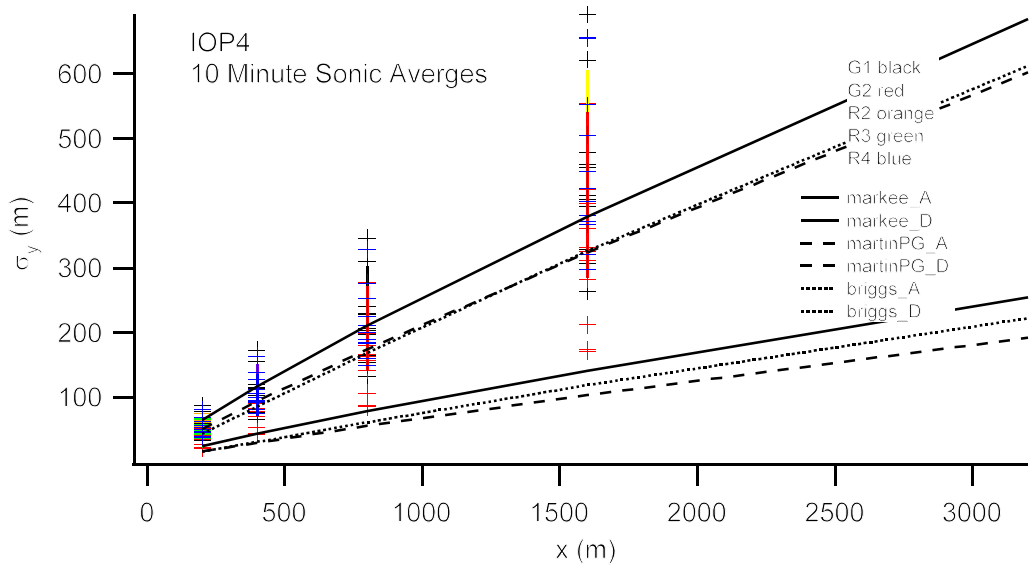


Figure 206c.

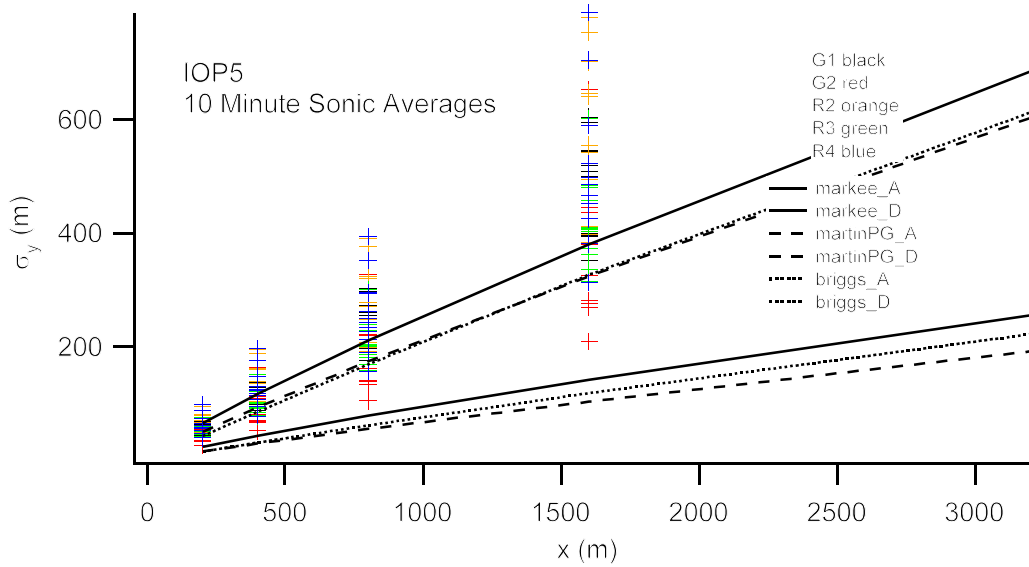


Figure 206d.

PSB1 σ_θ and Turbulence Intensity Measurements

The range of σ_θ measured during PSB1 is summarized in Fig. 207. PSB1 σ_θ were calculated in Campbell CR23X dataloggers using the Yamartino method (Yamartino, 1984) with 1-second sampling and 5-minute averaging periods. The cup anemometers and wind vanes on the GRI, COC, and TOW towers gave generally consistent results for wind speed, wind direction, and σ_θ across the study area. The σ_θ results for IOPs 2, 3, and 4 are representative of the range of values observed during PSB1 (Fig. 208). While temporal variation in σ_θ was sometimes observed across the study area, the overall tendency was toward horizontal homogeneity.

Vertical profiles from GRI of σ_θ , measured by wind vane, and turbulence intensity (σ_v/U), measured by sonic anemometer, are shown in Fig. 209. The wind vane results have been converted to radians for the purpose of comparison with the turbulence intensities. The ranges of turbulence intensities measured by the sonic anemometers during PSB1 were consistent with the σ_θ measured by the wind vanes. The sharp kinks in the sonic anemometer profiles are mostly due to transitions between WSULAR and ARLFRD sonics. The WSULAR sonics were collocated with an IRGA, which might have contributed to the larger values often associated with the WSULAR sonics relative to the ARLFRD sonics (no IRGA). There were also three makes of sonic involved (CSAT3 at 2, 8, 16, and 60 m; Gill at 4 and 30 m; R.M. Young at 45 m).

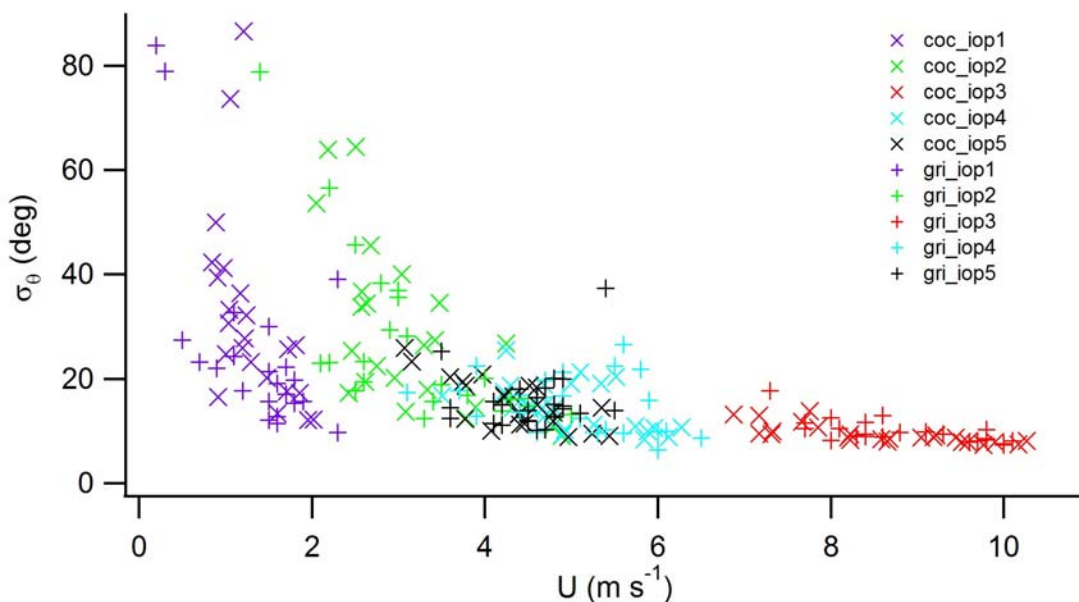


Figure 207. 5-minute average cup and vane σ_θ for all IOPs from COC and GRI at 10 m AGL as function of wind speed.

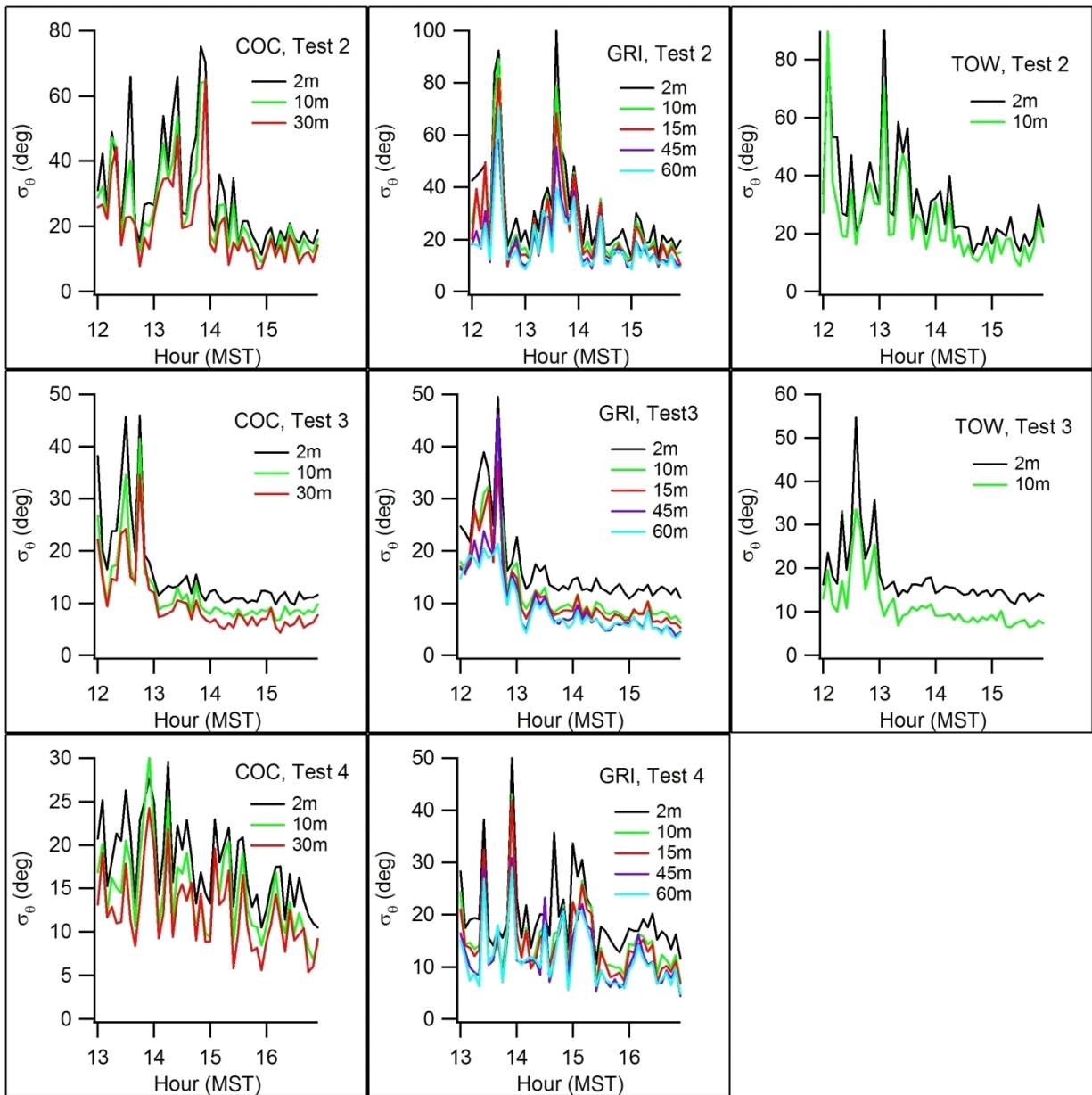


Figure 208. Wind vane anemometer measurements of σ_θ during IOPs 2, 3, and 4 during PSB1.

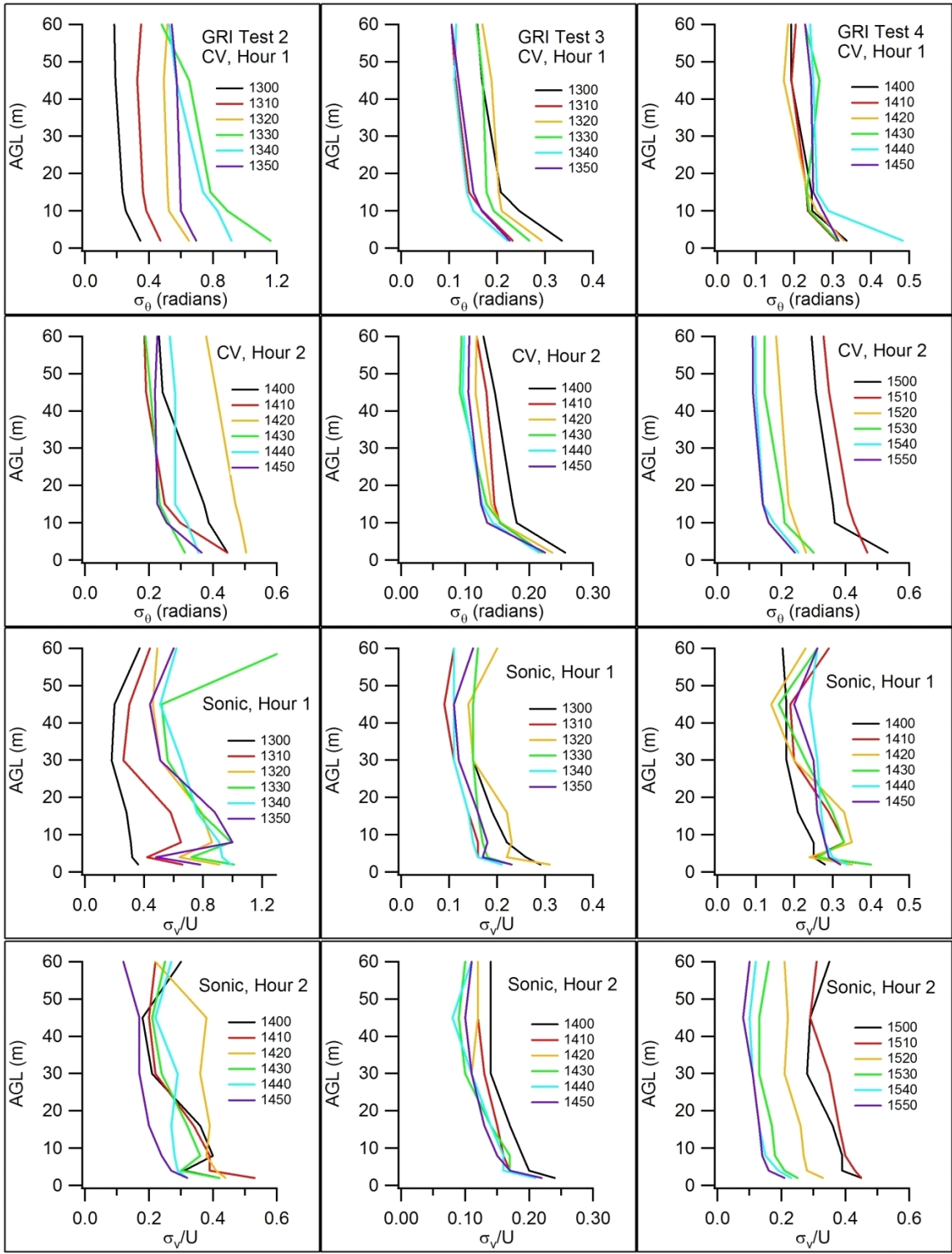


Figure 209. Comparisons between GRI cup and vane (CV) σ_θ measurements, converted to radians, and sonic anemometer measurements of turbulence intensity for each 10-minute period of IOPs 2, 3, and 4. Times indicated in the legends are MST start times

There is no evidence of anemometer instrumentation problems during PSB1 or that the σ_θ measurements were flawed or anomalous. The cup anemometers and wind vanes on the GRI, COC, and TOW towers gave consistent results for wind speed, wind direction, and σ_θ (Figs. 64, 65, 92, 93, 120, 121, 148, 149, 174, and 175). The sonic anemometer measurements of wind speed, wind direction, and turbulence on the GRI tower and along the 3200 m arc were consistent with other measurements at comparable heights and provided evidence of horizontal homogeneity. The cup anemometers and wind vanes are modern instruments that had been checked and calibrated to modern standards days prior to the experiments. Sonic anemometer measurements of turbulence intensity provide an independent check on the cup and vane measurements of σ_θ . The ranges of turbulence intensities measured by the sonic anemometers during the PSB1 IOPs were consistent with the σ_θ measured by the cup and vane anemometers (compare Figs. 80 and 83, 108 and 111, 136 and 139, 164 and 167, 190 and 193). Furthermore, the WSULAR and ARLFRD sonics at GRI provided independent checks on each other and the cup and vane results. While there were some differences, the overall ranges and magnitudes were consistent among the cup anemometers and wind vanes, WSULAR sonics, and ARLFRD sonics.

In the course of this preliminary investigation it was found that there is no discernible difference in daytime measurements between σ_θ determined by both sonic anemometers and wind vanes during fall, 2013 at the INL test site and wind vanes during Project Prairie Grass. While a greater fraction of the σ_θ measurements during PSB1 fell within the more unstable P-G stability classifications than during the daytime Project Prairie Grass experiments, as determined by the EPA method, the overall range of daytime variation of σ_θ was similar for the two sites. However, it was found that there were large differences between the two sites at nighttime. This distinction will be more fully developed in subsequent work.

Miscellaneous Observations and Calculations of σ_y

Figure 210 shows calculated PSB1 σ_y as a function of σ_θ for different distances and averaging periods. There is a suggestion of a linear dependence of σ_y on σ_θ for values of σ_θ up to about 18 degrees. The value of σ_y appears to be independent of σ_θ for values of σ_θ greater than about 18 degrees.

It has been posited that there is rough conformity to a "universal" relation between the ratio σ_y/σ_θ and downwind distance, irrespective of surface roughness and stability (Pasquill, 1976). The data indicate that the σ_y measured during PSB1 were larger than those found in many of the field studies done in previous decades but the observed σ_θ were similar to the daytime Project Prairie Grass. Figure 211 is a plot of the ratios of σ_y/σ_θ as a function of downwind distance for PSB1. The PSB1 results tend to fall near the upper limit or above the range of values found in previous field experiments (compare Fig. A-1, Pasquill (1976); Fig. 4.21 with σ_θ in degrees, Slade (1968)). There is a greater tendency for PSB1 ratios to exceed the bounds of the range with increasing downwind distance.

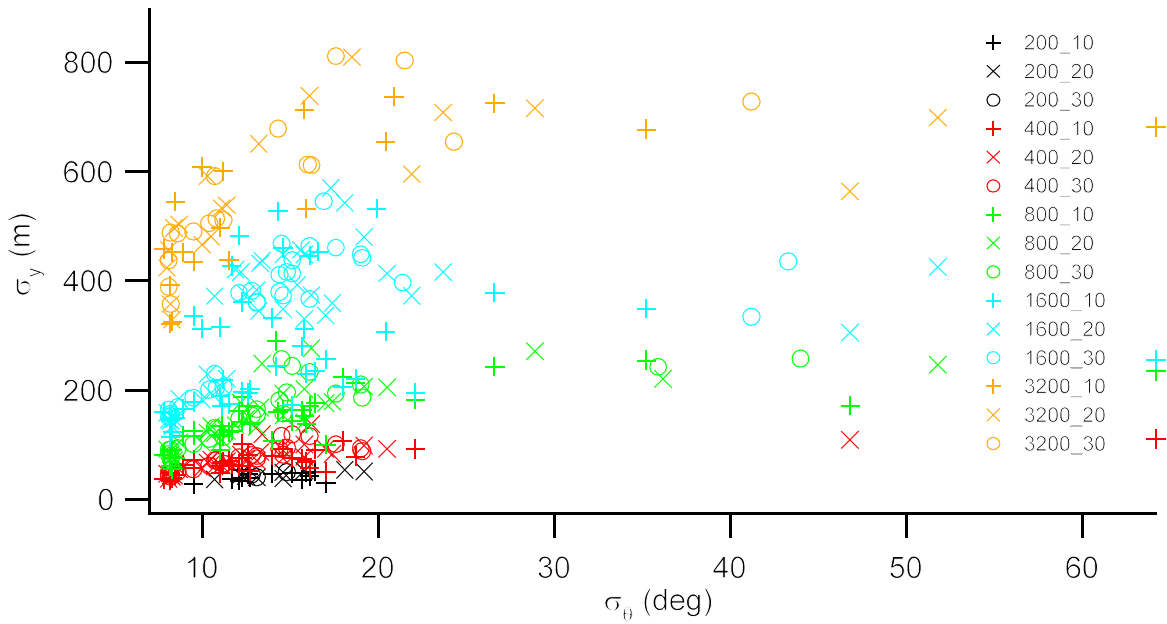


Figure 210. σ_y calculated by second moment method on non-truncated profiles for IOPs 2-5 as a function of σ_θ for different distances and averaging periods (dist_ap).

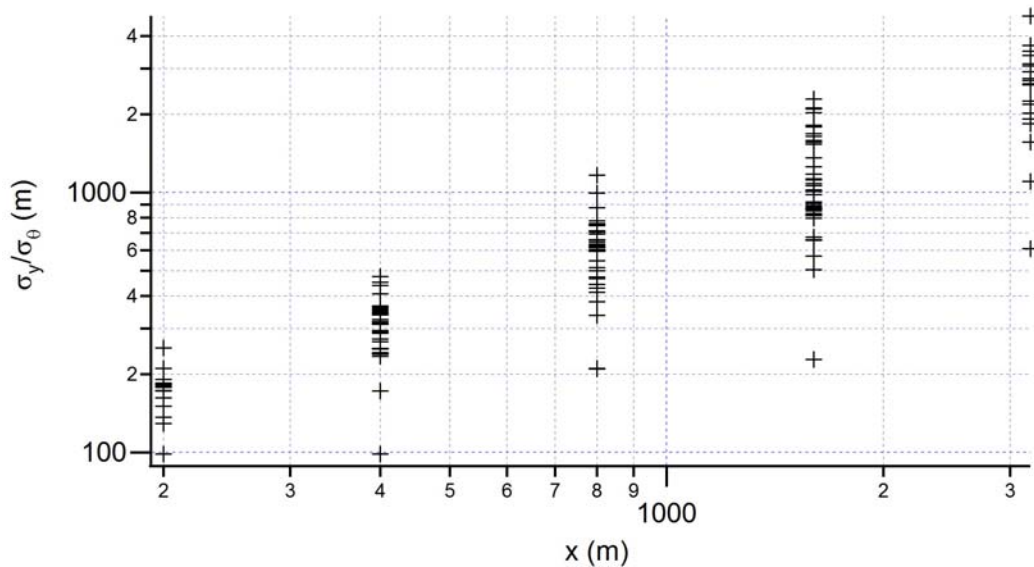


Figure 211. Plot of σ_y/σ_θ for non-truncated cross-sections. These results are roughly consistent with the “universal” relation posited by Pasquill (1976) although they tend to lie near or just above the upper bound of the range shown there.

Another question raised by this investigation into σ_y relates to translation of σ_y determined along an arc in polar coordinates into the traditional definition of σ_y in a rectangular coordinate system. In the limiting case where the small angle approximation is valid, any discrepancies are negligible. However, assumption of the small angle approximation was often inappropriate for PSB1 given the large observed plume spreads and σ_θ values. Furthermore, it can be demonstrated using Lagrangian particle experiments that dispersion deviates from the assumed Gaussian behavior at large turbulence intensities. If it is assumed that the distribution of the particles is Gaussian in time, then the particle distribution is not Gaussian at a specified downwind distance. The deviation from Gaussian increases as turbulence intensity increases.

Alternative ways of examining σ_y include as a function of the M-O similarity stability parameter z/L (Fig. 212). The σ_y shown were determined by the second moment method using qualified, non-truncated plume cross-sections. The z/L values are from the R3 and R4 sonic anemometers on the 3200 m arc. There is a clear pattern of a log-linear increase in σ_y as z/L decreases from zero to about -0.3 and then σ_y become roughly constant with further decreases in z/L .

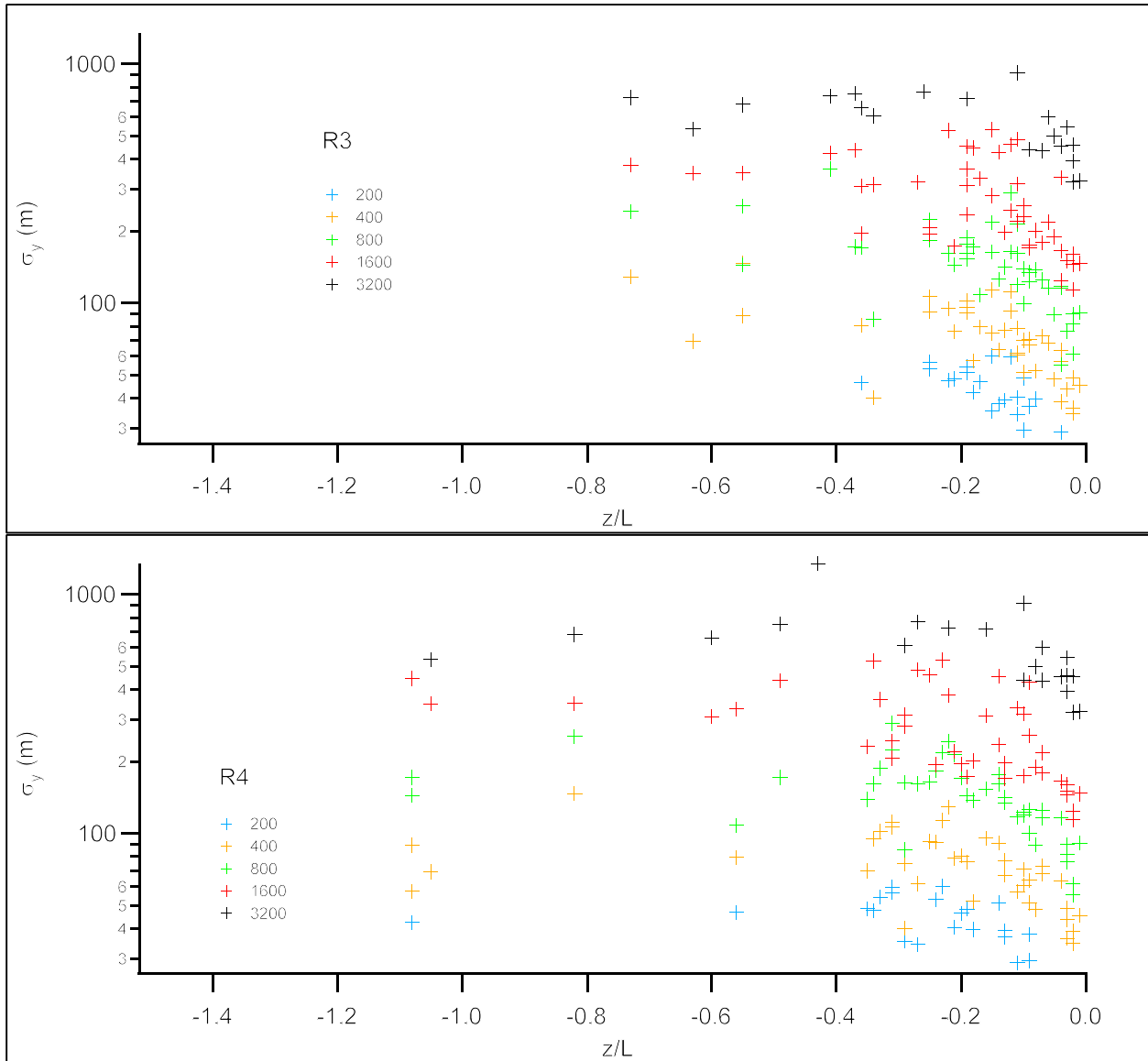


Figure 212. σ_y calculated on non-truncated cross-sections by the second moment method as a function of the stability parameter z/L for the five downwind distances in PSB1. The z/L were determined at the sonic anemometers R3 and R4 on the 3200 m arc.

DETERMINATION OF σ_z

Any concentration cross-sections with evidence of truncation were excluded as described above in the section on determination of σ_y . The 10-minute bag samples were averaged over 20, 30, 40, and 60 minute periods for each arc position for successive periods without interruption by truncated cross-sections. The wind speeds and σ_θ were also averaged as described earlier for each of the qualifying averaging periods and stability class determined using the EPA (2000c) σ_θ

method. The σ_y were determined for each qualifying arc profile and averaging period using the second moment method.

The mean and maximum concentration mixing ratios (pptv) for each averaging period were converted to mean and maximum concentrations ($\mu\text{g m}^{-3}$). The mean temperature (K) and pressure (atm) at GRI during the two hour release period were used to convert mixing ratio to concentration. The results for all of the qualifying data were combined and binned by stability class and averaging period. The mean wind speeds and mean σ_θ for each averaging period were used to determine the P-G stability class. The maximum concentrations, mean wind speeds, and σ_y for each averaging period were used to calculate the best-fit values of σ_z by iteration with the Gaussian plume formula:

$$C = \frac{Q}{2\pi u \sigma_y \sigma_z} \exp\left(-\frac{y^2}{2\sigma_y^2}\right) \left\{ \exp\left(-\frac{(z-H)^2}{2\sigma_z^2}\right) + \exp\left(-\frac{(z+H)^2}{2\sigma_z^2}\right) \right\} \quad (6)$$

In this analysis, the release height $H = 1.5$ m, the sampling height z is 1.0 m, C is the maximum plume centerline concentration ($\mu\text{g m}^{-3}$), $y = 0$ as it was nominally on the plume centerline, Q is the point source release rate ($\mu\text{g s}^{-1}$), and u (m s^{-1}) is the mean wind speed for the averaging period.

The resulting best-fit values of σ_z showed large variability (Fig. 213). This was due, at least in part, to the fact that many profiles were non-Gaussian, even after averaging. They often exhibited multiple peaks, and it was only the single maximum representing the nominal plume centerline that was used.

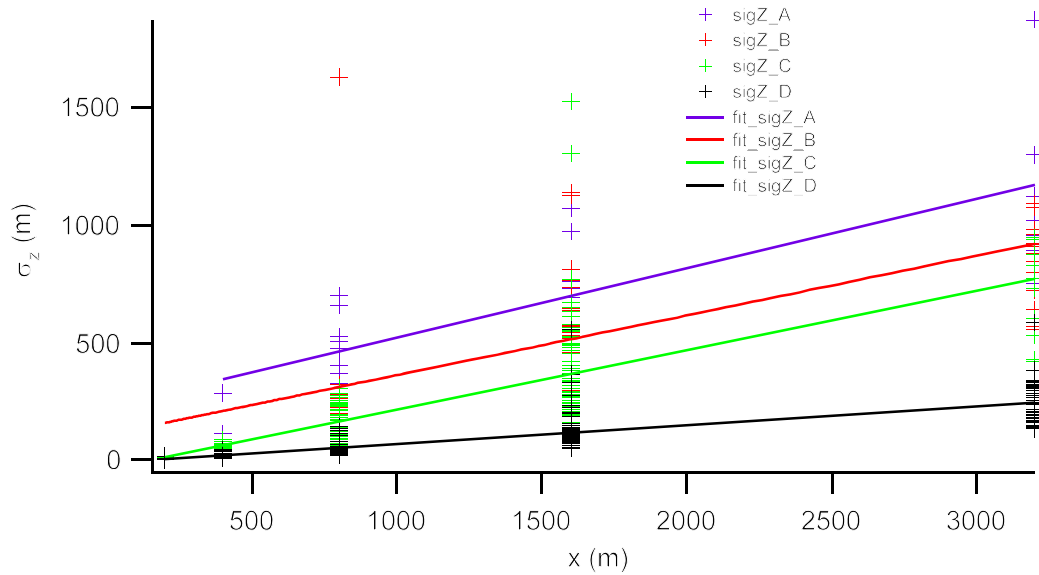


Figure 213. Calculated σ_z with linear best-fit lines for stability classes A, B, C, and D including all averaging periods for each class. Truncated profiles excluded.

A more detailed look at the σ_z results by stability class and averaging period is shown in Fig. 214 together with comparisons to some published dispersion curves. Two features are salient. One is that the calculated PSB1 σ_z results are consistently high relative to the published dispersion curves shown. This is likely at least partly due to the numerous profiles used that lacked well-defined Gaussian form with a single, nominal maximum concentration. A larger maximum concentration would have forced lower σ_z values.

The other feature is that averaging time makes relatively little difference in the values of σ_z . This can be more clearly seen in Fig. 215. Discounting the very large scatter, there is a suggestion of a trend toward lower σ_z as averaging time increases but it is a relatively small effect.

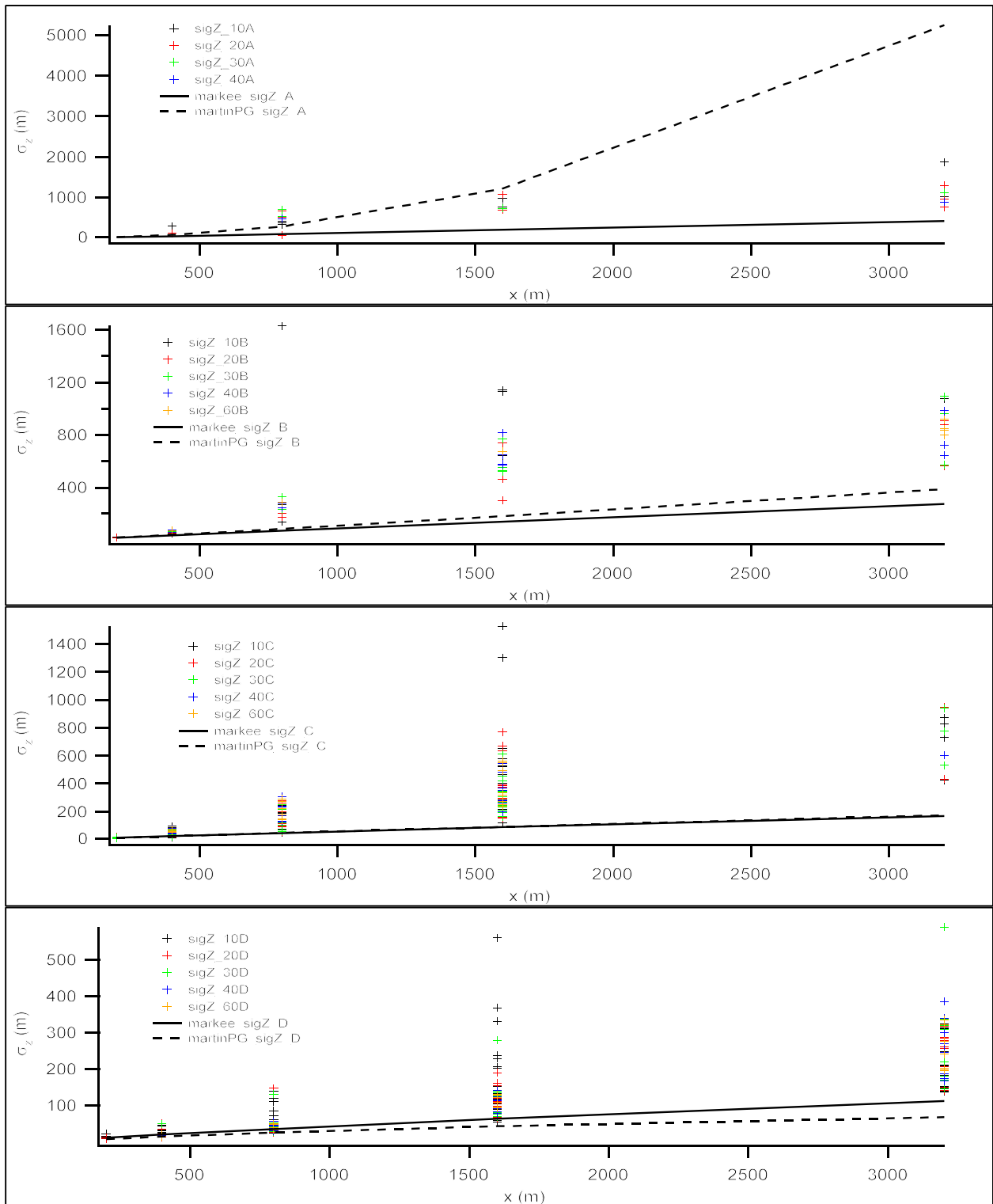


Figure 214. Plots of PSB1 σ_z results for qualifying profiles binned by stability class (A, B, C, D) and averaging period (10, 20, 30, 40, 60 minutes). The dispersion curves for Markee and PG (Turner, 1969, 1970; Martin, 1976) are shown for comparison.

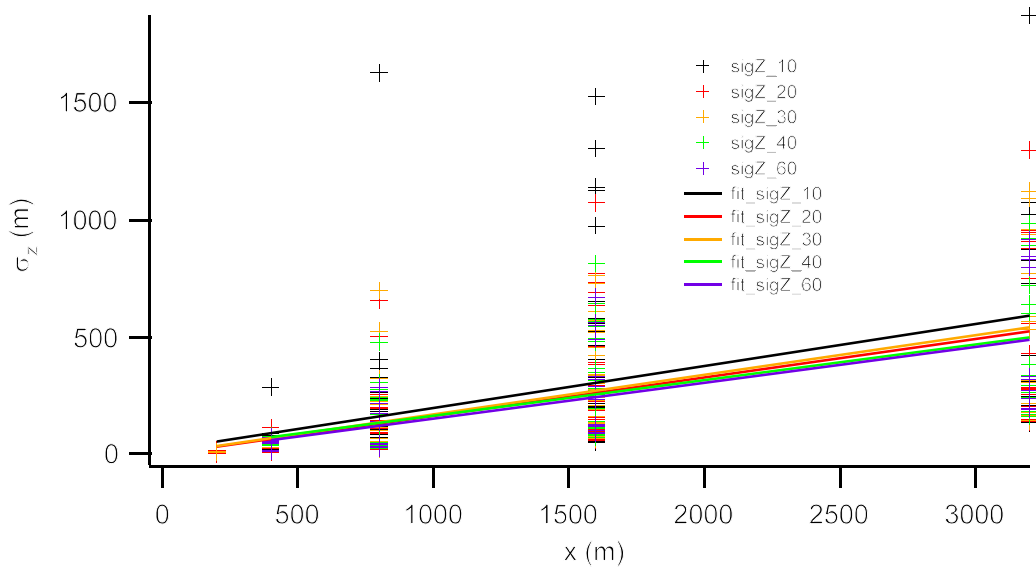


Figure 215. Calculated PSB1 σ_z results for qualifying profiles binned by averaging period (10, 20, 30, 40, and 60 minutes).

TOWER DATA COMPARISONS

A comparison was made between the measured concentrations of SF₆ on the towers to the calculated concentrations of SF₆ for IOPs 2 and 5. The latter were calculated using the Gaussian plume formula, the values of σ_y and σ_z estimated from the curves on Figs. 203 and 213, the mean temperature and pressure for the two-hour period, and y estimated as the arc distance between the location of the tower and location of the maximum concentration at the nearest arc distance for which data was available. The results are shown in Fig. 216.

The discrepancies between the measured and calculated concentrations are very large, often orders of magnitude. This is particularly true for lower measured concentrations. For higher concentrations there is much better agreement, commonly within a factor of 2 to 3 up to about an order of magnitude. There are numerous possible explanations that could contribute to the large discrepancies. There are large uncertainties in the estimates of σ_y and σ_z due to the wide spread of data used in their estimation. There are uncertainties related to the arc distance y due to the irregular, non-Gaussian plume cross-sections, often with multiple major concentration maxima. All of these are related to the variability that was potentially introduced by a quasi-steady state concentration field. The gaps exhibited by the calculated values relative to the measured concentrations reflects a combination of the tower measurement heights and the use of discrete values for the input parameters of the calculations.

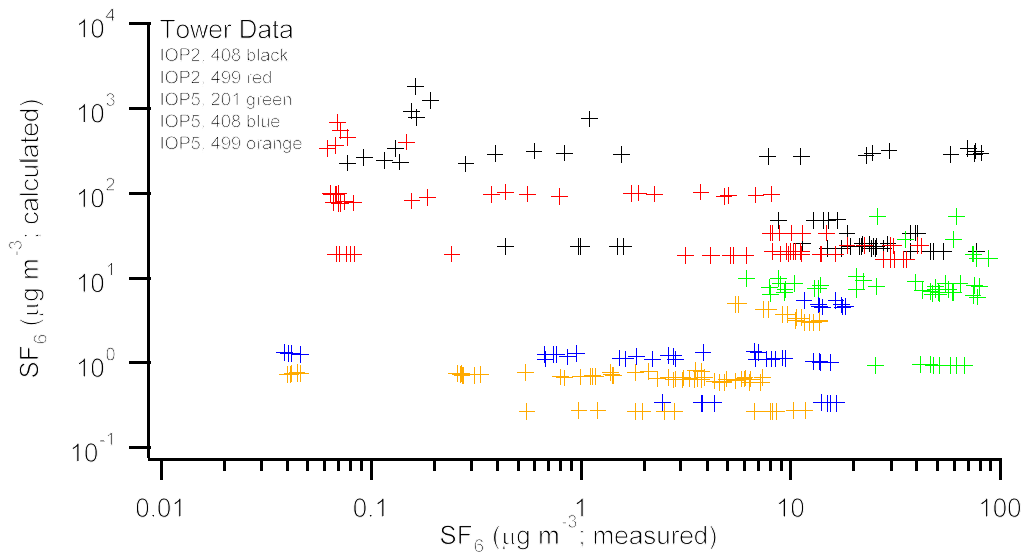


Figure 216. Comparison between concentrations measured at the towers to concentrations calculated by the Gaussian plume formula for IOPs 2 and 5.

FAST RESPONSE ANALYZER ANALYSES

A summary of a preliminary analysis of the PSB1 fast response concentration measurements is shown in Table 24. The calculations were completed with the following assumptions: flag=0 accepted as good values; flag=1 accepted as estimated non-zero values; flag=2 accepted and set to zero; flag=3 accepted as estimated values; flag=4 excluded; flag=5 accepted as zeros; all other flags excluded. The calculations covered the 2 h sampling period with the exception of IOP1. For IOP1 the periods when the plume was largely absent from the sampling array were excluded and the calculations are only for 1500-1600 h. Calculations were not performed on the IOP3 results due to the large amount of data affected by railing. The concentration fluctuation intensity is defined as the standard deviation of concentration divided by the mean concentration (σ_c/C). The unconditional concentration fluctuation intensity calculations used all accepted values. The conditional calculations used all accepted values excluding zeros. Both the 95th percentile and absolute maximum peak-to-mean ratios, denoted P:M, are shown in Table 24. The results are graphically presented in Fig. 217. Figure 218 shows that unconditional fluctuation intensity and unconditional P:M were inversely related to the fraction of time the fast response analyzer was in the plume while the conditional fluctuation intensity and P:M were largely independent of the fraction of time in plume. These results could be anticipated based on the premise of conditional sampling.

Table 24. Summary of fast response analyses. Peak:Mean (P:M) values of 19.9 represent ratios ≥ 20 . ‘U’ represents unconditional calculations (all valid values), ‘C’ represents conditional calculations (zeros excluded), and ‘c’ represents concentration.

IOP	Location		Intermittency (non-zero, fraction in plume)	Peak:Mean (P:M) 95 th percentile		P:M Max		Unconditional Fluctuation Intensity $(\sigma_c/\bar{c})_u$	Conditional Fluctuation Intensity $(\sigma_c/\bar{c})_c$
				U	C	U	C		
	Arc	Angle							
1	400	25	0.92	3.9	3.7	5.3	4.9	1.15	1.07
1	400	55	0.78	4.3	4.1	8.7	6.7	1.51	1.25
1	800	25	0.79	3.9	3.1	14.1	10.7	1.27	1.03
1	800	55	0.56	4.1	3.5	9.9	5.5	1.68	1.07
1	1600	55	0.47	3.3	1.9	4.7	2.3	1.27	0.49
2	400	31	0.49	6.9	5.5	13.3	6.5	2.59	1.67
2	400	61	0.24	6.9	3.9	19.9	7.5	3.38	1.40
2	800	31	0.52	5.5	4.1	10.5	5.5	1.99	1.26
2	800	61	0.30	5.9	3.9	19.9	7.1	2.99	1.40
2	1600	61	0.35	5.1	4.1	19.9	10.5	3.18	1.68
4	400	31	0.70	4.5	3.3	5.1	3.5	1.43	1.07
4	400	55	0.23	5.9	3.5	19.9	8.5	3.49	1.43
4	800	31	0.71	5.5	4.7	13.3	9.3	2.00	1.59
4	800	57	0.15	3.1	4.1	19.9	7.3	4.14	1.34
4	1600	31	0.55	3.7	3.9	19.9	15.5	2.75	1.92
4	1600	55	0.16	3.1	3.9	19.9	6.5	4.15	1.36
5	400	25	0.37	6.1	4.5	16.5	6.1	2.60	1.37
5	400	55	0.46	5.7	4.1	15.1	6.9	2.34	1.40
5	800	25	0.24	5.5	3.9	19.9	7.3	3.26	1.32
5	800	57	0.48	5.9	3.7	19.5	9.3	2.22	1.36
5	1600	25	0.12	7.1	2.5	19.9	3.3	3.33	0.70
5	1600	55	0.50	5.1	3.1	10.9	5.5	1.71	0.98

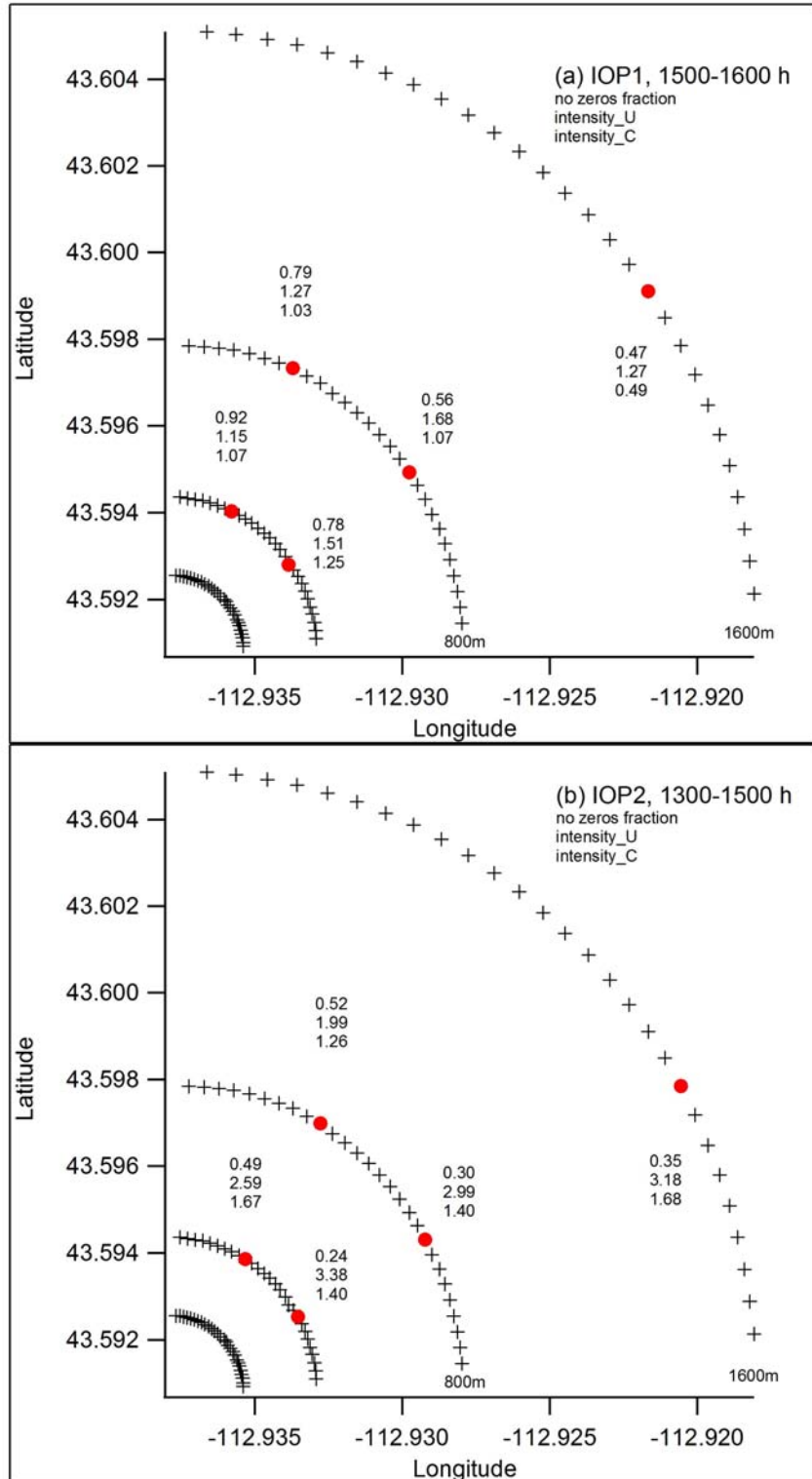


Figure 217. Intermittency (no zeros fraction) and unconditional (U) and conditional (C) concentration fluctuation intensities for IOPs 1 (a) and 2 (b). Intermittency is equivalent to time in plume.

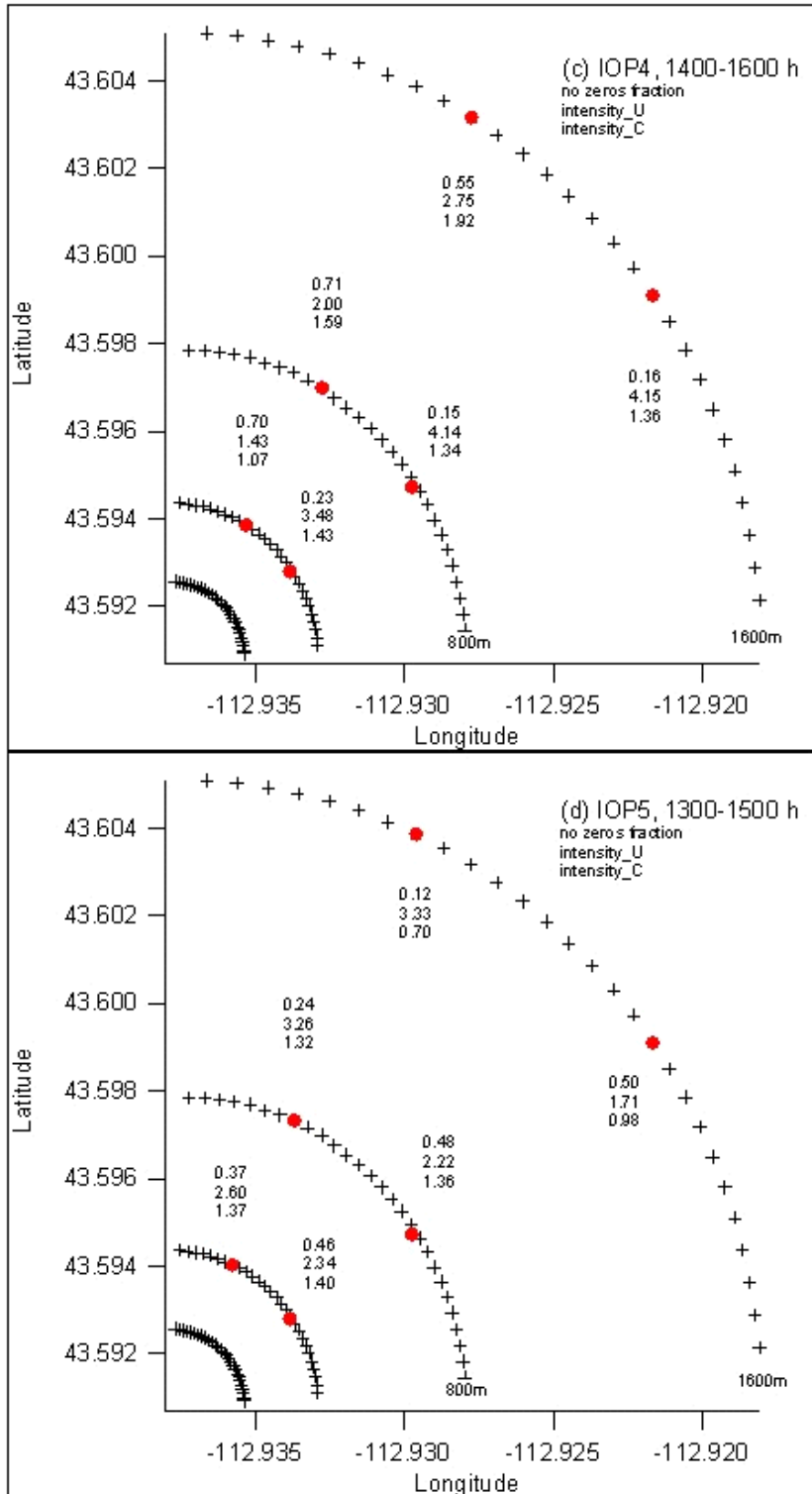


Figure 217 continued (c and d, IOPs 4 and 5).

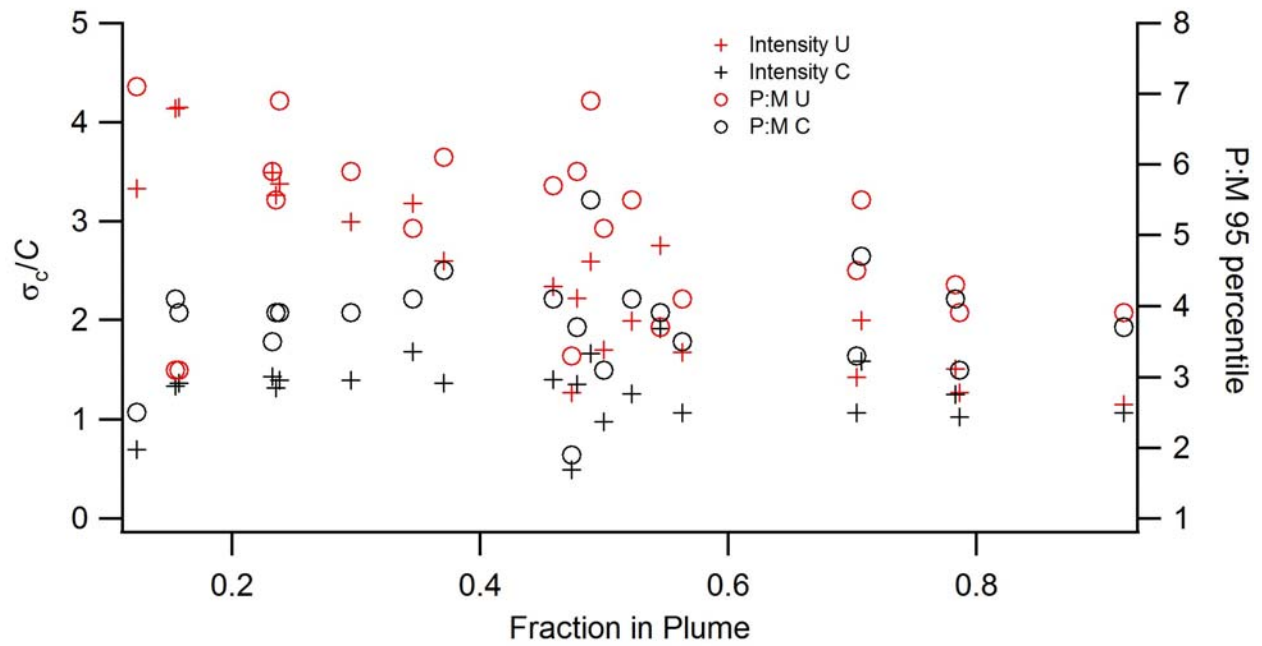


Figure 218. Unconditional (U) and conditional (C) concentration fluctuation intensities and 95th percentile P:M as a function of intermittency (fraction of time in plume).

This page is intentionally left blank.

REFERENCES

- ANSI/ANS-3.11, 2005. *Determining Meteorological Information at Nuclear Facilities*. American Nuclear Society, La Grange Park, IL, 31 pp.
- ANSI/ANS-3.2, 2006. *Administrative Controls and Quality Control Assurance for the Operational Phase of Nuclear Power Plants*. American Nuclear Society, La Grange Park, IL, 37 pp.
- Aubinet, M., A. Grelle, and others, 2000. Estimates of the annual net carbon and water exchange of forests: the EUROFLUX methodology. *Advances Ecological Res.*, **30**, 113-175.
- Barad, M. L. (Ed.), 1958. *Project Prairie Grass, a Field Program in Diffusion*, Volume I–III of *Geophysical Research Papers No. 59*. Air Force Cambridge Research Center, AFCRC-TR-58-235, USAF, Bedford, MA.
- Benner, R.L., and B. Lamb, 1985: A Fast Response Continuous Analyzer for Halogenated Atmospheric Tracers. *J. Atmos. Oceanic Technol.*, **2**, 582-589.
- Briggs, G.A., 1974. Diffusion estimation for small emissions, *in* Environmental Research Laboratories, Air Resources Laboratory, Atmosphere Turbulence and Diffusion Laboratory 1973 Annual Report, USAEC Report ATDL-106, NOAA, Oak Ridge, TN.
- Burba, G.G., D.K. McDermitt, and others, 2008. Addressing the influence of instrument surface heat exchange on the measurements of CO₂ flux from open-path gas analyzers. *Global Change Biology*, **14**, 1854-1876.
- Carter, R.G., 2003. *ARLFRD ATGAS Software Operator's Manual*. NOAA Air Resources Laboratory Field Research Division, Idaho Falls, ID, 26 pp.
- Clawson, K.L., R.G. Carter, and others, 2004. *URBAN 2000 SF₆ Atmospheric Tracer Field Tests*. NOAA Tech. Memo OAR ARL-253, Air Resources Laboratory, Idaho Falls, ID.
- Clawson, K.L., R.G. Carter, and others, 2005. *Joint Urban 2003 (JU03) SF₆ Atmospheric Tracer Field Tests*. NOAA Tech. Memo OAR ARL-254, Air Resources Laboratory, Idaho Falls, ID.
- Clawson, K.L., R.M. Eckman, and others, 2007. *Climatography of the Idaho National Laboratory, 3rd edition*. NOAA Tech. Memo OAR ARL-259, Air Resources Laboratory, Idaho Falls, ID.
- Clawson, K.L., R.M. Eckman, and others, 2009. *Roadside Sound Barrier Tracer Study 2008*. NOAA Tech. Memo OAR ARL-260, NOAA Air Resources Laboratory, Idaho Falls, ID, 212 pp.

Cramer, H.E., G.M. DeSanto, and others, 1964. *Meteorological Prediction Techniques and Data System*, Report GCA-64-3-G, Geophysical Corporation of America, Bedford, MA.

DOD, 2002. *Department of Defense Quality Systems Manual for Environmental Laboratories*, Final Version 2. U.S. Department of Defense, Environmental Data Quality Workgroup, Department of the Navy, Lead Service, 167 pp.

DOE, 2004. DOE/EH0173T Chapter 4, *Environmental Regulatory Guide for Radiological Effluent Monitoring and Environmental Surveillance*. U.S. Department of Energy, Office of Air, Water and Radiation Protection Policy & Guidance, 16 pp.

DOE, 2005. DOE Order 151.1C, *Comprehensive Emergency Management System*, U.S. Department of Energy, Office of Emergency Operations. Washington, D.C., 90 pp.

Eckman, R.M., 1994. Re-examination of empirically derived formulas for horizontal diffusion from surface sources. *Atmos. Environ.*, **28**, 265-272.

EPA, 2000a. *Guidance for Data Quality Assessment-Practical Methods for Data Analysis*. U.S. Environmental Protection Agency, QA/G-9, EPA/600/R-96/084.

EPA, 2000b. *Quality Systems. National Environmental Laboratory Accreditation Conference (NELAC)*. U.S. Environmental Protection Agency, QA/G-9, EPA/600/R-00/084, NTIS PB2001-104049.

EPA, 2000c. *Meteorological Monitoring Guidance for Regulatory Modeling Applications*. U.S. Environmental Protection Agency, EPA-454/R-99-005, 171 pp.

EPA, 2004. *Revised Assessment of Detection and Quantitation Approaches*. U.S. Environmental Protection Agency, EPA-821-B-04-005, Engineering and Analysis Division, Office of Science and Technology, Office of Water (4303T).

Finn, D., K. L. Clawson, R. G. Carter, J. D. Rich, R. M. Eckman, S. G. Perry, V. Isakov, and D. K. Heist, 2010. Tracer studies to characterize the effects of roadside noise barriers on near-road pollutant dispersion under varying atmospheric stability conditions. *Atmos. Environ.*, **44**, 204–214.

Foken, T., Leuning, R., Oncley, S., Mauder, M., & Aubinet, M., 2012. Corrections and Data Quality Control. In M. Aubinet, T. Vesala, & D. Papale (Eds.), *Eddy Covariance* (pp. 85–131). Springer Netherlands.

Fuquay, J. J., C. L. Simpson, and W. T. Hinds, 1964. Prediction of environmental exposures from sources near the ground based on Hanford experimental data. *J. Appl. Meteor.*, **3**, 761–770.

- Garodz, L. J., and K. L. Clawson, 1991: *Vortex Characteristics of C5A/B, C141B, and C130E aircraft applicable to ATC terminal flight operations, tower fly-by data*. NOAA/ERL/ARLFRD, Idaho Falls, Idaho, 250 pp.
- Garodz, L. J., and K. L. Clawson, 1993: *Volume 1, Vortex Wake Characteristics of B757-200 and B767-200 Aircraft Using the Tower Fly-By Technique. Volume 2, Appendices*. NOAA/ERL/ARLFRD, Idaho Falls, ID.
- Gifford, F.A., 1961. Use of routine meteorological observations for estimating atmospheric dispersion. *Nuclear Safety*, **2**, 47-51.
- Gifford, F.A., 1976. Turbulent diffusion-typing schemes; a review. *Nuclear Safety*, **17**, 68-86.
- Haugen, D. A. and J. J. Fuquay (Eds.), 1963. *The Ocean Breeze and Dry Gulch Diffusion Programs*, Volume I-II. Air Force Cambridge Research Laboratories, AFCRL-63-791.
- Islitzer, N. F. and R. K. Dumbauld, 1963. Atmospheric diffusion-deposition studies over flat terrain. *Intern. J. Air Water Pollution*, **7**, 999-1022.
- International Organization on Standardization (ISO), 1990: General Requirements for the Competence of Calibration and Testing Laboratories. *ISO/IEC Guide 25-1990*. 3 pp.
- Keith, L.H., W. Crummett, J. Deegan, R.A. Libby, J.K. Taylor, and G. Wentler, 1983. Principles of Environmental Analysis. *Analytical Chemistry*, **55**, 2210-2218.
- Martin, D.O., 1976. Comment on the change of concentration standard deviations with distance. *J. Air Pollut. Control Assoc.*, **26**, 145-146.
- Pasquill, F., 1961. The estimation of the dispersion of windborne material. *Meteorol. Mag.*, **90**, 33-49.
- Pasquill, F., 1975. *Some Topics Relating to Modeling of Dispersion in Boundary Layer*. EPA-650/4-75-015, U.S. Environmental Protection Agency, Washington, D.C.
- Pasquill, F., 1976. *Atmospheric Dispersion Parameters in Gaussian Plume Modeling, Part II: Possible Requirements for Change in the Turner Workbook Values*. U.S. Environmental Protection Agency, EPA-600/4-76-030b, 52 pp.
- Sagendorf, J. F. and C. R. Dickson, 1974. *Diffusion under low windspeed, inversion conditions*. NOAA Tech. Memo ERL ARL-52, Air Resources Laboratory, Idaho Falls, ID.
- Sagendorf, J. F., R. G. Carter, and K. L. Clawson, 2001. *MDIFF Transport and Diffusion Models*. NOAA Tech. Memorandum OAR ARL-238, Air Resources Laboratory, Idaho Falls, ID.

Schotanus, P., Nieuwstadt, F.T.M., De Bruin, H.A.R., 1983. Temperature measurement with a sonic anemometer and its application to heat and moisture fluxes. *Bound.-Layer Meteorol.* **26**, 81–93. doi:10.1007/BF00164332.

Slade, D. H. (Ed.), 1968. *Meteorology and Atomic Energy*. U. S. Atomic Energy Commission, Office of Information Services. Available as TID-24190 from National Technical Information Service.

Start, G. E., J. F. Sagendorf, G. R. Ackermann, J. H. Cate, N. F. Hukari, and C. R. Dickson. 1984. *Idaho Field Experiment 1981, Volume II: Measurement data, NUREG/CR-3488 Vol 2*.

Start, G.E., and L.L. Wendell, 1974. *Regional effluent dispersion calculations considering spatial and temporal meteorological variations*. NOAA Tech. Memo, ERLARL-44, 63 p.

Taylor, G.I., 1921. Diffusion by continuous movements. *Proc. London Math. Soc.*, **20**, 196-211.

Turner, D.B., 1969. *Workbook of Atmospheric Diffusion Estimates*. USEPA 999-AP-26, U. S. Environmental Protection Agency, Washington, DC., 84 pp.

Turner, D.B., 1970. *Workbook of Atmospheric Dispersion Estimates*. U.S. Environmental Protection Agency, Washington, D.C.

Vickers, D., and L. Mahrt, 1997. Quality control and flux sampling problems for tower and aircraft data. *J. Atmos. Oceanic Technol.*, **14**, 512-526.

Webb, E. K., Pearman, G. L., Leuning, R., 1980. Correction of flux measurements for density effects due to heat and water vapour transfer. *Q. J. R. Meteorol. Soc.* **106**, 85-100. doi:10.1002/qj.49710644707.

Yamartino, R.J., 1984. A comparison of several "single-pass" estimators of the standard deviation of wind direction. *J. Climate Appl. Meteor.*, **23**, 1362-1366.